frontiers | Research Topics

Plant-rhizobia symbiosis and nitrogen fixation in legumes

Edited by
Senjuti Sinharoy, Jesus Montiel and Chang Fu Tian

Published in
Frontiers in Plant Science

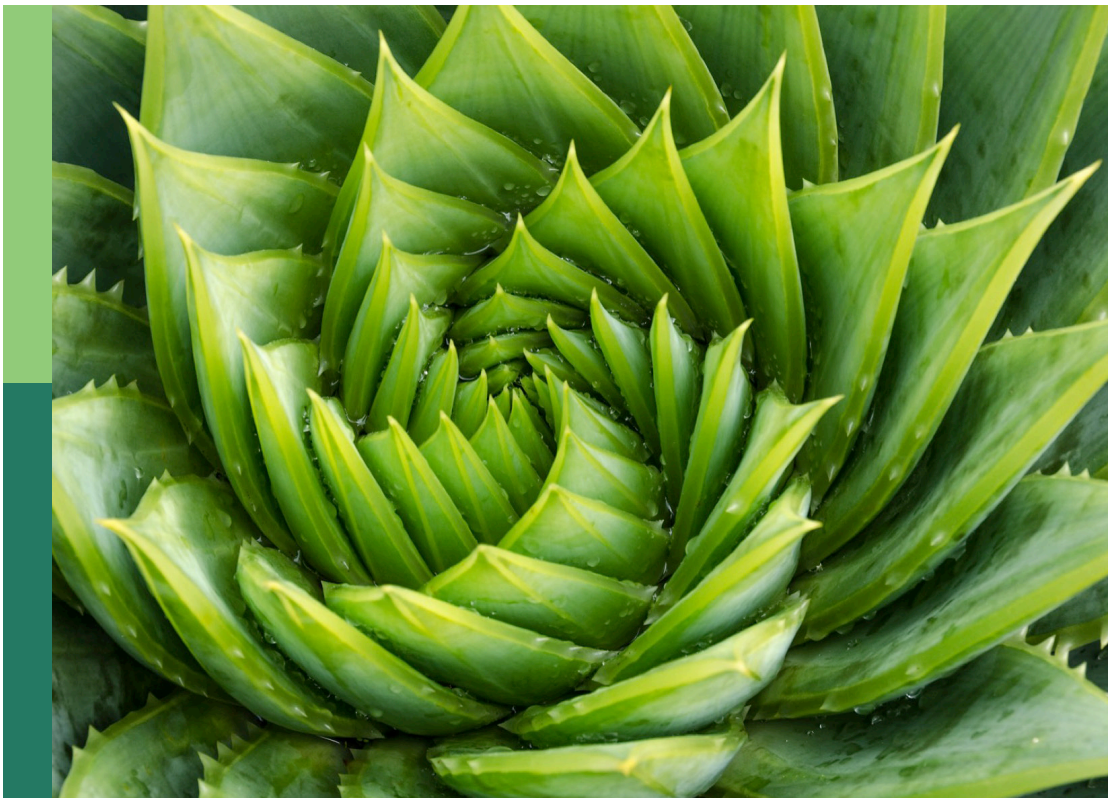

ISSN 1664-8714
ISBN 978-2-8325-4648-2
DOI 10.3389/978-2-8325-4648-2

About Frontiers

Frontiers is more than just an open access publisher of scholarly articles: it is a pioneering approach to the world of academia, radically improving the way scholarly research is managed. The grand vision of Frontiers is a world where all people have an equal opportunity to seek, share and generate knowledge. Frontiers provides immediate and permanent online open access to all its publications, but this alone is not enough to realize our grand goals.

Frontiers journal series

The Frontiers journal series is a multi-tier and interdisciplinary set of open-access, online journals, promising a paradigm shift from the current review, selection and dissemination processes in academic publishing. All Frontiers journals are driven by researchers for researchers; therefore, they constitute a service to the scholarly community. At the same time, the *Frontiers journal series* operates on a revolutionary invention, the tiered publishing system, initially addressing specific communities of scholars, and gradually climbing up to broader public understanding, thus serving the interests of the lay society, too.

Dedication to quality

Each Frontiers article is a landmark of the highest quality, thanks to genuinely collaborative interactions between authors and review editors, who include some of the world's best academicians. Research must be certified by peers before entering a stream of knowledge that may eventually reach the public - and shape society; therefore, Frontiers only applies the most rigorous and unbiased reviews. Frontiers revolutionizes research publishing by freely delivering the most outstanding research, evaluated with no bias from both the academic and social point of view. By applying the most advanced information technologies, Frontiers is catapulting scholarly publishing into a new generation.

What are Frontiers Research Topics?

Frontiers Research Topics are very popular trademarks of the *Frontiers journals series*: they are collections of at least ten articles, all centered on a particular subject. With their unique mix of varied contributions from Original Research to Review Articles, Frontiers Research Topics unify the most influential researchers, the latest key findings and historical advances in a hot research area.

Find out more on how to host your own Frontiers Research Topic or contribute to one as an author by contacting the Frontiers editorial office: frontiersin.org/about/contact

Plant-rhizobia symbiosis and nitrogen fixation in legumes

Topic editors

Senjuti Sinharoy — National Institute of Plant Genome Research (NIPGR), India
Jesus Montiel — National Autonomous University of Mexico, Mexico
Chang Fu Tian — China Agricultural University, China

Citation

Sinharoy, S., Montiel, J., Tian, C. F., eds. (2024). *Plant-rhizobia symbiosis and nitrogen fixation in legumes*. Lausanne: Frontiers Media SA.
doi: 10.3389/978-2-8325-4648-2

Table of contents

frontiers | Frontiers in Plant Science

TYPE Editorial
PUBLISHED 11 March 2024
DOI 10.3389/fpls.2024.1392006

OPEN ACCESS

EDITED AND REVIEWED BY
Andrea Genre,
University of Turin, Italy

*CORRESPONDENCE
Senjuti Sinharoy
ssinharoy@nipgr.ac.in
Chang-Fu Tian
cftian@cau.edu.cn
Jesús Montiel
jmontiel@ccg.unam.mx

RECEIVED 26 February 2024
ACCEPTED 28 February 2024
PUBLISHED 11 March 2024

CITATION
Sinharoy S, Tian C-F and Montiel J (2024) Editorial: Plant-rhizobia symbiosis and nitrogen fixation in legumes. *Front. Plant Sci.* 15:1392006. doi: 10.3389/fpls.2024.1392006

Editorial: Plant-rhizobia symbiosis and nitrogen fixation in legumes

Senjuti Sinharoy[1]*, Chang-Fu Tian[2]* and Jesús Montiel[3]*

[1]Plant-Microbe Interaction, National Institute of Plant Genome Research (NIPGR) New Delhi, New Delhi, India, [2]State Key Laboratory of Plant Environmental Resilience, College of Biological Sciences, China Agricultural University, Beijing, China, [3]Center for Genomic Sciences, National Autonomous University of Mexico, Cuernavaca, Mexico

KEYWORDS

legumes, symbiosis, nodule, rhizobia, nitrogen fixation

Editorial on the Research Topic
Plant-rhizobia symbiosis and nitrogen fixation in legumes

Nitrogen (N) is essential for life, but eukaryotes lack the ability to access this element, as only prokaryotic enzymes can convert N to ammonia. The Haber-Bosch process revolutionized agriculture by enabling synthetic N-fertilizer production, but its overuse and mismanagement created significant environmental challenges (Rockstrom et al., 2009; Richardson et al., 2023). Biological Nitrogen Fixation (BNF) by diazotrophic bacteria and symbiotic nitrogen fixation (SNF) by N-fixing plants offer age-old solutions to the N-problem (Adams et al., 2018).

In this context, legumes represent a valuable biological resource to migrate into a sustainable agriculture, since in N-deficient soil, they engage in symbiosis with rhizobia. In the rhizosphere, nodulation factors (NFs) secreted by rhizobia prompt mitotic activity in the root cortex cells, triggering de-differentiation and nodule formation. Concurrently, rhizobia invade root hair cells, guided by plant-derived infection threads (ITs), towards dividing plant cells. Once inside, rhizobia are endocytosed and become enclosed by plant membrane leading to the formation of 'symbiosomes', where they multiply and function as nitrogen-fixing entities. This Research Topic encompasses eleven articles addressing both bacterial and plant aspects essential for SNF (Kang et al., 2016; Roy et al., 2020), and the agronomical benefits of this mutualistic association.

Legumes

It is estimated that around 25% of nodulating legumes employ an alternative rhizobial colonization process, called intercellular infection, where bacteria invade the host plant between the epidermal cells or by crack entry (Quilbe et al., 2022). Since the molecular basis of this mechanism is largely unknown, García-Soto et al. conducted a large-scale mutant screening to discover genes recruited in the intercellular symbiotic colonization of the

Agrobacterium pusense strain IRBG74 on *Lotus japonicus* roots. The forward genetic approach was followed by sequencing the flanking regions of the mutagen to locate the potential causative genes.

Iron is crucial for various rhizobial and plant enzymes essential for BNF, including regulatory proteins like FixL and FixJ (Gilles-Gonzalez et al., 1991), nitrogen fixing enzymes NifH and NifDK (Dixon, 1998) and plant protein leghemoglobin (Wang et al., 2019; Brear et al., 2013). Iron transfer to nodules occurs through both apoplastic and symplastic routes and involves several transporters (Brear et al., 2013; Kryvoruchko et al., 2018; Tejada-Jiménez et al., 2015). MtVTL8 (Vacuolar Iron Transporter (VIT)-Like) is a major transporter responsible for delivering iron to the symbiosome in *Medicago truncatula* (Walton et al., 2020). In this Research Topic, Cai et al. highlights MtVTL8's unconventional mechanism of iron transport across the symbiosome membrane (SM), as revealed through genetic, structural prediction, and biochemical analyses.

The SNF imposes a significant energy burden on plants due to its high photosynthetic cost. Legumes regulate nodule number using a systemic signalling called autoregulation of nodulation (AON). The SUPER NUMERARY NODULES (MtSUNN), a leucine-rich repeat receptor-like kinase in the shoot, perceives root-derived peptide signals (MtCLE12 and MtCLE13) (Kang et al., 2016; Kassaw et al., 2017; Imin et al., 2018). *MtCLE12/13* is activated in the root by the master transcription factor of nodulation, Nodule Inception (NIN) (Laffont et al., 2020). Thomas and Frugoli discuss in this Research Topic, how the MtBAM2 protein, an ortholog of the Arabidopsis BARELY ANY MERISTEM family, collaborates with SUNN, crucial for nodule meristem establishment. Additionally, Shen and Feng provide a review detailing NIN's multifaceted role from infection to symbiosome development and AON.

Legumes also inhibit nodule formation under nitrogen sufficient condition (Kang et al., 2016) and interestingly, this effect can be partially alleviated by the organic macromolecule humic acid (HA). Zhang et al. further explored this phenomenon, by analysing the transcriptomic response of soybean nodules treated with HA under high nitrogen levels. Limited availability of phosphorus has a negative impact on nodule formation (Sulieman et al., 2013). Molecular studies using Arabidopsis have elucidated mechanisms controlling inorganic phosphate homeostasis. Under phosphate sufficiency, PHOSPHATE2 (PHO2) protein facilitate phosphate transporter degradation, limiting uptake. In phosphate deficiency, *microRNA399* (*miR399*) promotes PHO2 degradation (Aung et al., 2006; Bari et al., 2006). Huertas et al. demonstrated that MtPHO2b and MtPHO2c genes play a crucial role in regulating SNF by modulating plant phosphate homeostasis. Importantly, the complex molecular network in the legume-rhizobia symbiosis includes posttranscriptional regulation of gene expression by small RNAs (Roy et al., 2020), which are associated to ARGONAUTE proteins. Sánchez-Correa et al. explored the impact of RNAi-mediated silencing of Argonaute5 in roots and nodules of *Phaseolus vulgaris*. Additionally, they detected small RNAs bound to PvAGO5 at different stages of the nodulation process.

Rhizobia

Rhizobial nodulation factors (NFs) and type III secretion effectors (T3SEs) are key players in NF-dependent and NF-independent nodulation processes, respectively. It is not rare for rhizobia to harbour both nodulation genes and genes encoding type III secretion system (T3SS) and T3SEs. Available evidence from the intensively studied species *Sinorhizobium fredii* supports a regulatory network for these key symbiosis genes involving transcriptional factors NodD1, SyrM, NodD2, NolR and TtsI. In this Research Topic, Navarro-Gómez et al. compared transcriptional profiles, symbiotic performance and NF composition of *S. fredii* HH103 derivatives related to these regulatory genes, and proposed an updated regulatory model. NodD1 activates the transcription of nodulation genes and TtsI that in turn upregulates T3SS/T3SE genes. On the other hand, NodD1 can also activate the transcription of *syrM-nodD2* and *syrM-nolR* modules, and NodD2 and NolR negatively regulate TtsI and NodD1 regulons. Moreover, negative regulation of *nodD2* by NolR, feedback repression of *syrM* by NodD2 and NolR, antagonistic repression between TtsI and SyrM, and autoregulation of NodD1, SyrM, NolR and TtsI were proposed. Further *in vivo* and *in vitro* protein-DNA interaction evidence can be helpful for clarifying these regulatory effects as direct and/or indirect output. The work by Navarro-Gómez et al. provides novel insight into the overlooked complexity in the regulation network of key symbiosis genes, which deserves further exploration to guide engineering elite rhizobial inoculants.

Rhizobia can live saprophytically in bulk soils, colonize rhizosphere and rhizoplane, live as host endophytes, enter intracellular symbiosis with compatible legume plants, and release from senescent nodules. In this Research Topic, Agudelo et al. reviewed related literatures on the role of direct or indirect microbial interactions that alter rhizobial fitness in rhizosphere, during nodulation and within nodules. This is a timely summary of multipartite interactions involving legumes, rhizobia and other microorganisms. Authors further highlighted several understudied issues e.g. the significance of microbial interactions within nitrogen-fixing and senescent nodules, and after nodule senescence; genetic bases and eco-evolutionary dynamics underlying microbial interactions. Further efforts in addressing these questions by recruiting a multidisciplinary strategy involving genetics, physiology, molecular biology, ecology and evolution can be helpful.

Agricultural impact

In the last decades the benefits of SNF in agriculture has been largely documented. However, this extraordinary mutualistic association can be further exploited. In this regard, Xu et al. discovered that a mixed planting of *Medicago sativa* and *Bromus inermis* resulted in significantly higher hay yield compared to a monoculture grassland. For farmers, a key aspect to implement SNF

in the field, is the prediction of the expected yield. This represents a challenging task, considering the biotic and abiotic factors that influence SNF. However, Jemo et al. conducted a multifactorial analysis using mapped soil properties and weather variables, to predict by machine-learning techniques soybean yield in fields supplemented with phosphorus and inoculated with rhizobium.

Author contributions

SS: Conceptualization, Writing – original draft, Writing – review & editing. C-FT: Conceptualization, Writing – original draft, Writing – review & editing. JM: Conceptualization, Writing – original draft, Writing – review & editing.

Funding

The author(s) declare that financial support was received for the research, authorship, and/or publication of this article. NIPGR core grant and SERB Power Grant (SPG/2022/000171) to SS National Key Research and Development Program of China (grant number 2022YFA0912100) and the 2115 Talent Development Program of China Agricultural University to C-FT Dirección General de Asuntos del Personal Académico (DGAPA)-Universidad Nacional Autónoma de México (UNAM) – Programa de Apoyo a Proyectos de Investigación e Innovación Tecnológica (PAPIIT, grant IA200723) to JM.

Conflict of interest

The authors declare that the research was conducted in the absence of any commercial or financial relationships that could be construed as a potential conflict of interest.

The author(s) declared that they were an editorial board member of Frontiers, at the time of submission. This had no impact on the peer review process and the final decision.

Publisher's note

References

Adams, M. A., Buchmann, N., Sprent, J., Buckley, T. N., and Turnbull, T. L. (2018). Crops, nitrogen, water: are legumes friend, foe, or misunderstood ally? *Trends Plant Sci.* 23, 539–550. doi: 10.1016/j.tplants.2018.02.009

Aung, K., Lin, S. I., Wu, C. C., Huang, Y. T., Su, C. L., and Chiou, T. J. (2006). pho2, a phosphate overaccumulator, is caused by a nonsense mutation in a microRNA399 target gene. *Plant Physiol.* 141, 1000–1011. doi: 10.1104/pp.106.078063

Bari, R., Datt Pant, B., Stitt, M., and Scheible, W. R. (2006). PHO2, microRNA399, and PHR1 define a phosphate-signaling pathway in plants. *Plant Physiol.* 141, 988–999. doi: 10.1104/pp.106.079707

Brear, E. M., Day, D. A., and Smith, P. M. (2013). Iron: an essential micronutrient for the legume-rhizobium symbiosis. *Front. Plant Sci.* 4. doi: 10.3389/fpls.2013.00359

Dixon, R. (1998). The oxygen-responsive NIFL-NIFA complex: a novel two-component regulatory system controlling nitrogenase synthesis in gamma-proteobacteria. *Arch. Microbiol.* 169, 371–380. doi: 10.1007/s002030050585

Gilles-Gonzalez, M. A., Ditta, G. S., and Helinski, D. R. (1991). A haemoprotein with kinase activity encoded by the oxygen sensor of Rhizobium meliloti. *Nature* 350, 170–172. doi: 10.1038/350170a0

Imin, N., Patel, N., Corcilius, L., Payne, R. J., and Djordjevic, M. A. (2018). CLE peptide tri-arabinosylation and peptide domain sequence composition are essential for SUNN-dependent autoregulation of nodulation in Medicago truncatula. *New Phytol.* 218, 73–80. doi: 10.1111/nph.15019

Kang, Y., Li, M., Sinharoy, S., and Verdier, J. (2016). A snapshot of functional genetic studies in Medicago truncatula. *Front. Plant Sci.* 7. doi: 10.3389/fpls.2016.01175

Kassaw, T., Nowak, S., Schnabel, E., and Frugoli, J. (2017). ROOT DETERMINED NODULATION1 is required for. *Plant Physiol.* 174, 2445–2456. doi: 10.1104/pp.17.00278

Kryvoruchko, I. S. I. S., Routray, P., Sinharoy, S., Torres-Jerez, I., Tejada-Jiménez, M., Finney, L. A. L. A., et al. (2018). An iron-activated citrate transporter, MtMATE67, is required for symbiotic nitrogen fixation. *Plant Physiol.* 176, 2315–2329. doi: 10.1104/pp.17.01538

Laffont, C., Ivanovici, A., Gautrat, P., Brault, M., Djordjevic, M. A., and Frugier, F. (2020). The NIN transcription factor coordinates CEP and CLE signaling peptides that regulate nodulation antagonistically. *Nat. Commun.* 11, 3167. doi: 10.1038/s41467-020-16968-1

Quilbe, J., Montiel, J., Arrighi, J. F., and Stougaard, J. (2022). Molecular mechanisms of intercellular rhizobial infection: novel findings of an ancient process. *Front. Plant Sci.* 13. doi: 10.3389/fpls.2022.922982

Richardson, K., Steffen, W., Lucht, W., Bendtsen, J., Cornell, S. E., Donges, J. F., et al. (2023). Earth beyond six of nine planetary boundaries. *Sci. Adv.* 9, eadh2458. doi: 10.1126/sciadv.adh2458

Rockstrom, J., Steffen, W., Noone, K., Persson, A., Chapin, F. S. 3rd, Lambin, E. F., et al. (2009). A safe operating space for humanity. *Nature* 461, 472–475. doi: 10.1038/461472a

Roy, S., et al. (2020) 32, 15–41. NLM (Medline).

Sulieman, S., Ha, C. V., Schulze, J., and Tran, L. S. (2013). Growth and nodulation of symbiotic Medicago truncatula at different levels of phosphorus availability. *J. Exp. Bot.* 64, 2701–2712. doi: 10.1093/jxb/ert122

Tejada-Jiménez, M., Castro-Rodríguez, R., Kryvoruchko, I., Lucas, M. M., Udvardi, M., Imperial, J., et al. (2015). Medicago truncatula natural resistance-associated macrophage Protein1 is required for iron uptake by rhizobia-infected nodule cells. *Plant Physiol.* 168, 258–272. doi: 10.1104/pp.114.254672

Walton, J. H., Kontra-Kováts, G., Green, R. T., Domonkos, Á., Horváth, B., Brear, E. M., et al. (2020). The Medicago truncatula Vacuolar iron Transporter-Like proteins VTL4 and VTL8 deliver iron to symbiotic bacteria at different stages of the infection process. *New Phytol.* 228, 651–666. doi: 10.1111/nph.16735

Wang, L., Rubio, M. C., Xin, X., Zhang, B., Fan, Q., Wang, Q., et al. (2019). CRISPR/Cas9 knockout of leghemoglobin genes in Lotus japonicus uncovers their synergistic roles in symbiotic nitrogen fixation. *New Phytol.* 224, 818–832. doi: 10.1111/nph.16077

frontiers | Frontiers in Plant Science

TYPE Original Research
PUBLISHED 17 November 2022
DOI 10.3389/fpls.2022.1034419

OPEN ACCESS

EDITED BY
Juan Manuel Ruiz-Lozano,
Spanish National Research Council (CSIC), Spain

REVIEWED BY
Maria Eugenia Zanetti,
National University of La Plata, Argentina
Anca Macovei,
University of Pavia, Italy

*CORRESPONDENCE
Oswaldo Valdés-López
oswaldovaldesl@unam.mx
Damien Formey
formey@ccg.unam.mx

†PRESENT ADDRESS
María del Rocío Reyero-Saavedra,
Centro de Ciencias Genómicas, Universidad Nacional Autónoma de México, Cuernavaca, Morelos, Mexico

SPECIALTY SECTION
This article was submitted to Plant Symbiotic Interactions, a section of the journal Frontiers in Plant Science

RECEIVED 01 September 2022
ACCEPTED 19 October 2022
PUBLISHED 17 November 2022

CITATION
Sánchez-Correa MdS, Isidra-Arellano MC, Pozas-Rodríguez EA, Reyero-Saavedra MdR, Morales-Salazar A, del Castillo SML-C, Sanchez-Flores A, Jiménez-Jacinto V, Reyes JL, Formey D and Valdés-López O (2022) Argonaute5 and its associated small RNAs modulate the transcriptional response during the rhizobia-*Phaseolus vulgaris* symbiosis. *Front. Plant Sci.* 13:1034419. doi: 10.3389/fpls.2022.1034419

Argonaute5 and its associated small RNAs modulate the transcriptional response during the rhizobia-*Phaseolus vulgaris* symbiosis

María del Socorro Sánchez-Correa[1], Mariel C. Isidra-Arellano[1], Eithan A. Pozas-Rodríguez[1], María del Rocío Reyero-Saavedra[1†], Alfredo Morales-Salazar[1], Sarah Melissa Lugo-Caro del Castillo[2], Alejandro Sanchez-Flores[3], Verónica Jiménez-Jacinto[3], Jose L. Reyes[4], Damien Formey[2*] and Oswaldo Valdés-López[1*]

[1]Laboratorio de Genómica Funcional de Leguminosas, Facultad de Estudios Superiores Iztacala, Universidad Nacional Autónoma de México, Tlalnepantla, Estado de México, Mexico, [2]Centro de Ciencias Genómicas, Universidad Nacional Autónoma de México, Cuernavaca, Morelos, Mexico, [3]Unidad Universitaria de Secuenciación Masiva y Bioinformática, Instituto de Biotecnología, Universidad Nacional Autónoma de México, Cuernavaca, Morelos, Mexico, [4]Departamento de Biología Molecular de Plantas, Instituto de Biotecnología, Universidad Nacional Autónoma de México, Cuernavaca, Morelos, Mexico

Both plant- and rhizobia-derived small RNAs play an essential role in regulating the root nodule symbiosis in legumes. Small RNAs, in association with Argonaute proteins, tune the expression of genes participating in nodule development and rhizobial infection. However, the role of Argonaute proteins in this symbiosis has been overlooked. In this study, we provide transcriptional evidence showing that Argonaute5 (AGO5) is a determinant genetic component in the root nodule symbiosis in *Phaseolus vulgaris*. A spatio-temporal transcriptional analysis revealed that the promoter of *PvAGO5* is active in lateral root primordia, root hairs from rhizobia-inoculated roots, nodule primordia, and mature nodules. Transcriptional analysis by RNA sequencing revealed that gene silencing of *PvAGO5* affected the expression of genes involved in the biosynthesis of the cell wall and phytohormones participating in the rhizobial infection process and nodule development. PvAGO5 immunoprecipitation coupled to small RNA sequencing revealed the small RNAs bound to PvAGO5 during the root nodule symbiosis. Identification of small RNAs associated to PvAGO5 revealed miRNAs previously known to participate in this symbiotic process, further supporting a role for AGO5 in this process. Overall, the data presented shed light on the roles that PvAGO5 plays during the root nodule symbiosis in *P. vulgaris*.

KEYWORDS

argonaute proteins, microRNAs, rhizobial tRNA-derived sRNA fragments, root nodule symbiosis, legumes

Introduction

Legumes can fulfill their nitrogen needs by forming endosymbiosis with nitrogen-fixing soil bacteria collectively known as rhizobia. This symbiosis involves the modification of lateral roots to form the so-called root nodules (Schiessl et al., 2019; Soyano et al., 2019). These organs provide the appropriate environment for rhizobial nitrogenase to convert atmospheric nitrogen into ammonium. The formation of the root nodules requires the simultaneous and coordinated activation of two genetic programs. These programs allow the reactivation of cell division of the root cortex to form the nodule meristem and the infection of nodule cells by the rhizobia (Roy et al., 2020).

Legumes and rhizobia must communicate through diffusible signal molecules to activate the signaling networks required to establish the root nodule symbiosis. Legumes release flavonoids to the rhizosphere, where compatible rhizobia detect them (Phillips et al., 1992; Liu and Murray, 2016). In response, rhizobia release lipochitooligosaccharides (LCOs) that the legume host perceives through a set of plasma-membrane-located LysM domain receptor kinases (Dénarié et al., 1996; Broghammer et al., 2012; Murakami et al., 2018). Upon sensing these rhizobia-derived LCOs, a series of molecular responses are activated (Roy et al., 2020). Among them are rapid and continuous oscillations in nuclear and perinuclear calcium concentrations (Ehrhardt et al., 1996; Kosuta et al., 2008). Calcium-Calmodulin Kinase further decodes these calcium signatures, subsequently phosphorylating the transcription factor (TF) CYCLOPS (Lévy et al., 2004; Singh and Parniske, 2012). CYCLOPS, through the action of DELLA proteins, forms a large complex with the TFs Nodule Signaling Pathway 2 (NSP2) and NSP1 to activate the expression of the *Nodule INception* (*NIN*) TF gene (Oldroyd and Long, 2003; Hirsch et al., 2009; Cerri et al., 2012; Jin et al., 2016). NIN, in turn, controls the expression of genes participating in the rhizobial infection, nodule development, and regulation of nodule number per root (Hirsch et al., 2009; Cerri et al., 2012; Soyano et al., 2014; Jin et al., 2016).

The root nodule symbiosis is also finely tuned by diverse small RNA (sRNA) classes, with microRNAs (miRNAs) being the most studied (Tiwari et al., 2021). miRNAs are approximately 21-nt long and control gene expression by mRNA cleavage, translational inhibition, or DNA methylation (Wang et al., 2019). miRNAs have a determinant role in regulating nodule development and, to some extent, the colonization of root nodule cells by rhizobia (Tiwari et al., 2021). For instance, miR169 targets the *Nuclear Factor-YA1* gene (formerly called *HAP2*), which controls nodule meristem persistence and the progression of rhizobial infection in *Medicago truncatula* (Combier et al., 2006). miR171c plays a role during the rhizobial infection stage by targeting the *NSP2* TF gene in *Lotus japonicus* (De Luis et al., 2012). Evidence in *L. japonicus* and *M. truncatula* indicates that miR2111 is a mobile miRNA required to trigger the nodule development program (Tsikou et al., 2018; Okuma et al., 2020).

Modulating the legume host defense is also crucial for a successful symbiosis with rhizobia (Berrabah et al., 2015; Wang et al., 2016; Berrabah et al., 2019). Evidence in *Glycine max* and *M. truncatula* indicates that miR482, miR2109, and miR2118, which target *NB-LRR* genes – encoding receptors that recognize specific pathogen effectors and trigger plant resistance responses – modulate the legume immune response during the root nodule symbiosis (Li et al., 2010; Sós-Hegedus et al., 2020). This symbiosis is not only regulated by legume-derived sRNAs. Recently, it was reported that rhizobial transfer RNA (tRNA)-derived sRNA fragments (tRFs) help regulate the expression of host genes participating in the rhizobial infection and nodule development in *G. max* (Ren et al., 2019).

ARGONAUTE proteins (AGOs) are present in eukaryotes and associate with sRNAs to form the RNA-induced silencing complex (RISC) which regulates the expression of sRNA target genes (Hutvagner and Simard, 2008). Eukaryotic AGOs are structurally conserved and contain four domains: a variable N-terminal domain, PIWI-ARGONAUTE-ZWILLE (PAZ), MIDdle (MID), and PIWI (Tolia and Joshua-Tor, 2007). The PAZ domain binds sRNAs, while the MID domain recognizes the 5' nucleotide of sRNAs. The PIWI domain adopts an RNase H-like fold, allowing most AGOs to cleave target messenger RNAs complementary to the bound sRNAs (Song et al., 2004). The number of AGO genes present in plant genomes is variable and is plant species-dependent. For instance, the *Arabidopsis thaliana* genome encodes 10 AGOs (Vaucheret, 2008). In contrast, there are 17 in maize (Qian et al., 2011), 19 in rice (Kapoor et al., 2008), and 14 in *Phaseolus vulgaris* (Reyero-Saavedra et al., 2017).

In plants, both sRNAs and AGOs tune diverse developmental processes and coordinate adaptation to the environment by serving as sequence-specific regulators of genes (Manavella et al., 2019). For instance, the expression of seventeen maize AGOs is differentially regulated in response to cold, salinity, drought, and abscisic acid addition, suggesting that AGOs are determinant in the adaptation to these stresses (Zhai et al., 2019). The participation of diverse sRNAs during nodule development suggests that AGOs also play roles in the root nodule symbiosis. Indeed, we previously reported that AGO5 expression increases in response to rhizobia in both *P. vulgaris* and *G. max* and demonstrated that silencing *AGO5* reduces both nodule size and the number of rhizobia-infected nodule cells (Reyero-Saavedra et al., 2017). We therefore hypothesize that AGO5 plays roles in coordinating the genetic programs involved in rhizobial infection and nodule development.

In this study, we provide new evidence demonstrating that AGO5 contributes to regulation of the rhizobial infection process and nodule development in *P. vulgaris*. A spatio-temporal analysis in *P. vulgaris promoterPvAGO5:GUS (pPvAGO5:GUS)* transgenic roots revealed that *AGO5* is

expressed in root hairs in response to rhizobia. This analysis also indicates that the *PvAGO5* promoter has strong activity in nodule primordia and mature nodules. Further transcriptional analysis by genome-wide mRNA sequencing revealed that gene silencing of *PvAGO5* affects the expression of key nodulation genes as well as others related to the biosynthesis of the cell wall and phytohormones involved in the rhizobial infection process and nodule development. PvAGO5 immunoprecipitation coupled with sRNA sequencing revealed the sRNAs bound into AGO5 during the root nodule symbiosis. Among the sRNA associated to AGO5 were members of miR166, miR319, miR396, and miR2118 miRNA families, all of which were previously shown to participate in the root nodule symbiosis in different legumes. We also observed that AGO5's sRNA cargo in mature nodules contains rhizobial-derived tRFs that target *P. vulgaris* genes also implicated in this symbiosis. The data presented shed new light on AGO5's participation during the root nodule symbiosis in *P. vulgaris*.

Material and methods

Plant materials

P. vulgaris cultivar Negro Jamapa was used in this study. Seeds were surface sterilized and germinated as reported in Reyero-Saavedra et al. (2017). Two-day-old seedlings were transferred to 2 L pots containing moist perlite, kept in a growth chamber at 25-27°C, and watered with Summerfield nutrient solution (Summerfield et al., 1977) every three days.

Bacterial strains and culture conditions

Rhizobium tropici CIAT 899 strain was used to inoculate *P. vulgaris* seedlings. *R. tropici* cells were grown for two days at 30°C on PY medium (5 g/L peptone; 3 g/L yeast extract) supplemented with 0.7 M $CaCl_2$ and 20 µg/mL nalidixic acid. After two days, *R. tropici* cells were harvested and resuspended in sterile water at $O.D_{600nm}$= 0.3. One mL of this bacterial suspension was used to inoculate *P. vulgaris* seedlings individually.

Empty binary vectors pKGWFS7 and pTDT-DC-RNAi were propagated in *Escherichia coli* DB3.1, *promoterPvAGO5::GUS::GFP*, and the RNA interference (RNAi) against *PvAGO5* (see below for details of these genetic constructs) were propagated in DH5α.

Agrobacterium rhizogenes K599 strain was used to generate transgenic roots in *P. vulgaris* plants (see below for details). *A. rhizogenes* cells were grown on Luria-Bertani (LB) plates for two days at 30°C. 100 µg/mL spectinomycin was added to select for the presence of plasmid vectors.

Plasmid construction

To analyze *PvAGO5* promoter activity, a 1,800 bp DNA fragment upstream of the start codon was PCR-amplified from genomic DNA of *P. vulgaris* var. Negro Jamapa using specific primers. The amplified fragment was then cloned into the pENTR-D-TOPO (Thermo Fisher Scientific) vector. The resulting pENTR-*pPvAGO5* plasmid was recombined into the pKGWFS7 binary vector containing *GUS* and *GFP* CDS, yielding the transcriptional *pPvAGO5::GUS::GFP* fusion.

A previously generated and reported RNAi construct was used to silence the expression of *PvAGO5* (Reyero-Saavedra et al., 2017).

All constructs were verified by DNA sequencing. Primer sequences for plasmid constructions are shown in Supplementary Table 1.

Agrobacterium rhizogenes-mediated transformation

Binary vectors with *pPvAGO5:GUS-GFP* or *PvAGO5*-RNAi constructs were mobilized into *A. rhizogenes* K599 strain by electroporation. The empty vectors pKGWFS7 or pTDT-DC-RNAi were used as controls. *A. rhizogenes*-mediated transformation was performed according to Estrada-Navarrete et al. (2007). *P. vulgaris* composite plants (plants with the transformed root system and untransformed shoot system) were grown in 2 L pots containing wet perlite. Tandem Double Tomato (TDT) or GFP fluorescence in transgenic roots was observed with a fluorescence stereomicroscope.

Lateral root phenotype under non-symbiotic conditions

To evaluate the effect of the gene silencing of *PvAGO5* in the lateral root development under non-symbiotic conditions, *A. rhizogenes*-mediated *pPvAGO5*-RNAi transgenic roots were generated in the *P. vulgaris* as described above. Transgenic roots expressing an empty vector were used as a control. Composite plants were watered with 5 mM KNO_3-supplemented Summerfield nutrient solution. After three weeks, transgenic roots showing TDT fluorescence were collected to evaluate the number, density and length of lateral roots. Lateral root density was calculated by dividing the number of lateral roots on each transgenic root with the length of the root. For these experiments, ten biological replicates, each one containing ten transgenic roots from independent composite plants, were included.

Nodulation assays in common bean wild type and composite plants

Two-day-old *P. vulgaris* wild-type or composite plants expressing the empty vector or the *PvAGO5*-RNAi construct were transferred to 2 L pots containing wet perlite and inoculated with 1 mL of *R. tropici* ($O.D._{600nm}$= 0.3). Plants were watered with nitrogen-free Summerfield nutrient solution (Summerfield et al., 1977) every three days. Inoculated plants were kept in a growth chamber at 25-27°C. Ten and twenty days after rhizobial inoculation, roots with nodule primordia and nitrogen-fixing nodules (mature nodules) were collected separately and immediately processed for PvAGO5 Immunoprecipitation assays or RNA-seq analyses (see below for details). For these experiments, three biological replicates containing six independent wild-type or composite plants were included.

AGO5 promoter activity under non-symbiotic conditions

To evaluate *PvAGO5* promoter activity under non-symbiotic conditions, *A. rhizogenes*-mediated *pPvAGO5:GUS-GFP* transgenic roots were generated in the *P. vulgaris* as described above. Composite plants were watered with 5 mM KNO_3-supplemented Summerfield nutrient solution. After three weeks, transgenic roots showing GFP fluorescence were collected for GUS staining as reported in (Isidra-Arellano et al., 2020). For this experiment, ten biological replicates containing ten composite plants and ten roots were included.

AGO5 promoter activity during the root nodule symbiosis

To evaluate *PvAGO5* promoter activity during the root nodule symbiosis, *A. rhizogenes*-mediated *pPvAGO5:GUS-GFP* transgenic roots were generated in the *P. vulgaris*. Composite plants were inoculated with 1 mL of *R. tropici* ($O.D._{600nm}$= 0.3). Rhizobia-inoculated plants were watered with nitrogen-free Summerfield nutrient solution. Upon one, ten and twenty days after rhizobia inoculation, transgenic roots, roots with nodule primordia and mature nodules were collected for GUS staining assays as reported in (Isidra-Arellano et al., 2020). For this experiment, ten biological replicates containing ten composite plants and ten roots were included.

RNA extraction and RT-qPCR analysis

To analyze the expression of genes listed in Supplementary Table 1, transgenic roots and mature nodules expressing the *PvAGO5*-RNAi construct and showing TDT fluorescence were immediately harvested in liquid nitrogen and stored at -80°C until used. Total RNA was isolated from roots and nodules from three different composite plants using the ZR Plant RNA miniprep (Zymo Research, USA) following the manufacturer's instructions. cDNA was synthesized from 1 µg of genomic DNA-free total RNA and used to analyze gene expression by RT-qPCR as we previously described in Isidra-Arellano et al. (2020). RT-qPCR primer sequences used in this study are provided in Supplementary Table 1. Three biological replicates, each one with six technical replicates, were included for this experiment.

Preparation of messenger RNA-Seq libraries and next-generation sequencing

Total RNA was isolated as described in the previous section from 0.5 g of one-day rhizobia- or mock-inoculated transgenic roots and transgenic mature nodules expressing an empty vector, or the *PvAGO5*-RNAi construct. Stranded messenger RNA-seq (mRNA-seq) libraries were generated from 1 µg of gDNA-free total RNA from each experimental condition and prepared using the TruSeq RNA Sample Prep kit (Illumina, San Diego, CA, USA) according to the manufacturer's instructions. For each experimental condition, three biological replicates containing six independent composite plants were included. Eighteen libraries were sequenced on an Illumina NextSeq 500 platform with a 150-cycle sequencing kit and a configuration of pair-end reads with a 75 bp read length. Library construction and sequencing were performed by the Unidad Universitaria de Secuenciación Masiva y Bioinformática (Instituto de Biotecnología, UNAM, México).

Mapping and processing messenger RNA-Seq reads

Adapter and contamination removal were carried out using in-house Perl scripts. Sequences were filtered based on quality (Q33, FASTQ Quality Filter v0.0.13, http://hannonlab.cshl.edu/fastx_toolkit/index.html). About ten million reads per sample were aligned to the *P. vulgaris* transcriptome (v2.1 from Phytozome v13) using Bowtie2 (v2.3.5) and the recommended parameters to match RSEM analysis input requirements (Langmead and Salzberg, 2012). Gene expression was calculated using the RNA-seq by Expectation Maximization (RSEM) method (v1.3.3) and the default parameters (Li and Dewey, 2011). Significantly Differentially Expressed Genes (DEGs: adjusted p-value ≤ 0.05) were identified using DESeq2, part of the Integrated Differential Expression Analysis MultiEXperiment (IDEAMEX) platform (Jiménez-Jacinto et al., 2019), with the RSEM expected counts. Gene Ontology (GO) term enrichment analysis was performed using AgriGO

(v2.0) and default parameters (FDR cutoff = 0.05) (Tian et al., 2017). Protein domain enrichment analysis was performed using PhytoMine tool from Phytozome (v13), with Holm-Bonferroni correction (FDR cutoff = 0.05). Heatmaps were created with ggplot2 and heatmap.2 libraries using R software (v4.1.2).

AGO5 immunoprecipitation, small RNAs isolation and sequencing

Uninoculated roots, roots bearing nodule primordia, and mature nodules from wild-type *P. vulgaris* were manually collected on ice. For each experimental condition, material from 100 plants was ground on ice with immunoprecipitation buffer (50 mM Tris-HCl pH7.5; 1.5 mM NaCl, 0.1% Nonidet P40, 4 mM $MgCl_2$, 2 mM DTT, and Sigma Protease inhibitor cocktail). Cell debris was removed by centrifugation twice for 15 min at 12,000 g at 4°C. Next, supernatants were precleared by incubation for 1 hour with 10 µl Protein A-Agarose (Roche). Samples were centrifuged at 1,500 g for 5 minutes at 4°C. Supernatants were incubated with Protein A-Agarose (Roche) supplemented with 2 µl anti-AGO5 for exactly 16 hours with rotation at 4°C. Samples were centrifuged at 1,500 g for 5 minutes at 4°C. The beads were washed three times with a washing buffer (50 mM Tris-HCl pH7.5, 150 mM NaCl, 0.1% Nonidet P40, 4 mM $MgCl_2$, 2 mM DTT, and Sigma Protease inhibitor cocktail). Next, beads were resuspended in 0.4 M NaCl and sRNAs were extracted by phenol:chloroform:iso-amyl alcohol extraction.

Nine small libraries (3 for uninoculated roots, 3 for roots bearing nodule primordia, and 3 for mature nodules) were generated from AGO5-bound sRNA using TruSeq small RNA Library Prep kit (Illumina, San Diego, CA, USA) according to the manufacturer's instructions. Libraries were sequenced on an Illumina NextSeq 500. Library construction and sequencing were performed by the Unidad Universitaria de Secuenciación Masiva y Bioinformática (Instituto de Biotecnología, UNAM, México).

Small RNA data analysis

Adapters and reads with quality mean lower than 33 were removed and the sequence redundancy collapsed using the FASTX-Toolkit suite (v0.0.13, http://hannonlab.cshl.edu/fastx_toolkit/index.html). Small RNAs were compared to Viridiplantae miRNAs from miRbase (v22), 277 P. *vulgaris* small RNAs previously identified and published in (Formey et al., 2015; Formey et al., 2016), and 10 tRFs from *Rhizobium etli* (Ren et al., 2019). Normalization was performed using DESeq2. Only the sRNAs lying within the top 1% of the most accumulated sequences in a given library, were selected for further analyses. Transcript targets for the identified sRNAs were predicted using psRNAtarget (V2) and default parameters (Dai et al., 2018). Venn diagrams were designed using DeepVenn (Hulsen et al., 2008).

Statistical analyses and graphics

Statistical analyses and graphic generation were conducted using R software 4.1.2. The specific tests performed are indicated in the legend of the corresponding figure.

Results

Down-regulation of *PvAGO5* increases the number and density of lateral roots under non-symbiotic conditions

Our previous transcriptional analyses by RT-qPCR showed that *PvAGO5* is preferentially expressed in *P. vulgaris* roots, compared to leaves (Reyero-Saavedra et al., 2017). However, these data do not provide spatiotemporal insights into *PvAGO5* expression in this essential organ for root nodule symbiosis. To tackle this, we cloned a 1.8 kb fragment of the *PvAGO5* promoter (*pPvAGO5*) and generated a transcriptional fusion to the *GUS* (β-glucuronidase) and *GFP* coding sequence. The Empty vector: *GUS-GFP* (control) or the *pPvAGO5:GUS-GFP* constructs were transfected separately into *P. vulgaris* using *A. rhizogenes*-mediated transformation (Estrada-Navarrete et al., 2007), and composite plants were grown and watered with nitrogen-containing Summerfield nutrient solution for three weeks. We observed no GUS activity in transgenic roots expressing the empty vector (Figures 1A, D). In contrast, in the absence of rhizobia, 65 out of 70 roots transformed with *pPvAGO5:GUS-GFP* displayed a weak GUS signal in the whole root, intensified to a strong signal in lateral root primordia and mature lateral roots (Figures 1B, E); whereas the other five roots showed the same GUS signal intensity through the entire root, (Figures 1C, F). GUS activity was absent in the root hairs of the 70 transgenic roots analyzed (Figures 1G, H).

The presence of *PvAGO5* activity in the lateral root primordia prompted us to compare the number, density, and length of lateral roots in *P. vulgaris* composite plants expressing an empty vector (control) or the *PvAGO5*-RNAi construct. This analysis indicated that the number of lateral roots and density was increased 15% in *PvAGO5*-RNAi transgenic roots compared to the empty vector controls, with no significant differences in root length (Figures 1I–K). Moreover, no growth defects in the root hairs were observed in *PvAGO5*-RNAi transgenic roots (Supplementary Figure 1). In summary, these data inform that *PvAGO5* is expressed mostly in lateral root primordia in the absence of rhizobia. Furthermore, they also suggest that AGO5 plays a role in lateral root development in *P. vulgaris*.

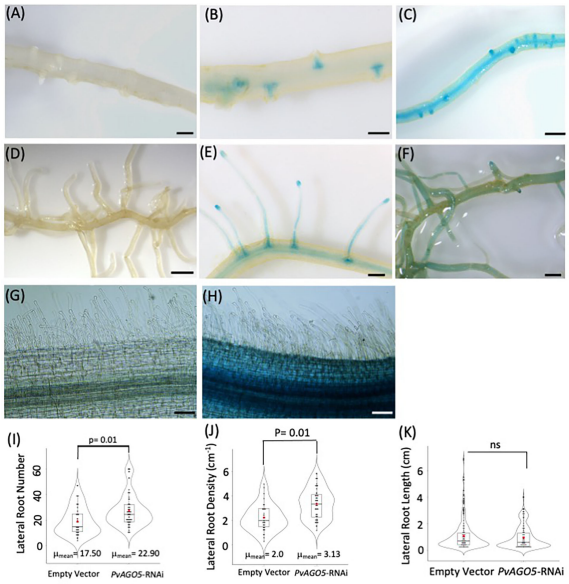

FIGURE 1
PvAGO5 is expressed in lateral roots under nonsymbiotic condition. *P. vulgaris composite* plants with transgenic roots expressing either the empty vector **(A, D, G)** or the *pPvAGO5:GUS-GFP* construct **(B, C, E, F, H)** were grown under optimal-nitrogen conditions for three weeks. Roots expressing the *pPvAGO5:GUS-GFP* displayed GUS signal in the lateral roots primordium and mature lateral roots **(B, C, E, F)**. Scale bars represent 500 μm. Images shown are representative of ten biological replicates, each one containing ten transgenic roots. Transgenic roots expressing the empty vector or *pPvAGO5:GUS-GFP* construct shown no GUS activity at the root hairs **(G, H)**. **(I)** Number and density **(J)** of lateral roots formed in transgenic roots expressing the empty vector or the *PvAGO5*-RNAi construct. **(K)** Lateral root length of *PvAGO5*-RNAi transgenic roots compared with the empty vector transgenic roots. Boxes indicate the second and third quartiles, with median and mean values indicated as a line and red dot, respectively. Data shown was obtained from ten biological replicates, each one containing ten transgenic roots. Statistical significance was obtained using Welch's *t*-test. ns, not significant

PvAGO5 is expressed in rhizobia-inoculated root hairs and nodules

We previously demonstrated by RT-qPCR that the expression of *PvAGO5* increases at one and three hours after inoculation with rhizobia as compared to non-inoculated roots, as well as in mature nodules (Reyero-Saavedra et al., 2017). To further understand the cellular expression pattern of *PvAGO5* across different stages of root nodule symbiosis, we evaluated its spatio-temporal promoter activity in common bean composite plants. These plants were inoculated with *R. tropici* and transgenic roots were harvested one, ten, and twenty days after inoculation to evaluate the *pPvAGO5:GUS* activity during the infection process, nodules primordia at the nodule emerging stage (nodule primordia), and in mature nodules, respectively. We observed no GUS activity in mock- and rhizobia-inoculated transgenic roots, or nodules expressing the empty vector (Figures 2A, B). Mock-inoculated *pPvAGO5:GUS-GFP* transgenic roots showed a weak GUS signal in the whole root (Figure 2A). After one day of rhizobial inoculation, *PvAGO5* is expressed in the entire root (Figure 2A). At this time-point, we also observed a faint but consistent GUS signal in the tips of root hairs from 60 out of 80 transgenic roots expressing the *pPvAGO5:GUS-GFP* construct (Figure 2A), whereas the other 20 roots showed no GUS activity in these cells (Supplementary Figure 2). Furthermore, at ten- and twenty-days post-inoculation with rhizobia, we observed a strong GUS activity in nodule primordia, mature nodules, and throughout the vasculature system (Figure 2B and Supplementary Figure 2). Altogether, our results show that *PvAGO5* expression is increased at early stages of the root nodule symbiosis. In addition, they demonstrate that the transcriptional activity of *PvAGO5* is further enhanced during the nodule development process.

Transcriptomic changes in *PvAGO5*-RNAi roots and mature nodules

To analyze global transcriptomic effects of *PvAGO5* down-regulation, empty vector (control) and *PvAGO5*-RNAi were analyzed from mock or *R. tropici*-inoculated roots at one day after inoculation and twenty-days-old nodules. For each time point, three biological replicates were analyzed using RNA-seq.

Overall, 10.7 to 12.2 million short sequence reads (2 X 75 bp) were generated from each of 18 RNA-seq libraries, with alignment rates to the reference genome ranging between 84-88%. Principal component analysis (PCA) showed a clustering of biological

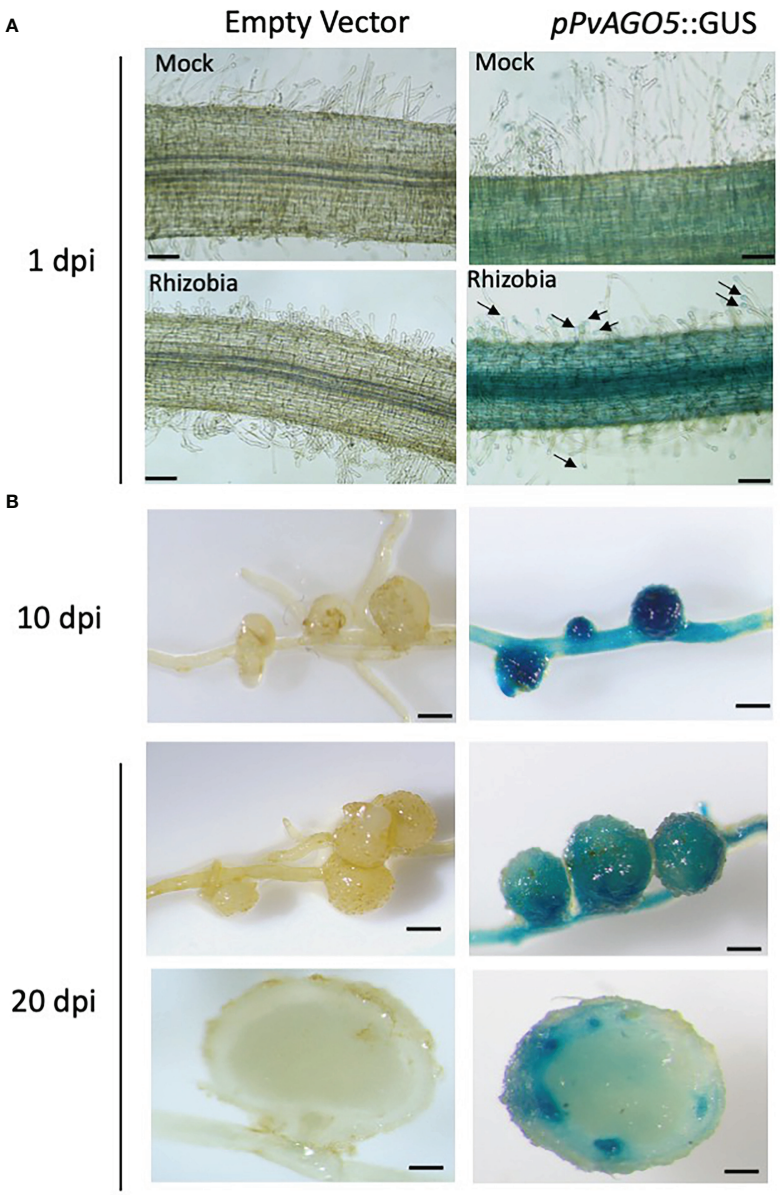

FIGURE 2
PvAGO5 is expressed in nodule primordia and mature nodules. *P. vulgaris composite* plants with transgenic roots expressing either the empty vector or the construct *pPvAGO5:GUS-GFP* were grown under low-nitrogen conditions and inoculated with *R. tropici* CIAT899. One **(A)**, ten and twenty days after inoculation with rhizobia, transgenic roots showing rhizobia-induced deformed root hairs **(A)**, or containing nodule primordia (**B**, middle panel) or mature nodules (**B**, last four panels) were collected and stained for three hours at 37°C. Roots expressing the *pPvAGO5:GUS-GFP* construct displayed GUS signal throughout the whole root and in the tip of root hairs (**A**, black arrows). A strong GUS signal was detected in nodule primordia and in mature nodules (**B**, middle panel). Scale bars represent 100 µm for pictures shown at panel A, and 1 mm for figures shown at panel B. Images shown are representative of ten biological replicates, each one containing ten transgenic roots.

replicates and silencing-dependent variation, with the first component explaining an average of ~54% of data variation (Supplementary Figure 3). Comparison of expression levels in each biological condition and at each time point (relative to the empty vector) revealed 2,295 differentially expressed genes (DEGs) with significant change in expression (adjusted $P < 0.05$), including 1,497 and 798 genes that were up- or down-regulated relative to empty vector, respectively (Supplementary Tables S3-S7). This transcriptional analysis confirmed the gene silencing of *PvAGO5* (two-fold reduction) in *PvAGO5*-RNAi transgenic roots and nodules. Furthermore, we observed that the expression of other AGO protein-encoding genes was not affected by the *PvAGO5*-

RNAi construct (Supplementary Table 2), which indicates that the gene silencing of *PvAGO5* was specific. To validate these transcriptional data sets, we randomly selected 11 genes and their expression levels were assessed by RT-qPCR. The results show similar trends between RNA-seq and RT-qPCR data (Supplementary Figure 4).

PvAGO5-RNAi roots show increased expression of cell wall- and jasmonic acid biogenesis-related genes, but decreased expression of transporter-encoding genes under non-symbiotic conditions

To gain insight into the role of AGO5 under non-symbiotic conditions, we compared the transcriptomes of transgenic roots carrying the *PvAGO5*-RNAi against the empty vector in the mock samples. This analysis led to the identification of 962DEGs, 598 up-regulated and 364 down-regulated genesin*PvAGO5*-RNAi roots, respectively (Figure 3 and Supplementary Table 3). Gene Ontology term enrichment analysis of the identified DEGs revealed that the most significant GO terms were those involved in cell wall biogenesis (Supplementary Table 8). Their upregulation in *PvAGO5*-RNAi transgenic roots suggests that AGO5 may play a role in negatively regulating the biogenesis of the cell wall during root development.

Further KEGG pathway functional classification not only confirmed the participation of AGO5 in cell wall biogenesis, but also revealed that gene silencing of *PvAGO5* increases the expression of genes related to the jasmonic acid biosynthesis and ethylene perception (Figures 4C, D and Supplementary Table 9). This functional classification analysis also indicated that the downregulation of *PvAGO5* diminished the expression of genes encoding diverse types of transporters, among them auxin-, cation-, carbohydrate- and amino acid transporters (Supplementary Figure 5). Altogether, this transcriptional

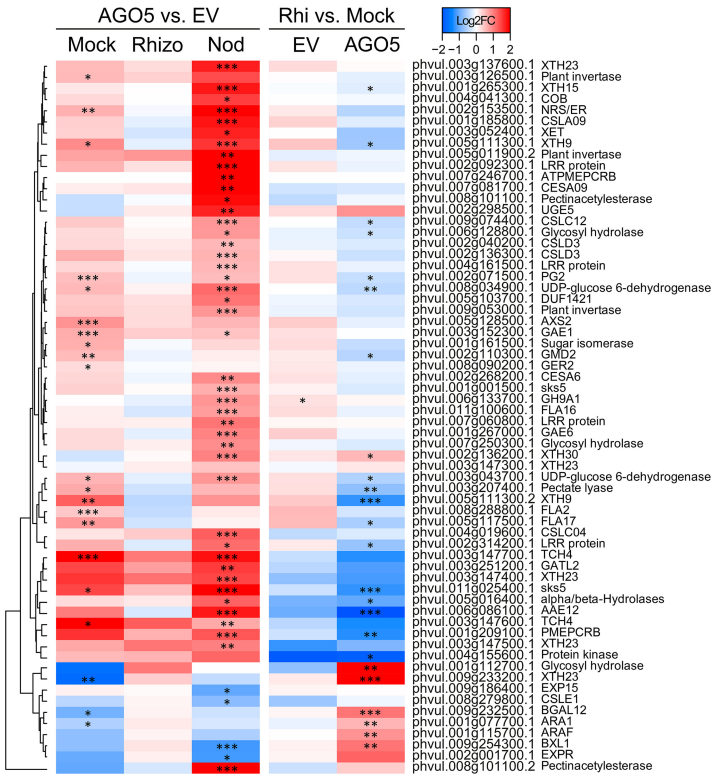

FIGURE 3
PvAGO5 modulates the expression of genes involved in the cell wall biosynthesis. Heatmap showing Log2 fold-change of gene transcripts involved in the biosynthesis and remodeling of the cell wall. Genes showing higher and lower expression difference are shown in different shades of red and blue, respectively. Labels at the top of the heatmap located on the left side indicate: Mock= uninoculated transgenic roots; Rhizo= rhizobia-inoculated transgenic roots, and Nod = mature nodules. In both cases the comparison between *PvAGO5*-RNAi vs Empty Vector is shown. Labels at the top of the heatmap located on the right side indicate: EV= transgenic roots expressing the empty vector (control), and AGO5: transgenic roots expressing the *PvAGO5*-RNAi construct. In both cases the comparison of rhizobia-inoculated roots vs mock-inoculated roots is shown. Asterisks indicate different levels of statistical significance of the comparisons (*: adjusted P-value<0.05; **= adjusted P-value<0.01; ***= adjusted P-value<0.001). Genes with no asterisk are not significantly differentially expressed. Dendrogram (left) represents the transcript clustering based on expression profile.

analysis implicates PvAGO5 in root development, likely through the regulation of genes involved in cell wall biogenesis and in the modulation of multiple phytohormones.

PvAGO5-RNAi roots show increased expression of defense-related genes during the first day of rhizobial interaction

Our spatio-temporal analyses indicated that *PvAGO5* is expressed in root hairs in response to rhizobia, suggesting that this AGO plays a role in the rhizobial infection process. To evaluate this hypothesis, we analyzed the transcriptional responses of *PvAGO5*-RNAi transgenic roots during the first day of interaction with *R. tropici*. Our transcriptome analyses revealed no overall drastic changes in the expression of canonical genes involved in the molecular dialogue between both symbionts and the rhizobial infection process when compared with rhizobia-inoculated transgenic roots expressing the empty vector. Instead, this transcriptome analysis revealed that the expression of genes related to plant defense, which must be modulated to allow the rhizobial infection (Berrabah et al., 2015; Wang et al., 2016; Berrabah et al., 2019), was significantly increased in *PvAGO5*-

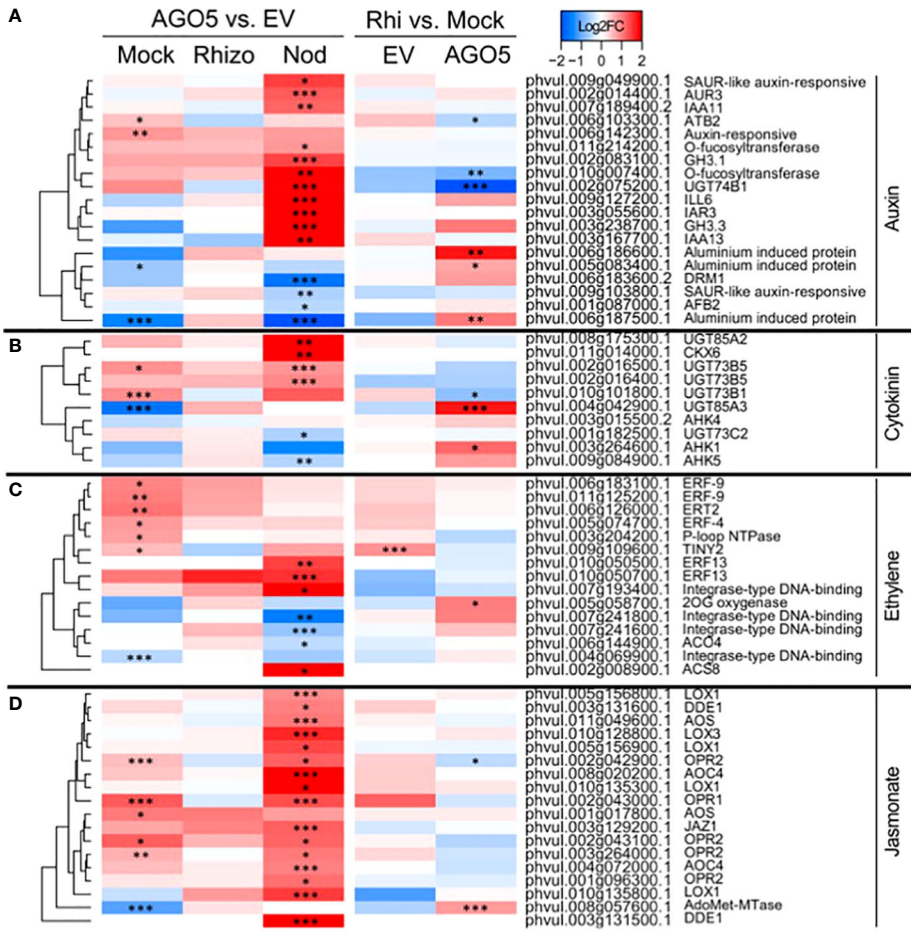

FIGURE 4
PvAGO5 modulates the expression of genes participating in the biosynthesis and signaling of phytohormones. Heatmaps showing Log2 fold-change of gene transcripts involved in the biosynthesis and signaling of auxins **(A)**, cytokinins **(B)**, ethylene **(C)**, and jasmonate **(D)**. Fold-changes are false-colored. Genes showing higher and lower expression difference are shown in different shades of red and blue, respectively. Labels at the top of the heatmap located on the left side indicate: Mock= uninoculated transgenic roots; Rhizo= rhizobia-inoculated transgenic roots, and Nod = mature nodules. In both cases the comparison between *PvAGO5*-RNAi vs Empty Vector is shown. Labels at the top of the heatmap located on the right side indicate: EV= transgenic roots expressing the empty vector (control), and AGO5: transgenic roots expressing the *PvAGO5*-RNAi construct. In both cases the comparison of rhizobia-inoculated roots vs mock-inoculated roots is shown. Asterisks indicate different levels of statistical significance of the comparisons (*: adjusted P-value<0.05; **= adjusted P-value<0.01; ***= adjusted P-value<0.001). Genes with no asterisk are not significantly differentially expressed. Dendrogram (left) represents the transcript clustering based on expression profile.

RNAi transgenic roots during the first day of interaction with rhizobia (Figure 5). We observed that the expression of genes encoding NBC-ARC domain-containing disease resistance proteins (e.g., Phvul.008g071500.1 and Phvul.001g133400.1) or LRR Receptor-Like Serine/Threonine-Protein Kinase (e.g., Phvul.005g162000.1 and Phvul.002g187300.1) increased two-fold in response to rhizobia (Figure 5). These transcriptional data indicate that the downregulation of *PvAGO5* activates the expression of plant defense-related genes in response to rhizobia.

The expression of phytohormone-, plant defense-, and cell wall biogenesis-related genes is affected in mature *PvAGO5*-RNAi nodules

Gene silencing of AGO5 significantly reduces nodule size and the number of rhizobial-infected nodule cells (Reyero-Saavedra et al., 2017). To explore the basis of this phenotype, we analyzed the transcriptome of mature nodules expressing the *PvAGO5*-RNAi or the empty vector. This analysis led us to the identification of 1,006 DEGs, of which 766 were upregulated and 240 downregulated in *PvAGO5*-RNAi nodules.

Functional classification of the DEGs indicated that many of the up-regulated genes were related to plant defense (Figure 5). For example, we found that oxidative burst-associated genes (i.e., *PvRbohA*: Phvul006g090200.1) or genes encoding resistance and pathogenesis-related (PR) proteins were significantly upregulated in *PvAGO5*-RNAi nodules (Figure 5). Interestingly, we also identified a three-fold induction of an *Rj4* orthologue (Phvul.002g107900) which encodes a thaumatin-like pathogenesis-protein known to restrict nodulation to specific rhizobial strains in soybean (Supplementary Figure 6 and Supplementary Table 7) (Tang et al., 2016).

Silencing of *PvAGO5* in mature nodules resulted in the significant upregulation of genes involved in the biosynthesis and signaling of the phytohormones auxin, ethylene, and jasmonic acid (Figure 4 and Supplementary Table 9). In contrast, genes involved in cytokinin degradation were up-regulated, whereas genes participating in its perception and signaling were downregulated in mature *PvAGO5*-RNAi nodules (Figure 4 and Supplementary Table 9).

Furthermore, we observed that the expression of genes participating in cell wall biogenesis and remodeling significantly increased (Figure 3 and Supplementary Table 7, 8). However, we also observed that some genes belonging to this category were downregulated. For instance, the expression of the gene *Increasing Nodule Size1* (*INS1*: Phvul.003g016300.1), which encodes for a UDP-Glycosyltransferase/trehalose-phosphatase, was significantly diminished in *PvAGO5*-RNAi nodules (Supplementary Figure 6 and Supplementary Table 7). Altogether, these transcriptional data indicate that PvAGO5 regulates nodule development and functioning by modulating the expression of genes involved in the phytohormone balance, control of the plant defense response, and cell wall biogenesis, which is determinant for this symbiosis.

The expression of mineral nutrient transporter-related genes is affected in *PvAGO5*-RNAi mature nodules

Legume hosts constantly translocate different mineral nutrients to the nodules to sustain an effective symbiosis. Defects in this mineral nutrient exchange compromise the symbiosis (Liu et al., 2020; Castro-Rodríguez et al., 2021). Hence, we investigated whether *PvAGO5* downregulation affects the expression of genes encoding mineral nutrient transporters in mature nodules. We found that the expression of genes encoding Fe^{2+}-, Mn^{2+}, and K^{+} transporters was significantly diminished in *PvAGO5*-RNAi mature nodules (Supplementary Figure 5). We also observed that the expression of Phvul.007g275300.1 that encodes the PHO1 transporter, which is required to transfer phosphate from infected nodule cells to bacteroids (Nguyen et al., 2021), was significantly downregulated. In contrast, genes encoding different ABC and MATE transporter family members, as well as sugars- and amino acid- transporters, were upregulated. Altogether, these transcriptional data indicate that PvAGO5 regulates nodule functioning by modulating the expression of genes involved in mineral nutrient transport underpinning the symbiosis.

The sRNA cargo of PvAGO5 is dynamic during root nodule development

To obtain further insights into the roles of PvAGO5 in the root nodule symbiosis and to determine changes in sRNA associations during this symbiosis, we isolated, sequenced, and compared PvAGO5-bound sRNA pools from nodule primordia and mature nodules. We choose mature nodules because of the strong transcriptional activity of the *PvAGO5* promoter during this stage of development. We also included nodule primordia and non-inoculated roots to capture those sRNAs that accumulate during nodule development. For each experimental condition, we included three biological replicates. For downstream analyses, we focused only on those sRNAs present in the three libraries from each of the three experimental conditions.

PvAGO5-associated sRNAs consisted of 18-22 nt sRNAs, with a 5' C and U bias, and an enrichment and a depletion of the sequence shorter and longer than 21-nt, respectively, compared to the starting dataset (Figures 6A, B). We identified 76 sRNAs, 72 of them were miRNAs and the rest rhizobial-derived tRFs. Sixty-nine of the identified miRNAs were grouped into 26 known miRNA families. The other three miRNAs were classified as *P. vulgaris*-specific miRNAs. 50% of these 72 miRNAs were grouped into only seven families, corresponding

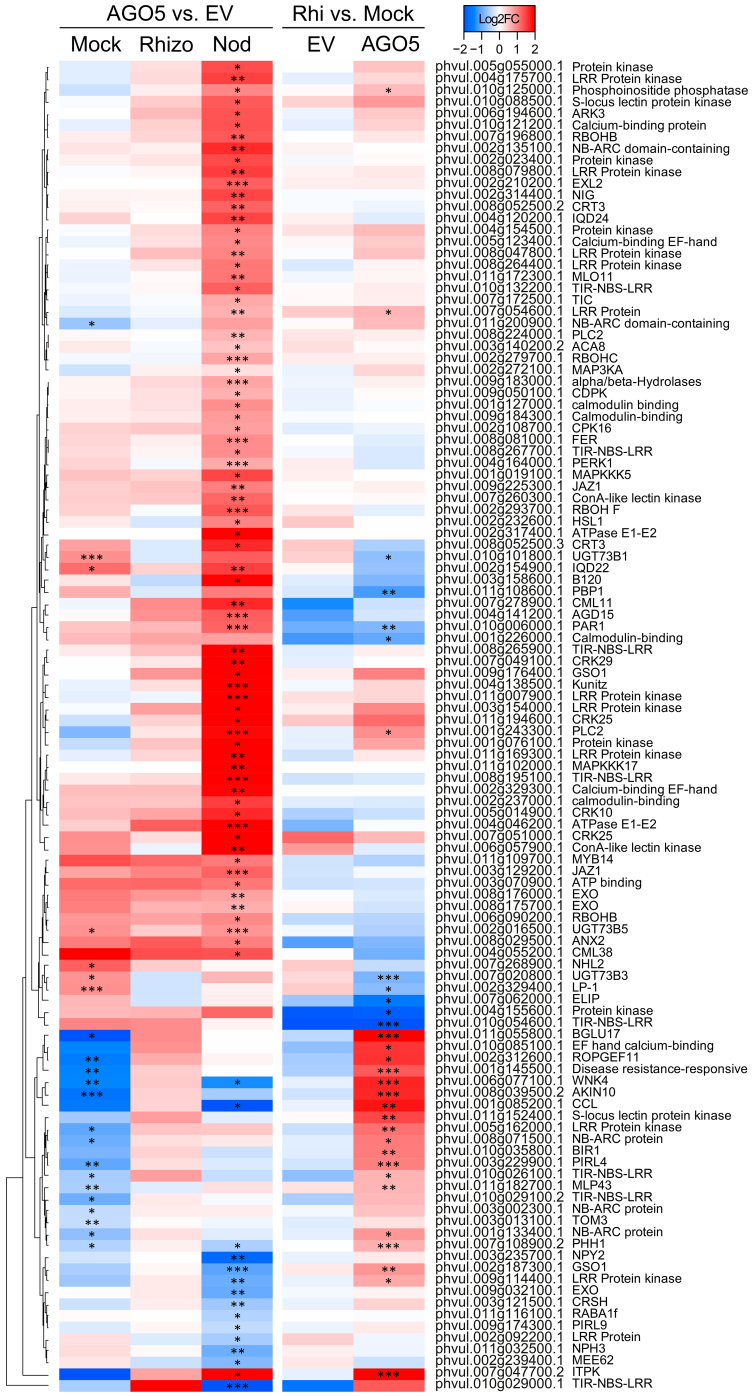

FIGURE 5
Down-regulation of *PvAGO5* increases the expression of plant-defense related genes. Heatmap showing Log2 fold-change of gene transcripts involved in plant defense response in uninoculated- (Mock) and rhizobia-inoculated roots (rhizobia), as well as in mature nodules (Nod). Genes showing higher and lower expression differences are shown in different shades of red and blue, respectively. Labels at the top of the heatmap located on the left side indicate: Mock= uninoculated transgenic roots; Rhizo= rhizobia-inoculated transgenic roots, and Nod = mature nodules. In both cases the comparison between *PvAGO5*-RNAi vs Empty Vector is shown. Labels at the top of the heatmap located on the right side indicate: EV= transgenic roots expressing the empty vector (control), and AGO5: transgenic roots expressing the *PvAGO5*-RNAi construct. In both cases the comparison of rhizobia-inoculated roots vs mock-inoculated roots is shown. Asterisks indicate different levels of statistical significance of the comparisons (*: adjusted P-value<0.05; **= adjusted P-value<0.01; ***= adjusted P-value<0.001). Genes with no asterisk are not significantly differentially expressed. Dendrogram (left) represents the transcript clustering based on expression profile.

to miR156, miR159, miR166, miR167, miR168, miR319, and miR396. (Supplementary Table 10).

A comparison between the PvAGO5-bound sRNAs from the three experimental conditions revealed that 23 out of the 76 sRNAs were present in the three tested biological samples (uninoculated roots, root bearing nodule primordia, and mature nodules), whereas the rest were present in at least two biological conditions (i.e., present in roots and in nodule primordia) or unique for a particular condition (i.e., specific to mature nodules) (Figure 6C). Among the 23 miRNAs present in the three experimental conditions, Pvu-miR482a-5p, Pvu-miR166a-3p, Gmax-miR1511, gma-miR6300, Pvu-miR166h-3p, Pvu-miR396c-5p, Pvi-miR156a-5p, Gmax-miR156a, Pvu-miR396b-5p, Pvu-miR1511-3p, Cme-miR168, hbr-miR156,

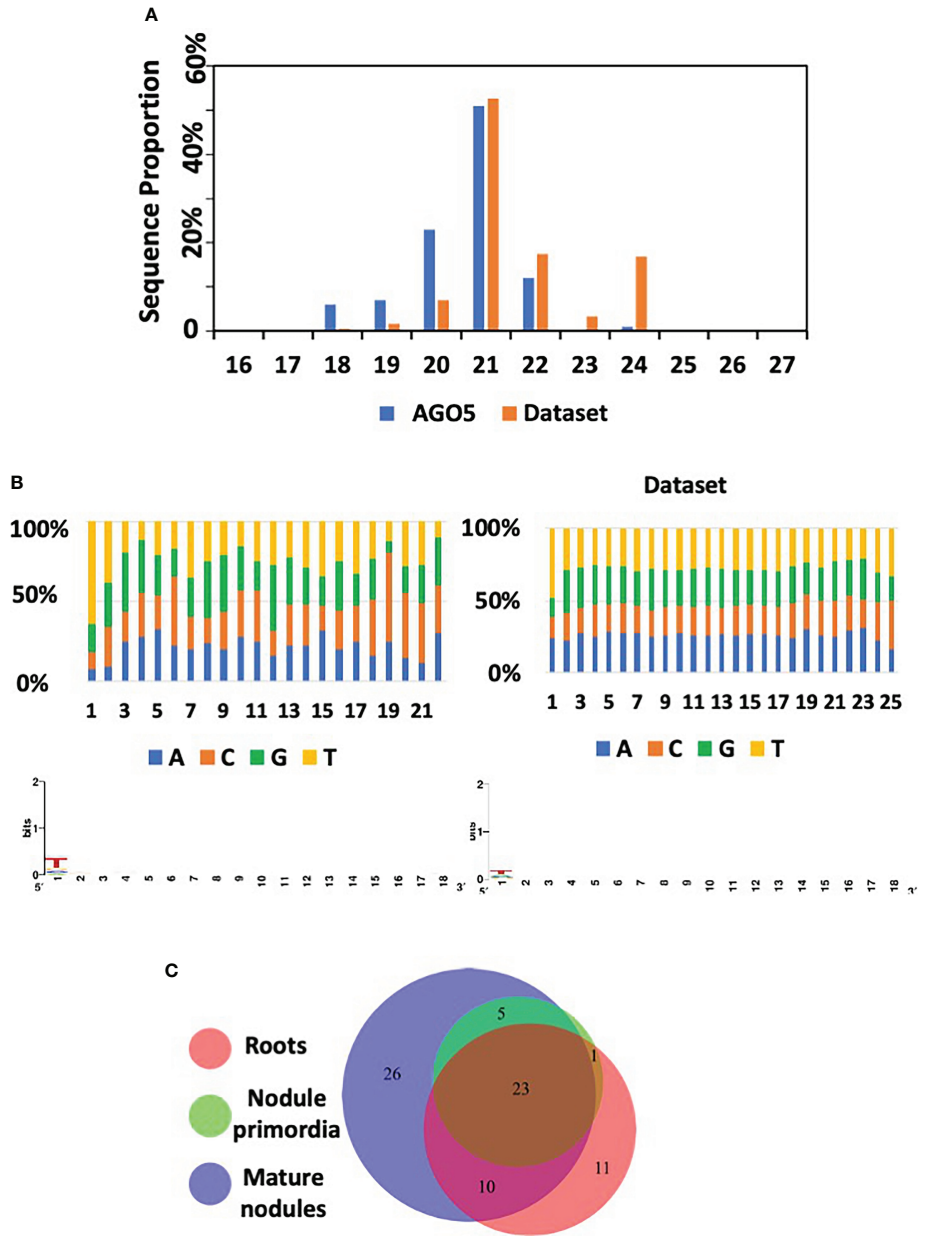

FIGURE 6
AGO5 sRNA cargo dynamically changes through the nodule development. **(A)** Length distribution of mapped sRNA reads isolated from AGO5 and the corresponding starting dataset. Starting dataset refers to the set of small RNA sequences used as reference for annotation of the sequencing results. **(B)** Read nucleotide distribution and 5′ bias of AGO5-associated sRNAs. **(C)** Number of sRNA associated in AGO5 from uninoculated roots, roots bearing nodule primordia, and mature nodules.

and Pvu-miRN95, were the most abundant miRNAs (Figure 6 and Supplementary Table 10). Most of these microRNA families are known to be involved in the regulation of pathways that are found altered in our transcriptomic data analysis between *PvAGO5*-RNAi and EV plants and could therefore explain the observed phenotypic. Some of these families are directly related to nodulation such as miR482, miR166 and miR156 (Boualem et al., 2008; Li et al., 2010; Wang et al., 2015). In the case of miR156 and miR396 families, they are involved in flavonoid biosynthesis (Yang et al., 2022) which could partly explain that, when we alter the production of AGO5, these microRNAs being associated, the biosynthesis of flavonoids is altered. Finally, an important candidate for the explanation of nodulation alteration is miR1511, that has been shown to regulate root growth under abiotic stresses, *via* iron homeostasis and ROS accumulation in roots (Martin-Rodriguez et al., 2021). As iron and ROS are components regulating rhizobial symbiosis at different stages of its establishment, it is likely that, by altering AGO5, we alter the function of miR1511, the corresponding iron and ROS accumulations and, ultimately, nodulation.

We found eleven, zero, and twenty-six miRNAs that were uniquely bound to PvAGO5 from uninoculated roots, roots bearing nodule primordia, and mature nodules, respectively (Supplementary Table 11). Among the 26 unique sRNAs bound to PvAGO5 from mature nodules, four of them were tRFs from *R. tropici*, which represents a 33-times enrichment compared to the original dataset (Supplementary Table 11). Interestingly, this type of sRNAs was recently shown to play a role in the root nodule symbiosis in soybean (Ren et al., 2019).

Next, we predicted putative target genes of AGO5-bound sRNAs by using psRNAtarget V2 using default parameters (Dai et al., 2018). Sixty-four out of 76 identified sRNA were predicted to target at least one mRNA (Supplementary Table 12). Although no GO terms nor any pathway were significantly enriched in the identified target gene set, analysis of protein domain enrichment reveals that AGO5-bound sRNAs preferentially target genes containing domains related to defense (e.g., NB-ARC, Leucine-rich repeat and Toll/interleukin-1 receptor), growth and development process (e.g., ZPR1-type TFs, SPB-box TFs, and Growth-regulating factor) or nodulation (e.g., Nodulin) (Supplementary Table 13). Next, we analyzed the expression of the predicted target genes in our transcriptome data set. Interestingly, the majority of the predicted target genes were up-regulated instead of the canonical down-regulation expected for sRNA target genes (Supplementary Table 12).

In summary, these data indicate that PvAGO5 can bind sRNA, both plant- and rhizobia-derived, that may play a role in the nodule development and functioning. The fact that the predicted target genes were up-regulated suggests that AGO5 may play a role in negatively regulating the protein production of sRNA targets, as well as the principal miRNA effector protein AGO1. However, further investigation is required to confirm this hypothesis.

Discussion

sRNAs recruited into the multiprotein complex RISC play an important role in regulating the root nodule symbiosis in diverse legumes. However, to date, the role of AGOs, the main protein component of RISC, in this symbiosis has been overlooked. Publicly available transcriptional data indicate that *PvAGO1*, *PvAGO5*, and *PvAGO10*, the genes coding for the three AGOs constituting a phylogenetic clade, are expressed in different *P. vulgaris* tissues, including leaves, shoots, pods, roots, and nodules (Supplementary Figure 8). *PvAGO1* is the most expressed, followed by *PvAGO5* and *PvAGO10*, except in the shoots where *PvAGO10* is more expressed than *PvAGO5*. Neither correlation nor contrast in the expression of these genes seems to occur in the analyzed tissues. Proportionally to the expression of *PvAGO1*, *PvAGO5* shows its greatest relative expression in effective nodules, compared to other tissues, and its accumulation is systematically greater in nodules or inoculated roots compared to the corresponding controls (Supplementary Figure 8). We previously confirmed by RT-qPCR that the expression of *PvAGO5* increases in nodules compared to leaves and uninoculated roots (Reyero-Saavedra et al., 2017). This transcriptional data suggested that PvAGO5 plays a role in the root nodule symbiosis. Indeed, we previously showed that the silencing of *AGO5* negatively affects nodule formation and reduces the number of rhizobia-infected nodule cells in *G. max* and *P. vulgaris* (Reyero-Saavedra et al., 2017). In this study, we provide additional transcriptional evidence supporting the notion that AGO5 modulates the expression of diverse genes involved in the rhizobial infection process, nodule development, and nodule functioning (Figure 7).

AGO5 and, therefore, its cargo sRNAs play different physiological and developmental roles. For instance, AGO5 modulates part of the plant defense responses against the *Potato virus X* and aphids in *A. thaliana* and wheat, respectively (Brosseau and Moffett, 2015; Sibisi and Venter, 2020). AGO5 also participates in the seed coat pigmentation in *G. max* (Cho et al., 2017). Additionally, AGO5 controls flowering time by modulating the expression of the transcription factor *Squamosa Binding Protein-Like* (*SPL*) through the action of miR156 in *A. thaliana* (Roussin-Léveillée et al., 2020). Recent evidence also indicates that AGO5 along with AGO9 bind to transposon-derived sRNAs to mark an early-segregating germline in *A. thaliana* (Bradamante et al., 2022). In this study, we provide a range of evidence for the participation of AGO5 in several aspects of root nodule symbiosis in *P. vulgaris*. This conclusion is supported by the expression of *PvAGO5* during the rhizobial infection and throughout the nodule development process. Furthermore, the downregulation of *PvAGO5* activates the expression of genes related to the plant defense response and the biosynthesis of phytohormones that negatively affects this symbiosis, as previously reported in both *P. vulgaris* and *G. max* (Reyero-Saavedra et al., 2017) (Figure 7).

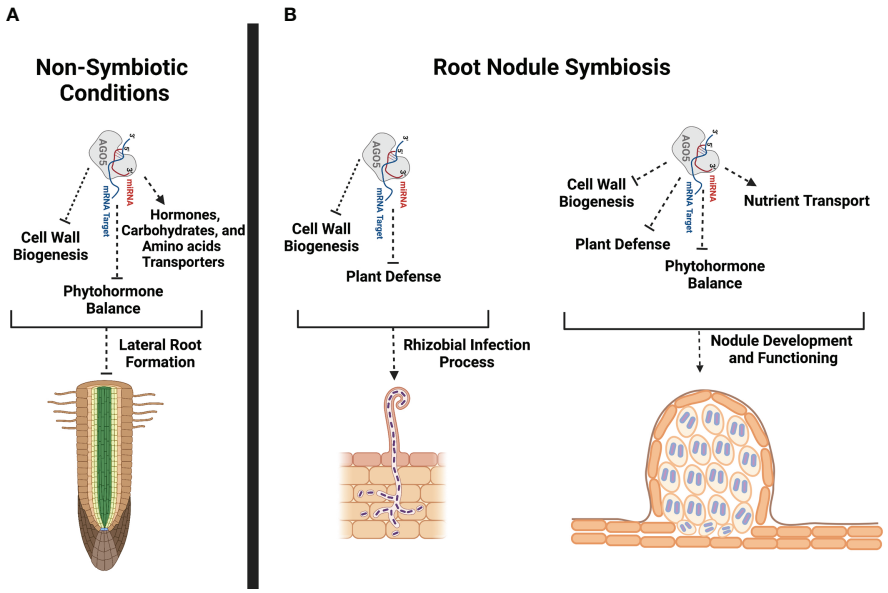

FIGURE 7
Schematic representation of potential PvAGO5 roles in lateral root formation and root nodule symbiosis. **(A)** Based on transcriptional data and phenotype from *PvAGO5*-RNAi transgenic roots growing under non-symbiotic conditions, PvAGO5 might modulates the expression of genes involved in the cell wall biogenesis, phytohormone balance and transportation. Modulation of the expression of these genes may be required to control the number and density of lateral roots in *P. vulgaris*. **(B)** In contrast, AGO5 acts as a positive regulator of the root nodule symbiosis in *P. vulgaris*. PvAGO5 modulates the expression of genes participating in the flavonoid biosynthesis, cell wall remodeling, and plant defense. It is likely that PvAGO5 participates in the cell wall remodeling, which is required to sustain the root hair curling that is crucial for rhizobial entrapping. Likewise, PvAGO5 may modulate the plant defense response to ensure the rhizobial infection and colonization. At late stages of this symbiosis, PvAGO5 may participate in cell wall remodeling and phytohormone balance allowing a proper nodule formation. Additional, PvAGO5 may also contribute to the nodule functioning by controlling the expression of nutrient transporter-encoding genes. Finally, it is likely that AGO5 also modulates the plant defense to host rhizobia during the nitrogen-fixation process. This figure was created with Biorender.com.

There is mounting evidence that *AGO5* is expressed in egg and sperm cells of mature gametophytes, developing carpels, axillary meristems, the subepidermal layer of the shoot apical meristem, and in the root apical meristem of *A. thaliana* (Borges et al., 2011; Tucker et al., 2012; Bradamente et al., 2022; Jullien et al., 2022). Based on the *A. thaliana* transcriptome atlas (https://www.arabidopsis.org), *AGO5* is also expressed in the xylem pole pericycle during lateral root initiation. In this study, we observed that *PvAGO5* is expressed in the lateral root primordium and throughout lateral root under non-symbiotic conditions. Additionally, the downregulation of *PvAGO5* led to an 15% increase in the number and density of lateral roots (Figures 1I–K). Hence, our data support earlier observations indicating that *AGO5* is active in root meristems, and we provide new evidence suggesting that AGO5 plays a role in lateral root formation.

Our transcriptome analysis of uninoculated *PvAGO5*-RNAi transgenic roots revealed that the expression of genes participating in jasmonic acid and cell wall biogenesis is increased when compared with control roots. Jasmonic acid is an essential phytohormone for the activation of the plant defense response. However, this phytohormone also promotes lateral root formation in a dose-dependent manner in *A. thaliana* (Sun et al., 2009; Raya-González et al., 2012; Cai et al., 2014). To sustain root growth, the cell wall must be modified and rebuilt during this process (Somssich et al., 2016). Hence, our transcriptional data indicate that the increase in the expression of genes associated with jasmonic acid and cell wall biogenesis may promote and sustain the formation of lateral roots observed in *PvAGO5*-RNAi transgenic roots. However, the role and mechanism of action of PvAGO5 in the formation of lateral roots need to be experimentally validated (Figure 7).

In the root nodule symbiosis context, we detected a specific expression of *PvAGO5* in the root hair tips at one-day post-inoculation with rhizobia (Figure 2). At this stage, root hair cell wall is softened allowing the entrance of rhizobia *via* the so-called infection thread (van Spronsen et al., 1994). Our transcriptomic data shows a significant increase in the expression of cell wall biosynthesis-related genes in *PvAGO5*-RNAi transgenic roots, indicating a role of PvAGO5 in their regulation. Altogether, these observations confirm that PvAGO5 plays a role in the early rhizobial infection process. Furthermore, these data provide lines of evidence that explain the reduced rhizobial infection observed in *PvAGO5*-RNAi transgenic roots (Reyero-Saavedra et al., 2017). This phenotype may be partly attributed to the lack of PvAGO5-mediated regulation of cell wall biosynthesis-related genes at the infection pocket and

infection thread initiation site. This defect may prevent the proper cell wall softening and rhizobial infection (Figure 7).

At late stages of the root nodule symbiosis, we observed that *PvAGO5* is also expressed in nodule primordia and mature nodules. These observations add more evidence supporting the notion that AGO5 is determinant in the nodule development. This hypothesis is supported by the fact that the downregulation of *PvAGO5*-RNAi results into a significant reduction in the number and size of nodules in *P. vulgaris* (Reyero-Saavedra et al., 2017). Studies in different legumes have identified different genetic components that regulate nodule development and size. For example, *INS1*, which encodes a cell wall β-expansin and is expressed in nodules, is a regulator of nodule development in *G. max* by positively controlling the enlargement of nodules and infection cells (Li et al., 2018). In this study, we found that the expression of *INS1* was significantly diminished in *PvAGO5*-RNAi mature nodules. Hence, the reduction in the number of nodules and their size, observed in *PvAGO5*-RNAi composite plants, can partially be explained by the altered expression of this regulator.

During the root nodule symbiosis, the plant defense response is finely tuned. Mounting evidence indicates that a sustained plant defense response compromises this symbiosis (Berrabah et al., 2015; Berrabah et al., 2019). In this study, we observed that genes related to the plant defense were significantly upregulated and enriched in rhizobia-inoculated *PvAGO5*-RNAi transgenic roots and mature nodules. One of these genes were *Rj4*, which encodes a Thaumatin-like protein (Hayashi et al., 2014). Rj4 restricts the rhizobial infection process and nodule development in incompatible interactions between *G. max* and rhizobia (Hayashi et al., 2014). Similarly, our transcriptomic analyses also revealed that the expression of flavonoid biosynthesis-related genes was significantly upregulated in *PvAGO5*-RNAi transgenic roots and nodules (Supplementary Figure 7). Flavonoids participate in different steps of the root nodule symbiosis, from early secreted signals to auxin balance during nodule organogenesis (Liu and Murray, 2016). Flavonoids also have a role in the plant resistance against bacterial infection (Mierziak et al., 2014) Hence, it is likely that the activation of the plant defense response may compromise the establishment of the root nodule symbiosis, particularly affecting the rhizobial infection process in *P. vulgaris*. This hypothesis is supported by the observation that *AGO5* down-regulation affects the rhizobial colonization in both root and nodule cells in *P. vulgaris* and *G. max* (Reyero-Saavedra et al., 2017).

Phytohormones play a determinant role in each step of the root nodule symbiosis (Lin et al., 2020). According to studies across diverse legumes, in an optimal balance, auxin and cytokinin are positive regulators of this symbiosis (Lin et al., 2020). For instance, cytokinins are required for nodule organogenesis and development (Heckmann et al., 2011; Reid et al., 2017). Additionally, disruption of auxin transport inhibits nodule formation (Huo et al., 2006). In contrast, several lines of evidence indicate that ethylene, jasmonic acid, and abscisic acid negatively affect the establishment of the root nodule symbiosis (Lin et al., 2020). Here, we observed that the down-regulation of *PvAGO5* decreases the expression of genes involved in auxin and cytokinin biosynthesis and signaling in rhizobia-inoculated roots. In contrast, the expression of genes participating in the biosynthesis and signaling of jasmonic acid and ethylene was significantly increased in *PvAGO5*-RNAi rhizobia-inoculated roots and nodules. Furthermore, it has been demonstrated that the miR319d/TCP10 node regulates the rhizobial infection process through the modulation of genes involved in the jasmonic acid biosynthesis in *P. vulgaris* (Martín-Rodríguez et al., 2018). Reduction in the miR319d level led to a significant reduction in the number of rhizobial-induced deformed root hairs and nodules (Martín-Rodríguez et al., 2018). Our data reveals that miR319 is one of the families most associated with AGO5, linking the jasmonic acid-related transcriptomic response, and the observed phenotype, to AGO5 cargo. Thus, the reduction in both rhizobial infection and number of nodules previously observed (Reyero-Saavedra et al., 2017) can be explained by the activation of jasmonic acid biosynthesis- and signaling related genes, likely due to the lack of miR319/AGO5 association.

Effective root nodule symbiosis depends on efficient nutrient exchange. Recent studies indicate that the Phosphate Transporter1.1 (PHO1.1) and PHO1.2 translocate phosphate from the infected cell to nitrogen-fixing bacteroids in *M. truncatula* (Nguyen et al., 2021). Similarly, different types of iron transporters, among them Yellow Stripe-Like and Vacuolar Iron Transporter Like, aid the translocation of iron from infected nodule cells to nitrogen-fixing bacteria (Liu et al., 2020; Castro-Rodríguez et al., 2021). Nutrient transporter failure negatively affects the functioning of mature nodules (Liu et al., 2020; Castro-Rodríguez et al., 2021; Nguyen et al., 2021). In this study, we observed that the expression of genes coding for mineral nutrient transporters, including different iron transporters and the phosphate transporter PHO1, was diminished in both *PvAGO5*-RNAi rhizobia-inoculated roots and nodules. The downregulation of these mineral nutrient transporters, essential for nodule functioning, by the repression of *PvAGO5* suggests that is likely that PvAGO5 sustains an effective root nodule symbiosis by modulating the expression of mineral nutrient transporters in mature nodules.

Studies in different legumes attest to the relevance of miRNAs in nodule development (Tiwari et al., 2021). All the phenotypic and transcriptomic alterations observed in *PvAGO5*-RNAi transgenic roots, in a nodulation context or not, are likely derived from the sRNA-guided AGO5 activity. Here, we found that 19 of the 26 conserved miRNAs cargo of PvAGO5 (e.g.: miR156, miR166, miR169, miR171, miR172, miR319, miR390, miR393, and miR482) have previously been demonstrated to play a role in regulating the rhizobial symbiosis and/or modulating the plant defense response (Tiwari et al., 2021). However, most of the target genes predicted for the identified sRNAs, which display a significant differential expression in *PvAGO5*-RNAi roots compared to EV, are not canonical targets and are not known to participate in the symbiotic process. From the gene set of targets showing significant

differential expression, we observed that around 93% of them showed an up-regulation in *PvAGO5*-RNAi mature nodules. Hence, our data suggest that sRNAs bound to AGO5 guide the negative regulation of genes required for effective root nodule symbiosis, a function similar to that of the other principal member of the same AGO clade, AGO1.

Recent evidence in *G. max* also attests the participation of rhizobia-derived tRFs in the root nodule symbiosis. tRFs were 33-fold enriched in the sRNA cargo of PvAGO5 from mature nodules. Three of them are predicted to target previously undescribed targets that are significantly up-regulated in our *PvAGO5*-RNAi root samples: *Early-Responsive to Dehydratation* (*ERD*), *Early NODulin-Like protein 17* (*ENOD17*), and *HEMA1*, a Glutamyl-tRNA reductase. The last two are likely to be related to nodulation. *ENOD17* encodes a nodulin-like protein, and *HEMA* is a homolog of *HEMA* genes encoding a Glutamyl-tRNA reductase known to participate in the heme synthesis of leghemoglobins in *L. japonicus* nodules (Wang et al., 2019). Hence, our data suggest that AGO5 and its sRNA cargo regulate the expression of diverse genes that are crucial for the rhizobial infection process as well as for nodule development and functioning. Furthermore, the role of the tRFs bound to AGO5 in the root nodule symbiosis must be experimentally tested.

Conclusions

Overall, the data presented in this study lead us to conclude that PvAGO5 and its associated sRNA modulate the expression of genes with diverse functions that are crucial for the development and maintenance of an effective root nodule symbiosis. The observation that the downregulation of *PvAGO5* has opposite effects in the lateral root versus nodule development, suggests that this AGO modulates the expression of genes required for the developmental programs of these distinct organs according to the nitrogen needs of *P. vulgaris* (Figure 7).

Data availability statement

The original contributions presented in the study are publicly available. The data presented in the study are deposited in the BioProject repository, accession number PRJNA835127 (https://www.ncbi.nlm.nih.gov/bioproject/PRJNA835127).

Author contributions

OV-L, DF, and JR proposed and designed the study. MS-C, MI-A, EP-R, and MR-S generated common bean composite plants. EP-R and MR-S generated the *pPvAGO5::GUS* and *PvAGO5*-RNAi constructs. OV-L, MI-A and MS-C generated the transgenic tissues used in this study. OV-L, MI-A, and MS-C purified total RNA from *P. vulgaris* tissues. OV-L, MI-A, and MDSS-C performed the AGO5 immunoprecipitation and sRNA purification. AS-F and VJ-J, prepared and sequenced the mRNA and sRNA libraries. DF, AS-F, VJ-J, SC, and AM-S analyzed the RNAseq data. OV-L, MI-A, and EP-R confirmed the RNAseq data by RT-qPCR. OV-L, DF, SC, and AM-S generated figures and performed statistical analyses. OV-L, DF, and JR wrote the manuscript. All authors read and approved the manuscript.

Funding

This work was supported by the Consejo Nacional de Ciencia y Tecnología (CONACyT grant No. A1-S-9454 and No. A1-S-16129) and by the Programa de Apoyo a Proyectos de Investigación e Inovación Tecnológica (PAPIIT-UNAM grant No. IN201320 and No. IA201522) to OV-L and DF, respectively. Research in JR laboratory is supported by a grant from PAPIIT-UNAM IN202918. MI-A is a doctoral student from Programa de Doctorado en Ciencias Biológicas, Universidad Nacional Autónoma de México, and received a doctoral student fellowship from CONACyT (CVU: 919676). SC is a doctoral student from the Programa de Doctorado en Ciencias Biomédicas, Universidad Nacional Autónoma de México, and has received CONACyT fellowship #1002252.

Acknowledgments

We thank Dr. Caspar C.C. Chater (Royal Botanic Gardens, Kew) and Dr. Georgina Hernández (Centro de Ciencias Genomicas-UNAM, Mexico) for constructive discussion.

Conflict of interest

The authors declare that the research was conducted in the absence of any commercial or financial relationships that could be construed as a potential conflict of interest.

Publisher's note

Supplementary material

The Supplementary Material for this article can be found online at: https://www.frontiersin.org/articles/10.3389/fpls.2022.1034419/full#supplementary-material

References

Berrabah, F., Ratet, P., and Bourion, B. (2019). Legume nodules: Massive infection in the absence of defense induction. *Mol. Plant Microbe Interact.* 32, 35–44. doi: 10.1094/MPMI-07-18-0205-FI

Berrabah, F., Ratet, P., and Gourion, B. (2015). Multiple steps control immunity during the intracellular accommodation of rhizobia. *J. Exp. Bot.* 66, 1977–1985. doi: 10.1093/jxb/eru545

Borges, F., Pereira, P. A., Slotkin, R. K., Martienssen, R. A., and Becker, J. D. (2011). MicroRNA activity in the arabidopsis male germline. *J. Exp. Bot.* 62, 1611–1620. doi: 10.1093/jxb/erq452

Boualem, A., Laporte, P., Jovanovic, M., Laffont, C., Plet, J., Combier, J.-P., et al. (2008). MicroRNA166 controls root and nodule development in. *Medicago truncatula Plant J.* 54, 876–887. doi: 10.1111/j.1365-313X.2008.03448.x

Bradamante, G., Nguyen, V. H., Incarbone, M., Meir, Z., Bente, H., Donà, M., et al. (2022). Two AGO proteins with transposon-derived sRNA cargo mark the germline in arabidopsis. *bioRxiv*. doi: 10.1101/2022.01.25.477718

Broghammer, A., Krusell, L., Blaise, M., Sauer, J., Sullivan, J. T., Maolanon, N., et al. (2012). Legume receptors perceive the rhizobial lipochitin oligosaccharides signal molecules by direct binding. *Proc. Natl. Acad. Sci. U.S.A.* 109, 13859–13864. doi: 10.1073/pnas.1205171109

Brosseau, C., and Moffett, P. (2015). Functional and genetic analysis identify a role for arabidopsis ARGONAUTE5 in antiviral RNA silencing. *Plant Cell.* 27, 1742–1754. doi: 10.1105/tpc.15.00264

Cai, X. T., Xu, P., Zhao, P. X., Liu, R., Yu, L. H., and Xiang, C. B. (2014). *Arabidopsis* ERF109 mediates cross-talk between jasmonic acid and auxin biosynthesis during lateral root formation. *Nat. Commun.* 5, 5833. doi: 10.1038/ncomms6833

Castro-Rodríguez, R., Escudero, V., Reguera, M., Gil-Perez, P., Quintana, J., Prieto, R. I., et al. (2021). *Medicago truncatula yellow stripe-Like7* encodes a peptide transporter in symbiotic nitrogen fixation. *Plant Cell Environ.* 44, 1908–1920. doi: 10.1111/pce.14059

Cerri, M. R., Frances, L., Laloum, T., Auriac, M. C., Niebel, A., Oldroyd, G. E. D., et al. (2012). *Medicago truncatula* ERN transcription factors: Regulatory interplay with NSP1/NSP2 GRAS factors and expression dynamics throughout rhizobial infection. *Plant Physiol.* 160, 2155–2172. doi: 10.1104/pp.112.203190

Cho, Y. B., Jones, S. I., and Vodkin, L. O. (2017). Mutations in *Argonaute5* illuminate epistatic interactions of the *K1* and *I* loci leading to saddle seed color patterns in *Glycine max*. *Plant Cell.* 29, 708–725. doi: 10.1105/tpc.17.00162

Combier, J. P., Frugier, F., de Billy, F., Boualem, A., Vernié, T., Ott, T., et al. (2006). *MtHAP2-1* is a key transcriptional regulator of symbiotic nodule development regulated by microRNA160 in *Medicago truncatula*. *Genes Dev.* 20, 3084–3088. doi: 10.1101/gad.402806

Dai, X., Zhuang, Z., and Zhao, X. (2018). psRNATarget: A plant small RNA target analysis server, (2017 Release). *Nucleic Acids Res.* 46, W49–W54. doi: 10.1093/nar/gky316

De Luis, A., Markmann, K., Cognat, V., Holt, D. B., Charpentier, M., Parniske, M., et al. (2012). Two microRNAs linked to nodule infection and nitrogen-fixing ability in the legume *Lotus japonicus*. *Plant Physiol.* 160, 2137–2154. doi: 10.1104/pp.112.204883

Dénarié, J., Debellé, F., and Promé, J. C. (1996). Rhizobium lipo-chitooligosaccharide nodulation factors: Signaling molecules mediating recognition and morphogenesis. *Annu. Rev. Biochem.* 65, 673–681. doi: 10.1146/annurev.bi.65.070196.002443

Ehrhardt, D. W., Wais, R., and Long, S. R. (1996). Calcium spiking in plant root hairs responding to rhizobium nodulation signals. *Cell* 85, 673–681. doi: 10.1016/s0092-8674(00)81234-9

Estrada-Navarrete, G., Alvarado-Affantrager, X., Olivares, J. E., Guillén, G., Díaz-Camino, C., Campos, F., et al. (2007). Fast, efficient and reproducible genetic transformation of *Phaseolus* spp. by *Agrobacterium rhizogenes*. *Nat. Prot.* 2, 1819–1824. doi: 10.1038/nprot.2007.259

Formey, D., Iñiguez, L. P., Peláez, P., Li, Y. F., Sunkar, R., Sánchez, F., et al. (2015). Genome-wide identification of the *Phaseolus vulgaris* sRNAome using small RNA and degradome sequencing. *BMC Genomics* 16, 423. doi: 10.1186/s12864-015-1639-5

Formey, D., Martín-Rodríguez, J. A., Leija, A., Santana, O., Quinto, C., Cárdenas, L., et al. (2016). Regulation of small RNAs and corresponding targets in nod factor-induced *Phaseolus vulgaris* root hair cells. *Int. J. Mol. Sci.* 17, 887. doi: 10.3390/ijms17060887

Hayashi, M., Shiro, S., Kanamori, H., Mori-Hosokawa, S., Sasaki-Yamagata, H., Sayama, T., et al. (2014). A thaumatin-like protein, Rj4, controls nodule symbiotic specificity in soybean. *Plant Cell Physiol.* 55, 1679–1689. doi: 10.1093/pcp/pcu099

Heckmann, A. B., Sandal, N., Bek, A. S., Madsen, L. H., Jurkiewics, A., Nielsen, M. W., et al. (2011). Cytokinin induction of root nodule primordia in *Lotus japonicus* is regulated by a mechanism operating in the root cortex. *Mol. Plant Microbe Interact.* 24, 1385–1395. doi: 10.1094/MPMI-05-11-0142

Hirsch, S., Kim, J., Muños, A., Heckmann, A. B., Downie, A., and Oldroyd, G. E. D. (2009). GRAS proteins form a DNA binding complex to induce gene expression during nodulation signaling in *Medicago truncatula*. *Plant Cell.* 21, 545–557. doi: 10.1105/tpc.108.064501

Hulsen, T., de Vlieg, J., and Alkema, W. (2008). BioVenn – a web application for the comparison and visualization of biological lists using area-proportional Venn diagrams. *BMC Genomics* 9, 488. doi: 10.1186/1471-2164-9-488

Huo, X., Schnabel, E., Hughes, K., and Frugoli, J. (2006). RNAi phenotypes and the localization of a protein::GUS fusion imply a role for *Medicago truncatula* PIN genes in nodulation. *J. Plant Growth Regul.* 25, 156–165. doi: 10.1007/s00344-005-0106-y

Hutvagner, G., and Simard, M. J. (2008). Argonaute proteins: Key players in RNA silencing. *Nat. Rev. Mol. Cell.* 9, 22–32. doi: 10.1038/nrm2321

Isidra-Arellano, M. C., Pozas-Rodríguez, E. A., Reyero-Saavedra, M. D. R., Arroyo-Canales, J., Ferrer-Orgaz, S., Sánchez-Correa, M. D. S., et al. (2020). Inhibition of legume nodulation by pi deficiency is dependent on the autoregulation of nodulation (AON) pathway. *Plant J.* 103, 1125–1139. doi: 10.1111/tpj.14789

Jiménez-Jacinto, V., Sanchez-Flores, A., and Vega-Alvarado, L. (2019). Integrative differential expression analysis for multiple experiments (IDEAMEX): A web server tool for integrated RNA-seq data analysis. *Front. Genet.* 10. doi: 10.3389/fgene.2019.00279

Jin, Y., Liu, H., Luo, D., Yu, N., Dong, W., Wang, C., et al. (2016). DELLA proteins are common components of symbiotic rhizobial and mycorrhizal signalling pathways. *Nat. Commun.* 7, 12433. doi: 10.1038/ncomms12433

Jullien, P. E., Schöder, J. A., Bonnet, D. M. V., Pimplin, N., and Voinnet, O. (2022). Asymmetric expression of argonautes in reproductive tissues. *Plant Physiol.* 188, 38–63. doi: 10.1093/plphys/kiab474

Kapoor, M., Arora, R., Lama, T., Nijhawan, A., Khurana, J. P., Tyagi, A. K., et al. (2008). Genome-wide identification, organization and phylogenetic analysis of dicer-like, argonaute and RNA-dependent RNA polymerase gene families and their expression analysis during reproductive development and stress in rice. *BMC Genomics* 9, 451. doi: 10.1186/1471-2164-9-451

Kosuta, S., Hazledine, S., Sun, J., Miwa, H., Morris, R. J., Downie, J. A., et al. (2008). Differential and chaotic calcium signatures in the symbiosis signaling pathway of legumes. *Proc. Natl. Acad. Sci. U.S.A.* 105, 9823–9828. doi: 10.1073/pnas.0803499105

Langmead, B., and Salzberg, S. L. (2012). Fast gapped-read alignment with bowtie 2. *Nat. Methods* 9, 357–359. doi: 10.1038/nmeth.1923

Lévy, J., Bres, C., Geurts, R., Chalhoub, B., Kulikova, O., Duc, G., et al. (2004). A putative Ca^{2+} and calmodulin-dependent protein kinase required for bacterial and fungal symbioses. *Science* 303, 1361–1364. doi: 10.1126/science.1093038

Li, H., Deng, Y., Wu, T., Subramanian, S., and Yu, O. (2010). Misexpression of miR482, miR1512, and miR1515 increases soybean nodulation. *Plant Physiol.* 153, 1759–1770. doi: 10.1104/pp.110.156950

Li, B., and Dewey, C. N. (2011). RSEM: Accurate transcript quantification from RNA-seq data with or without a reference genome. *BMC Bioinf.* 12, 323. doi: 10.1186/1471-2105-12-323

Lin, J., Frank, M., and Reid, D. (2020). No home without hormones: How plant hormones control legume nodule organogenesis. *Plant Commun.* 1, 100104. doi: 10.1016/j.xplc.2020.100104

Liu, S., Li, L., Nie, M. M., Peng, W. T., Zhang, M. S., Lei, J. N., et al. (2020). A VIT-like transporter facilitates iron transport into nodule symbiosomes for nitrogen fixation in soybean. *N. Phytol.* 226, 1413–1428. doi: 10.1111/nph.16506

Liu, C. W., and Murray, J. D. (2016). The role of flavonoids in nodulation host-range specificity: An update. *Plants (Basel)* 5, 33. doi: 10.3390/plants5030033

Li, X., Zheng, J., Yang, Y., and Liao, H. (2018). *INCREASING NODULE SIZE1* expression is required for normal rhizobial symbiosis and nodule development. *Plant Physiol.* 178, 1233–1248. doi: 10.1104/pp.18.01018

Manavella, P. A., Yang, S. W., and Palatnik, J. (2019). Keep calm and carry on: miRNA biogenesis under stress. *Plant J.* 99, 832–843. doi: 10.1111/tpj.14369

Martin-Rodriguez, J. A., Ariani, A., Leija, A., Elizondo, A., Fuentes, S. I., Ramirez, M., et al. (2021). *Phaseolus vulgaris* MIR1511 genotypic variations differentially regulate plant tolerance to aluminum toxicity. *Plant J.* 105, 1521–1533. doi: 10.1111/tpj.15129

Martín-Rodríguez, J.Á., Leija, A., Formey, D., and Hernández, G. (2018). The microRNA319d/TCP10 node regulates the common bean- rhizobia nitrogen-fixing symbiosis. *Front. Plant Sci.* 9. doi: 10.3389/fpls.2018.01175

Mierziak, J., Kostyn, K., and Kulma, A. (2014). Flavonoids as important molecules of plant interactions with the environment. *Molecules* 19, 16240–16260. doi: 10.3390/molecules191016240

Murakami, E., Cheng, J., Gysel, K., Bozsoki, Z., Kawaharada, Y., Hjuler, C. T., et al. (2018). Epidermal LysM receptor ensures robust symbiotic signaling in *Lotus japonicus*. *ELife* 7, e33506. doi: 10.7554/eLife.33506

Nguyen, N. N. T., Clua, J., Vetal, P. V., Vuarambon, D. J., De Bellis, D., Pervent, M., et al. (2021). PHO1 family memebers transport phosphate from infected nodule cells to bacteroids in *Medicago truncatula*. *Plant Physiol.* 185, 196–209. doi: 10.1093/plphys/kiaa016

Okuma, N., Soyano, T., Suzaki, T., and Kawaguchi, M. (2020). MIR2111-5 locus and shoot-accumulated mature miR2111 systemically enhance nodulation depending on HAR1 in *Lotus japonicus*. *Nat. Commun.* 11, 5192. doi: 10.1038/s41467-020-19037-9

Oldroyd, G. E. D., and Long, S. (2003). Identification and characterization of *Nodulation-signaling pathway 2*, a gene of *Medicago truncatula* involved in nod factor signaling. *Plant Physiol.* 131, 1027–1032. doi: 10.1104/pp.102.010710

Phillips, D. A., Joseph, C. M., and Maxwell, C. A. (1992). Trigolline and stachydrine released from alfalfa seeds activate NodD2 protein in *Rhizobium meliloti*. *Plant Physiol.* 99, 1526–1531. doi: 10.1104/pp.99.4.1526

Qian, Y., Cheng, Y., Cheng, X., Jian, H., Zhu, S., and Cheng, B. (2011). Identification and characterization of dicer-like, argonaute and RNA-dependent RNA polymerase gene families in maize. *Plant Cell Rep.* 30, 1347–1363. doi: 10.1007/s00299-011-1046-6

Raya-González, J., Pelagio-Flores, R., and López-Bucio, J. (2012). The jasmonate receptor COI1 plays a role in jasmonate-induced lateral root formation and lateral root positioning in *Arabidopsis thaliana*. *J. Plant Physiol.* 169, 1348–1358. doi: 10.1016/j.jplph.2012.05.002

Reid, D., Nadzieja, M., Novák, O., Heckmann, A. B., Sandal, N., and Stougaard, J. (2017). Cytokinin biosynthesis promotes cortical cell responses during nodule development. *Plant Physiol.* 175, 361–375. doi: 10.1104/pp.17.00832

Ren, B., Wang, X., Duan, J., and Ma, J. (2019). Rhizobial tRNA-derived small RNAs are signal molecules regulating plant nodulation. *Science* 365, 919–922. doi: 10.1126/science.aav8907

Reyero-Saavedra, M. D. R., Qiao, Z., Sánchez-Correa, M. D. S., Diaz-Pineda, M. E., Reyes, J. L., Covarrubias, A. A., et al. (2017). Gene silencing of *Argonaute5* negatively affects the establishment of the legume-rhizobia symbiosis. *Genes (Basel)* 8, 352. doi: 10.3390/genes8120352

Roussin-Léveillée, C., Silva-Martins, G., and Moffet, P. (2020). ARGONAUTE5 represses age-dependent induction of flowering through physical and functional interaction with miR156 in *Arabidopsis*. *Plant Cell Physiol.* 61, 957–966. doi: 10.1093/pcp/pcaa022

Roy, S., Liu, W., Nandety, R. S., Crook, A., Mysore, K. S., Pislariu, C. I., et al. (2020). Celebrating 20 years of genetic discoveries in legume nodulation and symbiotic nitrogen fixation. *Plant Cell.* 32, 15–41. doi: 10.1105/tpc.19.00279

Schiessl, K., Lilley, J. L. S., Lee, T., Tamvakis, I., Kohlen, W., Bailey, P. C., et al. (2019). *NODULE INCEPTION* recruits the lateral root development program for symbiotic nodule organogenesis in *Medicago truncatula*. *Curr. Biol.* 29, 3657–3668. doi: 10.1016/j.cub.2019.09.005

Sibisi, P., and Venter, E. (2020). Wheat *Argonaute 5* functions in aphid-plant interaction. *Front. Plant Sci.* 11. doi: 10.3389/fpls.2020.00641

Singh, S., and Parniske, M. (2012). Activation of calcium- and calmodulin-dependent protein kinase (CCaMK), the central regulator of plant root nodule development. *Curr. Opin. Plant Biol.* 15, 444–453. doi: 10.1016/j.pbi.2012.04.002

Somssich, M., Khan, G. A., and Persson, S. (2016). Cell wall heterogeneity in root development of *Arabidopsis*. *Front. Plant Sci.* 7. doi: 10.3389/fpls.2016.01242

Song, J. J., Smith, S. K., Hannon, G. J., and Joshua-Tor, L. (2004). Crystal structure of argonaute and its implications for RISC slicer activity. *Science* 305, 1434–1437. doi: 10.1126/science.1102514

Sós-Hegedus, A., Domokos, A., Tóth, T., Gyula, P., Kaló, P., and Szittya, G. (2020). Suppression of *NB-LRR* genes by miRNAs promotes nitrogen-fixing nodule development in *Medicago truncatula*. *Plant Cell Environ.* 43, 117–1129. doi: 10.1111/pce.13698

Soyano, T., Hirakawa, H., Sato, S., Hayashi, M., and Kawaguchi, M. (2014). NODULE INCEPTION creates a long-distance negative feedback loop involved in homeostatic regulation of nodule organ production. *Proc. Natl. Acad. Sci. U.S.A.* 111, 14607–14612. doi: 10.1073/pnas.1412716111

Soyano, T., Shimoda, Y., Kawaguchi, M., and Hayashi, M. (2019). A shared gene drives lateral root development and root nodule symbiosis pathways in *Lotus*. *Science* 366, 1021–1023. doi: 10.1126/science.aax2153

Summerfield, R. J., Huxley, P. A., and Minchin, F. R. (1977). Plant husbandry and management techniques for growing grain legumes under stimulated tropical conditions in controlled environments. *Exp. Agricult.* 13 (1), 81–92. doi: 10.1017/S0014479700007638

Sun, J., Xu, Y., Ye, S., Jiang, H., Chen, Q., Liu, F., et al. (2009). *Arabidopsis* ASA1 is important for jasmonate-mediated regulation of auxin biosynthesis and transport during lateral root formation. *Plant Cell.* 21, 1495–1511. doi: 10.1105/tpc.108.064303

Tang, F., Yang, S., Liu, J., and Zhu, H. (2016). *Rj4*, a gene controlling nodulation specificity in soybeans, encodes a thaumatin-like protein but not the one previously reported. *Plant Physiol.* 170, 26–32. doi: 10.1104/pp.15.01661

Tian, T., Liu, Y., Yan, H., You, Q., Yi, X., Du, Z., et al. (2017). agriGO v2.0: A GO analysis toolkit for the agricultural community 2017 update. *Nucleic Acids Res.* 45, W122–W129. doi: 10.1093/nar/gkx382

Tiwari, M., Pandey, V., Singh, B., and Bhatia, S. (2021). Dynamics of miRNA mediated regulation of legume symbiosis. *Plant Cell Environ.* 44, 1279–1291. doi: 10.1111/pce.13983

Tolia, N. H., and Joshua-Tor, L. (2007). Slicer and the argonautes. *Nat. Chem. Biol.* 3, 36–43. doi: 10.1038/nchembio848

Tsikou, D., Yan, Z., Holt, D. B., Abel, N. B., Reid, D. E., Madsen, L. H., et al. (2018). Systemic control of legume susceptibility to rhizobial infection by a mobile microRNA. *Science* 362, 233–236. doi: 10.1126/science.aat6907

Tucker, M. R., Okada, T., Hu, Y., Scholefield, A., Taylor, J. M., and Koltunow, A. M. (2012). Somatic small RNA pathways promote the mitotic events of megagametogenesis during female reproductive development in *Arabidopsis*. *Development* 139, 1399–1404. doi: 10.1242/dev.075390

van Spronsen, P. C., Bakhuizen, R., van Brussel, A. A., and Kijne, J. W. (1994). Cell wall degradation during infection thread formation by the root nodule bacterium *Rhizobium leguminosarum* is a two-step process. *Eur. J. Cell Biol.* 64, 88–94.

Vaucheret, H. (2008). Plant ARGONAUTES. *Trends Plant Sci.* 13, 305–308. doi: 10.1016/j.tplants.2008.04.007

Wang, J., Mei, J., and Ren, G. (2019). Plant microRNAs: Biogenesis, homeostasis, and degradation. *Front. Plant Sci.* 10. doi: 10.3389/fpls.2019.00360

Wang, L., Rubio, M. C., Xin, X., Zhang, B., Fan, Q., Wang, Q., et al. (2019). CRISPR/CAS9 knockout of leghomoglobins genes in *Lotus japonicus* uncovers their synergistic roles in symbiotic nitrogen fixation. *N. Phytol.* 224, 818–832. doi: 10.1111/nph.16077

Wang, Y., Wang, Z., Amyot, L., Tian, L., Xu, Z., Gruber, M. Y., et al. (2015). Ectopic expression of miR156 represses nodulation and causes morphological and developmental changes in. *Lotus japonicus Mol. Genet. Genomics* 290, 471–484. doi: 10.100/s00438-014-0931-4

Wang, C., Yu, H., Luo, L., Duan, L., Cai, L., He, X., et al. (2016). *NODULES WITH ACTIVATED DEFENSE 1* is required for maintenance of rhizobial endosymbiosis in *Medicago truncatula*. *N. Phytol.* 212, 176–191. doi: 10.1111/nph.1407

Yang, K., Han, H., Li, Y., Ye, J., and Xu, F. (2022). Significance of miRNA in enhancement of flavonoid biosynthesis. *Plant Biol.* 24, 217–226. doi: 10.1111/plb.13361

Zhai, L., Teng, F., Zheng, K., Xiao, J., Deng, W., and Sun, W. (2019). Expression analysis of argonaute genes in maize (*Zea mays* l.) in response to abiotic stress. *Hereditas* 156, 27. doi: 10.1186/s41065-019-0102-z

frontiers | Frontiers in Plant Science

TYPE Original Research
PUBLISHED 31 January 2023
DOI 10.3389/fpls.2023.1088849

OPEN ACCESS

EDITED BY
Bo Zhang,
Chinese Academy of Sciences (CAS), China

REVIEWED BY
Mianhai Zheng,
Chinese Academy of Sciences (CAS), China
Guanghui L.V.,
Xinjiang University, China

*CORRESPONDENCE
Qianmin Jia
guqm@lzu.edu.cn
Fujiang Hou
cyhoufj@lzu.edu.cn

SPECIALTY SECTION
This article was submitted to Plant Nutrition, a section of the journal Frontiers in Plant Science

RECEIVED 04 November 2022
ACCEPTED 05 January 2023
PUBLISHED 31 January 2023

CITATION
Xu R, Shi W, Kamran M, Chang S, Jia Q and Hou F (2023) Grass-legume mixture and nitrogen application improve yield, quality, and water and nitrogen utilization efficiency of grazed pastures in the loess plateau. *Front. Plant Sci.* 14:1088849. doi: 10.3389/fpls.2023.1088849

Grass-legume mixture and nitrogen application improve yield, quality, and water and nitrogen utilization efficiency of grazed pastures in the loess plateau

Ranran Xu[1,2,3], Wei Shi[1], Muhammad Kamran[1], Shenghua Chang[1], Qianmin Jia[1*] and Fujiang Hou[1*]

[1]State Key Laboratory of Herbage Improvement and Grassland Agro-ecosystems; Key Laboratory of Grassland Livestock Industry Innovation, Ministry of Agriculture and Rural Affairs; Engineering Research Center of Grassland Industry, Ministry of Education; College of Pastoral Agricultural Science and Technology, Lanzhou University, Lanzhou, China, [2]Tropical Crops Genetic Resources Institute, Chinese Academy of Tropical Agricultural Sciences, Haikou, China, [3]Hainan Key Laboratory for Sustainable Utilization of Tropical Bioresources, College of Tropical Crops, Hainan University, Haikou, China

Grazing on cultivated grassland is a green agricultural model. However, in China's Loess Plateau, the type of cultivated grassland suitable for grazing and the amount of nitrogen application is still unclear, which has led to the failure of this model to be widely implemented. In this context, we set up an experiment using three grass planting types, including monoculture of alfalfa (Medicago sativa L.), monoculture of brome (Bromus inermis L.), and mixed planting of the two forages. Under each planting type, there were six management measures: grazing and no nitrogen application (GN1), grazing and 80 kg ha^{-1} nitrogen application (GN2), grazing and 160 kg ha^{-1} nitrogen application (GN3), cutting and no nitrogen application (MN1), cutting and 80 kg ha^{-1} nitrogen application (MN2), and cutting and 160 kg ha^{-1} nitrogen application (MN3). To explore the impacts of these treatments on pastures, we studied the effects on the yield, quality, and water use efficiency of the three cultivated grasslands. Results showed that alfalfa monoculture and alfalfa-brome mixed sowing grassland resulted in significantly higher hay yield, crude protein yield, water use efficiency (WUE), precipitation use efficiency (PUE), nitrogen use efficiency (NUE), and agronomic efficiency of nitrogen (AEN) as compared to brome monoculture grassland. In addition, the crude protein, ether extract, and crude ash content of alfalfa monoculture and alfalfa-brome mixture were increased significantly while the contents of neutral detergent fiber (NDF) were reduced, thereby increasing the relative feed value (RFV) during the two years. The forage hay yield, crude protein yield, ether extract, crude ash content, RFV, PUE, and WUE were significantly higher with GN1, GN2, and GN3 treatments than that with MN1 treatment. In contrast, the NDF and acid detergent fiber (ADF) content was significantly lower than the MN1 treatment. Furthermore, the fresh forage yield, crude protein yield, PUE, and WUE of GN3 treatment were significantly higher than that of GN1 and GN2 treatments in both years, while the

NUE and AEN were significantly higher in GN2 and GN3 treatments than that of MN3 treatment. Based on these results, alfalfa-brome mixed cropping with the application of 160 kg ha^{-1} nitrogen under grazing conditions is an appropriate management practice for improving the forage yield, quality, and water- and nitrogen utilization efficiency of cultivated grassland in the Loess Plateau of China. This integrated management model is applicable to the cultivation and utilization of mixed grassland on nutrient-poor land in the Loess Plateau.

KEYWORDS

grazing, water and nitrogen utilization efficiency, alfalfa, forage yield, quality

1 Introduction

Soil erosion has resulted in a gradual increase in land barrenness and deterioration of the ecological environment, severely restricting the development of local industrial and agricultural production (Zhou et al., 2013). Planting perennial pastures in the loess plateau region is of practical importance because it will not only relieve the grazing pressure of natural grasslands but will also solve the problem of insufficient forage for livestock in the winter and spring seasons (Hou et al., 2008). In addition, cultivating grasslands in the Loess Plateau is an effective way of changing the land use patterns in the region and promoting ecological and economic development (Komarek et al., 2015). Compared to monoculture grasses, alfalfa and gramineous mixed grassland can not only increase the forage yield (Sanderson et al., 2005; Deak et al., 2009) but will also improve the nutritional quality of pasture (Tekeli and Ates, 2005). In addition, grazing on the grass-legume mixed grassland can improve grassland productivity by better-storing moisture and inorganic salt in the soil (Pykälä, 2005). In alfalfa-brome mixed sowing grassland, brome can utilize the nitrogen fixed by alfalfa, improve the N_2 fixation efficiency of alfalfa, and promote the absorption of nitrogen by brome (Lahiri et al., 2009; Li et al., 2011).

In addition, fertilization is one of the important agronomic measure for improving the yield and quality of pastures. Nitrogen application in cultivated grassland can improve the yield and crude protein content of dry matter, thus improving the nutritional quality of pasture (Mbatha and Ward, 2010; Tomić et al., 2012). Nitrogen is a major component of protein synthesis, and increased application of nitrogen fertilizer has been known to have positive effects on the nutrient absorption and utilization of cultivated grassland (Xiong et al., 2013; Gou et al., 2016). However, nitrogen application has a threshold effect in regulating crop growth, i.e. excessive nitrogen application is not conducive to improving crop growth and yield (Mon et al., 2016; Wang et al., 2017; Wang H. et al., 2018). The crude protein content and yield of Urochloa brizantha and Marandu pastures were increased with the increase in nitrogen application rates during each grazing cycle, while the content of neutral detergent fiber (NDF) was reduced, and in the case of continuous grazing, moderate nitrogen application (180 kg^{-1} N) resulted in high yield and quality forage (Campos et al., 2016; Delevatti et al., 2019). Brueck et al. (2010) showed that nitrogen application can improve the water use efficiency (WUE) of pasture regardless of water supply (Mckenzie et al., 2006; Brueck et al., 2010). However, Li et al. (2003) suggested that measuring soil nitrogen supply capacity and plant nitrogen demand at different stages, and providing timely and appropriate nitrogen fertilizer supply can improve the soil nutrient status, production performance, and sustainable productivity of cultivated grassland.

Moderate grazing is an effective way of managing grassland vegetation (Huntsinger et al., 2007). Moderate grazing is not only a management measure for preventing habitat loss or fragmentation but also a way for improving grassland biodiversity (Bartolome et al., 2014). Previous studies have found an increase in the biomass and crude protein content of the above-ground plants with the increase in the stocking rate (Schönbach et al., 2012a; Müller et al., 2014; Ren et al., 2016), while the content of neutral detergent fiber only decreased in the short term with the increase of stocking rate (Schönbach et al., 2009). Schönbach et al., 2012a showed that compared with light and heavy grazing, the available feed biomass under moderate grazing increased by 2 to 3 times, and plant nutrients were improved. However, some studies have reported that grazing has little impact on forage nutritional quality, but forages in grazing land had higher crude protein content in the late rainy season (Mbatha and Ward, 2010). Grazing not only increases the forage yield and improves nutritive quality but also the water use efficiency (Fenetahun et al., 2020). Peng et al. (2007) reported that the water use efficiency (WUE) of Cleistogenes squarrosa, Agropyron cristatum, and Potentilla acaulis increased significantly as the grazing intensity increased, reaching the highest value at moderate grazing intensity. Because of trampling disturbs soil by enhancing evaporation of water, sheep's dunk or urine might contribute to increase soil moisture (Peng et al., 2007). Under grazing conditions, *Leymus chinensis* is more sensitive to water deficit. It responds to grazing disturbance by reducing transpiration rate and improving WUE (D'Andrea et al., 2017). Grazing improves the water use efficiency of pasture, possibly due to the concentration of grazing grass roots to the surface soil, thus increasing the absorption and utilization of water by plant roots (Zheng et al., 2011).

Intensive grazing not only increase stocking rates and reduce costs but also improve soil moisture status and reduce soil erosion (Sone et al., 2020). Several studies have shown that grazing in the Loess Plateau, where "returning cropland to grassland" is practiced, significantly reduced soil erosion and improved soil characteristics (Wang et al., 2009; Chen et al., 2015; Yang and Lu, 2018). The results

of Yu et al. (2019) also showed that light grazing not only reduced soil erosion but also protected natural resources. Without disrupting the soil environment, grazing management may benefit the economic development of local animal husbandry and increase the income of local farmers to ensure food security and resolve conflicts of interest between agricultural development and nature protection (Sparovek et al., 2010; Spera, 2017). In the Loess Plateau of China, reasonable grazing of cultivated grassland is a sustainable grassland management model, and one of the strategies to achieve the dual goals of ecological and economic benefits (Wang and Zhang, 2003). However, most studies on grazing activities are concentrated on natural grasslands. There are few studies on grazing management of cultivated grasslands in the Loess Plateau, and the appropriate amount of nitrogen fertilizer for grass-legume mixed grassland is still uncertain. Therefore, this study explored the effect of grazing combined with nitrogen application on the yield, quality, water, and nitrogen utilization of cultivated grassland under the grassland types of monoculture alfalfa, monoculture brome, and mixed planting of the two forages. The objectives were to (a) explore the advantages of grass-legume mixed grassland compared with pasture monoculture; (b) clarify the appropriate management measures for improving the yield, quality, WUE, and NUE of cultivated grassland in the Loess Plateau.

2 Materials and methods

2.1 Overview of the research area

The study area is located in Huan xian Grassland Agricultural Experiment Station of Lanzhou University, Qingyang City, Gansu Province (36° 17′10″ N, 107° 31′36 ″E), with an altitude of 1218 m. It is a hilly and gully area on the Loess Plateau in eastern Gansu, with a typical river valley agricultural production system and semi-arid continental climate. The average annual rainfall is 430 mm and is mostly concentrated in July-September, accounting for 58.2% of the total annual precipitation. The annual potential evaporation reaches 1850 mm; the annual mean temperature is 9.2°C. The frost-free period is 165 days and the annual mean sunshine duration is 2596.2 hours. Compared with the 30-year average rainfall, 2019 (505.5 mm) was considered as a wet year, while 2020 (434.1 mm) as a normal year. Before the commencement of the experiment, the soil (0-20 cm soil layer) had the following soil properties; pH value of 8.5, soil organic carbon of 4.9 g kg^{-1}, the total nitrogen content of 0.67 g kg^{-1}, the available phosphorus content of 11.6 mg kg^{-1}, available potassium content 142 mg kg^{-1}.

2.2 Experimental design and field management

This study was arranged in a split-plot design. The main plot factor includes three grassland types: monoculture of alfalfa, monoculture of brome, and mixed cropping of alfalfa and brome. The sub-plot factor included six management measures: grazing and 0 kg ha^{-1} nitrogen application level of (GN1), grazing and 80 kg ha^{-1} nitrogen application level of (GN2), grazing and 160 kg ha^{-1} nitrogen application level of (GN3), cutting and 0 kg ha^{-1} nitrogen application level (MN1), cutting and 80 kg ha^{-1} nitrogen application level (MN2), and cutting and 160 kg ha^{-1} nitrogen application level (MN3). In this way the experiment consisted of a total of 18 treatments with three replications, resulting in a total of 54 treatment plots. The area of each treatment plot was 40 m^2 (5 m × 8 m), separated by a 1 m wide isolation belt. In addition, fences were set up around the grazing plots. The grassland was planted in August 2017, and 225 kg ha^{-1} diammonium hydrogen phosphate was used as the base fertilizer for each sowing plot. No irrigation was provided during the experimental period. The alfalfa variety Qianjing (*Medicago sativa* L. 'Vison'), and the brome American variety (*Bromus inermis* L. 'Vns') were used in the experiment. Before planting, ploughing (30 cm depth) was employed for removing weeds. Seeds were sown by drill sowing method at a row spacing of 30 cm, and planting depth of 2 to 3 cm. The seeding rate for monoculture alfalfa was 30 kg ha^{-1}, for monoculture brome was 45 kg ha^{-1}, while that of alfalfa and brome mixed grassland was 15.0 and 22.5 kg ha^{-1}, respectively. In both years, no fertilizers were applied to the N1 treated plots. The N2 plots were fertilized on 3rd June 2019 and 8th June 2020; while the N3 plots were fertilized on 3rd June and 1st August 2019, and 8th June and 5th August 2020. Urea (CH_4N_2O) was used as a nitrogen source and 80 kg N ha^{-1} was applied in trenches each time. Rotational grazing was carried out approximately every 30 days. There were 81 sheep in total and 9 sheep were allotted to each plot, and all the forages in the plot were grazed. Overall, 12 grazing cycles were performed during the two years. The cutting treatment was carried out at the flowering stage of the leguminous family or the heading period of the gramineous family. The stubble height was maintained at 5 cm, and 6 cuttings were carried out in two years, corresponding to May 21, July 23, September 24 in 2019, and May 24, July 15, and September 6 in 2020.

2.3 Sampling and measurements

2.3.1 Determination of forage yield and nutritional quality

For grazing treatments, samplings were carried out before each grazing, and for cutting treatments, samplings were performed at the leguminous flowering period or gramineous heading period. For cutting, 1 m^2 area was randomly selected at three different locations in each plot and immediately weighed for the fresh weight. The samples were put in a mesh bag, transported to the lab, and later oven-dried at 65°C for 48 h or until constant weight, and dry matter yield was determined. The seasonal total fresh grass and hay yields were the sum of the fresh and hay yields of each cutting throughout the growing period. The crude protein yield was calculated using the following formula:

$$Y_P\left(\mathrm{t\ ha^{-1}}\right) = C_P \times Y \times 0.01$$

where Y_P is crude protein yield (t·ha^{-1}), C_P is crude protein content (%), Y is hay yield (kg ha^{-1}).

The dried samples were crushed and were analyzed for the determination of nutrient values. The content of ether extract (ether extract, EE) was determined by the Soxhlet ether extraction method using an ether extract analyzer (XT15, Ankom, America) (Association of Official Analytical Chemists, 2000). Crude protein (CP) content was determined by the Kjeldahl method using the nitrogen analyzer (Kjeltec 2300, Foss Tecator, Sweden) (Jee, 1995). The crude ash content was determined by the incineration method in a muffle furnace (LE14/16/R6, Nabertherm, Germany) at 550°C (Van Soest, 1994). The content of neutral detergent fiber (NDF) and acid detergent fiber (ADF) was measured in a fiber analyzer (2000, Ankom, America) using the paradigm detergent fiber analysis method (Van Soest et al., 1991). The relative feeding value (RFV) was calculated using the following formulae (Kamran et al., 2022; Kamran et al., 2023):

$$RFV = (120/NDF) \times (88.9 - 0.799ADF)/1.29$$

Whereas NDF and ADF represent the neutral and acid detergent fiber, respectively.

2.3.2 Water utilization status

To determine the soil quality content of the soil samples were collected at recovering and withering date of the pasture A soil drill was used for collecting soil samples from 0-200 cm soil layer, each with a 20 cm increment. The soil was placed aluminum box and oven-dried at 105°C for 24 h or to a constant weight. The soil moisture contents in terms of soil water storage (SWS) were calculated following the formula (Wu et al., 2015):

$$SWS(mm) = \sum_1^n h_i \times p_i \times b_i$$

Where SWS is the soil water storage capacity (mm), hi is the depth of the soil layer (cm); p_i is the soil bulk density of the soil layer (g cm^{-3}); b_i is the absolute soil of the soil layer Mass moisture content (%); n is the number of soil layers.

The water consumption in terms of evapotranspiration (ET) from the field was calculated using the formula (Huang et al., 2005) is as follows:

$$ET\ (mm) = P + I + C + W1 - W2 - D - R$$

Where P (mm) is the rainfall during the growth period, I (mm) is the irrigation volume, C (mm) is the amount of groundwater at the roots zones, and W1 (mm) is the water storage at recovering date of 0-200 cm soil layer, W2 (mm) is the water storage at the withering date of 0-200 cm soil layer, D (mm) is the water discharge outside the roots, and R (mm) is the surface runoff loss. However, the runoff loss can be ignored as the test site is relatively flat, and ridges around the plot prevent runoff. The groundwater level of the test site was deeper than 80 m. As no irrigation was provided, therefore, the amount of groundwater flowing into the roots, rainfall-runoff loss, irrigation, and water discharge beyond the roots can be ignored (Zhao et al., 2014).

The calculation formulas for precipitation use efficiency and water use efficiency (are as follows Huang et al., 2005):

$$PUE\ (kg\ ha^{-1}\ mm^{-1}) = Y/P$$

$$WUE\ (kg\ ha^{-1}\ mm^{-1}) = Y/ET$$

Whereas PUE is the precipitation use efficiency (kg ha^{-1} mm^{-1}), WUE is water use efficiency (kg ha^{-1} mm^{-1}), Y is hay yield (kg ha^{-1}), and ET is field water consumption (mm), P is the rainfall during the growth period (mm).

2.3.3 Nitrogen utilization status

Determination of forage nitrogen content was carried out using FOSS-NIRS DS 2500 (Denmark) Near-Infrared Spectrometer. The nitrogen uptake, nitrogen use efficiency, and agronomic efficiency of nitrogen were calculated using the following formulas (Guo et al., 2014):

$$N_U\ (kg\ \ ha^{-1}) = N_C{\star}Y$$

$$NUE\ (kg\ \ kg^{-1}) = (U_N - U_0)/F_N$$

$$AEN\ (kg\ \ kg^{-1}) = (Y_N - Y_0)/F_N$$

where, N_U and Nc are nitrogen absorption (kg ha^{-1}) and nitrogen content (%); NUE is nitrogen utilization efficiency (kg kg^{-1}), U_N and U_0 are nitrogen absorption (kg ha^{-1}) in the nitrogen application treatment and no nitrogen application treatment; AEN is nitrogen agronomic efficiency (kg kg^{-1}), Y_N and Y_0 are yield (kg ha^{-1}) of nitrogen application treatment and no nitrogen application treatment; and F_N is the N rate (kg ha^{-1}) in N application treatments.

2.4 Data processing and statistical methods

Microsoft Excel 2010 was used to process the data and draw figures. After testing the data normality and homogeneity of variance, the data follows normal distribution and meets the homogeneity test of variance, the statistical software SPSS 24 (IBM, Chicago, IL, USA) was employed for the analysis of variance. To analyze the effects of different treatments on fresh hay yield, nutrient content, crude protein yield, relative feed value, water use efficiency, precipitation use efficiency, nitrogen use efficiency, and agronomic efficiency of nitrogen of forage, the Tukey significant difference test was employed for multiple comparisons ($P \leq 0.05$). Figures 1, 2.

3 Results

3.1 Fresh hay yield

The ANOVA results indicated significant effects ($P \leq 0.01$) of the year (Y), grassland type (GT), and management style (MM) on fresh biomass of pastures (Table 1). The interaction effects were also significant ($P \leq 0.01$). The fresh biomass yield of all treatments in 2019 was significantly higher by 20.5% than that in 2020. Among the grassland types, alfalfa-brome mixed sowing resulted in the highest fresh biomass compared to their monocultures (Table S1). In addition, the GN3 showed the most significant effect among the various management styles (Table S1).

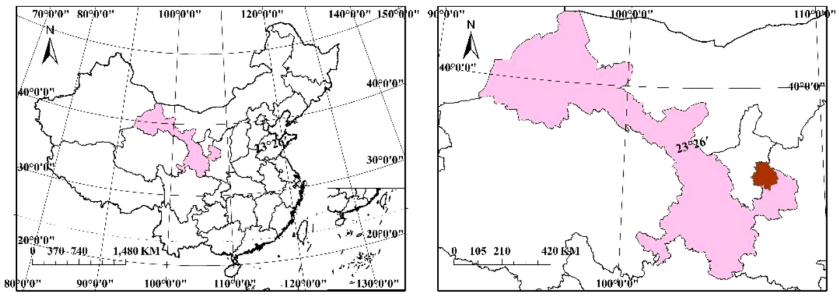

FIGURE 1
The geographical location of Huanxian test station.

When analyzed the interactive effects, the GN3 treatment in alfalfa-brome mixed sowing grassland achieved the highest fresh forage biomass (70.84 and 52.60 t ha^{-1}), and in alfalfa monoculture grassland (66.35 and 52.63 t ha^{-1}) in 2019 and 2020, respectively (Figure 3). In alfalfa-brome mixed pastures, the GN3 treatment increased the fresh biomass by 44.4 and 34.3%, 10.4 and 12.3%, 110.4 and 111.7%, 56.0 and 110.2%, 42.7 and 83.7% as compared to GN1, GN2, MN1, MN2, and MN3 treatments. Whereas in alfalfa monoculture, GN3 treatment increased the fresh biomass by 41.0 and 31.0%, 10.6 and 14.8%, 98.4 and 129.8%, 56.1 and 95.8%, 43.4 and 43.9% compared to GN1, GN2, MN1, MN2, and MN3 treatments.

The hay yield was significantly affected ($P \leq 0.01$) by year (Y), grassland type (GT), and management style (MM) on of pastures (Table 1). The interaction effects were also significant ($P \leq 0.01$). The hay yield of all treatments in 2019 was significantly higher by 4.5% than that in 2020. Among the grassland types, compared to brome monoculture, the hay yield in alfalfa-brome mixed sowing and alfalfa monoculture were significantly increased (Table S1). In addition, the GN3 showed the most significant effect among the various management styles (Table S1). For the interactive effects, the GN3 treatment showed the most significant effects on increasing hay yield in all grassland types compared to rest of the treatments in 2019 and 2020 (Figure 4). Among all the treatments, the GN3 treatment in alfalfa-brome mixed sowing grassland achieved the highest hay yield (14.58 and 11.45 t ha^{-1}), and in alfalfa monoculture grassland (12.96 and 12.00 t ha^{-1}) in 2019 and 2020, respectively (Figure 4). In alfalfa-brome mixed pastures, the GN3 treatment increased the hay yield by and 54.8%, and 32.8%, 16.0 and 4.0%, 120.2 and 69.1%, 63.5 and 61.7%, 44.8 and 46.2% as compared to GN1, GN2, MN1, MN2, and MN3 treatments. Whereas in alfalfa monoculture, GN3 treatment increased the hay yield by 47.9 and 35.4%, 12.3 and 11.0%, 107.7 and 96.7%, 57.1 and 59.8%, 41.9 and 19.2% compared to GN1, GN2, MN1, MN2, and MN3 treatments.

3.2 Crude protein yield

The crude protein yield was significantly affected ($P \leq 0.01$) by year (Y), grassland type (GT), and management style (MM) on of pastures (Table 1). The various interaction effects were also significant ($P \leq 0.01$). Crude protein yield of all treatments in 2019 was significantly higher by 5.4% than that in 2020. Among the grassland types, alfalfa-brome mixed sowing resulted in the highest crude protein yield whereas for management styles, GN3 showed the most significant effect (Table S1).

When analyzed the interactive effects, the GN3 treatment showed the most significant effects on increasing crude protein yield in all grassland types, compared to other treatments in both years (Figure 5). Among all the treatments, the GN3 treatment in alfalfa-brome mixed sowing grassland achieved the highest crude protein yield (2.97 and 2.50 t ha^{-1}), and in alfalfa monoculture grassland (2.72 and 2.53 t ha^{-1}) in 2019 and 2020, respectively (Figure 5). In alfalfa-brome mixed pastures, the GN3 treatment increased the crude protein yield by 66.9 and 35.9%, 149.6 and 100.0%, 74.7 and 82.5%,

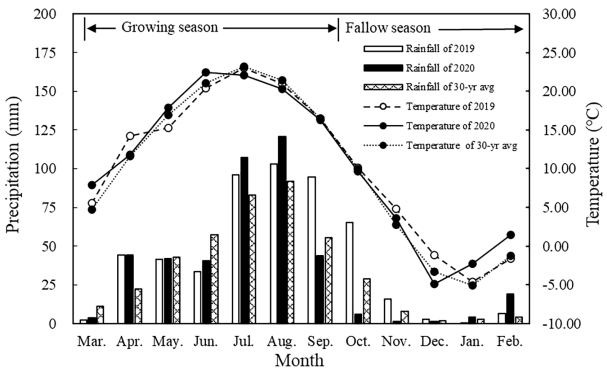

FIGURE 2
Monthly average precipitation and temperature in Huanxian experimental station.

TABLE 1 ANOVA results for the effect of the year, grassland type, management style, and their interactions on fresh forage biomass, hay yield, crude protein yield, the content of crude protein, crude fat, crude ash, acid detergent fiber (ADF), neutral detergent fiber (NDF), and relative feed value (RFV); soil water storage, evapotranspiration, water use efficiency (WUE), precipitation use efficiency (PUE); nitrogen uptake, nitrogen content, nitrogen use efficiency (NUE) and agronomic efficiency of nitrogen (AEN) in 2019-2020.

Parameters	Year (Y)	Grassland Type (GT)	Management Style (MM)	Y×GT	Y×MM	GT×MM	Y×GT×MM
Fresh forage biomass	335.63**	1545.99**	383.22**	211.68**	9.39**	12.98**	4.43**
Hay yield	36.79**	1221.14**	347.26**	35.61**	6.42**	9.96**	4.38**
Crude protein yield	20.25**	2131.82**	441.93**	18.55**	7.06**	25.20**	4.64**
Crude protein	3.99*	438.56**	17.67**	0.72^{ns}	1.14^{ns}	1.44^{ns}	0.16^{ns}
Crude fat	842.18**	410.89**	32.01**	36.81**	3.12*	0.31^{ns}	0.20^{ns}
Crude ash	174.03**	777.14**	11.42**	64.73**	3.07*	1.09^{ns}	0.85^{ns}
ADF	31.29**	11.38**	33.22**	6.59**	3.26*	0.46^{ns}	0.43^{ns}
NDF	25.51**	243.17**	15.56**	54.68**	0.90^{ns}	0.41^{ns}	0.34^{ns}
RFV	81.74**	292.27**	40.81**	75.51**	3.45**	0.74^{ns}	0.76^{ns}
Soil water storage at recovering	0.76^{ns}	103.99**	17.96**	55.35**	7.57**	2.12*	2.06*
Soil water storage at withering	4.97*	188.75**	24.40**	21.77**	13.45**	2.46*	2.62**
Evapotranspiration	292.60**	0.85^{ns}	0.15^{ns}	10.03**	1.23^{ns}	0.57^{ns}	0.69^{ns}
WUE	120.74**	1078.40**	325.50**	31.12**	3.95**	8.38**	2.40*
PUE	71.40**	1083.96**	311.00**	17.03**	4.32**	8.84**	3.81**
Nitrogen uptake	19.75**	2086.36**	432.58**	18.15**	6.91**	24.55**	4.53**
Nitrogen content	3.71^{ns}	411.68**	16.66**	0.67^{ns}	1.06^{ns}	1.35^{ns}	0.15^{ns}
NUE	827.29**	1322.13**	2115.48**	230.82**	117.16**	207.49**	43.21**
AEN	819.49**	1108.27**	2018.08**	210.72**	132.71**	193.87**	48.49**

* Significant at 5% probability level; ** Significant at 1% probability level; ^{ns}, Not significant.

50.8 and 64.5% as compared to GN1, MN1, MN2, and MN3 treatments. Whereas in alfalfa monoculture, GN3 treatment increased the crude protein yield by 47.9 and 35.4%, 107.7 and 96.7%, 57.1 and 59.8%, 41.9 and 19.2% compared to GN1, MN1, MN2, and MN3 treatments.

3.3 Nutritional quality

Our data portrayed significant effects ($P \leq 0.01$) of the grassland type and management style on crude protein content of forage (Table 1). Year (Y), GT, MM and Y×GT had a highly significant ($P \leq 0.01$) effect on crude fat content, crude ash content, acid detergent fiber (ADF) and neutral detergent fiber (NDF) content of the forage. Y, GT and MM had highly significant ($P \leq 0.01$) effects on RFV of forages, the interaction effects were also significant ($P \leq 0.01$), except that of GT× MM and Y×GT×MM (Table 1).

The crude protein content and RFV of all treatments in 2020 was significantly higher than that in 2019. Among the grassland types, alfalfa-brome mixed sowing and alfalfa monoculture resulted in significantly higher crude protein content and RFV compared to brome monoculture (Table S1) In addition, the crude protein content and RFV of GN3 showed the most significant effect among the various management styles (Table S1). Among the interactive effects, in alfalfa monoculture and alfalfa-brome mixed sowing grassland, there was no significant difference in the crude protein content of each treatment in both years, while in brome monoculture grassland, the GN3 treatment showed significant effects on increasing crude protein content compared to GN1 treatment in both years (Table 2). In brome monoculture grassland, the GN3 treatment showed significant effects on increasing ether extract content compared to GN1 and MN1 treatments in both years. However, in alfalfa monoculture and alfalfa-brome mixed sowing grassland, the GN3 treatment showed significant effects on increasing ether extract content only in 2019.

In brome monoculture grassland, the GN3 treatment showed significant effects on increasing crude ash content compared to GN1 and MN1 treatments in both years, while in alfalfa-brome mixed sowing grassland, the GN3 treatment showed significant effects on increasing crude ash content in 2020. In alfalfa monoculture and brome monoculture grassland, the MN1 treatment showed significant effects on increasing ADF content compared to GN2 and GN3 treatments in both years, while in alfalfa-brome mixed sowing grassland, the MN1 treatment showed significant effects on increasing ADF content compared to GN3 treatment in both years. In brome monoculture grassland, the MN1 treatment showed significant effects on increasing NDF content compared to GN3 treatment in both years, whereas in alfalfa monoculture and alfalfa-brome mixed sowing grassland, the MN1 treatment showed significant effects on increasing NDF content in 2020.

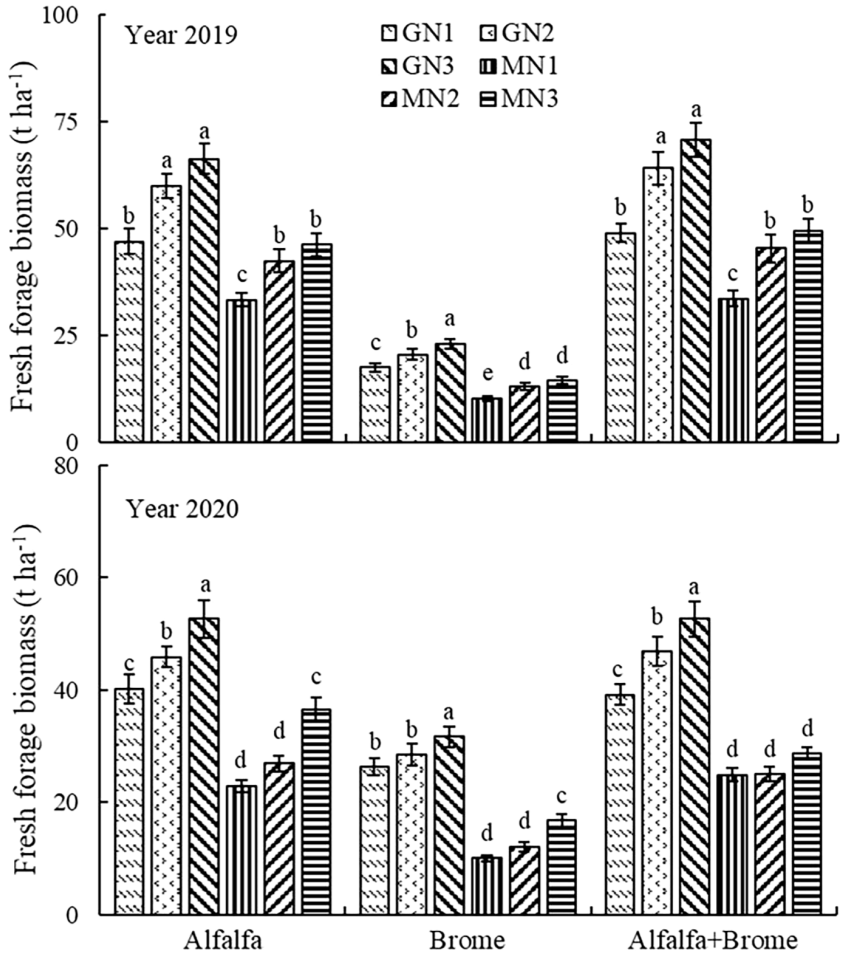

FIGURE 3
Fresh forage biomass of pasture under different treatments Note: The different lowercase letters indicate a significant difference among different treatment at $P \leq 0.05$. GT denotes grassland type, MM denotes field management measures, and GT×MM denotes the interaction between grassland type and field management measures. The GN1, GN2, GN3, MN1, MN2, and MN3 treatments indicate no nitrogen application under grazing, 80 kg ha^{-1} nitrogen application under grazing, 160 kg ha^{-1} nitrogen applications under grazing, no nitrogen application under cutting, 80 kg ha^{-1} nitrogen application under cutting, and 160 kg ha^{-1} nitrogen application under cutting, respectively.

The GN3 treatment showed significant effect on increasing RFV compared to MN1 treatment in 2019 among all the grassland types, whereas in 2020, the GN3 treatment showed significant differences compared to MN1 and MN2 treatments. Among all the treatments, the GN3 treatment in alfalfa-brome mixed sowing grassland achieved the highest crude protein content (20.36 and 21.76%), and in alfalfa monoculture grassland (20.97 and 21.76%) in 2019 and 2020, respectively (Table 2). The GN3 treatment in alfalfa-brome mixed sowing grassland achieved the RFV (154.49 and 178.28%), and in alfalfa monoculture grassland (157.63 and 201.72%) in 2019 and 2020, respectively. In brome monoculture grassland, the GN3 treatment increased the crude protein content by 16.7 and 24.7% as compared to MN1 treatment in 2019 and 2020. In alfalfa monoculture, brome monoculture and alfalfa-brome mixed pastures, the GN3 treatment increased the RFV by 19.8, 22.2 and 20.1% as compared to MN1 treatment in 2019; GN3 treatment increased the RFV by 31.7 and 25.7%, 29.4 and 15.4%, 23.1 and 16.1% as compared to MN1 and MN2 treatments in 2020.

3.4 Water use status

The ANOVA results indicated significant effects ($P \leq 0.01$) of the grassland type, management style, Y×GT and Y×MM on the soil water storage (WS) at withering and soil water storage at recovering (Table 1). Y and Y×GT had highly significant ($P \leq 0.01$) effects on evapotranspiration. Y, GT and MM had highly significant ($P \leq 0.01$) effects on water use efficiency (WUE), and precipitation use efficiency (PUE), the interaction effects were also significant ($P \leq 0.01$). Alfalfa-brome mixed sowing and alfalfa monoculture resulted in high WUE and PUE compared to brome monoculture (Table S1). In addition, the WUE and PUE of GN3 showed the most significant effect among the various management styles (Table S1).

When analyzed the interactive effects, under three grassland types, the MN1, MN2 and MN3 treatments showed significant effects on increasing the WS at recovering and withering date compared to GN1, GN2 and GN3 treatments in alfalfa monoculture and alfalfa-brome mixed sowing grassland in 2020

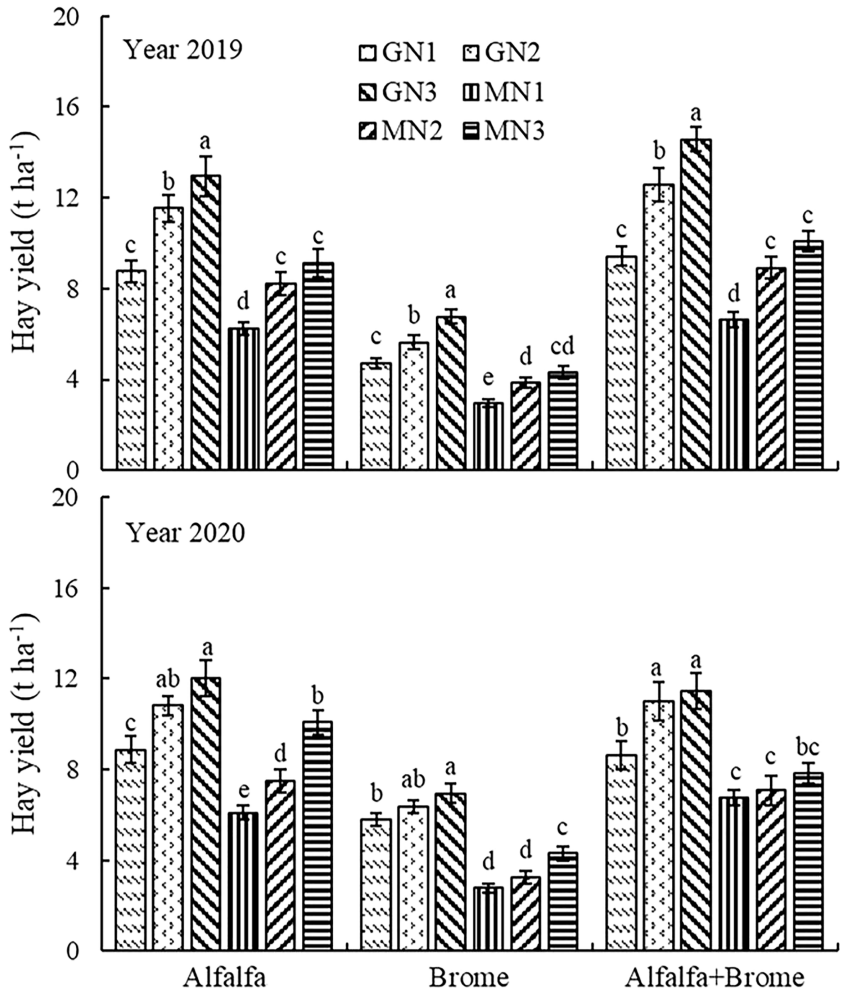

FIGURE 4
Hay yield of pasture under different treatments Note: The different lowercase letters indicate a significant difference among different treatment at $P \leq 0.05$. GT denotes grassland type, MM denotes field management measures, and GT×MM denotes the interaction between grassland type and field management measures. The GN1, GN2, GN3, MN1, MN2, and MN3 treatments indicate no nitrogen application under grazing, 80 kg ha^{-1} nitrogen application under grazing, 160 kg ha^{-1} nitrogen application under grazing, no nitrogen application under cutting, 80 kg ha^{-1} nitrogen application under cutting, and 160 kg ha^{-1} nitrogen application under cutting, respectively.

(Table 3). In brome monoculture grassland, there was no significant difference in the WS at recovering date of all treatments, While the MN2 and MN3 treatments showed significant effects on increasing the WS at withering date compared to GN1 treatment in 2020. However, the MN1 treatment showed significant effects on increasing the WS at withering date compared to GN3 treatment in alfalfa monoculture and alfalfa-brome mixed sowing grassland in 2019. the GN3 treatment showed significant effects on increasing WUE and PUE compared to GN1, GN2, MN1, MN2 and MN3 treatments in 2019 under three grassland types. The GN2 and GN3 treatments showed significant effects on increasing WUE and PUE compared to GN1, MN1, MN2 and MN3 treatments in 2020 under three grassland types. Among all the treatments, the GN3 treatment in alfalfa-brome mixed sowing grassland achieved the highest WUE (28.49 and 27.78 kg.ha^{-1}·mm^{-1}), and in alfalfa monoculture grassland (24.66 and 29.84 kg.ha^{-1}·mm^{-1}) in 2019 and 2020, respectively (Table 3). the GN3 treatment in alfalfa-brome mixed sowing grassland achieved the PUE (30.48 and 28.33 kg.ha^{-1}·mm^{-1}), and in alfalfa monoculture grassland (27.09 and 29.70 kg.ha^{-1}·mm^{-1}) in 2019 and 2020, respectively. In alfalfa-brome mixed sowing grassland, the GN3 treatment increased the WUE by 52.5 and 37.6%, 114.0 and 83.6%, 61.9 and 61.4%, 42.8 and 47.5% as compared to GN1, MN1, MN2 and MN3 treatments in 2019 and 2020. Whereas the GN3 treatment increased the PUE by 54.7 and 32.8%, 120.4 and 69.2%, 63.4 and 61.7%, 44.7 and 46.2% as compared to GN1, MN1, MN2 and MN3 treatments in 2019 and 2020. In alfalfa monoculture, the GN3 treatment increased the WUE by 44.4 and 35.8%, 104.3 and 103.1%, 57.8 and 64.8%, 42.1 and 24.9% as compared to GN1, MN1, MN2 and MN3 treatments in 2019 and 2020. Whereas the GN3 treatment increased the PUE by 47.9 and 35.4%, 107.6 and 96.7%, 57.8 and 59.8%, 42.0 and 19.2% as compared to GN1, MN1, MN2 and MN3 treatments in 2019 and 2020.

3.5 Nitrogen utilization status

In brome monoculture grassland, the GN3 treatment showed significant effects on increasing the nitrogen content compared to

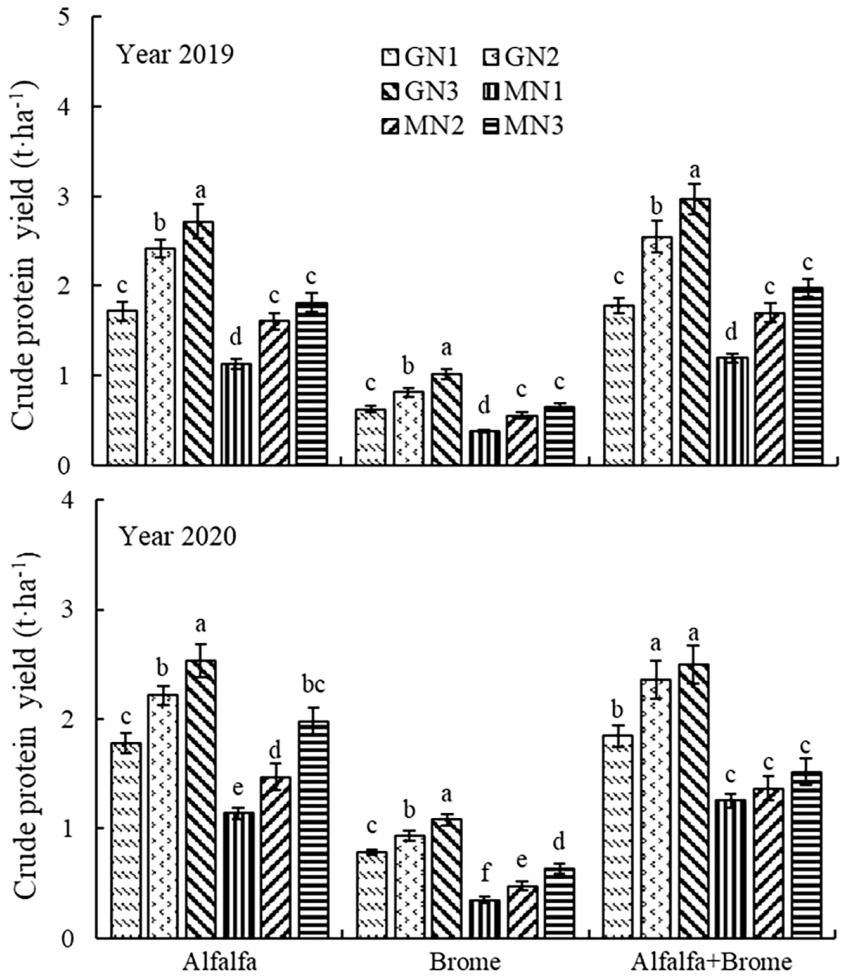

FIGURE 5
Crude protein yield of pasture under different treatments Note: The different lowercase letters indicate a significant difference among different treatment at $P \leq 0.05$. GT denotes grassland type, MM denotes field management measures, and GT×MM denotes the interaction between grassland type and field management measures. The GN1, GN2, GN3, MN1, MN2, and MN3 treatments indicate no nitrogen application under grazing, 80 kg ha^{-1} nitrogen application under grazing, 160 kg ha^{-1} nitrogen application under grazing, no nitrogen application under cutting, 80 kg ha^{-1} nitrogen application under cutting, and 160 kg ha^{-1} nitrogen application under cutting, respectively.

MN1 treatment in 2019 (Table 4); while the GN3 treatment showed significant effects on increasing the nitrogen content compared to GN1 and MN1 treatments in 2020. In alfalfa monoculture grassland, the GN3 treatment showed significant effects on increasing the nitrogen content compared to MN1 treatment in 2020. In alfalfa-brome mixed sowing grassland, the GN3 treatment showed significant effects on increasing the nitrogen content compared to GN1 treatment in 2020. In alfalfa monoculture and brome monoculture grassland, the GN3 treatment showed significant effects on increasing the nitrogen uptake compared to GN1, GN2, MN1, MN2 and MN3 treatments in 2019 and 2020. In alfalfa-brome mixed sowing grassland, the GN3 treatment showed significant effects on increasing the nitrogen uptake compared to GN1, GN2, MN1, MN2 and MN3 treatments in 2019, whereas the GN3 treatment showed significant effects on increasing the nitrogen uptake compared to GN1, MN1, MN2 and MN3 treatments in 2020.

In brome monoculture, The GN2, GN3 MN2 treatments showed significant effects on increasing the NUE and AEN compared to MN3 treatment in 2019. While in alfalfa monoculture and alfalfa-brome mixed sowing grassland, the GN2 treatment showed significant effects on increasing NUE and AEN compared to GN3 and MN2 treatments in 2019 and 2020. However, the GN2, GN3 and MN3 treatments showed significant effects on increasing NUE compared to MN2 treatment in 2020 under brome monoculture. The MN3 treatment showed significant effects on increasing AEN compared to GN2, GN3 and MN2 treatments in 2020 under brome monoculture. Among all the treatments, the GN2 treatment in alfalfa-brome mixed sowing grassland achieved the highest NUE (1.53 and 1.04 kg kg^{-1}), and in alfalfa monoculture grassland (1.39 and 0.88 kg kg^{-1}) in 2019 and 2020, respectively (Table 4). the GN3 treatment in alfalfa-brome mixed sowing grassland achieved the AEN (39.36 and 29.84 kg kg^{-1}), and in alfalfa monoculture grassland (34.68 and 24.29 kg kg^{-1}) in 2019 and 2020, respectively. In alfalfa-brome mixed sowing grassland, the GN2 treatment increased the NUE by 28.6 and 60%, 50 and 372.7%, 96.2 and 300% as compared to GN3, MN2, and MN3 treatments in 2019 and 2020. Whereas the GN2 treatment increased the AEN by 22.1 and 68.8%, 36.8 and 659.3%, 82.1 and 349.6% as compared to GN3, MN2 and MN3 treatments in 2019 and 2020. In alfalfa monoculture, the GN2 treatment increased the NUE by 39.0 and 17.3%, 46.3 and 31.3% as compared to GN3 and MN2 treatments in 2019 and 2020. Whereas the GN2 treatment increased

TABLE 2 The content of crude protein, crude fat, crude ash, acid detergent fiber, neutral detergent fiber and relative feed value of pasture under different treatments in 2019 and 2020.

Year	Grassland type	Management style	Crude protein(%)	Crude fat(%)	Crude ash(%)	Acid detergent fiber (%)	Neutral detergent fiber (%)	Relative feed value
2019	Alfalfa	GN1	19.58a	2.84bc	13.34a	30.76ab	44.02a	139.01ab
		GN2	20.90a	3.07ab	13.90a	28.73b	40.96a	152.76a
		GN3	20.97a	3.26a	13.98a	27.73b	40.31a	157.63a
		MN1	18.15a	2.57c	13.69a	32.45a	45.06a	131.56b
		MN2	19.58a	2.91abc	14.39a	30.07ab	42.37a	143.94ab
		MN3	19.82a	3.07ab	14.53a	29.24ab	41.06a	150.67a
	Brome	GN1	13.19b	2.25bc	6.64c	32.35ab	50.18ab	118.48bc
		GN2	14.50ab	2.48ab	7.76ab	29.51bc	46.40ab	133.05ab
		GN3	15.08a	2.64a	8.08a	27.85c	44.98b	139.66a
		MN1	12.92b	2.02c	6.92bc	33.11a	51.40a	114.27c
		MN2	14.39ab	2.28bc	7.86ab	30.34abc	48.38ab	125.55abc
		MN3	15.06a	2.38ab	8.22a	29.07bc	47.15ab	130.78ab
	Alfalfa + Brome	GN1	18.91a	2.62bc	12.31a	31.01ab	45.44a	134.30bc
		GN2	20.24a	2.82ab	13.14a	28.93ab	42.11a	148.68ab
		GN3	20.36a	2.97a	13.36a	27.69b	41.32a	154.49a
		MN1	18.02a	2.43c	12.62a	32.24a	46.48a	128.66c
		MN2	19.07a	2.73abc	13.33a	29.85ab	43.28a	142.51abc
		MN3	19.58a	2.84ab	13.52a	28.72ab	42.26a	148.09ab
2020	Alfalfa	GN1	21.33ab	3.08a	11.20ab	26.73b	36.65ab	174.23bcd
		GN2	21.44ab	3.16a	10.95ab	25.64bc	35.24ab	185.64ab
		GN3	21.76a	3.71a	11.52ab	22.57c	33.99b	201.72a
		MN1	18.61b	3.07a	10.10b	30.50a	39.66a	153.18d
		MN2	19.59ab	3.08a	10.73ab	29.16ab	38.52ab	160.51cd
		MN3	19.62ab	3.66a	12.15a	26.28b	36.32ab	177.48bc
	Brome	GN1	13.54ab	2.52bc	7.23b	29.62b	53.89ab	112.71bc
		GN2	14.60a	2.64abc	7.59ab	27.46b	51.94ab	120.79ab
		GN3	15.57a	2.93a	8.33a	26.49b	48.47b	129.50a
		MN1	12.49b	2.58c	7.25b	33.67a	56.70a	100.09c

(Continued)

10.3389/fpls.2023.1088849

TABLE 2 Continued

Year	Grassland type	Management style	Crude protein(%)	Crude fat(%)	Crude ash(%)	Acid detergent fiber (%)	Neutral detergent fiber (%)	Relative feed value
		MN2	14.58a	2.58abc	7.91ab	30.20b	52.24ab	112.23bc
		MN3	14.71a	2.74ab	8.44a	29.76b	50.25ab	121.37ab
	Alfalfa + Brome	GN1	20.11a	2.68a	11.54ab	28.22abc	37.41ab	166.19ab
		GN2	20.56a	2.73a	11.72ab	27.59bc	37.41ab	169.32ab
		GN3	21.08a	3.07a	12.19a	26.28c	35.92b	178.28a
		MN1	18.54a	2.66a	10.42b	31.68a	41.22a	144.86c
		MN2	19.30a	2.69a	10.56b	30.07ab	39.79ab	153.51bc
		MN3	19.36a	2.88a	11.21ab	29.41abc	38.61ab	159.17abc

The different lowercase letters indicate a significant difference among different treatment at $P \leq 0.05$. The GN1, GN2, GN3, MN1, MN2 and MN3 treatments were no nitrogen applied under grazing, 80 kg ha^{-1} nitrogen applied under grazing, 160 kg ha^{-1} nitrogen applied under grazing, no nitrogen applied under cutting, 80 kg ha^{-1} nitrogen application under cutting and 160 kg ha^{-1} nitrogen application under cutting, respectively. GT denotes grassland type, MM denotes field management measures, and GT×MM denotes the interaction between grassland type and field management measures.

the AEN by 32.3 and 23.9%, 41.1 and 38.4% as compared to GN3 and MN2 treatments in 2019 and 2020.

4 Discussion

4.1 Effects of grass-legume on forage yield, quality, water, and nitrogen utilization

Several studies have shown that the grass-legume mixed grassland results in higher forage yield than that of monoculture grassland (Nyfeler et al., 2011). Our research also shows that the fresh/hay yield of mixed cropping of grasses with alfalfa and brome was significantly higher than that of monoculture of brome. This may be due to the grass-legume mixed grassland that improved the resource utilization efficiency (such as light, moisture, and soil nutrients). Ajayi et al. (2009) reported that grass-legume mixed grassland not only increases the yield of forage but also improves the nutritional quality of forage. The results of Carpici (2017) also showed that compared with monoculture grassland, oat-pea mixed grassland have a lower content of neutral detergent fiber and acid detergent fiber, and a higher relative feed value. Our results corroborated these findings, as the two-year mixed grassland with alfalfa and brome significantly reduced the neutral detergent fiber content of the forage and increased the relative feed value, and improved the nutritional quality of forage (Table 2). Compared with the monoculture of gramineous or leguminous crops, grass-legume mixed grassland has advantages such as balanced feeding value, improved resource utilization efficiency, and increased forage yield (Phelan et al., 2015).

Studies have shown that mixed sowing of grass-legume increase the crude protein and dry matter yields of forages, and increases WUE to a certain extent (Zhang et al., 2018). A previous study by Dhakal et al. (2020) showed that the forage yield and nitrogen yield under alfalfa/gramineous grasses mixed sowing increased respectively by 35% and 96% compared with the monoculture of gramineous grasses. The WUE of alfalfa-gramineous mixed grassland was higher than that of monoculture of gramineous grasses, compared with the monoculture of gramineous grasses increased by 25%. Our results are similar to the findings from the above mentioned study. Under monoculture of alfalfa and mixed cropping of grasses with alfalfa and brome, the crude protein yield and WUE in both were significantly higher than those of monoculture of brome. This is due to the mixed sowing of gramineous grasses and alfalfa which can increase forage yield and increase nitrogen absorption, thereby increasing forage crude protein yield and WUE (Dhakal et al., 2020). At the same time, the strong root system of legumes forage and the shading effect of gramineous forage leaves promote the absorption and utilization of moisture by plants (Wang et al., 2015). Génard et al. (2017) showed that the nitrogen content of rape (*Brassica napus* L.) respectively intercropped with lupine (*Lupinus micranthus* Guss), clover (*Trifolium*), and Vetch (*Vicia sepium* L.) was higher than that of rape monoculture, which was increased by 34%, 140%, and 290%, respectively. The results showed that the nitrogen content of the mixed grassland of Leguminosae and Brassica was significantly higher than that of monoculture. In agreement with these finding our results

10.3389/fpls.2023.1088849

TABLE 3 Soil water storage, evapotranspiration, water use efficiency (WUE) and precipitation use efficiency (PUE) under different treatments in 2019 and 2020.

Year	Grassland type	Management style	Soil water storage at recovering (mm)	Soil water storage at withering (mm)	Evapotranspiration (mm)	WUE (kg ha^{-1} mm^{-1})	PUE (kg ha^{-1} mm^{-1})
2019	Alfalfa	GN1	295.12a	260.27ab	513.16a	17.08c	18.32c
		GN2	287.53a	246.04ab	519.79a	22.20b	24.12b
		GN3	280.00a	232.74b	525.55a	24.66a	27.09a
		MN1	305.39a	266.40a	517.29a	12.07d	13.05d
		MN2	298.16a	251.07ab	525.39a	15.63c	17.17c
		MN3	290.59a	243.11ab	525.77a	17.36c	19.08c
	Brome	GN1	312.19a	310.93a	479.56a	9.84c	9.87c
		GN2	305.71a	296.55a	487.46a	11.57b	11.79b
		GN3	293.81a	281.36a	490.75a	13.78a	14.14a
		MN1	320.71a	316.93a	482.07a	6.08e	6.13e
		MN2	311.33a	305.92a	483.71a	7.95d	8.04d
		MN3	304.98a	289.30a	493.98a	8.72cd	9.00cd
	Alfalfa + Brome	GN1	300.52a	274.65ab	504.17a	18.68c	19.70c
		GN2	285.25a	255.26ab	508.30a	24.73b	26.28b
		GN3	273.62a	240.25b	511.68a	28.49a	30.48a
		MN1	304.01a	285.19a	497.11a	13.31d	13.83d
		MN2	296.46a	268.04ab	506.71a	17.60c	18.65c
		MN3	285.62a	259.05ab	504.87a	19.95c	21.06c
2020	Alfalfa	GN1	289.18b	241.34bc	403.36a	21.98b	21.94c
		GN2	240.60bc	216.02c	401.59a	26.91a	26.74ab
		GN3	213.51c	183.06d	402.11a	29.84a	29.70a
		MN1	181.07a	293.92a	415.34a	14.69d	15.10e
		MN2	305.16a	280.79a	414.47a	18.11c	18.58d
		MN3	291.16a	270.31ab	421.27a	23.90b	24.91bc
	Brome	GN1	287.48a	290.39b	466.78a	12.38c	14.30b
		GN2	353.07a	322.49ab	438.53ab	14.53b	15.77ab
		GN3	356.92a	336.01ab	417.37ab	16.62a	17.17a
		MN1	349.28a	331.36ab	425.30ab	6.51e	6.85d
		MN2	352.56a	364.03a	424.42ab	7.64e	8.03d
		MN3	384.35a	373.94a	402.08b	10.70d	10.64c
	Alfalfa + Brome	GN1	371.92b	225.79b	426.90a	20.19b	21.33b
		GN2	248.59b	224.04b	407.00a	27.05a	27.24a
		GN3	226.94b	214.44b	412.21a	27.78a	28.33a
		MN1	222.55a	275.39a	447.28a	15.13c	16.74c
		MN2	318.57a	290.11a	411.43a	17.21bc	17.52c
		MN3	297.44a	277.31a	415.97a	18.83b	19.38bc

The different lowercase letters indicate a significant difference among different treatment at $P \leq 0.05$. The GN1, GN2, GN3, MN1, MN2 and MN3 treatments were no nitrogen applied under grazing, 80 kg ha^{-1} nitrogen applied under grazing, 160 kg ha^{-1} nitrogen applied under grazing, no nitrogen applied under cutting, 80 kg ha^{-1} nitrogen application under cutting and 160 kg ha^{-1} nitrogen application under cutting, respectively. GT denotes grassland type, MM denotes field management measures, and GT×MM denotes interaction between grassland type and field management measures.

TABLE 4 Nitrogen uptake, nitrogen content, nitrogen use efficiency and agronomic efficiency of nitrogen under different treatments in 2019 and 2020.

Year	Grassland type	Management style	Nitrogen content (%)	Nitrogen uptake (kg ha^{-1})	Nitrogen use efficiency (kg kg^{-1})	Agronomic efficiency of nitrogen (kg kg^{-1})
2019	Alfalfa	GN1	3.13a	274.53c		
		GN2	3.34a	385.88b	1.39a	34.68a
		GN3	3.36a	434.81a	1.00b	26.22b
		MN1	2.90a	181.35d		
		MN2	3.13a	257.22c	0.95b	24.58b
		MN3	3.17a	289.35c	0.68c	18.01c
	Brome	GN1	2.11ab	99.55c		
		GN2	2.32ab	130.84b	0.39a	11.54a
		GN3	2.41a	163.15a	0.40a	12.78a
		MN1	2.07b	60.61d		
		MN2	2.30ab	88.53c	0.35a	11.39a
		MN3	2.41a	103.75c	0.27b	8.58b
	Alfalfa + Brome	GN1	3.03a	285.00c		
		GN2	3.24a	407.10b	1.53a	39.36a
		GN3	3.26a	474.98a	1.19b	32.24b
		MN1	2.88a	190.73d		
		MN2	3.05a	272.12c	1.02c	28.78c
		MN3	3.13a	315.53c	0.78d	21.61d
2020	Alfalfa	GN1	3.41ab	284.17c		
		GN2	3.43ab	354.93b	0.88a	24.29a
		GN3	3.48a	404.71a	0.75b	19.61b
		MN1	2.98b	181.75d		
		MN2	3.13ab	235.30d	0.67c	17.55b
		MN3	3.14ab	316.02c	0.84a	24.78a
	Brome	GN1	2.17bc	125.11c		
		GN2	2.34ab	148.89b	0.30a	7.44b
		GN3	2.49a	172.90a	0.30a	7.26b
		MN1	2.00c	55.33f		
		MN2	2.33ab	75.64e	0.25b	5.93c
		MN3	2.35ab	101.21d	0.29a	9.57a
	Alfalfa + Brome	GN1	3.22b	294.85b		
		GN2	3.29a	377.80a	1.04a	29.84a
		GN3	3.37a	399.22a	0.65b	17.68b
		MN1	2.97a	200.75d		
		MN2	3.09a	218.59cd	0.22c	3.93d
		MN3	3.10a	242.57c	0.26c	6.66c

The different lowercase letters indicate a significant difference among different treatment at $P \leq 0.05$. The GN1, GN2, GN3, MN1, MN2 and MN3 treatments were no nitrogen applied under grazing, 80 kg ha^{-1} nitrogen applied under grazing, 160 kg ha^{-1} nitrogen applied under grazing, no nitrogen applied under cutting, 80 kg ha^{-1} nitrogen application under cutting and 160 kg ha^{-1} nitrogen application under cutting, respectively. GT denotes grassland type, MM denotes field management measures, and GT×MM denotes interaction between grassland type and field management measures.

also showed that the nitrogen content and NUE of the two-year alfalfa monoculture and the alfalfa- brome mixed grassland were significantly higher than those of the brome monoculture. In explanation, the biological nitrogen fixation of alfalfa not only provides a nitrogen source for its growth but also provides a nitrogen source for the growth of brome, which effectively increases the NUE of forage (Nyfeler et al., 2011).

4.2 Effects of grazing on forage yield, quality, and water use

Patton et al. (2007) showed that light and moderate grazing levels can increase forage yields compared to no grazing. Our research has also found that grazing significantly increased the fresh/hay yield of forages compared to cutting treatments. A possible reason for higher yield could be higher nutrient use efficiency of plants in the grazing plot compared with cutting treatments, which promotes the restoration of grassland productivity (Deléglise et al., 2015). In addition, animal manure can provide higher nutrients for grazing grassland compared with cutting management, which could be another possible reason for higher forage yields (De Boeck et al., 2010). Wilson et al. (2011) reported that pasture is frequently used under grazing management usually reduces the annual dry matter yield of pasture, but increases the crude protein content of pasture compared with cutting treatment. The results of this experiment showed that the crude protein content and yield of grazing forages were significantly higher than those of conventional cutting. This is because grazing keeps plants in the active growth and tillering stage rather than achieving the natural maturity, improving the nutritional value of forage (Bruinenberg et al., 2002).

Grazing can not only increase grassland productivity and improve forage quality but also increase the WUE of grassland (Fenetahun et al., 2020). Peng et al. (2007) found that the WUE of *Cleistogenes squarrosa*, *Agropyron cristatum*, and *Potentilla acaulis* reached the highest value under moderate grazing intensity. Our experiment results are similar to the above research, grazing significantly improves the WUE and precipitation use efficiency of forages compared with cutting treatments. This is because the trampling of livestock may increase the compaction and sealing of the soil, thereby affecting infiltration, leading to the concentration of forage roots in the surface soil, thus increasing the absorption and utilization of moisture by plant roots (Sone et al., 2020). Our research results showed that grazing significantly increased the hay yield of mixed grassland compared with cutting, but there was no significant increase in soil evapotranspiration, thus increasing the WUE of mixed grassland. The results of Zhang et al. (2020) showed that the ammonia produced by fresh chicken manure under aerobic conditions was significantly lower than that under anaerobic conditions (Schmidt et al., 2002), therefore, adding chicken grazing to rice fields significantly increased the total nitrogen content and nitrogen uptake during rice growth. The results of this experiment were similar to those of the previous study as the nitrogen content, nitrogen uptake, NUE, and AEN under the two-year grazing treatment were significantly higher than those under the conventional cutting treatment. The possible reason for these results might be the increase in soil nitrogen availability under grazing mainly through two pathways. Firstly, animal urine and feces under grazing are converted into nitrogen, so plants can more readily absorb it (Frank, 2020). Furthermore, grazing increase the labile organic compounds, stimulating microbial activity and enhancing the rate of nitrogen mineralization, and hence, inorganic nitrogen availability in the rhizosphere (Hamilton et al., 2008).

4.3 Effects of nitrogen application on forage yield, quality, and water use

China is among the countries with high nitrogen fertilizer usage in the world, with the average annual nitrogen fertilizer application accounting for about 30% of global nitrogen fertilizer usage (Li et al., 2003). Undeniably, nitrogen application is essential for improving the yield and quality of different crops (Varga et al., 2007; Izsaki, 2007; Kamran et al., 2022; Kamran et al., 2023). According to Ayub et al. (2009), the highest fresh yield (67.14 t ha^{-1}) and hay yield (19.83 t ha^{-1}) were achieved with the nitrogen application rate of 180 kg ha^{-1}. Leto et al. (2008) reported that the application of 150 kg ha^{-1} nitrogen fertilizer can increase the total hay yield of forage by 9% compared with no nitrogen application. In agreement, our results indicated that 160 kg ha^{-1} nitrogen application significantly increased the fresh and hay yield of forage compared with control (no N) and 80 kg ha^{-1} nitrogen application. Szeman (2007) also found that increasing the application of nitrogen fertilizer on the grassland reduced the number and diversity of species on the grassland, but increased the forage feed value and yield of forage. However, nitrogen application shows a threshold effect in regulating crop growth and yield, i.e., excessive nitrogen application may not be conducive to the improvement of crop growth and yield (Mon et al., 2016; Kamran et al., 2023). In this experiment, the maximum nitrogen application rate (160 kg ha^{-1}) may not exceed the threshold, thus as the nitrogen application rate increased, the fresh hay yield of the pasture consistently increased.

The results of Rostamza et al. (2011) also showed that nitrogen application can significantly increase the crude protein content of forages. This is because the increase in nitrogen application improves plants' nitrogen absorption, thereby increasing the crude protein content. Our results also depicted higher crude protein content under the nitrogen treatment than that of no nitrogen application. We also found that nitrogen application significantly reduced acid and neutral detergent fiber content compared with no nitrogen application, and improved the relative feed value. This is because the increased application of nitrogen fertilizer promotes the increase of soluble substances such as protein, which accumulates in the plant cell body and leads to the dilution of the cell wall, reducing the acid detergent fiber content (Peyraud and Astigarraga, 1998). In the early autumn period, when nitrogen was applied to the grassland, the crude protein content of the forage is greater by about 20%. The combination of higher crude protein content and lower neutral detergent fiber content can further improve the nutritional quality of the forage (Méndez et al., 2019; Kamran et al., 2022). Tomić et al. (2011) found that fertilization significantly increased the crude protein yield of monoculture and mixed grassland by 194.1 and 323.2 kg ha^{-1} respectively when compared with no fertilization. Our research results are similar to Tomić et al. (2011), indicating that nitrogen application significantly increased the crude protein yield of

forage compared with no nitrogen application, and the crude protein yield of forage under 160 kg ha^{-1} nitrogen application was significantly higher than that of 80 kg ha^{-1} nitrogen treatment. This may be because increased nitrogen application increased the hay yield (Figure 4) and crude protein content of the forage. The results of Cohen et al. (2004) also showed that the crude protein content increased with the increase of nitrogen level, which may be caused by the increase in amino acid and protein synthesis.

Several studies have reported that nitrogen application can increase the water use efficiency of cultivated grassland (Gu et al., 2017). Mariotti et al. (2015) showed that the WUE of the high-fertilizer treatment was significantly higher than that of the low-fertilizer treatment under the same grassland type. Our results are similar to the above research. The application of 160 kg ha^{-1} nitrogen significantly increased the precipitation use efficiency and WUE of forage compared with the application of 80 kg ha^{-1} nitrogen and control treatments. Because fertilization can improve water and nutrients uptake by plants, thereby maximizing the forage yield (Wang C. et al., 2018). In addition, nitrogen application improves plant growth and canopy structure, decreases direct solar radiation to the ground, reduces soil evapotranspiration (ET), and thereby increases the WUE of forage (Gu et al., 2016).

Previously, Xie et al. (2015) found that nitrogen fertilization significantly increased the nitrogen content of brome in monoculture and mixed grasslands compared with no nitrogen application. Consistently, our results showed that under the same grassland type, nitrogen application of 160 kg ha^{-1} significantly increased the nitrogen content of forage compared with no nitrogen application in both years. This may be because the nitrogen use status of forages is affected by both water and nitrogen (Soon et al., 2008). Silva et al. (2021) showed that the NUE of *Tithonia diversifolia* was the highest when nitrogen application was 100kg ha^{-1}. This study showed that NUE and AEN were significantly higher with nitrogen application of 160 kg ha^{-1} than without nitrogen application and with nitrogen application of 80 kg ha^{-1}. This may be due to competitive, complementary, or facilitative interactions in Grass-Legume mixed grasslands that increase the NUE of forages (Jensen et al., 2020). However, Lv et al. (2011) studied the effects of 0, 120, 240, 360, 360, 480, 600, and 720 kg ha^{-1} 7 nitrogen levels on maize and found that when the nitrogen application was higher than 360 kg ha^{-1}, the agronomic efficiency, absorption and utilization rate of nitrogen fertilizer were decreased significantly. Our results differ from those reported by Lv et al. (2011). Possibly, the maximum nitrogen application (160 kg·ha^{-1}) rate used in our experiment might not exceed the threshold value, and hence, the NUE of pasture showed an increase with the increase of nitrogen application rates.

5 Conclusion

During the two years, monoculture alfalfa and the alfalfa and brome mixed cropping resulted in insignificantly higher fresh hay yield, crude protein yield, WUE, PUE, NUE, AEN, crude protein, ether extract, and crude ash content, reduced NDF content and increase RFV compared with the monoculture of brome. The fresh hay yield, crude protein yield, WUE, PUE, NUE, and AEN of 160 kg ha^{-1} nitrogen application was significantly higher than that of no nitrogen application and 80 kg ha^{-1} nitrogen application. The application of 160 kg ha^{-1} nitrogen significantly increased the crude protein, ether extract, crude ash content, and RFV, and reduced the NDF and ADF content compared with no nitrogen application. In addition, the fresh hay yield, crude protein yield, WUE, PUE, NUE, and AEN under the grazing treatment were significantly higher than those under the conventional cutting treatment. Therefore, the mixed cropping of alfalfa and brome and nitrogen application of 160 kg ha^{-1} under grazing conditions can be adopted as an efficient management practice for improving the forage yield, nutritional quality, and water and nitrogen utilization efficiency of cultivated grassland in the Loess Plateau of China. This integrated management model is applicable to the cultivation and utilization of mixed grassland on nutrient-poor land in the Loess Plateau. However, this experiment has only been conducted for two years, Therefore, our research results and conclusions have some limitations and should be verified by long-term experiments in the future.

Data availability statement

The raw data supporting the conclusions of this article will be made available by the authors, without undue reservation.

Author contributions

The paper is co-authored by RX, WS, MK, SC, QJ, FH. All authors have contributed to field measurements and writing of the manuscript. All authors contributed to the article and approved the submitted version.

Funding

This work was supported by the Project of the Second Tibetan Plateau Scientific Expedition and Research Program (2019QZKK0302-02), the National Natural Science Foundation of China (31901389), the Strategic Priority Research Program of Chinese Academy of Sciences (XDA2010010203), the 111 Project (B12002), Scientific research start-up cost of team construction funds of "Double First-Rate" guiding project of Lanzhou University (561119204).

Acknowledgments

We are grateful to Liye Yang and Xiaoming Xiao for their help during the experimental period and thank Elsevier Language Editing Services for the English language editing.

Conflict of interest

The authors declare that the research was conducted in the absence of any commercial or financial relationships that could be construed as a potential conflict of interest.

Publisher's note

All claims expressed in this article are solely those of the authors and do not necessarily represent those of their affiliated organizations, or those of the publisher, the editors and the reviewers. Any product that may be evaluated in this article, or claim that may be made by its manufacturer, is not guaranteed or endorsed by the publisher.

Supplementary material

The Supplementary Material for this article can be found online at: https://www.frontiersin.org/articles/10.3389/fpls.2023.1088849/full#supplementary-material

References

Ajayi, F. T., Babayemi, O. J., and Taiwo, A. A. (2009). Mineral solubility of panicum maximum with four herbaceous forage legume mixtures incubated in the rumen of n' dama steers. *Anim. Sci. J.* 80 (3), 250–257. doi: 10.1111/j.1740-0929.2009.00636.x

Ayub, M., Nadeem, M. A., Tahir, M., Ibrahim, M., and Aslam, M. N. (2009). Effect of nitrogen application and harvesting intervals on forage yield and quality of pearl millet (*Pennisetum americanum* l.). *Pak. J. Life Soc Sci.* 7, 185–189.

Bartolome, J. W., Allen-Diaz, B. H., Barry, S., Ford, L. D., Hammond, M., Hopkinson, P., et al. (2014). Grazing for biodiversity in californian mediterranean grasslands. *Rangelands.* 36 (5), 36–43. doi: 10.2111/Rangelands-D-14-00024.1

Brueck, H., Erdle, K., Gao, Y., Giese, M., Zhao, Y., Peth, S., et al. (2010). Effects of n and water supply on water use-efficiency of a semiarid grassland in inner mongolia. *Plant Soil.* 328 (s1-2), 495–505. doi: 10.1007/s11104-009-0128-5

Bruinenberg, M. H., Valk, H., Korevaar, H., and Struik, P. C. (2002). Factors affecting digestibility of temperate forages from seminatural grasslands: a review. *Grass. Forage. Sci.* 57, 292–301. doi: 10.1046/j.1365-2494.2002.00327.x

Campos, F. P., Nicácio, D. R. O., Sarmento, P., Cruz, M. C. P., Santos, T. M., Faria, A. F. G., et al. (2016). Chemical composition and *in vitro* ruminal digestibility of hand-plucked samples of *Xaraes palisade* grass fertilized with incremental levels of nitrogen. *Anim. Feed. Sci. Technol.* 215, 1–12. doi: 10.1016/j.anifeedsci.2015.12.013

Carpici, E. B. (2017). Determination of forage yield and quality of mixtures of hairy vetch with some cereals (oat, barley and wheat) grown as catch crop. *Legume. Res.* 40, 1088–1092. doi: 10.18805/lr.v0i0.8402

Chen, J., Hou, F., Chen, X., Wan, X., and Millner, J. (2015). Stocking rate and grazing season modify soil respiration on the loess plateau, China. *Rangeland Ecol. Manag.* 68 (1), 48–53. doi: 10.1016/j.rama.2014.12.002

Cohen, R. D. H., Wright, S. B. M., Thomas, L. R., McCaughey, W. P., and Howard, M. D. (2004). Current and residual effects of nitrogen fertilizer applied to grass pasture on production of beef cattle in central Saskatchewan. *Can. J. Anim. Science.* 84, 91–104. doi: 10.4141/A03-050

D'Andrea, E., Trotta, C., Collalti, A., Rezaie, N., Scartazza, A., Battipaglia, G., et al. (2017). Different method to assess water use efficiency in a mediterranean beech forest. In *IUFRO 125th Anniversary congress 2017-Side event Seminar "Water use efficiency under drought" 18 September 2017* Centre Inra Grand Est-Nancy, Champenoux, France

Deak, A., Hall, M. H., and Sanderson, M. (2009). Grazing schedule effect on forage production and nutritive value of diverse forage mixtures. *Agron. J.* 101 (2), 408–414. doi: 10.2134/agronj2007.0365

De Boeck, H. J., Dreesen, F. E., Janssens, I. A., and Nijs, L. (2010). Whole-system responses of experimental plant communities to climate extremes imposed in different seasons. *New Phytol.* 189, 806–817. doi: 10.1111/j.1469-8137.2010.03515.x

Deléglise, C., Meisser, M., Mosimann, E., Spiegelberger, T., Signarbieux, C., Jeangros, B., et al. (2015). Drought-induced shifts in plants traits, yields and nutritive value under realistic grazing and mowing managements in a mountain grassland. agriculture. *Ecosyst. Environ.* 213, 94–104. doi: 10.1016/j.agee.2015.07.020

Delevatti, L. M., Cardoso, A. S., Barbero, R. P., Leite, R. G., and Reis, R. A. (2019). Effect of nitrogen application rate on yield, forage quality, and animal performance in a tropical pasture. *Sci. Rep.* 9 (1). doi: 10.1038/s41598-019-44138-x

Dhakal, M., West, C. P., Villalobos, C., Brown, P., and Green, P. E. (2020). Interseeding alfalfa into native grassland for enhanced yield and water use efficiency. *Agron. J.* 112 (3), 1931–1942. doi: 10.1002/agj2.20147

Fenetahun, Y., Xu, X. W., You, Y., and Wang, Y. D. (2020). Effects of vegetation cover, grazing and season on herbage species composition and biomass: a case study of yabello rangeland, southern Ethiopia. *J. Resour. Ecol.* 11 (02), 159–170. doi: 10.5814/j.issn.1674-764x.2020.02.004

Frank, D. A. (2020). Grazing effects on plant nitrogen use in a temperate grassland. *Rangeland. Ecol. Management.* 73 (4), 482–490. doi: 10.1016/j.rama.2020.03.002

Génard, T., Etienne, P., Diquélou, S., Yvin, J. C., Revellin, C., and Laîné, P. (2017). Rapeseed-legume intercrops: Plant growth and nitrogen balance in early stages of growth and development. *Heliyon* 3 (3), e00261. doi: 10.1016/j.heliyon.2017.e00261

Gou, F., Van, I. M., Wang, G. Y., Van, D. P., and Van, D. W. (2016). Yield and yield components of wheat and maize in wheat-maize intercropping in the Netherlands. *Eur. J. Agronomy.* 76, 17–27. doi: 10.1016/j.eja.2016.01.005

Gu, X. B., Li, Y. N., and Du, Y. D. (2017). Optimized nitrogen fertilizer application improves yield, water and nitrogen use efficiencies of winter rapeseed cultivated under continuous ridges with film mulching. *Ind. Crops Products.* 109, 233–240. doi: 10.1016/j.indcrop.2017.08.036

Gu, X. B., Li, Y. N., Du, Y. D., Zhou, C. M., Yin, M. H., and Yang, D. (2016). Effects of water and nitrogen coupling on nitrogen nutrition index and radiation use efficiency of winter oilseed rape (*Brassica napus* l.). *Trans. Chin. Soc Agric. Mach.* 47, 122–132. doi: 10.6041/j.issn.1000-1298.2016.02.017

Guo, Z. J., Zhang, Y. L., Zhao, J. Y., Shi, Y., and Yu, Z. W. (2014). Nitrogen use by winter wheat and changes in soil nitrate nitrogen levels with supplemental irrigation based on measurement of moisture content in various soil layers. *Field Crops Res.* 164, 117–125. doi: 10.1016/j.fcr.2014.05.016

Hamilton, E. W.III, Frank, D. A., Hinchey, P. M., and Murray, T. R. (2008). Defoliation induces root exudation and triggers positive rhizospheric feedbacks in a temperate grassland. *Soil Biol. Biochem.* 40, 2865–2873. doi: 10.1016/j.soilbio.2008.08.007

Hou, F. J., Nan, Z. B., Xie, Y. Z., Li, X. L., Lin, H. L., and Ren, J. Z. (2008). Integrated crop-livestock production systems in China. *Rangeland. J.* 30 (2), 221–231. doi: 10.1071/RJ08018

Huang, Y. L., Chen, L. D., Fu, B. J., Huang, Z. L., and Gong, J. (2005). The wheat yields and water-use efficiency in the loess plateau: straw mulch and irrigation effects. *Agric. Water Management.* 72 (3), 209–222. doi: 10.1016/j.agwat.2004.09.012

Huntsinger, L., Bartolome, J. W., and D'Antonio, C. M. (2007). "Grazing management on california's Mediterranean grasslands," in *The California grasslands*. Ed. M. R. Stromberg (California: University of California Press), 233–253.

Izsaki, Z. (2007). N and p impact on yield of maize in long-term trial. *Cereal Res. Commun.* 35 (4), 1701–1711. doi: 10.1556/CRC.35.2007.4.16

Jee, M. H. (1995). Official methods of analysis of AOAC international (16th edn); official and standardized methods of analysis (3rd edn). *Trends Food Sci. Technol.* 6 (11), 382–383. doi: 10.1016/S0924-2244(00)89213-4

Jensen, E. S., Carlsson, G., and Hauggaard-Nielsen, H. (2020). Intercropping of grain legumes and cereals improves the use of soil n resources and reduces the requirement for synthetic fertilizer n: A global-scale analysis. *Agron. Sustain. Dev.* 40 (1), 1–9. doi: 10.1007/s13593-020-0607-x

Kamran, M., Yan, Z., Chang, S., Ning, J., Lou, S., Ahmad, I., et al. (2023). Interactive effects of reduced irrigation and nitrogen fertilization on resource use efficiency, forage nutritive quality, yield, and economic benefits of spring wheat in the arid region of Northwest China. *Agric. Water Management.* 275, 108000. doi: 10.1016/j.agwat.2022.108000

Kamran, M., Yan, Z., Jia, Q., Chang, S., Ahmad, I., and Ghani, M. U. (2022). Irrigation and nitrogen fertilization influence on alfalfa yield, nutritive value, and resource use efficiency in an arid environment. *Field Crops Res.* 284, 108587. doi: 10.1016/j.fcr.2022.108587

Komarek, A. M., Bell, L. W., Whish, J., Robertson, M. J., and Bellotti, W. D. (2015). Whole-farm economic, risk and resource-use trade-offs associated with integrating forages into crop–livestock systems in western China. *Agric. Syst.* 133, 63–72. doi: 10.1016/j.agsy.2014.10.008

Lahiri, D., Khalid, S., Sarkar, T., Raychaudhuri, A. K., and Sharma, S. M. (2009). Barley intercropping for efficient symbiotic N2-fixation, soil n acquisiton and use of other nutrients in Europe organic cropping systems. *Field Crops Res.* 113, 64–71. doi: 10.1016/j.fcr.2009.04.009

Leto, J., Knežević, M., Bošnjak, K., Vranić, M., and Gunjača, J. (2008). Changes in grassland yield and botanical composition under contrasting managements. *Cereal Res. Commun.* 36, 867–870. doi: 10.1556/CRC.36.2008.Suppl.B.63

Li, L., Zhang, F., Li, X., Christie, P., Sun, J., Yang, S., et al. (2003). Interspecific facilitation of nutrient uptake by intercropped maize and faba bean. *Nutr. Cycl. Agroecosys.* 65 (1), 61–71. doi: 10.1023/A:1021885032241

Li, C. J., Li, Y. Y., Yu, C. B., Sun, J. H., Christie, P., An, M., et al. (2011). Crop nitrogen use and soil mineral nitrogen accumulation under different crop combinations and patterns of strip intercropping in northwest China. *Plant Soil.* 342 (1-2), 221–231. doi: 10.1007/s11104-010-0686-6

Lv, P., Zhang, J. W., Liu, W., Yang, J., Su, K., Liu, P., et al. (2011). Effects of nitrogen application on yield and nitrogen use efficiency of summer maize under super - high yielding conditions. *Plant Nutr. Fertilizer. Sci.* 17 (4), 852–860. doi: 10.1007/s11104-010-0686-6

Mariotti, M., Masoni, A., Ercoli, L., and Arduini, I. (2015). Nitrogen leaching and residual effect of barley/field bean intercropping. *Plant. Soil Environ.* 61 (2), 60–65. doi: 10.17221/832/2014-PSE

Mbatha, K. R., and Ward, D. (2010). The effects of grazing, fire, nitrogen and water availability on nutritional quality of grass in semi-arid savanna, south Africa. *J. Arid. Environ.* 74 (10), 1294–1301. doi: 10.1016/j.jaridenv.2010.06.004

Mckenzie, F. R., Jacobs, J. L., and Ward, G. N. (2006). Irrigated dairy pasture yield and water use efficiency responses to summer applied nitrogen. *In. Proc. New Z. Grassland. Assoc.* 68, 161–164. doi: 10.33584/jnzg.2006.68.2653

Méndez, R., Fernández, J. A., and Yáñez, E. A. (2019). Efecto de la fertilización nitrogenada sobre la producción y composición de cynodon plectostachyus. *Rev. veterinaria.* 30 (1), 48–53.

Mon, J., Bronson, K. F., Hunsaker, D. J., Thorp, K. R., White, J. W., and French, A. N. (2016). Interactive effects of nitrogen fertilization and irrigation on grain yield, canopy temperature, and nitrogen use efficiency in overhead sprinkler-irrigated durum wheat. *Field Crops Res.* 191, 54–65. doi: 10.1016/j.fcr.2016.02.011

Müller, K., Dickhoefer, U., Lin, L., Glindemann, T., Wang, C., Schönbach, P., et al. (2014). Impact of grazing intensity on herbage quality, feed intake and live weight gain of sheep grazing on the steppe of inner Mongolia. *J. Agric. Science.* 152 (1), 153–165. doi: 10.1017/S0021859613000221

Van Soest, P. J. (1994). *Nutritional Ecology of the Ruminant*. Cornell University Press

Van Soest, P. V., Robertson, J. B., and Lewis, B. A. (1991). Methods for dietary fiber, neutral detergent fiber, and nonstarch polysaccharides in relation to animal nutrition. *J. dairy. science.* 74 (10), 3583–3597. doi: 10.3168/jds.S0022-0302(91)78551-2

Nyfeler, D., Huguenin-Elie, O., Suter, M., Frossard, E., and Lüscher, A. (2011). Grass-legume mixtures can yield more nitrogen than legume pure stands due to mutual stimulation of nitrogen uptake from symbiotic and non-symbiotic sources. *Agricult. Ecosyst. Environ.* 140, 155–163. doi: 10.1016/j.agee.2010.11.022

Patton, B. D., Dong, X., Nyren, P. E., and Nyren, A. (2007). Effects of grazing intensity, precipitation, and temperature on forage production. *Rangeland. Ecol. Management.* 60 (6), 656–665. doi: 10.2111/07-008R2.1

Peng, Y., Jiang, G. M., Liu, X. H., Niu, S. L., Liu, M. Z., and Biswas, D. K. (2007). Photosynthesis, transpiration and water use efficiency of four plant species with grazing intensities in hunshandak sandland, China. *J. Arid. Environ.* 70 (2), 304–315. doi: 10.1016/j.jaridenv.2007.01.002

Peyraud, J., and Astigarraga, L. (1998). Review of the effect of nitrogen fertilization on the chemical composition, intake, digestion and nutritive value of fresh herbage: Consequences on animal nutrition and n balance. anim. *Feed. Sci. Technol.* 72, 235–259. doi: 10.1016/S0377-8401(97)00191-0

Phelan, P., Moloney, A. P., McGeough, E. J., Humphreys, J., Bertilsson, J., O'Riordan, E. G., et al. (2015). Forage legumes for grazing and conserving in ruminant production systems. *Crit. Rev. Plant Sci.* 34 (1-3), 281–326. doi: 10.1080/07352689.2014.898455

Pykälä, J. (2005). Plant species responses to cattle grazing in mesic semi-natural grassland. *Agric. Ecosyst. Environ.* 108 (2), 109–117. doi: 10.1016/j.agee.2005.01.012

Ren, H. Y., Han, G. D., Schoenbach, P., Gierus, M., and Taube, F. (2016). Forage nutritional characteristics and yield dynamics in a grazed semiarid steppe ecosystem of inner Mongolia. *China. Ecol. Indic.* 60, 460–469. doi: 10.1016/j.ecolind.2015.07.027

Rostamza, M., Chaichi, M. R., Jahansouz, M. R., and Alimadadi, A. (2011). Forage quality, water use and nitrogen utilization efficiencies of pearl millet (*Pennisetum americanum* l.) grown under different soil moisture and nitrogen levels. *Agric. Water Management.* 98 (10), 1607–1614. doi: 10.1016/j.agwat.2011.05.014

Sanderson, M. A., Soder, K. J., Muller, L. D., Klement, K. D., Skinner, R. H., and Goslee, S. C. (2005). Forage mixture productivity and botanical composition in pastures grazed by dairy cattle. *Agron. J.* 97 (5), 1465–1471. doi: 10.2134/agronj2005.0032

Schmidt, I., Sliekers, O., Schmid, M., Cirpus, I., Strous, M., Bock, E., et al. (2002). Aerobic and anaerobic ammonia oxidizing bacteria – competitors or natural partners? FEMS microbiol. *Ecol.* 39 (3), 175–181. doi: 10.1111/j.1574-6941.2002.tb00920.x

Schönbach, P., Wan, H., Gierus, M., Loges, R., Müller, K., Lin, L., et al. (2012a). Effects of grazing and precipitation on herbage production, herbage nutritive value and animal performance in continental steppe. *Grass. Forage. Science.* 67 (4), 535–545. doi: 10.1111/j.1365-2494.2012.00874.x

Schönbach, P., Wan, H., Schiborra, A., Gierus, M., Bai, Y., Müller, K., et al. (2009). Short-term management and stocking rate effects of grazing sheep on herbage quality and productivity of inner Mongolia steppe. *Crop Pasture Science.* 60 (10), 963–974. doi: 10.1071/CP09048

Silva, A. M., Santos, M. V., Silva, L. D., Santos, J. B., Ferreira, E. A., and Santos, L. D. T. (2021). Effects of irrigation and nitrogen fertilization rates on yield, agronomic efficiency and morphophysiology in tithonia diversifolia. *Agric. Water Management.* 248, 106782. doi: 10.1016/j.agwat.2021.106782

Sone, J. S., Oliveira, P. T. S., Euclides, V. P. B., Montagner, D. B., de Araujo, A. R., Zamboni, P. A. P., et al. (2020). Effects of nitrogen fertilisation and stocking rates on soil erosion and water infiltration in a Brazilian cerrado farm. *Agricult. Ecosyst. Environ.* 304, 107–159. doi: 10.1016/j.agee.2020.107159

Soon, Y. K., Malhi, S. S., Wang, Z. H., Brandt, S., and Schoenau, J. J. (2008). Effect of seasonal rainfall, n fertilizer and tillage on n utilization by dryland wheat in a semi-arid environment. *Nutrient. Cycling. Agroecosyst.* 82 (2), 149–160. doi: 10.1007/s10705-008-9176-0

Sparovek, G., Berndes, G., Klug, I. L. F., and Barretto, A. G. O. P. (2010). Brazilian Agriculture and environmental legislation: Status and future challenges. *Environ. Sci. Technol.* 44 (16), 6046–6053. doi: 10.1021/es1007824

Spera, S. (2017). Agricultural intensification can preserve the Brazilian cerrado: Applying lessons from mato grosso and goiás to brazil's last agricultural frontier. *Trop. Conserv. Sci.* 10, 1940082917720662. doi: 10.1177/1940082917720662

Szeman, L. (2007). Environmental consequences of sustainability on grasslands. *Cereal Res. Commun.* 35 (2), 1157–1160. doi: 10.1556/CRC.35.2007.2.248

Tekeli, S. A., and Ates, E. (2005). Yield potential and mineral composition of white clover (*Trifolium repens* l.) and tall fescue (*Festuca arundinacea* schreb.) mixtures. *J. Cent. Eur. Agricult.* 6 (1), 27–34. doi: 10.5513/jcea.v6i1.243

Tomić, Z., Bijelić, Z., Žujović, M., Simić, A., Kresović, M., Mandić, V., et al. (2011). Dry matter and protein yield of lucerne, cocksfoot, meadow fescue, perennial ryegrass and their mixtures under the influence of various doses of nitrogen fertilizer. *Biotechnol. Anim. Husbandry.* 27 (1), 1219–1226. doi: 10.2298/BAH1103219T

Tomić, Z., Bijelić, Z., Žujović, M., Simić, A., Kresović, M., Mandić, V., et al. (2012). The effect of nitrogen fertilization on quality and yield of grass-legume mixtures. grassland-a European resource? *Gen. Meeting Eur. Grassland. Federation.* 17, 187–189.

Varga, B., Svečnjak, Z., Jurković, Z., and Pospišil, M. (2007). Quality responses of winter wheat cultivars to nitrogen and fungicide applications in Croatia. *Acta Agronomica Hungarica.* 55 (1), 37–48. doi: 10.1556/AAgr.55.2007.1.5

Wang, H., Wu, L., Cheng, M., Fan, J., Zhang, F., Zou, Y., et al. (2018). Coupling effects of water and fertilizer on yield, water and fertilizer use efficiency of drip-fertigated cotton in northern xinjiang, China. *Field Crops Res.* 219, 169–179. doi: 10.1016/j.fcr.2018.02.002

Wang, C., Wu, S., Tankari, M., Zhang, X., Li, L., Gong, D., et al. (2018). Stomatal aperture rather than nitrogen nutrition determined water use efficiency of tomato plants under nitrogen fertigation. *Agric. Water Manage.* 209, 94–101. doi: 10.1016/j.agwat.2018.07.020

Wang, B., Yang, Q., and Liu, Z. (2009). Effect of conversion of farmland to forest or grassland on soil erosion intensity changes in yanhe river basin, loess plateau of China. *Front. For. China.* 4 (1), 68–74. doi: 10.1007/s11461-009-0015-5

Wang, G. H., and Zhang, X. S. (2003). Supporting of potential forage production to the herbivore-based pastoral farming industry on the loess plateau. *Plant J.* 45 (10), 1186–1194.

Wang, H., Zhang, Y., Chen, A., Liu, H., Zhai, L., Lei, B., et al. (2017). An optimal regional nitrogen application threshold for wheat in the north China plain considering yield and environmental effects. *Field Crops Res.* 207, 52–61. doi: 10.1016/j.fcr.2017.03.002

Wang, Z. K., Zhao, X. N., Wu, P. T., and Chen, X. L. (2015). Effects of water limitation on yield advantage and water use in wheat (Triticum aestivum l.)/maize (Zea mays l.) strip intercropping. *Eur. J. Agronomy.* 71, 149–159. doi: 10.1016/j.eja.2015.09.007

Wilson, R. L., Jensen, K. S., Etter, S. J., and Ahola, J. K. (2011). Variation in nutritive quality and mineral content of grazed and clipped forage from native range in southwest Idaho. *Prof. Anim. Scientist.* 27 (5), 435–448. doi: 10.15232/S1080-7446(15)30516-7

Wu, Y., Jia, Z., Ren, X., Zhang, Y., Chen, X., Bing, H., et al. (2015). Effects of ridge and furrow rainwater harvesting system combined with irrigation on improving water use efficiency of maize (Zea mays l.) in semi-humid area of China. *Agric. Water management.* 158, 1–9. doi: 10.1016/j.agwat.2015.03.021

Xie, K., Li, X., Feng, H., Zhang, Y., Wan, L., David, B., et al. (2015). Effect of nitrogen fertilization on yield, n content, and nitrogen fixation of alfalfa and smooth bromegrass grown alone or in mixture in greenhouse pots. *J. Integr. Agricult.* 14 (9), 1864–1876. doi: 10.1016/S2095-3119(15)61150-9

Xiong, H. C., Shen, H. Y., Zhang, L. X., Zhang, Y. X., Guo, X. T., Wang, P. F., et al. (2013). Comparative proteomic analyses for assessment of the ecological significance of maize and peanut intercropping. *J. Proteomics.* 78, 447–460. doi: 10.1016/j.jprot.2012.10.013

Yang, K., and Lu, C. (2018). Evaluation of land-use change effects on runoff and soil erosion of a hilly basin–the yanhe river in the Chinese loess plateau. *Land. Degradation. Dev.* 29 (4), 1211–1221. doi: 10.1002/ldr.2873

Yu, H., Li, Y., Oshunsanya, S. O., Are, K. S., Geng, Y., Saggar, S., et al. (2019). Re-introduction of light grazing reduces soil erosion and soil respiration in a converted grassland on the loess plateau, China. *Agricult. Ecosyst. Environ.* 280, 43–52. doi: 10.1016/j.agee.2019.04.020

Zhang, Q. P., Bell, L. W., Shen, Y. Y., and Whish, J. P. M. (2018). Indices of forage nutritional yield and water use efficiency amongst spring-sown annual forage crops in north-west China. *Eur. J. Agronomy.* 93 (1), 1–10. doi: 10.1016/j.eja.2017.11.003

Zhang, L., Zhou, L., Wei, J., Xu, H., Tang, Q., and Tang, J. (2020). Integrating cover crops with chicken grazing to improve soil nitrogen in rice fields and increase economic output. *Sci. Total. Environ.* 713, 135218. doi: 10.1016/j.scitotenv.2019.135218

Zhao, H., Wang, R. Y., Ma, B. L., Xiong, Y. C., Qiang, S. C., Wang, C. L., et al. (2014). Ridge-furrow with full plastic film mulching improves water use efficiency and tuber yields of potato in a semiarid rain-fed ecosystem. *Field Crops Res.* 161, 137–148. doi: 10.1016/j.fcr.2014.02.013

Zheng, S., Lan, Z., Li, W., Shao, R., Shan, Y., Wan, H., et al. (2011). Differential responses of plant functional trait to grazing between two contrasting dominant C3 and C4 species in a typical steppe of inner Mongolia, China. *Plant Soil.* 340 (1), 141–155. doi: 10.1007/s11104-010-0369-3

Zhou, P., Wen, A. B., Zhang, X. B., and He, X. B. (2013). Soil conservation and sustainable eco-environment in the loess plateau of China. *Environ. Earth Sci.* 68 (3), 633–639. doi: 10.1007/s12665-012-1766-0

frontiers | Frontiers in Plant Science

TYPE Original Research
PUBLISHED 11 April 2023
DOI 10.3389/fpls.2023.1120826

OPEN ACCESS

EDITED BY
Cesar Arrese-Igor,
Public University of Navarre, Spain

REVIEWED BY
Liming Ye,
Ghent University, Belgium
Robert C. Abaidoo,
Kwame Nkrumah University of Science and Technology, Ghana

*CORRESPONDENCE
Martin Jemo
Martin.Jemo@um6p.ma

SPECIALTY SECTION
This article was submitted to Plant Symbiotic Interactions, a section of the journal Frontiers in Plant Science

RECEIVED 10 December 2022
ACCEPTED 13 March 2023
PUBLISHED 11 April 2023

CITATION
Jemo M, Devkota KP, Epule TE, Chfadi T, Moutiq R, Hafidi M, Silatsa FBT and Jibrin JM (2023) Exploring the potential of mapped soil properties, rhizobium inoculation, and phosphorus supplementation for predicting soybean yield in the savanna areas of Nigeria. *Front. Plant Sci.* 14:1120826. doi: 10.3389/fpls.2023.1120826

Exploring the potential of mapped soil properties, rhizobium inoculation, and phosphorus supplementation for predicting soybean yield in the savanna areas of Nigeria

Martin Jemo[1]*, Krishna Prasad Devkota[2], Terence Epule Epule[3], Tarik Chfadi[3], Rkia Moutiq[4], Mohamed Hafidi[1,5], Francis B. T. Silatsa[6] and Jibrin Mohamed Jibrin[7]

[1]AgroBiosciences Program, College for Sustainable Agriculture and Environmental Sciences, Mohammed VI Polytechnic University (UM6P), Bengeurir, Morocco, [2]Soil, Water, and Agronomy (SWA) Program, International Center for Agricultural Research in the Dry Areas (ICARDA), Rabat-institute, Rabat, Morocco, [3]International Water Research Institute (IWRI), College for Sustainable Agriculture and Environmental Sciences, Mohammed VI Polytechnic University (UM6P), Bengeurir, Morocco, [4]National Institute of Agronomical Research (INRA), Regional Center of Kenitra, Kenitra, Morocco, [5]Cadi Ayad University, Laboratory of Microbial Biotechnologies, Agrosciences and Environment, Faculty of Science Semlalia, Marrakesh, Morocco, [6]Center of Excellence for Soil and Fertilizer Research in Africa (CESFRA), College for Sustainable Agriculture and Environmental Sciences, Mohammed VI Polytechnic University (UM6P), Benguerir, Morocco, [7]Centre for Dryland Agriculture, Bayero University, Kano, Nigeria

Rapid and accurate soybean yield prediction at an on-farm scale is important for ensuring sustainable yield increases and contributing to food security maintenance in Nigeria. We used multiple approaches to assess the benefits of rhizobium (Rh) inoculation and phosphorus (P) fertilization on soybean yield increase and profitability from large-scale conducted trials in the savanna areas of Nigeria [i.e., the Sudan Savanna (SS), Northern Guinea Savanna (NGS), and Southern Guinea Savanna (SGS)]. Soybean yield results from the established trials managed by farmers with four treatments (i.e., the control without inoculation and P fertilizer, Rh inoculation, P fertilizer, and Rh + P combination treatments) were predicted using mapped soil properties and weather variables in ensemble machine-learning techniques, specifically the conditional inference regression random forest (RF) model. Using the IMPACT model, scenario analyses were employed to simulate long-term adoption impacts on national soybean trade and currency. Our study found that yields of the Rh + P combination were consistently higher than the control in the three agroecological zones. Average yield increases were 128%, 111%, and 162% higher in the Rh + P combination compared to the control treatment in the SS, NGS, and SGS agroecological zones, respectively. The NGS agroecological zone showed a higher yield than SS and SGS. The highest training coefficient of determination (R^2 = 0.75) for yield prediction was from the NGS dataset, and the lowest coefficient (R^2 = 0.46) was from the SS samples. The results from the IMPACT model showed a reduction of

10% and 22% for the low (35% adoption scenario) and high (75% adoption scenario) soybean imports from 2029 in Nigeria, respectively. A significant reduction in soybean imports is feasible if the Rh + P inputs are large-scaled implemented at the on-farm field and massively adopted by farmers in Nigeria.

KEYWORDS

bradyrhizobium inoculation, foresight IMPACT model, Nigeria savanna agroecologies, participatory on-farm experiment, random forest model

1 Introduction

Soybean [*Glycine max* (L.) Merr.] is an important component in smallholder cropping systems due to its rich source of edible proteins, amino acids, and micronutrients, which are indispensable to addressing food insecurity and quality problems (Chigeza et al., 2019; Siamabele, 2021; Alabi et al., 2022). In Africa, soybeans are grown over more than 2.5 million hectares, and Nigeria is the second-largest producer after South Africa (FAOSTAT, 2022). Its cultivation confers several environmental benefits, such as biological nitrogen fixation (BNF) that converts atmospheric nitrogen gas (N_2) into soil nitrogen (N) for plant uptake (Thilakarathna and Raizada, 2018; Herridge et al., 2022; Ladha et al., 2022). This process contributes to alleviating N deficiencies and improving soil health, soil fertility, and crop productivity (Grönemeyer and Reinhold-Hurek, 2018). In Africa, the promotion of BNF can significantly increase soybean yield, where it is the lowest (only 1.2 t ha^{-1}) as compared to the world average (2.8 t ha^{-1}), the Americas (3.2 t ha^{-1}), Europe (2.0 t ha^{-1}), and Asia (1.4 t ha^{-1}) (FAOSTAT, 2022).

Seed inoculation with *Bradyrhizobium japonicum* elite strain is a proven strategy to improve soybean yield (Hungria et al., 2017). However, higher biological N fixation and yield response are reported when the legume plants are fertilized with a moderate phosphorus (P) rate, particularly in many soils and climatic conditions in Africa where available P in the soil is low (Jemo et al., 2010). The use of an appropriate strain of Rh inoculant and P fertilization practices to improve BNF legume production has been the subject of numerous studies in Sub-Saharan Africa (Ronner et al., 2016; Ulzen et al., 2018; van Heerwaarden et al., 2018; Buenor et al., 2022). Those studies have reported yield increases ranging from 452 to 815 kg ha^{-1} and a net economic benefit of about 400 USD ha^{-1} through the combined application of Rh inoculants and P fertilizer. Despite the above-mentioned advantages from the combined application of Rh inoculants and P supplementation to soybeans, there are obstacles to achieving higher yields due to the divergent impacts of many abiotic and biotic factors like drought, nutrient availability, and crop genotypes (Alves et al., 2003; Jemo et al., 2006; Ulzen et al., 2018; Khaki et al., 2020).

In Africa, the import of soybean products has witnessed an exponential increase, with more than 14 million USD spent on soybean imports in 2020 alone for Nigeria (FAOSTAT, 2022). As a consequence, the country is highly dependent on international soybean trade, which places pressure on household resources and negatively impacts food security and nutrition. Therefore, it is imperative to increase the yield of the crop per hectare of land to meet national and regional food demands with minimal environmental damage (Helfenstein et al., 2020). Yield prediction is complex, but accurate prediction provides timely import and export decisions to policymakers and provides year-to-year management and financial decisions to farmers (Smidt et al., 2016; Khaki and Wang, 2019). Yield prediction of crops, including soybeans, has been the subject of studies, but the prediction results, in general, are often challenging due to the interactions among numerous complex factors such as crop genetics, weather, soil input and crop management, and socio-economic conditions (Smidt et al., 2016; Khaki et al., 2020; Alabi et al., 2022; Bebeley et al., 2022). When using soil properties to predict soybean yield, soil available P, organic matter, soil available water supply in the upper 100 cm, and soil K were the major yield determinants (Smidt et al., 2016). In sub-Saharan Africa, using multispectral high-resolution unmanned aerial vehicles, Alabi et al. (2022) estimated soybean grain yield in on-station trials, focusing on varietal evaluation approaches and rapid high throughput phenotypic workflows. Another recent modeling study evaluated the CROPGRO–soybean model for assessing optimum sowing windows of soybean in the Nigeria Savannas and found that sowing dates between 15 June and 5 July accurately predicted the yields of genotypes TGX1951–3F and TGX1835–10E (Bebeley et al., 2022). However, limited studies have accounted for integrated soil properties, weather, and crop management practices for soybean yield prediction across Nigerian agroecology. Public availability of prediction datasets, the associated high costs, time consumption for analyses, and the sample size curtail acute prediction in such studies (Hengl et al., 2021; Wang et al., 2022). Thanks to a recent Soil Information System for Africa (iSDAsoil) mapped at 30 m resolution that is now making it possible to integrate them into models for predictions of African crops. The iSDAsoil platform provides detailed pan-african soil macro and mincronutrients maps at fine spatial resolutions (Hengl et al., 2021). However, for crops like soybeans, an important food security crop that has rapidly expanded in Africa, yield prediction is yet to be implemented.

Ensemble learning, which is a combination of several machine learning models, has made it feasible to combine several factors for predicting yields with robust results. Various techniques of

ensemble learning, such as regression, decision trees, association rule mining, artificial neural networks, and random forest (RF) models, provide results by combining several base models and datasets. Multivariate regression and random forest machine learning approaches have been recently applied to crop yield prediction (Khaki and Wang, 2019; Khaki et al., 2020). A salient feature of machine learning models is the holistic assessment of the input variables, which are often non-linear and complex functions of the output variable, such as crop yield (Khaki and Wang, 2019; Khaki et al., 2020). Machine learning techniques such as RF regression have been previously used to quantify the predictors of importance to outputs and identify the optimal input ranges as an entry point for closing the yield gap sustainably (Breiman, 2001; Devkota et al., 2021).

Furthermore, global food security is challenged by rapid changes in population, income, and climate change. Achieving and maintaining these threats and designing possible solutions requires a robust multidisciplinary approach (Robinson et al., 2015; Islam et al., 2016). The International Model for Policy of Agricultural Commodities Trade (IMPACT) model was developed by the International Food Policy Research Institute (IFPRI) links economic, water, and crop modules to simulate domestic and international agricultural markets and support needs under changing biophysical and socio-economic conditions and provides in-depth analysis and decision-making support to policymakers (Mason-D'Croz et al., 2016).

The adoption of Rh + P fertilizer technology can sustainably increase soybean yield per hectare at the national and regional scales, aid in reducing dependency on the international market for soybean products and contribute to food security maintenance. Therefore, the objectives of the present study were to: (a) examine the soybean yield variation as affected by Rh + P application across three agroecological zones of northern Nigeria; (b) predict soybean yield change using digitalized soil properties data and machine learning techniques; and (c) explore the scenarios of adoption of the combination Rh + P impacts on soybeans, reducing imports by 2050.

2 Materials and methods

2.1 Experimental site

On-farm demonstration trials were conducted for two years (2012–2013) in three agroecological zones of northern Nigeria (9° 05' to 11° 54' N and from 6° 38' to 8° 17' E), particularly covering the Sudan Savanna (SS), northern Guinea Savanna (NGS), and southern Guinea Savanna (SGS) regions (Figure 1). Long-term rainfall ranges from 600 to 1,000 mm (mean of 744.5 mm) in the SS, from 1,000 to 1,300 mm (mean of 1,179 mm) in the NGS, and from 1,100 to 1,400 mm (mean of 1,270 m) in the SGS (Ishaku and Majid, 2010; Umar and Bako, 2019). The extracted cumulative precipitation, average minimum, and maximum temperature are reported in Table 1.

2.2 Experimental design, treatments, and crop management practices

A total of 350 on-farm demonstration experiments were conducted across three agroecological zones in Nigeria. Those on-farm experiments were conducted using a randomized complete block design (RCBD), considering each farmer's field as a replicate. Each plot measured 6 × 4 m^2, and 350 experimental fields were established in the three agroecological zones. The seeds of a soybean variety were hand-drilled at 2 cm depth at 0.75 m between rows and 0.05 m within rows, recovered with soil, and thinned to 5 cm distance between plants after 15 days to maintain a uniform population density of 266,667 plants per hectare. Four treatments (Trt) were evaluated: Trt 1: Control (farmer practice) without

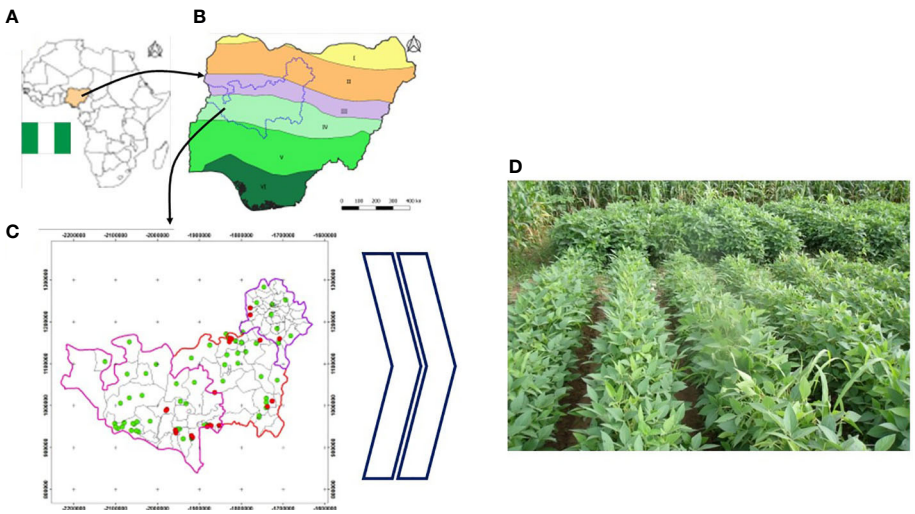

FIGURE 1
Map of Africa **(A)** and the different agroecological zones in Nigeria **(B)**, on-farm demonstrations areas **(C)**, and different field operations **(D)** field Rhizobia + P fertilizer combination and non-inoculated plots.

TABLE 1 Minimal (min), median, and maximum (max) of cumulative monthly precipitation (mm), average of minimal and maximal temperature, and covered administrative local governments of studies in the Sudan, Northern Guinea, and Southern Guinea Savannas of Nigeria recorded for 2012 and 2013 growing seasons.

Agroecological zones		Cumulative annual precipitation (mm)		Average minimum temperature (°C)[1]		Average maximum temperature (°C)		Covered administrative local governments
		2012	2013	2012	2013	2012	2013	
Sudan Savanna	Min	320.2	358.6	16.6	16.8	35.2	35.6	DANJA, GEZAWA, GWARZO, KARA, KARAYE, KURA, RANO, SOBA, and UNGOGO
	Median	390.3	413.6	18.0	19.5	37.9	37.5	
	Max	420.0	580.1	19.0	20.4	39.1	39.1	
Northern Guinea Savanna	Min	569.6	437.7	16.3	16.3	33.7	34.1	GIWA, IGABI, JEMA'A, KUDAN, Sabon GARI, and Zango KATAF
	Median	659.8	597.4	17.1	16.9	35.5	35.4	
	Max	712.5	754.1	18.0	18.0	35.8	36.1	
Southern Guinea savanna	Min	390.3	580.1	16.6	16.5	32.9	33.5	ABAJI, AGAIE, BOSSO, GURARA, IGABI, KATCHA, MUYA, SHIRORO, SULEJA, TUFA, and WUSHISHI
	Median	1252.1	680.6	18.5	18.0	33.9	33.8	
	Max	1629.5	717.2	19.7	20.7	37.9	35.5	

inoculation and no P application (non-treated); Trt 2: P-fertilizer application at 20 kg P ha^{-1} (P) in the form of triple superphosphate (TSP) (Ronner et al., 2016); Trt 3: Rh inoculation at 5 g kg^{-1} seed; and Trt 4: Combined application of Rh and P. Soybean seeds were treated with a commercial Rh inoculant (legume-fix) containing 10^{10} bacteria cells of *B. japonicum* strain 532c per gram of solid before sowing. The Rh inoculant was coated onto the seeds with gum arabic as a sticker and air-dried for 30 min under shade before sowing. The P fertilizer was applied by hand-broadcast within rows at sowing. The trained extensionists and farmers managed the experimental plots subsequently. Weed management was carried out through regular hand weeding every 30 days at intervals in consultation with the extensionist. Farmer groups and rural community members regularly visited the experimental plots during field days organized at the vegetative growth stage to demonstrate the treatment differences with the support of Village Promoter Agents (VPAs).

2.3 Pre-campaign training of village promoter agents and farmers groups for on-farm experimentation

Village promoter agents (VPAs) were recruited by the area manager staff of the Notore Limited group in Nigeria to monitor the trials. The VPAs were local farmers based in the villages with previous working experience in monitoring demonstration trials, good communication skills in Hausa local language with farmers, and an interest in participatory technology dissemination to rural farmers. Notore Limited is an established private sector company based in Nigeria with a recruited area manager who daily supervises the work of VPAs in the deployed areas. Each VPA received adequate training at the early stages before the on-farm demonstration establishment of trials regarding the handling of rhizobial inoculants, coating seeds, and P applications in the respective areas. Twenty-five (25) VPAs were trained for handling rhizobial inoculants, P fertilizer applications, and general monitoring of the trials. Collaborative farmer groups and community contact persons for participatory research were registered and trained. Identified fields to establish the demonstration trials were delimited, and the geographical coordinates of each field were recorded (Figure 1). Thereafter, farmer groups were subsequently trained to handle rhizobium inoculant for seed coating techniques in the respective locations, ensuring limited risks of cross-contamination. The sowing order was control, P treated, Rh inoculated, and Rh + P fertilizer plots, respectively. Farmers' groups and VPA regularly visited the demonstration plots at various growth stages, from sowing to harvest.

2.4 Soybean varieties and rhizobium inoculant

Three improved soybean varieties of different maturity groups developed by the International Institute of Tropical Agriculture (IITA) in Nigeria and released by the Nigeria National Research System (https://www.seedportal.org.ng) were used for the trials. The varieties were derivatives of a tropical *G. max* (TGx) series of cultivars bred for their promiscuous nodulation in a wide range of environments. The soybean varieties TGx 1987-62F (reg.: NGGM 10-19) and TGx 1987-10F (reg. NGGM 10-18) were released in 2010 and are resistant to Cercospora leaf spot and bacteria pustules. The TGx 1987-62F variety is a medium maturity group (90–110 days to maturity) and was used in demonstration plots in NGS agroecology. This variety had an average grain yield of 2.1 t ha^{-1} in on-station rainfed trials in Nigeria (https://www.seedportal.org.ng). The soybean variety TGx 1987-10F is also highly resistant to

Cercospora leaf spot and bacterial pustules, with a yield range of 1.5–2 t ha^{-1} under rainfed conditions. It is an early maturity variety (90–95 days to maturity) and was used in the experimental plots in the SS agroecology. The third variety, TGx 1448-2E, was released in 1992 and registered in 1996 under the Nigerian national code NGGM-96-15. It has an average grain yield of 2.4 t ha^{-1}, is frog-leaf resistant and belongs to the late maturity group (115–120 days); this variety was used in the SGS agroecology.

2.5 Data acquisition, preparation, and random forest and IMPACT models implementation

2.5.1 Grain yield

The soybean plants were harvested at maturity 90 to 110 days after sowing. Dried plants were harvested from the entire plot (24 m^2). Grains were separated from pods and sun-dried, and the dry weight of the seeds was recorded. The grain yield expressed in kg ha^{-1} was computed using Equation 1 (Eq. 1).

$$Yield\ (kg/ha) = [(Net\ plot\ yield\ (g) / 1,000\ (g) \times ((Area\ (ha)\ 10,000\ (m^2)/Net\ plot\ area\ (m^2) \times ((100 - MC)/88)]$$

where MC is moisture content (%). (Eq. 1) (Awuni et al., 2020).

2.5.1 Soil properties and weather data for predicting yield

Soil properties for each experimental site at 30 m spatial resolution were extracted from the iSDAsoil (https://www.isda-africa.com/isdasoil/) platforms using the "raster," "rgeos," "maptools," "rgdal," "shapefiles," and "PBS mapping" functions of the R packages (R version 4.2.1). The minimum median and maximum values of the extracted soil properties are given in Table 2. Specifically, soil pH, organic carbon (C), and total nitrogen (N), total carbon, effective cation exchange capacity (ECEC), available phosphorus (P), exchangeable potassium (K), exchangeable calcium (Ca), exchangeable magnesium (Mg), sulfur (S), sodium (Na), iron (Fe), zinc (Zn), silt, clay, and sand variables were extracted for each experimental site (Table 2). Monthly precipitation, temperature, and solar radiation for each site during the crop-growing season were extracted from the NASA platform (https://power.larc.nasa.gov/data-access-viewer/).

2.6 Random forest machine learning for yield prediction

A logical framework for the model's implementation, calibration, and training is displayed in Figure 2. A conditional inference regression RF machine learning approach was implemented for predicting yield variability from each

TABLE 2 Maximum (Max), median and minimum (Min) of soil properties from all sampled sites, Sudan, northern Guinea, and southern Guinea Savannas of Nigeria.

	All sites			Sudan Savanna			Northern Guinea Savanna			Southern Guinea Savanna		
	Min	Median	Max	Min	Median	Max	Min	Median	Max	Min	Median	Max
Effective Cation Exchange Capacity [cmol (+) kg^{-1}]	7.4	12.2	16.4	9.0	13.5	16.4	7.4	13.5	14.9	7.4	9.0	16.4
Exchangeable Ca [cmol (+) kg^{-1}]	0.90	3.0	7.3	2.7	2.7	6.02	2.0	4.5	7.3	1.0	3.6	5.4
Fe content (mg kg^{-1})	27.1	33.1	54.6	27.1	27.1	40.4	27.1	32.7	40.4	30.0	3.6	54.6
Exchangeable Mg [cmol (+) kg^{-1}]	0.49	1.0	2.0	0.66	0.99	1.34	0.60	0.90	2.00	0.45	0.98	1.64
Av-Pi content (mg P kg^{-1})	6.0	7.4	10.0	6.0	6.6	10.	6.0	7.4	9.0	6.0	7.4	10.0
Exchangeable K [cmol (+) kg^{-1}]	0.48	0.6	0.74	0.49	0.66	0.74	0.49	0.60	0.74	0.45	0.54	0.67
Su content (mg kg^{-1})	3.7	4.95	6.7	3.7	4.9	6.0	4.1	5.0	5.0	3.7	4.5	6.7
Zn content (mg kg^{-1})	1.5	2.2	4.1	1.5	2.2	2.7	1.5	2.4	3.3	1.5	1.8	4.1
Organic carbon content (g kg^{-1})	4.1	5.5	13.5	4.1	5.5	10.0	4.1	4.9	10.0	4.5	4.9	13.5
Total Nitrogen content (g kg^{-1})	1.3	1.7	2.2	1.4	1.6	2.2	1.3	1.7	2.1	1.4	1.7	2.2
pH (H_2O)	5.1	5.7	6.1	5.5	5.7	6.0	5.3	5.7	6.1	5.1	5.6	5.8
Clay content (%)	16.0	24.0	32.0	18.0	22.6	26.0	16.0	25	30.0	19.0	23	32.0
Silt content (%)	43.0	54.0	67.	45.0	54.0	60.0	43.0	52	67.0	46.0	56	61.0
Sand content (%)	15.0	20.0	26.0	18.0	23.4	24.0	18.0	22.4	26.0	15.0	18	23.0

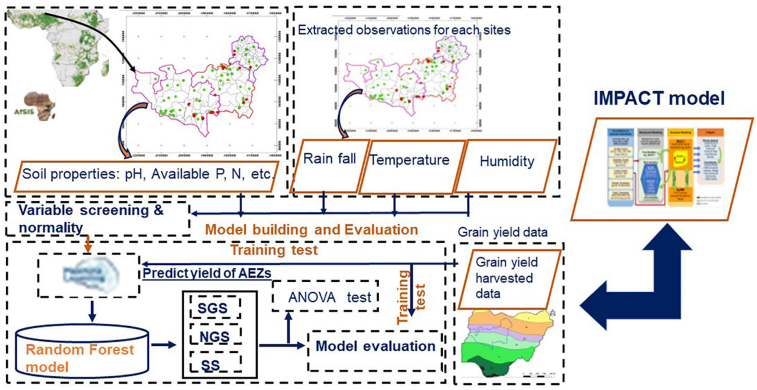

FIGURE 2
Framework of the model implementation approach. ANOVA, Analysis of variance; SGS, southern Guinea Savanna; NGS, northen Guinea Savanna; SS, Sudan Savanna; AEZs, Agroecological zones.

agroecological zone. The conditional RF captures the linear and non-linear effects of the estimator variables (soil, weather, and factor variables) on the yield response and quantifies the marginal effect of individual inputs. The inference regression RF is a powerful non-parametric decision ensemble learning method for regression classification that operates by constructing multiple artificial trees to predict and fit response variables without overfitting during the training process. To assess the model's performance, the root mean square error (RMSE), training coefficient of determination (R^2), and validation RMSE were computed for the datasets of each agroecoregion. The predicted values against the actual and variables of importance for each model were visualized. The normalized RMSE (NRMSE) was calculated using the formula:

$$NRMSE\,(\%) = [RMSE/(y_{max} - y_{min})] \times 100$$

(Eq. 2, Alabi et al., 2022),

where y_{max} and y_{min} are the maximum and minimum yield.

2.6.1 Screening variables of importance for the better prediction

Variables with low importance were discriminated from the principal component analysis check to reduce dimensionality in the number of input variables in the training dataset. A forward selection of explanatory variables for yield was performed, and predicted variables with a *P*-value below<0.05 were retained and included in the training dataset. Twenty-eight estimators from a total of 66 variables aggregated as predictors were retained for yield prediction of datasets from all agroecological zones, whereas 26 estimators were screened for model training for each agroecological zone dataset.

2.6.2 Training, testing, and model fitting

The training dataset was built with 70% of the dataset (by dividing the 1,400 observations by 0.7) and tested on 30% of the remaining dataset in the R package (version 4.2.1). The "cforest" functions of the partykit package in R were used for the model fit using unconditional subclasses, 200 as a number of trees, and 5 input variables randomly sampled as candidates at each node.

2.7 Application of IMPACT model

2.7.1 Model framework

The foresight IMPACT model (https://www.ifpri.org/project/ifpri-impact-model) was used to explore soybean marketing and import scenarios during 2017–2050 through the adoption of rhizobium inoculation and supplemental application of P fertilizer. The IMPACT model framework considers components of climate models (Earth System Models), crop models (Decision Support System for Agrotechnology Transfer, DSSAT), water models (hydrology, water basin management, and water stress models), land-use models (pixel-level land use) and integrates them into the multi-market model. The IMPACT model computes the effects of national and international demand and prices and is designed for scenario analysis rather than forecasting (Robinson et al., 2015).

2.7.2 Model integration, model inputs, and scenario analysis

In the IMPACT model, crop yield is a function of commodity price, input prices, available water, climate, and market variables. The model integrates five modules (climate, crop, water, land use, and market) to assess changes in yields. The model assumes a scenario of underlying improvements in yields due to the adoption of technology and simulates crop yields in specific areas as functions of the introduction of technology (Eq. 2).

$$Yield_{it} = \sum(Soy\_adtech_{it} \times Soytech\_Yield_{it})$$

Eq. 2. (Robinson et al., 2015)

Where, *Soy_adtech* = Soybean adoption technology for a country *i* at the period *t*, and *Soy_tech* = Soybean inoculation technology for a country i at the period *t* and under no climate change effect.

Two future scenarios were assessed in this study:

- a moderate adoption scenario where the adoption rate of the Rh + P fertilizer combination among farmers stops at 35%, and

- a more extensive scenario in which the adoption rate of the Rh + P fertilizer combination reaches 75%.

For both scenarios, it was assumed that the adoption of the Rh + P fertilizer technology would happen gradually between 2017 (the first year of beginning adoption) and 2050 (the year in which the model is calibrated for inputs). The effect of improved soybean inoculation technology and P fertilization was simulated by reducing imports and saving currency in Nigeria.

2.8 Statistical analysis

General statistical analysis was carried out for the three agroecological zones), and yield prediction using machine learning with 68 constructed explanatory variables and a single yield response variable was carried out. The extracted soil properties used to predict yield were tested for normality, skewness, and the kurtosis test, which reported a P value of<0.05. Descriptive statistics (maximum, median, and minimum) were computed for the yield variable. A one-way analysis of variance (ANOVA) was carried out to assess the effect of treatment on grain yield change using the JMP statistical software (JMP, 2019). The treatment mean differences were analyzed using the least significant difference (LSD) at 5% and 1% of the level of significance when the Fischer (F) value was significant from the ANOVA (P<0.05). Levels of significance are given by "ns" (not significant, P >0.05), *P<0.05, **P<0.01, and ***P<0.001. The RF analysis was computed using R Studio version 2022.12.0 (R version 4.2.1).

3 Results

3.1 Soil properties

Descriptive statistics of extracted soil properties used for model training and validation are presented in Table 2. Averaged across the agroecological zones, the available P ranged from 6.0 to 10.0 mg kg^{-1} and from 6 to 9 mg kg^{-1} in the NGS, with a right skew data distribution range (Table 2 and Table S1). Similarly, for the three agroecological zones, the pH ranged from 5.1 to 6.1, 5.5–6.0 in SS, 5.3–6.1 in NGS, and 5.1–5.8 in SGS, with a left (negative) skew data distribution (Table S1). The range of clay contents varied from 16% to 32% for all agroecological zones: 18%–30% in SS, 16%–30% in NGS, and 19%–32% in SGS. Similarly, the silt contents ranged from 43% to 67% across the three agroecological zones: 45%–60% in the SS, 43%–67% in the NGS, and 46%–61% in the SGS agroecology. Other extracted soil property summary statistics, such as their skewness and kurtosis values are reported in Table 2 and Table S1.

3.2 Soybean yield response as affected by Rh inoculation and P application

A one-way ANOVA testing the effect of the treatment on grain yield was highly significant for the SS (F = 65.4, P<0.001), NGS (F = 86.6, P<0.001), and SGS (F = 127.3, P<0.001) agroecological zones, respectively (Figure 3). The yield data for the combined application of Rh + P fertilizer was normally distributed in the SS, right-skewed in the NGS, and left-skewed in the SGS agroecological zones

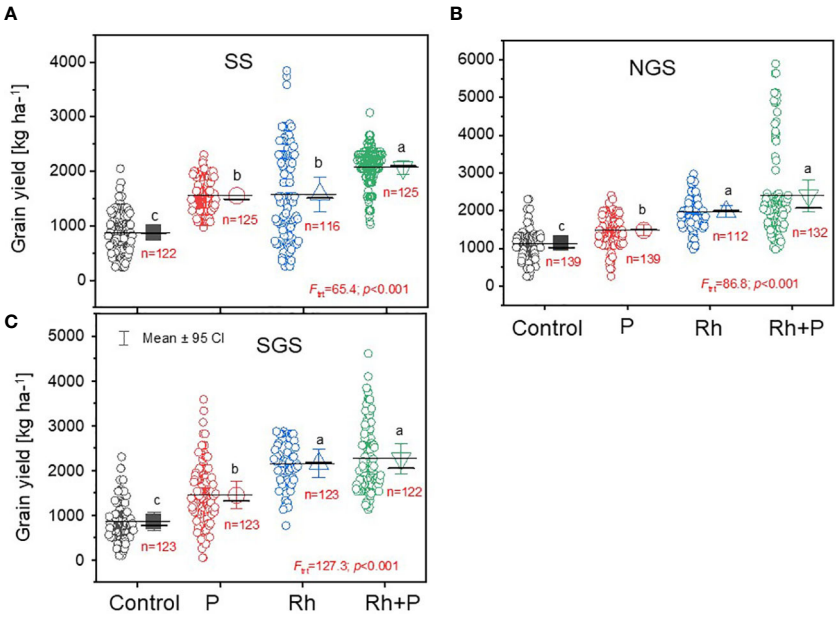

FIGURE 3
Boxplots of the soybean yield (kg ha^{-1}) for the control, phosphorus (P) fertilizer, rhizobia (Rh) inoculants, and the Rh + P combination in the **(A)** Sudan Savanna (SS), **(B)** Northern Guinea Savanna (NGS), and **(C)** Southern Guinea Savanna (SGS) of agroecology of Nigeria. Mean and ±95% confidence intervals are presented. Mean values appended by a different letter indicate significant differences at P<0.05.

10.3389/fpls.2023.1120826

(Figures 3A–C). The soybean yield of the Rh + P fertilizer treatment was always higher than that of the control treatment in the three agroecological zones of northern Nigeria (Figure 3). Average across all on-farm demonstration yield increments of 128%, 111%, and 162% were observed under the Rh + P combination compared to the control in SS, NGS, and SGS, respectively, and the overall increment for all agroecological zones of the established demonstration trial was 134% (Figures 3A–C). The average grain yield for the control treatment was the lowest in SGS compared to the SS and NGS agroecologies (Figures 3A–C). When inoculated with Rh alone, soybean yield was always higher in the Rh treatment than in the control treatment in the respective agroecological zones (Figures 3A–C). Similarly, the yield of the P fertilized treatment was higher than the control in the SS, NGS, and SGS agroecological zones, respectively (Figures 3A–C).

3.3 Soybean yield prediction using random forest machine learning

The results from RF models of data from the three agroecological zones and separately from each agroecological zone are presented in Table 3 and Figure 4 with their NRMSE and R^2 values. Among the three agroecological zones, NGS provided the highest trained R^2 value of 0.74 (Table 3). The trained NRMSE for NGS samples was 8.8 (Table 3). The validated R^2 and NRMSE were 0.52 and 6.0 (Table 3). For the SGS, the trained R^2 was the lowest (0.58) and the trained NRMSE was the highest (12.7) compared to the SS, NGS, and overall samples (Table 3). The validated R^2 and NRMSE were 0.53 and 8.9, respectively (Table 3). For the overall dataset, we found trained RMSE and R^2 values of 8.8 and 0.64, while the validated NRMSE and R^2 were 6.2 and 0.57, respectively (Table 3). The highest trained NRMSE was observed in SGS samples, and the reported R^2 was 0.58 (Table 3). The validated NRMSE and R^2 for SGS samples were 9.9 and 0.56 (Table 3). The biplots of the predicted and observed samples showed more dense points in the overall datasets and the NGS samples (Figures 4A, C).

The input variables of importance to predicting yield in the three agroecological zones are presented in Figure 5. For the three agroecological zones, the top five variables (based on importance) for predicting yield include the combined application of Rh + P fertilizer, year-to-year growing conditions, silt content in the soil, rhizobium inoculation, and the minimal temperature in the month of August (Figure 5A). The top five predicting variables of importance to soybean yield in the Sudan Savanna were crop management practices, combined application of Rh and P fertilizer, rhizobium inoculation, sand content in the soil, and soil available P (Figure 5B). The top six predictor variables for yield in the NGS were Rh + P combination, P fertilizer, year-to-year soybean cultivation, crop management practices, P fertilizers, and silt content in the soil (Figure 5C). Similarly, the RF model found crop management practices, Rh + P combination, P fertilizer, year-to-year cultivation, and effective cation exchange capacity as the top five yield predictor variables in SS (Figure 5D).

3.4 Food security and import through the adoption of rhizobium and P fertilizers

The simulation using the IMPACT model showed that soybean yield increases through the combined application of Rh and P fertilizer will reduce national trade through the less imports and result in currency savings in Nigeria by 2050. We implemented the model using an average yield increase of 134% (all agroecological zones) and 111% in the NGS and two scenarios of adoption rates: low (35% adoption rate) and high (75% adoption rate) (Figure 6A). The model was implemented using the dataset from the NGS agroecological zone because it had the highest prediction and accuracy from the RF model. Considering the average yield increase performance of 134% (averaged across three agroecological zones), results from the IMPACT model

TABLE 3 Training normalized root mean square error (NRMSE) and coefficient of determination (R^2), validated NRMSE, validated R^2, sample size, and number used estimators that predicting yield response of soybean from all sample sets, Sudan, Northern Guinea, and Southern Guinea Savannas of Nigeria.

Dataset	Training normalized root mean square error (NRMSE)	Training coefficient of determination (R^2)	Normalized validation (NRMSE	Validation coefficient of determination (R^2)	Sample size		Number of estimators
					Training	Tested	
All agroecological zones	8.8	0.64	6.2	0.57	980	420	28
Sudan Savanna	10.1	0.46	8.9	0.53	258	110	26
Northern Guinea Savanna	8.0	0.75	6.0	0.52	419	179	26
Southern Guinea Savanna	12.7	0.58	9.9	0.56	304	130.2	26

10.3389/fpls.2023.1120826

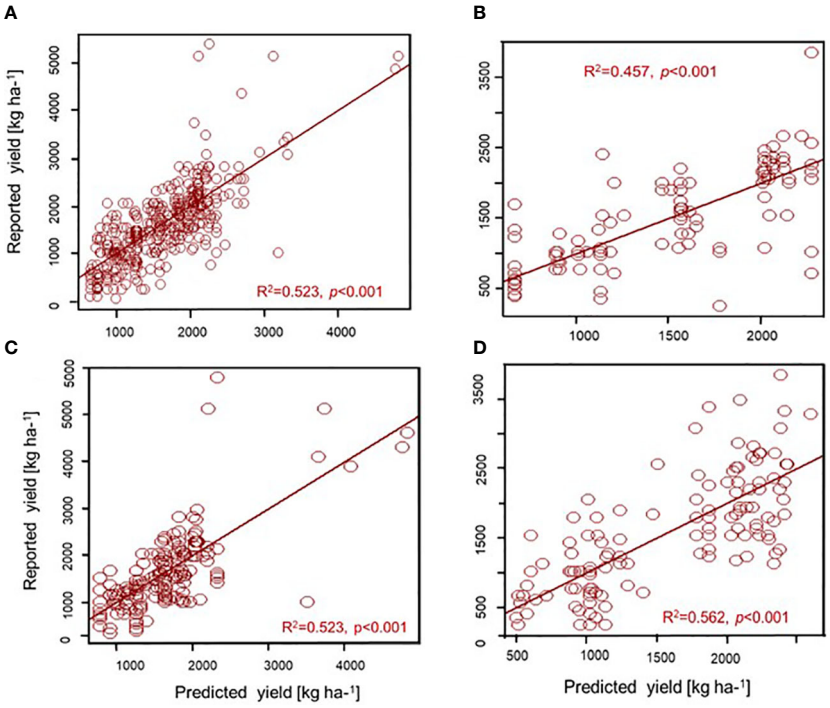

FIGURE 4
Scatter plots of the soybean predicted and reported yields validation from all sample sets **(A)**, Sudan **(B)**, Northern Guinea **(C)**, and Southern Guinea **(D)** Savannas of Nigeria. The validated coefficient of determination (R^2) of each sample set is indicated.

scenario showed that the quantity of soybeans imported in the country can be reduced by −10% (35% maximum) and by −22% (75% maximum adoption scenario) if the combined application of Rh and P fertilizer technology is adopted (Figure 6B). With an average yield increase of 111% from the combined application of Rh + P (observed in NGS), importation can be reduced by 8.4% (under a low adoption scenario) and by 18% (under a high adoption scenario) by 2030 in the country (Figure 6C).

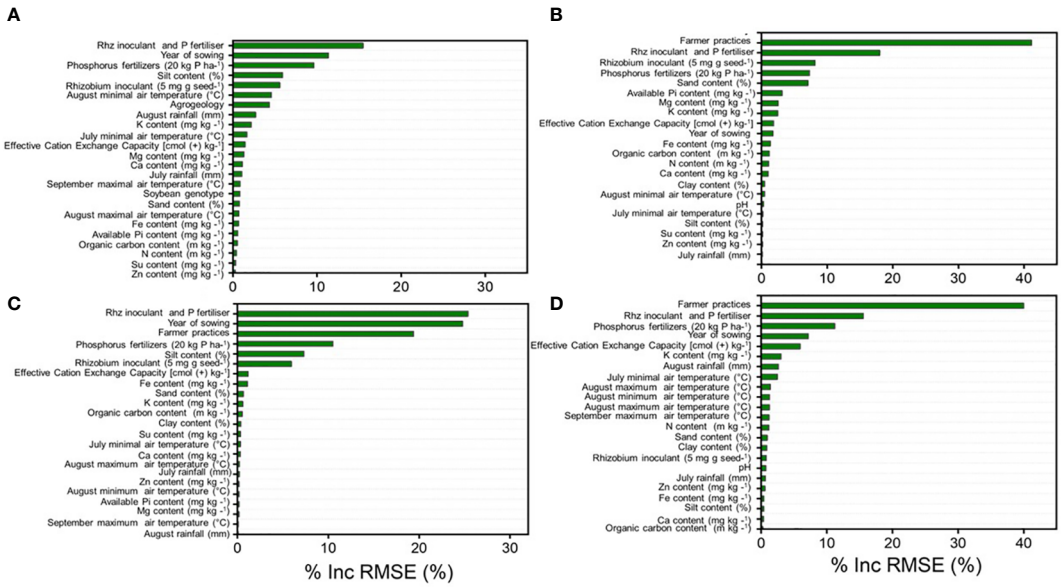

FIGURE 5
Best inputs variable of importance from soil, weather, and factorial estimators used to predict soybean yields from all sample sets **(A)**, Sudan **(B)**, Northern Guinea **(C)**, and Southern Guinea **(D)** Savannas of Nigeria.

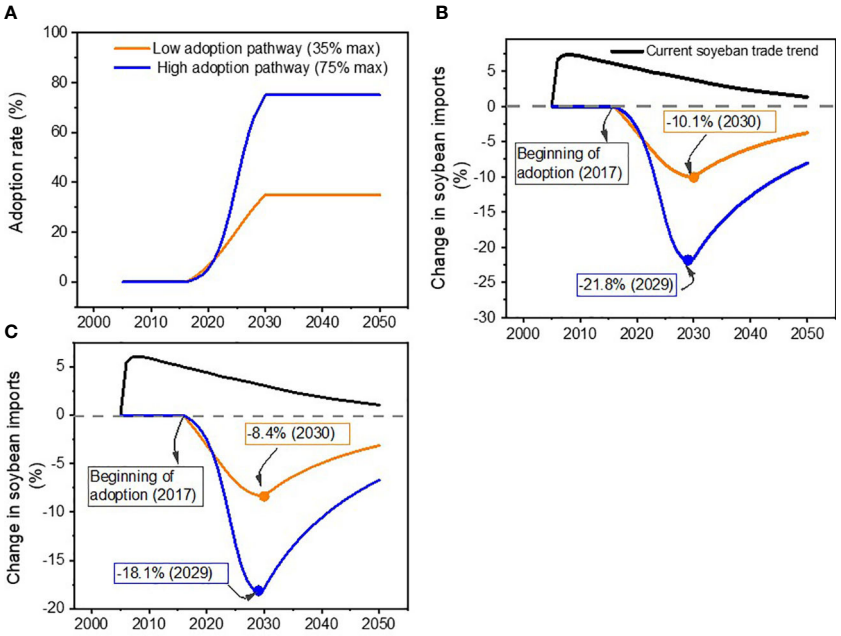

FIGURE 6
Scenario outlooks (2010–2050) of adoption of the combined rhizobia and phosphorus fertilizers technology based on average yield increase by 133.7% from the Nigeria savannas and by 111% in the Northern Guinea Savanna on-farm demonstrations plots **(A)** adoption profile by 35% and by 75% with with projectd impact under scenario, **(B)** for all sample sets and **(C)** Northern Guinea Savanna.

4 Discussion

Agricultural technologies focusing on increasing productivity, improving farmers' profitability, and enhancing sustainability are urgently needed to enhance the household food security of smallholders, particularly in SSA countries (Helfenstein et al., 2020). Such technologies are to be market-oriented, affordable, adapted to smallholder needs, and help to bridge gaps by integrating proper delivery mechanisms. This study demonstrated that on-farm improved soybean rhizobia inoculation technologies tested in collaboration with extension agents can help improve yield and profit, reduce soybean imports, and contribute to food security maintenance in Nigeria. Our results, in accordance with previous studies (Ronner et al., 2016), also demonstrated that yield increments from the combined application of Rh + P fertilizer were always higher than the control (farmer practice) in all three areas of Nigeria. Soybean yield at NGS sites was well predicted by the RF compared to the SS and SGS agroecological zones. A significant reduction in soybean imports in Nigeria could be made through yield increments from the combined application of Rh inoculant and P fertilizer. However, a rapid implementation strategy and massive adoption by farmers are required.

4.1 Yield response of soybean as affected by rhizobium inoculation and P application

A series of on-farm demonstration experiments showed soybean yield increased through the combined application of Rh + P (always higher in under-treated conditions than in non-treated conditions), irrespective of the agroecological zones and soil types. In the absence of Rh inoculation, P fertilizer, or Rh + P combination, the average yield in control was 1,084 kg ha^{-1} in the NGS sites, while the yield increased in the Rh + P inoculated plants by 2.3-, 2.1-, and 2.6-fold as compared to the non-treated plants (Figure 1). Earlier work demonstrated increased soybean yields with the combination of Rh inoculants and P fertilizer in West African soils. The observed higher yields of 1,188 kg ha^{-1} in SS, 1,203 kg ha^{-1} in NGS, and 1,397 kg ha^{-1} in SGS for the Rh + P application in West Africa (Ronner et al., 2016; Ulzen et al., 2018; Buenor et al., 2022). The authors reported an average yield increment of 815 kg ha^{-1} from the combined application of Rh + P, along with an increment in farmers' net profit. Several factors accounted for the higher yield under the Rh + P application, such as regular field monitoring by Notore extension agents, high-performing rhizobia microbes, and careful crop management by the engaged farmers during the implementation of the project activities. It is indicated that education, research, and extension in agriculture remain the vehicles to achieve sustainability in the modern food system. The NGS agroecological zone showed a favorable niche for rapidly increase of soybean yield using appropriate management interventions for food security in Nigeria and the sub-region. This high yield can be explained by suitable rainfall and soil fertility conditions. Suitable conditions for optimal soybean production require about 1,000 mm of water in rainfall-based production systems. The SS agroecological zone is a more drought-prone area that often limits yield. The SGS agroecology is the domain of acidic soils and low-P in Nigeria, which are limiting conditions to a high soybean yield (Jemo et al., 2015).

Farmer-managed participatory interventions and extension agents' engagement certainly facilitated the timely establishment of

on-farm demonstrations and weeding at critical crop developmental stages, *inter alia*. Thus, investments in information/knowledge dissemination, input fertilizers, and other technologies are crucial for the sustainable intensification of SSA.

Rhizobia inoculants are perishable commercial products, and this project secured standard and high-quality Rh inoculum with stable self-life from Legume Tech, UK. The inoculant was formulated with bacterial cell concentrations above 10^{10} cells g^{-1} with lyophilized *B. japonicum* that was kept in the Notore stores and delivered to VPAs only a few days before soybean sowing. It is worth mentioning policy decisions aiming to accelerate the manufacturing units, the marketing of high-quality rhizobia inoculants with a satisfying minimum of bacteria cell concentration of 10^9 cells g^{-1}, and the longer shelf-life of rhizobium to accelerate soybean production in Africa, as shown in the success study developed in Brazil (Bomfim et al., 2021). Other incentive measures to increase soybean production in SSA are the institutionalization of P fertilizers and their dissemination to rapidly address pressing food security issues.

4.2 Soybean yield prediction using random forest machine learning

Accurate yield prediction is of great importance to global food production. Using digitally soil-mapped properties and extracted weather and management variables, we predicted yield for the three agroecological zones using the RF machine-learning algorithm tools. The highest training R^2 (0.74) was achieved using samples from the NGS sites (Table 3). Alabi et al. (2022) predicted soybean yield using the vegetation index and soil texture information in the RF model. We lacked a comparable study on predicting soybean yield using soil properties in Nigerian Savanna conditions. The results of this study showed that NGS is the predominant agroecology for soybean production in terms of the required soil properties for growth. A better yield prediction in NGS can be explained by symmetrical data distribution (−0.42–0.58) of the extracted soil properties in the NGS agroecological (Table S1). The implications are that the soil and climatic conditions of NGS are favored for better growth and less drought effect during the growth stage. Bebeley et al. (2022) evaluated long–term seasonal analysis of soybean yield among the same three agroecological zones for deriving optimal sowing times for different soybean varieties, where yields were simulated in the NGS sites compared to other agroecological zones. In this study, the low R^2 values of the training dataset from SS and SGS agroecological zones could be attributed to normal data distributions of yield variables, making the yield data from SS and SGS less reliable for their good prediction using soil properties and extracted variables.

Predictions of soybean yield using datasets from the three agroecological zones (i.e., SS, NGS, and SGS) reported that the Rh + P combination has the topmost importance to increase yield under challenging environmental conditions. Also, P-fertilizer and Rh inoculation alone were also among the top variables in importance, but their relative importance varied depending on the agroecology. The available P of the soils was revealed as an important variable for soybean yield in the SS. The results imply that the supply of P fertilizers is largely required if farmers are to grow soybeans in the SS, SGS, and NGS soils. Other important soil properties, such as silt and sand contents and ECEC, were also predictors of soybean yield (Figure 5). The present study extracted an average silt content of 53.3% and a sand content of 19.9% (Table 2). Apart from precipitation, temperature, and macro- and micronutrients, crop yields are also dependent on soil properties such as soil texture that influence water retention at the root zones and improve nutrient diffusion and crop yield (Huang et al., 2021). Fine-textured or silty loam soil provides a higher water holding capacity and more resistance to plant water uptake in wet conditions compared to sandy soils and can be poorly drained and susceptible to waterlogging, which can lead to denitrification and yield loss (Huang et al., 2021). The interactions between physical soil properties and soybean yields are not well quantified across the agroecological zones of Nigeria and deserve further research and investigation. Such information is necessary to design key indicators to improve soil structure and carbon stocks to increase soil availability for water storage and nutrient retention and promote energy conservation around the soybean root zones.

The minimum air temperature recorded in August was among the top five predictors of importance to soybean yield. These temperatures correlated with the soybean pod filling stages and were in the range of 17–20°C, which was above the air temperature (15°C) reported to inhibit seed filling. The optimum temperatures for soybean are 15–22°C at the emergence stage, 20–25°C at the flowering stage, and 15–22°C at the maturity stage, and seed yield and yield formation of soybean are frequently reduced by temperatures below 15°C and above 30°C (Zhang et al., 2016).

In the present study, we observed that the R^2 for actual and predicted yields was less than 60% (Table 3 and Figure 3). The results imply that all the aggregated soil and weather variables partly explained the observed yield variation. Other biotic or abiotic factors that were not aggregated in the independent variables, such as competitions with native species that were incompatible with the introduced rhizobia, impaired the nodulation and affected yield. On the other hand, the rate of P applied was only 20 kg ha^{-1}, which was insufficient to achieve optimal soybean yield. Future studies to address the "non-compatible hypothesis" and the optimal P rate for each agroecological zone will deserve further research investigations.

4.3 Soybean import reduction through the adoption of Rh inoculant and P fertilizers

Linking biophysical and economic models is important in a world facing the complexities of increasing crop production under pressing climate change threats (Islam et al., 2016). We conducted a two-scenario analysis of the Rh + P combination treatment, evaluated the possibility of adoptions that could take place in the future, and assessed the impacts on Nigerian food security and soybean trade. Results from the IMPACT model showed that the Rh + P combination has the potential to reduce the current soybean importation demand by a maximum and reverse the importation

trend from 2029 if maximally adopted. The scenario analysis through the adoption of promising agricultural technology on yield by 2050 has been implemented in several commodities, including rainfed maize in Africa, irrigated rice in South Asia, rainfed potato in rainfed sorghum in India, and rainfed groundnut in Africa and Southeast Asia (Islam et al., 2016). In many of these studies, the authors observed that promising technologies tested in many regions/or ecologies showed a partial to complete offset of the deleterious impacts on yield through the adoption of technology (Islam et al., 2016). In the present study, we have opted for large adoption as many demonstrations, including many participating farmers, in various steps of soybean production and training in inoculation technology with the goal of rapid adoption, were implemented to increase soybean production and improve food security.

Possible gaps and limitations in the modeling for agricultural systems as presently conducted in this work are the bias generated from the model tools and environmental conditions such as soil and climate that are heterogeneous, especially in Sub-Saharan Africa. These gaps certainly decrease statistical robustness and bias upward the values obtained for decision variables, which could often be unachievable in the real world. To avoid these aggregated biases resulting from the model, the natural conditions of the independent variables were tested for data homogeneity. To minimize the biases from human heterogeneity at on-farms, we trained the engaged farmers to use Rh inoculant and P fertilizer technology, and VPs supervised their work regularly before trial establishments in the respective areas. Overall, the present results underscore the fact that innovative interventions should be tested across a wide range of AEZ, capturing all possible variables for wider adoption. Our results strongly suggest that the application of rhizobium inoculation is affordable, and represents a low-cost agricultural intensification strategy when combined with P fertilization and VPA technical assistance.

5 Conclusions

This study used a comprehensive mix-methodological approach integrating large-scale on-farm demonstrations and the engagement of local extension agents and farmers, as well as a machine learning approach, to identify the major determinants of yield variability in three savanna agroecological zones in Nigeria. The IMPACT model simulates the effect of the adoption of Rh + P on food security and imports to develop sustainable soybean production technology. Our result demonstrates a superior benefit from the combination of Rh inoculant and P fertilizer to improve soybean yield in the farmer field conditions of northern Nigeria. Soybean yield was well predicted from the combination of soil, climate, inputs, and crop management parameters in the northern Guinea Savanna agroecological zone, implying that the NGS offers a suitable production environment for soybean production among the three agroecological zones. If the combination of Rh inoculation and P fertilization demonstrated by this study as best practices and promoted by policymakers and maximally adopted by farmers in Nigeria, the country will reverse its dependency on soybean trade to about 21% by 2029 and become a self-sufficient producer by 2050 in the absence of climate change threats.

Data availability statement

The raw data supporting the conclusions of this article will be made available by the authors, without undue reservation.

Author contributions

Writing original draft: MJ. Methodology: MJ, KD, TE, TC, RM, MH, FS, and JJ. Manuscript review and inputs: MJ, KD, TE, TC, RM, MH, FS, and JJ. All authors contributed to the article and approved the submitted version.

Funding

The experimental work was conducted with the support of the Notore Limited Group, Nigeria. The project was financially supported partly by a grant from the Bill and Melinda Gates Foundation to support the on-farm demonstrations in Nigeria. Special thanks to extension agents from the Notore group and the collaborative farmers who participated in the on-farm demonstration trials. MJ was financially supported by a grant from OCP AFRICA to the University of Mohammed VI Polytechnic (UM6P) to develop sustainable grain legume production in Africa.

Conflict of interest

The authors declare that the research was conducted in the absence of any commercial or financial relationships that could be construed as a potential conflict of interest.

Publisher's note

Supplementary material

The Supplementary Material for this article can be found online at: https://www.frontiersin.org/articles/10.3389/fpls.2023.1120826/full#supplementary-material

References

Alabi, T. R., Abebe, A. T., Chigeza, G., and Fowobaje, K. R. (2022). Estimation of soybean grain yield from multispectral high-resolution UAV data with machine learning models in West Africa. *Remote Sens. Appl. Soc Environ.* 27, 100782. doi: 10.1016/j.rsase.2022.100782

Alves, B. J. R., Boddey, R. M., and Urquiaga, S. (2003). The success of BNF in soybean in Brazil. *Plant Soil* 252, 1–9. doi: 10.1023/A:1024191913296

Awuni, G. A., Reynolds, D. B., Goldsmith, P. D., Tamimie, C. A., and Denwar, N. N. (2020). Agronomic and economic assessment of input bundle of soybean in moderately acidic savanna soils of Ghana. *Agrosystems Geosci. Environ.* 3. doi: 10.1002/agg2.20085

Bebeley, J. F., Kamara, A. Y., Jibrin, J. M., Akinseye, F. M., Tofa, A. I., Adam, A. M., et al. (2022). Evaluation and application of the CROPGRO-soybean model for determining optimum sowing windows of soybean in the Nigeria savannas. *Sci. Rep.* 12, 6747. doi: 10.1038/s41598-022-10505-4

Bomfim, C. A., Coelho, L. G. F., do Vale, H. M. M., de Carvalho Mendes, I., Megías, M., Ollero, F. J., et al. (2021). Brief history of biofertilizers in Brazil: From conventional approaches to new biotechnological solutions. *Braz. J. Microbiol.* 52, 2215–2232. doi: 10.1007/s42770-021-00618-9

Breiman, L. (2001). Random forests. *Mach. Learn.* 45, 5–32. doi: 10.1023/A:1010933404324

Buenor, A. B., Kabiru, M. R., Bechtaoui, N., Jibrin, M. J., Asante, M., Bouraqqadi, A., et al. (2022). Grain legumes yields responses to rhizobia inoculants and phosphorus supplementation under Ghana soils: A meta-synthesis. *Front. Plant Sci*. doi: 10.3389/fpls.2022.877433

Chigeza, G., Boahen, S., Gedil, M., Agoyi, E., Mushoriwa, H., Denwar, N., et al. (2019). Public sector soybean (Glycine max) breeding: Advances in cultivar development in the African tropics. *Plant Breed.* 138, 455–464. doi: 10.1111/pbr.12682

Devkota, K. P., Devkota, M., Paudel, G. P., and McDonald, A. J. (2021). Coupling landscape-scale diagnostics surveys, on-farm experiments, and simulation to identify entry points for sustainably closing rice yield gaps in Nepal. *Agric. Syst.* 192, 103182. doi: 10.1016/j.agsy.2021.103182

FAOSTAT (2018) *FAOSTAT*. Available at: http://www.fao.org/faostat/en/#data/QC (Accessed November 26, 2020).

FAOSTAT (2022) *FAOSTAT*. Available at: http://www.fao.org/faostat/en/#data/QC (Accessed December 10, 2022).

Grönemeyer, J. L., and Reinhold-Hurek, B. (2018). Diversity of bradyrhizobia in subsahara Africa: A rich resource. *Front. Microbiol.* 9. doi: 10.3389/fmicb.2018.02194

Helfenstein, J., Diogo, V., Bürgi, M., Verburg, P., Swart, R., Mohr, F., et al. (2020). "Conceptualizing pathways to sustainable agricultural intensification," in *Advances in Ecological Research* (Elsevier), 161–192. doi: 10.1016/bs.aecr.2020.08.005

Hengl, T., Miller, M. A. E., Križan, J., Shepherd, K. D., Sila, A., Kilibarda, M., et al. (2021). African Soil properties and nutrients mapped at 30 m spatial resolution using two-scale ensemble machine learning. *Sci. Rep.* 11, 6130. doi: 10.1038/s41598-021-85639-y

Herridge, D. F., Giller, K. E., Jensen, E. S., and Peoples, M. B. (2022). Quantifying country-to-global scale nitrogen fixation for grain legumes II. Coefficients, templates and estimates for soybean, groundnut, and pulses. *Plant Soil*. 1–15. doi: 10.1007/s11104-021-05166-7

Huang, J., Hartemink, A. E., and Kucharik, C. J. (2021). Soil-dependent responses of US crop yields to climate variability and depth to groundwater. *Agric. Syst.* 190, 103085. doi: 10.1016/j.agsy.2021.103085

Hungria, M., Araujo, R. S., Silva Júnior, E. B., and Zilli, J.É. (2017). Inoculum rate effects on the soybean symbiosis in new or old fields under tropical conditions. *Agron. J.* 109, 1106–1112. doi: 10.2134/agronj2016.11.0641

Ishaku, H. T., and Majid, M. R. (2010). X-Raying rainfall pattern and variability in northeastern Nigeria: Impacts on access to water supply. *J. Water Resour. Prot.* 02, 952–959. doi: 10.4236/jwarp.2010.211113

Islam, S., Cenacchi, N., Sulser, T. B., Gbegbelegbe, S., Hareau, G., Kleinwechter, U., et al. (2016). Structural approaches to modeling the impact of climate change and adaptation technologies on crop yields and food security. *Glob. Food Secur.* 10, 63–70. doi: 10.1016/j.gfs.2016.08.003

Jemo, M., Abaidoo, R. C., Nolte, C., Tchienkoua, M., Sanginga, N., and Horst, W. J. (2006). Phosphorus benefits from grain-legume crops to subsequent maize grown on acid soils of southern Cameroon. *Plant Soil* 284, 385–397. doi: 10.1007/s11104-006-0052-x

Jemo, M., Nolte, C., Tchienkoua, M., and Abaidoo, R. C. (2010). Biological nitrogen fixation potential by soybeans in two low-p soils of southern Cameroon. *Nutr. Cycl. Agroecosystems* 88, 49–58. doi: 10.1007/s10705-008-9187-x

Jemo, M., Nwoke, C., Pypers, P., and Vanlauwe, B. (2015). Response of maize (*Zea mays*) to the application of foliar fertilizers in the Sudan and Guinea savanna zone of Nigeria. *J. Plant Nutr. Soil Sci.* 178, 374–383. doi: 10.1002/jpln.201400524

Khaki, S., and Wang, L. (2019). Crop yield prediction using deep neural networks. *Front. Plant Sci.* 10. doi: 10.3389/fpls.2019.00621

Khaki, S., Wang, L., and Archontoulis, S. V. (2020). A CNN-RNN framework for crop yield prediction. *Front. Plant Sci.* 10. doi: 10.3389/fpls.2019.01750

Ladha, J. K., Peoples, M. B., Reddy, P. M., Biswas, J. C., Bennett, A., Jat, M. L., et al. (2022). Biological nitrogen fixation and prospects for ecological intensification in cereal-based cropping systems. *Field Crops Res.* 283, 108541. doi: 10.1016/j.fcr.2022.108541

Mason-D'Croz, D., Vervoort, J., Palazzo, A., Islam, S., Lord, S., Helfgott, A., et al. (2016). Multi-factor, multi-state, multi-model scenarios: Exploring food and climate futures for southeast Asia. *Environ. Model. Software* 83, 255–270. doi: 10.1016/j.envsoft.2016.05.008

Robinson, S., Rosegran, M., Mason-D'Croz, D., Islam, S., Sulser, T. B., Robertson, R., et al. (2015). "The international model for policy analysis of agricultural commodities and trade (IMPACT)," in *IFPRI technical report* (Washington, DC: International Food Policy Research Institute (IFPRI)). Available at: http://ebrary.ifpri.org/cdm/ref/collection/p15738coll2/id/129825

Ronner, E., Franke, A. C., Vanlauwe, B., Dianda, M., Edeh, E., Ukem, B., et al. (2016). Understanding variability in soybean yield and response to p-fertilizer and rhizobium inoculants on farmers' fields in northern Nigeria. *Field Crops Res.* 186, 133–145. doi: 10.1016/j.fcr.2015.10.023

Siamabele, B. (2021). The significance of soybean production in the face of changing climates in Africa. *Cogent Food Agric.* 7, 1933745. doi: 10.1080/23311932.2021.1933745

Smidt, E. R., Conley, S. P., Zhu, J., and Arriaga, F. J. (2016). Identifying field attributes that predict soybean yield using random forest analysis. *Agron. J.* 108, 637–646. doi: 10.2134/agronj2015.0222

Thilakarathna, M., and Raizada, M. (2018). Challenges in using precision agriculture to optimize symbiotic nitrogen fixation in legumes: Progress, limitations, and future improvements needed in diagnostic testing. *Agronomy* 8, 78. doi: 10.3390/agronomy8050078

Ulzen, J., Abaidoo, R. C., Ewusi-Mensah, N., and Masso, C. (2018). On-farm evaluation and determination of sources of variability of soybean response to bradyrhizobium inoculation and phosphorus fertilizer in northern Ghana. *Agric. Ecosyst. Environ.* 267, 23–32. doi: 10.1016/j.agee.2018.08.007

Umar, A. T., and Bako, M. M. (2019). Recent rainfall trends and variability in sudano-sahelian region of nigeria, (1986– 2015). *Ghana J. Geogr.* 11, 33–57. doi: 10.4314/gjg.v11i1.3

van Heerwaarden, J., Baijukya, F., Kyei-Boahen, S., Adjei-Nsiah, S., Ebanyat, P., Kamai, N., et al. (2018). Soyabean response to rhizobium inoculation across sub-Saharan Africa: Patterns of variation and the role of promiscuity. *Agric. Ecosyst. Environ.* 261, 211–218. doi: 10.1016/j.agee.2017.08.016

Wang, L., Zhou, Y., Liu, J., Liu, Y., Zuo, Q., and Li, Q. (2022). Exploring the potential of multispectral satellite images for estimating the contents of cadmium and lead in cropland: The effect of the dimidiate pixel model and random forest. *J. Clean. Prod.* 367, 132922. doi: 10.1016/j.jclepro.2022.132922

Zhang, L., Zhu, L., Yu, M., and Zhong, M. (2016). Warming decreases photosynthates and yield of soybean [Glycine max (L.) Merrill] in the north China plain. *Crop J.* 4, 139–146. doi: 10.1016/j.cj.2015.12.003

frontiers | Frontiers in Plant Science

TYPE Original Research
PUBLISHED 13 June 2023
DOI 10.3389/fpls.2023.1211107

OPEN ACCESS

EDITED BY
Chang Fu Tian,
China Agricultural University, China

REVIEWED BY
Pascal Ratet,
UMR9213 Institut des Sciences des Plantes de Paris Saclay (IPS2), France
Deqiang Duanmu,
Huazhong Agricultural University, China

*CORRESPONDENCE
Michael Udvardi
m.udvardi@uq.edu.au
Raul Huertas
raul.huertas@hutton.ac.uk

†PRESENT ADDRESS
Raul Huertas,
Environmental and Biochemical Sciences, The James Hutton Institute, Dundee, United Kingdom
Ivone Torres-Jerez,
Institute for Agricultural Biosciences, Oklahoma State University, Ardmore, OK, United States
Michael Udvardi,
Queensland Alliance for Agriculture and Food Innovation, University of Queensland, Brisbane, QLD, Australia

RECEIVED 24 April 2023
ACCEPTED 22 May 2023
PUBLISHED 13 June 2023

CITATION
Huertas R, Torres-Jerez I, Curtin SJ, Scheible W and Udvardi M (2023) *Medicago truncatula PHO2* genes have distinct roles in phosphorus homeostasis and symbiotic nitrogen fixation. *Front. Plant Sci.* 14:1211107. doi: 10.3389/fpls.2023.1211107

Medicago truncatula PHO2 genes have distinct roles in phosphorus homeostasis and symbiotic nitrogen fixation

Raul Huertas[1*†], Ivone Torres-Jerez[1†], Shaun J. Curtin[2,3,4,5], Wolf Scheible[1] and Michael Udvardi[1*†]

[1]Noble Research Institute LLC, Ardmore, OK, United States, [2]United States Department of Agriculture, Plant Science Research Unit, St. Paul, MN, United States, [3]Department of Agronomy and Plant Genetics, University of Minnesota, St. Paul, MN, United States, [4]Center for Plant Precision Genomics, University of Minnesota, St. Paul, MN, United States, [5]Center for Genome Engineering, University of Minnesota, St. Paul, MN, United States

Three *PHO2*-like genes encoding putative ubiquitin-conjugating E2 enzymes of *Medicago truncatula* were characterized for potential roles in phosphorous (P) homeostasis and symbiotic nitrogen fixation (SNF). All three genes, *MtPHO2A, B and C*, contain miR399-binding sites characteristic of *PHO2* genes in other plant species. Distinct spatiotemporal expression patterns and responsiveness of gene expression to P- and N-deprivation in roots and shoots indicated potential roles, especially for *MtPHO2B*, in P and N homeostasis. Phenotypic analysis of *pho2* mutants revealed that MtPHO2B is integral to Pi homeostasis, affecting Pi allocation during plant growth under nutrient-replete conditions, while MtPHO2C had a limited role in controlling Pi homeostasis. Genetic analysis also revealed a connection between Pi allocation, plant growth and SNF performance. Under N-limited, SNF conditions, Pi allocation to different organs was dependent on MtPHO2B and, to a lesser extent, MtPHO2C and MtPHO2A. MtPHO2A also affected Pi homeostasis associated with nodule formation. Thus, *MtPHO2* genes play roles in systemic and localized, i.e., nodule, P homeostasis affecting SNF.

KEYWORDS

phosphorus, symbiotic nitrogen fixation (SNF), *Medicago truncatula*, *PHO2*, nitrogen

Introduction

Nitrogen (N) and phosphorus (P) are essential macronutrients for plant growth and development. Low availability of these nutrients in most soils limits crop production necessitating the use of fertilizers to secure food production. Symbiotic nitrogen fixation (SNF) in legumes is the primary natural source of nitrogen in agroecosystems, although industrial nitrogen-fertilizers now provide most of the nitrogen for crop production. Use and loss to the environment of industrial N-fertilizer is not sustainable and more needs to be done to

boost the use of legumes and N derived from SNF in agriculture to remedy this (Udvardi et al., 2021).

SNF results from a mutualistic symbiosis between soil bacteria, called rhizobia, and legumes during which the bacteria reduce atmospheric di-nitrogen into ammonia within specialized root organs called nodules. In exchange for ammonia provided to the plant, the bacteria receive carbon (C) in the form of organic acids and other nutrients, including P for instance (Udvardi & Poole, 2013). Complex regulatory networks have evolved to control acquisition and allocation of C, N, P and other essential nutrients for optimal growth, development and functioning of plant organs and the plant as a whole (Gautrat et al., 2021; Helliwell, 2022), although our understanding of these networks remains incomplete.

SNF is sensitive to environmental stress, including P-deficiency. Nodules contain relatively high concentrations of P especially in nucleic acids (plant and bacterial DNA and RNA), which underpin protein synthesis and high metabolic activity, including SNF (Sulieman et al., 2013; Cabeza et al., 2014). P limitation severely inhibits root nodule organogenesis and SNF (Hernandez et al., 2009). Maintenance of P homeostasis in nodules is considered a main adaptive strategy to maintain symbiotic performance under P-deficiency, although underlying mechanisms are poorly understood. (Cabeza et al., 2014; Nasr Esfahani et al., 2017).

In non-legumes, there is growing evidence for crosstalk between P and N regulation of nutrient acquisition, growth and metabolism (Hu et al., 2019; Medici et al., 2019; Ueda et al., 2020). In Arabidopsis and other species, P homeostasis is systemically regulated by the transcriptional activators Phosphate Starvation Response 1 (PHR1/PHL) (Rubio et al., 2001; Bustos et al., 2010), the negative regulator SPX-like (Puga et al., 2014; Wang et al., 2014), and tuned by the balance of specific microRNAs (miR399 and miR827) (Chiou et al., 2006; Lin et al., 2013) and long non-coding RNAs (IPS-like) (Franco-Zorrilla et al., 2007) in coordination with PHOSPHATE2 (PHO2) (Aung et al., 2006; Bari et al., 2006; Lin et al., 2008). PHO2 is a ubiquitin-conjugating (UBC) E2 enzyme involved in the degradation of multiple type of Pi transporters including members of the PHT1/PT (PHOSPHATE TRANSPORTER 1) protein family, PHOSPHATE 1 (PHO1) and PHF1 (PHOSPHATE TRANSPORTER TRAFFIC FACILITATOR 1) (Bari et al., 2006; Liu et al., 2012; Cao et al., 2014; Park et al., 2014; Ouyang et al., 2016; Pacak et al., 2016). The PHO2-miR399-IPS1 and PHO2-NLA-miR827 regulatory modules (Franco-Zorrilla et al., 2007; Kant et al., 2011; Lin et al., 2013) function independently but cooperatively, regulating acquisition and root-to-shoot translocation of Pi in response to P and N availability, protecting aboveground organs from excessive Pi accumulation. The physiological role of PHO2 protein in maintaining whole-plant Pi-homeostasis has been described for rice (Cao et al., 2014), wheat (Ouyang et al., 2016) and Arabidopsis (Bari et al., 2006). Further, Arabidopsis PHO2 is considered a local and systemic integrator of N availability in phosphate systemic signaling (Medici et al., 2019).

Although the mechanisms of N and P crosstalk in legumes related to nodule development and SNF are largely unknown, there is evidence that systemic signaling pathways controlling N fixation and acquisition are linked to phosphate systemic signaling. Phosphorus deficiency influence rhizobial infection and nodulation through miR2111/Too Much Love (TML), PHR (Phosphate Starvation Response) - RICs (Rhizobium-induced CLE Peptides) - NARK (Nodulation Autoregulation Receptor Kinase) and through PHR depending on P homeostasis regulatory modules in legumes (Gautrat et al., 2021; Zhong et al., 2023 and references therein). Some Phosphate Transporter (PHT/PT) and PHOSPHATE1 (PHO1)-type P transporters, downstream targets of PHR transcription factors, have been assigned an important role in maintaining Pi homeostasis in nodules, supporting SNF (Qin et al., 2012; Chen et al., 2019; Nguyen et al., 2021). Likewise, two alfalfa PHO2 genes have been implicated in systemic P-homeostasis, although their roles during symbiosis have not been explored (Miller et al., 2022) A *Medicago truncatula PHO2*-like gene contributes to quantitative variation in nodulation in this species, but the underlying mechanism remains unknown (Curtin et al., 2017). *Medicago truncatula* has two other *PHO2*-like genes, although their roles, if any, in P-homeostasis and SNF also remain unknown (Miller et al., 2022).

Here, we explore the roles of the three *Medicago truncatula PHO2-like* genes in P homeostasis and SNF. Our results implicate PHO2 proteins in systemic Pi homeostasis and the support of SNF.

Materials and methods

Plant material

Medicago truncatula ecotype R108 (HM340) was used in all experiments as a wild-type control as this is the genetic background of the *Tnt1*, CRISPR/Cas9 and TALEN *pho2* mutants. Offspring of the CRISPR/Cas9 line WPT210-9, described previously (Curtin et al. (2017), were screened to isolate homozygous *pho2-*A_{CRISPR} and *pho2-*B_{CRISPR} mutants. Similarly, offspring of TALEN line WPT52-4-8 (Cermak et al. (2017), were used to identify the homozygous mutant *pho2-*B_{TALEN}. Offspring of self-pollinated plants from the WPT210-9 and WPT52-4-8 lines were genotyped by combining PCR amplification and NlaIV and HaeIII restriction enzyme digestion assays, respectively. Changes in genomic DNA were confirmed by Sanger sequencing of undigested PCR products of the homozygous mutant lines and wild-type plants. Sequence comparisons were performed using Geneious software.

The *pho2-*A_{Tnt1} homozygous line was obtained from *Tnt1* line NF12360 (Curtin et al., 2017). *Tnt1* line NF16248 was used to isolate the homozygous exonic mutant allele *pho2-*C_{Tnt1} by PCR genotyping. *Tnt1*-specific and gene-specific primers are listed in Supplementary Table 2. *Pho2-*A_{CRISPR}, *pho2-*B_{CRISPR} and *pho2-*C_{Tnt1} were the mutant alleles selected for phenotypic analysis, while the *pho2-*A_{Tnt1} and *pho2-*B_{TALEN} mutant alleles were used to confirm phenotypes (Supplementary Figure 6).

Plant growth under non-symbiotic and symbiotic conditions

Seeds were sterilized, scarified, and stratified as described before (Kryvoruchko et al., 2018). Seedlings with fully opened cotyledons and similar radicles were individually transferred into 2” x 7” plastic

cones (Stuewe & Sons Inc.) containing a mixture (3:1, v/v) of sterilized Turface (calcined [illite] clay) and Vermiculite (Sun Gro Horticulture). Seedlings were fertilized with one-half-strength B&D solution (Broughton & Dilworth, 1971). Seven days after transplanting, seedlings were watered with full-strength modified B&D nutrient solution. Nitrogen was supplied as a 2:1 mixture of KNO_3 and NH_4NO_3, while phosphorus was supplied as KH_2PO_4. The different treatments and final concentrations were "control" (8 mM N and 0.5 mM P), "reduced-P" (8 mM N and 20 µM P), "$control_{sym}$" (0.25 mM N and 0.5 mM P) and "reduced-P_{sym}" (0.25 mM N and 20 µM P). K_2SO_4 was used to balance the potassium concentration in the reduced-P and reduced-P_{sym} solutions. All other macro- and micro-nutrients of the B&D nutrient solution were provided as specified (Broughton & Dilworth, 1971).

For the non-symbiotic experiments, plants were watered with control or reduced-P nutrient solutions, while for the symbiotic experiments they were inoculated with 50 mL suspension (OD_{600} ~0.02) of *Sinorhizobium meliloti* strain 1021 (Meade et al., 1982) in $control_{sym}$ or reduced-P_{sym} nutrient solutions. Plants were grown under controlled conditions of light (200 µmol m^{-2} s^{-1}, 16h day/8h night), constant temperature of 22°C, and 40% relative humidity, and irrigated twice per week - once with the corresponding nutrient solution and once with B&D without N or P, to avoid accumulation of N or P. Plants were harvested four weeks after starting treatments. Each plant was removed from its cone and the root carefully washed with water to remove substrate while avoiding loss of roots and nodules. Independent plant tissues were frozen in liquid nitrogen and stored at −80°C for later use, or oven dried at 60°C and weighed. Total plant dry weight (DW) was the sum of the shoot and root dry weights.

Symbiotic nitrogen fixation traits

The acetylene reduction assay (ARA) was carried out as previously described (Hardy et al., 1968). Briefly, four weeks after inoculation, entire root systems were transferred onto sterile Whatman paper strips placed inside 12-mL glass vials containing 2 mL of sterile distilled water. The tubes were sealed with rubber stoppers. Each tube contained roots from independent plants. Samples were incubated in dark in the presence of 10% (v/v) acetylene at 28°C for up to 16 h. Ethylene and acetylene concentrations were measured using an Agilent 7890A gas chromatograph (Agilent Technologies). Serial dilutions of a known quantity of ethylene were used to make standard curves of GC chromatogram peak area to calculate the amount of ethylene produced. The amount of ethylene produced was determined by measuring the area of the ethylene peak relative to background. Nitrogenase activity was calculated as the amount of ethylene produced per unit root dry weight. The number and biomass of the nodules was determined by detaching them from the roots.

RNA isolation and quantitative PCR (qPCR) analyses

Four weeks after treatments, roots, shoots, and nodules were collected into liquid nitrogen. After grinding in liquid nitrogen, total RNA was extracted using the TRIzol reagent (Life Technologies). Residual genomic DNA was removed using Turbo DNase I (Ambion). RNA was quantified using a Nanodrop Spectrophotometer ND-100 (NanoDrop Technologies). For qPCR, reverse transcription was carried out using SuperScript III Reverse Transcriptase (Invitrogen) and oligo(dT)20 primer, as describe previously. Transcript levels were normalized using the geometric mean of three housekeeping genes, MtPI4K (Medtr3g091400), MtPTB2 (Medtr3g090960), and MtUBC28 (Medtr7g116940), whose transcript levels were stable across all the samples analyzed (Kakar et al., 2008). Three biological replicates were included per gene. qPCR cycle threshold (Ct) values were analyzed using the ΔΔCt method (Livak & Schmittgen, 2001). Primer sequences used in this analysis are listed in Supplementary Table 2. Sequence alignments and the design of gene specific primers were performed using Geneious software.

Bioinformatics and phylogenetic analysis

The genome assembly of Jemalong A17 (Mt4.0 v1) and Medicago R108 (v0.95) ecotypes from Phytozome and the Legume Information System (LIS) were consulted to retrieve DNA sequences and gene structures. The Integrative Genomics Viewer (IGV) software (https://igv.org) was used to visualize the original raw RNA-seq data used for the MtSSPdb (https://mtsspdb.zhaolab.org/database) (Boschiero et al., 2020) and confirm the 5' and 3' UTR regions as well as the expression profiles.

Precursor sequences of the pre-miR399s from several plant species were obtained from miRBase (www.mirbase.org) and used to identify *Medicago truncatula* miR399. The miR399 sequences and the potential miR399-binding sites (miR399BS) were validated using psRNATarget with default parameters (Dai et al., 2018). The consensus miR399 sequence, miR399 sequence logo, potential PHO-like ([G(G/T/A) (C/T/A)GTGG]; Mukatira et al., 2001) and P1BS (GnATATnC; Rubio et al., 2001) cis-regulatory elements were generated using Geneious software.

Protein sequences were extracted from Phytozome and NCBI Protein databases. The circular phylogenetic tree was constructed from a ClustalW multiple sequence alignment of the full-length protein sequences in Geneious software using Juker-Cantor as the genetic distance model and the unweighted pair group method with arithmetic mean (UPGMA) as a tree build method with 500 replicates and 60% of support threshold. The gene IDs encoding each protein are described in Supplementary Table 1.

Measurements of soluble phosphate concentration

Soluble inorganic phosphate (Pi) was measured in four-week-old plants after treatments according to Miller et al. (2022), with minor modifications. Briefly, frozen tissue samples (leaves, roots and nodules) were ground. Deionized water was added to the homogenized samples, mixed, and centrifuged at 13,000 g for 3 minutes, and the clarified supernatant was transferred to a clean tube to quantify Pi content. Aliquots were diluted appropriately and mixed in 96 deep-well plates with HCl and malachite green reagent. After 15 minutes of incubation at room temperature, light absorbance was measured at 660 nm. The sample Pi concentration was determined by reference to a calibration curve using K_2HPO_4. Pi concentration was calculated based on fresh weight of samples. Measurements were performed in triplicate in three independent biological replicates.

Statistical analysis and graphs

Data on gene expression, biomass, Pi content, etc. were analyzed statistically for mean comparisons, between wild type and mutant alleles or between control and treatment conditions, by one-way analysis of variance (ANOVA) and *t*-tests ($P<0.05$). Statistical analyses and graphs were generated using GraphPad Prism software.

Results

Identification of *PHO2* genes in *Medicago truncatula* and phylogenetic analysis

M. truncatula PHO2 genes were identified *via* BLASTP searches using the Phytozome and the Legume Information System (LIS) as databases and known plant PHO2 proteins as queries (Supplementary Table 1). Three separate genes were identified and named *MtPHO2-A* (Medtr4g020620), *MtPHO2-B* (Medtr2g013650) and *MtPHO2-C* (Medtr4g088835) (Figure 1A), keeping Medtr4g020620 as -A, the first *PHO2* gene described in *M. truncatula* (Curtin et al., 2017). Note that Wang et al. (2017) described *Medtr2g013650* as the only *PHO2* gene in Medicago, which we named *MtPHO2-B* to distinguish it from the other two *PHO2* genes we identified.

Detailed *in silico* analysis of the annotated DNA sequences and visualization of raw RNA-seq data (Boschiero et al., 2020), with the Integrative Genomics Viewer (IGV) (Robinson et al., 2011), were used to validate gene structures. These three *MtPHO2* genes shared the typical number (7-9) and arrangement of exons and regulatory elements in the proximal promoter region/5'-UTR (Figure 1A).

Analyses of the 5′-UTR of the three *MtPHO2* genes showed five putative miR399-binding sites (miR399-BS) and PHO-like elements, while only t*MtPHO2-B* presented putative PHR1 binding sites (P1BS) in its 5′-UTR (Figure 1A; Supplementary Figure 2A). Using mature and stem-loop sequences of known miRNA399s obtained from miRbase (www.mirbase.org), up to 10 different miRNA399 species (miR399a to j) were identified in the *M. truncatula* genome. Sequence alignment distinguished up to 5 different variants of miR399 (Supplementary Figure 2B) that potentially could target the miR399BS identified within the 5′-UTR of the *MtPHO2* genes. Depending on the miR399BS, mismatches were identified in the central or toward the 3′ ends of the miR399s sequences.

The *MtPHO2-A* gene was predicted to have three splicing isoforms (Supplementary Figure 1A). Amino acid sequence alignment and phylogenetic analysis of the 81 PHO2 proteins identified in the sequenced plant genomes revealed phylogenetic patterns, grouping into clades. Except for the Poales order, most of the PHO2 identified in the databases fell into different plant orders of Eudicots. Gene duplication events were identified in monocots and eudicots, with close evolutionary relationships (92-98% homology). In legumes (order Fabales), two distinct branches associated with the well-known genome duplication event (Cannon et al., 2006) were identified. MtPHO2-A and MtPHO2-B appeared clustered together showing 84% homology at the protein level, while MtPHO2-C clustered in a duplicated branch (Figure 1B) sharing 68% homology with MtPHO2-B and 60% with MtPHO2-A (data not shown).

A detailed analysis revealed that four of the five possible MtPHO2 protein variants (including the three MtPHO2-A variants) conserve the distinctive ubiquitin-conjugating catalytic (UBCc) domain at the C-terminus, including E3 ligase interaction residues and the E2 active site cysteine according to PROSITE database (https://prosite.expasy.org/). MtPHO2-A.3 protein variant was the only exception, lacking the UBCc domain (Supplementary Figure 1B).

MtPHO2 expression is regulated by P and N availability

We investigated the spatial-temporal expression patterns of *MtPHO2* genes. Relative transcript levels, based on sequence fragments per kilobase of transcript per million reads mapped (FPKM) (MtSSPdb; https://mtsspdb.zhaolab.org/database), revealed that *MtPHO2* genes were ubiquitously expressed in different organs and pod developmental stages, although their expression was consistently higher in the root. *MtPHO2-B* had the highest expression level in all the organs evaluated, followed by *MtPHO2-C*. *MtPHO2-A* expression was relatively low in all organs (Figure 2A). Similar expression differences between these genes were detected during nodulation, with only slight changes between 10- and 28-days post inoculation (dpi). Again, *MtPHO2-A* expression levels were very low compared to the other two *MtPHO2* genes (Figure 3A).

Expression profiles determined by qPCR confirmed that in the absence of nutritional deficits, *MtPHO2-B* was the primary *PHO2* transcript in roots and shoots, followed by *MtPHO2-C* and *MtPHO2-A* (Figure 2B). P-limitation resulted in lower transcript levels of *MtPHO2-B* and *MtPHO2-C* in roots. In shoots, only *MtPHO2-B* was down-regulated under P-limitation while *MtPHO2-C* was up-regulated (Figure 2B; Supplementary Figure 3A). N-limitation resulted in up-regulation of *MtPHO2-B* and *MtPHO2-C* in roots and shoots, but no significant change in *MtPHO2-A* transcript levels (Supplementary Figure 3B).

10.3389/fpls.2023.1211107

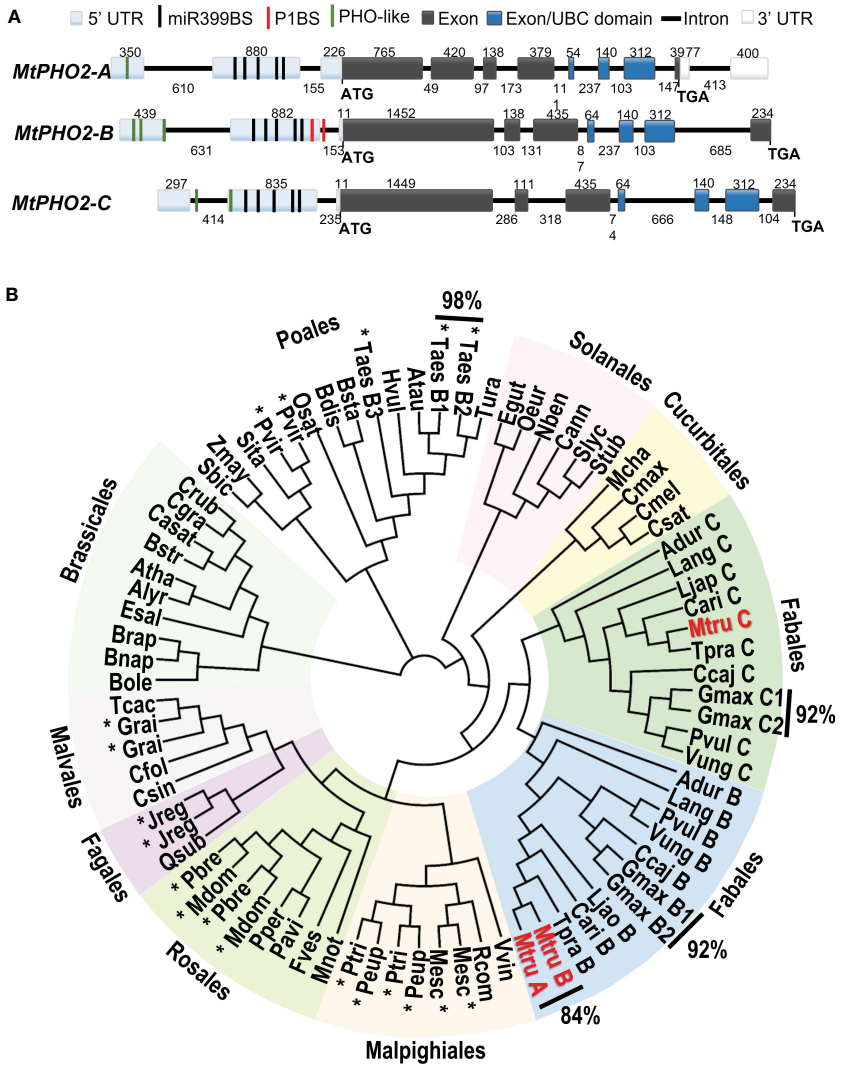

FIGURE 1
Gene structure and phylogenetic relationships of *Medicago truncatula PHO2*-like genes. **(A)** Gene structure of the three *PHO2* genes present in the A17 *Medicago truncatula* genome (Mt4.0v1) and validated using RNA-seq data. Only splicing variant *MtPHO2-A.2* is shown here (see Supplementary Figure 1A for other slicing variants). Exons are shown as grey or darker blue boxes, with the latter encoding the ubiquitin-conjugating (UBC) domain (see also Supplementary Figure 1B). UTRs are shaded light blue (5' of the coding sequence) or white boxes (3' of the coding sequence). The black, green and red lines depict the position within the 5' UTR of the five potential miR399-binding sites (miR399BS), PHO-like elements, and the PHR1 binding sites (P1BS). Promoters and cis-regulatory motifs are detailed in Supplementary Figure 2. Gene structures are drawn to scale, and the associated numbers indicate sizes (numbers above exons and below introns). **(B)** Phylogenetic tree of the *PHO2-like* gene family in plants. The different orders are marked next to different colored backgrounds. The *Medicago truncatula PHO2* genes are indicated in red (MtruA, *MtPHO2-A*; MtruB, *MtPHO2-B*; MtruC, *MtPHO2-C*). The * indicates gene duplication events outside of the order Fabales. Values outside of the Phylogenetic tree show the percentages of homology between MtPHO2A and B proteins as well as some other plant species. The protein sequences were extracted from Phytozome and NCBI Protein databases. The circular phylogenetic tree was constructed from a ClustalW alignment of the full-length protein sequences in Geneious software using Juker-Cantor as the genetic distance model and UPGMA as a tree build method with 500 replicates and 60% of support threshold. The gene IDs encoding each protein are described in Supplementary Table S1.

Expression profiles of the three *MtPHO2* genes in symbiotic, nitrogen-fixing plants were similar to those of non-symbiotic plants, with *MtPHO2-B* exhibiting the highest transcript levels in roots, shoots, and nodules, followed by *MtPHO2-C* and *MtPHO2-A* (Figure 3B; Supplementary Figure 3A). P-limitation under symbiotic conditions down-regulated *MtPHO2-B* in roots and nodules but not shoots. *MtPHO2-B* and *MtPHO2-C*, but not *MtPHO2-A*, were down-regulated in nodules in response to P-limitation (Figure 3B).

Functional characterization of the *MtPHO2* genes under optimal, non-symbiotic conditions

To explore the function of the MtPHO2 proteins, homozygous *pho2-A*$_{CRISPR}$, *pho2-B*$_{CRISPR}$, *pho2-A*$_{Tnt1}$, *pho2-B*$_{TALEN}$ and *pho2-C*$_{Tnt1}$ mutants were used (Supplementary Figure 4). Under optimal, nutrient-replete conditions, lack of MtPHO2-B or MtPHO2-C reduced root and shoot growth, especially in the case of the *pho2-B*$_{CRISPR}$ mutant

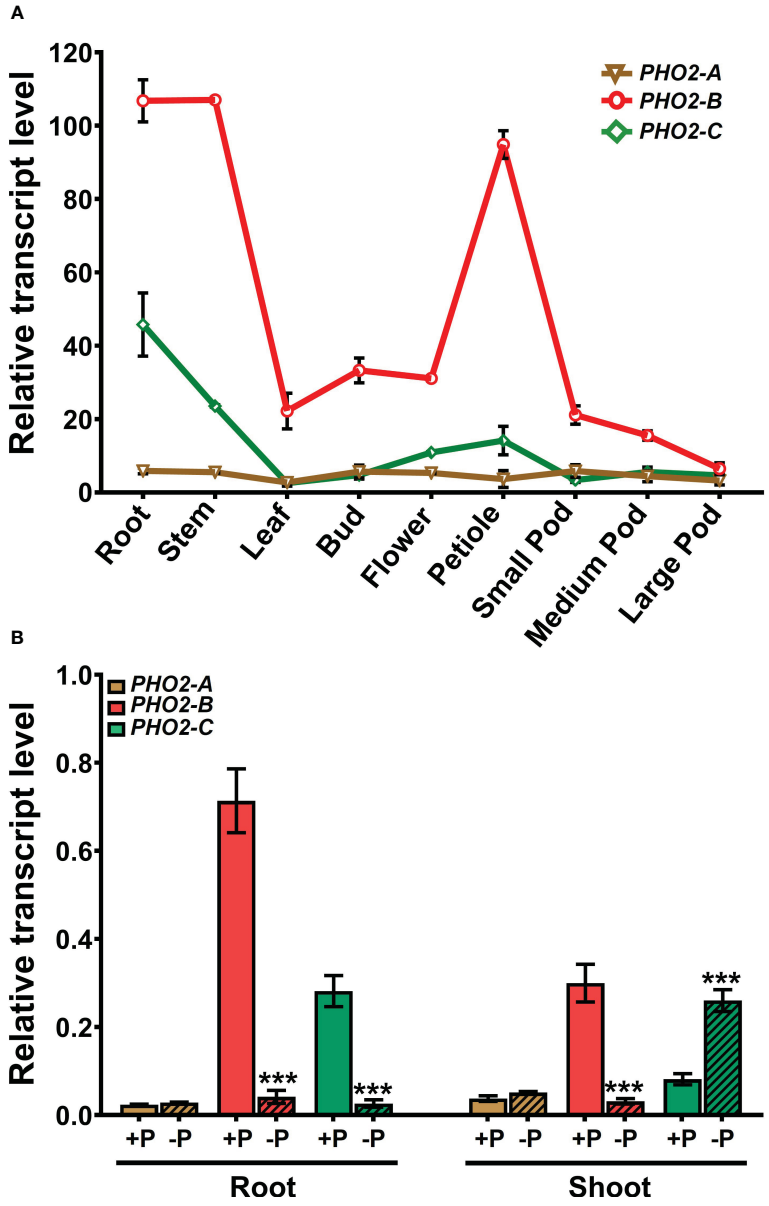

FIGURE 2
Expression profiles of *Medicago truncatula PHO2*-like genes in various organs and treatments.**(A)** Relative transcript levels of *MtPHO2-A*, *B*, *C* in different organs derived from RNA-seq data with numbers indicating fragments per kilobase of transcript per million reads mapped (FPKM) and represent the average of three biological replicates with standard errors. Further details are given in Boschiero et al. (2020) and the *M. truncatula* SSP database (MtSSPdb). **(B)** Relative transcript levels of *MtPHO2-A*, *B* and *C*, determined by qRT-PCR analysis of roots and shoots of four-week-old plants grown under optimal P-nutrition (+P, 0.5 mM Pi) and limiting-P (-P, 20 μM Pi) conditions, as shown in Figure 4 and as described in the methodology. PCR primer sequences are presented in Supplementary Table S2. Data shown are the mean and SEM of three independent experiments (n=6). For each replicate, transcript levels were normalized against two housekeeping genes, *MtPTB2* and *MtPDF2*; asterisks indicate significant differences between the optimal and reduced P (*p < 0.05, **p < 0.01, ***p < 0.001) calculated using two-tailed Student's t-tests.

(Figures 4A, B). Measurement of Pi accumulation in roots, young leaves and fully expanded mature leaves revealed that only the *pho2-B*$_{CRISPR}$ mutant had significantly higher Pi accumulation in mature leaves, compared to the WT, while the *pho2-C*$_{Tnt1}$ mutant showed a slight but significant reduction in Pi content in such leaves (Figure 4C). Plants of each mutant line were also grown in rich soil (Metro-Mix) in a greenhouse under optimal nutritional conditions for analysis of late developmental phenotypes and seed replication. All three mutants grew less than WT plants, although the *pho2-B*$_{CRISPR}$ mutant was the most severely affected, followed by *pho2-C*$_{Tnt1}$ and *pho2-A*$_{CRISPR}$ mutants (Supplementary Figure 5). Stunted growth was accompanied by a decrease in seed production in both the *pho2-B*$_{CRISPR}$ and *pho2-C*$_{Tnt1}$ mutants, especially the former, which also displayed symptoms of necrosis in its mature leaves (Supplementary Figure 5).

10.3389/fpls.2023.1211107

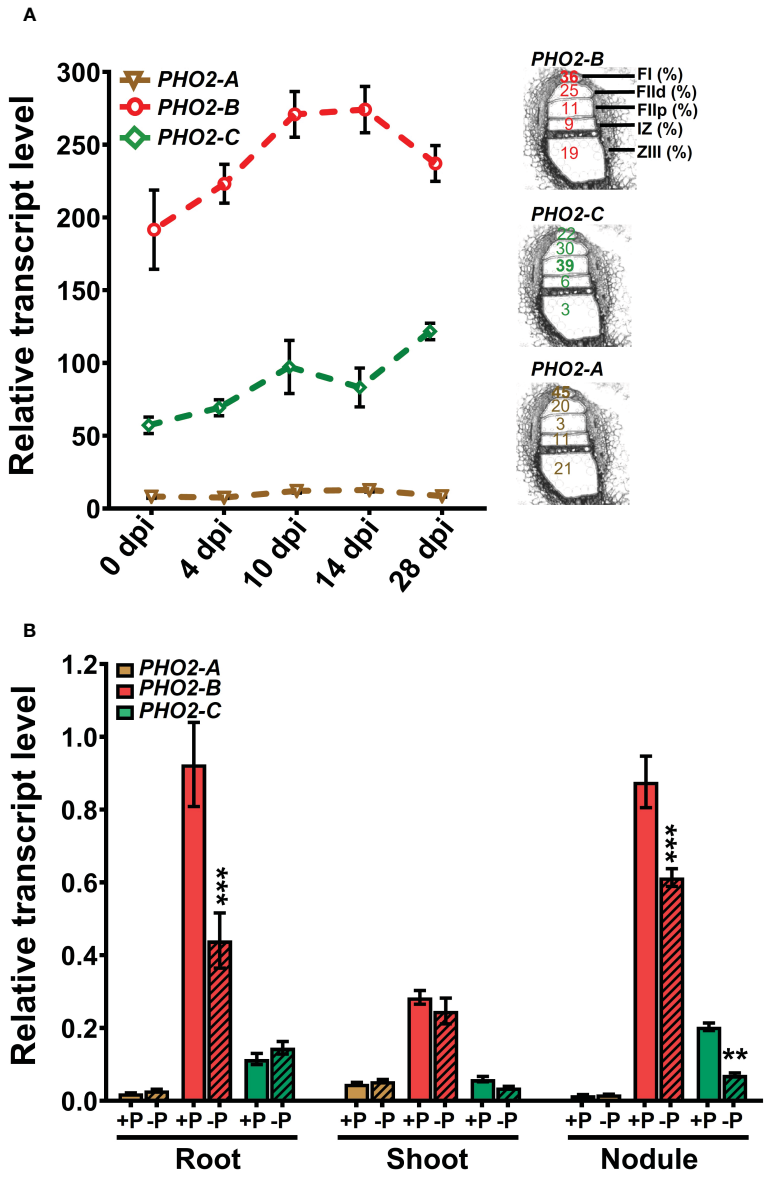

FIGURE 3
Expression profiles of *Medicago truncatula PHO2* genes in various organs and treatments during nodulation. **(A)** Relative transcript levels of *MtPHO2-A*, *B* and *C* in nodules over time. Left, RNA-seq data expressed as fragments per kilobase of transcript per million reads mapped (FPKM) represent the average of three biological replicates with standard errors. Further details are given in the MtSSPdb (Boschiero et al. (2020). Right: scheme of the five laser micro-dissected regions of *M. truncatula* nodules, containing the percentage of normalized counts per region for each *PHO2* gene, according to Roux et al. (2014). **(B)** Relative transcript levels, quantified by qRT-PCR, of *MtPHO2-A*, *B* and *C* genes in four-week-old roots, shoots and nodules of plants grown under symbiotic nitrogen fixation conditions (0.5 mM N and inoculated with *S. meliloti* strain Sm1021) with optimal-P (+P, 0.5 mM P) or reduced-P (-P, 20 µM P), under the same conditions as those shown in Figures 5–8. PCR primer sequences are presented in Supplementary Table 2. Data are the mean and SEM of three independent experiments (n=6 for root and shoot, n=18 for nodules). For each replicate, transcript levels were normalized against two housekeeping genes (*MtPTB2* and *MtPDF2*); asterisks indicate significant differences between optimal- and reduced-P, calculated using two-tailed Student's t-tests (*p < 0.05, **p < 0.01, ***p < 0.001).

Functional characterization of MtPHO2 genes under symbiotic nitrogen fixation conditions

All three mutants, *pho2-A*$_{CRISPR}$, *pho2-B*$_{CRISPR}$ and *pho2-C*$_{Tnt1}$ exhibited reduced growth and biomass under optimal symbiotic conditions, including high Pi (0.5 mM; Figure 5). Again, mature leaves of the *pho2-B*$_{CRISPR}$ mutant, but not the other mutants, exhibited necrotic symptoms (Figures 5A, B). Measurements of organ Pi content revealed hyper-accumulation of Pi in young and especially mature leaves of the *pho2-B*$_{CRISPR}$, which was mirrored by a drastic decrease in Pi content of its roots. Pi also accumulated in older leaves of both the *pho2-A*$_{CRISPR}$ and *pho2-C*$_{Tnt1}$ mutants relative to the WT (Figure 5C).

Traits related to SNF were differentially affected in the three mutants. The *pho2-A*$_{CRISPR}$ mutant showed a reduced number of nodules compared to the WT, but with similar biomass and nitrogenase activity (Figures 6A-E). The *pho2-B*$_{CRISPR}$ mutant was

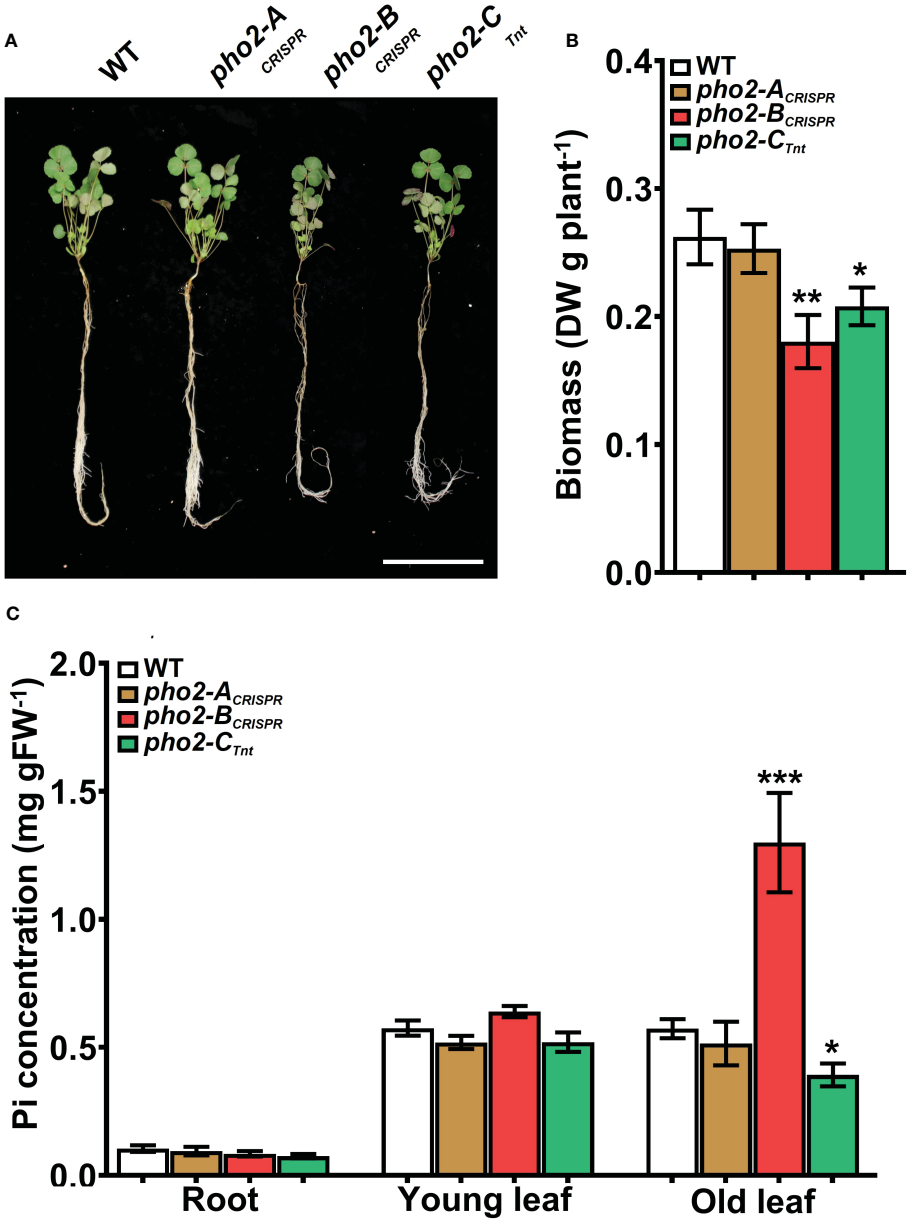

FIGURE 4
Performance of the *pho2* mutants under optimal nutritional conditions. **(A)** Representative four-week-old plants growth under optimal nutritional conditions, including 0.5 mM Pi. Scale bar = 10 cm. **(B)** Plant dry weight. **(C)** Free phosphate (Pi) concentration in roots, young and old leaves. Data shown are the mean and SEM of three independent experiments (n=5 per experiment). Asterisks indicate significant differences between the wild type and the mutants calculated using two-tailed Student's t-tests (*p < 0.05, **p < 0.01, ***p < 0.001).

affected in all the traits evaluated, with reduced number and biomass of nodules, as well as nitrogen fixation capacity. Likewise, *pho2-*C_{Tnt1} exhibited reduced nodule number, biomass and nitrogen fixation (Figures 6A-E). Loss of gene function had a variable effect on nodule Pi concentration, with the *pho2-*B_{CRISPR} accumulating less, *pho2-*A_{CRISPR} accumulating more, and *pho2-*C_{Tnt1} accumulating the same concentration as the WT (Figure 6B).

P-limitation reduced WT plant growth, biomass, nodule number and biomass, nitrogen fixation, and Pi concentration in all organs relative to P-replete plants (compare Figures 7, 8 with Figures 5, 6, respectively). Even so, *pho2-*B_{CRISPR} and *pho2-*C_{Tnt1} mutants were smaller than the WT under P-limiting conditions (Figures 7A, B). The reduced size of these two mutants was accompanied by a moderate but significant accumulation of Pi in mature leaves compared to the WT (Figure 7C). *pho2-*B_{CRISPR} and *pho2-*C_{Tnt1} mutants also exhibited defects in symbiotic traits, including reduced nodule biomass and nitrogen fixation (Figures 8C-E). Interestingly, reduced nodule biomass resulted

10.3389/fpls.2023.1211107

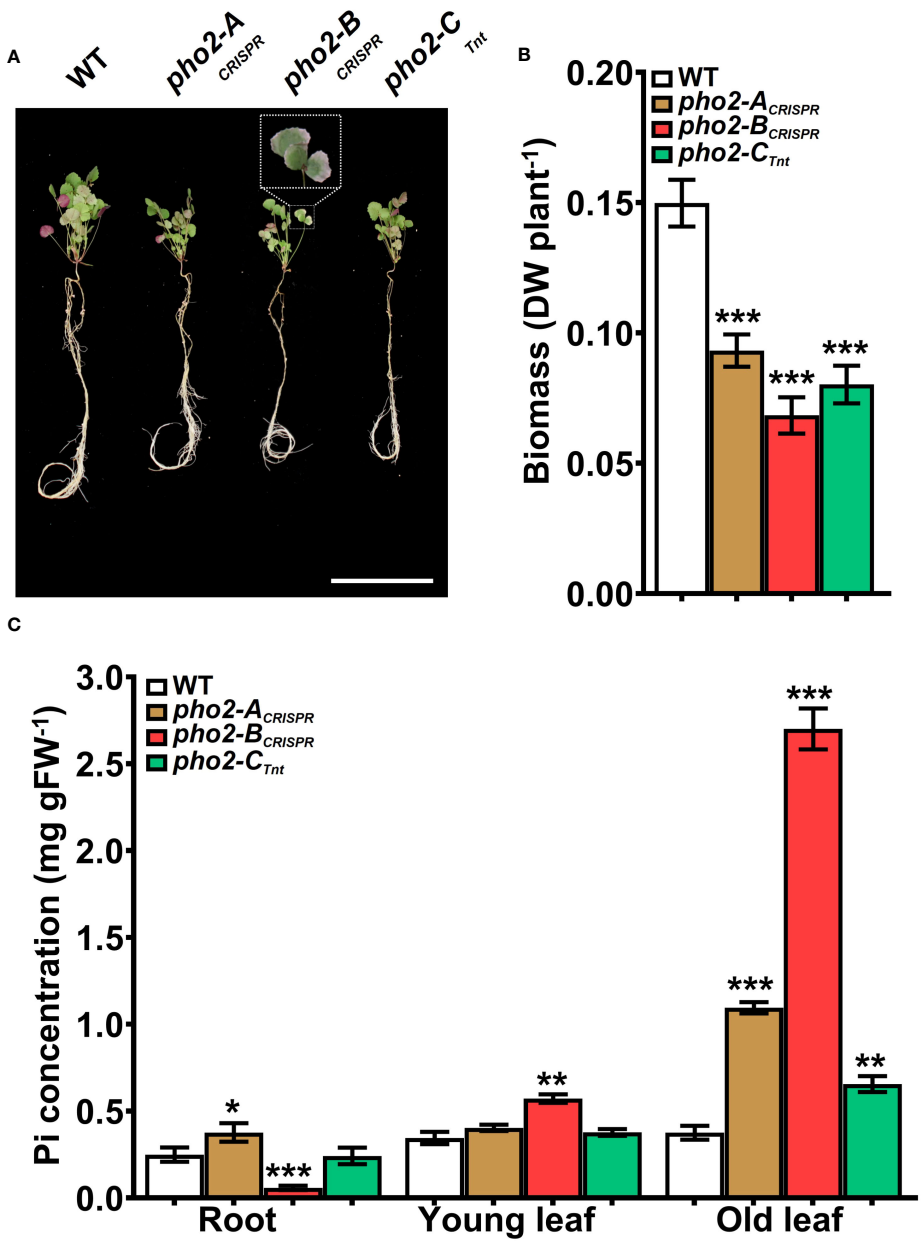

FIGURE 5
Performance of the Mt*pho2* mutants under symbiotic nitrogen fixation conditions. Plants were inoculated with *S. meliloti* strain Sm1021 and given optimal-P (0.5 mM Pi). **(A)** Representative four-week-old plants. Scale bar = 10 cm. **(B)** Plant dry weight. **(C)** Free phosphate (Pi) concentration in roots, young and old leaves. Data shown are the mean and SEM of three independent experiments (n=5/experiment). Asterisks indicate significant differences between the wild type and the mutants calculated using two-tailed Student's t-tests (*p < 0.05, **p < 0.01, ***p < 0.001).

from reduced nodule number of *pho2-*C_{Tnt1} but not *pho2-*B_{CRISPR}, which produced the same number of nodules as the wild-type, albeit smaller (Figure 8).

Transcriptomic responses associated with Pi content modifications

To better understand the role of PHO2 homologs in Pi homeostasis, we measured the expression levels of eight *MtPT/PHT1-like*, five *MtPHO1-like*, three nitrogen limitation adaptation (NLA) and three PHR1-like genes in roots and shoots of WT and mutant plants (Supplementary Table 2). Quantification of expression levels by qPCR revealed that all *MtPT/PHT1-like* and *MtPHO1-like* transporters were induced by P-limitation (data not shown). In the absence of nutritional deficits, *MtPT5*, *MtPT3* and *MtPT13* transporters were highly upregulated in roots and/or shoots of *pho2-*B_{CRISPR} plants compared to the WT plants, whereas *MtPT5* was slightly upregulated in shoots of *pho2-*A_{CRISPR} plants (Figure 9A). Under symbiotic conditions without P limitation, the three mutant alleles presented deregulation of the expression levels of *MtPT/PHT1-like* transporters. The expression

10.3389/fpls.2023.1211107

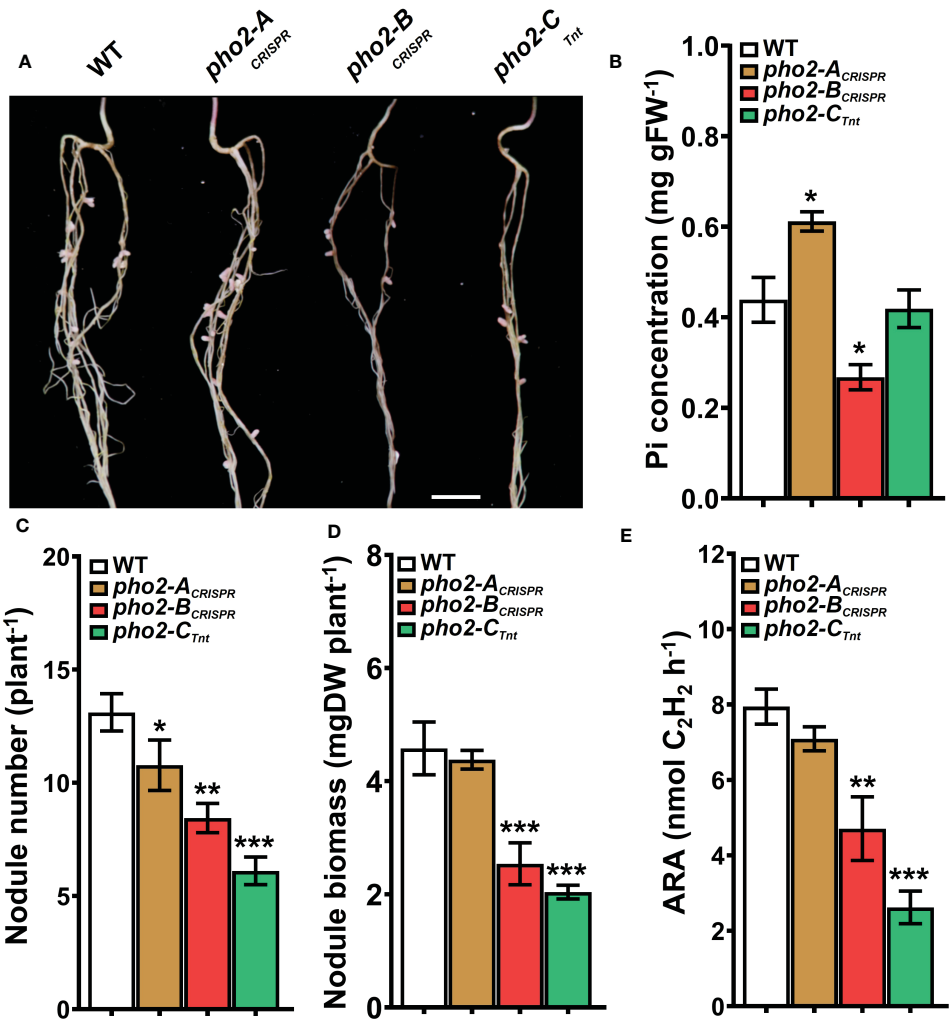

FIGURE 6
Symbiotic phenotypes of the Mt*pho2* mutants with optimal-P. **(A)** Nodulated roots at 21 dpi with *S. meliloti* strain Sm1021. Scale bar = 1 cm. **(B)** Free phosphate (Pi) concentration in nodules **(C)** Average nodule number. **(D)** Average nodule biomass. **E)** Acetylene reduction assay (ARA) on whole nodulated roots. Data shown are the mean and SEM of three independent experiments (n=5/experiment). Asterisks indicate significant differences between the wild type and mutants calculated using two-tailed Student's t-tests (*p < 0.05, **p < 0.01, ***p < 0.001).

levels of *MtPT5*, *MtPT3*, *MtPT6* and *MtPHO1;3* transporters were deregulated in roots and/or shoots of *pho2-B*$_{CRISPR}$ plants compared to the WT plants. These transporters, except for *MtPHO1;3*, also showed deregulation in their expression levels in *pho2-A*$_{CRISPR}$ plants, but more moderate than those in *pho2-A*$_{CRISPR}$ plants. Similarly, *MtPT5*, *MtPT6* and *MtPHO1;3* transporters were deregulated in roots and/or shoots of *pho2-C*$_{CRISPR}$ plants compared to the WT plants. Although *MtPT6* was upregulated at different levels in roots and shoots of all the three mutants, it was the only transporter upregulated in the nodule of the *pho2-A*$_{CRISPR}$ mutant compared with the WT plants (Figure 9B).

Discussion

PHOSPHATE2 (*PHO2*) genes encode PHO2/Ubiquitin-Conjugating E2 24 (UBC24) proteins. The role of PHO2 proteins in regulating inorganic phosphate (Pi) homeostasis and Pi translocation and remobilization has been illuminated using mutants of Arabidopsis (Bari et al., 2006), rice (Cao et al., 2014), common wheat (Ouyang et al., 2016), and alfalfa (Miller et al., 2022), and transient silencing in barley (Pacak et al., 2010; Pacak et al., 2016) and citrus (Wang et al., 2020). The regulatory role of PHO2 in Pi homeostasis is based on its joint action with E3 ligases to polyubiquitinate and degrade Pi transporters, thus controlling Pi translocation, accumulation and/or remobilization in plant tissues when P is not limiting. Under P limitation, turnover of Pi transporters is prevented by undermining PHO2 protein production *via* microRNA399 (miR399)-guided*PHO2* mRNA degradation, orchestrated by the transcription factor PHOSPHATE STARVATION RESPONSE 1 (PHR1) (Aung et al., 2006; Bari et al., 2006).

Although some species, e.g. Arabidopsis and rice (Bari et al., 2006; Cao et al., 2014), have a single *PHO2* gene, others have more than one, which begs the question of their roles in P-homoeostasis or other plant processes. For instance, autotetraploid alfalfa has two

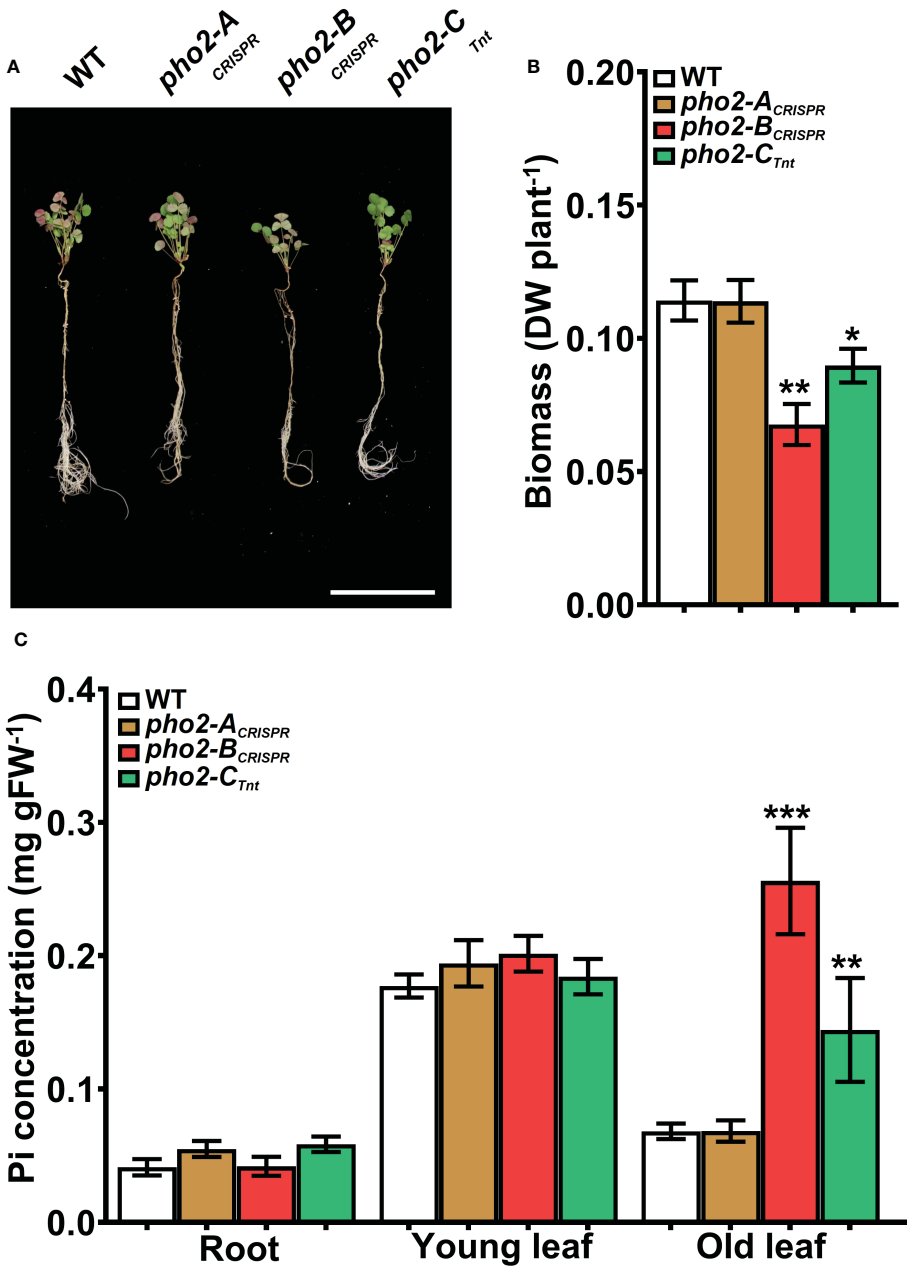

FIGURE 7
Performance of the *Mtpho2* mutants under symbiotic nitrogen fixation conditions. Plants were inoculated with *S. meliloti* strain Sm1021 and given reduced-P (20 µM Pi). **(A)** Representative four-week-old plants. Scale bar = 10 cm. **(B)** Plant dry weight. **(C)** Free phosphate (Pi) concentration in roots, young and old leaves. Data shown are the mean and SEM of three independent experiments (n=5/experiment). Asterisks indicate significant differences between the wild type and the mutants calculated using two-tailed Student's t-tests (*p < 0.05, **p < 0.01, ***p < 0.001).

PHO2 genes, with multiple haplotypes of each. However, only one of the two alfalfa PHO2 proteins seems to have a role in P-homeostasis (Miller et al., 2022).

Here, we used sequence and phylogenomic analysis to identify three different *PHO2* genes in the *Medicago truncatula*, encoding up to five possible PHO2 proteins, including splice variants (Figure 1; Supplementary Figure 1). In addition to having three *PHO2* genes, the presence of splicing isoforms adds an extra level of complexity that may have biological significance. Alternate splicing to produce different functional proteins is a tightly regulated process essential for plants development and adaptation to environment (Huertas et al., 2019). In fact, *PHO2* transcript splicing is regulated by P stress in rice (Secco et al., 2013), while Arabidopsis produces a shorter spliced form of its single *PHO2* gene transcript that does not contain miR399 binding sites, to escape from miR399 mediated target degradation (Scheible et al., 2023). Two splice variants of different length have been reported for *PHO2* in barley (Pacak et al., 2016) but have not been characterized. Interestingly, detailed study of splicing events in tomato under P stress revealed none in *SlPHO2* (Tian et al., 2021), suggesting that alternative splicing of *PHO2* transcript may not occur in all species and/or conditions. It is interesting that one of the Medicago splice variants, Mt*PHO2-A.3*, which lacks its UBC catalytic domain sequences

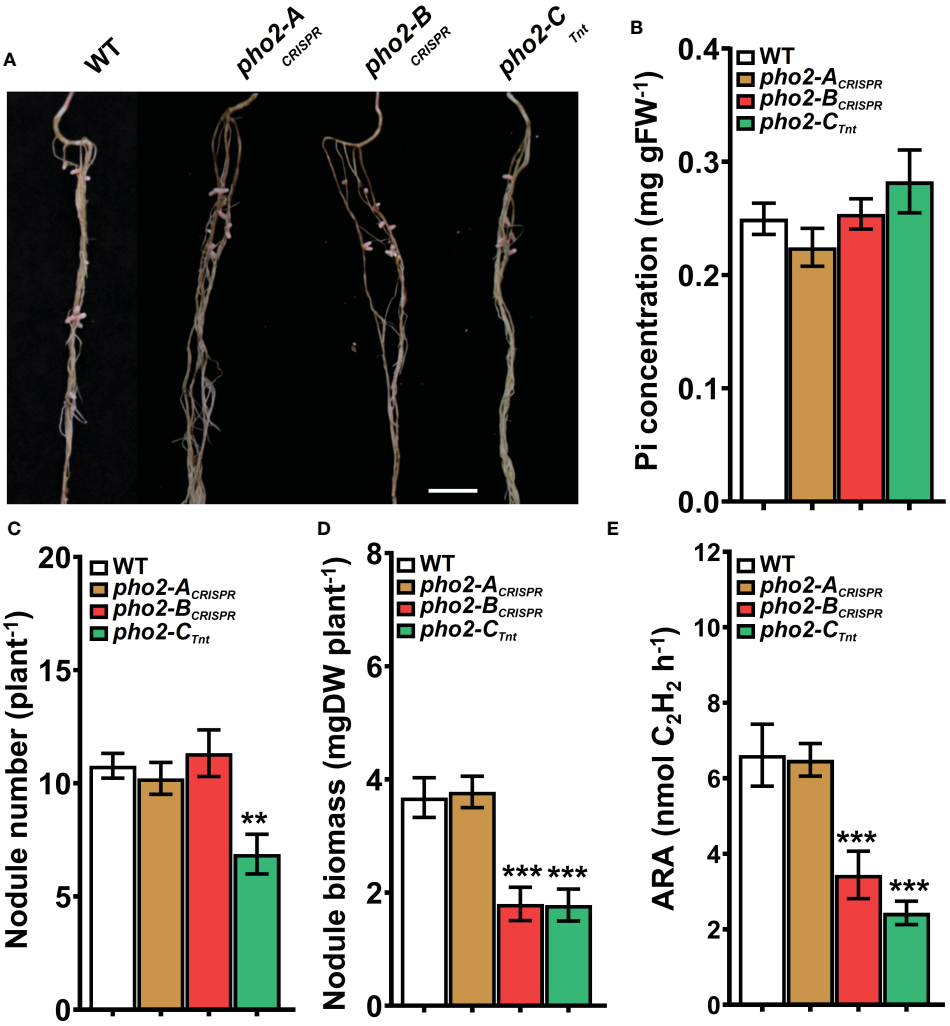

FIGURE 8
Symbiotic phenotypes of the *Mtpho2* mutants with reduced-P. **(A)** Nodulated roots at 21 dpi with *S. meliloti* strain Sm1021. Scale bar = 1 cm. **(B)** Free phosphate (Pi) concentration in nodules **(C)** Average nodule number. **(D)** Average nodule biomass. **(E)** Acetylene reduction activity (ARA) of whole nodulated roots. Data shown are the mean and SEM of three independent experiments (n=5/experiment). Asterisks indicate significant differences between the wild type and mutants calculated using two-tailed Student's t-tests (*p < 0.05, **p < 0.01, ***p < 0.001).

(Supplementary Figure 1), has a counterpart in rice (Dong et al., 2018). Further work is required to understand what role, if any, such a protein plays in Medicago and rice.

Transcript expression levels of the *PHO2* genes are modulated by nutritional status, being normally repressed in roots and shoots by P limitation (Bari et al., 2006; Hackenberg et al., 2013; Cao et al., 2014; Ouyang et al., 2016; Wang et al., 2017; Miller et al., 2022; Santoro et al., 2022). Recent reports in Arabidopsis, tomato and barley revealed that *PHO2* genes also can alter their expression as a function of N levels, indicating their integrative role between P and N homeostasis (de Souza Campos et al., 2019; Medici et al., 2019; Marro et al., 2022). Remarkably, some *PHO2* genes, however, have different time-, intensity-, and genotype-dependent transcriptomic responses under P limitation (de Souza Campos et al., 2019; Gamir et al., 2020), indicating complex spatial-temporal Pi starvation signaling. Modulation of *PHO2* transcripts requires recognition of *PHO2* mRNAs by miR399s, regulated in turn by the transcription factor PHR1. Thus, the presence of five different miR399-BS conserved in the 5′-UTR of the three *MtPHO2* genes underscores their likely role in P regulation (Figure 1A; Supplementary Figure 2). The high identity between the 10 *Medicago truncatula* miR399s and miR399-BSs on their 5′-UTR (Supplementary Figure 2) suggests their potential to cleave *MtPHO2* mRNAs. Although we did not validate miR399 cleavage, the high homology of the Medicago miR399 and miR399-BS sequences with those of other plant species already validated *in vitro* (Aung et al., 2006; Bari et al., 2006; Hackenberg et al., 2013; Xu et al., 2013; Miller et al., 2022) or by transient expression (Ouyang et al., 2016), strongly suggest their cleavage capabilities. Indeed, regulation of expression of *MtPHO2-B* by a miR399 has already demonstrated indirectly through the mutation of the Medicago *PDIL1* (Wang et al., 2017), a Pi deficiency-responsive At4-like lncRNA that suppresses the effect of miR399 by acting as mimics of PHO2 (Franco-Zorrilla et al., 2007). Interestingly, *MtPHO2-B* gene also contain a PHR1-binding DNA sequence (P1BS) motif. To our knowledge, this is the first description of the P1BS motif in a *PHO2* gene, suggesting direct PHR1-dependent regulation in addition of the mediated regulation by the various

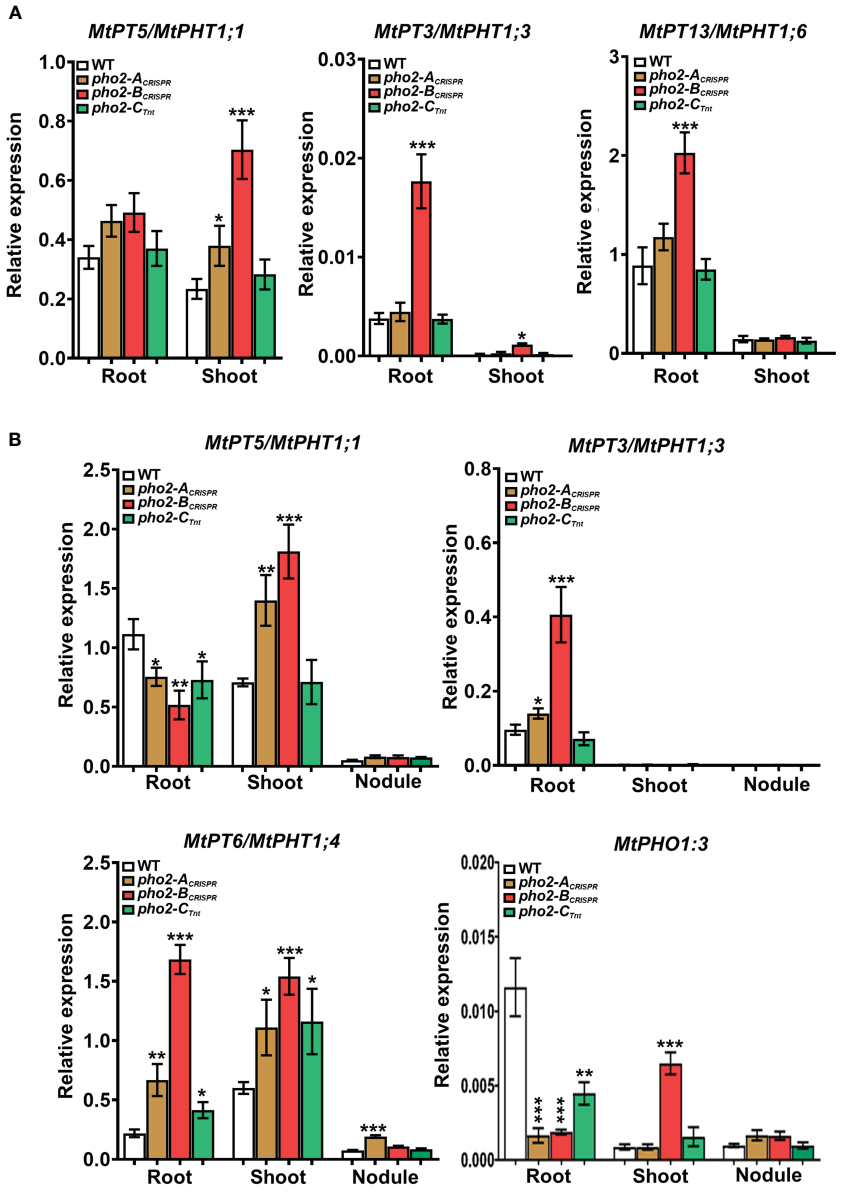

FIGURE 9
Relative expression levels, quantified by qPCR, of *MtPHT1-like* genes in various experimental conditions and organs **(A)** Optimal-P. **(B)** Symbiotic nitrogen fixation with optimal-P. PCR primers used are included in Supplementary Table S2. Data shown are the mean and SEM of three independent experiments. Plants were grown under the same conditions as those shown on Figures 4–8. For each replica, copy numbers were normalized using the mean average of two housekeeping genes (MtPTB2 and MtPDF2); asterisks indicate significant differences between the WT and mutants in each tissue of the same condition calculated using two-tailed Student's t-tests (*$p < 0.05$, **$p < 0.01$, ***$p < 0.001$). Double nomenclature (PT/PHT) due to Breuillin-Sessoms et al., 2015. Plant Cell. 27(4):1352-66.999.

miR399s. The presence of miR399s variants and cis-regulatory elements (Figure 1A; Supplementary Figure 2) could lead to different post-transcriptional regulations that could explain the different levels of expression and/or transcriptomic responses between the *MtPHO2-B* and *MtPHO2-C* genes to the P nutritional status in the plant (Figures 2, 4), suggesting then a differential role for both genes. Likewise, Mt*PHO2-B*, and to a much lesser extent *MtPHO2-C*, are induced by N limitation in roots and shoots (Supplementary Figure 3), suggesting a similar regulation dependent on the N status of the plant.

The impaired growth observed under control conditions by the lack of the protein MtPHO2-B can directly be associated with un unbalanced Pi homeostasis due to Pi hyperaccumulation in old mature leaves (Figure 4). This is the result of a deficiency PHO2-dependent degradation of Pi transporters, altering Pi movement between tissues and organs and preventing Pi from being used properly by the plant (Huang et al., 2013; Park et al., 2014). Taken together, our results identify MtPHO2-B as the functional ortholog of the characterized PHO2 proteins (Aung et al., 2006; Bari et al.,

2006; Cao et al., 2014; Ouyang et al., 2016; Miller et al., 2022), integral to Pi homeostasis in the absence of nutritional deficits. Similarly, the reduced plant growth in the absence of the protein MtPHO2-C can also be associated with an imbalanced P homeostasis. However, since *pho2* mutants are described as Pi hyperaccumulators (Aung et al., 2006; Bari et al., 2006) and the *M. truncatula* mutant has a marginal, albeit significant, reduction in Pi content in old leaves (Figure 4), our results implies that *MtPHO2-C* is not a functional ortholog of the characterized PHO2, although it does appear to have a role in Pi homeostasis. The proposed secondary role controlling Pi homeostasis is in line with results recently described for the alfalfa homologous *PHO2-C*, where mutations of the different haplotypes lead to limited Pi hyperaccumulation possibility because to the inability of miR399s to cleave *MtPHO2-C* mRNAs (Miller et al., 2022). Demonstrating the role of the MtPHO2-C proteins in Pi homeostasis, regardless of any putative role in plant development (Supplementary Figure 5), will require further experiments. Likewise, the reduced expression levels and lack of transcriptomic response to P limitation suggest a limited role in controlling Pi homeostasis, or compensation by the other two MtPHO2 proteins. This is partially supported by the absence of phenotypes in the mutant alleles during the early stages of development but does not rule out a long-term role in regulating certain levels of Pi necessary to support plant growth (Supplementary Figure 5). In fact, *Medicago truncatula* is more sensitive to elevated Pi content compared with most other leguminous and non-leguminous plant species (Sulieman et al., 2013), so it is possible to reason that it also requires a finely tuned Pi homeostasis, controlled by multiple PHO2 activities.

Symbiotic nitrogen fixation (SNF) is a complex series of physical and chemical interactions built upon the trading of reduced carbon (C) from a legume for reduced N from the compatible symbiont. Atmospheric nitrogen (N_2), once fixed in the root nodules, is partially transported to the aerial parts of the plant supporting multiple metabolic processes (Roy et al., 2020). The intensive C turnover during nodule development and N_2 fixation are energy-consuming processes, requiring a large amount of P (Cabeza et al., 2014), as well as a limited presence of mineral N to promote nodule development without actually inhibiting N_2 fixation (Ferguson et al., 2019). Under this condition of mineral N deprivation, most of the N available for plant use is obtained from the N_2 fixation, so plants need a fine adjustment of Pi homeostasis in the nodule coordinated with the whole-plant Pi homeostasis (Sulieman & Tran, 2015; Sulieman et al., 2019). Such level of coordination in *Medicago truncatula* seems to be provided by the three MtPHO2 proteins, although the protein PHO2-B has a leading role in maintaining Pi homeostasis, as evidenced by the huge Pi hyperaccumulation not only in old leaves but also in young leaves, while it locally disappears from the roots (Figure 5C) and nodules (Figure 6B) in the *pho2-B* mutant. To our knowledge, this is the first time that a *pho2* mutant imbalances Pi throughout the whole plant, including nodules. The abnormal distribution of Pi impacts nodule formation and development, causing the reduction in N_2 fixation activity (Figures 6C, D) (Hernandez et al., 2009), impairing plant growth (Figures 5A, B). Thus, although plants preferentially distribute available Pi to the nodules to maintain symbiotic N_2 fixation (Cabeza et al., 2014; Sulieman & Tran, 2015), our results confirm that nodule Pi homeostasis is subordinated to the whole-plant Pi homeostasis. Nevertheless, Pi homeostasis under SNF is not regulated by a single *MtPHO2* gene. Even if at a lower scale than MtPHO2-B, the proteins MtPHO2-C and MtPHO2-A are also necessary to maintain whole-plant Pi homeostasis, the latter controlling Pi accumulation in roots and old leaves (Figure 5), and specially regulating Pi content for the formation of nodules (Figures 6B, D). The fact that neither the diploid nor the tetraploid alfalfa genome contains an orthologous *MtPHO2-A* gene while it is present in the wild relative *Medicago ruthenica* (Wang et al., 2021; Miller et al., 2022) and in *Medicago truncatula* genomes, evidence the evolutionary importance of this gene controlling quantitative variation for nodule formation (Stanton-Geddes et al., 2013; Curtin et al., 2017). Therefore, we can speculate that MtPHO2-A gene diverged from MtPHO2-B (Figure 1B) to support a finely tuned Pi homeostasis, especially in root nodules.

Symbiotic nitrogen fixation under limited mineral P is severely impacted by reducing the formation and the development of nodules, reducing the fixed N_2 to be used by the plant (Figure 8) (Sulieman et al., 2013). In these conditions, MtPHO2-A protein does not seem to play a relevant role in the whole-plant Pi homeostasis while MtPHO2-B and MtPHO2-C proteins continue to exert some Pi regulatory capacity (Figure 7), necessary to regulate SNF traits (Figure 8). This, which could be somewhat unexpected since the role of PHO2 proteins, associated with the regulation of Pi when it is in excess, is necessary to coordinate N and P homeostasis (Liese et al., 2017; Medici et al., 2019) of the nodules to use Pi efficiently according to N availability. However, the reduced SNF due to P limitation also involves a lower degree of N_2 assimilation, and therefore it is expected that plants exhibit local and/or systemic N-limited-related responses. As mentioned earliest, *MtPHO2-B* and *MtPHO2-C* genes are both induced by N deficiency (Supplementary Figure 3), but their tissue-dependent transcriptomic responses to mineral N and P limitation suggest common functions within the nodule, but also some type of speciation between tissues (Figure 3B). In tomato, for example, Pi starvation signaling depends on the plant's N status, such that the downregulation of *SlPHO2* by Pi deficiency happens only under optimal N conditions, whereas it can be upregulated by N deficiency only under optimal P conditions (Marro et al., 2022). Our results point here, indicating that both proteins MtPHO2-B and MtPHO2-C have a similar role, coordinating whole-plant P and N homeostasis to sustain plant growth.

Overall, our results confirm that under mineral N deprivation, the fine adjustment of Pi homeostasis is primarily due to the integral action of MtPHO2-B, assisted by the action of MtPHO2-C and MtPHO2-A. The latter also seems to have a specific role regulating nodule Pi homeostasis associated to nodule formation.

Tissue hyperaccumulation of Pi in *pho2* mutants is known to result in local Pi limitation in other plant tissues and organs. To compensate for this local Pi limitation, these plants alter the expression levels of PHO1-like and PT/PHT1-like transporters, components of the P starvation response (PSR) (Aung et al., 2006; Bari et al., 2006; Hu et al., 2011; Liu et al., 2012; Huang et al., 2013; Ouyang et al., 2016). In fact, some of the PT/PHT1 transporters targeted by the PHO2-E3 complex to be degraded can

increase their mRNA levels in the pho2 mutants (Huang et al., 2013; Lin et al., 2013). Under non-limiting nutritional conditions, only the lack of MtPHO2-B protein resulted in a higher expression of MtPT5, MtPT3 and MtPT13 in roots and/or shoots compared to WT (Figure 9A), affirming that PHO2-B is the main regulator of Pi homeostasis in Medicago truncatula. Although it is not possible to know if these changes are directly or indirectly linked to MtPHO2-B activity, the fact that there are no differences in the others individual mutants, points at these Pi transporters as PHO2-E3 targets for future experiments in *Medicago truncatula*.

The different patterns of Pi hyperaccumulation also lead to transcriptomic responses of the PSR components during SNF. Interestingly, although the genes *MtPHO2-B* and *MtPHO2-C* are the more abundant *MtPHO2* genes within the nodules (Figure 3) (Roux et al., 2014), the lack of these individual proteins did not alter the expression of any of the Mt*PHO1-like* and Mt*PT/PHT1-like* genes in the nodules, but in roots and/or shoots (Figure 9B), supporting their role in maintaining whole-plant Pi homeostasis instead of nodule Pi homeostasis. These results contrast with the fact that some of the *PHO1-like* and *PT/PHT1-like* transporters, expressed between the root vascular system and vascular bundles of nodules, are crucial to maintain the Pi reallocation and homeostasis in young and mature nodules (Qin et al., 2012; Chen et al., 2019; Lu et al., 2020; Nguyen et al., 2021). On the contrary, the lack of the protein MtPHO2-A altered the expression of Mt*PT6/PHT1;4* in nodules (Figure 9B), one of the two *PT/PHT1-like* transporters that are induced during nodulation according to the MtSSPdb (Boschiero et al., 2020; https://mtsspdb.zhaolab.org/atlas-internal), which support the unique role of MtPHO2-A in maintaining Pi homeostasis in the nodule. New studies are needed to determine the role of MtPT6-like in SNF and the different variants of the MtPHO2-A protein, and a much more specific approach is required to determine the ubiquitination targets of the MtPHO2-E3 complex during SNF without P limitation.

Data availability statement

The original contributions presented in the study are included in the article/Supplementary Material. Further inquiries can be directed to the corresponding authors.

Author contributions

RH: conceptualization, methodology, investigation, formal analysis – tables and figures, writing - original draft, review and editing final manuscript; IT-J: methodology (RNA isolation and qPCR reactions); SJC: methodology (provided the biological material to isolate some of the mutant alleles) and editing; WS: supervision and editing; MU: review and editing final manuscript, supervision and funding. All authors contributed to the article and approved the submitted version.

Funding

This work was supported by the Noble Research Institute LLC. Noble Research Institute was not involved in the study design, collection, analysis, interpretation of data, the writing of this article, or the decision to submit it for publication. SJC was supported by the U.S. Department of Agriculture, Agricultural Research Service. Mention of any trade names or commercial products in this article is solely for the purpose of providing specific information and does not imply recommendation or endorsement by the U. S. Department of Agriculture. USDA is an equal opportunity provider and employer, and all agency services are available without discrimination.

Conflict of interest

Authors RH, IT-J, WS and MU are/were employed by the Noble Research Institute, LLC.

All the authors declare that the research was conducted without any commercial or financial relationships that could be construed as a potential conflict of interest.

Publisher's note

Supplementary material

The Supplementary Material for this article can be found online at: https://www.frontiersin.org/articles/10.3389/fpls.2023.1211107/full#supplementary-material

References

Aung, K., Lin, S. I., Wu, C. C., Huang, Y. T., Su, C. L., and Chiou, T. J. (2006). pho2, a phosphate overaccumulator, is caused by a nonsense mutation in a microRNA399 target gene. *Plant Physiol.* 141 (3), 1000–1011. doi: 10.1104/pp.106.078063

Bari, R., Datt Pant, B., Stitt, M., and Scheible, W. R. (2006). PHO2, microRNA399, and PHR1 define a phosphate-signaling pathway in plants. *Plant Physiol.* 141 (3), 988–999. doi: 10.1104/pp.106.079707

Boschiero, C., Dai, X., Lundquist, P. K., Roy, S., Christian de Bang, T., Zhang, S., et al. (2020). MtSSPdb: the medicago truncatula small secreted peptide database. *Plant Physiol.* 183 (1), 399–413. doi: 10.1104/pp.19.01088

Breuillin-Sessoms, F, Floss, DS, Gomez, SK, Pumplin, N, Ding, Y, Levesque-Tremblay, V,, et al. (2015). Suppression of arbuscule degeneration in Medicago truncatula phosphate transporter4 mutants is dependent on the ammonium

transporter 2 family protein AMT2; 3. *The Plant Cell*. 27(4):1352-66. https://doi.org/10.1105/tpc.114.131144

Broughton, W. J., and Dilworth, M. J. (1971). Control of leghaemoglobin synthesis in snake beans. *Biochem. J.* 125 (4), 1075–1080. doi: 10.1042/bj1251075

Bustos, R., Castrillo, G., Linhares, F., Puga, M. I., Rubio, V., Perez-Perez, J., et al. (2010). A central regulatory system largely controls transcriptional activation and repression responses to phosphate starvation in arabidopsis. *PloS Genet.* 6 (9), e1001102. doi: 10.1371/journal.pgen.1001102

Cabeza, R. A., Liese, R., Lingner, A., von Stieglitz, I., Neumann, J., Salinas-Riester, G., et al. (2014). RNA-Seq transcriptome profiling reveals that medicago truncatula nodules acclimate N(2) fixation before emerging p deficiency reaches the nodules. *J. Exp. Bot.* 65 (20), 6035–6048. doi: 10.1093/jxb/eru341

Cannon, S. B., Sterck, L., Rombauts, S., Sato, S., Cheung, F., Gouzy, J., et al. (2006). Legume genome evolution viewed through the medicago truncatula and lotus japonicus genomes. *Proc. Natl. Acad. Sci. U.S.A.* 103 (40), 14959–14964. doi: 10.1073/pnas.0603228103

Cao, Y., Yan, Y., Zhang, F., Wang, H. D., Gu, M., Wu, X. N., et al. (2014). Fine characterization of OsPHO2 knockout mutants reveals its key role in pi utilization in rice. *J. Plant Physiol.* 171 (3-4), 340–348. doi: 10.1016/j.jplph.2013.07.010

Cermak, T., Curtin, S. J., Gil-Humanes, J., Cegan, R., Kono, T. J. Y., Konecna, E., et al. (2017). A multipurpose toolkit to enable advanced genome engineering in plants. *Plant Cell* 29 (6), 1196–1217. doi: 10.1105/tpc.16.00922

Chen, L., Qin, L., Zhou, L., Li, X., Chen, Z., Sun, L., et al. (2019). A nodule-localized phosphate transporter GmPT7 plays an important role in enhancing symbiotic N(2) fixation and yield in soybean. *New Phytol.* 221 (4), 2013–2025. doi: 10.1111/nph.15541

Chiou, T. J., Aung, K., Lin, S. I., Wu, C. C., Chiang, S. F., and Su, C. L. (2006). Regulation of phosphate homeostasis by MicroRNA in arabidopsis. *Plant Cell* 18 (2), 412–421. doi: 10.1105/tpc.105.038943

Curtin, S. J., Tiffin, P., Guhlin, J., Trujillo, D. I., Burghart, L. T., Atkins, P., et al. (2017). Validating genome-wide association candidates controlling quantitative variation in nodulation. *Plant Physiol.* 173 (2), 921–931. doi: 10.1104/pp.16.01923

Dai, X., Zhuang, Z., and Zhao, P. X. (2018). psRNATarget: a plant small RNA target analysis server (2017 Release). *Nucleic Acids Res.* 46 (W1), W49–W54. doi: 10.1093/nar/gky316

de Souza Campos, P. M., Cornejo, P., Rial, C., Borie, F., Varela, R. M., Seguel, A., et al. (2019). Phosphate acquisition efficiency in wheat is related to root:shoot ratio, strigolactone levels, and PHO2 regulation. *J. Exp. Bot.* 70 (20), 5631–5642. doi: 10.1093/jxb/erz349

Dong, C., He, F., Berkowitz, O., Liu, J., Cao, P., Tang, M., et al. (2018). Alternative splicing plays a critical role in maintaining mineral nutrient homeostasis in rice (Oryza sativa). *Plant Cell* 30 (10), 2267–2285. doi: 10.1105/tpc.18.00051

Ferguson, B. J., Mens, C., Hastwell, A. H., Zhang, M., Su, H., Jones, C. H., et al. (2019). Legume nodulation: the host controls the party. *Plant Cell Environ.* 42 (1), 41–51. doi: 10.1111/pce.13348

Franco-Zorrilla, J. M., Valli, A., Todesco, M., Mateos, I., Puga, M. I., Rubio-Somoza, I., et al. (2007). Target mimicry provides a new mechanism for regulation of microRNA activity. *Nat. Genet.* 39 (8), 1033–1037. doi: 10.1038/ng2079

Gamir, J., Torres-Vera, R., Rial, C., Berrio, E., de Souza Campos, P. M., Varela, R. M., et al. (2020). Exogenous strigolactones impact metabolic profiles and phosphate starvation signalling in roots. *Plant Cell Environ.* 43 (7), 1655–1668. doi: 10.1111/pce.13760

Gautrat, P., Laffont, C., Frugier, F., and Ruffel, S. (2021). Nitrogen systemic signaling: from symbiotic nodulation to root acquisition. *Trends Plant Sci.* 26 (4), 392–406. doi: 10.1016/j.tplants.2020.11.009

Hackenberg, M., Shi, B.-J., Gustafson, P., and Langridge, P. (2013). Characterization of phosphorus-regulated miR399 and miR827 and their isomirs in barley under phosphorus-sufficient and phosphorus-deficient conditions. *BMC Plant Biol.* 13 (1), 1–17. doi: 10.1186/1471-2229-13-214

Hardy, R. W., Holsten, R. D., Jackson, E. K., and Burns, R. C. (1968). The acetylene-ethylene assay for n(2) fixation: laboratory and field evaluation. *Plant Physiol.* 43 (8), 1185–1207. doi: 10.1104/pp.43.8.1185

Helliwell, K. E. (2022). Emerging trends in nitrogen and phosphorus signalling in photosynthetic eukaryotes. *Trends Plant Sci.* 28 (3), 208–2111. doi: 10.1016/j.tplants.2022.10.004

Hernandez, G., Valdes-Lopez, O., Ramirez, M., Goffard, N., Weiller, G., Aparicio-Fabre, R., et al. (2009). Global changes in the transcript and metabolic profiles during symbiotic nitrogen fixation in phosphorus-stressed common bean plants. *Plant Physiol.* 151 (3), 1221–1238. doi: 10.1104/pp.109.143842

Hu, B., Jiang, Z., Wang, W., Qiu, Y., Zhang, Z., Liu, Y., et al. (2019). Nitrate–NRT1.1B–SPX4 cascade integrates nitrogen and phosphorus signalling networks in plants. *Nat. Plants* 5 (4), 401–413. doi: 10.1038/s41477-019-0384-1

Hu, B., Zhu, C., Li, F., Tang, J., Wang, Y., Lin, A., et al. (2011). LEAF TIP NECROSIS1 plays a pivotal role in the regulation of multiple phosphate starvation responses in rice. *Plant Physiol.* 156 (3), 1101–1115. doi: 10.1104/pp.110.170209

Huang, T. K., Han, C. L., Lin, S. I., Chen, Y. J., Tsai, Y. C., Chen, Y. R., et al. (2013). Identification of downstream components of ubiquitin-conjugating enzyme PHOSPHATE2 by quantitative membrane proteomics in arabidopsis roots. *Plant Cell* 25 (10), 4044–4060. doi: 10.1105/tpc.113.115998

Huertas, R., Catalá, R., Jiménez-Gómez, J. M., Mar Castellano, M., Crevillén, P., Piñeiro, M., et al. (2019). Arabidopsis SME1 regulates plant development and response to abiotic stress by determining spliceosome activity specificity. *Plant Cell* 31 (2), 537–554. doi: 10.1105/tpc.18.00689

Kakar, K., Wandrey, M., Czechowski, T., Gaertner, T., Scheible, W. R., Stitt, M., et al. (2008). A community resource for high-throughput quantitative RT-PCR analysis of transcription factor gene expression in Medicago truncatula. *Plant Methods* Dec;4(1):1-2. doi.org/10.1186/1746-4811-4-18

Kant, S., Peng, M., and Rothstein, S. J. (2011). Genetic regulation by NLA and microRNA827 for maintaining nitrate-dependent phosphate homeostasis in arabidopsis. *PloS Genet.* 7 (3), e1002021. doi: 10.1371/journal.pgen.1002021

Kryvoruchko, I. S., Routray, P., Sinharoy, S., Torres-Jerez, I., Tejada-Jiménez, M., Finney, L. A., et al. (2018). An iron-activated citrate transporter, MtMATE67, is required for symbiotic nitrogen fixation. *Plant Physiol.* 176 (3), 2315–2329. doi: 10.1104/pp.17.01538

Liese, R., Schulze, J., and Cabeza, R. A. (2017). Nitrate application or p deficiency induce a decline in medicago truncatula N(2)-fixation by similar changes in the nodule transcriptome. *Sci. Rep.* 7, 46264. doi: 10.1038/srep46264

Lin, S.-I., Chiang, S.-F., Lin, W.-Y., Chen, J.-W., Tseng, C.-Y., Wu, P.-C., et al. (2008). Regulatory network of microRNA399 and PHO2 by systemic signaling. *Plant Physiol.* 147 (2), 732–746. doi: 10.1104/pp.108.116269

Lin, W. Y., Huang, T. K., and Chiou, T. J. (2013). Nitrogen limitation adaptation, a target of microRNA827, mediates degradation of plasma membrane-localized phosphate transporters to maintain phosphate homeostasis in arabidopsis. *Plant Cell* 25 (10), 4061–4074. doi: 10.1105/tpc.113.116012

Liu, T. Y., Huang, T. K., Tseng, C. Y., Lai, Y. S., Lin, S. I., Lin, W. Y., et al. (2012). PHO2-dependent degradation of PHO1 modulates phosphate homeostasis in arabidopsis. *Plant Cell* 24 (5), 2168–2183. doi: 10.1105/tpc.112.096636

Livak, K. J., and Schmittgen, T. D. (2001). Analysis of relative gene expression data using real-time quantitative PCR and the 2– ΔΔCT method. *methods* 25 (4), 402–408. doi: 10.1006/meth.2001.1262

Lu, M., Cheng, Z., Zhang, X. M., Huang, P., Fan, C., Yu, G., et al. (2020). Spatial divergence of PHR-PHT1 modules maintains phosphorus homeostasis in soybean nodules. *Plant Physiol.* 184 (1), 236–250. doi: 10.1104/pp.19.01209

Marro, N., Lidoy, J., Chico, M. A., Rial, C., Garcia, J., Varela, R. M., et al. (2022). Strigolactones: new players in the nitrogen-phosphorus signalling interplay. *Plant Cell Environ.* 45 (2), 512–527. doi: 10.1111/pce.14212

Meade, H. M., Long, S. R., Ruvkun, G. B., Brown, S. E., and Ausubel, F. M. (1982). Physical and genetic characterization of symbiotic and auxotrophic mutants of rhizobium meliloti induced by transposon Tn5 mutagenesis. *J. Bacteriol.* 149 (1), 114–122. doi: 10.1128/jb.149.1.114-122.1982

Medici, A., Szponarski, W., Dangeville, P., Safi, A., Dissanayake, I. M., Saenchai, C., et al. (2019). Identification of molecular integrators shows that nitrogen actively controls the phosphate starvation response in plants. *Plant Cell* 31 (5), 1171–1184. doi: 10.1105/tpc.18.00656

Miller, S. S., Dornbusch, M. R., Farmer, A. D., Huertas, R., Gutierrez-Gonzalez, J. J., Young, N. D., et al. (2022). Alfalfa (Medicago sativa l.) pho2 mutant plants hyperaccumulate phosphate. *G3 (Bethesda)* 12 (6). doi: 10.1093/g3journal/jkac096

Mukatira, U. T., Liu, C., Varadarajan, D. K., and Raghothama, K. G. (2001). Negative regulation of phosphate starvation-induced genes. *Plant Physiol.* 127 (4), 1854–1862. doi: 10.1104/pp.010876

Nasr Esfahani, M., Inoue, K., Chu, H. D., Nguyen, K. H., Van Ha, C., Watanabe, Y., et al. (2017). Comparative transcriptome analysis of nodules of two mesorhizobium-chickpea associations with differential symbiotic efficiency under phosphate deficiency. *Plant J.* 91 (5), 911–926. doi: 10.1111/tpj.13616

Nguyen, N. N. T., Clua, J., Vetal, P. V., Vuarambon, D. J., De Bellis, D., Pervent, M., et al. (2021). PHO1 family members transport phosphate from infected nodule cells to bacteroids in medicago truncatula. *Plant Physiol.* 185 (1), 196–209. doi: 10.1093/plphys/kiaa016

Ouyang, X., Hong, X., Zhao, X., Zhang, W., He, X., Ma, W., et al. (2016). Knock out of the PHOSPHATE 2 gene TaPHO2-A1 improves phosphorus uptake and grain yield under low phosphorus conditions in common wheat. *Sci. Rep.* 6, 29850. doi: 10.1038/srep29850

Pacak, A., Barciszewska-Pacak, M., Swida-Barteczka, A., Kruszka, K., Sega, P., Milanowska, K., et al. (2016). Heat stress affects pi-related genes expression and inorganic phosphate Deposition/Accumulation in barley. *Front. Plant Sci.* 7. doi: 10.3389/fpls.2016.00926

Pacak, A., Geisler, K., Jorgensen, B., Barciszewska-Pacak, M., Nilsson, L., Nielsen, T. H., et al. (2010). Investigations of barley stripe mosaic virus as a gene silencing vector in barley roots and in brachypodium distachyon and oat. *Plant Methods* 6, 26. doi: 10.1186/1746-4811-6-26

Park, B. S., Seo, J. S., and Chua, N. H. (2014). NITROGEN LIMITATION ADAPTATION recruits PHOSPHATE2 to target the phosphate transporter PT2 for degradation during the regulation of arabidopsis phosphate homeostasis. *Plant Cell* 26 (1), 454–464. doi: 10.1105/tpc.113.120311

Puga, M. I., Mateos, I., Charukesi, R., Wang, Z., Franco-Zorrilla, J. M., de Lorenzo, L., et al. (2014). SPX1 is a phosphate-dependent inhibitor of phosphate starvation response 1 in arabidopsis. *Proc. Natl. Acad. Sci.* 111 (41), 14947–14952. doi: 10.1073/pnas.140465411

Qin, L., Zhao, J., Tian, J., Chen, L., Sun, Z., Guo, Y., et al. (2012). The high-affinity phosphate transporter GmPT5 regulates phosphate transport to nodules and nodulation in soybean. *Plant Physiol.* 159 (4), 1634–1643. doi: 10.1104/pp.112.199786

Robinson, J. T., Thorvaldsdottir, H., Winckler, W., Guttman, M., Lander, E. S., Getz, G., et al. (2011). Integrative genomics viewer. *Nat. Biotechnol.* 29 (1), 24–26. doi: 10.1038/nbt.1754

Roux, B., Rodde, N., Jardinaud, M. F., Timmers, T., Sauviac, L., Cottret, L., et al. (2014). An integrated analysis of plant and bacterial gene expression in symbiotic root nodules using laser-capture microdissection coupled to RNA sequencing. *Plant J.* 77 (6), 817–837. doi: 10.1111/tpj.12442

Roy, S., Liu, W., Nandety, R. S., Crook, A., Mysore, K. S., Pislariu, C. I., et al. (2020). Celebrating 20 years of genetic discoveries in legume nodulation and symbiotic nitrogen fixation. *Plant Cell* 32 (1), 15–41. doi: 10.1105/tpc.19.00279

Rubio, V., Linhares, F., Solano, R., Martín, A. C., Iglesias, J., Leyva, A., et al. (2001). A conserved MYB transcription factor involved in phosphate starvation signaling both in vascular plants and in unicellular algae. *Genes Dev.* 15 (16), 2122–2133. doi: 10.1101/gad.204401

Santoro, V., Schiavon, M., Visentin, I., Martin, M., Said-Pullicino, D., Cardinale, F., et al. (2022). Tomato plant responses induced by sparingly available inorganic and organic phosphorus forms are modulated by strigolactones. *Plant Soil* 474 (1-2), 355–372. doi: 10.1007/s11104-022-05337-0

Scheible, W. R., Pant, P., Pant, B. D., Krom, N., Allen, R. D., and Mysore, K. S. (2023). Elucidating the unknown transcriptional responses and PHR1 mediated biotic and abiotic stress tolerance during phosphorus-limitation. *J. Exp. Bot.* 74(6):2083–2111 doi: 10.1093/jxb/erad009

Secco, D., Jabnoune, M., Walker, H., Shou, H., Wu, P., Poirier, Y., et al. (2013). Spatio-temporal transcript profiling of rice roots and shoots in response to phosphate starvation and recovery. *Plant Cell* 25 (11), 4285–4304. doi: 10.1105/tpc.113.117325

Stanton-Geddes, J., Paape, T., Epstein, B., Briskine, R., Yoder, J., Mudge, J., et al. (2013). Candidate genes and genetic architecture of symbiotic and agronomic traits revealed by whole-genome, sequence-based association genetics in medicago truncatula. *PloS One* 8 (5), e65688. doi: 10.1371/journal.pone.0065688

Sulieman, S., Ha, C. V., Schulze, J., and Tran, L. S. (2013). Growth and nodulation of symbiotic medicago truncatula at different levels of phosphorus availability. *J. Exp. Bot.* 64 (10), 2701–2712. doi: 10.1093/jxb/ert122

Sulieman, S., Kusano, M., Ha, C. V., Watanabe, Y., Abdalla, M. A., Abdelrahman, M., et al. (2019). Divergent metabolic adjustments in nodules are indispensable for efficient N(2) fixation of soybean under phosphate stress. *Plant Sci.* 289, 110249. doi: 10.1016/j.plantsci.2019.110249

Sulieman, S., and Tran, L.-S. P. (2015). Phosphorus homeostasis in legume nodules as an adaptive strategy to phosphorus deficiency. *Plant Sci.* 239, 36–43. doi: 10.1016/j.plantsci.2015.06.018

Tian, P., Lin, Z., Lin, D., Dong, S., Huang, J., and Huang, T. (2021). The pattern of DNA methylation alteration, and its association with the changes of gene expression and alternative splicing during phosphate starvation in tomato. *Plant J.* 108 (3), 841–858. doi: 10.1111/tpj.15486

Udvardi, M., Below, F. E., Castellano, M. J., Eagle, A. J., Giller, K. E., Ladha, J. K., et al. (2021). A research road map for responsible use of agricultural nitrogen. 5, 660155 doi: 10.3389/fsufs.2021.660155

Udvardi, M., and Poole, P. S. (2013). Transport and metabolism in legume-rhizobia symbioses. *Annu. Rev. Plant Biol.* 63 (64), 781–805. doi: 10.1146/annurev-arplant-050312-120235

Ueda, Y., Kiba, T., and Yanagisawa, S. (2020). Nitrate-inducible NIGT1 proteins modulate phosphate uptake and starvation signalling *via* transcriptional regulation of SPX genes. *Plant J.* 102 (3), 448–466. doi: 10.1111/tpj.14637

Wang, R., Fang, Y. N., Wu, X. M., Qing, M., Li, C. C., Xie, K. D., et al. (2020). The miR399-CsUBC24 module regulates reproductive development and Male fertility in citrus. *Plant Physiol.* 183 (4), 1681–1695. doi: 10.1104/pp.20.00129

Wang, T., Ren, L., Li, C., Zhang, D., Zhang, X., Zhou, G., et al. (2021). The genome of a wild medicago species provides insights into the tolerant mechanisms of legume forage to environmental stress. *BMC Biol.* 19 (1), 1–17. doi: 10.1186/s12915-021-01033-0

Wang, Z., Ruan, W., Shi, J., Zhang, L., Xiang, D., Yang, C., et al. (2014). Rice SPX1 and SPX2 inhibit phosphate starvation responses through interacting with PHR2 in a phosphate-dependent manner. *Proc. Natl. Acad. Sci.* 111 (41), 14953–14958. doi: 10.1073/pnas.1404680111

Wang, T., Zhao, M., Zhang, X., Liu, M., Yang, C., Chen, Y., et al. (2017). Novel phosphate deficiency-responsive long non-coding RNAs in the legume model plant medicago truncatula. *J. Exp. Bot.* 68 (21-22), 5937–5948. doi: 10.1093/jxb/erx384

Xu, F., Liu, Q., Chen, L., Kuang, J., Walk, T., Wang, J., et al. (2013). Genome-wide identification of soybean microRNAs and their targets reveals their organ-specificity and responses to phosphate starvation. *BMC Genomics* 14, 66. doi: 10.1186/1471-2164-14-66

Zhong, Y., Tian, J., Li, X., and Liao, H. (2023). Cooperative interactions between nitrogen fixation and phosphorus nutrition in legumes. *New Phytol.* 237 (3), 734–745. doi: 10.1111/nph.18593

frontiers | Frontiers in Plant Science

TYPE Original Research
PUBLISHED 26 July 2023
DOI 10.3389/fpls.2023.1196939

OPEN ACCESS

EDITED BY
Senjuti Sinharoy,
National Institute of Plant Genome Research (NIPGR), India

REVIEWED BY
Manish Tiwari,
University of Wisconsin-Madison, United States
Oswaldo Valdes-Lopez,
National Autonomous University of Mexico, Mexico

*CORRESPONDENCE
Tongguo Gao
gtgrxf@163.com

†These authors have contributed equally to this work

RECEIVED 30 March 2023
ACCEPTED 06 July 2023
PUBLISHED 26 July 2023

CITATION
Zhang W, Li J, Li H, Zhang D, Zhu B, Yuan H and Gao T (2023) Transcriptomic analysis of humic acid in relieving the inhibitory effect of high nitrogen on soybean nodulation.
Front. Plant Sci. 14:1196939.
doi: 10.3389/fpls.2023.1196939

Transcriptomic analysis of humic acid in relieving the inhibitory effect of high nitrogen on soybean nodulation

Wenhua Zhang[1†], Jia Li[1†], Hongya Li[1], Dongdong Zhang[1], Baocheng Zhu[1], Hongli Yuan[2] and Tongguo Gao[1*]

[1]Hebei Engineering Research Center for Resource Utilization of Agricultural Waste, College of Life Sciences, Hebei Agricultural University, Baoding, China, [2]State Key Laboratory of Agrobiotechnology and Key Laboratory of Soil Microbiology, Ministry of Agriculture, College of Biological Sciences, China Agricultural University, Beijing, China

Introduction: Nitrogen fertilizer intake promotes soybean growth before the formation of nodules, but excess nitrogen has an inhibitory effect on soybean nodulation. It is important to balance nitrogen levels to meet both growth and nodulation needs.

Methods: the nitrogen level suitable for soybean growth and nodulation was studied, the role of humic acid (HA) in alleviating the inhibition of high nitrogen on soybean nodulation was analyzed, and transcriptomic analysis was performed to understand its mechanism.

Results: The results showed that a lower level of nitrogen with 36.4 mg urea per pot could increase the number of nodules of soybean, and a higher level of nitrogen with 145.9 mg urea per pot (U4 group) had the best growth indicators but inhibited nodulation significantly. HA relieved the inhibitory effect at high nitrogen level, and the number of nodules increased by 122.1% when 1.29 g HA was added (H2 group) compared with the U4 group. The transcriptome analysis was subsequently performed on the H2 and U4 groups, showing that there were 2995 differentially expressed genes (DEGs) on the 25th day, accounting for 6.678% of the total annotated genes (44,848) under the test conditions. These DEGs were enriched in mitogen-activated protein kinase signaling pathway-plant, flavonoid biosynthesis, and plant hormone signal transduction based on the −log10 ($P_{adjusted}$) value in the Kyoto Encyclopedia of Genes and Genomes pathway (KEGG).

Discussion: HA balanced the nitrogen level through the above pathways in soybean planting to control the number of nodules.

KEYWORDS

high nitrogen, humic acid, nodulation, relieve inhibition, transcriptome

Abbreviations: NSP1, Nodulation signaling pathway 1; ERN1, Ethylene response factor required for nodulation 1; NIN, including nodule inception.

1 Introduction

Nitrogen fertilizer application can make up for the lack of nitrogen before nodulation and promote soybean growth. However, excessive nitrogen in the external environment can not only inhibit the number of nodules and nitrogen fixation efficiency of soybean but also cause environmental pollution (Nishida and Suzaki, 2018; Du et al., 2020). Slow-release nitrogen is extremely important for soybean growth and nodulation.

Nitrogen is an indispensable element for plants. About 78% of nitrogen in the atmosphere exists in the form of nitrogen and cannot be directly used by plants. Biological nitrogen fixation can convert nitrogen in the air into ammonia and nitric acid available to plants (Bulen, 1965). The symbiotic nitrogen fixation (SNF) system formed by legumes and rhizobia has the strongest nitrogen fixation ability, which can meet 50%–80% of the total nitrogen required for the growth of legumes, among which the soybean and rhizobia system accounts for 77% of the total symbiotic nitrogen fixation (Herridge et al., 2008).

In soybeans, the nitrogen produced by symbiotic fixation is not always sufficient for achieving high yields (Kunert et al., 2016). When cultured in a nitrogen-free medium, the root nodules appeared as the early senescence type and could not form normal nodules (Banba et al., 2001). Therefore, applying appropriate amounts of nitrogen can supplement the nitrogen required by legumes before nodulation, play a "start-up effect," and promote the formation of root nodules and their nitrogen fixation capacity (Afza et al., 1987; Sincik et al., 2009). High-nitrogen conditions due to the excessive use of nitrogen fertilizer suppress nodulation and nitrogen fixation, negatively affecting soybean yield. Both nodule formation and nitrogen fixation processes are energetically expensive processes. In the case of enough external nitrogen, a long-distance signaling known as autoregulation of nodulation (AON) should strictly control the number of nodules in host plants and inhibit rhizobia infection (Tiwari et al., 2021; Mengke et al., 2020), root nodule formation and development, and nitrogenase activity (Eaglesham, 1989). This even results in overgrown plants and a fall in productivity and grain quality, creating a disease-prone environment (Petricka et al., 2012; Almeida et al., 2016; Wang et al., 2021). Different form of high-level chemical nitrogen had an inhibitory effect on nodulation of soybean (Yamashita et al., 2019). Urease of soil microorganisms catalyzes the hydrolysis of urea to ammonium, which has a less inhibitory effect on nodulation than nitrate (Paradiso et al., 2015).

Humic acid (HA) is an organic macromolecule produced though chemical or biological decomposition of animal and plant debris and microbial cells (Hayes, 1997). The main constituents of HAs are aromatic rings, aliphatic groups, and other functional groups such as carboxyl group, alcohol hydroxyl group, sulfonic acid group, phenol hydroxyl group, methoxy group, ketone group, enol group, and quinone group (Schulten and Schnitzer, 1993). HA can participate in the transformation of inorganic matter and the mineralization of organic matter, and also promote the absorption, transportation, and distribution of nitrogen by plants and biological nitrogen fixation (Gao et al., 2020). Because of its hydroxyl structure, HA can adsorb bound ammonia, maintain NH_4^+ in soil, resist microbial nitrification and denitrification, reduce its volatilization, and regulate soil nitrogen (Burge and Broadbent, 1961; Susilawati et al., 2009). Introducing HA into the interlayer space of bentonite and then combining it with urea released nitrogen slowly, which ultimately led to increased wheat yield and nitrogen uptake (Shen et al., 2020a). Further, HA could also form a complex with urea having phenolic hydroxyl and carboxyl groups to form HA–urea complex, which could alleviate urea hydrolysis. Urea is mainly hydrolyzed into ammonia and carbon dioxide by urease in soil. HA can not only inhibit and stabilize urease activity (Serban and Nissenbaum, 1986) but also alleviate ammonia volatilization after urea hydrolysis. Previous studies have shown that low-molecular-weight HA inhibits urease activity, while high-molecular-weight HA stabilizes urease activity (Marzadori et al., 2000).

There is general consensus that HAs can promote plant growth in an eco-friendly manner. Moreover, HAs, as biostimulants, increase the number of nodules of legumes and improve nitrogen fixation efficiency (Haghighi et al., 2011; Gao et al., 2015). Water-soluble humic materials (WSHM) at a concentration of 500 mg/L significantly promoted nodulation and nitrogen fixation in soybean and increased the biomass, plant height, and root length of soybean, as well as the chlorophyll content. WSHM increased the number of nodules in soybean by 30.5%, the nodule fresh weight by 36%, and the activity of nitrogenase by 30% (Gao et al., 2015). The structure of HA was determined using the pyrolysis gas chromatography–mass spectrometry (py-GC-MS), and flavonoid analogues were observed, which might have a positive effect on soybean nodulation.

HAs can stimulate the growth of legumes and improve the number of nodules and yield under low-nitrogen conditions. However, no studies reported the role of HA on the growth and nodulation of legumes at high-nitrogen level. This study hypothesized that HA alleviated the release of urea and the inhibition of high nitrogen on soybean nodulation under high-nitrogen conditions.

2 Materials and methods

2.1 HA and strain

HA chosen in this study was the product of *Penicillium* sp. P6 fermentation of lignite, as previously described (Dong and Yuan, 2009), comprising 45.5% HA and 11.7% WSHM. The HA in biodegraded lignite had 2.28% nitrogen, 54.56% carbon, 3.82% hydrogen, and 38.85% oxygen.

Sinorhizobium fredii strain CCBAU45436 was provided by Rhizobium Research Center, China Agricultural University, Beijing, China (Zhang et al., 2011). This strain was cultured aerobically at 28°C, 180 r/min in yeast malt broth (Gao et al., 2015).

2.2 Effect of urea on soybean nodulation

Urea was used to determine the concentration of nitrogen to study the role of HA in relieving high-nitrogen inhibition of

soybean nodulation (The experimental sketch map is shown in Supplementary figure 1A).

Soybean seeds were sterilized on the surface through a two-step process involving a 30-second treatment with 95% ethanol followed by a 5-minute treatment with 0.2% $HgCl_2$, and then washed six times using sterile water. The seeds were germinated on 0.8% agar-water plates in the dark at 25°C for 24 hours. Once germinated, they were planted in nitrogen-free nutrient solution moisturized vermiculite (Lyu et al., 2019) and 20 mg KH_2PO_4 and 1 mL bacterial culture (approximately 10^6 cells) were added in pots (500 mL). The pots were divided into five parallel treatments, and different amounts of urea were added: U1 (18.2 mg), U2 (36.4 mg), U3 (72.9 mg), U4 (145.9 mg), and U5 (291.8 mg). All the plants were grown under a photoperiod of 16/8-h light/dark cycles at 23°C in a light incubator for 21 days. Three biological replicates were established for each treatment, and 5 plants were randomly selected from each replicate to measure the number, fresh weight, and leghemoglobin content of nodules, as well as the growth index of soybean. The leghemoglobin content was determined as proposed by Becana (Becana et al., 1986) and Riley (Riley and Dilworth, 1985).

2.3 Alleviating effect of HA

The effect of HA in terms of relieving the inhibition of high nitrogen on soybean nodulation was examined by the method discussed in Section 2.2. Different amounts of HA were added to potted soybean under high-nitrogen conditions, and the aforementioned high-concentration urea was used as the control group (Supplementary figure 1B). Four treatment groups with different amounts of HA were set: H1 (0.43 g HA), H2 (1.29 g HA), H3 (2.16 g HA), and H4 (4.31 g HA). The growth index, number, fresh weight, and leghemoglobin content of nodules were measured. The chlorophyll content in soybean leaves was determined using an SPAD-502 chlorophyll meter (Konica Minolta, Tokyo, Japan).

2.4 Urea, ammonium nitrogen, and urease in vermiculite

The residual urea, ammonium nitrogen, and urease activity in vermiculite were determined by diacetyl monoxime colorimetry (Reay et al., 2019), phenol-sodium hypochlorite colorimetry (Kere et al., 2018) and colorimetry (Khan et al., 2020), respectively, to evaluate the hydrolytic ability of urea.

2.5 RNA extraction, sequencing, and analysis

After 25 days of cultivation as described previously, the nodules under high-nitrogen conditions treated with and without HA were collected for transcriptomic analysis. The total RNA of nodules was isolated using the TRIzol reagent (Invitrogen, CA, USA) following the manufacturer's protocol. The quality and integrity of total RNA were examined using the Nanodrop 2000 spectrophotometer (Thermo Fisher Scientific) and the Bioanalyzer 2100 systems (Agilent). The mRNA enrichment, fragmentation into small pieces, cDNA library construction, sequencing, data filtering, and mapping were performed commercially by Meiji Biotechnology Co., Ltd., Shanghai, China. Sequencing was performed on the Illumina HiSeq X Ten platform. After sequencing, Fastp software (0.19.5) was used for quality control of sequencing data. The original paired end reads were pruned and quality-controlled using SeqPrep and Sickle. The quality-controlled Clean Reads were mapped onto the *Glycine_max* genome (reference genome Version: Wm82.a4) using HISAT2 (Version 2.1.0) (http://ccb.jhu.edu/software/hisat2/index.shtml). The mapped reads were spliced using

Cufflinks software (http://cole-trapnell-lab.github.io/cufflinks/). The expression level of each transcript was calculated according to the TPM (the transcripts per million reads) method, false discovery rate (FDR) <0.05 and |log2FC (fold-change) | ≥ 1 were set as the cutoff criteria to identify differentially expressed genes (DEGs) using DESeq2. RNA-seq by expectation maximization (RSEM) was used to quantify gene abundances. (http://cole-trapnell-lab.github.io/cufflinks/) (Trapnell et al., 2010), the mapped reads of each sample were assembled using StringTie (Kim et al., 2015). Function annotation and enrichment analysis of genes were performed based on Gene Ontology (GO, http://www.geneontology.org/) (Young et al., 2010) and Kyoto Encyclopedia of Genes and Genomes (KEGG) Orthology (http://www.genome.jp/kegg/) (Kanehisa et al., 2008). KOBAS software (Mao et al., 2005) was used to test the statistical enrichment of DEGs in the KEGG pathway. All sequencing data are available in the National Center for Biotechnology Information Sequence Read Archive under the accession number PRJNA918980.

2.6 Quantitative real-time polymerase chain reaction verification

Total RNA was extracted from nodules using the TRIzol reagent for verifying gene expression (Invitrogen, Carlsbad, CA, USA), and the cDNA was synthesized using the HiScript III RT SuperMix for quantitative polymerase chain reaction (qPCR) (+gDNA wiper) following the manufacturer's protocols (Vazyme Biotech, Nanjing, China). The Bio-Rad CFX qPCR instrument (Bio-Rad Hercules, CA, USA) was used for quantitative real-time PCR (qRT-PCR), and the data were analyzed using Bio-Rad CFX Manager 3.0 software (Bio-Rad). The expression of target genes was verified using *Actin11* and *CYP2* as internal reference genes (Le et al., 2012).

2.7 Statistical analysis

All assays were performed in triplicate, and each experiment was replicated at least three times. The experimental data were presented as the means ± standard deviation (SD). Statistical analyses were carried out using the SPSS Statistics 23.0 software.

10.3389/fpls.2023.1196939

3 Results

3.1 Effect of different urea levels on soybean nodules and growth

Figure 1A shows the impact of urea dosage on the number of nodules and fresh weight of soybean. The number and fresh weight of soybean nodules initially increased, followed by a decline with increasing concentration of urea. Compared to the U1 group, the U2 group exhibited a 25.9% increase in nodule numbers, while significantly decreasing by 43.4% and 81.1% in the U4 and U5 groups, respectively. The effect of urea dosage on the fresh weight of nodules was consistent with the change in the number of nodules. The fresh weight of nodules in the U2 group increased by 60.5% compared to that of the U1 group, and the fresh weight of root nodules in the U4 and U5 groups was significantly lower than that in the U1 group ($P < 0.05$).

The leghemoglobin content of soybean nodules under different urea levels is shown in Figure 1B. The OD_{540} value of the U2 group was 22.6% higher than that of the U1 group, which was also significantly higher than that in the U4 and U5 groups. Both the fresh and dry weights of above-ground exhibited an increasing trend followed by a decreasing trend with the increasing application of urea (Table 1). The U4 group outperformed significantly, with an increase of nearly 109% in the above-ground fresh weight and 59% in the above-ground dry weight compared with the U1 group. The U3 group reached the maximum in terms of root fresh and dry weights, exhibiting a 66.7% and 73.3% increase compared to the control group, respectively. The chlorophyll content in leaves increased with the increase in urea dosage. Based on the aforementioned experiments, U4 significantly reduced the number of nodules and improved the growth index compared to the control group. Therefore, the U4 group was considered in this study as the control group with a high level of nitrogen to investigate the potential alleviating effect of HAs on soybean nodulation inhibition caused by high nitrogen.

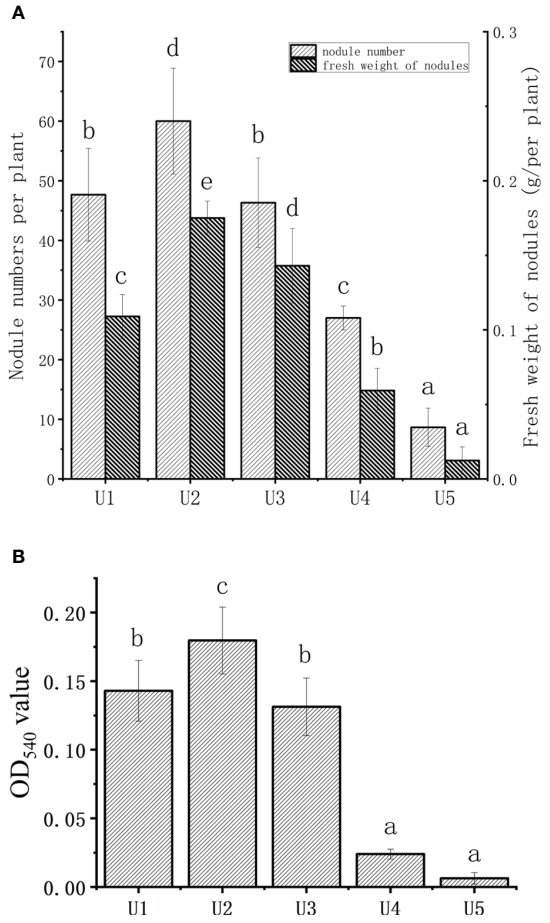

FIGURE 1
Effect of different urea levels on the number and fresh weight of soybean nodules **(A)**, and leghemoglobin of soybean nodules **(B)**. U1, treated with 18.2 mg urea; U2, treated with 36.4 mg urea; U3, treated with 72.9 mg urea; U4, treated with 145.9 mg urea; U5, treated with 291.8 mg urea. The data were presented as the means ± standard deviation. Different letters indicated significant differences ($P < 0.05$) among groups.

3.2 HA relieved the inhibition of high nitrogen on soybean nodulation

Figure 2A illustrates the alleviating effect of HA on soybean nodulation inhibition under a high level of nitrogen. The number of nodules in the four treatment groups (H1, H2, H3, and H4) with HA significantly increased by 59.1%, 122.1%, 47.4%, and 45.5%, respectively, compared with that in the control group (U4 group) treated with urea only. The number of nodules reached the maximum value of 114.0 in the H2 group (1.29 g HA added).

TABLE 1 Effect of urea dosage on soybean growth index.

	Plant height(cm)	Root length (cm)	Above ground fresh weight (g)	Root fresh weight (g)	Aboveground dry weight (g)	Root dry weight (g)	Chlorophyll (SPAD value)
U1	28.87 ± 0.32a	19.50 ± 0.67a	1.94 ± 0.06a	0.91 ± 0.06a	0.32 ± 0.03a	0.08 ± 0.006a	25.35 ± 3.84a
U2	31.83 ± 1.74a	24.37 ± 1.00c	3.09 ± 0.16b	1.92 ± 0.07b	0.60 ± 0.05b	0.23 ± 0.001c	30.70 ± 3.76b
U3	29.23 ± 1.29a	21.73 ± 0.50b	3.68 ± 0.14bc	2.73 ± 0.03c	0.76 ± 0.02c	0.30 ± 0.009d	35.75 ± 2.73c
U4	40.10 ± 1.80b	22.78 ± 0.87bc	4.06 ± 0.21c	2.08 ± 0.22b	0.78 ± 0.03c	0.22 ± 0.021c	35.00 ± 1.71c
U5	28.33 ± 2.50a	23.68 ± 0.34bc	3.85 ± 0.28c	1.77 ± 0.21b	0.71 ± 0.02c	0.15 ± 0.019b	40.00 ± 3.20d

U1: Treated with 18.2 mg urea; U2: Treated with 36.4 mg urea; U3: Treated with 72.9 mg urea; U4: Treated with 145.9 mg urea; U5: Treated with 291.8 mg urea. The means followed by different letters were significantly different at $P < 0.05$, which was indicated by the means ± standard deviation (n = 3).

10.3389/fpls.2023.1196939

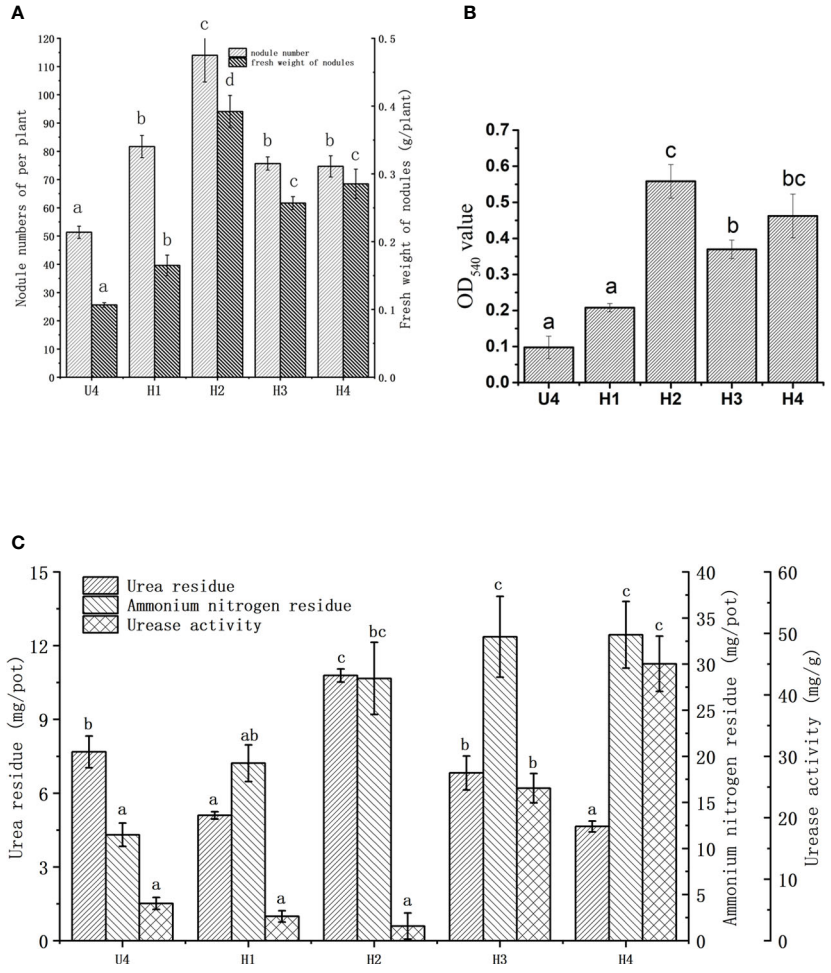

FIGURE 2
Effects of HA on the number **(A)** and fresh weight **(B)** of root nodules, urea residues, ammonium nitrogen residues, and urease activity in vermiculite **(C)** under the high level of nitrogen. U4, the control group; H1, treated with 0.43 g HA; H2, treated with 1.29 g HA; H3, treated with 2.16 g HA; H4, treated with 4.31 g HA. The data were presented as the means ± standard deviation. Different letters indicated significant differences ($P < 0.05$) among groups.

The treatment with HA increased the fresh weight of nodules compared with that in the control group (Figure 2A); especially, the fresh weight in the H2 group reached the maximum value of 0.39 g, representing a significant rise of 267.5% compared to the control group. The fresh weight of root nodules in other HA treatment groups also exhibited significantly increases compared to the control group. In general, the change pattern in the number of soybean nodules and fresh weight was consistent.

The leghemoglobin content of nodules increased on adding HA. The most significant increase was observed in the H2 group with an OD_{540} value of 0.558, followed by that in the H4 and H3 groups. HA had a relieving effect on the leghemoglobin content after urea treatment (Figure 2B). At the same time, in order to ensure meaningful leghemoglobin content, the nitrogenase activity was tested (Supplementary figure 2). The results of this part prove that soybean leghemoglobin content is valuable, indicating that the nodules had nitrogen fixation activity. The influence of HA on the soybean growth index under a high level of nitrogen is depicted in Table 2. The addition of HA did not change the chlorophyll content of the plants under a high level of nitrogen. The root length, above-ground fresh weight, and root fresh weight of soybean increased significantly in the H2 group compared with the control group. Among these, the H2 group demonstrated a 28.14% increase in above-ground fresh weight and a 57.8% increase in root fresh weight compared to the control group, respectively. The plant height in the H3 and H4 groups showed significant differences compared with that in the control group, which increased by 41.4% and 39.2%, respectively.

3.3 Relationship between HAs and hydrolyzed urea

Urea is decomposed by urease to form ammonia. The urea residue, urease activity, and ammonia nitrogen content in vermiculite were determined to investigate the role of HA in this chemical process (Figure 2C). Proper amounts of HA could slow down the hydrolysis of urea. Among all the treatment groups, the

10.3389/fpls.2023.1196939

TABLE 2 Effect of HA on soybean growth index under a high level of nitrogen.

	Chlorophyll (SPAD value)	Plant height (cm)	Root length (cm)	Aboveground fresh weight (g)	Root fresh Weight (g)
U4	50.27 ± 0.71ab	29.07 ± 3.47a	23.67 ± 0.43a	3.02 ± 0.11a	2.25 ± 0.14a
H1	48.50 ± 0.49a	35.40 ± 3.23ab	26.33 ± 0.54ab	3.35 ± 0.12ab	2.93 ± 0.09b
H2	51.93 ± 0.28b	34.53 ± 2.26ab	28.17 ± 1.92b	3.87 ± 0.07d	3.55 ± 0.21c
H3	50.83 ± 1.49ab	41.10 ± 2.40b	27.53 ± 1.77ab	3.45 ± 0.14bc	2.82 ± 0.19ab
H4	51.23 ± 1.39ab	40.47 ± 1.95b	28.47 ± 1.25b	3.82 ± 0.16cd	3.72 ± 0.29c

U4: the control group; H1: treated with 0.43 g HA; H2: treated with 1.29 g HA; H3: treated with 2.16 g HA; H4: treated with 4.31 g HA. The means followed by different letters were significantly different at $P < 0.05$, which was indicated by the means ± standard deviation (n = 3).

H2 group showed a significantly higher urea residue content of up to 10.79 mg/pot compared to others. The urea residues in the H1 and H4 groups were 33.7% and 39.45% lower than those in the control group, respectively, and there was no significant difference between the H3 group and the control group. The HA in the H2 group exhibited a slow-release effect on urea. The residual ammonium nitrogen level increased with the increase in HA, and was higher in all HA groups compared to the control groups. The level of residual ammonium nitrogen in the H1, H2, H3, and H4 groups was 67.6%, 147.7%, 187%, and 189% higher than that in the U4 group, respectively. Although not significant, the urease activity in the H1 and H2 groups was lower than that in the control group. The urease activity in the H3 and H4 groups was 186.9% and 188.9% higher than that in the control group, respectively.

3.4 Transcriptomic analysis of HA in relieving the inhibition of high nitrogen on nodulation

A comparative transcriptomic analysis of soybean nodules was performed with and without HA at a high level of urea to reveal the candidate genes involved in HA, relieving the inhibition of high urea content. RNA paired-end sequencing was carried out using the Illumina Solexa platform, resulting in a high proportion of high-quality reads (approximately 93%). The heat map of the correlation between samples verified the scientific validity of biological replicates (Figures 3A, B). Upon trimming the raw data, a total of 43,739,118 clean reads were obtained for the U4 sample and 46,537,918.67 clean reads were obtained for the H2 sample (Table S1). All clean reads were then mapped to the soybean reference genome, with an average of 84.46% of the reads being uniquely mapped.

The assay results were screened using differential significance criteria, with a two-fold difference as the threshold for identifying differentially expressed genes (DEGs) with FDR ≤ 0.05. A total of 2995 DEGs were identified, which accounted for 5.66% of the total annotated genes (44,848). Among these DEGs identified, 2036 genes were found to be upregulated while 959 genes were downregulated after adding HA (Figure 3C). GO functional annotation analysis of DEGs revealed 7 items associated with biological process, 7 items with cellular component and 6 items with molecular function (Supplementary figure 3). The majority of biological processes were comprised of DEGs that participate in metabolic process, cellular process and biological regulation. The cell part, membrane part and organelle part account for the majority of cellular component. In the terms of molecular function, the significant proportion of DEGs were associated with binding, catalytic activity and transporter activity. Only the top 30 enriched GO terms were displayed in upregulated and downregulated genes. The smaller the $P_{adjusted}$ value (<0.5), the more significant it became. The most significant term in the upregulated genes' GO terms was "flavonoid metabolic process," followed by "response to cytokinin" and "response to wounding" (Figure 4A). Increasing the Rich factor leads to a corresponding increase in the degree of enrichment. "Response to cytokinin," "naringenin-chalcone synthase activity," and "polyamine catabolic process" were the top three enrichment terms with richness factor greater than 0.4 in the upregulated genes. In the downregulated genes, "tricarboxylic acid biosynthetic process," "nicotianamine metabolic process," "nicotianamine biosynthetic process," and "nicotianamine synthase activity" were the terms with the same Rich factor (0.8) at the top enrichment degree (Figure 4B). These 30 terms were significantly upregulated or downregulated ($P_{adjusted} \leq 0.05$).

The KEGG database showed a significant enrichment of the "mitogen-activated protein kinase (MAPK) signaling pathway–plant," positively regulating nodule organogenesis in *Lotus japonicus* (Chen et al., 2012), which was enriched with 46 genes (Figure 4C), followed by the pathway "flavonoid biosynthesis" with 20 genes and "alpha-linolenic acid metabolism" with 20 genes [$-\log10\ (P_{adjusted}) > 5$]. The three most significantly enriched gene/transcript pathways were "MAPK signaling pathway–plant," "plant hormone signal transduction" with 41 enriched genes, and "plant–pathogen interaction" with 34 enriched genes. Among these, "zeatin biosynthesis" was significantly upregulated with HA treatment ($P_{adjusted} = 0.016503162$), which is a type of cytokinin that plays a central role in nodule development (Lin et al., 2020). There were 33 enriched genes in the phenylpropanoid pathway, which is responsible for the synthesis of flavonoids as secondary metabolites. Further, the metabolism of some amino acids, such as cysteine and methionine, tyrosine, and propanoate, was significantly upregulated ($P_{adjusted} < 0.05$). Plant–pathogen interaction terms "phenylpropanoid biosynthesis," "plant

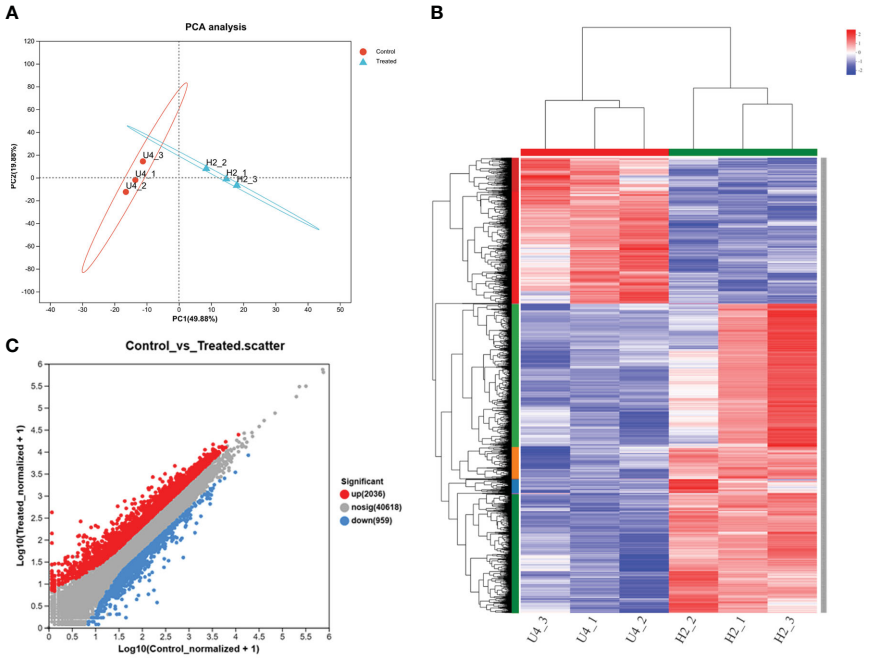

FIGURE 3
PCA **(A)**, Pearson correlation coefficient analysis of all expressed genes **(B)**, and differential fold of gene expression **(C)** in the treatment groups with and without HA at the high nitrogen level. Numbers within parentheses indicated the percentage of variance explained by each component. Each dot in the graph represents a specific gene: red dots indicate significantly upregulated genes, blue dots indicate significantly downregulated genes, and gray dots indicate non-significantly different genes. All treatments included three parallel samples. Control referred to the U4 group with the high nitrogen level, and treated referred to the H2 group treated with HA at the high nitrogen level on day 25.

hormone signal transduction," and "protein processing in endoplasmic reticulum" were significantly enriched in the downregulated KEGG pathway ($P_{adjusted} < 0.5$) (Figure 4D). The results indicated that HA-triggered mode of action and alterations regulated the expression levels of genes involved in hormone metabolism and signal activity in soybean, and the transcriptome results were consistent with those of root nodules produced on adding HA slow-release nitrogen fertilizer.

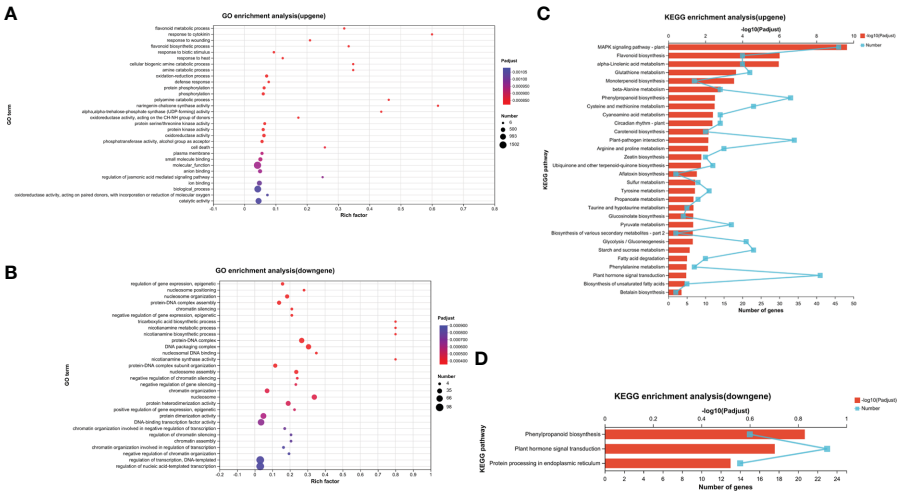

FIGURE 4
GO enrichment analysis of upregulated genes **(A)** and downregulated genes **(B)**, and KEGG enrichment analysis of upregulated genes **(C)** and downregulated genes **(D)**. Each GO term is represented by a dot, the size of which indicates the number of genes/transcripts in this GO term, and the color of the dot corresponds to a different $P_{adjusted}$ range. Different points on the line indicate the number of genes/transcripts in the pathway, and the higher the −log10 ($P_{adjusted}$) value, the more significantly the KEGG pathway was enriched. Only the top 30 enrichment results were shown by $P_{adjusted} < 0.5$.

3.5 RT- PCR verification

To validate the expression analysis of RNA sequencing data, 23 key DEGs were selected for qPCR. Of 23 DEGs (Table 3), 5 DEGs (*Glyma.10G036300*, *Glyma.19G164100*, *Glyma.20G203700*, *Glyma.08G133600*, and *Glyma.09G204100*) were involved in MAPK signaling pathway–plant, 4 DEGs (*Glyma.09G131500*, *Glyma.16G214500*, *Glyma.07G101100*, and *Glyma.13G252600*) were involved in plant–pathogen interaction, 4 DEGs (*Glyma.10G219800*, *Glyma.18G055600*, *Glyma.05G125900*, and *Glyma.18G211100*) were involved in phenylpropanoid biosynthesis, 2 DEGs (*Glyma.02G268200* and *Glyma.05G2407*) were involved in cysteine and methionine metabolism, 4 DEGs (*Glyma.01G118000*, *Glyma.18G204200*, *Glyma.01G116300*, and *Glyma.18G257700*) were involved in glycolysis/gluconeogenesis, and 4 DEGs (*Glyma.13G361100*, *Glyma.03G224800*, *Glyma.03G128600*, and *Glyma.04G150500*) were involved in plant hormone signal transduction. Figure 5 displays the qPCR results. The correlation analysis indicated high consistency between qPCR and RNA sequencing data ($R^2_{(CYP2)}$ = 0.9946, $R^2_{(Actin11)}$ = 0.9921), which demonstrated the reliability of the data.

4 Discussion

4.1 HA inhibited urease activity

Exposure of nodulated roots to high concentrations of combined nitrogen, known as the nitrogen inhibitory effect, represses the development of root nodules and nitrogen fixation activity, which acts *via* mechanisms that are largely unknown (Gibson and Harper, 1985; Xu et al., 2021). In comparison to soybean that didn't receive nitrogen, the addition of nitrogen led to a decrease of 19% and 52% in below-ground biomass and number of nodules, respectively, across soils. Among all factors influencing root growth parameters, the nitrogen rate was found to be the most critical one (Namvar et al., 2011; McCoy et al., 2018). Lyu et al. (Lyu et al., 2019) used a dual-root soybean system to investigate the impact of nitrogen application on root nodule growth, nitrogenase activity, and nitrogen accumulation, which indicated that high nitrogen application led to a contact-dependent local inhibition of these parameters. The specific nitrogenase activity was systematically regulated throughout the whole plant, and high levels of nitrogen inhibition were found to be recoverable.

Urea fertilizers are extensively utilized due to their ability to significantly increase soil nitrogen levels (Saeed et al., 2017). The SPAD meter is a prevalent tool for non-destructive and efficient measurement of leaf chlorophyll concentrations (Dong et al., 2019). The SPAD value is related to various factors, among which nitrogen is one of the most important factors. SPAD value was positively correlated with nitrogen uptake by plants (Xiong et al., 2015; Yuan et al., 2016). In this study, chlorophyll content increases with the use of urea (Table 1), which was consistent with the above conclusion. Humic acid has positive effect on the growth of plant in Table 2, which was verified in many reports (Arancon et al., 2006; Maji et al., 2016; Ampong et al., 2022). Urease inhibitors existed in the fertilizers, ensuring the long-term nitrogen release and improvement in nitrogen uptake by plants and nitrogen storage in seeds and silage (Folina et al., 2021). Lignin was an excellent carrier of nutrients for slow-release fertilizers, adsorbing and encapsulating nutrients to achieve the slow-release property (Mulder et al., 2011).

HA formed a complex through carboxyl and phenolic hydroxyl groups. The HA–urea complex could slow down the decomposition of urea and play a slow-release role in urea. Low-molecular-weight HA inhibited the urease activity, and high-molecular-weight HA stabilized the urease activity (Marzadori et al., 2000). However, the urease activity increased with the increase in the ratio between HA and urease (Liu et al., 2019). The hydroxyl group in HA adsorbed and bound ammonia to maintain NH_4^+ in soil and reduced ammonia volatilization (Susilawati et al., 2009). Moreover, the greater the amount of HA added to urea fertilizer, the stronger its ability becomes to inhibit ammonia volatilization (Mohd et al., 2009; Shen et al., 2020b). In this study, urease activity was the lowest in the H2 group and the highest in the H3 and H4 groups, which was consistent with the result of urea residue. The amount of residual ammonium nitrogen also increased with an increase in the amount of HA.

4.2 HA promoted nodulation by regulating initial nodulation signal transduction

Many studies confirmed that HA could increase the number of nodules of leguminous plants (Capstaff et al., 2020; da Silva et al., 2021). However, no reports explored the effect of HA on the nodulation ability of soybean under high-nitrogen conditions. HA relieved the inhibition of nodulation under high-nitrogen conditions, thereby increasing the number of soybean nodules. Transcriptomics was used to explain this phenomenon. According to KEGG analysis, genes related to the MAPK signaling pathway, flavonoid biosynthesis, α-linolenic acid metabolism, and so on were upregulated, while genes related to plant hormone signal transduction and protein processing in endoplasmic reticulum were downregulated. MAPK cascades acted as a signal transduction pathway, including hormone responses. Yin et al. (Yin et al., 2019) discovered SIP2, an MAP kinase kinase, which interacts with SymRK to promote nodule organogenesis in *L. japonicus*. This suggests that an MAPK cascade might be involved in *Rhizoium*–legume symbiosis. MAPKs play significant roles in nodulation; for instance, MAPKK4 is a positive regulator of nodule formation (Chen et al., 2012), while the pathway involving MKK5 and MPK3/MPK6 negatively regulates the transcription factors NSP1 and ERN1 to inhibit the initial stages of nodule formation (Komis et al., 2018). The activation of the MKK5–MPK3/MPK6–NSP1/ERN1 pathways controls the formation of symbiotic root nodules in *Medicago truncatula* (Ryu et al., 2017). Lee et al. (Lee et al., 2008) prepared genistein induced culture filtrate (GCF) of *Bradyrhizobium japonicum* by Nod factor to induce the early reaction of soybean root hair. It was found that GCF could induce root hair deformation, so the antibody against *GMK1* (*Glycine max* MAP kinase 1) was used to verify that GMK1 was the activated kinase after GCF-treated. The

10.3389/fpls.2023.1196939

TABLE 3 Annotation of the 23 validated genes.

Gene name	Primer for Q-PCR	Log_2FC (Treated/ Control)	Regulate	Pathway definition
Glyma.10G036300	F: CTCCACAGCACCAACAACAGAAG R: CAGTGTCAAAGGTTCCAAGCCAAA	4.491097	up	MAPK signaling pathway - plant; Plant hormone signal transduction
Glyma.19G164100	F: GTCACTACCGTTGCTGCCTTCG R: TGCGGCTTCGGCTGTGTCAA	2.172373	up	MAPK signaling pathway - plant; Plant hormone signal transduction
Glyma.20G203700	F: TTCTCCTCCGAATCTTCCTCTCCG R: CGCACACCTCTGTACGACTTCTTC	2.286828	up	MAPK signaling pathway - plant; Plant hormone signal transduction
Glyma.08G133600	F: ATTCAGTGAGGACGAGGCGAGAT R: CGTGGTGCTGAGCTTCCATCTAG	-1.518029	down	MAPK signaling pathway - plant; Plant hormone signal transduction
Glyma.09G204100	F: ACACCGTCGTCCTCGAATCCTAC R: ACCGTCGCCGTTGGTTCCTT	-1.525996	down	MAPK signaling pathway - plant; Plant hormone signal transduction
Glyma.13G361100	F: TACCGCAAGAAGAACACCGTCAA R: TCAGCATTCTCCGCATCCTTCAA	2.834028	up	Plant hormone signal transduction
Glyma.03G224800	F: CCCGCTAGTTCTTCCTCTTCCTCT R: ATGCCGAGTCCAAGCCTGAGAT	2.417607	up	Plant hormone signal transduction
Glyma.03G128600	F: CAGTAGCAGCAGCGGCAACAAC R: CTCTCGTCCTCAGCGTTATCCAGT	-1.438246	down	Plant hormone signal transduction
Glyma.04G150500	F: GAGCCGCTGGATAAGTGGAGGAAG R: AAGCCGAAGCCGCAATGAGAGG	-1.803954	down	Plant hormone signal transduction
Glyma.09G131500	F: TGAGGATGTTGACGAGGAGAAGG R: CCAGTCATTGGTGAGGCTCTTGT	4.206525	up	Plant-pathogen interaction; Protein processing in endoplasmic reticulum
Glyma.16G214500	F: ATGTTGCCGATCTGCCTGTTGAA R: CCTCCACCTCTCCAGCAGTTGT	2.134464	up	Plant-pathogen interaction; Phosphatidylinositol signaling system; MAPK signaling pathway - plant
Glyma.07G101100	F: TTCAACCGCTTCGACGCCAAC R: GCGAACTCTGTGAGGCTGATGAAG	-1.314561	down	Plant-pathogen interaction
Glyma.13G252600	F: CCAGACTGCAACCTCGAACACT R: CAGGCACTCATCATGGACACAAG	-1.884467	down	MAPK signaling pathway - plant; Plant-pathogen interaction; Plant hormone signal transduction
Glyma.10G219800	F: TGACATTGTAGCAGTAGCAGCAC R: ATCGTCTGTGAATCGTGGAAGGT	4.451012	up	Phenylpropanoid biosynthesis
Glyma.18G055600	F: ATCCTTGCTCCGTCTTCATTTCCA R: GGACAAGCACTCTCCAACTGACTT	4.067622	up	Phenylpropanoid biosynthesis
Glyma.05G125900	F: GTGCTGACAATGTTCGAGATGCTA R: TGCCTCCACCACCTCCTCTTAT	-2.154422	down	Phenylpropanoid biosynthesis
Glyma.18G211100	F: TGCTCTTGGTGGACCTAGTTGGA R: TTTCTGCGGTGGTGAGACCTTTG	-2.083624	down	Phenylpropanoid biosynthesis
Glyma.02G268200	F: AGATTGAAGACGCTTGCCAGAACT R: CGACTGCCTCCTTGAACCTGTT	3.120259	up	Cysteine and methionine metabolism
Gene name	Primer for Q-PCR	Log_2FC (Treated/ Control)	Regulate	Pathway definition
Glyma.05G240700	F: CATCGCCGTCAATCGTGGAAC R: ATGGTGGAGCAATTAGGGTTAGCA	-1.181538	down	Cysteine and methionine metabolism; Lysine biosynthesis; Glycine, serine and threonine metabolism; Monobactam biosynthesis
Glyma.01G118000	F: CAGTGGAAGCAGCAGCAGAGTT R: ATGGCATCACAGCAAATGGATAGC	2.385361	up	Glycolysis/Gluconeogenesis
Glyma.18G204200	F: CGGAGCGTACAGCGAGAACTT R: ACAGCCTGGAAGCAAGTAATGGT	2.377114	up	Glycolysis/Gluconeogenesis
Glyma.01G116300	F: ATGGCGATGGCGACCTCAATC R: ACAGAGAGACCCACAGCACCTAA	-2.319937	down	Glycolysis/Gluconeogenesis; Fatty acid degradation; Tyrosine metabolism
Glyma.18G257700	F: CGGGTTGCTAACAGAATTGGAGGA R: CTGAAGGTAATGCTGGGACTTGGA	-1.113815	down	Glycolysis/Gluconeogenesis; Galactose metabolism

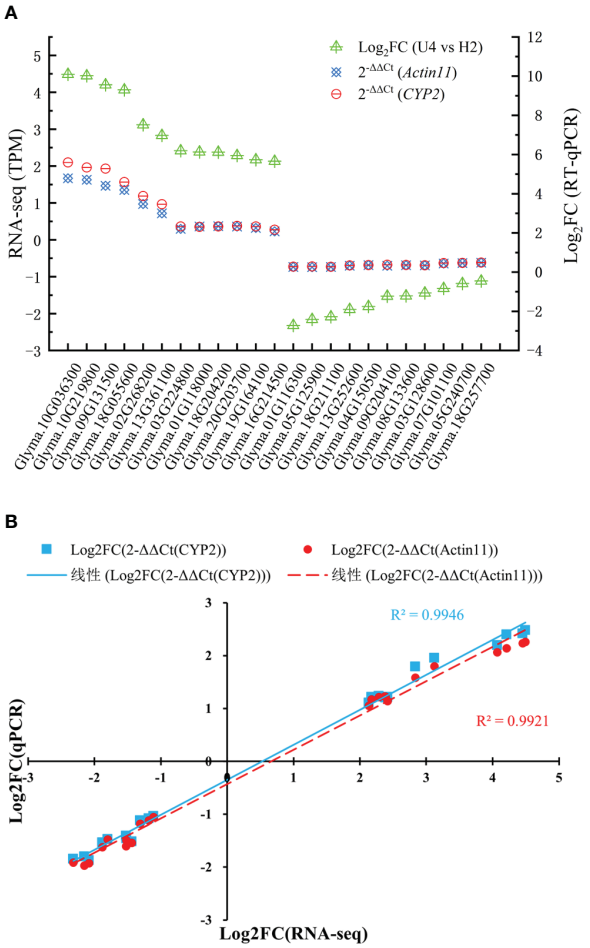

FIGURE 5
qRT-PCR results showing the mRNA expression level of 23 genes **(A)** and the linear regression **(B)**. Expression levels were normalized to *Actin11* and *CYP2* and were presented relative to controls, which were calculated using $2^{-\triangle\triangle Ct}$ (mean ± standard deviation).

results indicated that MAPK plays a role in establishment of symbiosis between soybean and *B. japonicum*.

4.3 HA affected cytokinin signaling in early soybean nodulation

The beneficial role of cytokinins in the initiation of nodule organogenesis has been demonstrated. Nod factors produced by rhizobia induce nodule formation in legumes. This signaling cascade leads to activation of cytokinin signaling and an increase in cytokinin concentration at the nodule initiation site in *Medicago truncatula* (van Zeijl et al., 2015). Although rhizobia can secrete bioactive cytokinins, it cannot replace the role of Nod factors (Podlešáková et al., 2013). In the absence of rhizobia infection, nodule-like structures were found in the roots of chickpea seedlings exogenously treated with appropriate concentration of cytokinin, indicating that cytokinin was sufficient to induce nodular organs (Tiwari et al., 2022). Cytokinin signaling involves regulating the expression of cytokinin primary response genes through type-B response regulator (RRB). Sovanna et al. significantly reduced the number of nodules formed by RNA interference or mutation of *MtRRB3*, which is the RRB-encoding gene most strongly expressed in *M. truncatula* roots and nodules (Tan et al., 2020). Among the various phytohormones that govern cell cycle checkpoints, cytokinins play the most crucial role in limiting cell proliferation at the meristems (Wong et al., 2020). Guinel et al. (Guinel, 2015) clearly illustrated the role of ethylene in nodule organogenesis, functioning, and senescence. The findings demonstrate that ethylene is a crucial component at the center of this highly effective symbiotic relationship. It was reported that nodulation could be affected by the application of ethylene to rhizobia-inoculated root cultures of beans. The results showed a significant reduction, not only in the number of nodules formed but also the amount of fixed nitrogen (Grobbelaar et al., 1971). Pizzeghello et al. highlighted that humic substances (HS) contain a physiologically active concentrations of the cytokinin isopentenyladenosine (IPA), which can enhance plant metabolism (Pizzeghello et al., 2013). Ng et al. investigated the failure to initiate nodulation in the cytokinin perception mutant *cre1* of *M. truncatula*, and proposed that cytokinin signaling mediated CRE1 is essential in regulating flavonoid accumulation, altering auxin transport and auxin accumulation required for nodule initiation in *M. truncatula* (Ng et al., 2015). In addition, cytokinin biosynthesis in shoots may participate in AON system to regulate nodule organogenesis (Gamas et al., 2017). Therefore, it is assumed that humic acid affects the autoregulation of nodulation system and changes the nodulation situation by changing the transport and content of cytokinin in long distances between shoot and root, as observed by Mora et al. 's application of humic acid to cucumber (Mora et al., 2010). But so far, there are no reports on the relationship between HA and AON pathways.

4.4 HA affected the secondary metabolism of soybean

The transcriptome KEGG enrichment results in this study indicated that HA upregulated the phenylpropane biosynthesis pathway. Flavonoids, the secondary metabolites of the phenylpropanoid pathway, have been identified as key players in the establishment of legume root nodule symbiosis. Flavonoids act as signal molecules that trigger rhizobial nodulation initiation signals and act as inhibitors of polar auxin transport in nodule organogenesis (Gifford et al., 2018). Cinnamic acid 4-hydroxylase, a major rate-limiting component in the biosynthesis of phenanthrene, was significantly differentially expressed in *M. sativa* (Gifford et al., 2018). Gene-specific qRT-PCR was used to quantify the expression of isoflavone synthesis genes in soybean (*Glycine max* L). Chalcone synthase 7, chalcone synthase 8, and isoflavone synthase 1 displayed high basal expression levels in roots compared with hypocotyls. Hence, these genes could be responsible for encoding the isoenzymes that play a major role in the principal substrate flux toward specific isoflavone synthesis in roots (Pregelj

et al., 2010). However, this class of genes also showed a significant upregulation trend in HA-treated root nodules, indicating that HA promoted the phenylpropane metabolic pathway, stimulated the production of flavonoids, and enhanced signal expression. The activation of *nod* genes in rhizobia is attributed to daidzein and genistein (Bosse et al., 2021). HA has been considered as a candidate for the auxin effect because it can induce certain enzyme-encoding genes associated with secondary nutrient transport proteins (such as nitrate transporter) (Quaggiotti et al., 2004). LjSWEET3, a member of the SWEET transporter family, shows a significant increase during the development of root nodules in *L. japonicus* and has the highest expression level in mature nodules (Sugiyama et al., 2017). In a high-urea environment, humic acid was found to upregulate the expression of sugar transporter genes (*Glyma.08G010000*; *Glyma.03G149267*), suggesting that humic acid can promote nodulation and provide a source of carbon when soybean is inhibited by high concentrations of urea. Application of fulvic acid resulted in an increase in the number of pink nodules without affecting the nutrient composition (Capstaff et al., 2020). Roomi et al. treated *Arabidopsis* roots with HA and performed proteomic analysis (Roomi et al., 2018). The results of functional annotation analysis indicated that the main molecular functions are binding of copper and manganese ions, nutrient reservoir activity, and protease binding. These findings suggest that HA can stimulate plant energy metabolism and protein synthesis, and may have an impact on metabolic pathways and physiological processes in plants (Roomi et al., 2018). In this study, 6 genes (*Glyma.19G058900*; *Glyma.06G153900*; *Glyma.20G110100*; *Glyma.15G042100*; *Glyma.17G049800*; *Glyma.15G176900*) related to "nutrient reservoir activity" were annotated by GO, but how HA affects the nodulation process of legumes remains though transport pathway is not clear. All the aforementioned findings supported the results of the gene annotation of the transcriptome in this study. HS established transcriptional interactions with biochemical components and signaling pathways, eliciting dynamic signaling within the plant to regulate nodulation.

5 Conclusions

High concentrations of urea inhibited soybean nodulation, and HA alleviated the inhibitory effect on soybean nodulation and nitrogen fixation. Following transcriptomic analysis and validation, a more than two-fold variation in the expression levels of "response to cytokinin," "MAPK signaling pathway-plant," "flavonoid biosynthesis," "plant hormone signal transduction," and "phenylpropanoid biosynthesis" was observed. This demonstrates that HA can modify the cytokinin signal of soybean nodules and regulate the phenylpropyl pathway and MAPK signaling pathway under conditions of high nitrogen to maintain the normal level of nodulation and restores the nitrogen-fixing activity of soybean nodulation. Humic acid can alleviate the inhibitory effects of high levels of nitrogen on soybean nodulation.

Data availability statement

The datasets presented in this study can be found in online repositories. The names of the repository/repositories and accession number(s) can be found in the article/Supplementary Material.

Author contributions

This paper was co-written and analyzed by WZ and JL. TG took the lead in designing, researching and writing the paper. HL and DZ proofread all drafts. BZ gave preliminary guidance. HY conducted objective review of the paper. All authors have contributed to further revisions of this paper.

Funding

This work was supported by the Natural Science Foundation of Hebei Province (C2021204053), National Natural Science Foundation of China (41807037 and 31770541) and Key R & D projects in Hebei Province (20322907D).

Conflict of interest

The remaining authors declare that the research was conducted in the absence of any commercial or financial relationships that could be construed as a potential conflict of interest.

Publisher's note

Supplementary material

The Supplementary Material for this article can be found online at: https://www.frontiersin.org/articles/10.3389/fpls.2023.1196939/full#supplementary-material

SUPPLEMENTARY FIGURE 1
A flow chart with pictures describing the experimental design.

SUPPLEMENTARY FIGURE 2
Nitrogenase activity of nodules on adding HA. Acetylene reduction assay was used to detect nitrogenase activity.

SUPPLEMENTARY FIGURE 3
GO functional annotation analysis of DEGs.

References

Afza, R., Hardarson, G., Zapata, F., and Danso, S. K. A. (1987). Effects of delayed soil and foliar N fertilization on yield and and N_2 fixation of soybean. *Plant Soil.* 97 (3), 361–368. doi: 10.1007/BF02383226

Almeida, O., Melo, H. C. D., and Portes, T. D. (2016). Growth and yield of the common bean in response to combined application of nitrogen and Paclobutrazol. *Rev. Caatinga.* 29, 127–132. doi: 10.1590/1983-21252016v29n115rc

Ampong, K., Thilakaranthna, M. S., and Gorim, L. Y. (2022). Understanding the role of humic acids on crop performance and soil health. *Front. Agron.* 4, 848621. doi: 10.3389/fagro.2022.848621

Arancon, N. Q., Edwards, C. A., Lee, S., and Byrne, R. (2006). Effects of humic acids from vermicomposts on plant growth. *Eur. J. Soil Biol.* 42, S65–S69. doi: 10.1016/j.ejsobi.2006.06.004

Banba, M., Siddique, A.-B. M., Kouchi, H., Izui, K., and Hata, S. (2001). *Lotus japonicus* Forms Early Senescent Root Nodules with *Rhizobium etli*. *Mol. Plant Microbe Interact.* 14 (2), 173–180. doi: 10.1094/MPMI.2001

Becana, M., Gogorcena, Y., Aparicio-Tejo, P. M., and Sánchez-Díaz, M. (1986). Nitrogen fixation and leghemoglobin content during vegetative growth of alfalfa. *J. Plant Physiol.* 123 (2), 117–125. doi: 10.1016/S0176-1617(86)80132-8

Bosse, M. A., Silva, M. B. D., de Oliveira, N. G. R. M., de Araujo, M. A., Rodrigues, C., de Azevedo, J. P., et al. (2021). Physiological impact of flavonoids on nodulation and ureide metabolism in legume plants. *Plant Physiol. Biochem.* 166, 512–521. doi: 10.1016/j.plaphy.2021.06.007

Bulen, W. A. (1965). Biological nitrogen fixation. *Science* 147 (3655), 310–312. doi: 10.1126/science.147.3655.310

Burge, W. D., and Broadbent, F. E. (1961). Fixation of Ammonia by organic soils. *Soil Sci. Soc Am. J.* 25 (3), 199–204. doi: 10.2136/sssaj1961.03615995002500030018x

Capstaff, N. M., Morrison, F., Cheema, J., Brett, P., Hill, L., Muñoz-García, J. C., et al. (2020). Fulvic acid increases forage legume growth inducing preferential up-regulation of nodulation and signalling-related genes. *J. Exp. Bot.* 71 (18), 5689–5704. doi: 10.1093/jxb/eraa283

Chen, T., Zhu, H., Ke, D., Cai, K., Wang, C., Gou, H., et al. (2012). A MAP kinase kinase interacts with SymRK and regulates nodule organogenesis in *Lotus japonicus*. *Plant Cell.* 24 (2), 823–838. doi: 10.1105/tpc.112.095984

da Silva, M.S.R. d., de Melo Silveira dos Santos, B., Hidalgo Chávez, D. W., de Oliveira, R., Barbosa Santos, C. H., Oliveira, E. C., et al. (2021). K-humate as an agricultural alternative to increase nodulation of soybeans inoculated with *Bradyrhizobium*. *Biocatal. Agric. Biotechnol.* 36, 102129. doi: 10.1016/j.bcab.2021.102129

Dong, T., Shang, J., Chen, J. M., Liu, J., and Zhou, G. (2019). Assessment of portable chlorophyll meters for measuring crop leaf chlorophyll concentration. *Remote Sens.* 11 (22), 2706. doi: 10.3390/rs11222706

Dong, L., and Yuan, H. (2009). Nitrogen Incorporation into Lignite Humic Acids during Microbial Degradation. *Geomicrobiol. J.* 26 (7), 484–490. doi: 10.1080/01490450903061085

Du, M., Gao, Z., Li, X., and Liao, H. (2020). Excess nitrate induces nodule greening and reduces transcript and protein expression levels of soybean leghemoglobins. *Ann. Bot.* 126 (1), 61–72. doi: 10.1093/aob/mcaa002

Eaglesham, A. R. J. (1989). Nitrate inhibition of root-nodule symbiosis in doubly rooted soybean plants. *Crop Sci.* 29 (1), 115–119. doi: 10.2135/cropsci1989.0011183X002900010027x

Folina, A., Tataridas, A., Mavroeidis, A., Kousta, A., Katsenios, N., Efthimiadou, A., et al. (2021). Evaluation of various nitrogen indices in N-fertilizers with inhibitors in field crops: A review. *Agronomy* 11 (3), 418. doi: 10.3390/agronomy11030418

Gamas, P., Brault, M., Jardinaud, M. F., and Frugier, F. (2017). Cytokinins in symbiotic nodulation: when, where, what for? *Trends Plant Sci.* 22 (9), 792–802. doi: 10.1016/j.tplants.2017.06.012

Gao, G. T., Xu, Y. Y., Feng, J., Li, B. Z., Yang, J. S., Wang, E. T., et al. (2015). Nodulation characterization and proteomic profiling of *Bradyrhizobium liaoningense* CCBAU05525 in response to water-soluble humic materials. *Sci. Rep.* 5, 10836. doi: 10.1038/srep10836

Gao, T. G., Yuan, H. L., Hou, H. Y., Yao, Y. H., and Gao, F. (2020). The role of humic acid in nitrogen cycle: a review. *Humic acid.* 3, 11–18. doi: 10.19451/j.cnki.issn1671-9212.2020.03.001

Gibson, A. H., and Harper, J. E. (1985). Nitrate effect on nodulation of soybean by *Bradyrhizobium japonicum*[1]. *25* 3), 497–501. doi: 10.2135/cropsci1985.0011183X002500030015x

Gifford, I., Battenberg, K., Vaniya, A., Wilson, A., Tian, L., Fiehn, O., et al. (2018). Distinctive Patterns of Flavonoid Biosynthesis in Roots and Nodules of *Datisca glomerata* and Medicago spp. Revealed by Metabolomic and Gene Expression Profiles. *Front. Plant Sci.* 9, 1463. doi: 10.3389/fpls.2018.01463

Grobbelaar, N., Clarke, B., and Hough, M. C. (1971). The nodulation and nitrogen fixation of isolated roots of *Phaseolus vulgaris* L. *Plant Soil.* 35, 215–223. doi: 10.1007/BF02661851

Guinel, F. C. (2015). Ethylene, a hormone at the center-stage of nodulation. *Front. Plant Sci.* 6. doi: 10.3389/fpls.2015.01121

Haghighi, S., Saki Nejad, T., and Lack, S. (2011). Effect of biological fertilizer of humic acid on metabolic process of biological nitrogen fixation. *Life Sci. J.* 8 (3), 43–48.

Hayes, M. H. B. (1997). Emerging concepts of the compositions and structures of humic substances. M.H.B. Hayes, W.S. Wilson (Eds.), Humic Substances, Peats and Sludges: Health and Environmental Aspects, (London, UK: The Royal Society of Chemistry) 3–30. doi: 10.1016/B978-1-85573-805-8.50005-7

Herridge, D. F., Peoples, M. B., and Boddey, R. M. (2008). Global inputs of biological nitrogen fixation in agricultural systems. *Plant Soil.* 311 (1), 1–18. doi: 10.1007/s11104-008-9668-3

Kanehisa, M., Araki, M., Goto, S., Hattori, M., Hirakawa, M., Itoh, M., et al. (2008). KEGG for linking genomes to life and the environment. *Nucleic Acids Res.* 36 (Database issue), D480–D484. doi: 10.1093/nar/gkm882

Kere, T. A., Jadhav, V. R., and Soni, S. (2018). Comparative study of wet deposition at high altitude station. *Int. J. Innov. Res. Multidiscip. Field.* 4 (8), 118–124.

Khan, M. Q., Rahman, K.-u., Ghani, U., Basharat, A., Qamar, S. A., and Bilal, M. (2020). Synergistic effect of inhibitors (allylthiourea and 1,2,4-triazole) on the activity of wheat soil urease to reduce nitrogen loss. *Case Stud. Chem. Environ. Eng.* 2, 100059. doi: 10.1016/j.cscee.2020.100059

Kim, D., Langmead, B., and Salzberg, S. L. (2015). HISAT: a fast spliced aligner with low memory requirements. *Nat. Methods* 12, 357–360. doi: 10.1038/nmeth.3317

Komis, G., Šamajová, O., Ovečka, M., and Šamaj, J. (2018). Cell and developmental biology of plant mitogen-activated protein kinases. *Annu. Rev. Plant Biol.* 69, 237–265. doi: 10.1146/annurev-arplant-042817-040314

Kunert, K. J., Vorster, B. J., Fenta, B. A., Kibido, T., Dionisio, G., and Foyer, C. H. (2016). Drought stress responses in soybean roots and nodules. *Front. Plant Sci.* 7. doi: 10.3389/fpls.2016.01015

Le, D. T., Aldrich, D. L., Valliyodan, B., Watanabe, Y., Ha, C. V., Nishiyama, R., et al. (2012). Evaluation of candidate reference genes for normalization of quantitative RT-PCR in soybean tissues under various abiotic stress conditions. *PloS One* 7 (9), e46487. doi: 10.1371/journal.pone.0046487

Lee, H., Kim, J., Im, J. H., Kim, H. B., Oh, C. J., and An, C. S. (2008). Mitogen-activated protein kinase is involved in the symbiotic interaction between *Bradyrhizobium japonicum* USDA110 and soybean. *J. Plant Biol.* 51 (4), 291–296. doi: 10.1007/BF03036129

Lin, J., Frank, M., and Reid, D. (2020). No home without hormones: how plant hormones control legume nodule organogenesis. *Plant Commun.* 1 (5), 100104. doi: 10.1016/j.xplc.2020.100104

Liu, X., Zhang, M., Li, Z., Zhang, C., Wan, C., Zhang, Y., et al. (2019). Inhibition of urease activity by humic acid extracted from sludge fermentation liquid. *Bioresour. Technol.* 290, 121767. doi: 10.1016/j.biortech.2019.121767

Lyu, X., Xia, X., Wang, C., Ma, C., Dong, S., and Gong, Z. (2019). Effects of changes in applied nitrogen concentrations on nodulation, nitrogen fixation and nitrogen accumulation during the soybean growth period. *Soil Sci. Plant Nutr.* 65 (5), 479–489. doi: 10.1080/00380768.2019.1667213

Maji, D., Misra, P., Singh, S., and Kalra, A. (2016). Humic acid rich vermicompost promotes plant growth by improving microbial community structure of soil as well as root nodulation and mycorrhizal colonization in the roots of Pisum sativum. *Appl. Soil Ecol.* 110, 97–108. doi: 10.1016/j.apsoil.2016.10.008

Mao, X., Cai, T., Olyarchuk, J. G., and Wei, L. (2005). Automated genome annotation and pathway identification using the KEGG Orthology (KO) as a controlled vocabulary. *Bioinformatics* 21 (19), 3787–3793. doi: 10.1093/bioinformatics/bti430

Marzadori, C., Francioso, O., Ciavatta, C., and Gessa, C. (2000). Activity and stability of jack bean urease in the presence of peat humic acids obtained using different extractants. *Biol. Fertil. Soils.* 32 (5), 415–420. doi: 10.1007/s003740000272

McCoy, J. M., Kaur, G., Golden, B. R., Orlowski, J. M., Cook, D. R., Bond, J. A., et al. (2018). Nitrogen fertilization of soybean affects root growth and nodulation on two soil types in Mississippi. *Commun. Soil Sci. Plant Anal.* 49 (2), 181–187. doi: 10.1080/00103624.2017.1421649

Mohd, T., Osumanu, H. A., and Nik, M. (2009). Effect of enhancing urea-humic acid mixture with refined acid sulphate soil. *Am. J. Agric. Biol. Sci.* 6 (11), 1892–1896. doi: 10.3844/ajassp.2009.1892.1896

Mora, V., Bacaicoa, E., Zamarreño, A. M., Aguirre, E., Garnica, M., Fuentes, M., et al. (2010). Action of humic acid on promotion of cucumber shoot growth involves nitrate-related changes associated with the root-to-shoot distribution of cytokinins, polyamines and mineral nutrients. *J. Plant Physiol.* 167 (8), 633–642. doi: 10.1016/j.jplph.2009.11.018

Mulder, W. J., Gosselink, R. J. A., Vingerhoeds, M. H., Harmsen, P. F. H., and Eastham, D. (2011). Lignin based controlled release coatings. *Ind. Crops Prod.* 34 (1), 915–920. doi: 10.1016/j.indcrop.2011.02.011

Namvar, A., Sharifi, R. S., Sedghi, M., Zakaria, R. A., Khandan, T., and Eskandarpour, B. (2011). Study on the effects of organic and inorganic nitrogen fertilizer on yield, yield components, and nodulation state of chickpea (*Cicer arietinum* L.). *Commun. Soil Sci. Plant Anal.* 42 (9), 1097–1109. doi: 10.1080/00103624.2011.562587

Ng, J. L. P., Hassan, S., Truong, T. T., Hocart, C. H., Laffont, C., Frugier, F., et al. (2015). Flavonoids and Auxin Transport Inhibitors Rescue Symbiotic Nodulation in the *Medicago truncatula* Cytokinin Perception Mutant *cre1*. *Plant Cell.* 27 (8), 2210–2226. doi: 10.1105/tpc.15.00231

Nishida, H., and Suzaki, T. (2018). Nitrate-mediated control of root nodule symbiosis. *Curr. Opin. Plant Biol.* 44, 129–136. doi: 10.1016/j.pbi.2018.04.006

Paradiso, R., Buonomo, R., Dixon, M. A., Barbieri, G., and De Pascale, S. (2015). Effect of bacterial root symbiosis and urea as source of nitrogen on performance of soybean plants grown hydroponically for Bioregenerative Life Support Systems (BLSSs). *Front. Plant Sci.* 6. doi: 10.3389/fpls.2015.00888

Petricka, J. J., Winter, C. M., and Benfey, P. N. (2012). Control of *Arabidopsis* root development. *Annu. Rev. Plant Biol.* 63, 563–590. doi: 10.1146/annurev-arplant-042811-105501

Pizzeghello, D., Francioso, O., Ertani, A., Muscolo, A., and Nardi, S. (2013). Isopentenyladenosine and cytokinin-like activity of different humic substances. *J. Geochem. Explor.* 129, 70–75. doi: 10.1016/j.gexplo.2012.10.007

Podlešáková, K., Fardoux, J., Patrel, D., Bonaldi, K., Novák, O., Strnad, M., et al. (2013). Rhizobial synthesized cytokinins contribute to but are not essential for the symbiotic interaction between photosynthetic *Bradyrhizobia* and *Aeschynomene* legumes. *Mol. Plant Microbe Interact.* 26, 1232–1238. doi: 10.1094/MPMI-03-13-0076-R

Pregelj, L., McLanders, J. R., Gresshoff, P. M., and Schenk, P. M. (2010). Transcription profiling of the isoflavone phenylpropanoid pathway in soybean in response to bradyrhizobium japonicum inoculation. *Funct. Plant Biol.* 38 (1), 13–24. doi: 10.1071/FP10093

Quaggiotti, S., Ruperti, B., Pizzeghello, D., Francioso, O., Tugnoli, V., and Nardi, S. (2004). Effect of low molecular size humic substances on nitrate uptake and expression of genes involved in nitrate transport in maize (*Zea mays* L.). *J. Exp. Bot.* 55, 803–813. doi: 10.1093/jxb/erh085

Reay, M. K., Yates, C. A., Johnes, P. J., Arthur, C. J., Jones, D. L., and Evershed, R. P. (2019). High resolution HPLC-MS confirms overestimation of urea in soil by the diacetyl monoxime (DAM) colorimetric method. *Soil Biol. Biochem.* 135, 127–133. doi: 10.1016/j.soilbio.2019.04.015

Riley, I. T., and Dilworth, M. J. (1985). Cobalt requirement for nodule development and function in *Lupinus angustifolius L. New Phytol.* 100 (3), 347–359. doi: 10.1111/j.1469-8137.1985.tb02784.x

Roomi, S., Masi, A., Conselvan, G. B., Trevisan, S., Quaggiotti, S., Pivato, M., et al. (2018). Protein profiling of arabidopsis roots treated with humic substances: insights into the metabolic and interactome networks. *Front. Plant Sci.* 9. doi: 10.3389/fpls.2018.01812

Ryu, H., Laffont, C., Frugier, F., and Hwang, I. (20172017). MAP kinase-mediated negative regulation of symbiotic nodule formation in *Medicago truncatula*. *Mol. Cells* 40 (1), 17–23. doi: 10.14348/molcells.2017.2211

Saeed, A., Rehman, S.-u., Channar, P. A., Larik, F. A., Abbas, Q., Hassan, M., et al. (2017). Long chain 1-acyl-3-arylthioureas as jack bean urease inhibitors, synthesis, kinetic mechanism and molecular docking studies. *J. Taiwan Inst. Chem. Eng.* 77, 54–63. doi: 10.1016/j.jtice.2017.04.044

Schulten, H. R., and Schnitzer, M. (1993). A state of the art structural concept for humic substances. *Naturwissenschaften* 80 (1), 29–30. doi: 10.1007/BF01139754

Serban, A., and Nissenbaum, A. (1986). Humic acid association with peroxidase and catalase. *Soil Biol. Biochem.* 18 (1), 41–44. doi: 10.1016/0038-0717(86)90101-X

Shen, Y., Jiao, S., Ma, Z., Lin, H., Gao, W., and Chen, J. (2020a). Humic acid-modified bentonite composite material enhances urea-nitrogen use efficiency. *Chemosphere* 255, 126976. doi: 10.1016/j.chemosphere.2020.126976

Shen, Y., Lin, H., Gao, W., and Li, M. (2020b). The effects of humic acid urea and polyaspartic acid urea on reducing nitrogen loss compared with urea. *J. Sci. Food Agric.* 100 (12), 4425–4432. doi: 10.1002/jsfa.10482

Sincik, M., Göksoy, A. T., and Turan, Z. M. (2009). Soybean seed yield performances under different cultural practices. *Turk. J. Agric. For.* 33 (2), 111–118. doi: 10.3906/tar-0807-26

Sugiyama, A., Saida, Y., Yoshimizu, M., Takanashi, K., Sosso, D., Frommer, W. B., et al. (2017). Molecular characterization of ljSWEET3, a sugar transporter in nodules of *Lotus japonicus*. *Plant Cell Physiol.* 58 (2), 298–306. doi: 10.1093/pcp/pcw190

Susilawati, K., Osumanu, H. A., Nik, M., Mohd, K. Y., and Mohamadu, B. (2009). Effect of organic based N fertilizer on dry matter (*Zea mays* L.), ammonium and nitrate recovery in an acid soil of Sarawak, Malaysia. *Am. J. Appl. Sci.* 6 (7), 1289–1294. doi: 10.3844/AJASSP.2009.1289.1294

Tan, S., Sanchez, M., Laffont, C., Boivin, Stéphane, Le Signor, C., Thompson, R., et al. (2020). Cytokinin signaling type-B response regulator transcription factor acting in early nodulation. *Plant Physiol.* 183 (3), 1319–1330. doi: 10.1104/pp.19.01383

Tiwari, M., Pandey, V., Singh, B., Yadav, M., and Bhatia, S. (2021). Evolutionary and expression dynamics of LRR-RLKs and functional establishment of KLAVIER homolog in shoot mediated regulation of AON in chickpea symbiosis. *Genomics* 113 (6), 4313–4326. doi: 10.1016/j.ygeno.2021.11.022

Tiwari, M., Singh, B., Min, D., and Jagadish, S. V. K. (2022). Omics path to increasing productivity in less-studied crops under changing climate-lentil a case study. *Front. Plant Sci.* 13, 1239. doi: 10.3389/fpls.2022.813985

Trapnell, C., Williams, B. A., Pertea, G., Mortazavi, A., Kwan, G., van Baren, M. J., et al. (2010). Transcript assembly and quantification by RNA-Seq reveals unannotated transcripts and isoform switching during cell differentiation. *Nat. Biotechnol.* 28 (5), 511–515. doi: 10.1038/nbt.1621

van Zeijl, A., Op den Camp, R. H. M., Deinum, E. E., Charnikhova, T., Franssen, H., Op den Camp, H. J. M., et al. (2015). Rhizobium lipo-chitooligosaccharide signaling triggers accumulation of cytokinins in *Medicago truncatula* roots. *Mol. Plant* 8 (8), 1213–1226. doi: 10.1016/j.molp.2015.03.010

Wang, H., Ren, C., Cao, L., Jin, X., Wang, M., Zhang, M., et al. (2021). The mechanisms underlying melatonin improved soybean seedling growth at different nitrogen levels. *Funct. Plant Biol.* 48 (12), 1225–1240. doi: 10.1071/FP21154

Wong, W. S., Zhong, H. T., Cross, A. T., and Yong, J. W. H. (2020). Plant biostimulants in vermicomposts: Characteristics and plausible mechanisms. *Chem. Biol. Plant biostimulants* 6, 155–180. doi: 10.1002/9781119357254.ch6

Xiong, D., Chen, J., Yu, T., Gao, W. L., Ling, X. X., Li, Y., et al. (2015). SPAD-based leaf nitrogen estimation is impacted by environmental factors and crop leaf characteristics. *Rep* 5 (1), 13389. doi: 10.1038/srep13389

Xu, H., Li, Y., Zhang, K., Li, M., Fu, S., Tian, Y., et al. (2021). *miR169c-NFYA-C-ENOD40* modulates nitrogen inhibitory effects in soybean nodulation. *New Phytol.* 229 (6), 3377–3392. doi: 10.1111/nph.17115

Yamashita, N., Tanabata, S., Ohtake, N., Sueyoshi, K., Sato, T., Higuchi, K., et al. (2019). Effects of different chemical forms of nitrogen on the quick and reversible inhibition of soybean nodule growth and nitrogen fixation activity. *Front. Plant Sci.* 10. doi: 10.3389/fpls.2019.00131

Yin, J., Guan, X., Zhang, H., Wang, L., Li, H., Zhang, Q., et al. (2019). An MAP kinase interacts with LHK1 and regulates nodule organogenesis in *Lotus japonicus*. *Sci. China: Life Sci.* 62 (9), 1203–1217. doi: 10.1007/s11427-018-9444-9

Young, M. D., Wakefield, M. J., Smyth, G. K., and Oshlack, A. (2010). Gene ontology analysis for RNA-seq: accounting for selection bias. *Genome Biol.* 11 (2), R14. doi: 10.1186/gb-2010-11-2-r14

Yuan, Z., Ata-Ul-Karim, S. T., Cao, Q., Lu, Z. Z., and Cao, W. X. (2016). Indicators for diagnosing nitrogen status of rice based on chlorophyll meter readings. *Field Crops Res.* 185, 12–20. doi: 10.1016/j.fcr.2015.10.003

Zhang, Y. M., Li, Y., Chen, W. F., Wang, E. T., Tian, C. F., Li, Q. Q., et al. (2011). Biodiversity and Biogeography of Rhizobia associated with soybean plants grown in the north china plain. *Appl. Environ. Microbiol.* 77 (18), 6331–6342. doi: 10.1128/AEM.00542-11

frontiers | Frontiers in Plant Science

TYPE Review
PUBLISHED 09 October 2023
DOI 10.3389/fpls.2023.1277262

OPEN ACCESS

EDITED BY
Chang Fu Tian,
China Agricultural University, China

REVIEWED BY
Oswaldo Valdes-Lopez,
National Autonomous University of Mexico, Mexico
Maria Jose Soto,
Spanish National Research Council (CSIC), Spain

*CORRESPONDENCE
Philippe Remigi
philippe.remigi@inrae.fr

RECEIVED 14 August 2023
ACCEPTED 22 September 2023
PUBLISHED 09 October 2023

CITATION
Granada Agudelo M, Ruiz B, Capela D and Remigi P (2023) The role of microbial interactions on rhizobial fitness. *Front. Plant Sci.* 14:1277262. doi: 10.3389/fpls.2023.1277262

The role of microbial interactions on rhizobial fitness

Margarita Granada Agudelo, Bryan Ruiz, Delphine Capela and Philippe Remigi*

Laboratoire des Interactions Plantes Microbes Environnement (LIPME), Université de Toulouse, INRAE, CNRS, Castanet-Tolosan, France

Rhizobia are soil bacteria that can establish a nitrogen-fixing symbiosis with legume plants. As horizontally transmitted symbionts, the life cycle of rhizobia includes a free-living phase in the soil and a plant-associated symbiotic phase. Throughout this life cycle, rhizobia are exposed to a myriad of other microorganisms that interact with them, modulating their fitness and symbiotic performance. In this review, we describe the diversity of interactions between rhizobia and other microorganisms that can occur in the rhizosphere, during the initiation of nodulation, and within nodules. Some of these rhizobia-microbe interactions are indirect, and occur when the presence of some microbes modifies plant physiology in a way that feeds back on rhizobial fitness. We further describe how these interactions can impose significant selective pressures on rhizobia and modify their evolutionary trajectories. More extensive investigations on the eco-evolutionary dynamics of rhizobia in complex biotic environments will likely reveal fascinating new aspects of this well-studied symbiotic interaction and provide critical knowledge for future agronomical applications.

KEYWORDS

rhizobia, symbiosis, nitrogen fixation, microbial communities, microbe-microbe interactions, eco-evolutionary dynamics

1 Introduction

Ecological systems are complex. They involve a multitude of organisms that can interact with each other. These interactions, ranging from antagonism to mutualism, strongly influence the fitness of each individual and, consequently, the structure of the communities in which they live. Microbial communities, termed microbiomes, in particular have received much attention because of the fundamental role they play in Earth's biogeochemical cycles and in plant and animal health. Common mechanisms governing interactions within microbiomes include competition for resources, predation, the production of antagonistic/toxic molecules, cross-feeding processes, the production of public goods, or the formation of protection structures such as biofilms (Konopka, 2009; Pierce and Dutton, 2022). These interactions are particularly prevalent and significant in dense host-associated microbial communities, such as the mammalian gut or the

rhizosphere (Hassani et al., 2018; Coyte and Rakoff-Nahoum, 2019; Kern et al., 2021; Chepsergon and Moleleki, 2023). In these ecosystems, positive or negative interactions between microbiome members can allow or inhibit, respectively, the proliferation of pathogens or beneficial microbes, with important effects on host health. For example, some rhizospheric bacteria were shown to inhibit the growth of fungal pathogens and protect plants against disease (Carrión et al., 2018; Durán et al., 2018).

Notable members of the rhizosphere community are rhizobia. These bacteria are able to form mutualistic associations with legume plants, during which they fix atmospheric nitrogen to the benefit of the host, in exchange for carbon compounds from photosynthesis (Poole et al., 2018). Rhizobia are gram-negative bacteria classified in 18 different genera of Alpha- and Beta-proteobacteria including *Rhizobium, Sinorhizobium, Bradyrhizobium, Mesorhizobium, Azorhizobium, Cupriavidus*, and *Paraburkholderia* (Masson-Boivin et al., 2009; Tang and Capela, 2020). Rhizobia are horizontally-transmitted symbionts. Their biphasic life cycle is composed of a free-living saprophytic phase, where rhizobia are part of the soil and rhizosphere microbiomes, and a symbiotic phase in their host. Soil bacteria are attracted to the germinating seeds or the mature roots following the perception of chemoattractants present in plant exudates (Compton and Scharf, 2021). In the plant, rhizobia are hosted in specific root organs, called nodules. Nodule formation is initiated by the exchange of compatible signals between rhizobia and legumes (Walker et al., 2020). In most rhizobia, the expression of *nod* genes, responsible for the synthesis of lipochito-oligosaccharides called Nod Factors (NF), is induced by specific flavonoids exuded by host plants. NF, whose structures vary between rhizobium strains, are then specifically recognised by plant receptors. The perception of NF allows the entry of bacteria in root tissues, where they start to proliferate extracellularly. NF perception and downstream signaling also trigger a plant development program, which leads to nodule organogenesis. In most legumes of the Papilionoideae and Mimosoid clades (Sprent, 2009; De Faria et al., 2022), rhizobia are then engulfed in the cytoplasm of nodule cells, where they form structures surrounded by the plant plasma membrane called symbiosomes. Rhizobia differentiate into bacteroids that fix nitrogen, and persist for several weeks or months within nodule cells. In legumes of the Inverted Repeat-Lacking Clade and Dalbergioid clade, this differentiation is terminal, meaning that bacteroids cannot resume growth after nodule senescence (Mergaert et al., 2006; Czernic et al., 2015; Montiel et al., 2016). During nodule senescence, undifferentiated bacteria and non-terminally differentiated bacteroids present in nodules are released and can recolonise the soil and the rhizosphere. The ability of a given rhizobial strain to successfully complete the different steps of this complex life cycle will determine how fit it is in its current environment. Studying the different factors governing rhizobial fitness is critical to understand the diversity, ecology and evolution of these important plant symbionts.

All along their life cycle, rhizobia interact with other microorganisms composing the soil, rhizosphere and nodule microbiomes, and are therefore involved in a diversity of interactions that affect their fitness either directly or indirectly through plant-mediated mechanisms. This review focuses on how the microbial community context, *i.e.* the ecological interactions between rhizobia and other microorganisms, contributes to determining rhizobial fitness. We first discuss the notion of fitness in the case of rhizobia and then describe how the diverse rhizobia-microorganisms (including rhizobia-rhizobia) interactions affect the fitness of rhizobia and their evolutionary dynamics.

2 The multiple facets of rhizobial fitness

Fitness is a central notion in evolutionary biology, as it measures how well a genotype performs in terms of survival and reproduction in a given environment. Yet, experimental measurements of fitness can be challenging. Even in seemingly simple systems (Vasi et al., 1994), bacterial fitness is dependent on several phenotypic traits (called 'fitness components') that will determine a genotype's performance at the different steps of the life cycle (Orr, 2009). However, the life history traits that are measured and considered as best fitness proxies can differ between studies and experimenters. This is typically the case for rhizobia. The different measurable fitness components include (i) proliferation and survival in the soil and the rhizosphere, (ii) nodulation proficiency and competitiveness, (iii) proliferation and survival within nodules, and (iv) bacterial release from nodules during senescence. Below we highlight salient aspects of some of these different fitness measures.

Understandably, literature on rhizobial fitness has put a lot of emphasis on bacterial traits governing the association with host plants. First, the nodulation step is a major determinant of fitness for rhizobia, since it represents a strong selective bottleneck for rhizobial populations and rhizobia founding nodules will leave many more descendants than those staying in the rhizosphere (Denison and Kiers, 2011). Although nodules are usually considered to be founded by one single bacterium, mixed nodules, hosting several different rhizobial strains, can also be found in proportions that vary depending on the plant growth substrate or rhizobial density (Checcucci et al., 2016; Daubech et al., 2017; Mendoza-Suárez et al., 2020). The ability of rhizobia to form nodules can be measured during single inoculation experiments (nodulation proficiency) or in co-inoculation experiments (nodulation competitiveness). There can be significant discrepancies between these two types of assays, as the outcome of nodule occupancy following co-inoculations is unpredictable from data in single inoculation. Indeed nodulation competitiveness is a complex trait that involves a large number of bacterial genes and functions (see section 4) and that is not fully understood yet (Younginger and Friesen, 2019; Mendoza-Suárez et al., 2021). Rhizobial strains can be more competitive for nodulation if (i) they are more efficient at colonising the rhizosphere (for example by growing faster on the available nutrient sources or by producing antimicrobial compounds that inhibit the growth of sensitive competitor strains), (ii) they are faster to reach the root and induce nodulation, and/or (iii) they show an optimal compatibility with the host plant (Handelsman

et al., 1984; Kiers et al., 2013; Boivin and Lepetit, 2020; Mendoza-Suárez et al., 2021). Moreover, when the co-inoculated strains have different nitrogen fixation efficiencies, the absolute and relative numbers of nodules formed by one plant can be modulated by the mechanism of auto-regulation of nodulation (AON, see section 5). Indeed, in single inoculations, strains that are fixing large amounts of nitrogen may form a relatively small number of nodules (since the nitrogen needs of the plants will be covered with few nodules), while strains that fix low amounts of nitrogen may form a large number of nodules. Yet, co-inoculating these two types of strains may modulate the number of nodules formed by each strain (Daubech et al., 2017; Westhoek et al., 2017).

Second, bacterial proliferation within nodules can be assessed by harvesting, crushing surface-sterilised nodules and plating the resulting suspensions on selective media. An important aspect of these experiments is that only viable nodule bacteria will be detected. In certain legumes, bacteroids undergo a process of 'terminal differentiation' characterised by drastic morphological and physiological changes as well as a loss of viability (Mergaert et al., 2006). As a result, the proportion of viable bacteria within nodules can vary from less than 1% in pea or *Medicago* to almost 100% in plants where bacteroids are not terminally differentiated such as soybean, with intermediate cases (Gresshoff and Rolfe, 1978; Mergaert et al., 2006; Marchetti et al., 2011). When terminal differentiation occurs, viable bacteria that can be recovered from nodules most likely arise from bacteria that were still located in infection threads or intercellular spaces at the time of harvest.

In addition, the proliferation and/or viability of rhizobia within nodule cells can be affected by their nitrogen fixation activity. Since the first discovery that soybean can 'sanction' non-fixing rhizobia (Kiers et al., 2003) and thereby promotes fitness of nitrogen-fixing ones, ample experimental data from several model species has accumulated to support the idea that there is a positive correlation between nitrogen fixation and rhizobial fitness (Kiers et al., 2006; Oono et al., 2011; Friesen, 2012; Kimbrel et al., 2013; Berrabah et al., 2015; Daubech et al., 2017; Quides et al., 2017; Burghardt et al., 2018; Westhoek et al., 2021; Batstone et al., 2022; Epstein et al., 2023). Plants can even discriminate fixing versus non-fixing strains in mixed nodules, and only target non-fixing bacteria for premature degeneration (Daubech et al., 2017; Regus et al., 2017). However, there are exceptions, where non-fixing rhizobia show higher fitness than fixing ones [(Crook et al., 2012; Porter and Simms, 2014; Gano-Cohen et al., 2019) but see (Frederickson, 2020; Wendlandt et al., 2022) to ponder two of these examples]. Nodule size or weight are sometimes used as convenient proxies for bacterial fitness, but in certain cases, these values should be interpreted with caution. Indeed, the efficiency of nitrogen fixation (and the occurrence of plant 'sanctions', see below) or the accumulation of storage compounds can modify the relationship between nodule weight and the number of viable bacteria per nodule (Oono et al., 2011; Ratcliff et al., 2011). Another study showed, using a large collection of natural *S. meliloti* isolates, that nodule weight was positively correlated to the symbiotic fitness of the bacteria but only in one of the two plant genotypes tested (Batstone et al., 2022).

At the final stage of the symbiosis, nodules senesce and bacteria return to the soil where they can survive for months or even years before re-infecting a new host (Denison and Kiers, 2011). This extended phase of the rhizobial life cycle is crucial for the ecology and evolution of these bacteria, but remains largely understudied. In aged nodules of *M. sativa*, a population of saprophytic bacteria develop in the proximal zone (Timmers et al., 2000). A recent transcriptomic analysis showed that cell division and the general stress response are activated in rhizobia from senescent nodules (Sauviac et al., 2022). These results indicate that exiting nodules is an active process for rhizobia, but there are, to our knowledge, no study that analysed the determinants of rhizobial fitness during this phase. To persist in the soil, some bacteria may rely on previously accumulated carbon storage particles, such as polymers of poly-3-hydroxybutyrate (PHB) (Müller-Santos et al., 2021). Among rhizobial strains, some, but not all (Trainer and Charles, 2006; Chen et al., 2023), were shown to accumulate high amounts of PHB in nodules, which can represent up to 50% of the dry weight of the cells (Bergersen et al., 1995; Tavernier et al., 1997). This stored PHB can support several divisions of bacteria or a much longer survival of dormant cells without the need for any other carbon sources (Muller and Denison, 2018). Therefore, measuring PHB content in bacteroids could be a good proxy for estimating the ability of rhizobia to reproduce in soil, and an indicator of the 'quality' of the progenies released from nodules (Ratcliff et al., 2008; Ratcliff et al., 2011; Muller and Denison, 2018). Alternative polymers such as glycogen can also be produced by some rhizobia in nodules to store carbon and energy (Lodwig et al., 2005; Wang et al., 2007a). These processes, which consume significant amounts of energy resources, are thought to divert energy from nitrogen fixation (Lodwig and Poole, 2003) and thus induce plant sanctions (Oono et al., 2020). However, in the literature, mutants defective in the synthesis of PHB have shown contrasting nitrogen fixation phenotypes, ranging from increased to decreased nitrogen fixation (Cevallos et al., 1996; Lodwig et al., 2005; Wang et al., 2007a; Wang et al., 2007b; Crang et al., 2021). Considering the redox balance and oxygen-limiting conditions that prevail in nodules, the accumulation of PHB or other carbon polymers may indeed be required for the persistence of bacteroids in nodules (Terpolilli et al., 2016; Schulte et al., 2021). There may therefore be a trade-off between rhizobial survival in the soil, persistence in nodules and nitrogen fixation efficiency (Ratcliff et al., 2008), but these effects might be species-specific and host-plant dependent (Chen et al., 2023).

Beyond the analysis of individual fitness components, an important question relates to the potential couplings or trade-offs between the different phenotypic traits. In particular, there is no selection of nitrogen fixation at the nodulation step (since nitrogen fixation occurs at the late stages of the interaction) (Daubech et al., 2017; Westhoek et al., 2017), but several lines of evidence indicate that co-evolutionary processes may lead to the selection of strains that are both competitive for nodulation and efficient for nitrogen fixation on a given host genotype (Burghardt et al., 2018; Younginger and Friesen, 2019; Batstone et al., 2020; Fields et al., 2023; Rahman et al., 2023). This can occur through partner-fidelity feedback, a positive feedback loop acting on the fitness of the two

mutualistic partners as a result of repeated associations between these organisms (Sachs et al., 2004; Fujita et al., 2014).

Although most of the fitness measurements described above usually rely on traditional microbiological techniques [with potential new optimisations, e.g. (Mendoza-Suárez et al., 2020; Quides et al., 2023)], new approaches based on bacterial populations carrying short DNA tags, in combination with next generation sequencing, now enable to analyse rhizobial fitness in a high-throughput manner (Burghardt et al., 2018; Wheatley et al., 2020). These approaches are particularly powerful to gather integrative measures of fitness (*e.g.* encompassing all fitness components composing the entire life cycle) in genetically complex rhizobial populations, and open many opportunities to perform integrative fitness measurements in a variety of conditions (Burghardt, 2020; Burghardt et al., 2020; Burghardt et al., 2022).

Finally, it is worth remembering that measurements of bacterial fitness will likely be dependent on the abiotic and biotic environment during the experiment. Abiotic factors include experimental conditions (light, temperature, plant growth substrate…), and biotic factors include host plant genotype and microbial communities (composition and density), which is the focus of this review. In the next sections, we illustrate how microbial communities affect rhizobial fitness at the different steps of their life cycle (Figure 1; Table 1; Supplementary Table 1).

3 The rhizosphere microbiome: a hotspot for microbial interactions

The rhizosphere, which is the soil surrounding and under the influence of the roots, is characterised by a high microbial biomass and a great diversity of tens of thousands of species (Berendsen et al., 2012; De La Fuente Cantó et al., 2020). It is composed of eukaryotic microorganisms (protozoa, fungi, oomycetes, yeasts and nematodes), prokaryotic microorganisms (bacteria and archaea) and viruses (Philippot et al., 2013). This complex microbial community is highly dynamic and depends on the soil chemical and biochemical characteristics, the plant genotypes, and the type of interactions between plants and microorganisms (mutualistic, pathogenic, saprophytic, or commensal) (Philippot et al., 2013; Trivedi et al., 2020). In particular, exudates released by the roots, such as the secretion of aromatic organic acids that are preferentially consumed by rhizosphere bacteria have a major effect on microbial abundance and composition (Bais et al., 2006; Shi et al., 2011; Zhalnina et al., 2018). Abiotic factors such as pH, salinity, the presence of biofertilizers, heavy metals and carbon resource availability are also strong factors influencing the rhizobiome (Ofek et al., 2006; Bellabarba et al., 2019). In addition, microbial interactions among community members have a fundamental effect on the rhizobiome composition (Hassani et al., 2018; Chepsergon and Moleleki, 2023). Network community analyses have found co-occurrence and exclusion patterns suggesting positive and negative interactions between microorganisms (Han et al., 2020). Several mechanisms can explain these patterns. For instance, competition between organisms sharing the same ecological niche and exploiting the same resources can lead to the exclusion of some strains (Hibbing et al., 2010; Ghoul and Mitri, 2016). The secretion of antibiotics or metabolites or even predation (i.e. killing and consuming the prey) by members of the community also influence the abundance of the other members (Granato et al., 2019; Peterson et al., 2020). On the other hand, cooperation by the production of public goods (Smith and Schuster, 2019) and cross-feeding between microorganisms (D'Souza et al., 2018; Jacoby and Kopriva, 2019) can maintain the co-occurrence of some species in the community. Plant-mediated indirect interactions can also occur when microbes induce a modification in the secretion of root exudates, which in turn affects other members of the microbiome (De La Fuente Cantó et al., 2020; Korenblum et al., 2020).

The root-associated rhizobial density varies in nature (Yan et al., 2014). It depends on both positive and negative interactions with other microorganisms. Among negative interactions, predation by protozoa or bacteria (*Bdellovibrio* or *Myxococcus*) can alter rhizobial populations (Danso et al., 1975; Keya and Alexander, 1975; Ramirez and Alexander, 1980). Soil bacteriophages, which have been shown to rapidly adapt to local bacterial host communities, can also reduce the rhizobial density in the rhizosphere (Van Cauwenberghe et al., 2021). Finally, the presence of antimicrobial compounds produced by other rhizosphere microorganisms such as antibiotics produced by Actinomycetes is likely to inhibit the growth of rhizobia (Patel, 1974; Pugashetti et al., 1982). However, certain rhizobia have the means to survive to these attacks and compete with other microorganisms in the soil. In an *in vitro* experiment, Pérez et al. (2014) showed that some strains of *Sinorhizobium meliloti* that produce the exopolysaccharide (EPS) galactoglucan are more resistant to predation by *Myxococcus xanthus*. Given that EPS play a crucial role in plant recognition and early steps of symbiosis, it is possible that in the rhizosphere, EPS production has a dual ecological advantage in reducing predation and promoting interactions with compatible host plants. The production of melanin was also shown to favour resistance against predation by *Myxococcus xanthus* (Contreras-Moreno et al., 2020), and a transcriptomic analysis identified several other putative defense mechanisms, such as the production of surface polysaccharides and membrane lipids, the activation of efflux pumps or the induction of iron uptake (Soto et al., 2023).

In addition, studies have shown that type VI secretion systems (Bladergroen et al., 2003; De Campos et al., 2017) as well as the production of phages (Schwinghamer and Brockwell, 1978; Joglekar et al., 2023) or bacteriocins (Hirsch, 1979; Triplett and Barta, 1987; Oresnik et al., 1999) in rhizobia can play an important role in the direct inhibition of bacterial competitors. Among antagonistic molecules produced by rhizobia, diffusible quorum sensing molecules, in particular Acyl Homoserine Lactones (AHLs), can inhibit the growth of other rhizobial strains by activating LuxR-type regulators in the neighbouring strains and inducing genes leading to growth arrest (Schripsema et al., 1996; Wilkinson et al., 2002). The production of these antimicrobial compounds by rhizobia offers a competitive advantage in nutrient-limited environments but also for the establishment of symbiosis, by inhibiting other nodulating bacteria. A recent *in vitro* study suggests that both facilitative and

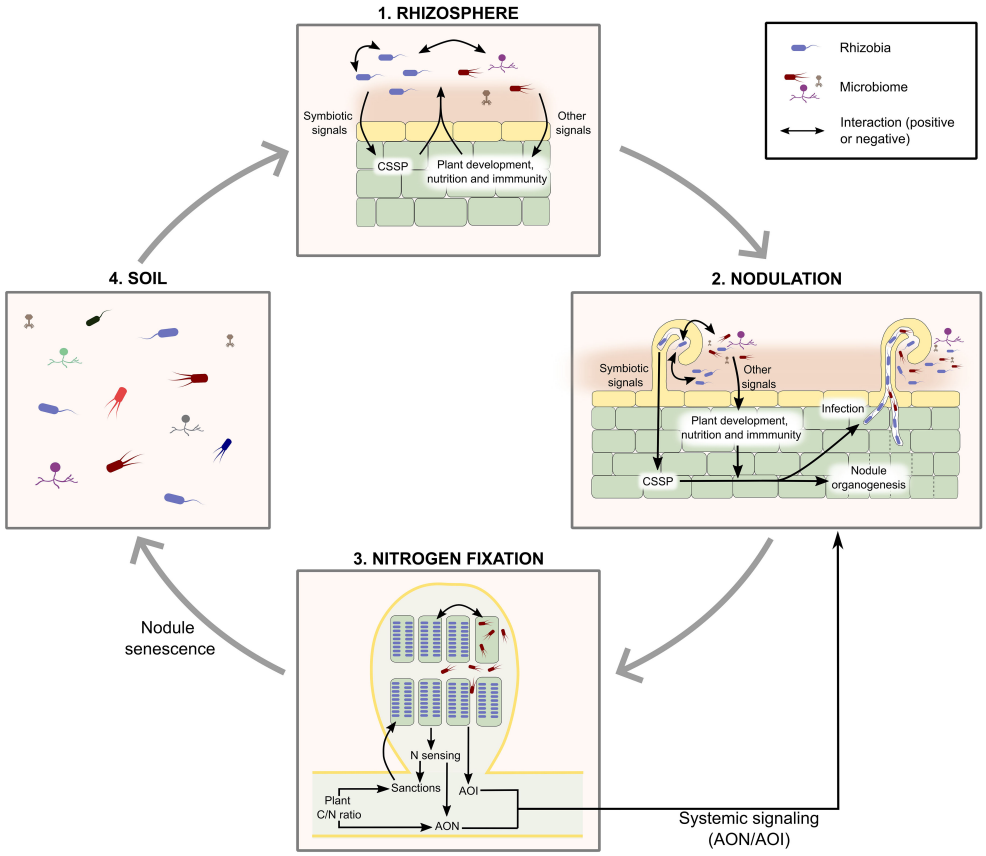

FIGURE 1
The life cycle of rhizobia and interactions with microbiome. A simplified view of the life cycle of rhizobia considers 4 successive steps: (1) colonisation of the rhizosphere, (2) initiation of nodulation, (3) nodule infection and nitrogen fixation, (4) nodule senescence and release of bacteria in the soil. Interactions with other microbes can occur at each step of the life cycle. (1) Rhizosphere: direct interactions (contact-dependent, or mediated by the secretion of beneficial or harmful chemical compounds) can occur as in any microbial community; indirectly, rhizobia and some members of the rhizosphere microbiome can modify the composition of their microbial community through plant-mediated effects: rhizobia and AMF through CSSP and non-rhizobia likely via other pathways linked to plant development, immunity, or nutrition. (2) Nodulation: rhizobia elicit plant symbiosis signaling pathways, more or less efficiently, which results in different levels of competitiveness. Other microbiome members can also induce physiological responses (for example through the secretion of plant hormones, or the modulation of hormone synthesis by the plant, or the synthesis of incompatible Nod Factors) that affect nodulation (positively or negatively, respectively). Direct physical or biochemical interactions between rhizobia and other microbes can also affect rhizobial nodulation success. (3) Nodule infection and nitrogen fixation: direct interactions can occur through the secretion of diffusible molecules (siderophores, antibiotics…) within nodules. Indirect interactions can result from the conditional sanctioning of rhizobia fixing less nitrogen than rhizobia present in other nodules. Of note, bacteria within nodules can influence the nodulation process (through AON, AOI, or the production of rhizobitoxin). AON, and probably conditional sanctioning, depend on the general physiological status of the plant (C/N ratio), which can be influenced by many biotic or abiotic factors. (4) Although we have not found any documented example (and are therefore not represented on this figure), it is also possible that in nodules indirect interactions between non-rhizobial endophytes and rhizobia occur, if nodule endophytes can activate plant signaling pathways that modify nodule physiology and rhizobial survival. Finally, although interactions likely occur during nodule senescence and bacterial release in the soil, we have not found any references on that topic. AOI, Auto-regulation of Infection; AON, Auto-regulation of Nodulation; CSSP, Common Symbiotic Signaling Pathway (induced by both AMF and rhizobium symbionts).

inhibitory interactions exist even between rhizobial genotypes of the same species (Fields et al., 2022).

Besides negative interactions, cases of cooperation between rhizobia and other microorganisms are frequently found. An example of positive interaction was recently observed in co-cultures of the rhizobium *Rhizobium etli* and the yeast *Saccharomyces cerevisiae*. This interaction led to the formation of mixed biofilms in which the growth of the rhizobium was promoted (Andrade-Domínguez et al., 2021). This study has shown that this synergism is an effect of commensal interactions, where the rhizobia benefit from compounds secreted by the yeast such as dicarboxylic acids that bacteria use for their nutrition, and sophoroside, an antimicrobial compound detoxified by *R. etli*, which can shape the composition of the microbial community associated with this yeast. In the rhizosphere, nutritional interdependencies and reciprocal exchange of metabolites between microorganisms are commonly found (Jacoby and Kopriva, 2019). For example, a feeding of rhizobia by *Actinobacteria* capable of hydrolyzing cellulose has been evidenced (Silva et al., 2019). Other synergistic interactions were observed between *Mesorhizobia* and *Actinobacteria* (Vo et al., 2021), and between *Sinorhizobia* and bacteria of the *Bacillus cereus* group (Han et al., 2020), which enhance the growth of rhizobia by mechanisms that have not yet been elucidated.

Finally, recent research has led to the discovery that plant functional genes, and in particular symbiotic signaling genes in legumes, are involved in modulating the structure of the root-

TABLE 1 Types of microbial interactions that can alter the fitness of rhizobia[a].

Compartment / lifecyle stage	Type of interactions	Effects/Mechanisms
Rhizosphere	Direct	A variety of microorganisms, such as rhizospheric bacteria (including Actinobacteria, nodule endophytes, or other rhizobia), yeasts, bacteriophages, protozoa or fungi, can directly interact with rhizobia in the rhizosphere, and promote or inhibit their growth. Antagonistic effects include predation, production of antimicrobial compounds, or contact-dependent inhibition, while positive interactions can occur through cross-feeding or protection by the production of biofilms.
Rhizosphere	Indirect	The composition of root exudates strongly affect microbial communities in the rhizosphere. Some rhizospheric bacteria can modify the secretion of root exudates and it is thus plausible (but, to our knowledge, remains to be shown) that these modifications can then alter the growth and survival of rhizobia in the rhizosphere.
Initiation of nodulation	Direct	Direct interactions specifically acting on the initiation of nodulation (i.e., not being a direct consequence of the rhizospheric stage) can occur through the modification of rhizobial gene expression, or the propagation of rhizobia towards infection sites thanks to fungal hyphae. Negative interactions can occur by competition for attachement sites on root hairs or the saturation of plant receptors with incompatible Nod Factors.
Initiation of nodulation	Indirect	The outcome of competition for nodulation between rhizobia will depend on the compatibility of bacterial factors (NF, LPS, EPS…) with the host plant. Cases of positive indirect interactions can occur when one rhizobial strain produces compatible diffusible signals (NF, EPS) that promote nodulation of another rhizobium (trans-complementation). Other microorganisms can interfere with nodulation by producing compounds, such as plant hormones, that favor or inhibit nodulation, or by providing nutrients that modify the global physiological status of the plant (e.g. phosphate supply by AMF).
Nodule	Direct	Nodule epiphytic bacteria assists the bacteroids in assimilating metals, likely by producing siderophores that sequester them and then transfer them to the bacteroids.
Nodule	Indirect	The persistence of rhizobia within nodules can be modified by the plant according to the nitrogen fixation level of the strains colonising the different nodules of a host plant (conditional sanctions). AMF reduces the effect of drought stress on nodule senescence by reducing oxidative stress. Rhizospheric bacteria or rhizobia can secrete molecules that interfere with plant hormonal pathways to delay nodule senescence.

[a]See Supplementary Table 1 for additional details on the interactions mentionned in this table.

associated microbiota and the interactions among these communities (Zgadzaj et al., 2016; Thiergart et al., 2019; Liu et al., 2023). Legumes can establish mutualistic interactions with rhizobia and arbuscular mycorrizal fungi (AMF) that induce symbiotic signaling pathways involving specific components but also sharing some common components (Oldroyd, 2013). Disruption of both common and specific components of the symbiotic pathways affects the relative abundance of many bacterial and fungal taxa in the rhizosphere. For example, *Lotus japonicus* mutants defective in rhizobial NF perception (*nfr5* mutants) or in rhizobium infection (*nin* mutants) associate with a different bacterial community than the wild-type *Lotus japonicus* accession, with several bacterial orders such as Flavobacteriales, Myxococcales, Pseudomonadales, Rhizobiales, and Sphingomonadales being depleted in the roots of mutant plant genotypes (Zgadzaj et al., 2016; Wippel et al., 2021). Furthermore, inactivation of both root nodule and arbuscular mycorrhizal symbiosis pathways (*symrk* and *ccamk* mutants) was surprisingly associated with the root microbiota network structure (increase in both network connectivity and degree centrality) suggesting a higher number of interactions between community members in the absence of both symbioses (Thiergart et al., 2019). Interestingly, the activation of the specific mycorrhizal symbiosis pathway in peanut was shown to promote the accumulation of rhizobia in the rhizosphere and stimulate nodulation (Wang et al., 2021). Altogether, these studies showed a broad role of plant symbiotic genes in shaping the structure of microbial communities on legume roots or rhizosphere and the interactions between members of these communities.

4 Microbial interactions interfering with the initiation of nodulation

The success of nodulation by rhizobia depends not only on the rhizobial density near the root but also on a process of selection mediated by the plant. In nature, legumes are usually nodulated by a diversity of rhizobial strains that produce NF with compatible structure. However, among compatible strains, even from the same species complex, some are more competitive than others to form nodules (Elliott et al., 2009; Melkonian et al., 2014; Batstone et al., 2017; Boivin et al., 2020; Boivin et al., 2021). This preferential association is dependent on both the plant genotype, the bacterial genotypes and the interaction between the plant and bacterial genotypes (Burghardt et al., 2017; Boivin et al., 2021; Fagorzi et al., 2021). On the bacterial side, using classical genetics or large-scale transposon insertion mutant libraries, several studies have shown that hundreds of genes are involved in the competitive ability of rhizobia to form nodules (Pobigaylo et al., 2008; Wheatley et al., 2020; Mendoza-Suárez et al., 2021). Beyond NF biosynthesis and regulatory genes, genes involved in motility and chemotaxis, or other functions that help bacteria to migrate near the roots (Caetano-Anollés et al., 1988; Wheatley et al., 2020; Ji et al., 2023), and in surface polysaccharide biosynthesis (Pobigaylo et al., 2008; Janczarek et al., 2009) were shown to be important for competitive nodule formation. Also, the bacterial capacity to metabolise components found in root exudates such as the homoserine or mimosine (Soedarjo and Borthakur, 1998;

Vanderlinde et al., 2014), particular sugars such as erythritol (Yost et al., 2006; Wheatley et al., 2020), rhamnose (Oresnik et al., 1998), myo-inositol (Fry et al., 2001) or amino acids such as proline (Jimenez-Zurdo, 1995) contribute to nodulation competitiveness. In addition, genes involved in purine biosynthesis (Xie et al., 2009; Wheatley et al., 2020) and nitrogen metabolism (Wheatley et al., 2020) play a role in competitive nodule occupancy. Although in nature strains that exhibit high competitiveness for nodulation often demonstrate high nitrogen fixation efficiency as well (Burghardt et al., 2018; Fields et al., 2023; Rahman et al., 2023), the capacity to fix atmospheric nitrogen itself does not contribute to nodulation competitiveness (Amarger, 1981; Hahn and Studer, 1986; Daubech et al., 2017; Westhoek et al., 2017; Bourion et al., 2018). Interestingly, co-inoculation of highly competitive and efficient nitrogen-fixing strains with another rhizobial strain can lead either to higher plant benefits than in single inoculation or, on the contrary, to a decrease in both nodulation and plant benefits, indicating the existence of positive and negative competitive interferences between the rhizobial strains (Heath and Tiffin, 2007; Montoya et al., 2023; Rahman et al., 2023). Other interactions negatively affecting nodulation initiation were described by Gano-Cohen et al. (2016), who showed that the presence of non-nodulating *Bradyrhizobium* reduced the number of nodules formed by nodulating *Bradyrhizobium* on the legume *Acmispon strigosus*, probably by directly competing for attachment sites on the root. In another study, a phenomenon called "competitive nodulation blocking" was observed in the presence of some rhizobial strains that produce high levels of NF of incompatible structure, thus inhibiting nodulation by other compatible symbionts (Hogg et al., 2002). The presence of plant pathogens can also inhibit nodule formation as shown under laboratory conditions by Benezech et al. (2021) using the *Medicago-Sinorhizobium-Ralstonia* model system.

On the other hand, direct cooperations between rhizobial strains are possible through the production of extracellular diffusible molecules that can functionally complement each other. For example, a *Mesorhizobium loti* strain deficient in NF production (R7A *nodA* mutant) and another one deficient in exopolysaccharide production (R7A *exoU* mutant) are both unable to nodulate *Lotus japonicus* but can complement each other to form functional nodules. In that case, 80% of nodules contained both strains (Kelly et al., 2013). Similar results were obtained with *nod* and *exo* mutants of *Sinorhizobium meliloti* nodulating alfalfa (Klein et al., 1988; Kapp et al., 1990). A more recent study showed that complementation of rhizobium EPS deficient strain can be done by non rhizobial nodule endophytic bacteria (Zgadzaj et al., 2015). Another example of cooperation has been observed between the *Phaseolus vulgaris* symbiont *R. etli* and a commensal rhizobium *R. fabae*. In this cooperation, *R. fabae* produces AHLs, quorum sensing molecules that are perceived by the CinR regulator of *R. etli* leading to changes in gene expression and optimisation of nodulation (Miao et al., 2018).

In addition, the presence of plant growth-promoting rhizobacteria (PGPR) in the soil can indirectly increase the nodulation efficiency of rhizobia by producing or decreasing the amounts of phytohormones known to interfere either positively or negatively with the nodulation process (Alemneh et al., 2020). For example, the production of indole-3-acetic acid (IAA), a plant hormone of the auxin class, by bacteria of the genera *Azospirillum*, *Micromonosperma*, *Pseudomonas* or *Bacillus*, increases nodule formation by rhizobia on legumes (see (Alemneh et al., 2020) for a review on bacteria able to synthesise IAA). Indeed, these molecules are known to increase lateral root growth (Casimiro et al., 2001), potentially providing more infection sites for rhizobia. IAA may also promote nodulation through induction of a rhizobium infection signaling pathway in root hairs (Breakspear et al., 2014). In addition, many PGPRs, such as bacteria of the genera *Serratia*, *Arthrobacter* or *Pseudomonas*, are able to produce 1-aminocyclopropane-1-carboxylate (ACC) deaminase which sequesters and cleaves the plant ethylene precursor ACC, reducing levels of ethylene, a negative regulator of nodule formation, and thus promoting nodulation (see (Alemneh et al., 2020) for a review on bacteria able to synthesise ACC deaminases). This process is even more important under stressful conditions, such as salinity stress, known to increase the levels of plant-produced ethylene (Ahmad et al., 2011). Finally, some PGPR can increase the availability of nutrients for rhizobia and can stimulate their growth *in vitro* (Le et al., 2016; Vo et al., 2021). An example of cooperation between *Streptomyces* and *Rhizobium* sp. was described by Tokala et al. (2002), where iron- and molybdate-sequestering siderophores produced by *Streptomyces* provide these metals to the rhizobium strain at early and late symbiotic stages, increasing both nodulation and nitrogen fixation.

Rhizobia can also interact with eukaryotic microorganisms such as fungi. A large number of studies have shown the positive effect of AMF on nodulation (Antunes and Goss, 2005; Barea et al., 2005; Pang et al., 2023; Tsikou et al., 2023). Phosphate supply by the fungus seems to be the main factor improving the rhizobium-legume symbiosis, although other factors such as the modulation of plant hormone levels by fungi, as described for PGPRs, also contribute to increase nodule number and plant biomass. Nevertheless, a meta-analysis showed that the synergistic effect between AMF and rhizobia is mostly observed in perennial plants but was not observed in annual plants (Primieri et al., 2022). These results suggest that the effect of the tripartite interaction between legumes, AMF and rhizobia can be influenced by the life history of the host plant. Additionally, these effects can vary based on the co-inoculated species, suggesting a particular compatibility between the symbionts is necessary to obtain combined positive effects in plants (Xavier and Germida, 2003), and on abiotic conditions (Afkhami et al., 2020). For example, under limited light, co-inoculation of rhizobia and AMF can lead to a reduction in plant growth, likely due to the important allocation of carbohydrates to the symbionts (Ballhorn et al., 2016). Finally, fungal mycelia form dispersion networks, which may facilitate root invasion. This was observed for a *Bradyrhizobium* strain, which initiates nodulation on peanut by a crack entry process and uses mycelia produced by a biotrophic fungus, *Phomopsis liquidambaris*, to migrate to legume rhizosphere and reach infection sites (Zhang et al., 2020).

5 Direct and indirect inter-bacterial interactions within nodules

Nodules represent a specific niche for rhizobia, in which they are largely shielded from competition with other soil bacteria. However, this isolation is not strict. The presence of non-rhizobial strains in nodules has been reported for a long time, but the recent advent of large-scale sequencing experiments provided some more complete and systematic descriptions of these 'nodule-associated bacteria' (NAB). These findings open the possibility that rhizobia may interact directly with other non-rhizobia within nodules.

Reported NAB belong to many different genera of Alpha-, Gamma- or Beta- proteobacteria (the latter now been included as a subset of Gamma-proteobacteria (Parks et al., 2018)) as well as to the Actinobacteria and Firmicutes phyla (Martínez-Hidalgo and Hirsch, 2017). NAB tend to have lower densities than rhizobia within nodules (Etesami, 2022), but their precise localisation within nodules is often unknown. Numerous studies have shown that NAB can affect the number of nodules formed by rhizobia and/or plant growth. In fact, many NAB seem to possess plant-growth promoting traits, making them good candidate as inoculants together with selected rhizobial strains (Martínez-Hidalgo and Hirsch, 2017; Velázquez et al., 2017; da Silva et al., 2023). Yet, there is little information currently available on the activity and biological relevance of these NAB within nodules.

In *Lotus*, NAB can enter nodules by co-colonising infection threads formed by the compatible rhizobium *Mesorhizobium loti* (Zgadzaj et al., 2015). A fluorescently labeled non-nodulating and non-fixing strain *Rhizobium mesosinicum* KAW12 was then shown to colonise both inter- and intra-cellular nodule spaces, when co-inoculated with *M. loti*. Colonisation was dependent on the symbiotic genetic program of the host plant, activated by the compatible NF from *M. loti*. Crosbie et al. (2022) later identified an antagonistic interaction between another intracellular nodule commensal (*Pseudomonas* sp.) and an ineffective *Rhizobium* strain. Indeed, *Pseudomonas* strains were detected in *L. japonicus* nodules formed by an efficient *M. loti* strain, but not in nodules formed by the non-fixing *Rhizobium* sp. BW8-2. Co-inoculating one of these *Pseudomonas* strains with *Rhizobium* sp. BW8-2 reduced the number of nodules formed by the latter strain, suggesting a negative effect of *Pseudomonas* on *Rhizobium* during the early stages of symbiosis. This effect was observed on *Lotus japonicus* but not on *L. burnetii*, showing that the host plant plays a role in the mediation of this rhizobium-NAB interaction.

Hansen et al. (2020) were also able to isolate cultivable NAB from *Medicago sativa* nodules formed by *S. meliloti*. These strains, representative of a simplified nodule microbial community established after three cycles of *in planta* selection, were used to perform functional studies on synthetic communities, by measuring the rate of nodule colonisation of each strain when co-inoculated with other members of this community (but always including *S. meliloti*). Both cooperative and antagonistic interactions between strains were identified in this system. Several interesting results emerge from this study. First, while two strains (*Pseudomonas* sp. and *Paenibacillus* sp.) showed a mutually beneficial effect on the rate of nodule colonisation, *Paenibacillus* sp. proliferation within nodules was reduced in the presence of *Pseudomonas* sp., showing that the type of interaction can be dependent on the phase of the life cycle. Second, all endophytes were able to antagonise *S. meliloti* in *in vitro* conditions and reduced nodule formation. However, co-inoculation of the entire community with *S. meliloti* reduced neither nodule formation nor plant growth, suggesting that higher-order interactions modify the effect of these NAB on *S. meliloti*. Finally, spatial metabolic analyses indicate that some antagonistic interactions might be mediated by the production of antibiotics by one of the nodule commensal strains.

Overall, these three studies gathered compelling evidence that rhizobia-NAB and rhizobia-plant-NAB interactions do occur within nodules. Future investigations on the precise effects of NAB on rhizobial fitness and nitrogen fixation will undoubtedly complete our understanding of these fascinating aspects of rhizobia biology.

Direct interactions between rhizobia and other bacteria may also occur at longer distance. A subset of rhizobial species produce rhizopines, a class of inositol-derived molecules synthesised in bacteroids (Murphy et al., 1995). Rhizopines are believed to be catabolised by rhizobia that are in the rhizosphere or infection threads and carry the corresponding degradation operons. In agreement with this hypothesis, rhizopine-catabolising strains have a fitness advantage over non-catabolizing strains during symbiosis (Gordon et al., 1996). However, this advantage was observed at early symbiotic stages, and it is therefore unclear if it arises from the ability to catabolise rhizopines produced by bacteroids, or other compounds produced by plants or bacteria in the rhizosphere. Nevertheless, the ability to catabolise rhizopines was also found in non-rhizobia (Gardener and De Bruijn, 1998), suggesting that other rhizospheric bacteria or possibly NAB may benefit from rhizopine produced by nodule bacteria and that rhizopines may represent a 'public good' for rhizospheric bacteria (although the capacity to catabolise it is restricted to a relatively small subset of bacteria). This consideration opens interesting evolutionary questions that have been addressed by mathematical modeling (Simms and Bever, 1998).

Indirect long-distance interactions also occur between rhizobia present within nodules and rhizobia located in the rhizosphere. The process of auto-regulation of infection (AOI) initiated by nodule rhizobia regulates root-hair infection by rhizospheric bacteria (Tian et al., 2012). This phenomenon involves complex signal exchanges between plants and nodule bacteria (Garnerone et al., 2018; Sorroche et al., 2019; Sorroche et al., 2020). However, the relevance of AOI for rhizobial fitness when plants are exposed to different rhizobial or non-rhizobial strains remains to be investigated. In addition, infection and nitrogen fixation by rhizobia have strong effects on plant physiology, and can lead to the production of systemic signals that modulate rhizobial fitness throughout the plant (Lepetit and Brouquisse, 2023). For example, the auto-regulation of nodulation (AON) allows the plant to block the nodulation process when its needs in nitrogen are covered by the functioning nodules (Ferguson et al., 2019). Long-distance interactions are also known to occur between rhizospheric microorganisms and nodule bacteria (Ruiz-Lozano et al., 2001;

Tokala et al., 2002). In soybean, symbiosis with the AMF *Glomus mosseae* protects nodules from drought-induced senescence (Ruiz-Lozano et al., 2001). The authors observed that AMF reduced the effect of drought on several markers associated with nodule senescence, such as the decreased nitrogen fixation activity and the early appearance of oxidative damages. It is likely that this protective effect also translates into better rhizobial fitness.

Finally, indirect interactions between rhizobia present in different nodules have recently been reported when plants are colonised by several different rhizobial strains. While it is now well established that rhizobial persistence within nodules depends on their rate of nitrogen fixation (see section 2), Whesthoek et al. (2021) showed that this effect can be modulated depending on the symbiotic effectiveness of the diverse strains nodulating the same host plant. Using a strain that fixes reduced amounts of nitrogen ('intermediate fixer'), the authors showed that bacterial load within mature nodules colonised by this strain is lower when the plant is co-inoculated with an efficient strain than with a non-fixing strain. These results show that plants are able to impose 'conditional sanctions' by comparing nitrogen output from the different nodules and responding accordingly in ways that affect rhizobial survival within nodules. This response seems to involve differential transport of sugars and di-carboxylic acids to the nodules, but the precise molecular mechanisms involved in the sensing of differential nitrogen fixation levels and the establishment of conditional sanctions remain to be discovered.

6 Towards the incorporation of ecological interactions into evolutionary processes

All the examples mentioned so far in this review (and also reviewed by others; (Barea et al., 2005; Afkhami et al., 2020; Checcucci and Marchetti, 2020; Burghardt and diCenzo, 2023)) show that rhizobial fitness can be modified by the presence of other microorganisms at the different steps of the life cycle. Therefore, microbial communities will change the selective pressures acting on rhizobial populations, and thus their evolutionary trajectories. Below we discuss two processes by which the biotic environment can affect rhizobial evolution: eco-evolutionary feedbacks and the alteration of the mechanisms of evolution. For more general perspectives on the evolution of rhizobia, we refer interested readers to the following recent reviews (Andrews et al., 2018; Burghardt, 2020; Denison and Muller, 2022; Remigi et al., 2016; Masson-Boivin and Sachs, 2018; Tian and Young, 2019; Tang and Capela, 2020; Provorov et al., 2022; Wardell et al., 2022; Liu S, et al., 2023).

Eco-evolutionary feedbacks refer to the interplay between the modification of selective pressures by ecological mechanisms (*e.g.* biotic interactions) and the modification of ecological interactions by evolutionary mechanisms (Schoener, 2011; Hendry, 2017; Ware et al., 2019). Eco-evolutionary feedbacks are expected to be particularly relevant when the time scales of ecological and evolutionary processes overlap, which is typically the case in microbial populations (Fields and Friman, 2022). In the case of rhizobia, the presence of a complex microbiome can shape not only the evolution of the interactions between rhizobia and other microbiome members, but also interactions between rhizobia and their host plant. This seems be the case for example with the emergence of phage-resistant rhizobia that survive better in the rhizosphere but show a decreased symbiotic performances on their host plant (Kleczkowska, 1950; Stacey et al., 1982; Handelsman et al., 1984; Mishra et al., 2004; Anand et al., 2012). In another example of eco-evolutionary feedback, the co-culture of *R. etli* with yeasts leads to the rapid appearance of bacterial phenotypic variants (Andrade-Domínguez et al., 2014). These variants carry diverse mutations that allow *R. etli* to grow in the presence of orotic acid, a metabolite secreted by yeasts and that inhibits the growth of wild-type bacteria. These variants then further evolved to become yeast antagonists, thus completely changing the nature of the interaction between these organisms. Although it is unknown whether these two strains interact with one another in their natural environment, this work nicely unravels how the presence of yeasts can rapidly affect the phenotypic and genetic composition of rhizobial populations.

Experimental evolution can also be used to study how plant-rhizobia interactions can change in a variety of ecological contexts (Remigi et al., 2019). Doin De Moura et al. (2023) analysed an evolution experiment designed to turn a plant pathogenic bacterium into a legume symbiont, following the artificial transfer of a symbiotic plasmid into the plant pathogenic ancestor (Doin de Moura et al., 2020). In the course of this experiment, multiple sub-populations of bacteria emerge and compete in the rhizosphere. Evolved bacteria (that are still not fixing nitrogen at the end of the experiment) predominantly improved their nodulation competitiveness. These results show that, in emerging rhizobia with poor symbiotic phenotypes, the selective bottleneck at the nodulation step exerts a strong selective pressure on bacterial populations.

Batstone et al. (2020) performed serial nodulation cycles on five lines of *M. truncatula* using a mix of two rhizobial strains as starting inoculum: one effective and one ineffective nitrogen-fixing strain. During this experiment, the effective strain increased in frequency in almost all lines, and became even more beneficial to the plant lines on which they evolved. An interesting follow-up of this experiment would be to evolve strains alone or in co-inoculation, to assess the effect of competition between multiple rhizobial strains on their respective evolutionary trajectories.

The presence of a complex microbial community can also modify the basic evolutionary mechanisms acting on a focal species, such as the rates of mutations and of horizontal gene transfer (HGT). Bacterial mutation rates are plastic (Ferenci, 2019; Matic, 2019; Pribis et al., 2022), and can be influenced by various stresses, nutrient availability (Maharjan and Ferenci, 2017), or cell density (Krašovec et al., 2017). Interestingly, in *E. coli*, the modulation of mutation rate by cell density depends on the quorum-sensing gene *luxS*, indicating a 'social-dependence' of mutation rate in this strain (Krašovec et al., 2014). Given that microbial communities can constitute stressful environments for bacteria (Hibbing et al., 2010; LeRoux et al., 2015; Traxler and Kolter, 2015; Granato et al., 2019), it is plausible that mutation rates

of rhizobia might be affected by other microorganisms. In addition, many symbiotic plasmids also carry stress-inducible error-prone DNA polymerases (Remigi et al., 2014). After transferring one of these plasmids (from the rhizobium *Cupriavidus taiwanensis*) into a non-symbiotic bacterium, the expression of error-prone DNA polymerases in stressful environments (the rhizosphere) induces transient bursts in mutation rate and accelerates adaptation to the symbiotic lifestyle. Antagonistic interactions between microbiome members can also lead to the selection of constitutive hypermutator strains (*e.g.*, that are defective in DNA repair systems). This has been documented for phage-bacteria interactions where lytic phages impose strong mortality in bacterial populations. Second-order selection of constitutive hypermutators can thus occur, as these strains will have a higher chance to become resistant to phages (Chevallereau et al., 2022).

HGT is another major driver of rhizobia evolution. Evidently, dense and diverse microbial communities, like those found in the rhizosphere, facilitate HGT due to both the elevated transfer rates and the extensive pool of genes that could potentially be transferred (Brito, 2021; Moura De Sousa et al., 2023; Sánchez-Salazar et al., 2023). Yet additional mechanisms exist that further increase HGT in rhizobia. The transfer rate of symbiotic integrative and conjugative elements (ICE) from *Azorhizobium caulinodans* to other rhizobia is elevated in the rhizosphere of several plants compared to empty soil (Ling et al., 2016). The perception of flavonoid compounds by a transcription regulator of the LysR family controls the expression of the ICE integrase, together with two other genes located on this symbiotic island (Ling et al., 2016; Li et al., 2022). Recently, the transfer of symbiotic plasmids from *R. etli* CFN42 to other rhizobia and NAB was also detected in bean nodules (Bañuelos-Vazquez et al., 2019; Bañuelos-Vazquez et al., 2020). These examples show that symbiosis genes are particularly prone to be transferred in the presence of host plants. Indeed, HGT of symbiosis genes has been extensively documented by phylogenetic studies (Remigi et al., 2016; Andrews et al., 2018; Wardell et al., 2022). In the field, non-symbiotic strains that are well adapted to the abiotic environment can become efficient symbionts by acquiring symbiotic ICE from 'elite' rhizobial inoculants that are not adapted to the soil conditions (Sullivan et al., 1995; Nandasena et al., 2007; Hill et al., 2021; Colombi et al., 2023). Moreover, the frequent re-arrangements and recombinations between symbiotic genes from different strains create a dynamic equilibrium where less cooperative strains regularly appear as well as strains with new or improved symbiotic abilities, illustrating how genetic diversity of rhizobial strains fuels the evolvability of symbiosis (Weisberg et al., 2022). Altogether, these studies demonstrate that incorporating the whole microbial communities will be crucial to understand the rate and patterns of rhizobial evolution.

7 Conclusion and perspectives

The rhizobium-legume symbiosis has long been a model system to study both the molecular and eco-evolutionary aspects of host-microbe interactions. In the recent years, we have witnessed an increased interest in incorporating the effect of complex microbial communities on the functioning of this symbiosis, and numerous interactions with a multitude of microbes have already been detected throughout the rhizobial life cycle in both laboratory and field conditions (Table 1).

However, certain stages of the rhizobial life cycle have been understudied. For instance, interactions within the nodule microbiome, although much less complex than the rhizosphere microbiome, still lack a comprehensive understanding. Similarly, interactions of bacteria released from senescent nodules with soil communities remain largely unknown. In addition, research has predominantly focused on pairwise interactions so far, while in nature, interspecies interactions occur in multispecies communities. In such complex ecosystems, higher-order interactions can profoundly impact the fitness of a focal strain (Levine et al., 2017). Another set of open questions relates to the genetic bases of inter-microbial interactions. Once we start to uncover the molecular mechanisms involved in these interactions and to describe the existing natural genetic variations in the life history traits, it will be particularly interesting to further test whether there are genetic trade-offs or couplings between these different traits, including those involved in the interaction with the host plant. In parallel, assessing the eco-evolutionary dynamics of these interactions with laboratory evolution or field experiments will provide complementary information on the selective pressures acting on rhizobial populations.

Therefore, we have probably only scratched the surface of the extent to which rhizobial-microbial interactions contribute to the establishment and functioning of legume-rhizobia symbioses. Additional discoveries are expected as research progresses on this topic, concerning both the mechanisms that mediate these interactions and their ecological and evolutionary consequences. A future challenge will be to integrate all these findings in a coherent framework, and use this knowledge to improve agricultural and ecosystem services that can be obtained from rhizobia. An ambitious goal would be to be able to design synthetic communities where microbial interactions enhance rhizobial fitness and symbiotic services, and mitigate the effects of plant pathogens. This will require cooperation between several disciplines (molecular microbiology, ecology and evolutionary biology, plant physiology, agronomy…) and cross-fertilisation between laboratory and field experiments.

Author contributions

MGA: Writing – original draft, Writing – review & editing. BR: Writing – original draft, Writing – review & editing. DC: Writing – original draft, Writing – review & editing. PR: Writing – original draft, Writing – review & editing.

Funding

The author(s) declare financial support was received for the research, authorship, and/or publication of this article. This work is funded by the French National Research Agency (ANR-21-CE02-

0019-01), the "Laboratoires d'Excellence (LABEX)" TULIP (ANR-10-LABX-41), and the "École Universitaire de Recherche (EUR)" TULIP-GS (ANR-18-EURE-0019).

Acknowledgments

We apologise to colleagues whose work could not be cited to keep the review concise.

Conflict of interest

The authors declare that the research was conducted in the absence of any commercial or financial relationships that could be construed as a potential conflict of interest.

Publisher's note

Supplementary material

The Supplementary Material for this article can be found online at: https://www.frontiersin.org/articles/10.3389/fpls.2023.1277262/full#supplementary-material

References

Afkhami, M. E., Almeida, B. K., Hernandez, D. J., Kiesewetter, K. N., and Revillini, D. P. (2020). Tripartite mutualisms as models for understanding plant–microbial interactions. *Curr. Opin. Plant Biol.* 56, 28–36. doi: 10.1016/j.pbi.2020.02.003

Ahmad, M., Zahir, Z. A., Asghar, H. N., and Asghar, M. (2011). Inducing salt tolerance in mung bean through coinoculation with rhizobia and plant-growth-promoting rhizobacteria containing 1-aminocyclopropane-1-carboxylate deaminase. *Can. J. Microbiol.* 57, 578–589. doi: 10.1139/w11-044

Alemneh, A. A., Zhou, Y., Ryder, M. H., and Denton, M. D. (2020). Mechanisms in plant growth-promoting rhizobacteria that enhance legume–rhizobial symbioses. *J. Appl. Microbiol.* 129, 1133–1156. doi: 10.1111/jam.14754

Amarger, N. (1981). Competition for nodule formation between effective and ineffective strains of *Rhizobium meliloti*. *Soil Biol. Biochem.* 13, 475–480. doi: 10.1016/0038-0717(81)90037-7

Anand, A., Jaiswal, S. K., Dhar, B., and Vaishampayan, A. (2012). Surviving and thriving in terms of symbiotic performance of antibiotic and phage-resistant mutants of *Bradyrhizobium* of soybean [*Glycine max* (L.) Merrill]. *Curr. Microbiol.* 65, 390–397. doi: 10.1007/s00284-012-0166-8

Andrade-Domínguez, A., Salazar, E., Del Carmen Vargas-Lagunas, M., Kolter, R., and Encarnación, S. (2014). Eco-evolutionary feedbacks drive species interactions. *ISME J.* 8, 1041–1054. doi: 10.1038/ismej.2013.208

Andrade-Domínguez, A., Trejo-Hernández, A., Vargas-Lagunas, C., and Encarnación-Guevara, S. (2021). Phenotypic plasticity and a new small molecule are involved in a fungal-bacterial interaction. *Sci. Rep.* 11, 19219. doi: 10.1038/s41598-021-98474-y

Andrews, M., De Meyer, S., James, E., Stępkowski, T., Hodge, S., Simon, M., et al. (2018). Horizontal transfer of symbiosis genes within and between rhizobial genera: Occurrence and importance. *Genes* 9, 321. doi: 10.3390/genes9070321

Antunes, P. M., and Goss, M. J. (2005). "Communication in the tripartite symbiosis formed by arbuscular mycorrhizal fungi, rhizobia and legume plants: A review," in *Roots and Soil Management: Interactions between Roots and the Soil*. Eds. R. W. Zobel and S. F. Wright (Madison, WI, USA: American Society of Agronomy, Crop Science Society of America, Soil Science Society of America), 199–222. doi: 10.2134/agronmonogr48.c11

Bais, H. P., Weir, T. L., Perry, L. G., Gilroy, S., and Vivanco, J. M. (2006). The role of root exudates in rhizosphere interactions with plants and other organisms. *Annu. Rev. Plant Biol.* 57, 233–266. doi: 10.1146/annurev.arplant.57.032905.105159

Ballhorn, D. J., Schädler, M., Elias, J. D., Millar, J. A., and Kautz, S. (2016). Friend or foe — Light availability determines the relationship between mycorrhizal fungi, rhizobia and Lima bean (*Phaseolus lunatus* L.). *PloS One* 11, e0154116. doi: 10.1371/journal.pone.0154116

Bañuelos-Vazquez, L. A., Cazares, D., Rodríguez, S., Cervantes-De la Luz, L., Sánchez-López, R., Castellani, L. G., et al. (2020). Transfer of the symbiotic plasmid of *Rhizobium etli* CFN42 to endophytic bacteria inside nodules. *Front. Microbiol.* 11, 1752. doi: 10.3389/fmicb.2020.01752

Bañuelos-Vazquez, L. A., Torres Tejerizo, G., Cervantes-De La Luz, L., Girard, L., Romero, D., and Brom, S. (2019). Conjugative transfer between *Rhizobium etli* endosymbionts inside the root nodule. *Environ. Microbiol.* 21, 3430–3441. doi: 10.1111/1462-2920.14645

Barea, J.-M., Pozo, M. J., Azcón, R., and Azcón-Aguilar, C. (2005). Microbial co-operation in the rhizosphere. *J. Exp. Bot.* 56, 1761–1778. doi: 10.1093/jxb/eri197

Batstone, R. T., Burghardt, L. T., and Heath, K. D. (2022). Phenotypic and genomic signatures of interspecies cooperation and conflict in naturally occurring isolates of a model plant symbiont. *Proc. R. Soc B Biol. Sci.* 289, 20220477. doi: 10.1098/rspb.2022.0477

Batstone, R. T., Dutton, E. M., Wang, D., Yang, M., and Frederickson, M. E. (2017). The evolution of symbiont preference traits in the model legume *Medicago truncatula*. *New Phytol.* 213, 1850–1861. doi: 10.1111/nph.14308

Batstone, R. T., O'Brien, A. M., Harrison, T. L., and Frederickson, M. E. (2020). Experimental evolution makes microbes more cooperative with their local host genotype. *Science* 370, 476–478. doi: 10.1126/science.abb7222

Bellabarba, A., Fagorzi, C., diCenzo, G. C., Pini, F., Viti, C., and Checcucci, A. (2019). Deciphering the symbiotic plant microbiome: Translating the most recent discoveries on rhizobia for the improvement of agricultural practices in metal-contaminated and high saline lands. *Agronomy* 9, 529. doi: 10.3390/agronomy9090529

Benezech, C., Le Scornet, A., and Gourion, B. (2021). *Medicago - Sinorhizobium - Ralstonia*: A model system to investigate pathogen-triggered inhibition of nodulation. *Mol. Plant-Microbe Interact.* 34, 499–503. doi: 10.1094/MPMI-11-20-0319-SC

Berendsen, R. L., Pieterse, C. M. J., and Bakker, P. A. H. M. (2012). The rhizosphere microbiome and plant health. *Trends Plant Sci.* 17, 478–486. doi: 10.1016/j.tplants.2012.04.001

Bergersen, F. J., Gibson, A. H., and Licis, I. (1995). Growth and N_2-fixation of soybeans inoculated with strains of *Bradyrhizobium japonicum* differing in energetic efficiency and PHB utilization. *Soil Biol. Biochem.* 27, 611–616. doi: 10.1016/0038-0717(95)98639-6

Berrabah, F., Ratet, P., and Gourion, B. (2015). Multiple steps control immunity during the intracellular accommodation of rhizobia. *J. Exp. Bot.* 66, 1977–1985. doi: 10.1093/jxb/eru545

Bladergroen, M. R., Badelt, K., and Spaink, H. P. (2003). Infection-blocking genes of a symbiotic *Rhizobium leguminosarum* strain that are involved in temperature-dependent protein secretion. *Mol. Plant-Microbe Interact.* 16, 53–64. doi: 10.1094/MPMI.2003.16.1.53

Boivin, S., Ait Lahmidi, N., Sherlock, D., Bonhomme, M., Dijon, D., Heulin-Gotty, K., et al. (2020). Host-specific competitiveness to form nodules in *Rhizobium leguminosarum* symbiovar viciae. *New Phytol.* 226, 555–568. doi: 10.1111/nph.16392

Boivin, S., and Lepetit, M. (2020). "Partner preference in the legume-rhizobia symbiosis and impact on legume inoculation strategies," in *Advances in Botanical Research*. Eds. P. Frendo, F. Frugier and C. Masson-Boivin (Cambridge, MA, USA: Academic Press), 323–348. doi: 10.1016/bs.abr.2019.09.016

Boivin, S., Mahé, F., Debellé, F., Pervent, M., Tancelin, M., Tauzin, M., et al. (2021). Genetic variation in host-specific competitiveness of the symbiont *Rhizobium leguminosarum* symbiovar viciae. *Front. Plant Sci.* 12, 719987. doi: 10.3389/fpls.2021.719987

Bourion, V., Heulin-Gotty, K., Aubert, V., Tisseyre, P., Chabert-Martinello, M., Pervent, M., et al. (2018). Co-inoculation of a pea core-collection with diverse rhizobial strains shows competitiveness for nodulation and efficiency of nitrogen fixation are distinct traits in the interaction. *Front. Plant Sci.* 8, 2249. doi: 10.3389/fpls.2017.02249

Breakspear, A., Liu, C., Roy, S., Stacey, N., Rogers, C., Trick, M., et al. (2014). The root hair "Infectome" of *Medicago truncatula* uncovers changes in cell cycle genes and reveals a requirement for auxin signaling in rhizobial infection. *Plant Cell* 26, 4680–4701. doi: 10.1105/tpc.114.133496

Brito, I. L. (2021). Examining horizontal gene transfer in microbial communities. *Nat. Rev. Microbiol.* 19, 442–453. doi: 10.1038/s41579-021-00534-7

Burghardt, L. T. (2020). Evolving together, evolving apart: Measuring the fitness of rhizobial bacteria in and out of symbiosis with leguminous plants. *New Phytol.* 228, 28–34. doi: 10.1111/nph.16045

Burghardt, L. T., and diCenzo, G. C. (2023). The evolutionary ecology of rhizobia: Multiple facets of competition before, during, and after symbiosis with legumes. *Curr. Opin. Microbiol.* 72, 102281. doi: 10.1016/j.mib.2023.102281

Burghardt, L. T., Epstein, B., Guhlin, J., Nelson, M. S., Taylor, M. R., Young, N. D., et al. (2018). Select and resequence reveals relative fitness of bacteria in symbiotic and free-living environments. *Proc. Natl. Acad. Sci. U.S.A.* 115, 2425–2430. doi: 10.1073/pnas.1714246115

Burghardt, L. T., Epstein, B., Hoge, M., Trujillo, D. I., and Tiffin, P. (2022). Host-associated rhizobial fitness: Dependence on nitrogen, density, community complexity, and legume genotype. *Appl. Environ. Microbiol.* 88, e00526–e00522. doi: 10.1128/aem.00526-22

Burghardt, L. T., Guhlin, J., Chun, C. L., Liu, J., Sadowsky, M. J., Stupar, R. M., et al. (2017). Transcriptomic basis of genome by genome variation in a legume-rhizobia mutualism. *Mol. Ecol.* 26, 6122–6135. doi: 10.1111/mec.14285

Burghardt, L. T., Trujillo, D. I., Epstein, B., Tiffin, P., and Young, N. D. (2020). A select and resequence approach reveals strain-specific effects of *Medicago* nodule-specific PLAT-domain genes. *Plant Physiol.* 182, 463–471. doi: 10.1104/pp.19.00831

Caetano-Anollés, G., Wall, L. G., De Micheli, A. T., Macchi, E. M., Bauer, W. D., and Favelukes, G. (1988). Role of motility and chemotaxis in efficiency of nodulation by *Rhizobium meliloti*. *Plant Physiol.* 86, 1228–1235. doi: 10.1104/pp.86.4.1228

Carrión, V. J., Cordovez, V., Tyc, O., Etalo, D. W., De Bruijn, I., De Jager, V. C. L., et al. (2018). Involvement of *Burkholderiaceae* and sulfurous volatiles in disease-suppressive soils. *ISME J.* 12, 2307–2321. doi: 10.1038/s41396-018-0186-x

Casimiro, I., Marchant, A., Bhalerao, R. P., Beeckman, T., Dhooge, S., Swarup, R., et al. (2001). Auxin transport promotes *Arabidopsis* lateral root initiation. *Plant Cell* 13, 843–852. doi: 10.1105/tpc.13.4.843

Cevallos, M. A., Encarnación, S., Leija, A., Mora, Y., and Mora, J. (1996). Genetic and physiological characterization of a *Rhizobium etli* mutant strain unable to synthesize poly-beta-hydroxybutyrate. *J. Bacteriol.* 178, 1646–1654. doi: 10.1128/jb.178.6.1646-1654.1996

Checcucci, A., Azzarello, E., Bazzicalupo, M., Galardini, M., Lagomarsino, A., Mancuso, S., et al. (2016). Mixed nodule infection in *Sinorhizobium meliloti–Medicago sativa* symbiosis suggest the presence of cheating behavior. *Front. Plant Sci.* 7, 835. doi: 10.3389/fpls.2016.00835

Checcucci, A., and Marchetti, M. (2020). The rhizosphere talk show: The rhizobia on stage. *Front. Agron.* 2, 591494. doi: 10.3389/fagro.2020.591494

Chen, W. F., Meng, X. F., Jiao, Y. S., Tian, C. F., Sui, X. H., Jiao, J., et al. (2023). Bacteroid development, transcriptome, and symbiotic nitrogen-fixing comparison of *Bradyrhizobium arachidis* in nodules of peanut (*Arachis hypogaea*) and medicinal legume *Sophora flavescens*. *Microbiol. Spectr.* 11, e01079–e01022. doi: 10.1128/spectrum.01079-22

Chepsergon, J., and Moleleki, L. N. (2023). Rhizosphere bacterial interactions and impact on plant health. *Curr. Opin. Microbiol.* 73, 102297. doi: 10.1016/j.mib.2023.102297

Chevallereau, A., Pons, B. J., Van Houte, S., and Westra, E. R. (2022). Interactions between bacterial and phage communities in natural environments. *Nat. Rev. Microbiol.* 20, 49–62. doi: 10.1038/s41579-021-00602-y

Colombi, E., Hill, Y., Lines, R., Sullivan, J. T., Kohlmeier, M. G., Christophersen, C. T., et al. (2023). Population genomics of Australian indigenous *Mesorhizobium* reveals diverse nonsymbiotic genospecies capable of nitrogen-fixing symbioses following horizontal gene transfer. *Microb. Genomics* 9. doi: 10.1099/mgen.0.000918

Compton, K. K., and Scharf, B. E. (2021). Rhizobial chemoattractants, the taste and preferences of legume symbionts. *Front. Plant Sci.* 12, 686465. doi: 10.3389/fpls.2021.686465

Contreras-Moreno, F. J., Muñoz-Dorado, J., García-Tomsig, N. I., Martínez-Navajas, G., Pérez, J., and Moraleda-Muñoz, A. (2020). Copper and melanin play a role in Myxococcus xanthus predation on *Sinorhizobium meliloti*. *Front. Microbiol.* 11, 94. doi: 10.3389/fmicb.2020.00094

Coyte, K. Z., and Rakoff-Nahoum, S. (2019). Understanding competition and cooperation within the mammalian gut microbiome. *Curr. Biol.* 29, R538–R544. doi: 10.1016/j.cub.2019.04.017

Crang, N., Borah, K., James, E. K., Jorrín, B., Green, P., Tkacz, A., et al. (2021). Role and regulation of poly-3-hydroxybutyrate in nitrogen fixation in *Azorhizobium caulinodans*. *Mol. Plant-Microbe Interact.* 34, 1390–1398. doi: 10.1094/MPMI-06-21-0138-R

Crook, M. B., Lindsay, D. P., Biggs, M. B., Bentley, J. S., Price, J. C., Clement, S. C., et al. (2012). Rhizobial plasmids that cause impaired symbiotic nitrogen fixation and enhanced host invasion. *Mol. Plant-Microbe Interact.* 25, 1026–1033. doi: 10.1094/MPMI-02-12-0052-R

Crosbie, D. B., Mahmoudi, M., Radl, V., Brachmann, A., Schloter, M., Kemen, E., et al. (2022). Microbiome profiling reveals that *Pseudomonas* antagonises parasitic nodule colonisation of cheater rhizobia in *Lotus*. *New Phytol.* 234, 242–255. doi: 10.1111/nph.17988

Czernic, P., Gully, D., Cartieaux, F., Moulin, L., Guefrachi, I., Patrel, D., et al. (2015). Convergent evolution of endosymbiont differentiation in Dalbergioid and inverted repeat-lacking clade legumes mediated by nodule-specific cysteine-rich peptides. *Plant Physiol.* 169, 1254–1265. doi: 10.1104/pp.15.00584

Danso, S. K. A., Keya, S. O., and Alexander, M. (1975). Protozoa and the decline of *Rhizobium* populations added to soil. *Can. J. Microbiol.* 21, 884–895. doi: 10.1139/m75-131

da Silva, T. R., Rodrigues, R. T., Jovino, R. S., Carvalho, J. R. D. S., Leite, J., Hoffman, A., et al. (2023). Not just passengers, but co-pilots! Non-rhizobial nodule-associated bacteria promote cowpea growth and symbiosis with (brady)rhizobia. *J. Appl. Microbiol.* 134, lxac013. doi: 10.1093/jambio/lxac013

Daubech, B., Remigi, P., Doin De Moura, G., Marchetti, M., Pouzet, C., Auriac, M.-C., et al. (2017). Spatio-temporal control of mutualism in legumes helps spread symbiotic nitrogen fixation. *eLife* 6, e28683. doi: 10.7554/eLife.28683

De Campos, S. B., Lardi, M., Gandolfi, A., Eberl, L., and Pessi, G. (2017). Mutations in two *Paraburkholderia phymatum* type VI secretion systems cause reduced fitness in interbacterial competition. *Front. Microbiol.* 8, 2473. doi: 10.3389/fmicb.2017.02473

De Faria, S. M., Ringelberg, J. J., Gross, E., Koenen, E. J. M., Cardoso, D., Ametsitsi, G. K. D., et al. (2022). The innovation of the symbiosome has enhanced the evolutionary stability of nitrogen fixation in legumes. *New Phytol.* 235, 2365–2377. doi: 10.1111/nph.18321

De La Fuente Cantó, C., Simonin, M., King, E., Moulin, L., Bennett, M. J., Castrillo, G., et al. (2020). An extended root phenotype: The rhizosphere, its formation and impacts on plant fitness. *Plant J.* 103, 951–964. doi: 10.1111/tpj.14781

Denison, R. F., and Kiers, E. T. (2011). Life histories of symbiotic rhizobia and mycorrhizal fungi. *Curr. Biol.* 21, R775–R785. doi: 10.1016/j.cub.2011.06.018

Denison, R. F., and Muller, K. E. (2022). An evolutionary perspective on increasing net benefits to crops from symbiotic microbes. *Evol. Appl.* 15, 1490–1504. doi: 10.1111/eva.13384

Doin De Moura, G. G., Mouffok, S., Gaudu, N., Cazalé, A.-C., Milhes, M., Bulach, T., et al. (2023). A selective bottleneck during host entry drives the evolution of new legume symbionts. *Mol. Biol. Evol.* 40, msad116. doi: 10.1093/molbev/msad116

Doin de Moura, G. G., Remigi, P., Masson-Boivin, C., and Capela, D. (2020). Experimental evolution of legume symbionts: What have we learnt? *Genes* 11, 339. doi: 10.3390/genes11030339

D'Souza, G., Shitut, S., Preussger, D., Yousif, G., WasChina, S., and Kost, C. (2018). Ecology and evolution of metabolic cross-feeding interactions in bacteria. *Nat. Prod. Rep.* 35, 455–488. doi: 10.1039/C8NP00009C

Durán, P., Thiergart, T., Garrido-Oter, R., Agler, M., Kemen, E., Schulze-Lefert, P., et al. (2018). Microbial interkingdom interactions in roots promote *Arabidopsis* survival. *Cell* 175, 973–983.e14. doi: 10.1016/j.cell.2018.10.020

Elliott, G. N., Chou, J.-H., Chen, W.-M., Bloemberg, G. V., Bontemps, C., Martínez-Romero, E., et al. (2009). *Burkholderia* spp. are the most competitive symbionts of *Mimosa*, particularly under N-limited conditions. *Environ. Microbiol.* 11, 762–778. doi: 10.1111/j.1462-2920.2008.01799.x

Epstein, B., Burghardt, L. T., Heath, K. D., Grillo, M. A., Kostanecki, A., Hämälä, T., et al. (2023). Combining GWAS and population genomic analyses to characterize coevolution in a legume-rhizobia symbiosis. *Mol. Ecol.* 32, 3798–3811. doi: 10.1111/mec.16602

Etesami, H. (2022). Root nodules of legumes: A suitable ecological niche for isolating non-rhizobial bacteria with biotechnological potential in agriculture. *Curr. Res. Biotechnol.* 4, 78–86. doi: 10.1016/j.crbiot.2022.01.003

Fagorzi, C., Bacci, G., Huang, R., Cangioli, L., Checcucci, A., Fini, M., et al. (2021). Nonadditive transcriptomic signatures of genotype-by-genotype interactions during the initiation of plant-rhizobium symbiosis. *mSystems* 6, e00974–e00920. doi: 10.1128/mSystems.00974-20

Ferenci, T. (2019). Irregularities in genetic variation and mutation rates with environmental stresses. *Environ. Microbiol.* 21, 3979–3988. doi: 10.1111/1462-2920.14822

Ferguson, B. J., Mens, C., Hastwell, A. H., Zhang, M., Su, H., Jones, C. H., et al. (2019). Legume nodulation: The host controls the party. *Plant Cell Environ.* 42, 41–51. doi: 10.1111/pce.13348

Fields, B., and Friman, V.-P. (2022). Microbial eco-evolutionary dynamics in the plant rhizosphere. *Curr. Opin. Microbiol.* 68, 102153. doi: 10.1016/j.mib.2022.102153

Fields, B., Moeskjær, S., Deakin, W. J., Moffat, E. K., Roulund, N., Andersen, S. U., et al. (2023). *Rhizobium* nodule diversity and composition are influenced by clover host selection and local growth conditions. *Mol. Ecol.* 32, 4259–4277. doi: 10.1111/mec.17028

Fields, B., Moffat, E. K., Harrison, E., Andersen, S. U., Young, J. P. W., and Friman, V.-P. (2022). Genetic variation is associated with differences in facilitative and competitive interactions in the *Rhizobium leguminosarum* species complex. *Environ. Microbiol.* 24, 3463–3485. doi: 10.1111/1462-2920.15720

Frederickson, M. E. (2020). No selection for cheating in a natural meta-population of rhizobia. *Ecol. Lett.* 23, 409–411. doi: 10.1111/ele.13293

Friesen, M. L. (2012). Widespread fitness alignment in the legume-rhizobium symbiosis. *New Phytol.* 194, 1096–1111. doi: 10.1111/j.1469-8137.2012.04099.x

Fry, J., Wood, M., and Poole, P. S. (2001). Investigation of myo-inositol catabolism in *Rhizobium leguminosarum* bv. viciae and its effect on nodulation competitiveness. *Mol. Plant-Microbe Interact.* 14, 1016–1025. doi: 10.1094/MPMI.2001.14.8.1016

Fujita, H., Aoki, S., and Kawaguchi, M. (2014). Evolutionary dynamics of nitrogen fixation in the legume–rhizobia symbiosis. *PloS One* 9, e93670. doi: 10.1371/journal.pone.0093670

Gano-Cohen, K. A., Stokes, P. J., Blanton, M. A., Wendlandt, C. E., Hollowell, A. C., Regus, J. U., et al. (2016). Nonnodulating Bradyrhizobium spp. modulate the benefits of legume-rhizobium mutualism. *Appl. Environ. Microbiol.* 82, 5259–5268. doi: 10.1128/AEM.01116-16

Gano-Cohen, K. A., Wendlandt, C. E., Stokes, P. J., Blanton, M. A., Quides, K. W., Zomorrodian, A., et al. (2019). Interspecific conflict and the evolution of ineffective rhizobia. *Ecol. Lett.* 22, 914–924. doi: 10.1111/ele.13247

Gardener, B. B. M., and De Bruijn, F. J. (1998). Detection and isolation of novel rhizopine-catabolizing bacteria from the environment. *Appl. Environ. Microbiol.* 64, 4944–4949. doi: 10.1128/AEM.64.12.4944-4949.1998

Garnerone, A.-M., Sorroche, F., Zou, L., Mathieu-Demazière, C., Tian, C. F., Masson-Boivin, C., et al. (2018). NsrA, a predicted β-Barrel outer membrane protein involved in plant signal perception and the control of secondary infection in *Sinorhizobium meliloti*. *J. Bacteriol.* 200, e00019-18. doi: 10.1128/JB.00019-18

Ghoul, M., and Mitri, S. (2016). The ecology and evolution of microbial competition. *Trends Microbiol.* 24, 833–845. doi: 10.1016/j.tim.2016.06.011

Gordon, D. M., Ryder, M. H., Heinrich, K., and Murphy, P. J. (1996). An experimental test of the rhizopine concept in *Rhizobium meliloti*. *Appl. Environ. Microbiol.* 62, 3991–3996. doi: 10.1128/aem.62.11.3991-3996.1996

Granato, E. T., Meiller-Legrand, T. A., and Foster, K. R. (2019). The evolution and ecology of bacterial warfare. *Curr. Biol.* 29, R521–R537. doi: 10.1016/j.cub.2019.04.024

Gresshoff, P. M., and Rolfe, B. G. (1978). Viability of *Rhizobium* bacteroids isolated from soybean nodule protoplasts. *Planta* 142, 329–333. doi: 10.1007/BF00385085

Hahn, M., and Studer, D. (1986). Competitiveness of a *nif* – *Bradyrhizobium japonicum* mutant against the wild-type strain. *FEMS Microbiol. Lett.* 33, 143–148. doi: 10.1111/j.1574-6968.1986.tb01228.x

Han, Q., Ma, Q., Chen, Y., Tian, B., Xu, L., Bai, Y., et al. (2020). Variation in rhizosphere microbial communities and its association with the symbiotic efficiency of rhizobia in soybean. *ISME J.* 14, 1915–1928. doi: 10.1038/s41396-020-0648-9

Handelsman, J., Ugalde, R. A., and Brill, W. J. (1984). *Rhizobium meliloti* competitiveness and the alfalfa agglutinin. *J. Bacteriol.* 157, 703–707. doi: 10.1128/jb.157.3.703-707.1984

Hansen, B. L., Pessotti, R., de, C., Fischer, M. S., Collins, A., El-Hifnawi, L., et al. (2020). Cooperation, competition, and specialized metabolism in a simplified root nodule microbiome. *mBio* 11, e01917–e01920. doi: 10.1128/mBio.01917-20

Hassani, M. A., Durán, P., and Hacquard, S. (2018). Microbial interactions within the plant holobiont. *Microbiome* 6, 58. doi: 10.1186/s40168-018-0445-0

Heath, K. D., and Tiffin, P. (2007). Context dependence in the coevolution of plant and rhizobial mutualists. *Proc. R. Soc B Biol. Sci.* 274, 1905–1912. doi: 10.1098/rspb.2007.0495

Hendry, A. P. (2017). *Eco-evolutionary dynamics* (Princeton: Princeton University Press). doi: 10.1515/9781400883080

Hibbing, M. E., Fuqua, C., Parsek, M. R., and Peterson, S. B. (2010). Bacterial competition: Surviving and thriving in the microbial jungle. *Nat. Rev. Microbiol.* 8, 15–25. doi: 10.1038/nrmicro2259

Hill, Y., Colombi, E., Bonello, E., Haskett, T., Ramsay, J., O'Hara, G., et al. (2021). Evolution of diverse effective N_2-fixing microsymbionts of *Cicer arietinum* following horizontal transfer of the *Mesorhizobium ciceri* CC1192 symbiosis integrative and conjugative element. *Appl. Environ. Microbiol.* 87, e02558–e02520. doi: 10.1128/AEM.02558-20

Hirsch, P. R. (1979). Plasmid-determined bacteriocin production by *Rhizobium leguminosarum*. *J. Gen. Microbiol.* 113, 219–228. doi: 10.1099/00221287-113-2-219

Hogg, B., Davies, A. E., Wilson, K. E., Bisseling, T., and Downie, J. A. (2002). Competitive nodulation blocking of cv. Afghanistan pea is related to high levels of nodulation factors made by some strains of *Rhizobium leguminosarum* bv. viciae. *Mol. Plant-Microbe Interact.* 15, 60–68. doi: 10.1094/MPMI.2002.15.1.60

Jacoby, R. P., and Kopriva, S. (2019). Metabolic niches in the rhizosphere microbiome: New tools and approaches to analyse metabolic mechanisms of plant–microbe nutrient exchange. *J. Exp. Bot.* 70, 1087–1094. doi: 10.1093/jxb/ery438

Janczarek, M., Jaroszuk-Ściseł, J., and Skorupska, A. (2009). Multiple copies of *rosR* and *pssA* genes enhance exopolysaccharide production, symbiotic competitiveness and clover nodulation in *Rhizobium leguminosarum* bv. trifolii. *Antonie Van Leeuwenhoek* 96, 471–486. doi: 10.1007/s10482-009-9362-3

Ji, Y.-Y., Zhang, B., Zhang, P., Chen, L.-C., Si, Y.-W., Wan, X.-Y., et al. (2023). Rhizobial migration toward roots mediated by FadL-ExoFQP modulation of extracellular long-chain AHLs. *ISME J.* 17, 417–431. doi: 10.1038/s41396-023-01357-5

Jimenez-Zurdo, J. I. (1995). Characterization of a *Rhizobium meliloti* proline dehydrogenase mutant altered in nodulation efficiency and competitiveness on alfalfa roots. *Mol. Plant Microbe Interact.* 8, 492. doi: 10.1094/MPMI-8-0492

Joglekar, P., Ferrell, B. D., Jarvis, T., Haramoto, K., Place, N., Dums, J. T., et al. (2023). Spontaneously produced lysogenic phages are an important component of the soybean *Bradyrhizobium* mobilome. *mBio* 14, e0029523. doi: 10.1128/mbio.00295-23

Kapp, D., Niehaus, K., Quandt, J., Muller, P., and Puhler, A. (1990). Cooperative action of *Rhizobium meliloti* nodulation and infection mutants during the process of forming mixed infected alfalfa nodules. *Plant Cell* 2, 139–151. doi: 10.1105/tpc.2.2.139

Kelly, S. J., Muszyński, A., Kawaharada, Y., Hubber, A. M., Sullivan, J. T., Sandal, N., et al. (2013). Conditional requirement for exopolysaccharide in the *Mesorhizobium-Lotus* symbiosis. *Mol. Plant-Microbe Interact.* 26, 319–329. doi: 10.1094/MPMI-09-12-0227-R

Kern, L., Abdeen, S. K., Kolodziejczyk, A. A., and Elinav, E. (2021). Commensal inter-bacterial interactions shaping the microbiota. *Curr. Opin. Microbiol.* 63, 158–171. doi: 10.1016/j.mib.2021.07.011

Keya, S. O., and Alexander, M. (1975). Regulation of parasitism by host density: The *Bdellovibrio-Rhizobium* interrelationship. *Soil Biol. Biochem.* 7, 231–237. doi: 10.1016/0038-0717(75)90044-9

Kiers, E. T., Ratcliff, W. C., and Denison, R. F. (2013). Single-strain inoculation may create spurious correlations between legume fitness and rhizobial fitness. *New Phytol.* 198, 4–6. doi: 10.1111/nph.12015

Kiers, E. T., Rousseau, R. A., and Denison, R. F. (2006). Measured sanctions: Legume hosts detect quantitative variation in rhizobium cooperation and punish accordingly. *Evol. Ecol. Res.* 8, 1077–1086.

Kiers, E. T., Rousseau, R. A., West, S. A., and Denison, R. F. (2003). Host sanctions and the legume-rhizobium mutualism. *Nature* 425, 78–81. doi: 10.1038/nature01931

Kimbrel, J. A., Thomas, W. J., Jiang, Y., Creason, A. L., Thireault, C. A., Sachs, J. L., et al. (2013). Mutualistic co-evolution of type III effector genes in *Sinorhizobium fredii* and *Bradyrhizobium japonicum*. *PloS Pathog.* 9, e1003204. doi: 10.1371/journal.ppat.1003204

Kleczkowska, J. (1950). A study of phage-resistant mutants of *Rhizobium trifolii*. *J. Gen. Microbiol.* 4, 298–310. doi: 10.1099/00221287-4-3-298

Klein, S., Hirsch, A. M., Smith, C. A., and Signer, E. R. (1988). Interaction of *nod* and *exo Rhizobium meliloti* in alfalfa nodulation. *Mol. Plant-Microbe Interact.* 1, 94–100. doi: 10.1094/mpmi-1-094

Konopka, A. (2009). What is microbial community ecology? *ISME J.* 3, 1223–1230. doi: 10.1038/ismej.2009.88

Korenblum, E., Dong, Y., Szymanski, J., Panda, S., Jozwiak, A., Massalha, H., et al. (2020). Rhizosphere microbiome mediates systemic root metabolite exudation by root-to-root signaling. *Proc. Natl. Acad. Sci. U.S.A.* 117, 3874–3883. doi: 10.1073/pnas.1912130117

Krašovec, R., Belavkin, R. V., Aston, J. A. D., Channon, A., Aston, E., Rash, B. M., et al. (2014). Mutation rate plasticity in rifampicin resistance depends on *Escherichia coli* cell–cell interactions. *Nat. Commun.* 5, 3742. doi: 10.1038/ncomms4742

Krašovec, R., Richards, H., Gifford, D. R., Hatcher, C., Faulkner, K. J., Belavkin, R. V., et al. (2017). Spontaneous mutation rate is a plastic trait associated with population density across domains of life. *PloS Biol.* 15, e2002731. doi: 10.1371/journal.pbio.2002731

Le, X. H., Franco, C. M. M., Ballard, R. A., and Drew, E. A. (2016). Isolation and characterisation of endophytic actinobacteria and their effect on the early growth and nodulation of lucerne (*Medicago sativa* L.). *Plant Soil* 405, 13–24. doi: 10.1007/s11104-015-2652-9

Lepetit, M., and Brouquisse, R. (2023). Control of the rhizobium–legume symbiosis by the plant nitrogen demand is tightly integrated at the whole plant level and requires inter-organ systemic signaling. *Front. Plant Sci.* 14, 1114840. doi: 10.3389/fpls.2023.1114840

LeRoux, M., Peterson, S. B., and Mougous, J. D. (2015). Bacterial danger sensing. *J. Mol. Biol.* 427, 3744–3753. doi: 10.1016/j.jmb.2015.09.018

Levine, J. M., Bascompte, J., Adler, P. B., and Allesina, S. (2017). Beyond pairwise mechanisms of species coexistence in complex communities. *Nature* 546, 56–64. doi: 10.1038/nature22898

Li, M., Chen, Q., Wu, C., Li, Y., Wang, S., and Chen, X. (2022). A novel module promotes horizontal gene transfer in *Azorhizobium caulinodans* ORS571. *Genes* 13, 1895. doi: 10.3390/genes13101895

Ling, J., Wang, H., Wu, P., Li, T., Tang, Y., Naseer, N., et al. (2016). Plant nodulation inducers enhance horizontal gene transfer of *Azorhizobium caulinodans* symbiosis island. *Proc. Natl. Acad. Sci. U.S.A.* 113, 13875–13880. doi: 10.1073/pnas.1615121113

Liu, Q., Cheng, L., Nian, H., Jin, J., and Lian, T. (2023). Linking plant functional genes to rhizosphere microbes: A review. *Plant Biotechnol. J.* 21, 902–917. doi: 10.1111/pbi.13950

Liu, S., Jiao, J., and Tian, C.-F. (2023). Adaptive evolution of rhizobial symbiosis beyond horizontal gene transfer: From genome innovation to regulation reconstruction. *Genes* 14, 274. doi: 10.3390/genes14020274

Lodwig, E. M., Leonard, M., Marroqui, S., Wheeler, T. R., Findlay, K., Downie, J. A., et al. (2005). Role of polyhydroxybutyrate and glycogen as carbon storage compounds in pea and bean bacteroids. *Mol. Plant-Microbe Interact.* 18, 67–74. doi: 10.1094/MPMI-18-0067

Lodwig, E., and Poole, P. (2003). Metabolism of *rhizobium* bacteroids. *Crit. Rev. Plant Sci.* 22, 37–78. doi: 10.1080/713610850

Maharjan, R. P., and Ferenci, T. (2017). A shifting mutational landscape in 6 nutritional states: Stress-induced mutagenesis as a series of distinct stress input–mutation output relationships. *PloS Biol.* 15, e2001477. doi: 10.1371/journal.pbio.2001477

Marchetti, M., Catrice, O., Batut, J., and Masson-Boivin, C. (2011). *Cupriavidus Taiwanensis* bacteroids in *Mimosa pudica* indeterminate nodules are not terminally differentiated. *Appl. Environ. Microbiol.* 77, 2161–2164. doi: 10.1128/aem.02358-10

Martínez-Hidalgo, P., and Hirsch, A. M. (2017). The nodule microbiome: N_2-fixing rhizobia do not live alone. *Phytobiomes J.* 1, 70–82. doi: 10.1094/PBIOMES-12-16-0019-RVW

Masson-Boivin, C., Giraud, E., Perret, X., and Batut, J. (2009). Establishing nitrogen-fixing symbiosis with legumes: How many rhizobium recipes? *Trends Microbiol.* 17, 458–466. doi: 10.1016/j.tim.2009.07.004

Masson-Boivin, C., and Sachs, J. L. (2018). Symbiotic nitrogen fixation by rhizobia - the roots of a success story. *Curr. Opin. Plant Biol.* 44, 7–15. doi: 10.1016/j.pbi.2017.12.001

Matic, I. (2019). Mutation rate heterogeneity increases odds of survival in unpredictable environments. *Mol. Cell* 75, 421–425. doi: 10.1016/j.molcel.2019.06.029

Melkonian, R., Moulin, L., Béna, G., Tisseyre, P., Chaintreuil, C., Heulin, K., et al. (2014). The geographical patterns of symbiont diversity in the invasive legume *Mimosa pudica* can be explained by the competitiveness of its symbionts and by the host genotype: Competition for nodulation in α- and β-rhizobia. *Environ. Microbiol.* 16, 2099–2111. doi: 10.1111/1462-2920.12286

Mendoza-Suárez, M., Andersen, S. U., Poole, P. S., and Sánchez-Cañizares, C. (2021). Competition, nodule occupancy, and persistence of inoculant strains: Key factors in the rhizobium-legume symbioses. *Front. Plant Sci.* 12, 690567. doi: 10.3389/fpls.2021.690567

Mendoza-Suárez, M. A., Geddes, B. A., Sánchez-Cañizares, C., Ramírez-González, R. H., Kirchhelle, C., Jorrin, B., et al. (2020). Optimizing *Rhizobium*-legume symbioses by simultaneous measurement of rhizobial competitiveness and N_2 fixation in nodules. *Proc. Natl. Acad. Sci. U.S.A.* 117, 9822–9831. doi: 10.1073/pnas.1921225117

Mergaert, P., Uchiumi, T., Alunni, B., Evanno, G., Cheron, A., Catrice, O., et al. (2006). Eukaryotic control on bacterial cell cycle and differentiation in the *Rhizobium* – legume symbiosis. *Proc. Natl. Acad. Sci. U.S.A.* 103, 5230–5235. doi: 10.1073/pnas.0600912103

Miao, J., Zhang, N., Liu, H., Wang, H., Zhong, Z., and Zhu, J. (2018). Soil commensal rhizobia promote *Rhizobium etli* nodulation efficiency through CinR-mediated quorum sensing. *Arch. Microbiol.* 200, 685–694. doi: 10.1007/s00203-018-1478-2

Mishra, A., Dhar, B., and Singh, R. M. (2004). Nodulation competitiveness between contrasting phage phenotypes of pigeonpea rhizobial strains. *Indian J. Exp. Biol.* 42, 611–615.

Montiel, J., Szűcs, A., Boboescu, I. Z., Gherman, V. D., Kondorosi, É., and Kereszt, A. (2016). Terminal bacteroid differentiation is associated with variable morphological changes in legume species belonging to the inverted repeat-lacking clade. *Mol. Plant-Microbe Interact.* 29, 210–219. doi: 10.1094/MPMI-09-15-0213-R

Montoya, A. P., Wendlandt, C. E., Benedict, A. B., Roberts, M., Piovia-Scott, J., Griffitts, J. S., et al. (2023). Hosts winnow symbionts with multiple layers of absolute and conditional discrimination mechanisms. *Proc. R. Soc B Biol. Sci.* 290, 20222153. doi: 10.1098/rspb.2022.2153

Moura De Sousa, J., Lourenço, M., and Gordo, I. (2023). Horizontal gene transfer among host-associated microbes. *Cell Host Microbe* 31, 513–527. doi: 10.1016/j.chom.2023.03.017

Muller, K. E., and Denison, R. F. (2018). Resource acquisition and allocation traits in symbiotic rhizobia with implications for life-history outside of legume hosts. *R. Soc Open Sci.* 5, 181124. doi: 10.1098/rsos.181124

Müller-Santos, M., Koskimäki, J. J., Alves, L. P. S., de Souza, E. M., Jendrossek, D., and Pirttilä, A. M. (2021). The protective role of PHB and its degradation products against stress situations in bacteria. *FEMS Microbiol. Rev.* 45, fuaa058. doi: 10.1093/femsre/fuaa058

Murphy, P. J., Wexler, W., Grzemski, W., Rao, J. P., and Gordon, D. (1995). Rhizopines—Their role in symbiosis and competition. *Soil Biol. Biochem.* 27, 525–529. doi: 10.1016/0038-0717(95)98627-Z

Nandasena, K. G., O'Hara, G. W., Tiwari, R. P., Sezmiş, E., and Howieson, J. G. (2007). *In situ* lateral transfer of symbiosis islands results in rapid evolution of diverse competitive strains of mesorhizobia suboptimal in symbiotic nitrogen fixation on the pasture legume *Biserrula pelecinus* L. *Environ. Microbiol.* 9, 2496–2511. doi: 10.1111/j.1462-2920.2007.01368.x

Ofek, M., Ruppel, S., and Waisel, Y. (2006). "Effects of salinity on rhizosphere bacterial communities associated with different root types of *Vicia faba* L," in *Biosaline Agriculture and Salinity Tolerance in Plants*. Eds. M. Öztürk, Y. Waisel, M. A. Khan and G. Görk (Basel: Birkhäuser Basel), 1–13. doi: 10.1007/3-7643-7610-4_1

Oldroyd, G. E. D. (2013). Speak, friend, and enter: Signalling systems that promote beneficial symbiotic associations in plants. *Nat. Rev. Microbiol.* 11, 252–263. doi: 10.1038/nrmicro2990

Oono, R., Anderson, C. G., and Denison, R. F. (2011). Failure to fix nitrogen by non-reproductive symbiotic rhizobia triggers host sanctions that reduce fitness of their reproductive clonemates. *Proc. R. Soc B Biol. Sci.* 278, 2698–2703. doi: 10.1098/rspb.2010.2193

Oono, R., Muller, K. E., Ho, R., Jimenez Salinas, A., and Denison, R. F. (2020). How do less-expensive nitrogen alternatives affect legume sanctions on rhizobia? *Ecol. Evol.* 10, 10645–10656. doi: 10.1002/ece3.6718

Oresnik, I. J., Pacarynuk, L. A., O'Brien, S. A. P., Yost, C. K., and Hynes, M. F. (1998). Plasmid-encoded catabolic genes in *Rhizobium leguminosarum* bv. trifolii: Evidence for a plant-inducible rhamnose locus involved in competition for nodulation. *Mol. Plant-Microbe Interact.* 11, 1175–1185. doi: 10.1094/MPMI.1998.11.12.1175

Oresnik, I. J., Twelker, S., and Hynes, M. F. (1999). Cloning and characterization of a *Rhizobium leguminosarum* gene encoding a bacteriocin with similarities to RTX toxins. *Appl. Environ. Microbiol.* 65, 2833–2840. doi: 10.1128/AEM.65.7.2833-2840.1999

Orr, H. A. (2009). Fitness and its role in evolutionary genetics. *Nat. Rev. Genet.* 10, 531–539. doi: 10.1038/nrg2603

Pang, J., Ryan, M. H., Wen, Z., Lambers, H., Liu, Y., Zhang, Y., et al. (2023). Enhanced nodulation and phosphorus acquisition from sparingly-soluble iron phosphate upon treatment with arbuscular mycorrhizal fungi in chickpea. *Physiol. Plant* 175, e13873. doi: 10.1111/ppl.13873

Parks, D. H., ChuvoChina, M., Waite, D. W., Rinke, C., Skarshewski, A., Chaumeil, P.-A., et al. (2018). A standardized bacterial taxonomy based on genome phylogeny substantially revises the tree of life. *Nat. Biotechnol.* 36, 996–1004. doi: 10.1038/nbt.4229

Patel, J. J. (1974). Antagonism of actinomycetes against rhizobia. *Plant Soil* 41, 395–402. doi: 10.1007/BF00017266

Pérez, J., Jiménez-Zurdo, J. I., Martínez-Abarca, F., Millán, V., Shimkets, L. J., and Muñoz-Dorado, J. (2014). Rhizobial galactoglucan determines the predatory pattern of *Myxococcus xanthus* and protects *Sinorhizobium meliloti* from predation. *Environ. Microbiol.* 16, 2341–2350. doi: 10.1111/1462-2920.12477

Peterson, S. B., Bertolli, S. K., and Mougous, J. D. (2020). The central role of interbacterial antagonism in bacterial life. *Curr. Biol.* 30, R1203–R1214. doi: 10.1016/j.cub.2020.06.103

Philippot, L., Raaijmakers, J. M., Lemanceau, P., and van der Putten, W. H. (2013). Going back to the roots: The microbial ecology of the rhizosphere. *Nat. Rev. Microbiol.* 11, 789–799. doi: 10.1038/nrmicro3109

Pierce, E. C., and Dutton, R. J. (2022). Putting microbial interactions back into community contexts. *Curr. Opin. Microbiol.* 65, 56–63. doi: 10.1016/j.mib.2021.10.008

Pobigaylo, N., Szymczak, S., Nattkemper, T. W., and Becker, A. (2008). Identification of genes relevant to symbiosis and competitiveness in *Sinorhizobium meliloti* using signature-tagged mutants. *Mol. Plant-Microbe Interact.* 21, 219–231. doi: 10.1094/MPMI-21-2-0219

Poole, P., Ramachandran, V., and Terpolilli, J. (2018). Rhizobia: From saprophytes to endosymbionts. *Nat. Rev. Microbiol.* 16, 291–303. doi: 10.1038/nrmicro.2017.171

Porter, S. S., and Simms, E. L. (2014). Selection for cheating across disparate environments in the legume-rhizobium mutualism. *Ecol. Lett.* 17, 1121–1129. doi: 10.1111/ele.12318

Pribis, J. P., Zhai, Y., Hastings, P. J., and Rosenberg, S. M. (2022). Stress-induced mutagenesis, gambler cells, and stealth targeting antibiotic-induced evolution. *mBio* 13, e01074–e01022. doi: 10.1128/mbio.01074-22

Primieri, S., Magnoli, S. M., Koffel, T., Stürmer, S. L., and Bever, J. D. (2022). Perennial, but not annual legumes synergistically benefit from infection with arbuscular mycorrhizal fungi and rhizobia: a meta-analysis. *New Phytol.* 233, 505–514. doi: 10.1111/nph.17787

Provorov, N. A., Andronov, E. E., Kimeklis, A. K., Onishchuk, O. P., Igolkina, A. A., and Karasev, E. S. (2022). Microevolution, speciation and macroevolution in rhizobia: Genomic mechanisms and selective patterns. *Front. Plant Sci.* 13, 1036943. doi: 10.3389/fpls.2022.1026943

Pugashetti, B. K., Angle, J. S., and Wagner, G. H. (1982). Soil microorganisms antagonistic towards *Rhizobium japonicum*. *Soil Biol. Biochem.* 14, 45–49. doi: 10.1016/0038-0717(82)90075-X

Quides, K. W., Lee, Y., Hur, T., and Atamian, H. S. (2023). Evaluation of qPCR to detect shifts in population composition of the rhizobial symbiont *Mesorhizobium japonicum* during serial in *planta* transfers. *Biology* 12, 277. doi: 10.3390/biology12020277

Quides, K. W., Stomackin, G. M., Lee, H.-H., Chang, J. H., and Sachs, J. L. (2017). *Lotus japonicus* alters in *planta* fitness of *Mesorhizobium* loti dependent on symbiotic nitrogen fixation. *PloS One* 12, e0185568. doi: 10.1371/journal.pone.0185568

Rahman, A., Manci, M., Nadon, C., Perez, I. A., Farsamin, W. F., Lampe, M. T., et al. (2023). Competitive interference among rhizobia reduces benefits to hosts. *Curr. Biol.* 33, 2988–3001.e4. doi: 10.1016/j.cub.2023.06.081

Ramirez, C., and Alexander, M. (1980). Evidence suggesting protozoan predation on rhizobium associated with germinating seeds and in the rhizosphere of beans (*Phaseolus vulgaris* L.). *Appl. Environ. Microbiol.* 40, 492–499. doi: 10.1128/aem.40.3.492-499.1980

Ratcliff, W. C., Kadam, S. V., and Denison, R. F. (2008). Poly-3-hydroxybutyrate (PHB) supports survival and reproduction in starving rhizobia: PHB increases rhizobium fitness. *FEMS Microbiol. Ecol.* 65, 391–399. doi: 10.1111/j.1574-6941.2008.00544.x

Ratcliff, W. C., Underbakke, K., and Denison, R. F. (2011). Measuring the fitness of symbiotic rhizobia. *Symbiosis* 55, 85–90. doi: 10.1007/s13199-011-0150-2

Regus, J. U., Quides, K. W., O'Neill, M. R., Suzuki, R., Savory, E. A., Chang, J. H., et al. (2017). Cell autonomous sanctions in legumes target ineffective rhizobia in nodules with mixed infections. *Am. J. Bot.* 104, 1299–1312. doi: 10.3732/ajb.1700165

Remigi, P., Capela, D., Clerissi, C., Tasse, L., Torchet, R., Bouchez, O., et al. (2014). Transient hypermutagenesis accelerates the evolution of legume endosymbionts following horizontal gene transfer. *PloS Biol.* 12, e1001942. doi: 10.1371/journal.pbio.1001942

Remigi, P., Masson-Boivin, C., and Rocha, E. P. C. (2019). Experimental evolution as a tool to investigate natural processes and molecular functions. *Trends Microbiol.* 27, 623–634. doi: 10.1016/j.tim.2019.02.003

Remigi, P., Zhu, J., Young, J. P. W., and Masson-Boivin, C. (2016). Symbiosis within symbiosis: evolving nitrogen-fixing legume symbionts. *Trends Microbiol.* 24, 63–75. doi: 10.1016/j.tim.2015.10.007

Ruiz-Lozano, J. M., Collados, C., Barea, J. M., and Azcón, R. (2001). Arbuscular mycorrhizal symbiosis can alleviate drought-induced nodule senescence in soybean plants. *New Phytol.* 151, 493–502. doi: 10.1046/j.0028-646x.2001.00196.x

Sachs, J. L., Mueller, U. G., Wilcox, T. P., and Bull, J. J. (2004). The evolution of cooperation. *Q. Rev. Biol.* 79, 135–160. doi: 10.1086/383541

Sánchez-Salazar, A. M., Taparia, T., Olesen, A. K., Acuña, J. J., Sørensen, S. J., and Jorquera, M. A. (2023). An overview of plasmid transfer in the plant microbiome. *Plasmid* 127, 102695. doi: 10.1016/j.plasmid.2023.102695

Sauviac, L., Rémy, A., Huault, E., Dalmasso, M., Kazmierczak, T., Jardinaud, M., et al. (2022). A dual legume-rhizobium transcriptome of symbiotic nodule senescence reveals coordinated plant and bacterial responses. *Plant Cell Environ.* 45, 3100–3121. doi: 10.1111/pce.14389

Schoener, T. W. (2011). The newest synthesis: understanding the interplay of evolutionary and ecological dynamics. *Science* 331, 426–429. doi: 10.1126/science.1193954

Schripsema, J., de Rudder, K. E., van Vliet, T. B., Lankhorst, P. P., de Vroom, E., Kijne, J. W., et al. (1996). Bacteriocin small of *Rhizobium leguminosarum* belongs to the class of N-acyl-L-homoserine lactone molecules, known as autoinducers and as quorum sensing co-transcription factors. *J. Bacteriol.* 178, 366–371. doi: 10.1128/jb.178.2.366-371.1996

Schulte, C. C. M., Borah, K., Wheatley, R. M., Terpolilli, J. J., Saalbach, G., Crang, N., et al. (2021). Metabolic control of nitrogen fixation in rhizobium-legume symbioses. *Sci. Adv.* 7, eabh2433. doi: 10.1126/sciadv.abh2433

Schwinghamer, E. A., and Brockwell, J. (1978). Competitive advantage of bacteriocin and phage-producing strains of *Rhizobium trifolii* in mixed culture. *Soil Biol. Biochem.* 10, 383–387. doi: 10.1016/0038-0717(78)90062-7

Shi, S., Richardson, A. E., O'Callaghan, M., DeAngelis, K. M., Jones, E. E., Stewart, A., et al. (2011). Effects of selected root exudate components on soil bacterial communities. *FEMS Microbiol. Ecol.* 77, 600–610. doi: 10.1111/j.1574-6941.2011.01150.x

Silva, V. M. A., Martins, C. M., Cavalcante, F. G., Ramos, K. A., Silva, L. L. D., Menezes, F. G. R. D., et al. (2019). Cross-feeding among soil bacterial populations: Selection and characterization of potential bio-inoculants. *J. Agric. Sci.* 11, 23. doi: 10.5539/jas.v11n5p23

Simms, E. L., and Bever, J. D. (1998). Evolutionary dynamics of rhizopine within spatially structured rhizobium populations. *Proc. R. Soc Lond. B Biol. Sci.* 265, 1713–1719. doi: 10.1098/rspb.1998.0493

Smith, P., and Schuster, M. (2019). Public goods and cheating in microbes. *Curr. Biol.* 29, R442–R447. doi: 10.1016/j.cub.2019.03.001

Soedarjo, M., and Borthakur, D. (1998). Mimosine, a toxin produced by the tree-legume leucaena provides a nodulation competition advantage to mimosine-degrading rhizobium strains. *Soil Biol. Biochem.* 30, 1605–1613. doi: 10.1016/S0038-0717(97)00180-6

Sorroche, F., Morales, V., Mouffok, S., Pichereaux, C., Garnerone, A. M., Zou, L., et al. (2020). The ex planta signal activity of a *Medicago* ribosomal uL2 protein suggests a moonlighting role in controlling secondary rhizobial infection. *PloS One* 15, e0235446. doi: 10.1371/journal.pone.0235446

Sorroche, F., Walch, M., Zou, L., Rengel, D., Maillet, F., Gibelin-Viala, C., et al. (2019). Endosymbiotic *Sinorhizobium meliloti* modulate *Medicago* root susceptibility to secondary infection via ethylene. *New Phytol.* 223, 1505–1515. doi: 10.1111/nph.15883

Soto, M. J., Pérez, J., Muñoz-Dorado, J., Contreras-Moreno, F. J., and Moraleda-Muñoz, A. (2023). Transcriptomic response of *Sinorhizobium meliloti* to the predatory attack of *Myxococcus xanthus*. *Front. Microbiol.* 14, 1213659. doi: 10.3389/fmicb.2023.1213659

Sprent, J. I. (2009). *Legume nodulation: a global perspective*. *1st ed* (Oxford, UK: Wiley-Blackwell). doi: 10.1002/9781444316384

Stacey, G., Paau, A. S., Noel, K. D., Maier, R. J., Silver, L. E., and Brill, W. J. (1982). Mutants of *Rhizobium japonicum* defective in nodulation. *Arch. Microbiol.* 132, 219–224. doi: 10.1007/BF00407954

Sullivan, J. T., Patrick, H. N., Lowther, W. L., Scott, D. B., and Ronson, C. W. (1995). Nodulating strains of *Rhizobium loti* arise through chromosomal symbiotic gene transfer in the environment. *Proc. Natl. Acad. Sci. U.S.A.* 92, 8985–8989. doi: 10.1073/pnas.92.19.8985

Tang, M., and Capela, D. (2020). Rhizobium diversity in the light of evolution, in: *Advances in Botanical Research*. Eds. P. Frendo, F. Frugier and C. Masson-Boivin. (Cambridge, MA, USA: Academic Press), 251–288. doi: 10.1016/bs.abr.2019.09.006

Tavernier, P., Portais, J., Nava, S., Courtois, J., Courtois, B., and Barbotin, J. (1997). Exopolysaccharide and poly-(beta)-hydroxybutyrate coproduction in two *Rhizobium meliloti* strains. *Appl. Environ. Microbiol.* 63, 21–26. doi: 10.1128/aem.63.1.21-26.1997

Terpolilli, J. J., Masakapalli, S. K., Karunakaran, R., Webb, I. U. C., Green, R., Watmough, N. J., et al. (2016). Lipogenesis and redox balance in nitrogen-fixing pea bacteroids. *J. Bacteriol.* 198, 2864–2875. doi: 10.1128/JB.00451-16

Thiergart, T., Zgadzaj, R., Bozsóki, Z., Garrido-Oter, R., Radutoiu, S., and Schulze-Lefert, P. (2019). *Lotus japonicus* symbiosis genes impact microbial interactions between symbionts and multikingdom commensal communities. *mBio* 10, e01833–e01819. doi: 10.1128/mBio.01833-19

Tian, C. F., Garnerone, A.-M., Mathieu-Demazière, C., Masson-Boivin, C., and Batut, J. (2012). Plant-activated bacterial receptor adenylate cyclases modulate epidermal infection in the *Sinorhizobium meliloti–Medicago* symbiosis. *Proc. Natl. Acad. Sci. U.S.A.* 109, 6751–6756. doi: 10.1073/pnas.1120260109

Tian, C. F., and Young, J. P. W. (2019). Genomics and evolution of rhizobia, in: Ecology and Evolution of Rhizobia. *Springer Singapore Singapore* pp, 103–119. doi: 10.1007/978-981-32-9555-1_4

Timmers, A. C. J., Soupène, E., Auriac, M.-C., De Billy, F., Vasse, J., Boistard, P., et al. (2000). Saprophytic intracellular rhizobia in alfalfa nodules. *Mol. Plant-Microbe Interact.* 13, 1204–1213. doi: 10.1094/MPMI.2000.13.11.1204

Tokala, R. K., Strap, J. L., Jung, C. M., Crawford, D. L., Salove, M. H., Deobald, L. A., et al. (2002). Novel plant-microbe rhizosphere interaction involving *Streptomyces lydicus* WYEC108 and the pea plant (*Pisum sativum*). *Appl. Environ. Microbiol.* 68, 2161–2171. doi: 10.1128/AEM.68.5.2161-2171.2002

Trainer, M. A., and Charles, T. C. (2006). The role of PHB metabolism in the symbiosis of rhizobia with legumes. *Appl. Microbiol. Biotechnol.* 71, 377–386. doi: 10.1007/s00253-006-0354-1

Traxler, M. F., and Kolter, R. (2015). Natural products in soil microbe interactions and evolution. *Nat. Prod. Rep.* 32, 956–970. doi: 10.1039/C5NP00013K

Triplett, E. W., and Barta, T. M. (1987). Trifolitoxin production and nodulation are necessary for the expression of superior nodulation competitiveness by *Rhizobium leguminosarum* bv. *trifolii* strain T24 on clover. *Plant Physiol.* 85, 335–342. doi: 10.1104/pp.85.2.335

Trivedi, P., Leach, J. E., Tringe, S. G., Sa, T., and Singh, B. K. (2020). Plant–microbiome interactions: from community assembly to plant health. *Nat. Rev. Microbiol.* 18, 607–621. doi: 10.1038/s41579-020-0412-1

Tsikou, D., Nikolaou, C. N., Tsiknia, M., Papadopoulou, K. K., and Ehaliotis, C. (2023). Interplay between rhizobial nodulation and arbuscular mycorrhizal fungal colonization in *Lotus japonicus* roots. *J. Appl. Microbiol.* 134, lxac010. doi: 10.1093/jambio/lxac010

Van Cauwenberghe, J., Santamaría, R. I., Bustos, P., Juárez, S., Ducci, M. A., Figueroa Fleming, T., et al. (2021). Spatial patterns in phage-*Rhizobium* coevolutionary interactions across regions of common bean domestication. *ISME J.* 15, 2092–2106. doi: 10.1038/s41396-021-00907-z

Vanderlinde, E. M., Hynes, M. F., and Yost, C. K. (2014). Homoserine catabolism by *Rhizobium leguminosarum* bv. *viciae* 3841 requires a plasmid-borne gene cluster that also affects competitiveness for nodulation. *Environ. Microbiol.* 16, 205–217. doi: 10.1111/1462-2920.12196

Vasi, F., Travisano, M., and Lenski, R. E. (1994). Long-term experimental evolution in *Escherichia coli*. II. Changes in life-history traits during adaptation to a seasonal environment. *Am. Nat.* 144, 432–456. doi: 10.1086/285685

Velázquez, E., Carro, L., Flores-Félix, J. D., Martínez-Hidalgo, P., Menéndez, E., Ramírez-Bahena, M.-H., et al. (2017). "The legume nodule microbiome: A source of plant growth-promoting bacteria," in *Probiotics and Plant Health*. Eds. V. Kumar, M. Kumar, S. Sharma and R. Prasad (Singapore: Springer Singapore), 41–70. doi: 10.1007/978-981-10-3473-2_3

Vo, Q. A. T., Ballard, R. A., Barnett, S. J., and Franco, C. M. M. (2021). Isolation and characterisation of endophytic actinobacteria and their effect on the growth and nodulation of chickpea (*Cicer arietinum*). *Plant Soil* 466, 357–371. doi: 10.1007/s11104-021-05008-6

Walker, L., Lagunas, B., and Gifford, M. L. (2020). Determinants of host range specificity in legume-rhizobia symbiosis. *Front. Microbiol.* 11, 585749. doi: 10.3389/fmicb.2020.585749

Wang, X., Feng, H., Wang, Y., Wang, M., Xie, X., Chang, H., et al. (2021). Mycorrhizal symbiosis modulates the rhizosphere microbiota to promote rhizobia–legume symbiosis. *Mol. Plant* 14, 503–516. doi: 10.1016/j.molp.2020.12.002

Wang, C., Saldanha, M., Sheng, X., Shelswell, K. J., Walsh, K. T., Sobral, B. W. S., et al. (2007a). Roles of poly-3-hydroxybutyrate (PHB) and glycogen in symbiosis of *Sinorhizobium meliloti* with Medicago sp. *Microbiology* 153, 388–398. doi: 10.1099/mic.0.29214-0

Wang, C., Sheng, X., Equi, R. C., Trainer, M. A., Charles, T. C., and Sobral, B. W. S. (2007b). Influence of the poly-3-hydroxybutyrate (PHB) granule-associated proteins (PhaP1 and PhaP2) on PHB accumulation and symbiotic nitrogen fixation in *Sinorhizobium meliloti* Rm1021. *J. Bacteriol.* 189, 9050–9056. doi: 10.1128/JB.01190-07

Wardell, G. E., Hynes, M. F., Young, P. J., and Harrison, E. (2022). Why are rhizobial symbiosis genes mobile? *Philos. Trans. R. Soc B Biol. Sci.* 377, 20200471. doi: 10.1098/rstb.2020.0471

Ware, I. M., Fitzpatrick, C. R., Senthilnathan, A., Bayliss, S. L. J., Beals, K. K., Mueller, L. O., et al. (2019). Feedbacks link ecosystem ecology and evolution across spatial and temporal scales: Empirical evidence and future directions. *Funct. Ecol.* 33, 31–42. doi: 10.1111/1365-2435.13267

Weisberg, A. J., Rahman, A., Backus, D., Tyavanagimatt, P., Chang, J. H., and Sachs, J. L. (2022). Pangenome evolution reconciles robustness and instability of rhizobial symbiosis. *mBio* 13, e00074–e00022. doi: 10.1128/mbio.00074-22

Wendlandt, C. E., Roberts, M., Nguyen, K. T., Graham, M. L., Lopez, Z., Helliwell, E. E., et al. (2022). Negotiating mutualism: A locus for exploitation by rhizobia has a broad effect size distribution and context-dependent effects on legume hosts. *J. Evol. Biol.* 35, 844–854. doi: 10.1111/jeb.14011

Westhoek, A., Clark, L. J., Culbert, M., Dalchau, N., Griffiths, M., Jorrin, B., et al. (2021). Conditional sanctioning in a legume-*Rhizobium* mutualism. *Proc. Natl. Acad. Sci. U.S.A.* 118, e2025760118. doi: 10.1073/pnas.2025760118

Westhoek, A., Field, E., Rehling, F., Mulley, G., Webb, I., Poole, P. S., et al. (2017). Policing the legume-*Rhizobium* symbiosis: a critical test of partner choice. *Sci. Rep.* 7, 1419. doi: 10.1038/s41598-017-01634-2

Wheatley, R. M., Ford, B. L., Li, L., Aroney, S. T. N., Knights, H. E., Ledermann, R., et al. (2020). Lifestyle adaptations of *Rhizobium* from rhizosphere to symbiosis. *Proc. Natl. Acad. Sci. U.S.A.* 117, 23823–23834. doi: 10.1073/pnas.2009094117

Wippel, K., Tao, K., Niu, Y., Zgadzaj, R., Kiel, N., Guan, R., et al. (2021). Host preference and invasiveness of commensal bacteria in the Lotus and Arabidopsis root microbiota. *Nat. Microbiol.* 6, 1150–1162. doi: 10.1038/s41564-021-00941-9

Wilkinson, A., Danino, V., Wisniewski-Dyé, F., Lithgow, J. K., and Downie, J. A. (2002). N -acyl-homoserine lactone inhibition of rhizobial growth is mediated by two quorum-sensing genes that regulate plasmid transfer. *J. Bacteriol.* 184, 4510–4519. doi: 10.1128/JB.184.16.4510-4519.2002

Xavier, L. J. C., Germida, J. J., et al. (2003). Selective interactions between arbuscular mycorrhizal fungi and *Rhizobium leguminosarum* bv. viceae enhance pea yield and nutrition. *Biol. Fertil. Soils.* 37, 261–267. doi: 10.1007/s00374-003-0605-6

Xie, B., Chen, D., Cheng, G., Ying, Z., Xie, F., Li, Y., et al. (2009). Effects of the purL gene expression level on the competitive nodulation ability of *Sinorhizobium fredii*. *Curr. Microbiol.* 59, 193–198. doi: 10.1007/s00284-009-9420-0

Yan, J., Han, X. Z., Ji, Z. J., Li, Y., Wang, E. T., Xie, Z. H., et al. (2014). Abundance and diversity of soybean-nodulating rhizobia in black soil are impacted by land use and crop management. *Appl. Environ. Microbiol.* 80, 5394–5402. doi: 10.1128/AEM.01135-14

Yost, C. K., Rath, A. M., Noel, T. C., and Hynes, M. F. (2006). Characterization of genes involved in erythritol catabolism in *Rhizobium leguminosarum* bv. *viciae*. *Microbiol.* 152, 2061–2074. doi: 10.1099/mic.0.28938-0

Younginger, B. S., and Friesen, M. L. (2019). Connecting signals and benefits through partner choice in plant–microbe interactions. *FEMS Microbiol. Lett.* 366, fnz217. doi: 10.1093/femsle/fnz217

Zgadzaj, R., Garrido-Oter, R., Jensen, D. B., Koprivova, A., Schulze-Lefert, P., and Radutoiu, S. (2016). Root nodule symbiosis in *Lotus japonicus* drives the establishment of distinctive rhizosphere, root, and nodule bacterial communities. *Proc. Natl. Acad. Sci. U.S.A.* 113, E7996–E8005. doi: 10.1073/pnas.1616564113

Zgadzaj, R., James, E. K., Kelly, S., Kawaharada, Y., De Jonge, N., Jensen, D. B., et al. (2015). A legume genetic framework controls infection of nodules by symbiotic and endophytic bacteria. *PloS Genet.* 11, e1005280. doi: 10.1371/journal.pgen.1005280

Zhalnina, K., Louie, K. B., Hao, Z., Mansoori, N., Da Rocha, U. N., Shi, S., et al. (2018). Dynamic root exudate chemistry and microbial substrate preferences drive patterns in rhizosphere microbial community assembly. *Nat. Microbiol.* 3, 470–480. doi: 10.1038/s41564-018-0129-3

Zhang, W., Li, X.-G., Sun, K., Tang, M.-J., Xu, F.-J., Zhang, M., et al. (2020). Mycelial network-mediated rhizobial dispersal enhances legume nodulation. *ISME J.* 14, 1015–1029. doi: 10.1038/s41396-020-0587-5

frontiers | Frontiers in Plant Science

TYPE Original Research
PUBLISHED 21 December 2023
DOI 10.3389/fpls.2023.1322435

OPEN ACCESS

EDITED BY
Jesus Montiel,
National Autonomous University of Mexico, Mexico

REVIEWED BY
Shaun Ferguson,
Aarhus University, Denmark
Barney Geddes,
North Dakota State University, United States

*CORRESPONDENCE
José-María Vinardell
jvinar@us.es
Sebastián Acosta-Jurado
sacojur@upo.es

RECEIVED 16 October 2023
ACCEPTED 04 December 2023
PUBLISHED 21 December 2023

CITATION
Navarro-Gómez P, Fuentes-Romero F, Pérez-Montaño F, Jiménez-Guerrero I, Alías-Villegas C, Ayala-García P, Almozara A, Medina C, Ollero F-J, Rodríguez-Carvajal M-Á, Ruiz-Sainz J-E, López-Baena F-J, Vinardell J-M and Acosta-Jurado S (2023)
A complex regulatory network governs the expression of symbiotic genes in *Sinorhizobium fredii* HH103.
Front. Plant Sci. 14:1322435.
doi: 10.3389/fpls.2023.1322435

A complex regulatory network governs the expression of symbiotic genes in *Sinorhizobium fredii* HH103

Pilar Navarro-Gómez[1,2], Francisco Fuentes-Romero[1], Francisco Pérez-Montaño[1], Irene Jiménez-Guerrero[1], Cynthia Alías-Villegas[1,2], Paula Ayala-García[1], Andrés Almozara[1], Carlos Medina[1], Francisco-Javier Ollero[1], Miguel-Ángel Rodríguez-Carvajal[3], José-Enrique Ruiz-Sainz[1], Francisco-Javier López-Baena[1], José-María Vinardell[1*] and Sebastián Acosta-Jurado[1,2*]

[1]Departamento de Microbiología, Universidad de Sevilla, Sevilla, Spain, [2]Departamento de Biología Molecular e Ingeniería Bioquímica, Centro Andaluz de Biología del Desarrollo, Universidad Pablo de Olavide/Consejo Superior de Investigaciones Científicas/Junta de Andalucía, Sevilla, Spain, [3]Departamento de Química Orgánica, Facultad de Química, Universidad de Sevilla, Sevilla, Spain

Introduction: The establishment of the rhizobium-legume nitrogen-fixing symbiosis relies on the interchange of molecular signals between the two symbionts. We have previously studied by RNA-seq the effect of the symbiotic regulators NodD1, SyrM, and TtsI on the expression of the symbiotic genes (the *nod* regulon) of *Sinorhizobium fredii* HH103 upon treatment with the isoflavone genistein. In this work we have further investigated this regulatory network by incorporating new RNA-seq data of HH103 mutants in two other regulatory genes, *nodD2* and *nolR*. Both genes code for global regulators with a predominant repressor effect on the *nod* regulon, although NodD2 acts as an activator of a small number of HH103 symbiotic genes.

Methods: By combining RNA-seq data, qPCR experiments, and b-galactosidase assays of HH103 mutants harbouring a *lacZ* gene inserted into a regulatory gene, we have analysed the regulatory relations between the *nodD1*, *nodD2*, *nolR*, *syrM*, and *ttsI* genes, confirming previous data and discovering previously unknown relations.

Results and discussion: Previously we showed that HH103 mutants in the *nodD2*, *nolR*, *syrM*, or *ttsI* genes gain effective nodulation with *Lotus japonicus*, a model legume, although with different symbiotic performances. Here we show that the combinations of mutations in these

genes led, in most cases, to a decrease in symbiotic effectiveness, although all of them retained the ability to induce the formation of nitrogen-fixing nodules. In fact, the *nodD2*, *nolR*, and *syrM* single and double mutants share a set of Nod factors, either overproduced by them or not generated by the wild-type strain, that might be responsible for gaining effective nodulation with *L. japonicus*.

KEYWORDS

rhizobium-legume symbiosis, Nod factors, *NodD1*, *NodD2*, *NolR*, *SyrM*, *TtsI*, symbiotic genes regulatory network

1 Introduction

Rhizobia are soil proteobacteria able to establish a symbiotic nitrogen-fixing interaction with legumes (Poole et al., 2018). These bacteria infect legume roots and induce the formation of new root organs called nodules. Later on, rhizobia colonize intracellularly these nodules and differentiate into bacteroids able to fix N_2. Bacteroids supply combined nitrogen to the plant and, in return, are fed with C and energy sources. The complete set of events that takes place in this symbiotic interaction is known as the nodulation process (Roy et al., 2020; Yang et al., 2022).

The nodulation process relies on a complex molecular dialogue established between both partners (Peck et al., 2013; López-Baena et al., 2016). The first step is exudation of flavonoids by plant roots. The interaction of appropriate flavonoids with the rhizobial protein NodD, which belongs to the LysR family of transcriptional regulators, will affect the expression of many bacterial genes related to symbiosis. Flavonoid-NodD complexes bind to conserved DNA sequences called *nod* boxes (NBs) that are located upstream of many rhizobial symbiotic genes. One of the set of genes regulated by NodD and flavonoids is that involved in the production and secretion of specific molecular signals called Nod factors (NFs). NFs are N-acetyl-glucosamine oligosaccharides harbouring different decorations, and each rhizobial strain produces a specific set of NFs (Ghantasala and Choudhury, 2022). These bacterial signals are perceived by LysM receptors located in the root hairs membrane. If NFs are compatible, this recognition event triggers bacterial infection and nodule organogenesis (Roy et al., 2020; Jhu and Oldroyd, 2023). Thus, the flavonoid/NodD and NF/LysM receptor interactions are key events for the establishment of the symbiotic interaction.

NFs are not the only rhizobial molecular signal involved in symbiosis. In some rhizobial strains, such as most of those belonging to the genus *Bradyrhizobium* spp. or to *Sinorhizobium fredii*, NodD and flavonoids also activate the production of effector proteins that are secreted into the cytoplasm of host cells by a type 3 secretion system (T3SS) (Jiménez-Guerrero et al., 2022; Teulet et al., 2022). This is because the expression of the transcriptional regulator TtsI is also activated by NodD and flavonoids. TtsI interacts with conserved DNA sequences called *tts* boxes (TBs) triggering the expression of genes coding both for the symbiotic type 3 secretion system (T3SS) machinery and for effector proteins (called T3Es). T3Es might alter host pathways or suppress host defense responses, with different effects in the symbiotic process (positive, neutral, negative) depending on the specific rhizobium-legume couple and, in some specific cases, can promote symbiosis even in the absence of NFs (Jiménez-Guerrero et al., 2022; Teulet et al., 2022). In addition to NFs and T3Es, various bacterial surface polysaccharides, such as exopolysaccharides (EPS), lipopolysaccharides (LPS), K-antigen capsular polysaccharides (KPS), and cyclic glucans (CG), may have significant roles in symbiosis. They can function as crucial molecules required for the progression of the infection and/or suppress plant defense responses (Downie, 2010; López-Baena et al., 2016; Acosta-Jurado et al., 2021).

Sinorhizobium fredii HH103 Rif^R (hereafter referred to as HH103) is a broad host-range rhizobial strain that nodulates many different legumes, including different species of the *Glycine* genus such as *G. soja* and *G. max*, its natural host plants (Margaret et al., 2011; Vinardell et al., 2015). In this strain, different RNA-seq studies have been performed to analyse the regulation of the expression of bacterial genes that might be involved in symbiosis with legumes. These studies have been carried out either in the presence of effective *nod* gene inducers such as genistein or in the presence of *Lotus japonicus* root exudates (Vinardell et al., 2004a; Pérez-Montaño et al., 2016; Acosta-Jurado et al., 2019; Acosta-Jurado et al., 2020). These studies showed that one hundred HH103 genes (the so-called *nod* regulon) respond to the presence of genistein and that NodD1 is the main positive regulator of the HH103 *nod* regulon. NodD1 activates the expression of those genes related to NFs and T3Es production as well as that of different secondary transcriptional regulators such as NodD2, SyrM, and TtsI (Pérez-Montaño et al., 2016). These studies also demonstrated that TtsI is a positive regulator responsible for the genistein-dependent induction of 35 genes involved in T3SS assembly and T3Es production. Additional RNA-seq studies showed that SyrM is a global regulator that affects the expression of 279 genes in the presence of genistein. The effect of SyrM on the *nod* regulon is variable, since this protein acts as a repressor of a number of genes

(including those related to NFs production) but as an activator of others (such as *nodD2*, and genes putatively related to indole-3-acetic acid synthesis and nitrogen fixation) (Acosta-Jurado et al., 2020). Other RNA-seq studies, performed in the presence of *L. japonicus* root exudates, have analysed the role of NodD2 and the global regulator NolR in HH103 (Acosta-Jurado et al., 2019). These studies showed that the absence of each of these proteins affected the expression of hundreds of genes indicating that not only NolR but also NodD2 is a global regulator in HH103. Regarding the *nod* regulon, NodD2 and NolR appeared to function as repressors of genes related to NFs production and the T3SS. However, these studies also showed that NodD2 acts as an activator of several genes belonging to this regulon. Some of the genes induced by NodD2 upon treatment with *L. japonicus* root exudates are also induced by SyrM in the presence of genistein, such as the previously mentioned genes putatively related to indole-3-acetic acid synthesis and nitrogen fixation.

HH103 NodD1 is essential for symbiosis with all the host-legumes tested so far (Margaret et al., 2011; López-Baena et al., 2016). However, the symbiotic relevance of NodD2, NolR, SyrM, and TtsI, which play important roles in the fine-tune modulation of the expression of the *nod* regulon, is variable. The lack of NodD2, NolR, SyrM, or TtsI provokes partial impairment in symbiosis with soybean (Vinardell et al., 2004b; López-Baena et al., 2008);. However, mutation of either *nodD2*, *nolR*, or *syrM* allows effective nodulation on two legumes in which wild-type HH103 only induces the formation of non-colonized ineffective nodules: the model legume *Lotus japonicus* and *Phaseolus vulgaris* (Acosta-Jurado et al., 2016a; Acosta-Jurado et al., 2019; Acosta-Jurado et al., 2020; Fuentes-Romero et al., 2022). This positive effect might be due to the increased NFs production observed in all these mutants. Interestingly, mutants in *ttsI* also gain effective nodulation in *L. japonicus* but not in *P. vulgaris* (Jiménez-Guerrero et al., 2020; Fuentes-Romero et al., 2022), indicating that some of the T3Es produced by HH103 block nodulation with the former plant.

In this work we have further investigated the complex regulatory network that governs the expression of the HH103 *nod* regulon. Thus, we have completed our analyses of the effect of genistein on HH103 gene expression by carrying out RNA-seq experiments in the HH103 *nolR* and *nodD2* mutant backgrounds. We have investigated the putative regulatory connections among the main regulatory genes of the *nod* regulon: *nodD1*, *nodD2*, *nolR*, *syrM*, and *ttsI*. In addition, we have studied the symbiotic abilities of HH103 *ttsI* mutant derivatives carrying an additional mutation in either *nodD2*, *nolR*, or *syrM*, as well as the production of NFs in the three possible combinations of HH103 double mutants in the *nodD2*, *nolR*, and *syrM* genes.

2 Materials and methods

2.1 Basic molecular and microbiological techniques

Table 1 contains all the bacterial strains and plasmids employed in this work. *Sinorhizobium fredii* strains were grown at 28 °C on

TABLE 1 Bacterial strains and plasmids used in this work.

Strain	Derivation and relevant properties[a]	Source or reference
Sinorhizobium fredii		
HH103 Rif^R (=SVQ269)	Spontaneous Rif^R derivative of HH103	Madinabeitia et al., 2002
SVQ318	HH103 Rif^R *nodD1*::Ω	Vinardell et al., 2004a
SVQ515	HH103 Rif^R *nodD2*::Ω	López-Baena et al., 2008
SVQ533	HH103 Rif^R *ttsI*::Ω	López-Baena et al., 2008
SVQ534	HH103 Rif^R *ttsI*::*lacZ*Δp-Gm^R	López-Baena et al., 2008
SVQ544	HH103 Rif^R *nodD1*::Ω *ttsI*::*lacZ*Δp-Gm^R	López-Baena et al., 2008
SVQ545	HH103 Rif^R *nodD2*::Ω *ttsI*::*lacZ*Δp-Gm^R	López-Baena et al., 2008
SVQ548	HH103 Rif^R *nolR*::*lacZ*Δp-Gm^R	Acosta-Jurado et al., 2016b
SVQ549	HH103 Rif^R *nodD1*::Ω *nolR*::*lacZ*Δp-Gm^R	López-Baena et al., 2008
SVQ550	HH103 Rif^R *ttsI*::Ω *nolR*::*lacZ*Δp-Gm^R	López-Baena et al., 2008
SVQ551	HH103 Rif^R *nodD2*::Ω *nolR*::*lacZ*Δp-Gm^R	López-Baena et al., 2008
SVQ553	HH103 Rif^R *nolR*::Ω *ttsI*::*lacZ*Δp-Gm^R	López-Baena et al., 2008
SVQ555	HH103 Rif^R *nodD1*::Ω n*odD2*:: *lacZ*Δp-Gm^R	Acosta-Jurado et al., 2019
SVQ556	HH103 Rif^R *ttsI*::Ω n*odD2*::*lacZ*Δp-Gm^R	López-Baena et al., 2008
SVQ557	HH103 Rif^R *nolR*::Ω	López-Baena, F.J.
SVQ724	HH103 Rif^R Δ*syrM*	Acosta-Jurado et al., 2019
SVQ727	HH103 Rif^R *syrM*::*lacZ*Δp-Gm^R	Acosta-Jurado et al., 2020
SVQ770	HH103 Rif^R Δ*syrM nodD2*::*lacZ*Δp-Gm^R	This work
SVQ786	HH103 Rif^R *nodD1*::*lacZ*Δp-Gm^R	This work
SVQ787	HH103 Rif^R *nodD2*::*lacZ*Δp-Gm^R	This work
SVQ788	HH103 Rif^R *nolR*::Ω *nodD1*::*lacZ*Δp-Gm^R	This work
SVQ789	HH103 Rif^R Δ*syrM nolR*::*lacZ*Δp-Gm^R	This work
SVQ811	HH103 Rif^R Δ*syrM nodD1*::*lacZ*Δp-Gm^R	This work
SVQ814	HH103 Rif^R *nodD1*::Ω *syrM*:: *lacZ*Δp-Gm^R	This work
SVQ817	HH103 Rif^R *ttsI*::Ω *nodD1*::*lacZ*Δp-Gm^R	This work
SVQ819	HH103 Rif^R *nodD2*::Ω *syrM*:: *lacZ*Δp-Gm^R	This work

(Continued)

10.3389/fpls.2023.1322435

TABLE 1 Continued

Strain	Derivation and relevant properties[a]	Source or reference
SVQ828	HH103 Rif^R *ttsI*::*lacZ*Δp-Gm^R *syrM*::pK18*mob*	This work
SVQ836	HH103 Rif^R *nodD2*::Ω *nodD1*::*lacZ*Δp-Gm^R	This work
SVQ837	HH103 Rif^R *nolR*::Ω *nodD2*::*lacZ*Δp-Gm^R	This work
SVQ842	HH103 Rif^R *ttsI*::Ω *syrM*::*lacZ*Δp-Gm^R	This work
SVQ843	HH103 Rif^R *nolR*::Ω *syrM*::*lacZ*Δp-Gm^R	This work
Escherichia coli		
DH5α	*supE44 ΔlacU169 hsdR17 racA1 endA1 gyr96 thi-1 relA1* Nx^R	Stratagene
BTH101	*cya-99, araD139, galE15, galK16, rpsL1* (Str^R), *hsdR2, mcrA1, mcrB1*	Euromedex, TwoHybrid (BACTH) System Kit
S17-1	*pro, res- hsdR17 (rK- mK+) recA-* with an integrated *RP4-2-Tc::Mu-Km::Tn7*, Tp^R	Simon, 1984
Plasmids		
pAB2001	Ap^R resistant vector containing the *lacZ*Δp-Gm^R cassette	Becker et al., 1995
pBluescript II SK+	Cloning and sequencing vector, Ap^R	Stratagene
pGEM-T-Easy	Cloning vector for PCR amplified fragments	Promega
pRK2013	Helper plasmid, Km^R	Figurski and Helinski, 1979
pBBR1MCS-2	Broad host-range cloning vector, Km^R	Kovach et al., 1995
pK18*mob*	Cloning vector, *sacB* gene, Km^R, suicide in rhizobia	Schäfer et al., 1994
pKT25	*B. pertussis cya* T25-expression plasmid, Km^R	Euromedex, TwoHybrid (BACTH) System Kit
pKNT25	*B. pertussis cya* NT25-expression plasmid, Km^R	Euromedex, TwoHybrid (BACTH) System Kit
pKT25-zip	*B. pertussis cya* T25-leucine zipper fusion, Km^R	Euromedex, TwoHybrid (BACTH) System Kit
pUT18	*B. pertussis cya* T18-expression plasmid, Km^R	Euromedex, TwoHybrid (BACTH) System Kit
pUT18C	*B. pertussis cya* T18C-expression plasmid, Km^R	Euromedex, TwoHybrid (BACTH) System Kit
pUT18C-zip	*B. pertussis cya* T18C-leucine zipper fusion, Km^R	Euromedex, TwoHybrid (BACTH) System Kit
pMUS296	pMP92 carrying a ~1,7 kb *EcoRV-ApaI* fragment containing the *nodD1* gene	Vinardell et al., 2004a
pMUS534	pK18*mob* carrying a 6,0 kb *Hind*III fragment containing the *nodD1*::*lacZ*Δp-Gm^R fusion	Vinardell et al., 2004a
pMUS672	pBluescript carrying a 2,547-bp *Eco*RI fragment containing HH103 *nolR*	Vinardell et al., 2004b
pMUS675	pMP92 carrying a ~2,5 kb *EcoRI* fragment containing the *nolR* gene	Vinardell et al., 2004b
pMUS741	pMP92 carrying a ~1,4 kb *EcoRI* fragment containing the *ttsI* gene and its *nod* box	López-Baena et al., 2008
pMUS746	pMP92 carrying a ~1,4 kb *EcoRI* fragment containing the *nodD2* gene	López-Baena et al., 2008
pMUS788	pGEM-T-Easy derivative carrying the *lacZ*Δp-Gm^R as a 4.3 kb *SmaI* fragment from pAB2001 into *nodD2*	Acosta-Jurado et al., 2019
pMUS789	pK18*mob* carrying a ~5,7 kb *EcoRI* fragment containing the *nodD2*::*lacZ*Δp-Gm^R fusion	This work
pMUS857	pMUS672 containing the *lacZ*Δp-Gm^R into the *Nco*I site of *nolR*	This work
pMUS859	pK18*mob* carrying a 7,0 kb *EcoRI* fragment containing the *nolR*::*lacZ*Δp-Gm^R fusion	This work
pMUS1232	pK18*mobsac* carrying a 1,5 kb *Hind*III-*BamH*I fragment containing the deleted version of the *syrM* gene	Acosta-Jurado et al., 2020
pMUS1234	pK18*mob* carrying a 2,0 kb *Hind*III-*BamH*I containing the *syrM*::*lacZ*Δp-Gm^R fusion	Acosta-Jurado et al., 2020
pMUS1447	pKT25 carrying a 1,0 kb *Kpn*I-*Xba*I fragment containing the *syrM* gene	This work
pMUS1449	pKT25 carrying a 1,0 kb *Kpn*I-*Xba*I fragment containing the *nodD1* gene	This work
pMUS1450	pKNT25 carrying a 1,0 kb *Kpn*I-*Xba*I fragment containing the *nodD1* gene	This work
pMUS1451	pUT18C carrying a 1,0 kb *Kpn*I-*Xba*I fragment containing the *nodD1* gene	This work
pMUS1452	pUT18 carrying a 1,0 kb *Kpn*I-*Xba*I fragment containing the *nodD2* gene	This work
pMUS1453	pUT18C carrying a 1,0 kb *Kpn*I-*Xba*I fragment containing the *nodD2* gene	This work
pMUS1454	pUT18 carrying a 1,0 kb *Kpn*I-*Xba*I fragment containing the *nodD1* gene	This work
pMUS1455	pKT25 carrying a 1,0 kb *Kpn*I-*Xba*I fragment containing the *nodD2* gene	This work

(Continued)

TABLE 1 Continued

Strain	Derivation and relevant properties[a]	Source or reference
pMUS1457	pKNT25 carrying a 1,0 kb *Kpn*I-*Xba*I fragment containing the *nodD2* gene	This work
pMUS1492	pK18*mob* carrying a *syrM* ~0,6kb *Eco*RI-*Xba*I internal fragment	This work
pMUS1514	pBBR1MCS-2 carrying a ~1,9 kb *Kpn*I-*Xba*I fragment containing the *syrM* gene	This work

TABLE 2 Primers used in polymerase chain reaction (PCR) experiments and quantitative PCR (*q*PCR).

Primer	Sequence (5´-3´)	Use
lacZintR	gcctcttcgctattacgcca	Checking of plasmids and mutants
OmegaintR	gggccttgatgttacccgaga	
M13puc-F	gttttcccagtcacgac	
M13puc-R	caggaaacagctatgac	
nodD2-F	ctaaccaagccggagga	
nodD2-R	ccgaagccgtgtacca	
Y4xi-F	taatcagcctggctgaca	
Y4xi-R	aacagaacgagcgcgtaga	
HHnodD1extF	ctttgagcggtttctcgcag	
HHnodD1extR	gagtatcgaagacggctggg	
nolRupst	ttagctacccccaattcttgc	
nolRdwst	gaaaaagccccgcgattgct	
HHsyrMextF	gtacatcacaagccctcgct	
HHsyrMextR	cgcttgaagggaacctgtga	
syrMintEcoRI-F	atcgaattcgcgtgacatgttcaatgacg	Construction of pMUS1492
syrMintXbaI-R	gcttctagagtggatctacaatagcgagc	
syrMPMP92bis-F KpnI	gccggtacctgagggaatggtggagaagg	Construction of pMUS1514
syrMPMP92bis-R XbaI	ctttctagaatcaatcgcacgcggtgtc	
rt16S-F2	gataccctggtagtccac	
rt16S-R2	taaaccacatgctccacc	
qnodA-F[a]	cgtcatgtatccggtgctgca	
qnodA-R[a]	cgttggcggcaggttgaga	
qnodD1-F	gcgagcacggactgcgaa	

(Continued)

TY medium (Beringer, 1974) or in yeast extract/mannitol (YM)

TABLE 2 Continued

Primer	Sequence (5´-3´)	Use
qnodD1-R	cgggaaaaatgggttgcgga	*q*PCR
qnodD2-F	acgctaaagccctccatcga	
qnodD2-R	atggtggaagtgccagtgga	
rt-nolR-F	ccaaaacgcctgctcatt	
rt-nolR-R	attctgggcacgcaactt	
qsyrM-F[a]	gttcaatgacgatctcttggt	
qsyrM-R[a]	attgccatagttaccttcgac	
qttsI-F	cggttggaagatcaactcta	
qttsI-R	gtcaattcaagaacgtagcc	
qpsfHH103d_161-F	agaatgtcgcatacctcttag	
qpsfHH103d_161-R	gtgaaggctgttatcccatc	
qpsfHH103d_208-F	gatctcaggctttcacagac	
qpsfHH103d_208-R	cgtcctctgacggtttcatg	
qpsfHH103d_229-F	gctacgcatcaaagtggaag	
qpsfHH103d_229-R	gttggggttctcaaagatgaa	
qpsfHH103d_255-F	aggcggttacattgctac	
qpsfHH103d_255-R	atcccactgcaccacttt	
qpsfHH103d_257-F	acagacagctaaattctctgc	
qpsfHH103d_257-R	gatgttgtcatcctctggata	
qpsfHH103d_275-F	gagcgcaatatcgcatgt	
qpsfHH103d_275-R	ctcaaccaacgacacgaa	
qpsfHH103d_292-F	gtggctttcaatatcggg	
qpsfHH103d_292-R	cggtgtagtttgtccaga	
qpsfHH103d_306-F	cttcacagttacggagga	
qpsfHH103d_306-R	gcgttcgcgagatcaaaa	
qpsfHH103d_327-F	gagctggatcatggcaa	
qpsfHH103d_327-R	atgctgccaatcaagca	
qpsfHH103d_373-F	tcgacgattcaataagggtg	
qpsfHH103d_373-R	catatcctctccgcaatagc	
qpsfHH103d_448-F	actctcaagagcaggattagg	
qpsfHH103d_448-R	accatcgggagtagtatcagt	
qpsfHH103d_3504-F	caaaggggggcatgga	
qpsfHH103d_3504-R	caaccgatcgaagagcta	
qSFHH103_00346-F	tgctgaattcctcggaag	

(Continued)

TABLE 2 Continued

Primer	Sequence (5´-3´)	Use
qSFHH103_00346-R	cagcatcgacttgacgaa	
qSFHH103_04163-F	acgtgggtggaaacga	
qSFHH103_04163-R	gacgaatctgtctcgaca	

[a]The gen ID of *nodA* and *syrM* are psfHH103d_126 and psfHH103d_367, respectively, in Supplementary Data Sheet 5.

medium (Vincent, 1970). *Escherichia coli* was cultured on LB medium (Sambrook and Russell, 2001) at 37 °C. Supplementation with antibiotics and/or genistein, when necessary, was carried out as described by Vinardell et al. (2004a).

Recombinant DNA techniques were performed as described by Sambrook and Russell (2001). Specific details about DNA-DNA hybridization and PCR amplifications can be found in previous works of our group (Vinardell et al., 2004b; Pérez-Montaño et al., 2016). For quantitative PCR (*q*PCR) experiments, total RNA (DNA free), obtained by using the High Pure RNA Isolation Kit (Roche) and the RNAase Free DNAse (Qiagen), was reverse transcribed to cDNA with the QuantiTec Reverse Transcription Kit (Qiagen). Quantitative PCR (*q*PCR) experiments were conducted as described by Pérez-Montaño et al. (2016). Normalization was carried out with the *S. fredii* HH103 RNA 16S gene. For each treatment, the fold changes showed in this work have been obtained by performing at least two independent experiments with three technical replicates and using the ΔΔCt method (Pfaffl et al., 2002). Table 2 summarizes all the primer pairs used in PCR/*q*PCR experiments in this work.

2.1.1 Construction of plasmids

Plasmid pMUS789 is a pK18*mob* (Schäfer et al., 1994) derivative carrying a *nodD2*::*lacZ*Δp-Gm^R fusion. For constructing pMUS789, a ~5,7 kb *Eco*RI fragment containing the *nodD2*::*lacZ*Δp-Gm^R fusion from pMUS788 (Acosta-Jurado et al., 2019) was subcloned into pK18*mob*.

Plasmid pMUS859 is a pK18*mob* derivative carrying a *nolR*::*lacZ*Δp-Gm^R fusion. For generating this plasmid, the *lacZ*Δp-Gm^R cassette from pAB2001 was subcloned as a 4.3 kb *Nco*I fragment into the *Nco*I site of pMUS672, a pBluescript derivative carrying HH103 *nolR* (Vinardell et al., 2004b), rendering plasmid pMUS857. Finally, a 7,0 kb *Eco*RI fragment containing the *nolR*::*lacZ*Δp-Gm^R fusion from pMUS857 was subcloned into pK18*mob*, generating plasmid pMUS859.

Plasmid pMUS1492 is a pK18*mob* (Schäfer et al., 1994) derivative carrying an internal fragment of the HH103 *syrM* gene. For constructing this plasmid, an internal fragment of *syrM* was PCR amplified by using primers syrMintEcoRI-F and syrMintXbaI-R, and gDNA of HH103 as template. The amplified fragment was digested with *Eco*RI and *Xba*I and subcloned into pK18*mob*, rendering plasmid pMUS1492.

For constructing a broad host-range containing the HH103 *syrM*, a fragment containing this gene and its NB was PCR amplified by using primers SyrMextBamHI-F and SyrMextXbaI-R, and HH103 gDNA as template. The amplified fragment was digested with *Bam*HI and *Xba*I and subcloned into pBBR1MCS-2 (Kovach et al., 1995), rendering plasmid pMUS1514.

2.1.2 Construction of *Sinorhizobium fredii* HH103 single and double mutants

In this work we have used a number of HH103 single or double mutants in the regulatory genes *nodD1*, *nodD2*, *nolR*, *ttsI*, and *syrM* (see Table 1). In all the double mutants, one of the genes was mutated by insertion of the *lacZ*Δp-Gm^R cassette (Becker et al., 1995), whereas the second gene was either deleted or inactivated by insertion of the Ω interposon (Prentki and Krisch, 1984) or the plasmid pK18*mob* (Schäfer et al., 1994). Although many of the mutants had been already constructed in our laboratory, others have been generated in this work. For that purpose, we have used mutated versions of one of the genes subcloned in pK18*mob*, a Km^R vector that is suicide in rhizobia, and transferring the corresponding plasmids from *E. coli* to rhizobia by triparental mating using the helper plasmid pRK2013 (Figurski and Helinski, 1979; Simon, 1984). The specific details of the mutants constructed in this work are provided in Supplementary Table S1. All these mutants were checked by hybridization and by PCR.

2.2 Transcriptomic analyses

Culture conditions and RNA extraction. Three strains of *Sinorhizobium fredii*, SVQ269 (= HH103 Rif^R), SVQ515 (= HH103 Rif^R *nodD2*::Ω) and SVQ548 (= HH103 Rif^R *nolR*::*lacZ*-Gm^R), were cultivated at 28°C until stationary phase (OD_{600} ≈ 1,2) on yeast extract mannitol medium (YM) supplemented with the appropriate antibiotics. Genistein at a concentration of 3.7 µM was added to the medium when required. Two independent total RNA extractions, carried out as describe above for *q*PCR experiments, were performed out for each condition.

RNA-seq experiments. RNA-seq experiments were conducted as previously described (Pérez-Montaño et al., 2016; Acosta-Jurado et al., 2019; Acosta-Jurado et al., 2020). Depletion of rRNA was performed with the MICROB Express Bacterial mRNA Purification kit (Ambion). RNA quality assays and sequencing was performed by Sistemas Genómicos (https://www.sistemasgenomicos.com/web_sg) by using an Illumina HiSeq 2000 sequencing instrument (Illumina). High-quality were mapped against HH103 genome (http://www.ncbi.nlm.nih.gov/assembly/GCF_000283895.1/).

Gene Prediction and Expression Analysis. Gene expression levels were quantified as previously described (Anders and Huber, 2010; Robinson et al., 2010; Trapnell et al., 2010; Anders et al., 2015). More details can be found in Pérez-Montaño et al. (2016) and Acosta-Jurado et al. (2019); Acosta-Jurado et al. (2020). We considered as differentially expressed genes (DEGs) those showing a fold-change lower than -3 or higher than +3 compared to the

value previously reported for HH103 grown in the absence of genistein, being the p-value lower than 0.05 (Pérez-Montaño et al., 2016).

RNA-seq data accession number. All the RNA-seq data used in this publication can be consulted in the Sequence Read Archive of NCBI (BioProject database, BioProject IDs PRJNA313151 and PRJNA413684.

2.3 Plant tests

Nodulation tests on *Lotus japonicus* ecotype Gifu were performed as described by Acosta-Jurado et al. (2016a). At least two independent assays were carried out for each strain, giving similar results. The figures included in this paper shows a representative experiment. In all the assays, *Mesorhizobium loti* MAFF 303099 was used as positive control of effective nodulation in *L. japonicus*. In each experiment, we used five Leonard jar assemblies containing four germinated seeds each per treatment (n = 20). The upper vessel contained 220 ml of sterilized vermiculite supplemented with the plant nutrient solution described by Rigaud and Puppo (1975), whereas the lower recipient was filled with 180 ml (pH 7.0) of the same solution. Each Leonard jar was inoculated with 1 mL of a medium exponential phase rhizobial culture (OD_{600} ≈ 0,5-0,6), containing approximately 10^8 bacteria. Upon inoculation, plants were grown for 9 weeks in a plant-growth chamber (16 h photoperiod, 25 °C in the light and 18 °C in the dark). Nitrogenase activity in nodules was estimated by acetylene reduction assays (ARA) as described by Buendía-Clavería et al., 1986.

2.4 Identification of Nod factors

Purification and LC-MS/MS determination of NFs produced by *S. fredii* strains were carried out as described by Acosta-Jurado et al. (2019). Two independent cultures in B- medium were used for each strain and condition (presence or absence of genistein). In previous works we showed that HPLC-HRMS signal areas reflect the relative abundance of each NF, allowing the estimation of quantitative variations for any individual NF. Samples used in this work were analysed the same day to minimize variations due to experimental conditions.

3 Results

3.1 Inactivation of either *nolR* or *nodD2* of *Sinorhizobium fredii* HH103 affects the expression of hundreds of genes in the presence of genistein

In previous works we investigated the effect of genistein in the transcriptomic profiles of HH103 and mutant derivatives affected in the symbiotic regulatory genes *nodD1*, *ttsI*, and *syrM* (Pérez-Montaño et al., 2016; Acosta-Jurado et al., 2020). These RNA-seq studies allowed us to define a set of 100 HH103 differentially expressed genes (DEGs) in the presence of that flavonoid, the so-called *nod* regulon (Pérez-Montaño et al., 2016). In order to better understand the effect of genistein in the expression of the *nod* regulon of HH103, in this work we have used a transcriptomic approach (RNA-seq) to study the effect of genistein in two other mutant derivatives in HH103 symbiotic regulatory genes: *nodD2* (strain SVQ515) and *nolR* (strain SVQ548). These analyses have been performed both in the absence and presence of genistein, and the data obtained have been compared to the results obtained for the wild-type strain. As we have done in previous transcriptomic studies, we considered as DEGs those genes that, in the presence of genistein, exhibited a fold-change in their expression lower than -3 (i. e., <0.33) or higher than +3 in comparison to the values obtained for the wild-type strain grown in the absence of genistein (Supplementary Data Sheets 1 and 2, respectively). The numbers of DEGs found in each mutant, 382 in HH103 *nodD2* and 201 in HH103 *nolR*, were higher than that found in the wild-type strain, 100 (Pérez-Montaño et al., 2016). These results indicate that both regulatory genes have a high impact in HH103 gene expression. The number of common DEGs found in these mutants was 122 (83 of them belonging to the *nod* regulon), whereas 79 and 260 genes were found as DEGs only in the *nolR* and in the *nodD2* mutant backgrounds, respectively (Supplementary Data Sheet 3).

The 100 DEGs found in the wild-type strain upon induction with genistein can be divided into different groups according to the presence of known motifs in their promoter sequences, such as NBs, TBs, or SyrM boxes (Pérez-Montaño et al., 2016; Acosta-Jurado et al., 2020) As mentioned above, 83 out of these 100 genes were also found as DEGs in both the *nolR* and *nodD2* mutants in the presence of genistein when compared to the wild-type strain grown in the absence of genistein, whereas 11 and 3 genes were found only in the *nolR* or in the *nodD2* mutant respectively. All these 97 genes are marked in bold letters in Supplementary Data Sheet 3. Supplementary Data Sheet 4 shows the expression level of the 100 DEGs found in HH103 upon treatment with genistein in the HH103 *nodD1*, *nodD2*, *nolR*, *syrM*, and *ttsI* mutants grown in the presence of this flavonoid, as well as the comparison to the values obtained in the wild-type strain. The expression levels for the *nodD1*, *ttsI*, and *syrM* mutants have been previously published by our group (Pérez-Montaño et al., 2016; Acosta-Jurado et al., 2020). We considered as overexpressed or repressed in the different mutants analysed those genes whose expression in the presence of genistein was more than three times higher or lower in the mutant than in the wild-type strain grown in the presence of genistein. The presence of well conserved NolR-binding boxes in the upstream region of these genes or operons (Acosta-Jurado et al., 2019) is also indicated in Supplementary Data Sheet 4. For validating RNA-seq data, we studied the expression of 16 out of these 100 genes by *q*PCR in the *nolR* and *nodD2* mutants. Supplementary Data Sheet 5 shows the fold-change values of these 16 genes (by both *q*PCR and RNA-seq) in both mutant strains in the presence of genistein with respect to their expression in the wild-type strain supplemented with genistein. In most cases, there is a good correlation between the two types of data. A heat map showing the effect of the lack of either

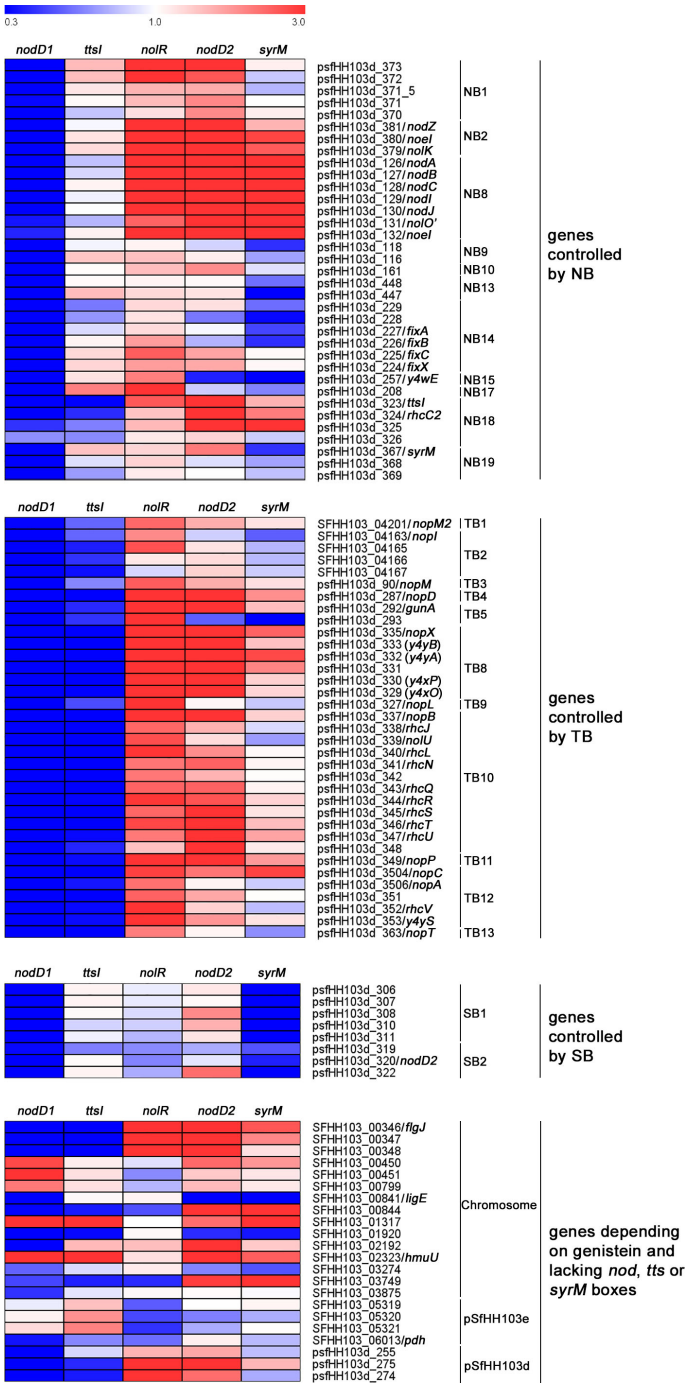

FIGURE 1
Heat map of the effect of the inactivation of either *nodD1*, *nodD2*, *nolR*, *syrM*, or *ttsI* on the expression of the HH103 *nod* regulon upon treatment with genistein when compared to the expression observed in the wild-type strain grown in the presence of this flavonoid.

NodD1, NodD2, NolR, SyrM, or TtsI on the expression of the 100 genes belonging to the HH103 *nod* regulon is provided in Figure 1.

Regarding genes depending on well-defined NBs, all HH103 genes that have been found to be related to Nod factor production (both common and specific) were overexpressed in the presence of genistein in the *nodD2* and *nolR* mutants, similarly to that previously observed for the *syrM* mutant (Acosta-Jurado et al., 2020): the *nodZnoeInolK* (NB2, involved in the fucosylation of NFs; Lamrabet et al., 1999) and *nodABCIJnolO'noeI* (NB8, responsible of the synthesis of the Nod factor backbone and the methylation of the fucosyl residue; Madinabeitia et al., 2002). Also in both mutants, the psfHH103d_373 gene (NB1) shows an expression level that is more than 3-fold higher when compared to the wild-type strain. This gene codes for a hypothetical protein that remains uncharacterized (Vinardell et al., 2015). In the *nolR* mutant, but not in the *nodD2* mutant, gene psfHH103d_208 (NB17) is also overexpressed. To our knowledge, the encoded product of this gene, the putative periplasmic component of an ABC-type transport system

(Vinardell et al., 2015), has not been studied in rhizobia so far. In coherence with the expression data, a well conserved NolR-binding box is present in the upstream region of all these genes/operons (Supplementary Data Sheet 4, Acosta-Jurado et al., 2019). On the other hand, psfHH103d_323 (NB18), which codes for TtsI (López-Baena et al., 2008), is clearly upregulated in the *nodD2* mutant (5.1 when compared to the wild-type) but only slightly in the *nolR* derivative (2.6-fold). Interestingly, psfHH103d_257 (NB15), which codes for an enzyme that participates in indole-3-acetic acid synthesis (Vinardell et al., 2015) is slightly overexpressed (2.3-fold) and repressed (0.4-fold) in the *nolR* and *nodD2* mutants, respectively. For both psfHH103d_323 and psfHH103d_257 a NolR-binding box has been located upstream of these genes.

Concerning genes depending on TBs, most of them were upregulated, some of them slightly, in both mutant backgrounds (Supplementary Data Sheet 4). These results reveal that, as expected, inactivation of either *nolR* or *nodD2* increases the expression of the HH103 symbiotic T3SS since both NolR and NodD2 repress *ttsI* expression. For genes under the control of TB2, 4, 5, 8, 9, 11, and 12, the presence of NolR-binding boxes in their promoter regions might also contribute to the observed increase in their expression in the *nolR* mutant background (Supplementary Data Sheet 4, Acosta-Jurado et al., 2019).

In *S. fredii*, HH103 only two groups of genes present a well-defined SyrM box in their upstream DNA sequences and, accordingly, its expression depends on the presence of SyrM (Supplementary Data Sheet 4, Acosta-Jurado et al., 2020). Inactivation of *nolR* had no effect on the expression of these genes, but that of *nodD2* slightly increased the expression of some of them.

Regarding genes lacking NBs, TBs, or SyrM boxes in their promoter sequences, both the chromosomal SFHH103_00346-SFHH103_00348 and the symbiotic plasmid psfHH103d_275-psfHH103d_274 genetic regions were upregulated in both the *nodD2* and *nolR* mutant backgrounds. SFHH103_00346, SFHH103_00347 and SFHH103_00348 codes for flagellar proteins (FlgJ, FlgN, and MotF), as described recently in *S. meliloti* (Sobe et al., 2022). The predicted products coded by psfHH103d_275 and psfHH103d_274 are hypothetical proteins. Three other genes were overexpressed in the *nodD2* but not in the *nolR* mutant: SFHH103_00844 (conserved hypothetical protein containing nucleic acid-binding domains), SFHH103_02192 (peptidase_M10_C and COG2931 domain-containing conserved hypothetical protein) and SFHH103_02323/*hmuU* (a putative iron ABC transporter permease). In addition, the SFHH103_00841/*ligE* (glutathione S-transferase etherase domain-containing protein) was clearly repressed in the *nodD2* mutant.

3.2 *Lotus japonicus* root exudates have a bigger impact in the transcriptomic profile of the HH103 *nodD2* and *nolR* mutants than genistein

In a previous work we reported the effect of *L. japonicus* root exudates on the global gene expression of HH103 and its *nodD2* and *nolR* mutant derivatives (Acosta-Jurado et al., 2019). In this work we have carried out these transcriptomic analyses upon treatment with genistein. The number of DEGs found in the presence of root exudates were higher than that found in the presence of genistein: 575 vs 382 and 279 vs 201 for HH103 *nodD2* and HH103 *nolR* respectively. Supplementary Data Sheet 6 summarizes the transcriptome data for both mutants in both conditions (genistein or *L. japonicus* root exudates).

In the case of the HH103 *nodD2* mutant, 371 and 178 DEGs were exclusively found upon treatment with *L. japonicus* root exudates and genistein respectively, whereas 204 DEGs were found in both conditions, 77 belonging to the *nod* regulon (Supplementary Data Sheet 7, Figure 2A). In the case of HH103 *nolR*, 177 and 99 DEGs were detected exclusively with root exudates and genistein, respectively, and the number of shared DEGs were 102, 79 belonging to the *nod* regulon (Supplementary Data Sheet 7, Figure 2B). For both mutants, most genes involved in NF production or T3SS functioning were affected by treatments with either genistein or *L. japonicus* root exudates.

3.3 Analysis of the expression of different HH103 symbiotic regulators (*nodD1*, *nodD2*, *nolR*, *syrM*, *ttsI*) by RNA-seq and *q*PCR

One of the main purposes of this work was to study the possible connections among different symbiotic regulators previously identified in HH103: *nodD1*, *nodD2*, *nolR*, *syrM*, and *ttsI*. Table 3 summarizes the fold-changes, as determined by RNA-seq, of the expression of these genes in the wild-type strain and in different individual mutants in the mentioned genes when grown in the presence of genistein, in comparison to the values obtained in the wild-type strain grown in the absence of genistein. The *nodA* gene, coding for one of the key enzymes participating in NF biosynthesis, was included as a control of a gene whose expression is affected by different symbiotic regulators. In addition, we performed *q*PCR analyses of the expression of all these six genes (*nodA* and the five symbiotic regulators previously mentioned) in the same genetic backgrounds as those employed in the RNA-seq analyses (Table 3).

As expected, both methodologies showed that *nodA* expression was strongly enhanced by genistein in a NodD1-dependent manner. The absence of either NodD2, NolR, or SyrM provoked strong increases of this expression, whereas lack of TtsI had no effects at all. Similarly to *nodA*, both *ttsI* and *syrM* are preceded by a NB (Vinardell et al., 2015). As shown in Table 3, the expression of these two regulatory genes is, as that of *nodA*, genistein-induced in a NodD1 dependent manner, and repressed (in a lesser extent in the case of *syrM*) by NolR and NodD2. In addition, both RNA-seq and *q*PCR data showed that SyrM and TtsI appear to repress the expression of each other. Regarding *nodD1*, its expression was slightly repressed by the presence of genistein both in the wild-type and in the *ttsI* mutant background, and slightly increased in the absence of NodD2. The *nodD2* gene also showed genistein-induction and dependence on the presence of functional copies of NodD1 and, to a lesser extent, SyrM. Regarding *nolR*, its expression was not affected by genistein nor by NodD1, NodD2, or TtsI. However, the absence of SyrM appeared to

10.3389/fpls.2023.1322435

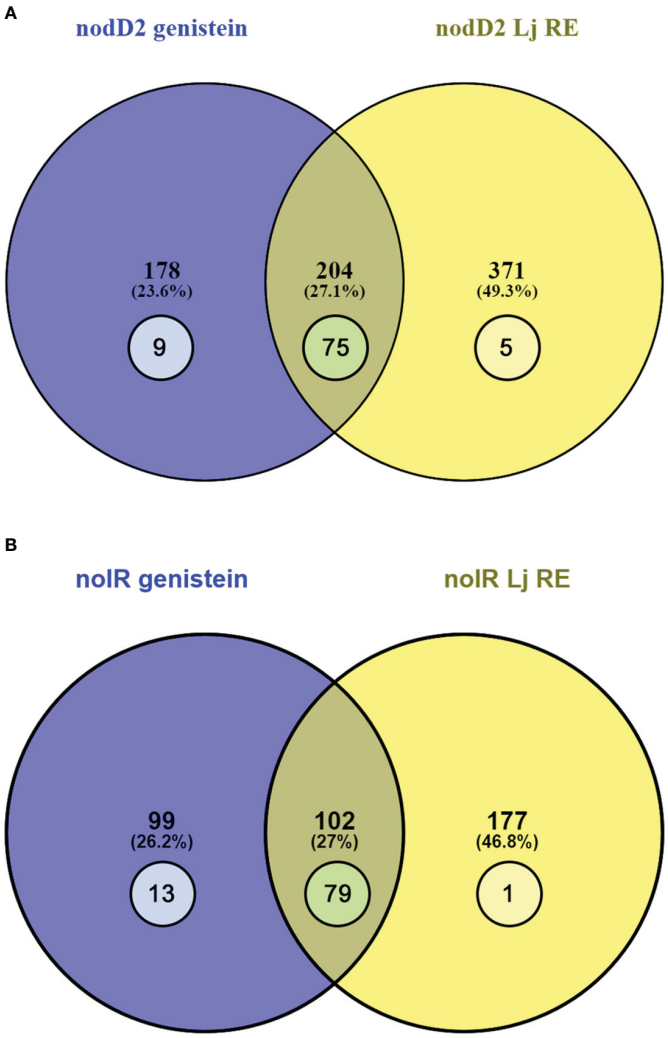

FIGURE 2
Venn diagram of the sets of the DEGs found in the HH103 *nodD2* **(A)** and *nolR* **(B)** mutants upon treatments with genistein (blue circle) and *L. japonicus* root exudates (yellow circle). The numbers represented inside circles correspond to genes belonging to the *nod* regulon.

negatively affect the level of transcripts of *nolR*, as scored by both RNA-seq and *q*PCR.

3.4 Assessing the fine-tuning modulation of the expression of *nodD1*, *nodD2*, *nolR*, *syrM* and *ttsI* by β-galactosidase assays

To further investigate the relationships among different symbiotic regulators (*nodD1*, *nodD2*, *nolR*, *syrM* and *ttsI*) of HH103, we performed β-galactosidase assays of HH103 mutants in each of these genes constructed by insertion of the *lacZ*Δp-Gm^R cassette (Becker et al., 1995). In these mutants, the cassette not only disrupts the gene of interest but also provides a readout for expression from the promoter activity of the mutated gene. We carried out two different series of experiments (Figure 3): (i) HH103 double mutants in two regulatory genes, one of them carrying the *lacZ*Δp-Gm^R cassette, and the other mutated by in frame deletion or by insertion of the Ω cassette (Prentki and Krisch, 1984), in order to analyse the effect of the lack of the latter gene on the expression of the former; (ii) HH103 mutants in a symbiotic regulatory gene with the *lacZ*Δp-Gm^R cassette and harbouring extra copies of each of the different symbiotic regulators carried on a plasmid stable in rhizobia, in order to analyse the effect of multiple copies of the latter gene on the expression of the former one. The differences were analysed by using the non-parametric test of Mann-Whitney. For the sake of clarity, only the statistical differences between each treatment and the control (the corresponding *lacZ*Δp-Gm^R mutant grown in the absence of genistein) are shown in Figure 3. When necessary, additional statistical comparisons are mentioned below.

Concerning *nodD1*, its expression was not affected by the absence of either *nodD2*, *ttsI*, or *syrM*, but it significantly increased (2.3-fold) in the absence of a functional copy of *nolR*. On the other hand, *nodD1* expression was significantly repressed in

TABLE 3 RNA-seq and *q*PCR analyses of the expression of *nodA* and several genes coding for symbiotic regulators of *S. fredii* HH103 when grown in genistein.

		Fold change in different genetic backgrounds in the presence of genistein[1]					
		Wild-type	*nodD1*	*ttsI*	*nodD2*	*nolR*	*syrM*
Gen ID	**Gene name**	**RNA-seq[2]**					
psfHH103d_126	*nodA*	17.65	0.72	14.68	233.98	102.56	77.22
psfHH103d_386	*nodD1*	0.80		0.76	1.36	0.96	0.85
psfHH103d_323	*ttsI*	10.09	0.82		51.79	26.68	17.76
psfHH103d_320	*nodD2*	6.60	0.92	6.95		4.38	2.56
SFHH103_02239	*nolR*	0.99	0.93	1.20	0.54		0.32
psfHH103d_367	*syrM*	5.81	0.86	9.29	13.36	8.23	
Gen ID	**Gene name**	***q*PCR[3]**					
psfHH103d_126	*nodA*	31.71	1.19	31.56	225.45	244.16	201.55
psfHH103d_386	*nodD1*	0.84		0.83	1.96	1.16	0.95
psfHH103d_323	*ttsI*	13.27	1.32		98.36	61.53	28.84
psfHH103d_320	*nodD2*	6.04	0.70	4.48		6.21	2.73
SFHH103_02239	*nolR*	1.18	1.24	1.45	1.36		0.79
psfHH103d_367	*syrM*	6.51	0.85	9.80	9.29	13.02	

[1]With regard to the expression in the wild-type strain in the absence of genistein.
[2]p values were lower than 10^{-3}.
[3]Standard deviations were less or equal than 15% of the average fold-change.

the presence of extra copies of either *nodD2*, *nolR* and, also, *nodD1* (2.1, 3.2, and 2.1-fold respectively), but not when multiple copies of either *ttsI* or *syrM* were present. All the effects on the expression of *nodD1* mentioned were found regardless of the absence or presence of genistein.

The expression of *nodD2* was slightly, but significantly, increased (1.6-fold) in the presence of genistein, but this induction did not take place in the absence of NodD1. The genistein-induction of *nodD2* was slightly, but significantly, higher (2.1-fold, $p<0.05$) and lower 1.4-fold, $p<0.002$)) in a *nolR* and a *syrM* mutant backgrounds, respectively, and not affected by the absence of TtsI. Upon treatment with genistein, the presence of extra copies of *nodD2* and *nodD1* slightly affected *nodD2* expression in a negative and positive way, respectively, but these expression changes were not significant. However, when multiple copies of *syrM* were present, the expression of *nodD2* enhanced significantly in the presence of genistein (2-fold, $p<0.002$) and was independent of the presence of genistein. On the other hand, the presence of extra copies of NolR negated the genistein-dependent induction of *nodD2* expression, provoking a significant difference with respect to the control strain ($p<0.002$).

The absence of either *nodD1*, *nodD2*, *syrM*, or *ttsI* did not significantly affect *nolR* expression, whereas the presence of extra copies of this gene, but not that of either *nodD1*, *nodD2*, *syrM*, or *ttsI*, clearly repressed its expression (4.3-fold).

The analysis of the β-galactosidase data in the *syrM*::*lacZ*ΔpGm^R mutant revealed that this gene is subjected to a complex regulation. On the one hand, the expression of *syrM* almost duplicated in the presence of genistein (1.84-fold) and it was dependent on the presence of NodD1. Also, when genistein was present, the absence of NolR provoked a slight but significant increase of *syrM* expression ($p<0.05$). On the other hand, the presence of extra copies of either *nodD2*, *nolR*, *syrM*, or *ttsI* exerted a significant repressor effect on *syrM* expression upon treatment with genistein ($p<0.002$ for extra copies of *nodD2*, *nolR*, and *ttsI*; $p<0.05$ for extra copies of *syrM*).

As expected, the expression of *ttsI* was enhanced in the presence of genistein (more than 3-fold) in a NodD1-dependent manner. This genistein-dependent expression was not affected by the absence of NodD2 or SyrM, but exhibited a slight but significant increase when NolR was not present ($p<0.05$). On the other hand, the presence of extra copies of *nolR*, *syrM*, or, to a lesser extent, *ttsI*, significantly reduced the expression of this gene upon treatment with genistein ($p<0.002$ in all cases).

3.5 Phenotype of HH103 symbiotic regulatory gene double mutants on *Lotus japonicus*

HH103 is a broad-host range rhizobial strain able to induce the formation of Fix$^+$ nodules in *Lotus burttii* but ineffective white empty nodules in *L. japonicus* (Acosta-Jurado et al., 2016a). However, HH103 mutants in the secondary symbiotic regulators *nodD2*, *nolR*, *syrM*, or *ttsI* gain the ability to fix nitrogen with *L. japonicus*, although they differ in their effectiveness (Acosta-

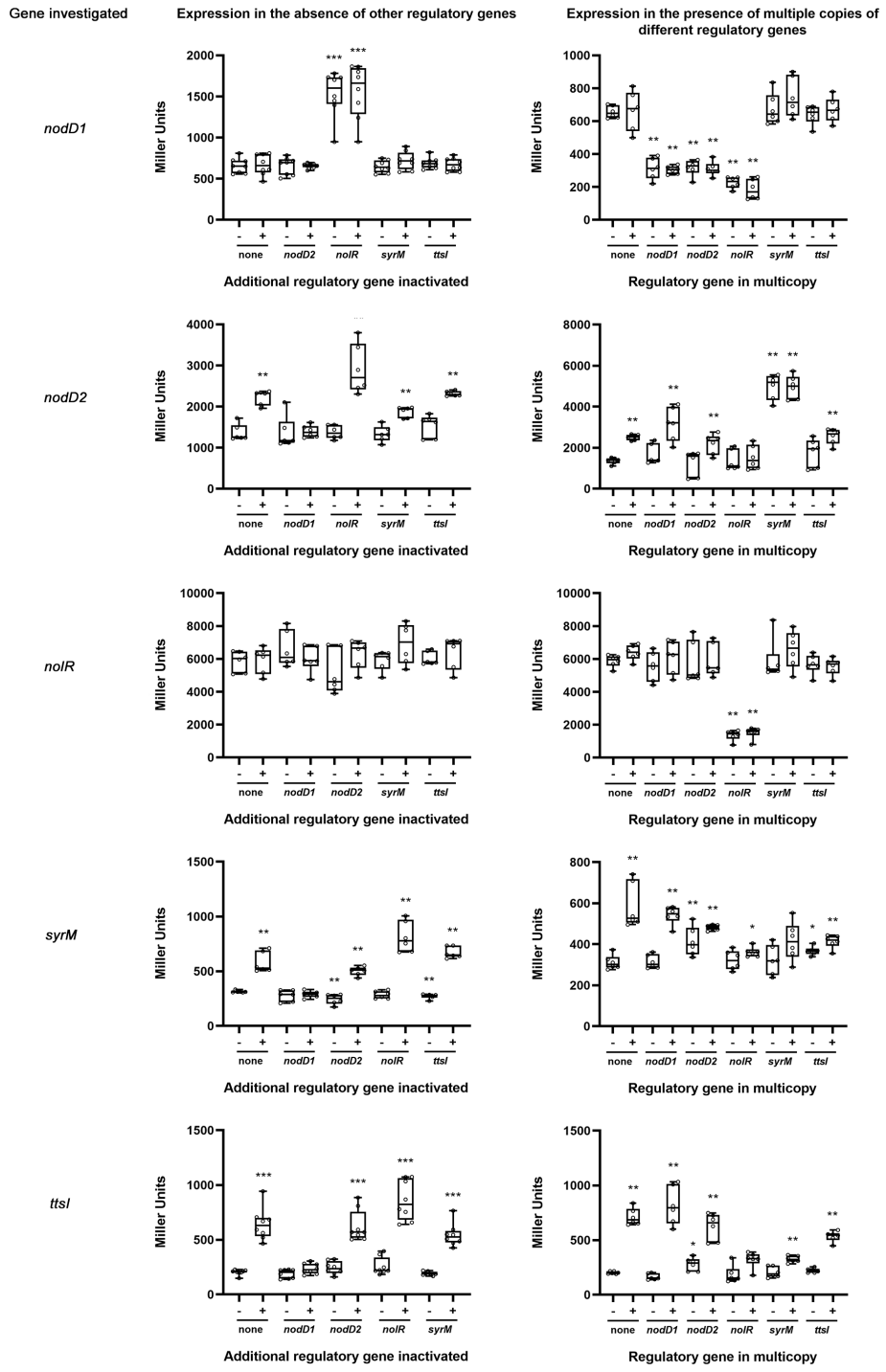

FIGURE 3
Analysis of *nodD1*, *nodD2*, *nolR*, *syrM*, and *ttsI* expression by β-galactosidase assays in the absence of an additional regulatory gene (left panels) or in the presence of multiple copies of different regulatory genes (right panels). These assays were carried out in the absence (-) or presence (+) of genistein 3.7 μM. Error bars show standard deviations. All the treatments were individually compared to the control values (none) obtained in the absence of flavonoids by using the non-parametric test of Mann-Whitney ($p<0.001$, ***; $p<0.002$, **, $p<0.05$, *). Other statistical analyses are indicated in the text.

Jurado et al., 2019; Acosta-Jurado et al., 2020; Jiménez-Guerrero et al., 2020). In order to shed light about this issue, in this work we have studied the symbiotic behaviour with *L. japonicus* of all the possible combinations of double mutants in the four genes mentioned above. Four different parameters were analysed (Figure 4): plant-top fresh weight (PTFW), number of white nodules, number of pink nodules, and nitrogenase activity (estimated by acetylene reduction assay, ARA). Supplementary

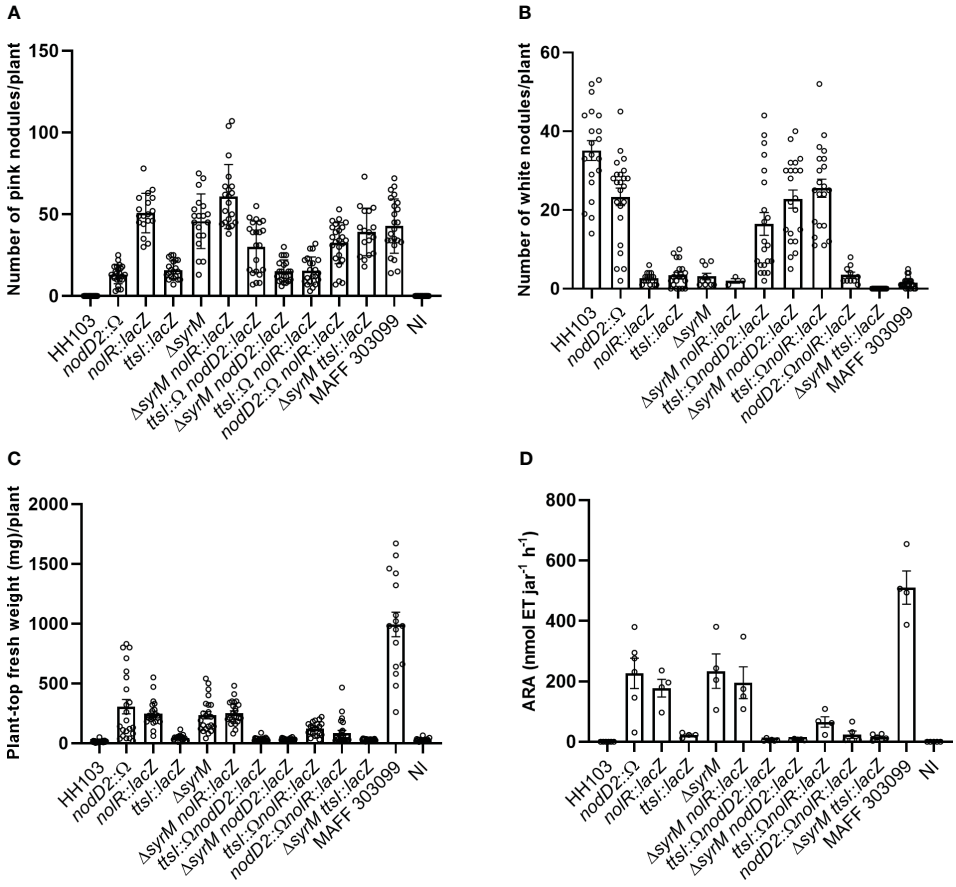

FIGURE 4
Symbiotic performance of *S. fredii* HH103 and different mutant derivatives with *L. japonicus*. **(A)** Number of pink nodules per plant. **(B)** Number of white nodules per plant. **(C)** Plant-top fresh weight per plant. **(D)** ARA per Leonard jar. Error bars show standard deviations. For each HH103 individual mutant in either *nodD2*, *nolR*, *syrM*, or *ttsI*, the values of these parameters were compared to those of their corresponding double mutants, the wild-type strain and the Non-inoculated plants (NI) by using the non-parametric test of Kruskal-Wallis.

Figure S1 provides individual analysis for strains sharing a mutation on each specific regulatory gene.

As previously observed, HH103 individual mutants in either *nodD2*, *nolR*, or *syrM* showed similar symbiotic performances (values of PTFW and ARA), which were higher than that of HH103 *ttsI*. In contrast to HH103, all the double mutants tested in this work were able to induce the formation of nitrogen-fixing nodules in *L. japonicus*, as well as white nodules (Figure 4), as HH103 did. However, the number of both types of nodules were highly variable among the different strains tested.

Regarding PTFW (Figure 4), the three double mutants lacking TtsI behaved similarly to the individual HH103 *ttsI* mutant. These results indicate that carrying a mutation in *ttsI* led to a decrease in the symbiotic performance of the HH103 mutants in either *nodD2*, *nolR*, or *syrM*. A similar pattern could be observed in the case of ARA (Figure 4). However, it is noticeable that the mutation of *nolR*, but not those of *nodD2* or *syrM*, increased the symbiotic performance (PTFW and ARA) of the HH103 *ttsI* mutant (Figure 4, Supplementary Figure S1).

Regarding the different combinations of double mutants of the *nodD2*, *nolR*, and *syrM* genes, only HH103 *nolR syrM* exhibited a symbiotic performance similar to that of the corresponding individual mutants. Instead, plants inoculated with either HH103 *nodD2 nolR* or HH103 *nodD2 syrM* exhibited values of PTFW and ARA that were clearly smaller than those exhibited by the corresponding individual mutants.

3.6 Production of Nod factors is *Sinorhizobium fredii* HH103 double mutants in the *nodD2*, *nolR* and, *syrM* genes

In previous works (Acosta-Jurado et al., 2019; Acosta-Jurado et al., 2020) we showed that the HH103 individual mutants in the *nolR*, *nodD2*, and *syrM* genes exhibit increased expression of genes involved in NF synthesis and, consequently, enhanced production of these signal molecules. In this work we have investigated the production of NFs in the different combinations of HH103 double mutants in the *nolR*, *nodD2*, and *syrM* genes and compared to that of the wild-type strain and the single mutants in these regulatory genes.

HPLC coupled with data-dependent High-Resolution Mass Spectrometry (HPLC-HRMS/MS) enabled the identification of

108 different NFs in HH103 cultures upon induction with genistein (as detailed in Supplementary Data Sheet 8). Interestingly, the number of different NFs was notably higher in double (129, 128 and 118 in *nolR nodD2*, *syrM nodD2*, and *syrM nolR*, respectively) and, particularly, in single mutants (158, 145 and 170 in *nodD2*, *nolR* and *syrM*, respectively) than in the wild-type strain (Table 4, Supplementary Data Sheet 8). All these mutants, single or double, share a common core of 65 different NFs with the parental strain (Supplementary Data Sheet 8). The signal area values registered by the mass spectrometer for a particular NF serves as a metric for comparing the production of these molecules among the tested strains subjected to identical treatment conditions, as previously shown by Acosta-Jurado et al. (2019); Acosta-Jurado et al. (2020) and Jiménez-Guerrero et al. (2020). In this context, most of the common NFs were detected at elevated concentrations in the *nodD2* (58), *nolR* (38), and *syrM* (44) single mutants when compared to those produced by the parental strain (Table 4, Supplementary Data Sheet 8). Interestingly, a different landscape emerges when analysing the relative amounts of NFs in the double mutants compared to *S. fredii* HH103. While certain shared NFs were also identified at elevated concentrations (31 for *nolR nodD2*, 16 for *syrM nodD2*, or 19 for *syrM nolR*) when compared to those produced by HH103, the majority of them were observed at similar or even lower levels than in the parental strain (36, 49, and 46 for *nolR nodD2*, *syrM nodD2*, and *syrM nolR*, respectively) (Table 4, Supplementary Data Sheet 8). Overall, these results indicate that a general overproduction of NFs in the presence of genistein is a characteristic shared by all single mutants but not conserved among double mutant strains. In Table 5, we have summarized the chemical structures of the NFs that were shared among all single and double mutants but were not produced by the parental strain, as well as those that were overproduced by all single and double mutants with respect to HH103.

TABLE 5 Chemical structures of Nod Factors categorized based on their presence and overproduction in the *nodD2*, *nolR*, and *syrM* single and double mutants of *Sinorhizobium fredii* HH103 in comparison to the parental strain.

NFs shared by all single and double mutants but not produced by HH103
III (C14:0, Ac, MeFuc), III (C14:1, Ac, MeFuc), III (C16:0, Ac, MeFuc), III (C16:1, Ac, MeFuc), III (C16:2-OH, MeFuc), III (C18:1-OH, MeFuc), III (C18:2-OH, MeFuc), IV (C14:0, Ac, MeFuc), IV (C16:1-OH, MeFuc)
NFs overproduced by all single and double mutants
II-Hex-GlcNAc-GlcNAc (C16:0, MeFuc), II-Hex-GlcNAc-GlcNAc (C18:1, MeFuc), III (C14:0, MeFuc), III (C16:0), III (C16:0, MeFuc), III (C16:0, NMe, MeFuc), III (C18:1, NMe, MeFuc), IV (C14:0, MeFuc
NFs overproduced only by all single mutants
III (C18:1, MeFuc), III (C16:0, Fuc), IV (C16:0, NMe, MeFuc), IV (C16:1), IV (C16:1, Ac, MeFuc), IV (C16:1, Fuc), IV (C16:1, MeFuc), IV (C16:1, NMe, MeFuc), IV (C18:2, MeFuc), IV (C18:1-OH, MeFuc), IV (C18:2-OH, MeFuc), V (C16:0, Fuc), V (C16:0, MeFuc)

4 Discussion

The rhizobia-legume symbiosis relies on a complex molecular dialogue between two symbionts (López-Baena et al., 2016; Roy et al., 2020; Ghantasala and Choudhury, 2022). The presence of appropriate signals from the plant (flavonoids) affects the expression of many bacterial genes involved in the establishment and progression of the symbiotic interaction (revised by Jiménez-Guerrero et al., 2018). The regulation of the expression of these bacterial symbiotic genes is complex and involves the participation of different transcriptional regulators (Barnett and Long, 2015; López-Baena et al., 2016). In HH103, a broad-host range strain, different transcriptomic studies (Pérez-Montaño et al., 2016; Acosta-Jurado et al., 2020) have revealed that one hundred genes, collectively known as the *nod* regulon, respond to the presence of genistein, an effective flavonoid for HH103 (Vinardell et al., 2004a). Although the LysR family regulator NodD1 acts as the main activator of the HH103 *nod* regulon, other transcriptional regulators, such as TtsI and SyrM, also participate in the genistein effect on the *nod* regulon. Additional transcriptomics studies carried out upon treatment with *L. japonicus* root exudates showed that two others transcriptional regulators, NodD2 and NolR, are also involved in the modulation of the expression of the HH103 *nod* regulon (Acosta-Jurado et al., 2019). In the present work, we show

TABLE 4 Number and average fold-change values of HPLC-HRMS signal areas for overproduced and decreased Nod Factors produced by single and double mutants of *Sinorhizobium fredii* HH103 in comparison to the parental strain.

HH103	*nodD2*	*nolR*	*syrM*	*nolR nodD2*	*syrM nodD2*	*syrM nolR*
Total number of detected NFs						
108	158	145	170	128	119	118
Number of common NFs						
Overproduced	56	35	38	31	16	19
Neutral	9	30	27	31	24	25
Decreased	0	0	0	3	25	21
Fold-change average of common NFs						
Overproduced	+19,1	+9,5	+6,5	+12,5	+11,0	+10,1
Decreased	–	–	–	-3,0	-9,0	-7,8

that these two regulatory proteins are also involved in the fine-tuning modulation of this regulon upon treatment with genistein. The number of DEGs found in the HH103 *nodD2* or *nolR* mutants are higher upon treatment with *L. japonicus* root exudates than upon treatment with genistein, suggesting that these two regulatory proteins are global regulators that, in addition to flavonoids, respond to other components that might be present in legume root exudates, such as phenolic acids, organic acids, fatty acids, galactosides, or aminoacids (Pantigoso et al., 2022; Shimamura et al., 2022). In any case, in both mutants a high number of genes belonging to the *nod* regulon are differentially expressed in both conditions (treatments with either genistein or root exudates from *L. japonicus*).

Regarding the effects of the different regulatory proteins analysed in the HH103 *nod* regulon (Figure 1, Supplementary Data Sheet 4), NodD1 affects positively the expression of 91 out of these 100 genes, including all the genes depending on NBs, TBs, and SyrM boxes, whereas TtsI induces the expression of the 35 genes depending on TBs (Pérez-Montaño et al., 2016; Supplementary Data Sheet 4). SyrM is required for the expression of the two operons harbouring a well-defined SyrM *box* in their promoter sequences but can activate or repress of a number of other genes belonging to the *nod* regulon (Acosta-Jurado et al., 2020; Supplementary Data Sheet 4). In this work we show that NodD2 have a similar behaviour that SyrM, although its predominant effect is repressor (Supplementary Data Sheet 4). NolR, instead, appears as the main repressor of the *nod* regulon, decreasing the expression of 55 different genes. NodD2, NolR, and SyrM share the repressor activity over the two operons (*nodABCIJnolO´noeI* and *nodZnoeLnolK*) that are involved in HH103 NFs biosynthesis and export, which may explain the increased NF production ability of the HH103 individual mutants affected in the coding genes of these transcriptional regulators (Tables 4, 5; Supplementary Data Sheet 8).

In previous works we have analysed the relations between the main regulatory proteins involved in the modulation of the expression of the HH103 *nod* regulon. In the presence of genistein, NodD1 induces the expression of TtsI (and consequently that of the T3SS) and SyrM (López-Baena et al., 2008; Pérez-Montaño et al., 2016) through its binding to NB18 and NB19 respectively. SyrM, in turn, activates the expression of *nodD2*, presumably due to its biding to a well-conserved SyrM box located upstream of this gene (Acosta-Jurado et al., 2020). As we show in this work, NodD2 represses the expression of many genes belonging to the *nod* regulon, presumably due to its previously demonstrated repressor effect on *nodD1* expression (MaChado et al., 1998). The nature of this repression (transcriptional or post-transcriptional) remains to be determined. Finally, NolR represses a high number of genes of the *nod* regulon, both because of its repressor effect on *nodD1* but also due to the presence of NolR boxes within the promoters of many of the genes of this regulon (Vinardell et al., 2004b; Acosta-Jurado et al., 2019, Supplementary Data Sheet 4), including *syrM* and *ttsI*. In this work we have further investigated these relations by integrating RNA-seq data of individual mutants for each of these regulators with *q*PCR analyses and β-galactosidase assays of individual mutants of these genes targeted with the *lacZ* gene (Table 3, Figure 3). In general, our data support all these previous observations, although we have also found new relations between some of these regulators previously not reported. The *nodD1* gene is repressed by NolR and NodD2, and it shows autorepression. Repression by NolR might be due to a well conserved NolR box located upstream of *nodD1* (Vinardell et al., 2004b), although this regulatory motif is inversely orientated with respect to *nodD1*. The presence of an inversely orientated NB upstream of *nodD1* might account for its auto-repression in the presence of genistein, as scored by *q*PCR and RNAseq analysis. The fact that the expression of the *nodD1*::*lacZ*Δp-Gm^R fusion in the single mutant was not influenced by the presence of genistein (Figure 3) might be due to the absence of a functional NodD1 protein in that mutant. The expression of *nodD2* is clearly dependent on NodD1 and enhanced by SyrM, coherently with the presence of a NB upstream of *syrM* and that of a SyrM box in the promoter region of *nodD2*.The repressor effect of NolR on *nodD2* expression might be the result of the repression of the expression of both *nodD1* and *syrM* by NolR. Regarding *nolR*, our β-galactosidase assays indicate that none of the other regulator proteins analysed in this work influence its expression. However, *nolR* shows a clear autorepression, that might be caused by the presence of a NolR box in its upstream region, although this motif is inversely orientated with regard to *nolR* (Vinardell et al., 2004b). In addition, both *q*PCR and RNA-seq analyses suggest a possible positive effect of SyrM in the level of *nolR* transcripts. This fact suggests that SyrM might have a positive effect on *nolR* expression at the posttranscriptional level, although further research would be needed to clarify this issue. In the case of the *syrM* gene, all our results corroborate previous findings that is transcription is dependent on NodD1 through a well-conserved NB (Pérez-Montaño et al., 2016), but also indicates that *syrM* expression is repressed by itself, NodD2, NolR, and surprisingly, by TtsI. The repressor effect of NolR could be due to the presence of a NolR box in the upstream region of *syrM*, and that of NodD2 might be the result of the repressor effect of this protein on *nodD1* expression. However, at present, we do not have clues about how SyrM or TtsI influence *syrM* expression. Finally, the positive and negative effects of NodD1 and NolR on *ttsI* expression can be justified by the presence of a NB and a NolR box in the upstream region of this gene. In addition, *ttsI* is repressed by NodD2and SyrM, but also by itself. Again, the negative effect of NodD2 might be due to its repressor activity on *nodD1*. At this moment, we do not know how SyrM and TtsI repress the expression of *ttsI*. In any case, our data indicate that *ttsI* and *syrM* seems to negatively regulate each other. Also, to our knowledge, this is the first time that TtsI is described as a repressor, in this case of *syrM* and itself., but also of other genes belonging to the *nod* regulon and, to our knowledge, non-related to the T3SS, such as SFHH103_01317 and SFHH103_02323. These results open the possibility that TtsI might act as a regulator not only of the T3SS but also of other processes that remains to be elucidated. Figure 5 shows the regulatory motifs located in the upstream regions of the five regulatory genes analysed in this work and summarizes the relations we found among those five regulators. This regulatory scheme might be even more complex since there is at least another

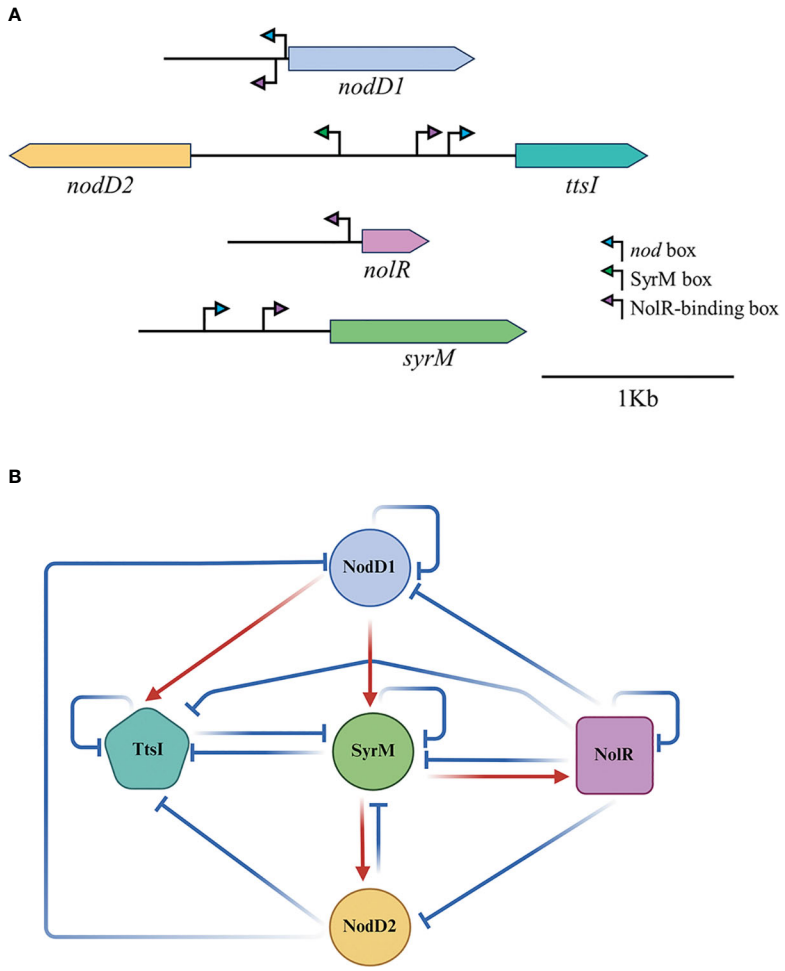

FIGURE 5
Regulatory relationships between NodD1, NodD2, NolR, SyrM and TtsI in HH103. **(A)** Regulatory motifs present in the upstream regions of the coding genes of these regulators. **(B)** A schematic model indicating the relations of induction (red arrows) or repression (blue lines) in the presence of genistein among the different HH103 symbiotic regulators analysed in this work (NodD1, NodD2, NolR, SyrM, and TtsI). This model does not distinguish the type of interaction (transcriptional or posttranscriptional). It only represents how a specific regulator modulates (positively or negatively) the level of expression of the genes coding for the other regulators.

regulator showing a clear influence in the HH103 *nod* regulon, MucR1 (Acosta-Jurado et al., 2016b), that has not been studied in this work.

Previous works of our group showed that inactivation of different regulatory genes extended the host-range of HH103 to *L. japonicus* and *P. vulgaris*, two legumes in which the wild-type strain is unable to nodulate effectively (Acosta-Jurado et al., 2019; Acosta-Jurado et al., 2020; Jiménez-Guerrero et al., 2020; Fuentes-Romero et al., 2022). In the specific case of *L. japonicus*, the gaining of effective nodulation can be achieved either by inactivation of *ttsI*, which avoids T3SS assembly and T3Es delivery, or that of *nodD2*, *nolR*, or *syrM*, which leads to an overproduction of NFs. The symbiotic performance of mutants in any of the three latter genes was better than that of the *ttsI* mutant (Acosta-Jurado et al., 2019; Acosta-Jurado et al., 2020; Jiménez-Guerrero et al., 2020). In this work we have investigated whether the different combination of two mutations among the four mentioned regulatory genes might affect the symbiotic performance with *L. japonicus* in comparison with the single mutants (Figure 4 and Supplementary Figure S1). All the double mutants tested in this work retained the ability to induce the formation of nitrogen-fixing (pink) nodules, as confirmed by ARA. In the case of the three double mutants harbouring an inactivated copy of *ttsI*, all of them showed worse symbiotic performances (values of PTFW and ARA) than the corresponding single mutants in either *nodD2*, *nolR*, or *syrM*, and similar to that of the *ttsI* single mutant (with the only exception of the double mutant *ttsI nolR*, which gives intermediate values of PTFW and ARA with regard to the single *nolR* and *ttsI* mutants). These results suggest that the gaining of infection ability caused by the absence of a functional T3SS predominates over the effect of the *nodD2*, *nolR* and *syrM* mutations, which most probably is the overproduction of NFs. One possibility to explain this fact would be that the *ttsI* mutation might negatively affect bacterial fitness. However, at least in laboratory conditions, bacterial growth is not affected when the *ttsI* gene is inactivated (López-Baena et al., 2008). However, we have recently found that bacterial motility is negatively affected in the absence of the T3SS (Alías-Villegas et al., 2022), so we may speculate that the T3SS mutant could be affected in root colonization. Alternatively,

since T3Es may act suppressing plant immune responses (Jiménez-Guerrero et al., 2022), we cannot exclude the possibility that some T3E might be required along with increased NF production for a better symbiotic performance with *L. japonicus*.

Regarding the combinations of double mutants among the three genes whose inactivation led to overproduction of NFs (*nolD2*, *nolR*, *syrM*), only the double mutant *nolR syrM* exhibited a similar performance to that of the corresponding single mutants. In the rest of the cases, plants inoculated with the double mutants exhibited PTFW and ARA values that were smaller than those of the plants inoculated with the corresponding single mutants. We have also compared the production of NFs by HH103 single and double mutants in the *nodD2*, *nolR* and *syrM* genes. As shown in Supplementary Data Sheet 8 and Table 4, overproduction of NFs was more evident in the single than in the double mutants, and this fact was also true for the only double mutant, *nolR syrM*, whose symbiotic performance was similar to that of the corresponding single mutants.

NF recognition is a key event for the establishment of the symbiosis (Radutoiu et al., 2007; Broghammer et al., 2012; Ghantasala and Choudhury, 2022). As discussed in a previous work (Acosta-Jurado et al., 2019), NFs produced by HH103 and the *Lotus* symbiont *Mesorhizobium loti* R7A are structurally related. Both set of NFs predominantly harbour C16 and C18 saturated or monounsaturated acyl groups and a fucosyl moiety linked to the N-acetyl-glucosamine residue located in the reducing end (Bek et al., 2010; Margaret et al., 2011). However, there are also differences: the presence of carbamoyl substitutions and 4-O-acetyl (or 3-O-acetyl) in *M. loti* NFs and that of 2-O-methyl substitutions in the fucosyl residues of HH103 NFs. The different HH103 single and double mutants in the *nodD2*, *nolR* and *syrM* genes share a set of common NFs that are either overproduced with regard to HH103 or absent in the parental strain (Table 5). HH103 is able to induce the formation of white nodules but unable to infect *L. japonicus* roots (Acosta-Jurado et al., 2016a), so the set and amounts of NF produced by this strain are able to trigger nodule organogenesis but not bacterial infection. Our current hypothesis is that some of the NFs overproduced or exclusively produced by the *nodD2*, *nolR* and *syrM* single and double mutants might be essential for triggering the infection of *L. japonicus* roots by *S. fredii* HH103. However, the inactivation of either *nodD2*, *nolR*, and *syrM*, affects the expression not only of genes related to NFs production, but also that of hundreds of other genes. Thus, these regulatory genes affect the production of other bacterial molecular signals such as the repression of the symbiotic T3SSs in the case of *nodD2* and *nolR* or that of EPS in the case of *syrM* (Acosta-Jurado et al., 2016c). Thus, the combination of two mutations among these three regulatory genes might affect differentially the expression of certain genes related with other traits relevant for symbiosis, such as a better capacity of infection or nitrogen-fixation ability, which would explain the observed differences in symbiotic performance among the *nodD2*, *nolR*, and *syrM* different single and double mutants. However, we cannot rule out the possibility that some of the NFs exclusively overproduced by the single mutants, such as some NFs harbouring fucosyl residues instead of methyl-fucosyl moieties (Table 5), might be responsible for the better symbiotic performance of these mutants when compared to the double mutants. Clearly, more research is required to clarify this issue.

Data availability statement

The datasets presented in this study can be found in online repositories. The names of the repository/repositories and accession number(s) can be found in the article/Supplementary Material.

Author contributions

PN-G: Writing – original draft, Conceptualization, Investigation, Methodology, Formal analysis. FF-R: Writing – original draft, Investigation, Methodology, Formal analysis. FM: Investigation, Methodology, Formal analysis, Writing – original draft, Writing – review & editing. IJ-G: Writing – original draft, Investigation, Methodology. CA-V: Writing – original draft, Investigation, Methodology. PA-G: Writing – original draft, Investigation, Methodology. AA: Writing – original draft, Investigation, Methodology. CM: Writing – original draft, Investigation, Methodology. FO: Investigation, Methodology, Writing – review & editing. MR-C: Writing – original draft, Investigation, Methodology. JR-S: Writing – original draft, Conceptualization. FL-B: Funding acquisition, Project administration, Writing – review & editing. JV: Conceptualization, Investigation, Methodology, Formal analysis, Funding acquisition, project administration, Supervision, Visualization, writing – original draft, Writing – review & editing. SJ: Conceptualization, Investigation, Methodology, Formal analysis, Supervision, Visualization, Writing – original draft, Writing – review & editing.

Funding

The author(s) declare financial support was received for the research, authorship, and/or publication of this article. This work was supported by grant PID2019-107634RB-I00 funded by MCIN/AEI/10.13039/501100011033. PN-G was recipient of a Ph.D. grant from the VPPI of the University of Seville. FF-R is recipient of a Ph.D. grant from the "Consejería de Transformación Económica, Industria, Conocimiento y Universidades" of the Andalusian Government.

Acknowledgments

We thank the Biology and Mass Spectrometry Research Services of the "Centro de Investigación, Tecnología e Innovación" (CITIUS) of the University of Seville.

Conflict of interest

The authors declare that the research was conducted in the absence of any commercial or financial relationships that could be construed as a potential conflict of interest.

Publisher's note

All claims expressed in this article are solely those of the authors and do not necessarily represent those of their affiliated organizations, or those of the publisher, the editors and the reviewers. Any product that may be evaluated in this article, or claim that may be made by its manufacturer, is not guaranteed or endorsed by the publisher.

Supplementary material

The Supplementary Material for this article can be found online at: https://www.frontiersin.org/articles/10.3389/fpls.2023.1322435/full#supplementary-material

References

Acosta-Jurado, S., Alias-Villegas, C., Navarro-Gómez, P., Almozara, A., Rodríguez-Carvajal, M. A., Medina, C., et al. (2020). *Sinorhizobium fredii* HH103 *syrM* inactivation affects the expression of a large number of genes, impairs nodulation with soybean and extends the host-range to Lotus japonicus. *Environ. Microbiol.* 22, 1104–1124. doi: 10.1111/1462-2920.14897

Acosta-Jurado, S., Alías-Villegas, C., Navarro-Gómez, P., Zehner, S., Murdoch, P. D., Rodríguez-Carvajal, M. A., et al. (2016b). The *Sinorhizobium fredii* HH103 MucR1 global regulator is connected with the *nod* regulon and is required for efficient symbiosis With *Lotus burttii* and *Glycine max* cv. Williams. *Mol. Plant Microbe Interact.* 29, 700–712. doi: 10.1094/MPMI-06-16-0116-R

Acosta-Jurado, S., Fuentes-Romero, F., Ruiz-Sainz, J. E., Janczarek, M., and Vinardell, J. M. (2021). Rhizobial exopolysaccharides: Genetic regulation of their synthesis and relevance in symbiosis with legumes. *Int. J. Mol. Sci.* 22, 6233. doi: 10.3390/ijms22126233

Acosta-Jurado, S., Navarro-Gómez, P., Murdoch, P., del, S., Crespo-Rivas, J. C., Jie., S., et al. (2016c). Exopolysaccharide production by *Sinorhizobium fredii* HH103 is repressed by genistein in a NodD1-dependent manner. *PloS One* 11, e0160499. doi: 10.1371/journal.pone.0160499

Acosta-Jurado, S., Rodríguez-Navarro, D. N., Kawaharada, Y., Perea, J. F., Gil-Serrano, A., Jin, H., et al. (2016a). *Sinorhizobium fredii* HH103 invades *Lotus burttii* by crack entry in a Nod factor-and surface polysaccharide-dependent manner. *Mol. Plant Microbe Interact.* 29, 925–937. doi: 10.1094/MPMI-09-16-0195-R

Acosta-Jurado, S., Rodríguez-Navarro, D. N., Kawaharada, Y., Rodríguez-Carvajal, M. A., Gil-Serrano, A., Soria-Díaz, M. E., et al. (2019). *Sinorhizobium fredii* HH103 *nolR* and *nodD2* mutants gain capacity for infection thread invasion of *Lotus japonicus* Gifu and *Lotus burttii*. *Environ. Microbiol.* 21, 1718–1739. doi: 10.1111/1462-2920.14584

Alías-Villegas, C., Fuentes-Romero, F., Cuéllar, V., Navarro-Gómez, P., Soto, M. J., Vinardell, J. M., et al. (2022). Surface motility regulation of *Sinorhizobium fredii* HH103 by plant flavonoids and the NodD1, TtsI, NolR, and MucR1 symbiotic bacterial regulators. *Int. J. Mol. Sci.* 23, 7698. doi: 10.3390/ijms23147698

Anders, S., and Huber, W. (2010). Differential expression analysis for sequence count data. *Genome Biol.* 11, R106. doi: 10.1038/npre.2010.4282.2

Anders, S., Pyl, P. T., and Huber, W. (2015). HTSeq–a Python framework to work with high-throughput sequencing data. *Bioinformatics* 31, 166–169. doi: 10.1093/bioinformatics/btu638

Barnett, M. J., and Long, S. R. (2015). The *Sinorhizobium meliloti* SyrM regulon: Effects on global gene expression are mediated by *syrA* and *nodD3*. *J. Bacteriol.* 197, 1792–1806. doi: 10.1128/JB.02626-14

Becker, A., Schmidt, M., Jager, W., and Puhler, A. (1995). New gentamicin-resistance and *lacZ* promoter-probe cassettes suitable for insertion mutagenesis and generation of transcriptional fusions. *Gene* 162, 37–39. doi: 10.1016/0378-1119(95)00313-u

Bek, A. S., Sauer, J., Thygesen, M. B., Duus, J.Ø., Petersen, B. O., Thirup, S., et al. (2010). Improved characterization of Nod factors and genetically based variation in LysM receptor domains identify amino acids expendable for Nod factor recognition in Lotus spp. *Mol. Plant Microbe Interact.* 23, 58–66. doi: 10.1094/MPMI-23-1-0058

Beringer, J. E. (1974). R factor transfer in *Rhizobium leguminosarum*. *J. Gen. Microbiol.* 84, 188–198. doi: 10.1099/00221287-84-1-188

Broghammer, A., Krusell, L., Blaise, M., Sauer, J., Sullivan, J. T., Maolanon, N., et al. (2012). Legume receptors perceive the rhizobial lipochitin oligosaccharide signal molecules by direct binding. *Proc. Natl. Acad. Sci. U.S.A.* 109, 13859–13864. doi: 10.1073/pnas.1205171109

Buendía-Clavería, A. M., Ruiz-Sainz, J. E., Cubo-Sánchez, T., and Pérez-Silva, J. (1986). Studies of symbiotic plasmids in *Rhizobium trifolii* and fast-growing bacteria that nodulate soybeans. *J. Appl. Bacteriol.* 61, 1–9. doi: 10.1111/j.1365-2672.1986.tb03752.x

Downie, J. A. (2010). The roles of extracellular proteins, polysaccharides, and signals in the interactions of rhizobia with legume roots. *FEMS Microbiol. Rev.* 34, 150–170. doi: 10.1111/j.1574-6976.2009.00205.x

Figurski, D. H., and Helinski, D. R. (1979). Replication of an origin-containing derivative of plasmid RK2 dependent on a plasmid function provided in *trans*. *Proc. Natl. Acad. Sci. U.S.A.* 76, 1648–1652. doi: 10.1073/pnas.76.4.1648

Fuentes-Romero, F., Navarro-Gómez, P., Ayala-García, P., Moyano-Bravo, I., López-Baena, F. J., Pérez-Montaño, F., et al. (2022). The *nodD1* gene of *Sinorhizobium fredii* HH103 restores nodulation capacity on bean in a *Rhizobium tropici* CIAT 899 *nodD1*/*nodD2* mutant, but the secondary symbiotic regulators *nolR*, *nodD2* or *syrM* prevent HH103 to nodulate with this legume. *Microorganisms* 10, 139. doi: 10.3390/microorganisms10010139

Ghantasala, S., and Choudhury, S. R. (2022). Nod factor perception: an integrative view of molecular communication during legume symbiosis. *Plant Mol. Biol.* 110, 485–509. doi: 10.1007/s11103-022-01307-3

Jhu, M. Y., and Oldroyd, G. E. D. (2023). Dancing to a different tune, can we switch from chemical to biological nitrogen fixation for sustainable food security? *PloS Biol.* 21, e3001982. doi: 10.1371/journal.pbio.3001982

Jiménez-Guerrero, I., Acosta-Jurado, S., del Cerro, P., Navarro-Gómez, P., López-Baena, F. J., Ollero, F. J., et al. (2018). Transcriptomic studies of the effect of *nod* gene-inducing molecules in rhizobia: Different weapons, one purpose. *Genes (Basel)* 9, 1. doi: 10.3390/genes9010001

Jiménez-Guerrero, I., Acosta-Jurado, S., Medina, C., Ollero, F. J., Alias-Villegas, C., Vinardell, J. M., et al. (2020). The *Sinorhizobium fredii* HH103 type III secretion system effector NopC blocks nodulation with *Lotus japonicus* Gifu. *J. Exp. Bot.* 71, 6043–6056. doi: 10.1093/jxb/eraa297

Jiménez-Guerrero, I., Medina, C., Vinardell, J. M., Ollero, F. J., and López-Baena, F. J. (2022). The rhizobial Type 3 secretion system: The Dr. Jekyll and Mr. Hyde in the rhizobium-legume symbiosis. *Int. J. Mol. Sci.* 23, 11089. doi: 10.3390/ijms231911089

Kovach, M. E., Elzer, P. H., Hill, D. S., Robertson, G. T., Farris, M. A., Roop, R. M. 2nd, et al. (1995). Four new derivatives of the broad-host-range cloning vector pBBR1MCS, carrying different antibiotic-resistance cassettes. *Gene* 166, 175–176. doi: 10.1016/0378-1119(95)00584-1

Lamrabet, Y., Ramón, A. B., Cubo, T., Espuny, R., Gil, A., and Krishnan, H. B. (1999). Mutation in GDP-fucose synthesis genes of *Sinorhizobium fredii* alters Nod Factors and significantly decreases competitiveness to nodulate soybeans. *Mol. Plat Microbe Interact.* 12, 207–217. doi: 10.1094/MPMI.1999.12.3.207

López-Baena, F. J., Ruiz-Sainz, J. E., Rodríguez-Carvajal, M. A., and Vinardell, J. M. (2016). Bacterial molecular signals in the *Sinorhizobium fredii*-soybean symbiosis. *Int. J. Mol. Sci.* 17, 755. doi: 10.3390/ijms17050755

López-Baena, F. J., Vinardell, J. M., Pérez-Montaño, F., Crespo-Rivas, J. C., Bellogín, R. A., Espuny, M. D. R., et al. (2008). Regulation and symbiotic significance of nodulation outer proteins secretion in *Sinorhizobium fredii* HH103. *Microbiol. (Reading)* 154, 1825–1836. doi: 10.1099/mic.0.2007/016337-0

MaChado, D., Pueppke, S. G., Vinardell, J. M., Ruiz-Sainz, J. E., and Krishnan, H. B. (1998). Expression of *nodD1* and *nodD2* in *Sinorhizobium fredii*, a nitrogen-fixing symbiont of soybean and other legumes. *Mol. Plant-Microbe Interact.* 11, 375–382. doi: 10.1094/MPMI.1998.11.5.375

Madinabeitia, N., Bellogín, R. A., Buendía-Clavería, A. M., Camacho, M., Cubo, T., Espuny, M. R., et al. (2002). *Sinorhizobium fredii* HH103 has a truncated *nolO* gene due to a -1 frameshift mutation that is conserved among other geographically distant *S. fredii* strains. *Mol. Plant Microbe Interact.* 15, 150–159. doi: 10.1094/MPMI.2002.15.2.150

Margaret, I., Becker, A., Blom, J., Bonilla, I., Goesmann, A., Göttfert, M., et al. (2011). Symbiotic properties and first analyses of the genomic sequence of the fast growing model strain *Sinorhizobium fredii* HH103 nodulating soybean. *J. Biotechnol.* 155, 11–19. doi: 10.1016/j.jbiotec.2011.03.016

Pantigoso, H. A., Newberger, D., and Vivanco, J. M. (2022). The rhizosphere microbiome: Plant-microbial interactions for resource acquisition. *J. Appl. Microbiol.* 133, 2864–2876. doi: 10.1111/jam.15686

Peck, M. C., Fisher, R. F., Bliss, R., and Long, S. R. (2013). Isolation and characterization of mutant *Sinorhizobium meliloti* NodD1 proteins with altered responses to luteolin. *J. Bacteriol.* 195, 3714–3723. doi: 10.1128/JB.00309-13

Pérez-Montaño, F., Jiménez-Guerrero, I., Acosta-Jurado, S., Navarro-Gómez, P., Ollero, F. J., Ruiz-Sainz, J. E., et al. (2016). A transcriptomic analysis of the effect of genistein on *Sinorhizobium fredii* HH103 reveals novel rhizobial genes putatively involved in symbiosis. *Sci. Rep.* 6, 31592. doi: 10.1038/srep31592

Pfaffl, M. W., Horgan, G. W., and Dempfle, L. (2002). Relative expression software tool (REST) for group-wise comparison and statistical analysis of relative expression results in real-time PCR. *Nucleic Acids Res.* 30, e36. doi: 10.1093/nar/30.9.e36

Poole, P., Ramachandran, V., and Terpolilli, J. (2018). Rhizobia: From saprophytes to endosymbionts. *Nat. Rev. Microbiol.* 16, 291–303. doi: 10.1038/nrmicro.2017.171

Prentki, P., and Krisch, H. M. (1984). *In vitro* insertional mutagenesis with a selectable DNA fragment. *Gene* 29, 303–313. doi: 10.1016/0378-1119(84)90059-3

Radutoiu, S., Madsen, L. H., Madsen, E. B., Jurkiewicz, A., Fukai, E., Quistgaard, E. M., et al. (2007). LysM domains mediate lipochitin-oligosaccharide recognition and Nfr genes extend the symbiotic host range. *EMBO J.* 26, 3923–3935. doi: 10.1038/sj.emboj.7601826

Rigaud, J., and Puppo, A. (1975). Indol-3-acetic catabolism by soybean bacteroids. *J. Gen. Microbiol.* 88, 223–228. doi: 10.1099/00221287-88-2-223

Robinson, M. D., McCarthy, D. J., and Smyth, G. K. (2010). edgeR: a Bioconductor package for differential expression analysis of digital gene expression data. *Bioinformatics* 26, 139–140. doi: 10.1093/bioinformatics/btp616

Roy, S., Liu, W., Nandety, R. S., Crook, A., Mysore, K. S., Pislariu, C. I., et al. (2020). Celebrating 20 years of genetic discoveries in legume nodulation and symbiotic nitrogen fixation. *Plant Cell.* 32, 15–41. doi: 10.1105/tpc.19.00279

Sambrook, J., and Russell, D. W. (2001). *Molecular cloning: A laboratory manual. 3rd Edition* Vol. 1 (New York: Cold Spring Harbor Laboratory Press).

Schäfer, A., Tauch, A., Jager, W., Kalinowski, J., Thierbach, G., and Puhler, A. (1994). Small mobilizable multi-purpose cloning vectors derived from the *Escherichia coli* plasmids pK18 and pK19: selection of defined deletions in the chromosome of *Corynebacterium glutamicum*. *Gene* 145, 69–73. doi: 10.1016/0378-1119(94)90324-7

Shimamura, M., Kumaki, T., Hashimoto, S., Saeki, K., Ayabe, S. I., Higashitani, A., et al. (2022). Phenolic acids induce nod factor production in *Lotus japonicus-Mesorhizobium* symbiosis. *Microbes Environ.* 37, ME21094. doi: 10.1264/jsme2.ME21094

Simon, R. (1984). High frequency mobilization of gram-negative bacterial replicons by the in *vivo* constructed Tn*5*-Mob transposon. *Mol. Gen. Genet.* 196, 413–4200. doi: 10.1007/BF00436188

Sobe, R. C., Gilbert, C., Vo, L., Alexandre, G., and Scharf, B. E. (2022). FliL and its paralog MotF have distinct roles in the stator activity of the *Sinorhizobium meliloti* flagellar motor. *Mol. Microbiol.* 118, 223–243. doi: 10.1111/mmi.14964

Teulet, A., Camuel, A., Perret, X., and Giraud, E. (2022). The versatile roles of type III secretion systems in rhizobium-legume symbioses. *Annu. Rev. Microbiol.* 76, 45–65. doi: 10.1146/annurev-micro-041020-032624

Trapnell, C., Williams, B. A., Pertea, G., Mortazavi, A., Kwan, G., van Baren, M. J., et al. (2010). Transcript assembly and quantification by RNA-Seq reveals unannotated transcripts and isoform switching during cell differentiation. *Nat. Biotechnol.* 28, 511–515. doi: 10.1038/nbt.1621

Vinardell, J. M., Acosta-Jurado, S., Zehner, S., Göttfert, M., Becker, A., Baena, I., et al. (2015). The *Sinorhizobium fredii* HH103 genome: A comparative analysis with *S. fredii* strains differing in their symbiotic behavior with soybean. *Mol. Plant Microbe Interact.* 28, 811–824. doi: 10.1094/MPMI-12-14-0397-FI

Vinardell, J. M., López-Baena, F. J., Hidalgo, A., Ollero, F. J., Bellogín, R. A., Espuny, M. R., et al. (2004a). The effect of FITA mutations on the symbiotic properties of *Sinorhizobium fredii* varies in a chromosomal-background-dependent manner. *Arch. Microbiol.* 181, 144–154. doi: 10.1007/s00203-003-0635-3

Vinardell, J. M., Ollero, F. J., Hidalgo, A., López-Baena, F. J., Medina, C., Ivanok, K., et al. (2004b). NolR regulates diverse symbiotic signals of *Sinorhizobium fredii* HH103. *Mol. Plant Microbe Interact.* 17, 676–685. doi: 10.1094/MPMI.2004.17.6.676

Vincent, J. M. (1970). "The modified Fåhraeus slide technique," in *A manual for the practical study of root nodule bacteria*, vol. 1970 . Ed. J. M. Vincent (Oxford, UK: Blackwell Scientific Publications), 144–145.

Yang, J., Lan, L., Jin, Y., Yu, N., Wang, D., and Wang, E. (2022). Mechanisms underlying legume-rhizobium symbioses. *J. Integr. Plant Biol.* 64, 244–267. doi: 10.1111/jipb.13207

frontiers | Frontiers in Plant Science

TYPE Original Research
PUBLISHED 04 January 2024
DOI 10.3389/fpls.2023.1306491

OPEN ACCESS

EDITED BY
Chang Fu Tian,
China Agricultural University, China

REVIEWED BY
Igor Kryvoruchko,
United Arab Emirates University,
United Arab Emirates
Teodoro Coba De La Peña,
Catholic University of the North, Chile

*CORRESPONDENCE
Rebecca Dickstein
beccad@unt.edu

†These authors have contributed equally to this work and share senior authorship

RECEIVED 03 October 2023
ACCEPTED 28 November 2023
PUBLISHED 04 January 2024

CITATION
Cai J, Longo A and Dickstein R (2024) Expression and mutagenesis studies in the *Medicago truncatula* iron transporter MtVTL8 confirm its role in symbiotic nitrogen fixation and reveal amino acids essential for transport.
Front. Plant Sci. 14:1306491.
doi: 10.3389/fpls.2023.1306491

Expression and mutagenesis studies in the *Medicago truncatula* iron transporter MtVTL8 confirm its role in symbiotic nitrogen fixation and reveal amino acids essential for transport

Jingya Cai, Antonella Longo† and Rebecca Dickstein*†

Department of Biological Sciences and BioDiscovery Institute, University of North Texas, Denton, TX, United States

The model legume *Medicago truncatula* establishes a symbiosis with soil bacteria (rhizobia) that carry out symbiotic nitrogen fixation (SNF) in plant root nodules. SNF requires the exchange of nutrients between the plant and rhizobia in the nodule that occurs across a plant-derived symbiosome membrane. One iron transporter, belonging to the Vacuolar iron Transporter-Like (VTL) family, MtVTL8, has been identified as essential for bacteria survival and therefore SNF. In this work we investigated the spatial expression of *MtVTL8* in nodules and addressed whether it could be functionally interchangeable with a similar nodule-expressed iron transporter, MtVTL4. Using a structural model for MtVTL8 and the previously hypothesized mechanism for iron transport in a phylogenetically-related Vacuolar Iron Transporter (VIT), EgVIT1 with known crystal structure, we identified critical amino acids and obtained their mutants. Mutants were tested *in planta* for complementation of an SNF defective line and in an iron sensitive mutant yeast strain. An extended phylogenetic assessment of VTLs and VITs showed that amino acids critical for function are conserved differently in VTLs vs. VITs. Our studies showed that some amino acids are essential for iron transport leading us to suggest a model for MtVTL8 function, one that is different for other iron transporters (VITs) studied so far. This study extends the understanding of iron transport mechanisms in VTLs as well as those used in SNF.

KEYWORDS

***Medicago truncatula*, symbiotic nitrogen fixation, iron transporter, site-directed mutagenesis, protein models, transporter function**

Abbreviations: *At*, *Arabidopsis thaliana*; CCC1, Cross-complements Ca^{2+} phenotype of csg1; *Eg*, *Eucaliptus grandis*; *Mt*, *Medicago truncatula*; SNF, symbiotic nitrogen fixation; VIT, Vacuolar iron transporter; VTL, Vacuolar iron transporter-like.

Introduction

Symbiotic nitrogen fixation (SNF) in legumes uses energy derived from photosynthesis to reduce N_2 gas to ammonia at normal temperature and pressure, and is thus, especially important for sustainable food production. Legumes form a symbiosis with bacteria called rhizobia, which are hosted in specialized root organs called nodules (Hirsch et al., 1992; Oldroyd et al., 2011). These form after a series of interactions between the legume root cells and rhizobia which results in the reprogramming and division of plant cortical cells to form nodule primordia. These primordial cells are colonized by rhizobia in infection threads that deliver the rhizobia to the cells (Oldroyd, 2013; Roy et al., 2020). Rhizobia enter the plant cells in a process resembling endocytosis in which rhizobia are surrounded by a plant-derived symbiosome membrane (SM), through which all plant-microbe nutrient exchange occurs (Udvardi and Poole, 2013). The internalized rhizobia surrounded by the SM and the symbiosome space form symbiosomes, novel organelle-like structures. Rhizobia within symbiosomes, now called bacteroids, grow and divide until tens of thousands fill the infected cells, which increase in ploidy depending on the legume species (Maróti and Kondorosi, 2014). The outer cells of nodules form a gas diffusion barrier resulting in a hypoxic nodule interior (Witty et al., 1987) protecting the rhizobially-encoded oxygen-labile nitrogenase enzyme. Paradoxically, high rates of respiration in nodules are required by rhizobia as well as plant mitochondria during SNF. Respiration is supported by the rapid binding and delivery of oxygen by leghemoglobin, lowering oxygen concentrations further in the nodule interior (Appleby, 1984; Ott et al., 2005).

Many legumes, like the model plant *Lotus japonicus* and soybean, form round, determinate nodules that only have a transient meristem. Others, like the model *Medicago truncatula* and pea, form oblong, indeterminate nodules with a persistent meristem. Both nodule types have a central zone of rhizobia infected cells interspersed with uninfected cells (Hirsch, 1992). Indeterminate nodules contain cells in a developmental gradient classified into zones. Zone I (ZI) is the meristem; zone II (ZII) is the invasion zone where rhizobia enter plant cells, divide and differentiate; the interzone (IZ) is where final maturation occurs; and zone III (ZIII) is where SNF takes place. Older nodules also have a senescent zone, zone IV (IV), which likely is involved in nutrient recycling (Vasse et al., 1990). Each zone has characteristic gene expression (Limpens et al., 2013; Roux et al., 2014).

The transition metal iron is a key essential nutrient required for SNF (Clarke et al., 2014; González-Guerrero et al., 2014; Day and Smith, 2021; González-Guerrero et al., 2023) and it accumulates to higher concentrations in nodules than other plant organs (Burton et al., 1998). Low iron levels can hinder SNF in nodules (O'Hara et al., 1988; Tang et al., 1992; Johnston et al., 2001). Iron is a cofactor of multiple metallo-enzymes directly or indirectly implicated in SNF in different stages of the symbiosis process. Rhizobial catalase, containing a catalytic heme iron, has been implicated as having a crucial role early in bacterial infection of nodule primordia (Jamet et al., 2003). Later in nodule development, heme iron is required by rhizobia to sense declining O_2 levels (Gilles-Gonzalez et al., 1991), signaling the rhizobia to develop into SNF-capable forms. As rhizobia mature to be able to fix nitrogen, they express nitrogenase comprising the iron-sulfur cluster containing NifH and the iron-molybdenum cofactor-containing NifDK (Hoffman et al., 2014; Einsle and Rees, 2020). Proteins essential for shuttling reducing equivalents to nitrogenase, e.g. FixABCX, contain iron cofactors (Ledbetter et al., 2017). Rhizobial proteins essential for respiration contain iron, either as heme iron (Preisig et al., 1996) or as iron-sulfur clusters. In the plant cell cytosol, leghemoglobin containing heme iron, is abundant, buffering and transporting oxygen to the respiring rhizobia and mitochondria (Appleby, 1984; Ott et al., 2005).

Evidence suggests that iron reaches the nodule via the xylem, chelated to citrate or to nicotianamine, where it is released from the vasculature into the apoplastic space in ZII, the infection and differentiation nodule zone (Rodríguez-Haas et al., 2013). The route from vasculature to infected cells crosses several cell layers, which the iron traverses using symplastic and apoplastic routes (Brear et al., 2013; Rodríguez-Haas et al., 2013; Day and Smith, 2021; González-Guerrero et al., 2023). *M. truncatula* NRAMP1, a member of the Natural Resistance-Associated Macrophage Protein (NRAMP) family, transports iron from the apoplast into the infected cells' cytosol (Tejada-Jiménez et al., 2015), potentially assisted by citrate efflux transporter MtMATE67 (Multidrug And Toxic Compound Extrusion) (Kryvoruchko et al., 2018). MtMATE67 transports citrate in an iron-activated manner and appears to enhance iron uptake into infected cells (Kryvoruchko et al., 2018). Once inside the cytoplasm of nodule cells, the iron needs to cross another membrane, the SM, to reach the internalized rhizobia. In *M. truncatula*, two different transporters have been implicated in the SM transport: MtVTL8 (*M. truncatula* Vacuolar Iron Transporter (VIT)-Like) (Walton et al., 2020; Cai et al., 2022), the subject of this study, and MtFPN2 (*M. truncatula* Ferroportin Protein2) (Escudero et al., 2020). Both MtVTL8 and MtFPN2 are ferrous iron efflux transporters. Plants with mutations in either protein's gene show defects in SNF (Escudero et al., 2020; Walton et al., 2020; Cai et al., 2022).

Rhizobia inside symbiosomes import iron from the symbiosome space. In rhizobia, iron uptake is regulated by the heme-regulated transcription repressor Irr, that represses *rirA*. RirA is a transcriptional activator of iron-uptake genes (O'Brian, 2015; Sankari et al., 2022). The nodule cysteine-rich peptide (NCR) NCR247 is secreted into symbiosomes and taken up by rhizobia in a *bacA*-dependent manner (Marlow et al., 2009; Farkas et al., 2014). NCR247 was recently found to bind to and sequester heme, inducing an iron starvation response in rhizobia, resulting in increased iron import (Sankari et al., 2022). Thus, NCR247 enables rhizobia to be better iron sinks.

MtVTL8 is a member of the Cross-Complements Ca^{2+} phenotype of the csg1/Vacuolar Iron Transporter (CCC1/VIT) family. Both it (encoded by Medtr4094335/MtrunA17Chr4g0050851) and the homolog MtVTL4 (encoded by Medtr4g09325/MtrunA17Chr4g0050811) are expressed in nodules, although their expression profiles are somewhat different temporally and spatially (Roux et al., 2014; Walton et al., 2020; Carrere et al., 2021). MtVTL8 was found to localize on the SM; while MtVTL4

localizes to the plasma membrane and membranes surrounding the infection thread (Walton et al., 2020). Plants with mutations in *MtVTL8* have profound defects in nodule development, while those with mutations in *MtVTL4* have only minor defects (Walton et al., 2020; Cai et al., 2022). The two *Tnt1 mtvtl4* mutants studied were not back-crossed and had similar vegetative growth defects in both low and high nitrogen conditions, with higher numbers of less-developed nodules, suggesting a developmental defect, not a symbiotic defect *per se* (Walton et al., 2020). *MtVTL8* is homologous to *L. japonicus LjSEN1* (Stationary Endosymbiont Nodule 1) and to soybean *GmVTL1a*, which when knocked down or mutated have similar phenotypes to *mtvtl8* mutants (Suganuma et al., 2003; Hakoyama et al., 2012; Brear et al., 2020; Liu et al., 2020). *MtVTL4*, *MtVTL8* and *GmVTL1a* are able to complement the yeast *Saccharomyces cerevisiae Δccc1* (*ScΔccc1*) mutant with a defect in a vacuolar ferrous iron transporter demonstrating their iron efflux activity (Brear et al., 2020; Walton et al., 2020). Two *mtvtl8* mutants are available. The first is *mtvtl8-1* or 13U, in the A17 genotype, having a large deletion on chromosome 4 that deletes both *MtVTL4* and *MtVLT8* (Walton et al., 2020). The second is *mtvtl8-2* derived from *Tnt1* line NF11322 in the R108 background with a homozygous *Tnt1* insertion in the exon of *MtVTL8* (Cai et al., 2022). Both *mtvtl8-1 and mtvtl8-2* form defective Fix^- white nodules with *Sinorhizobium* (*Ensifer*) *meliloti* (hereafter referred to as *S. meliloti*) under limited nitrogen conditions (Walton et al., 2020; Cai et al., 2022).

VIT transporters are predicted to fold into five transmembrane helices (TMH) with a long hydrophilic sequence between TMH2 and TMH3. Similarly, the related VTL transporters contain five TMHs but have a much shorter sequence between TMH2-3. Iron transporters with truncated sequences or VTLs are found among angiosperm plants, both monocots and eudicots (Sorribes-Dauden et al., 2020). Based on phylogenetic analysis of CCC1/VTL sequences, Sorribes-Dauden et al. (2020) proposed a different origin for VITs and VTLs: VITs originated from an ancestral horizontal transfer from bacteria while VTLs were transferred from an archaeal lineage with both transfers dating at the origin of the last common eukaryote ancestor.

The crystal structure of VIT1 from the rose gum *Eucalyptus grandis* was solved (Kato et al., 2019) and is so far the only solved iron transporter structure from the CCC1/VIT family. The structure confirmed the presence of five TMHs, with the N-terminal end located in the cytoplasm and the C-terminal end in the vacuolar space. In the structure, EgVIT1 is a dimer with TMH1 from each monomer at the center and TMH2-5 arranged clockwise around TMH1 to form the transmembrane domain (TMD). A cavity forms between the monomers and in the crystal structure is open toward the cytoplasm. The cytoplasmic TMH2-3 loop folds into three short α-helices, named H1, H2, and H3. Glutamic residues from H1 and H3 in combination with two glutamic acids from the extended cytoplasmic portion of TMH2 bind three metal ions in each monomer. This region was therefore defined as a metal binding domain (MBD). The dimeric interaction is mediated both by the TMD and the MBD. EgVIT1 as well as another member of the CCC1/VIT family, PfVIT, from the human malaria-causing parasite *Plasmodium falciparum*, were shown to be Fe^{2+}/H^+ antiporters with the exchange driven by the proton electrochemical potential (Labarbuta et al., 2017; Kato et al., 2019). Comparing the EgVIT1 structure with the VTL sequences suggests the absence of an MBD in the subfamily (Sorribes-Dauden et al., 2020).

In this work, we investigated the spatial expression of *MtVTL8* in WT and *mtvtl8-2* roots during nodulation. We then explored whether altering *MtVTL4*'s expression using the *MtVTL8 cis* elements would enable it to functionally complement *mtvtl8-2* roots. We used a comparison between the EgVIT1 structure to a structural model of MtVTL8 to identify potentially essential amino acids. We then performed mutagenesis studies to challenge our hypothesis. Our results confirm MtVTL8's unique role as an iron transporter in nodulation and suggest that it may function differently from previously characterized iron transporters. Models for potential mechanisms of transport are presented.

Materials and methods

MtVTL8 structural model

A structural model for MtVTL8 was obtained from the AlphaFold protein structure database (Jumper et al., 2021; Varadi et al., 2022) using MtVTL8's UniProt ID: A0A072UNI3. Structural analysis was limited to residues 40-235 due to the low confidence score for the N-terminal amino acids. Structures were visualized by the PyMOL Molecular Graphics System (Schrödinger, LLC). A dimer was generated within PyMOL by aligning the AlphaFold monomer with chains A and B of EgVIT1, pdb 6IU3 (Kato et al., 2019). Structures were positioned in the lipid membrane using the PPM web server (Lomize et al., 2012).

Primers and plasmids

Primers and plasmids used for this study are listed in Supplementary Tables S1, S2, respectively. Vectors pMU06 and pMU14 were generous gifts of Drs. Wei Liu and Michael Udvardi. pMU06 contains the *pAtUBI-DsRed* marker gene for detection of transformed roots using DsRed fluorescence, a site to insert a promoter upstream of *GUS*, the *GUS* gene, and the *35S 3'* terminator. pMU14 contains the *pAtUBI-DsRed* marker gene, the *35S* promoter, *GFP* and *35S 3'* terminator. All constructs were confirmed by sequencing.

Cloning *MtVTL8* and *MtVTL4* for expression in *M. truncatula*

For *in planta* complementation studies, *MtVTL*s were cloned in the binary vector pMU14 for expression in Medicago as in our previous study of the nitrate transporter MtNPF1.7 (Yu et al., 2021). To express *MtVTL8* with its native controlling elements the *MtVTL8* promoter (2629 bp), *MtVTL8* CDS (708 bp) and *MtVTL8* terminator (1083 bp) were amplified from *M. truncatula* R108 genomic DNA using Q5 High-Fidelity DNA polymerase (New England Biolabs) and primers JYC05-F1/JYC05-R1, JYC05-F2/JYC05-R2, and JYC05-F3/JYC05-R3 respectively. pMU14 was

digested with *Xho*I and *Hin*dIII-HF (New England Biolabs). The digested vector, the *MtVTL8* promoter, CDS, and terminator PCR fragments were assembled with the Gibson assembly method (NEBuilder HiFi DNA Assembly, New England Biolabs) to form pJYC05 (pMU14/p*MtVTL8*-Mt*VTL8-MtVTL8-t*). To obtain the *MtVTL4* gene driven by p*MtVTL8*, *MtVTL4* was amplified with forward primer JYC24F and reverse primer JYC24R from R108 gDNA. It was assembled with the pJYC05-*Spe*I/*Kpn*I fragment with the Gibson assembly method to form pJYC24 (pMU14/p*MtVTL8-MtVTL4-MtVTL8-t*). Plasmids were transformed into electrocompetent *Agrobacterium rhizogenes* MSU440 by electroporation using Gene Pulser Xcell™ electroporation system (Bio-rad, Hercules, CA, USA) (Valimehr et al., 2014).

Construct for p*MtVTL8-GUS* expression

The *GUS* CDS was amplified from the binary vector pMU06 by using primers JYC15-F and JYC15-R. The *GUS* CDS and JYC05-*Spe*I-*Kpn*I were assembled with the Gibson assembly method (NEBuilder HiFi DNA Assembly, New England Biolabs) to form pJYC15 (MU06/p*MtVTL8-GUS*). The construct was introduced into *A. rhizogenes* as above.

GUS staining and nodule sections

Plant roots transformed with p*MtVTL8-GUS* were selected by their red fluorescence, demonstrating presence of the transformed vector with the visible marker, at 0, 5 and 15 dpi. Transformed roots were harvested in 0.1 M PBS (Na_2HPO_4 and NaH_2PO_4, pH 7.0) and then transferred to GUS solution (44.5 mL of 100 mM PBS-Na pH 7.0, 2 mL of 50 mM $K_3Fe(CN)_6$, 2 mL of 50 mM $K_4Fe(CN)_6$, 1 mL of 0.5 M EDTA, 0.5 mL of 10% Triton X-100, 50 mg of X-Gluc salt mixed together) followed by vacuum infiltration for 1.5 h. Roots were kept at 37°C overnight. The samples were subsequently washed with 0.1 M PBS (Na_2HPO_4 and NaH_2PO_4, pH 7.0) at 4° C. Samples were observed under an Olympus BX50 microscope (Olympus, Tokyo, Japan). GUS-stained nodules were cut and fixed with 4% glutaraldehyde (made in 0.1 M PBS-Na, pH 7.0) under vacuum for 30 min. The samples were kept overnight at 4°C with gentle rotation. Then, the samples were washed three times with 0.1 M PBS-Na and dehydrated with a series of ethanol gradients (30%, 50%, 70%, 90%, 100%), each step was carried out with gentle rotation for 30 min at room temperature. The ethanol was replaced with ethanol: Technovit 7100 (Kulzer Technik, Hanau, Germany) (2:1/v:v) and rotated for one hour at room temperature, followed by ethanol: Technovit 7100 (1:2/v:v) for another hour. The liquid was replaced with 100% Technovit 7100 and rotated gently at room temperature overnight. The next day, the liquid was replaced with fresh Technovit 7100 and rotated at room temperature for 1 h. Resin was prepared by mixing Technovit 7100 with hardener II (15:1/v:v). Resin was added to the mold well and the nodule was placed in the resin. The well was covered with parafilm and left at room temperature for 1 h for polymerization. After polymerization, the parafilm was removed and the block was glued to an adaptor using the Technovit 3040 glue (Kulzer Technik, Hanau, Germany). Five micrometer nodule sections were sliced by a microtome (Leica HistoCore Multicut, Leica) and collected on glass slides. The slides were stained with ruthenium red staining solution (200 mg ruthenium red, 200 mL water) for 5 min followed by rinsing with water until the background was clear. The slides were dried on a hotplate and nodule sections were visualized with an Olympus BX50 microscope.

Mutagenesis of *MtVTL8* for expression in *M. truncatula*

Mutants of *MtVTL8* were constructed in pJYC05, replacing the *MtVTL8* cDNA with the mutated gene. Two PCR reactions were carried out resulting in two overlapping fragments, one containing the 5' end of *MtVTL8* to the desired mutation (using primers JYCmut-F and JYC19R2) and the other containing the desired mutation to the 3' end of *MtVTL8* (using primers JYC19F2 and JYCmut-R). The relevant primers for each construct are listed in Supplementary Table S3. Mutated *MtVTL8* fragments were subsequently assembled into pJYC05-*Spe*I/*Kpn*I vector with the Gibson assembly method to form pJYCmut. We obtained the following mutants: MtVTL8_R51A (pJYC16), MtVTL8_D59A (pJYC17), MtVTL8_G88E (pJYC18), MtVTL8_E100A (pJYC19), MtVTL8_E111A (pJYC20), and MtVTL8_K135A (pJYC21). Double mutants MtVTL8_R51E/E100R (pJYC22), and MtVTL8_E111K/K135E (pJYC23) were obtained by the assembly of three PCR fragments with pJYC05-*Spe*I/*Kpn*I vector.

Complementation experiments in *mtvtl8-2* plants

M. truncatula Tnt1 insertion mutant *mtvtl8-2* seeds and control wild type R108 seeds were scarified and germinated as described (Cai et al., 2023). Seedlings of *mtvtl8-2* and R108 were transformed with *A. rhizogenes* MSU440 containing either empty vector (EV) pMU14, pJYC05, or plasmids containing mutated *MtVTL8*. Transformants were transferred to Fåhraeus medium (Fåhraeus, 1957) containing 5 mg/L nystatin (Millipore-Sigma, Burlington, MA USA) for 5 d in growth chamber with 14 h/10 h (light/dark) at 24°C (Boisson-Dernier et al., 2001). Then, the plants were moved to a 1% MS medium (Millipore-Sigma) plate in between two filter papers covering the roots for 14 d in growth chamber with 14 h/10h (light/dark) at 24°C. Transformed roots were selected based on their expression of the DsRed fluorescent marker, contained in the pMU14 vector. This was done using a Leica MZ10F dissecting microscope (Leica, Deer Park, IL, USA). Non-transformed roots were excised. The plants with transgenic roots were transferred to the aeroponic system with Lullien's medium (Lullien et al., 1987) without a nitrogen source at 22°C with a 16 h/8 h light/dark photoperiod at 60 µmol $m^{-2}s^{-1}$ for 5 d (Barker et al., 2006; Cai et al., 2023). Then, the plants were inoculated with *S. meliloti* Rm41 (Kondorosi et al., 1980). Growth of the transformed plants was checked at 15 dpi and nodules were analyzed and documented

using the Leica MZ10F dissecting microscope. Nodules were photographed and their proxy 2-D surface areas were analyzed with Fiji software (Schindelin et al., 2012). For chlorophyll estimation, we followed the control method described (Liang et al., 2017). Briefly, leaves were collected at 28 dpi and frozen in liquid N_2. For extraction, 100 mg of leaves were ground under liquid N_2, 1.0 mL of 80% acetone was added and the mixture gently agitated for 24 h at room temperature, followed by 15,000*g* centrifugation for 5 min at 4°C. 100 µL of supernatant was mixed with 400 µL of 80% acetone. Absorbance of the supernatant was measured at wavelength of 645 nm (A645) and 663 nm (A663) with a Bio-Rad SmartSpec Plus spectrophotometer (Hercules, CA, USA) The total chlorophyll content was calculated following the Arnon's equation (Arnon, 1949): Total chlorophyll (µg/mL) = 20.2 (A645) + 8.02 (A663).

Cloning for yeast expression

The vector pYES2/CT (ThermoFisher Scientific) was digested with HindIII-HF and BamHI-HF (New England Biolabs). The *MtVTL8* gene and its eight different mutant versions were amplified from pJYC16-23 using primers JYC10.FOR and JYC10.REV and assembled with the pYES2/CT-HindIII/BamH1 fragment using the Gibson assembly method to form pJYC10 (*MtVTL8-wt*) and eight different *Mtvtl8-mut* versions (pYJYC16-23).

Fe^{2+} sensitivity in yeast

The *Saccharomyces cerevisiae* wild type strain DY150 and mutant strain Δ*ccc1*(*ura3, leu2, his3, ade2, can1, CCC1::HIS3*) (Li et al., 2001) in the DY150 background were grown in YPD medium at 30°C, 250 rpm for 16 h. Competent cells of DY150 and Δ*ccc1* were produced using the Frozen-EZ Yeast Transformation II kit (Zymo Research). pYES2/CT was transformed into the DY150. The mutant strain Δ*ccc1* was transformed with pYES2/CT, pYES2-*AtVTL1* (At1g21140, wild type), pJYC10 or pYJYC16-23. Single colonies, each with a specific construct, were cultured in SC-U+Gal medium at 28°C for 16 *h*. OD_{600} was monitored and adjusted to 1 for the spot assay. Ten µL of each culture and their serial dilutions were spotted on SC-U+Gal or SC-U+Gal + 5 mM ammonium ferrous sulfate plates, followed by incubation at 28°C for 3 d. Plates were observed to assess the yeast growth and photographed.

Sequence analysis and phylogenetic tree construction

Genes belonging to the *CCC1/VIT1* family were identified in the PANTHER18 family library of trees (Thomas et al., 2022) using the keyword PTHR31851. Sequences from one alga and selected plant genomes were retrieved from UniProt Knowledgebase (UniProtKB) (UniProt Consortium, 2023). Sequences for *Ceratopteris richardii* and *Lotus japonicus* were obtained on Phytozome v13 (Goodstein et al., 2012). We limited our analysis to the following genomes: *Chlamydomonas reinhardtii* (green alga); *Selaginella moellendorffii* (lycophyte); *Marchantia polymorpha* (liverwort); *Physcomitrella patens* (bryophyte); *Amborella trichopoda* (amborella); *Ceratopteris richardii* (pteridophyte); *Brachypodium distachyon*, *Hordeum vulgare*, *Musa acuminata*, *Oryza sativa*, *Setaria italica*, *Sorghum bicolor*, *Triticum aestivum*, *Tulipa gesneriana*, *Zea mays*, and *Zostera marina* (monocots); *Arabidopsis thaliana*, *Brassica napus*, *Capsicum annuum*, *Citrus sinensis*, *Cucumis sativus*, *Erythrante guttata*, *Eucalyptus grandis*, *Glycine max*, *Gossypium hirsutum*, *Helianthus annuus, Lactuca sativa, Lotus japonicus*, *Medicago truncatula*, *Nicotiana tabacum*, *Populus trichocarpa*, *Prunus persica*, *Ricinus communis*, *Solanum lycopersicum, Solanum tuberosum*, *Spinacia oleracea*, *Theobroma cacao*, and *Vitis vinifera* (eudicots). Sequences are listed in Supplementary Table S4. Multiple sequence alignment was obtained using ClustalW. WebLogo 3 was used to create the sequence logos (Crooks et al., 2014). The initial maximum-likelihood phylogenetic tree was calculated by ModelFinder (Kalyaanamoorthy et al., 2017) using the IQ-TREE multicore version 2.1.2 COVID-edition for Linux 64-bit. The best-fit model based on Bayesian Information Criterion was JTT+R6. Branch support for the maximum-likelihood tree was generated with ultrafast bootstrap (Hoang et al., 2018) (1000 replicates) implemented in the IQ-TREE software (Nguyen et al., 2015) Calculations were performed on the CIPRES (CyberInfrastructure for Phylogenetic Research) science gateway platform (Miller et al., 2010). The phylogenetic tree was visualized and annotated with iTOL (Letunic and Bork, 2021) and can be accessed here: https://itol.embl.de/tree/47187131203292916985088O6. Predicted protein structures, provided by AlphaFold within UniProtKB, were visually analyzed for each protein in the tree.

Results

Spatial expression of *MtVTL8* in *M. truncatula*

To determine when and where *MtVTL8* is expressed in roots and nodules, the coding sequence for the β-glucuronidase (GUS) enzyme (Jefferson et al., 1987) was cloned under the control of the *MtVTL8*-promoter (*pMtVTL8*). The *pMtVTL8*-GUS construct was transferred to an *A. rhizogenes* strain and expressed via hairy-root transformation in the roots of R108 wild type and *mtvtl8-2*, a *Tnt1* line with a homozygous *Tnt1* insertion in the exon of *MtVTL8* (Cai et al., 2022). Roots and nodules were examined at 0 dpi, 5 dpi and 15 dpi with *S. meliloti* Rm41 (Supplementary Figures S1, S2). Blue color was found in nodule primordia and nodules but not in the roots, demonstrating that the *MtVTL8* promoter highly and exclusively directs expression in these tissues (Supplementary Figures S1, S2). Longitudinal cross sections of the GUS stained nodules of R108 and *mtvtl8-2* at 15 dpi followed by light microscopy imaging showed that p*MtVTL8-GUS* was expressed from ZII to ZIII in both infected cells (IC) and uninfected cells (UC) with high

expression in the infection zone (IZ) (Figure 1; Supplementary Figure S3). Expression was not observed in the interzone (IZ). These results correspond to the RNA-seq data from the Symbimics database (Roux et al., 2014) and reinforce the idea that MtVTL8's role is to support SNF. Expression of p*MtVTL8-GUS* was not observed in the vascular system (Figures 1A, E; Supplementary Figures S3A, B). In *mtvtl8-2*, the *MtVTL8* expression was dramatically decreased in the premature senescent zone compared to the zones containing rhizobia (Supplementary Figure S3). However, the expression pattern in R108 was similar to that observed in *mtvtl8-2*, (Supplementary Figure S3), taking into consideration the developmental defects observed in these nodules due to the absence of *MtVTL8* (Walton et al., 2020; Cai et al., 2022). At the 15 dpi time point in R108 nodules, there is not yet a senescent zone; taken together, these results suggest that MtVTL8 may not have a role in reusing Fe^{2+} during senescence.

Functional complementation of a yeast Fe^{2+} mutant and *mtvtl8-2* nodulated roots

The yeast Cross-complements Ca^{2+} phenotype of the Csg1 family (*CCC1*) (Li et al., 2001) gene encodes an Fe^{2+}/Mn^{2+} vacuolar transporter. Yeast *Δccc1* mutants, containing a deletion of *CCC1*, show hypersensitivity to high concentrations of external Fe^{2+} because they fail to sequester the excess Fe^{2+} in their vacuoles (Li et al., 2001). The *ScΔccc1* strain has been used in complementation studies of several plant iron transporters belonging to the CCC1 family including MtVTL4 and MtVTL8 (Walton et al., 2020); AtVIT1 (Kim et al., 2006); AtVTL1, AtVTL2 and AtVTL5 (Gollhofer et al., 2014); TgVIT1 (Momonoi et al., 2009); OsVIT1 and OsVIT2 (Zhang et al., 2012); TaVIT2 (Connorton et al., 2017); EgVIT1 (Kato et al., 2019); GmVTL1a and GmVTL1b (Brear et al., 2020; Liu et al., 2020). Additionally the strain was used to test PfVIT from the *P. falciparum* parasite (Slavic et al., 2016). All tested transporters were able to complement the *ScΔccc1* mutation and restore the growth of the defective strain in high iron conditions.

The *S. cerevisiae* wild-type DY150 and mutant *Δccc1* strains transformed with empty vector (EV) pYES2/CT individually were able to grow on selective medium without Fe^{2+} (Figures 2A, B, left side). Mutant *ScΔccc1* were transformed with pYES2/CT harboring the genes for *AtVTL1*, a positive control, *MtVTL4*, or *MtVTL8* were able to grow on selective medium without Fe^{2+} (Figures 2C–E, left side). *ScΔccc1* transformed with EV was unable to grow on the selection plates supplied with 5 mM Fe^{2+} (Figure 2B, right side). In contrast, the growth of the *ScΔccc1* strain in the presence of 5 mM Fe^{2+} was partially restored by heterologous expression of *AtVTL1*, a positive control, *MtVTL4*, and *MtVTL8* (Figures 2C–E, right side). This confirms that both MtVTL8 and MtVTL4, as well as AtVTL1, are able to transport ferrous ions out of the cytosol either to the vacuole or across the plasma membrane in yeast.

In addition to the yeast assay, we performed *in planta* complementation using the SNF defective line *mtvtl8-2*. *In planta*

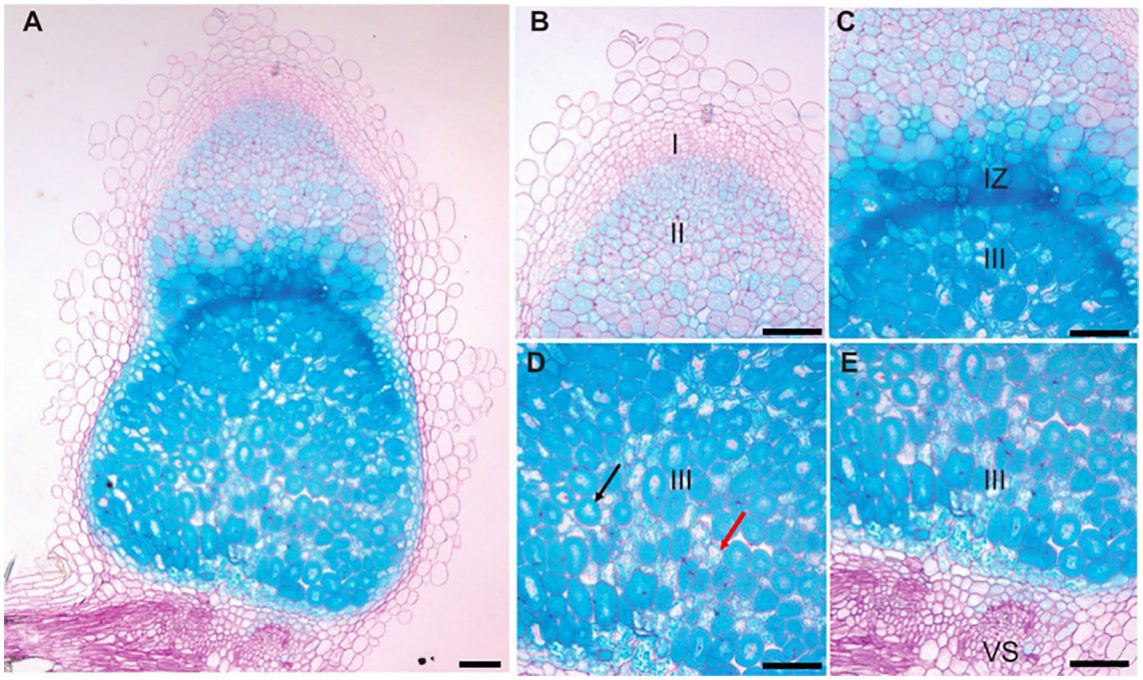

FIGURE 1
p*MtVTL8-GUS* is expressed from zone II to zone III in both infected and uninfected cells of *Medicago truncatula* genotype R108 nodules. Nodules were collected and stained for GUS followed by fixation with glutaraldehyde. Then they were embedded in Technovit 7100 (Kulzer Technik, Hanau, Germany) and sectioned at 5 µm. **(A)** Expression of p*MtVTL8-GUS* in the R108 nodule section at 15 dpi with *S. meliloti* Rm41. **(B-E)** Details from **(A)** for expression of p*MtVTL8-GUS* from Zone I to Zone III. VS, vasculature. I, zone I, meristem zone. II, zone II, infection zone. IZ, interzone, maturation zone. III, zone III, fixation zone. The black arrow indicates an infected cell. The red arrow indicates an uninfected cell. Scale bars represent 0.1 mm.

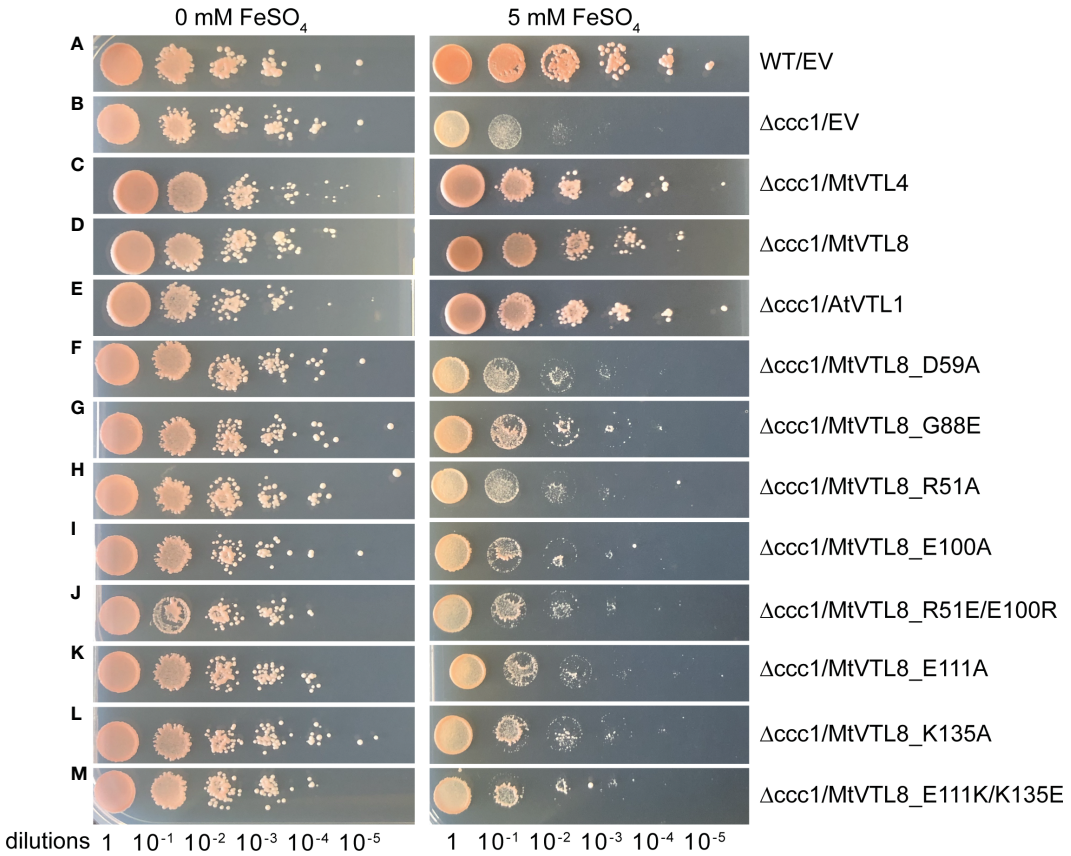

FIGURE 2
Spot assay of different mutants of *MtVTL8* expressed in the *S. cerevisiae Δccc1* strain. Spot assay with tenfold dilutions of overnight yeast cultures plated on at 0 or 5 mM ferrous sulfate (left and right panels, respectively) and incubated at 28°C for 3 days. From top to bottom: **(A)** wild-type strain DY150 transformed with empty vector (EV), **(B–M)** *Δccc1* strain transformed with EV and vector containing *MtVTL4, MtVTL8, AtVTL1* or specific *MtVTL8* mutant genes under the p*GAL1* promoter. *Δccc1* expressing *AtVTL1, MtVTL4* or *MtVTL8* are positive controls. Vector is pYES2/CT.

complementation is a good platform to investigate plant transporters and has been used in our lab to complement *M. truncatula* plants with defective nodulation due to a mutated nitrate transporter (Yu et al., 2021). Expression of MtVTL8 driven by its 2.8 kb MtVTL8 native promoter in the mtvtl8-2 root system was accomplished by A. rhizogenes mediated hairy-root transformation (Figures 3). Wildtype *MtVTL8* constructs successfully rescued the defective nodule phenotype from small Fix$^-$ white nodules with empty vector (Figures 3B, G) to wild-type like (WTL) pink nodules (Figures 3C, H; compare to WT with empty vector, Figures 3A, F). Complemented or control plants' nodule surface areas were assessed with the aim of determining if *MtVTL8*- complemented *mtvtl8-2* nodules produced statistically similar nodule surface areas to WT R108 nodules, larger than the non-complemented *mtvtl8-2* nodules. However, none were found to have statistically different sizes (Supplementary Figure S4). Chlorophyll content of composite *MtVTL8*- expressing *mtvtl8-2* plants was used to assess effective nitrogen fixation. Results showed similar chlorophyll content of plants with *MtVTL8*- expressing *mtvtl8-2* roots was similar to WT R108 plants, which was markedly higher than *mtvtl8-2* plants whose roots with an empty vector-transformed (Supplementary Figure S5). This demonstrates that complementation (pink color in nodule and leaf chlorophyll content) can be used to assess MtVTL8 functionality *in planta*.

MtVLT4 and misexpression of *MtVTL8* fail to rescue *Mtvtl8*'s defective phenotype

Two *M. truncatula* CCC1/VIT1 genes, MtVTL4 and MtVTL8, are exclusively and highly expressed in nodules. Sequence alignment shows that the two proteins are 55% identical and 72% positives. Expression of MtVTL4 or MtVTL8 was found to successfully rescue the toxicity of iron in yeast *ScΔccc1* mutants (Walton et al., 2020) and confirmed in our lab (Figures 2C, D). These results indicate that both transporters can transport ferrous ions out of the cytosol in yeast. While *mtvtl8* mutants, either *mtvtl8-1* with a large deletion spanning *MtVTL8* and *MtVTL4* (Walton et al., 2020), or with a homozygous *Tnt1* insertion in the *MtVTL8* exon (*mtvtl8-2*) (Cai et al., 2022) display defective white nodules, Walton et al. (2020) found that plants with a *Tnt1* homozygous insertion in the *MtVTL4* exon display wild-type like nodules, with an apparent developmental delay (Walton et al., 2020). Expression of *MtVTL8* under the control of its own promoter successfully

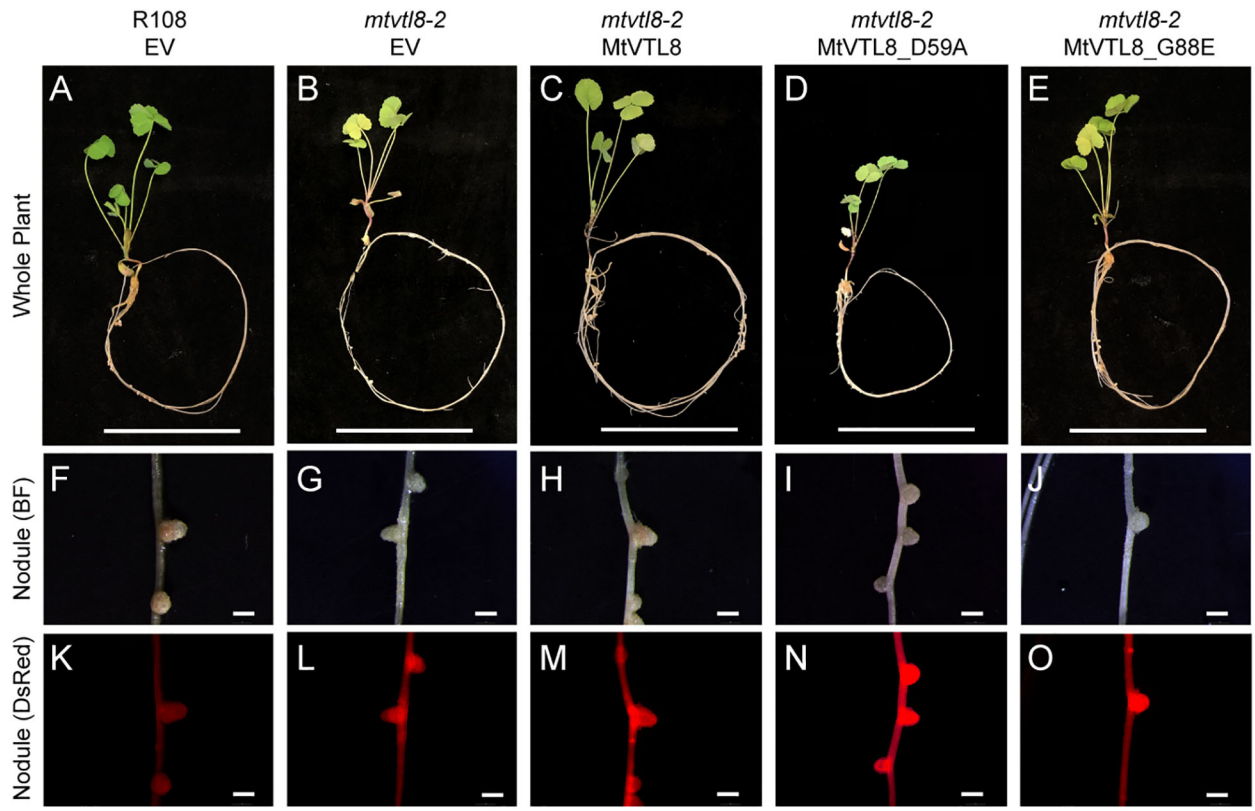

FIGURE 3
In planta complementation assays of the *mtvtl8-2* mutant with the wild-type *MtVTL8* and its different mutated versions affected in the transmembrane domain. **(A–E)** Images of *M. truncatula* plants transformed with different vectors expressing different mutated versions of *MtVTL8*. From left to right, **(A)** R108 plant roots transformed with empty vector (EV). **(B–E)** *Mtvtl8-2* plant roots transformed with **(B)** EV, **(C)** *MtVTL8* (WT), **(D)** *MtVTL8*_D59A, and **(E)** *MtVTL8*_G88E expressed under pMt*VTL8* promoter. **(F–J)** Bright field (BF) images of nodules corresponding to **(A–E)**. **(K–O)** DsRed fluorescence encoded by the *DsRed* gene under the p*AtUBI* constitutive promoter in the vector is observed in the transformed nodules corresponding to **(F–J)**. Scale bars represent 5 cm for **(A–E)** and 1 mm for **(F–O)**.

rescued the *mtvtl8-1* deletion mutant, but *MtVTL4* expression under the control of its own promoter did not have the same result (Walton et al., 2020).

Since both MtVTL4 and MtVTL8 transport Fe^{2+} in yeast, we wondered whether the failure of *MtVTL4* expression to complement *mtvtl8-1* (Walton et al., 2020) could have been caused by it being expressed at the wrong time and place in maturing nodules. To address this question, we expressed the *MtVTL4* gene driven by the constitutive *Arabidopsis thaliana* translation elongation factor (*AtEF1a*) promoter (Axelos et al., 1989; Auriac and Timmers, 2007) in the roots of *mtvtl8-2*. As a control, we expressed *MtVTL8* in the same vector. The results showed that expression of neither *MtVTL4* nor *MtVTL8* driven by the *AtEF1a* promoter in the roots of *mtvtl8-2* rescued the defective nodulation (Supplementary Figures S6D, E, I, J). While these results are not definitive for *MtVTL4*, they suggest that expression of *MtVTL8* in an inappropriate nodule location may be deleterious to nodule development. Alternatively, the *AtEF1a* promoter may not express well in the area(s) of the nodule where *MtVTL8* is needed.

Because *MtVTL4* and *MtVTL8* have different expression patterns within nodules (Roux et al., 2014; Walton et al., 2020) with *MtVTL4* expressed most highly in ZII and *MtVTL8* expressed most highly in the IZ and ZIII, we wondered if expressing *MtVTL4* under *MtVTL8*'s promoter might enable *MtVTL4* to functionally complement *mtvtl8*. However, expression of *MtVTL4* under the *MtVTL8* promoter displayed defective nodulation in *mtvtl8-2* (Supplementary Figures S7D, H). Plants with roots transformed with *MtVTL4* had leaves containing significantly less chlorophyll compared with the positive controls (Supplementary Figure S5). Thus, our data suggest that MtVTL4's localization to the plasma membrane and infection thread or other functional differences from MtVTL8 give these two transporters unique capabilities in nodules.

Structural model of MtVTL8 and identification of essential amino acids

We obtained a structural model for the monomer of MtVTL8 from the AlphaFold protein structure database (Jumper et al., 2021; Varadi et al., 2022). We then produced the dimeric form (Figure 4A) by overlapping the monomer on chains A and B of EgVIT1, pdb 6IU3 (Kato et al., 2019). The dimeric model for MtVTL8 shows the predicted five transmembrane helices (TMHs) from TMH1 to TMH5 (Figure 4B) contributing to form the transmembrane domain (TMD). A cavity forms at the interface

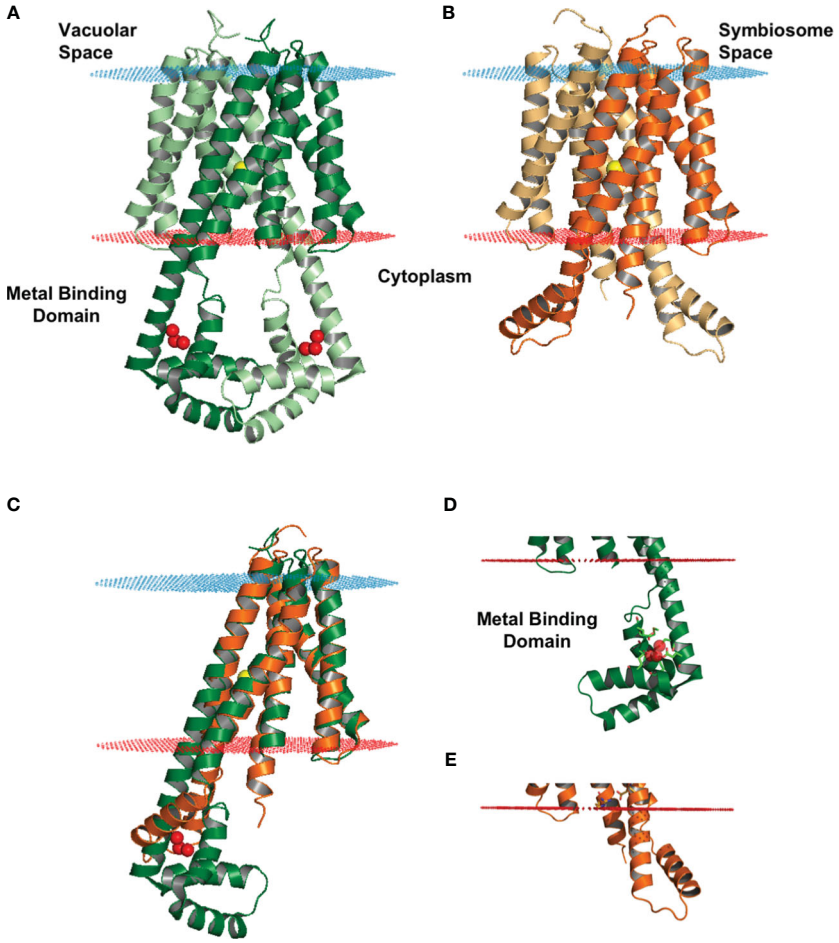

FIGURE 4
Structural model of MtVTL8 compared to the crystal structure of EgVIT1. **(A)** Crystal structure of EgVIT1, with monomer A in dark green and monomer B in light green, showing the TMD embedded in the membrane (blue and red dots) and the MBD in the cytoplasm. **(B)** AlphaFold model of MtVTL8, with monomer A in dark orange and monomer B in light orange, showing a conserved TMD and a reduced cytoplasmic region lacking a MBD. **(C)** Monomer A of MtVTL8 (dark orange) overlapped on monomer A of EgVIT1 (dark green). **(D)** Zoom into the MBD of EgVIT1 showing the side chains for the residues that bind the Fe^{2+} ions. **(E)** Zoom into the cytoplasmic region of MtVTL8 showing a shorter TMH2 and one α-helix. **(A–E)** Iron ion in the TMD is a yellow sphere; iron ions in the MBD are red spheres.

between the two monomers and in the model is open toward the cytoplasm, like in the EgVIT1 structure. The transmembrane region does not show remarkable differences between the two transporters (Figure 4C) (RMSD value of 1.23 for 650 atoms). The only exception is TMH2 that in the MtVTL8 model is slightly bent in the direction of TMH1 (Figures 4D, E). This may be due to constraints caused by a shortened sequence between TMH2 and 3. In contrast to the TMD region, structural alignment between the AlphaFold model of MtVTL8 and the crystal structure of EgVIT1 shows intriguing differences in the cytoplasmic region of the two proteins (Figure 4C). Like in EgVIT1, TMH2 in MtVTL8 is longer than the other TMHs and protrudes in the cytoplasm. However, in MtVTL8 the cytoplasmic portion of TMH2 is predicted to be seven residues shorter than TMH2 in EgVIT1 (Supplementary Figure S8A). Also, while in EgVIT1 the extended TMH2 connects with three additional cytoplasmic α-helices to form a metal binding domain (MBD) (Figures 4A, C, D), in MtVTL8 a shorter sequence, MtVTL8(124-138), between TMH2 and 3 is predicted to form one α-helix, H1 (Figures 4B, C, E). In the MtVTL8 model, TMH2 and H1 are almost parallel and are separated by a short loop of seven residues (Figures 4B, C, E; Supplementary Figure S8C). In summary, the overall topology of the transporter is changed from five transmembrane helices plus three cytoplasmic helices in EgVIT1 to five transmembrane helices plus one cytoplasmic helix in MtVTL8 (Supplementary Figures S8B, C).

In the EgVIT1 structure, five glutamic acid residues, Glu102 (TMH2), Glu105 (TMH2), Glu113 (H1), Glu116 (H1), and Glu153 (H3) and two methionines, Met149 and Met150 (H3), within the MBD are involved in binding and stabilizing transition metal ions like Fe^{2+} or Mg^{2+} (Supplementary Figure S8A, red arrowheads). Mutating any of the glutamic acids or the methionines failed to complement the growth inhibition phenotype of *Sc*△*ccc1* and decreased transport activity in liposomes made with the transporter mutant versions (Kato et al., 2019). Additionally, two

other residues, Glu32 and Asp36 (Supplementary Figure S8A, red arrowheads), located at the entrance of the ion-translocation pathway on TMH1, may play a role in guiding iron ions from the MBD to the TMD. With the exception of Glu102 on TMH2 (Asp118 in MtVTL8), no amino acid residues with similar biochemical properties in similar locations are found in the cytoplasmic domain of MtVTL8 (Supplementary Figure S8A). This suggests that MtVTL8 is not able to bind metal ions in the cytoplasm.

We used the MtVTL8 structural model to identify residues potentially important for transport activity in VTL. After identifying residues that may have a role in metal ion binding or transport, we studied the effect of point mutations on the transport properties of MtVTL8 in complementation studies in the *mtvtl8-2* mutated plant line and in *ScΔccc1*, the iron sensitive mutant yeast strain.

Complementation studies to test amino acids involved in the translocation pathway

In EgVIT1, two residues from each monomer in the translocation channel, Asp43 and Met80 are predicted to bind metal ions, followed by relaying the metal ions to Glu72 within the central translocation pathway (Kato et al., 2019). The three residues are all essential for EgVIT1 transport activity as demonstrated by yeast spot assay and liposomal essays. Based on sequence alignment between EgVIT1 and MtVTL8, residues Asp43 and Met80 of EgVIT1 correspond to residues Asp59 and Met96 of MtVTL8, respectively (Supplementary Figure S8A). However, Glu72 is not conserved in MtVTL8 as the equivalent position is occupied by a glycine, Gly88 (Supplementary Figure S8A).

To test its impact on the function of MtVTL8, we mutated the polar residue Asp59 to Ala to obtain the MtVTL8_D59A mutant. *A. rhizogenes-mediated* transformation of mtvtl8-2 mutant roots was used to express constructs of empty vector (EV), MtVTL8, and MtVTL8_D59A (Figures 3A–D, F–I, K–N). Our complementation experiments showed that *mtvtl8-2* roots transformed with the *MtVTL8_D59A* mutant gene displayed defective nodulation with white nodules (Figures 3D, I) compared with the pink nodules from the positive controls, wild type plant R108 transformed with EV (Figures 3A, F) or *mtvtl8-2* transformed with *MtVTL8* (Figures 3C, H). *Mtvtl8-2* plants transformed with *MtVTL8_D59A* had leaves that contained less chlorophyll compared with positive controls, and no significant difference was observed compared with the negative control (Supplementary Figure S5), suggesting defects in N supply. Taken together, our results indicate that *mtvtl8-2* roots transformed with *MtVTL8_D59A* showed defective SNF and did not complement the *mtvtl8-2* phenotype. Similarly, expression of the *MtVTL8_D59A* mutant failed to complement the yeast *ScΔccc1* strain (Figure 2F). Together these results suggest that Asp59 is essential to Fe^{2+} transport in MtVTL8.

In EgVIT1, Glu72 on TMH2 is an essential residue proposed to translocate the metal ions by displacing its bonded proton along the central ion translocation pathway (Kato et al., 2019). The corresponding residue in MtVTL8 is a glycine, Gly88. We speculated that adding back the glutamic acid in the place of Gly88 in MtVTL8 could have a positive effect on the function. Therefore, we replaced Gly88 with Glu to make the single mutant MtVT8_G88E. Expression of *MtVTL8_G88E* in *mtvtl8-2* hairy roots produced transgenic roots that displayed defective white nodules compared with the pink nodules from the positive controls (Figures 3E, J, O). *Mtvtl8-2* plants with roots transformed with *MtVTL8_G88E* had chlorotic leaves (Supplementary Figure S5). When evaluated in the yeast *ScΔccc1* mutant, the *MtVTL8_G88E* mutant failed to restore iron tolerance (Figure 2G). These data indicate that Gly88 is an essential residue for MtVTL8 function and mutating it to glutamic acid does not restore its putative role as proton transporter proposed for EgVIT1. Interestingly, MtVTL8 does not harbor other negatively chargeable amino acids in the substrate cavity that could potentially fulfill the same role as Glu72. These observations suggest that MtVTL8 may use a different mechanism for iron transport than that hypothesized for EgVIT1. It is also possible that another residue far from MtVTL8's Gly88 could function in proton transport if MtVTL8 is indeed an iron-proton antiporter.

Putative TMH1-TMH2 salt bridge formation in MtVTL8 TMD

In silico analysis of the MtVTL8 model indicates the formation of a salt bridge in the TMD between two oppositely charged residues, Arg51 located on TMH1 and Glu100 on TMH2 (Supplementary Figure S9A). Alignment of MtVTL8 with EgVIT1 shows the TMH1-TMH2 salt bridge is only possible in MtVTL8 and not EgVIT1 as the corresponding amino acids in EgVIT1 are Arg35 and Gly84 (Supplementary Figure S8A). Based on our observation that in MtVTL8, Arg51 and Glu100 could form a salt bridge, we constructed mutants with a single mutation of Arg51 or Glu100 into Ala. Expression of *MtVTL8_R51A* or *MtVTL8_E100A* in *mtvtl8-2* hairy roots produced plants that displayed defective nodulation and symbiotic nitrogen fixation phenotypes (Figures 5; Supplementary Figures S4, S5). Subsequently we tried to restore the putative salt bridge by swapping the charges and we obtained the R51E/E100R double mutant. However, the *MtVTL8_R51E/E100R* mutant gene failed to rescue the *mtvtl8-2* phenotype (Figures 5F, L). *Mtvtl8-2* plants transformed with *MtVTL8_R51A* or *MtVTL8_E100A* or the double mutant with swapped charges had nodules with no significant difference in size compared with the positive or negative controls (Supplementary Figure S4), whereas the leaves contained significantly less chlorophyll compared with the positive controls (Supplementary Figure S5), indicating a deficiency in SNF. In yeast, neither MtVTL8 proteins with R51A, E100A, nor R51E/E100R were able to rescue the *ScΔccc1* iron transport deficiency (Figures 2H–J). These data suggest that these two residues are essential for MtVTL8 function and their location in the protein is

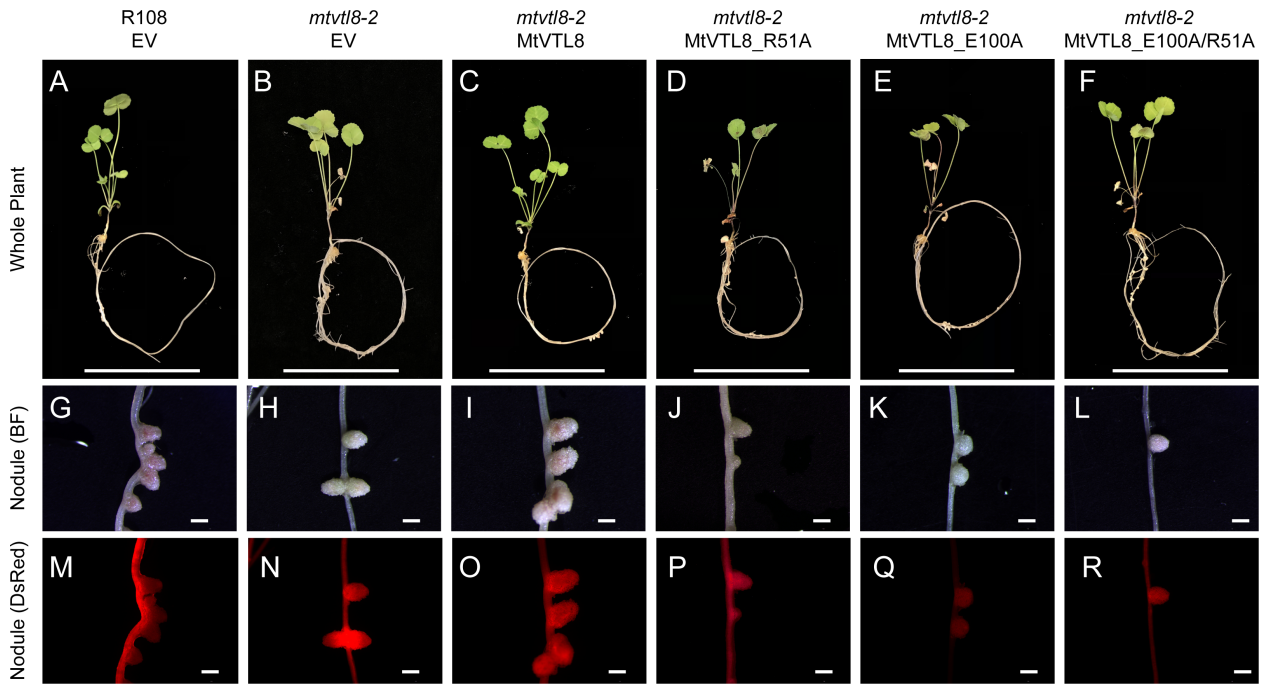

FIGURE 5
In planta complementation assays of the *mtvtl8-2* mutant with wild-type mutations and its different mutated versions affected in the putative TMH1-2 salt bridge. **(A–F)** Images of *M. truncatula* plants expressing different mutated versions of *MtVTL8*. From left to right, **(A)** R108 plant roots transformed with empty vector (EV); *Mtvtl8* plant roots transformed with **(B)** EV, **(C)** *MtVTL8* under p*MtVTL8* (WT), **(D)** *MtVTL8*_R51A, **(E)** *MtVTL8*_E100A, and **(F)** *MtVTL8*_R51E/E100R. **(G–L)** Bright field (BF) and **(M–R)** DsRed fluorescence images of transformed nodules corresponding to **(A–F)**. Scale bars represent 5 cm for **(A–F)** and 1 mm for **(G–R)**.

important as well, likely contributing to ionic interactions other than a salt bridge between the two residues.

MtVTL8's putative cytoplasmic salt bridge

Our model shows that the cytoplasmic portion of MtVTL8 is dramatically different from that of EgVIT1 with MtVTL8 harboring a lone α-helix MtVTL8(124-138) (H1) instead of the three α-helices as in EgVIT1 (Figure 3; Supplementary Figures S8B, C). In the model, H1 lies almost parallel to the cytoplasmic portion of TMH2. We observed that Lys135 from H1 is at a distance of 2.7 Å from Glu111 (TMH2) which is compatible with the formation of a salt bridge between the two residues (Supplementary Figure S9). In order to assess the role of Glu111 and Lys135, we created the single mutants *MtVTL8_E111A* and *MtVTL8_K135A* (Figure 6). The results showed that expression of *MtVTL8_E111A* in hairy roots of *mtvtl8-2* plants failed to rescue the defective nodulation phenotype (Figures 6D, J) whereas expression of *MtVTL8_K135A* successfully rescued the defective phenotype of *mtvtl8-2* (Figures 6E, K). Quantitation of nodule surface areas and leaf chlorophyll of composite plants showed no significant difference with the positive controls (Supplementary Figures S4, S5). To assess the restoration of the putative salt bridge between Glu111 and Lys135, we swapped the charges between the two residues creating the double mutant *K111E/E135K*. Expression of the double mutant with swapped charges failed to rescue the defective nodulation and nitrogen fixation phenotypes of *mtvtl8-2* (Figures 6F, L; Supplementary Figures S4, S5). This data suggests that Glu111 is an essential residue for MtVTL8 function as an Fe^{2+} transporter in yeast, whereas Lys135 is not *in planta*. It also suggests that trying to restore the putative salt bridge by swapping the charges in MtVTL8 is insufficient for function *in planta*. Similarly, when the single or double mutants were expressed in the *ScΔccc1* strain they were not able to rescue iron transport deficiency (Figures 2K–M).

Phylogenetic analysis of plant VITs and VTLs and conservation of essential amino acids

A thorough phylogenetic analysis of plant CCC1/VIT members is not available. Sorribes-Dauden et al. (2020) obtained a phylogenetic tree using 771 sequences from Archaea, bacteria, fungi, and plants showing that CCC1/VIT homologs can be classified in eight different groups. Groups I and II contain only Bacteria or Archaea proteins, respectively. Fungal VITs are clustered in Groups VI, VII and VIII. Plant VITs (69 sequences) belong to Group V, plant VTLs (111 sequences) belong to Group III. Group V also includes several bacterial VITs. Based on their phylogenetic analysis, Sorribes-Dauden et al. (2020) proposed that VITs and VTLs have a different origin: VITs originated from ancestral horizontal transfers from bacteria while VTLs emerged from an archaeal lineage, with both transfers dating at the origin of the last common eukaryote ancestor.

In this paper, we expanded the phylogenetic analysis to include VIT and VTL sequences from 37 plant genomes for a total of 306

FIGURE 6
In planta complementation assays of the *mtvtl8-2* mutant with wild-type *MtVTL8* and its different mutated versions with mutations affected in residues capable of forming a salt bridge on the cytosolic face of the membrane. **(A–F)** Images of *M. truncatula* plants expressing different mutated versions of *MtVTL8*. From left to right, **(A)** R108 plant roots transformed with empty vector (EV); *Mtvtl8-2* plant roots transformed with **(B)** EV, **(C)** *MtVTL8* under p*MtVTL8* (WT), **(D)** *MtVTL8*_E111A, **(E)** *MtVTL8*_K135A and **(F)** *MtVTL8*_E111K/K135E under p*VTL8*. **(G–L)** Bright field (BF) and **(M–R)** DsRed fluorescence images of transformed nodules corresponding to **(A–F)**. Scale bars represent 5 cm for **(A–F)** and 1 mm for **(G–R)**.

sequences (Supplementary Table S4). We also included two sequences from the alga *Chlamydomonas reinhardtii*. After multiple sequence alignment, we obtained a maximum-likelihood phylogenetic tree (Supplementary Figure S10). The phylogenetic tree supports two main clades: one clade includes transporters that harbor a MBD (purple stars in Supplementary Figure S10) corresponding to VITs (green labels); the other clade contains sequences that lack the MBD corresponding to VITs (orange labels). However, among VTLs, there is an exception with three VTLs that contain a MBD, MpoVTL1, PpaVTL1 and PpaVTL2 (Supplementary Figure S10). In addition, we divided the VITs in two subclades, Group I and II, as they display different structural features as described below.

To learn more about the conservation level of specific amino acids in VTLs and VITs and to validate the results of our mutagenesis experiments, we used our multiple sequence alignment to create separated LOGOs of specific regions for the two phylogenetic groups. We observed that residues corresponding to Asp43 and Met80 in EgVIT1 (Supplementary Figures S11A, C), Asp59 and Met96 in MtVTL8 (Supplementary Figures S11B, D) are strictly conserved in VITs and VTLS, respectively. Intriguingly, we observed that Asp72 which has been proposed to have a role in iron translocation as well as proton movement toward Asp43 (Kato et al., 2019), is only conserved in Group I VITs, while it is a Gln in the 22 VITs belonging to Group II (Supplementary Figure S11C). In VTLs, Asp72 is diverged to a glycine (Gly88 in MtVTL8) or other non-chargeable residue in VTLs (Supplementary Figure S11D).

Residues involved in metal binding in the MBD, Glu102, Glu105, Glu113, Glu116, Met149, Met150, and Glu153 are strictly conserved in Group I VITs (Supplementary Figures S11E–G). However, in Group II VITs, these residues are far less conserved. With the exception of Glu102 that corresponds to Asp118 in MtVTL8, the metal binding residues are absent in VTLs as they lack the MBD region. Note that TMH2 is shorter in MtVTL8 and Asp118 is the last residue of TMH2. On a side note, we should mention that the glutamic acids within the cytoplasmic MBD are conserved in PfVIT but functional expression of mutants with substitutions of glutamic acid residues in *ScΔccc1* showed iron tolerance (Sharma et al., 2021). Note that PfVIT was not included in our phylogenetic analysis. Additionally, two residues with a role in transferring iron ions from the MBD to the TMD, Glu32 and Asp36, are highly conserved in VITs, but are instead conserved non-polar residues in VTLs.

We also investigated if residues predicted to form two salt bridges, Arg51-Glu110 (TMH1-TMH2) and Glu111-Lys135 (TMH2-H1), in the MtVTL8's AlphaFold model are conserved in VTLs and VITs. We obtained different results for the two salt bridges. Arg51 is conserved in both VITs and VTLs (Supplementary Figures S12A, B). However, Glu100 is only conserved in VTLs (Supplementary Figure S12D) and in Group II VITs (Supplementary Figure S12C), while it is a glycine in Group I VITs (Supplementary Figure S12C). Therefore, a salt bridge between TMH1 and TMH2 could only form in VTLs and Group II VITs. Finally, Glu111 (TMH2) is strictly conserved in all VTLs

(Supplementary Figure S12D). The quality of alignment for the H1 region among VTLs was not enough to determine the conservation of Lys35 (H1).

These phylogenetic analyses reinforce the conclusions from our complementation studies with mutagenized MtVTL8 proteins. Together, they indicate that MtVTL8 and other VTLs operate by a mechanism that is distinct from that proposed for the VITs. Our analysis also indicates that a subset of VITs may have a different transport mechanism as they lack some of the structural features found in other well-characterized VITs.

Discussion and conclusions

Iron is an essential micronutrient for human nutrition and iron-deficiency anemia affects millions of people. Biofortification of crops such as wheat, corn and legumes has been indicated as a sustainable solution to combat malnutrition including iron deficiency (Garg et al., 2018; Ofori et al., 2022). Iron transporters from the CCC1/VIT family have been used to increase iron in the endosperm of wheat and barley by overexpression of TaVIT2 (Connorton et al., 2017) and in cassava roots by overexpression of AtVIT1 (Narayanan et al., 2015; Narayanan et al., 2019). Understanding the mechanism underlying iron transport by iron transporters including VTLs can result in future beneficial application for agronomic biofortification. Equally important is understanding the mechanisms of SNF that contribute to sustainable agriculture.

Our results show the spatial patterns of *MtVTL8*-promoter directed expression in roots in developing and mature nodules, with expression detected as early as 5 dpi in nodule primordia (Figure 1; Supplementary Figures S1, S2). The results in mature nodules (Figure 1) confirm previous results obtained by laser-capture dissection RNAseq for WT *M. truncatula* nodules (Roux et al., 2014) showing expression in the proximal areas of ZII, IZ and ZIII. Expression of *MtVTL8* was not observed in the vascular system (Figure 1; Supplementary Figures S1A, E, S2A, B, S3A, B). These results are somewhat different from those obtained in a study of the homologous *GmVTL1a* gene, in which expression was observed in cells surrounding the nodule vasculature and in infected nodule cells (Brear et al., 2020). In mutant *mtvtl8-2* nodules, expression was similar to WT (Supplementary Figures S2, S3 compare to Figure 1 and Supplementary Figure S1). It was expressed early in nodulation, in 5 dpi nodule primordia (Supplementary Figures S2H–J) and in the distal zones of the nodule, but much lower in the proximal zones, demarking the nodule zones where MtVTL8 is essential for nodule function (Supplementary Figures S1–3). This suggests that MtVTL8 is dispensable for early nodule development and only becomes essential after the bacteroids are enclosed by symbiosome membranes.

Because both *MtVTL4* and *MtVTL8* are expressed solely in nodules with different spatial expression patterns as assessed by RNAseq (Roux et al., 2014; Walton et al., 2020), with *MtVTL4* only expressed in cells where rhizobia are being released into symbiosomes, we were curious to see if expression of *MtVTL4* using *MtVTL8 cis* elements would complement the defect in *mtvtl8-2*; i.e., does MtVTL4 have similar functionality if expressed in place of MtVTL8? The p-*MtVTL8-MtVTL4* construct did not complement *mtvtl8-2* (Supplementary Figure S7), while expression of either gene in the yeast △*ccc1* mutant rescued the iron toxicity phenotype (Figures 2C, D), leading us to propose that MtVTL4 and MtVTL8 have distinct functions beyond iron transport per se. We note that our results may be caused by intracellular localization of MtVTL4 vs. MtVTL8 as well as differences in function between the two proteins.

Functional studies for PtVIT and EgVIT1 (Labarbuta et al., 2017; Kato et al., 2019) showed they are Fe^{2+}/H^{+} antiporters that exchange metal ions and protons on the opposite sides of lipid membranes. The solved crystal structure for EgVIT1, which captured the inside-open conformation, allowed the identification of essential amino acids for the transport of iron/protons (Kato et al., 2019). A model has been proposed in which the proton/iron transport cycle starts on the cytosolic side of the membrane where metal ions are captured by the MBD (Figure 7A). Conserved residues in the MBD and the TMD substrate channel entrance provide a pathway for the iron ions to translocate from the MBD to the TMD. Metal ions are transferred to a metal binding pocket in the TMD that is alternatively exposed to either side of the membrane. Two chargeable amino acids in the TMD, Asp43 and Glu72 are the initial iron and proton binding sides, respectively. After an exchange of position happens, irons are released in the vacuolar space and protons in the cytosol. We note that although most antiporters utilize a so-called single-site alternating-access mechanism, where the transporter can only associate with one substrate at a time, there are some examples of antiporters where ion and substrate binding sites were not overlapping, e.g. in the NorM transporters (Lu et al., 2013; Claxton et al., 2021). Despite the proposed model, many details of the mechanism of transport for EgVIT1 and for VITs in general are not fully understood. For instance, although a cooperative action is expected to take place between the TMD and the auxiliary cytoplasmic MBD, the role of the latter in transport is still not clear. Also, the stoichiometry of transport is not known.

In the absence of a crystal structure for VTLs, we obtained a model for MtVTL8. Using such model as a guide we identified amino acids potentially involved in iron transport in MtVTL8. We demonstrated that when mutated, the resulting protein cannot restore SNF in plants or iron tolerance in yeast confirming our hypotheses. We proposed that MtVTL8 could rely on a different transport mechanism from that proposed for VITs and suggested two alternative mechanisms. As discussed previously, VTLs, including MtVTL8, lack the cytoplasmic MBD and the amino acids that can capture metal ions in the cytoplasm. Additionally, they lack amino acids that guide the metal ions toward the binding pocket and an essential glutamic acid residue, Glu72, that has been indicated to work as relay for proton-iron exchange in the TMD. In VTLs, Glu72 is substituted with a glycine (Gly88 in MtVTL8) but our studies have shown that the MtVTL8_Gly88Glu mutant is not an active transporter (Figures 2H,3E, J, O). Based on these

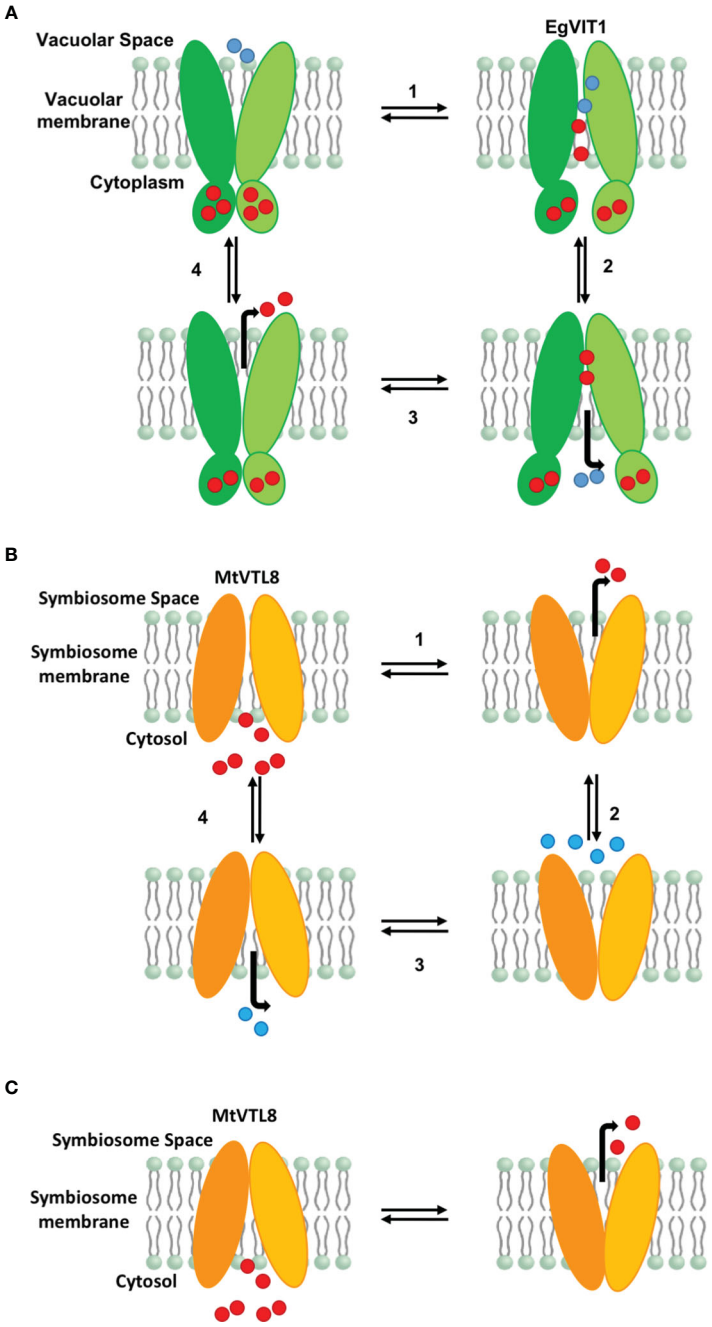

FIGURE 7
Proposed models for iron transport in plant VITs and VTLs. **(A)** Proposed model for EgVIT1 as a Fe^{2+}/H^{+} antiporter that utilizes a multiple-site alternating-access mechanism. Iron ions are captured in the cytosol and stored in the MBD. Iron ions and protons travel in opposite directions through the transporter simultaneously during the alternating access cycle. Protons enter the transport channel with the transporter in the conformation open toward the vacuolar space. Iron ions enter the transport channel in the cytosol open conformation. Iron ions protons are exchanged in the cavity and protons are released in the cytosol. When the transporter opens again toward the vacuolar space, iron ions are released. **(B)** Proposed model for MtVTL8 as a Fe^{2+}/H^{+} antiporter that utilizes a single-site alternating-access mechanism. Iron ions and protons do not travel simultaneously in the transport channel. As it lacks a MBD, MtVTL8 does not store iron ions. Instead iron ions enter the transporter channel when the protein is open toward the cytosol and are then released in the symbiosome space in the inward open conformation. Protons enter the transport channel and are released when the transporter opens again toward the cytoplasm. **(C)** Proposed model for MtVTL8 as a Fe^{2+} uniporter. In this model MtVTL8 operates as a uniporter and there is no transport of protons. **(A, B)** Numbers corresponds to the proposed order of events. EgVIT1 in green, MtVTL8 in orange. Iron ions are shown as red spheres, protons as blue spheres.

observations, we have two working hypotheses. Our first hypothesis is that MtVTL8 is a Fe^{2+}/H^{+} antiporter that uses the symbiosome proton gradient to fuel Fe^{2+} transport (Figure 7B). In this scenario, in MtVTL8, Asp59, the only membrane-embedded charged residue, is a common binding site for substrate and protons, and the occupancy of this site is mutually exclusive (Figure 7B). This is agreement with what was proposed for other antiporters and called single-site alternating-access mechanism of transport (Yerushalmi

and Schuldiner, 2000; Schuldiner, 2014). Another possibility is that MtVTL8 uses an antiporter mechanism similar to that proposed to EgVIT1 but uses an amino acid residue distant from Gly88 as a proton acceptor. Because we lack experimental evidence that MtVTL8 is an Fe^{2+}/H^{+} antiporter, there exists the less-likely possibility that MtVTL8 and other VTLs may operate as Fe^{2+} efflux channels instead of being active as active Fe^{2+}/H^{+} antiporters (Figure 7C). In this model, Fe^{2+} binds to the conserved Asp59 inside the channel and is transported without an exchange of protons. This hypothetical mechanism spares the pH gradient across the symbiosome membrane required for nitrogen fixation (Udvardi and Day, 1989; Pierre et al., 2013). The gradient is essential for the import of dicarboxylates for SNF and believed to be important for the import of other molecules. In this less-likely scenario, the recently identified sequestration of heme by *M. truncatula*'s NCR247 that overrides the bacteroids' negative Fe^{2+} regulation of Fe^{2+} import (Sankari et al., 2022) might result in a lowered Fe^{2+} concentration in the symbiosome space. That lowered Fe^{2+} concentration might be low enough to provide a sufficient driving force for Fe^{2+} movement across the symbiosome membrane from the cytosol without requiring an additional source of energy for transport. Additional studies are needed to address these hypotheses including molecular dynamics calculations, transport assays and experimental structures for VTLs.

Data availability statement

The original contributions presented in the study are included in the article/Supplementary Material. Further inquiries can be directed to the corresponding author.

Author contributions

JC: Conceptualization, Data curation, Formal analysis, Investigation, Methodology, Visualization, Writing – original draft. AL: Conceptualization, Data curation, Formal analysis, Investigation, Methodology, Validation, Writing – original draft, Writing – review & editing. RD: Conceptualization, Data curation, Funding acquisition, Investigation, Methodology, Project administration, Resources, Supervision, Writing – original draft, Writing – review & editing.

Funding

The author(s) declare financial support was received for the research, authorship, and/or publication of this article. This work was partially funded by US National Science Foundation, grant 2139351.

Acknowledgments

We thank Drs. Wei Liu and Michael Udvardi for the pMU vectors used in this work, Dr. Elinor Lichtenberg for help with statistics, and the reviewers for thoughtful and helpful comments.

Conflict of interest

The authors declare that the research was conducted in the absence of any commercial or financial relationships that could be construed as a potential conflict of interest.

Publisher's note

Supplementary material

The Supplementary Material for this article can be found online at: https://www.frontiersin.org/articles/10.3389/fpls.2023.1306491/full#supplementary-material

References

Appleby, C. A. (1984). Leghemoglobin and *rhizobium* respiration. *Annu. Rev. Plant Physiol.* 35, 443–478. doi: 10.1146/annurev.pp.35.060184.002303

Arnon, D. I. (1949). Copper enzymes in isolated chloroplasts, polyphenolexidase in *Beta vulgaris*. *Plant Physiol.* 24, 1–15. doi: 10.1104/pp.24.1.1

Auriac, M.-C., and Timmers, A. C. J. (2007). Nodulation studies in the model legume *Medicago truncatula*: Advantages of using the constitutive *EF1α* promoter and limitations in detecting fluorescent reporter proteins in nodule tissues. *Mol. Plant Microbe Interact.* 20, 1040–1047. doi: 10.1094/MPMI-20-9-1040

Axelos, M., Bardet, C., Liboz, T., Le Van Thai, A., Curie, C., and Lescure, B. (1989). The gene family encoding the *Arabidopsis thaliana* translation elongation factor EF-1α: Molecular cloning, characterization and expression. *Mol. Gen. Genet.* 219, 106–112. doi: 10.1007/BF00261164

Barker, D. G., Pfaff, T., Moreau, D., Groves, E., Ruffel, S., Lepetit, M., et al. (2006). "Growing *M. truncatula:* choice of substrates and growth conditions," in *The Medicago truncatula handbook*. Eds. U. Mathesius, E.-P. Journet and L. W Sumner. Available at: https://citeseerx.ist.psu.edu/document?repid=rep1&type=pdf&doi=9ff882f0d91b9e3bbb8217920c8f5eb94d9c3d2c.

Boisson-Dernier, A., Chabaud, M., Garcia, F., Becard, G., Rosenberg, C., and Barker, D. G. (2001). *Agrobacterium rhizogenes*-transformed roots of *Medicago truncatula* for the study of nitrogen-fixing and endomycorrhizal symbiotic associations. *Mol. Plant Microbe Interact.* 14, 695–700. doi: 10.1094/MPMI.2001.14.6.695

Brear, E. M., Bedon, F., Gavrin, A., Kryvoruchko, I. S., Torres-Jerez, I., Udvardi, M. K., et al. (2020). GmVTL1a is an iron transporter on the symbiosome membrane of soybean with an important role in nitrogen fixation. *New Phytol.* 228, 667–681. doi: 10.1111/nph.16734

Brear, E. M., Day, D. A., and Smith, P. M. C. (2013). Iron: an essential micronutrient for the legume-rhizobium symbiosis. *Front. Plant Sci.* 13, 359. doi: 10.3389/fpls.2013.00359

Burton, J. W., Harlow, C., and Theil, E. C. (1998). Evidence for reutilization of nodule iron in soybean seed development. *J. Plant Nutr.* 21, 913–927. doi: 10.1080/01904169809365453

Cai, J., Veerappan, V., Arildsen, K., Sullivan, C., Piechowicz, M., Frugoli, J., et al. (2023). A modified aeroponic system for growing small–seeded legumes and other plants to study root systems. *Plant Methods* 19, 21. doi: 10.1186/s13007-023-01000-6

Cai, J., Veerappan, V., Troiani, T., Mysore, K. S., Wen, J., and Dickstein, R. (2022). "Whole genome sequencing identifies a *Medicago truncatula Tnt1* insertion mutant in the *VTL8* gene that is essential for symbiotic nitrogen fixation," in *The Medicago truncatula Genome*. Eds. S. Sinharoy, Y. Kang and V. Benedito (Switzerland: Springer Nature Switzerland AG).

Carrere, S., Verdier, J., and Gamas, P. (2021). MtExpress, a comprehensive and curated RNAseq-based gene expression atlas for the model legume *Medicago truncatula*. *Plant Cell Physiol.* 62, 1494–1500. doi: 10.1093/pcp/pcab110

Clarke, V. C., Loughlin, P. C., Day, D. A., and Smith, P. M. C. (2014). Transport processes of the legume symbiosome membrane. *Front. Plant Sci.* 5, 699. doi: 10.3389/fpls.2014.00699

Claxton, D. P., Jagessar, K. L., and Mchaourab, H. S. (2021). Principles of alternating access in multidrug and toxin extrusion (MATE) transporters. *J. Mol. Biol.* 6, 166959. doi: 10.1016/j.jmb.2021.166959

Connorton, J. M., Jones, E. R., Rodríguez-Ramiro, I., Fairweather-Tait, S., Uauy, C., and Balk, J. (2017). Wheat vacuolar iron transporter TaVIT2 transports Fe and Mn and is effective for biofortification. *Plant Physiol.* 174, 2434–2444. doi: 10.1104/pp.17.00672

Crooks, G. E., Hon, G., Chandonia, J.-M., and Brenner, S. E. (2014). WebLogo: a sequence logo generator. *Genome Res.* 14, 1188–1190. doi: 10.1101/gr.849004

Day, D. A., and Smith, P. M. C. (2021). Iron transport across symbiotic membranes of nitrogen-fixing legumes. *Int. J. Mol. Sci.* 22, 432. doi: 10.3390/ijms22010432

Einsle, O., and Rees, D. C. (2020). Structural enzymology of nitrogenase enzymes. *Chem. Rev.* 120, 4969–5004. doi: 10.1021/acs.chemrev.0c00067

Escudero, V., Abreu, I., Tejada-Jiménez, M., Rosa-Núñez, E., Quintana, J., Prieto, R. I., et al. (2020). *Medicago truncatula* Ferroportin2 mediates iron import into nodule symbiosomes. *New Phytol.* 228, 194–209. doi: 10.1111/nph.16642

Fåhraeus, G. (1957). The infection of clover root hairs by nodule bacteria studied by a simple glass slide technique. *J. Gen. Microbiol.* 16, 374–381. doi: 10.1099/00221287-16-2-374

Farkas, A., Maróti, G., Dürgő, H., Györgypál, Z., Lima, R. M., Medzihradszky, K. F., et al. (2014). *Medicago truncatula* symbiotic peptide NCR247 contributes to bacteroid differentiation through multiple mechanisms. *Proc. Natl. Acad. Sci. U.S.A.* 111, 5183–5188. doi: 10.1073/pnas.1404169111

Garg, M., Sharma, N., Sharma, S., Kapoor, P., Kumar, A., Chunduri, V., et al. (2018). Biofortified crops generated by breeding, agronomy, and transgenic approaches are improving lives of millions of people around the world. *Front. Nutr.* 433, 166959. doi: 10.3389/fnut.2018.00012

Gilles-Gonzalez, M. A., Ditta, G. S., and Helinski, D. R. (1991). A haemoprotein with kinase activity encoded by the oxygen sensor of Rhizobium meliloti. *Nature* 350, 170–172. doi: 10.1038/350170a0

Gollhofer, J., Timofeev, R., Lan, P., Schmidt, W., and Buckhout, T. J. (2014). Vacuolar-Iron-Transporter1-Like proteins mediate iron homeostasis in Arabidopsis. *PloS One* 9, e110468. doi: 10.1371/journal.pone.0110468

González-Guerrero, M., Matthiadis, A., Sáez, Á., and Long, T. A. (2014). Fixating on metals: new insights into the role of metals in nodulation and symbiotic nitrogen fixation. *Front. Plant Sci.* 5, 45. doi: 10.3389/fpls.2014.00045

González-Guerrero, M., Navarro-Gómez, C., Rosa-Núñez, E., Echávarri-Erasun, C., Imperial, J., and Escudero, V. (2023). Forging a symbiosis: transition metal delivery in symbiotic nitrogen fixation. *New Phytol.* 239, 2113–2125. doi: 10.1111/nph.19098

Goodstein, D. M., Shu, S., Howson, R., Neupane, R., Hayes, R. D., Fazo, J., et al. (2012). Phytozome: A comparative platform for green plant genomics. *Nucleic Acids Res.* 40, D1178–D1186. doi: 10.1093/nar/gkr944

Hakoyama, T., Niimi, K., Yamamoto, T., Isobe, S., Sato, S., Nakamura, Y., et al. (2012). The integral membrane protein SEN1 is required for symbiotic nitrogen fixation in *Lotus japonicus* nodules. *Plant Cell Physiol.* 53, 225–236. doi: 10.1093/pcp/pcr167

Hirsch, A. M. (1992). Developmental biology of legume nodulation. *New Phytol.* 122, 211–237. doi: 10.1111/j.1469-8137.1992.tb04227.x

Hoang, D. T., Chernomor, O., von Haeseler, A., Minh, B. Q., and Vinh, L. S. (2018). UFBoot2: Improving the ultrafast bootstrap approximation. *Mol. Biol. Evol.* 35, 518–522. doi: 10.1093/molbev/msx281

Hoffman, B. M., Lukoyanov, D., Yang, Z.-Y., Dean, D. R., and Seefeldt, L. C. (2014). Mechanism of nitrogen fixation by nitrogenase: The next stage. *Chem. Rev.* 114, 4041–4062. doi: 10.1021/cr400641x

Jamet, A., Sigaud, S., Van de Sype, G., Puppo, A., and Hérouart, D. (2003). Expression of the bacterial catalase genes during *Sinorhizobium meliloti–Medicago sativa* symbiosis and their crucial role during the infection process. *Mol. Plant Microbe Interact.* 16, 217–225. doi: 10.1094/MPMI.2003.16.3.217

Jefferson, R., Kavanagh, T., and Bevan, M. (1987). GUS fusions: β-glucuronidase as a sensitive and versatile gene fusion marker in higher plants. *EMBO J.* 6, 3901–3907. doi: 10.1002/j.1460-2075.1987.tb02730.x

Johnston, A. W., Yeoman, K. H., and Wexler, M. (2001). Metals and the rhizobial-legume symbiosis–uptake, utilization and signalling. *Adv. Microbial. Physiol.* 45, 113–156. doi: 10.1016/S0065-2911(01)45003-X

Jumper, J., Evans, R., Pritzel, A., Green, T., Figurnov, M., Ronneberger, O., et al. (2021). Highly accurate protein structure prediction with AlphaFold. *Nature* 596, 583–589. doi: 10.1038/s41586-021-03819-2

Kalyaanamoorthy, S., Minh, B. Q., Wong, T. K. F., von Haeseler, A., and Jermin, L. S. (2017). ModelFinder: fast model selection for accurate phylogenetic estimates. *Nat. Methods* 14, 587–589. doi: 10.1038/nmeth.4285

Kato, T., Kumazaki, K., Wada, M., Taniguchi, R., Nakane, T., Yamashita, K., et al. (2019). Crystal structure of plant vacuolar iron transporter VIT1. *Nat. Plants* 5, 308–315. doi: 10.1038/s41477-019-0367-2

Kim, S. A., Punshon, T., Lanzirotti, A., Li, L., Alonso, J. M., Ecker, J. R., et al. (2006). Localization of iron in *Arabidopsis* seed requires the vacuolar membrane transporter VIT1. *Science* 314, 1295–1298. doi: 10.1126/science.1132563

Kondorosi, A., Vincze, E., Johnston, A. W. B., and Beringer, J. E. (1980). A comparison of three *Rhizobium* linkage maps. *Mol. Gen. Genet.* 178, 403–408. doi: 10.1007/BF00270491

Kryvoruchko, I. S., Routray, P., Sinharoy, S., Torres-Jerez, I., Tejada-Jiménez, M., Finney, L. A., et al. (2018). An iron-activated citrate transporter, MtMATE67, is required for symbiotic nitrogen fixation. *Plant Physiol.* 176, 2315–2329. doi: 10.1104/pp.17.01538

Labarbuta, P., Duckett, K., Botting, C. H., Chahrour, O., Malone, J., Dalton, J. P., et al. (2017). Recombinant vacuolar iron transporter family homologue PfVIT from human malaria-causing Plasmodium falciparum is a Fe2+/H+exchanger. *Sci. Rep.* 7, 42850. doi: 10.41038/srep42850

Ledbetter, R. N., Garcia Costas, A. M., Lubner, C. E., Mulder, D. W., Tokmina-Lukaszewska, M., Artz, J. H., et al. (2017). The electron bifurcating FixABCX protein complex from *Azotobacter vinelandii*: Generation of low-potential reducing equivalents for nitrogenase catalysis. *Biochemistry* 56, 4177–4190. doi: 10.1021/acs.biochem.7b00389

Letunic, I., and Bork, P. (2021). Interactive Tree Of Life (iTOL) v5: an online tool for phylogenetic tree display and annotation. *Nucleic Acids Res.* 49, W293–W296. doi: 10.1093/nar/gkab301

Li, L., Chen, O. S., Ward, D. M., and Kaplan, J. (2001). CCC1 is a transporter that mediates vacuolar iron storage in yeast. *J. Biol. Chem.* 276, 29515–29519. doi: 10.1074/jbc.M103944200

Liang, Y., Urano, D., Liao, K.-L., Hedrick, T. L., Gao, Y., and Jones, A. M. (2017). A nondestructive method to estimate the chlorophyll content of Arabidopsis seedlings. *Plant Methods* 13, 26. doi: 10.1186/s13007-017-0174-6

Limpens, E., Moling, S., Hooiveld, G., Pereira, P. A., Bisseling, T., Becker, J. D., et al. (2013). Cell- and tissue-specific transcriptome analyses of *Medicago truncatula* root nodules. *PloS One* 8, e64377. doi: 10.1371/journal.pone.0064377

Liu, S., Liao, L. L., Nie, M. M., Peng, W. T., Zhang, M. S., Lei, J. N., et al. (2020). A VIT-like transporter facilitates iron transport into nodule symbiosomes for nitrogen fixation in soybean. *New Phytol.* 225, 1413–1428. doi: 10.1111/nph.16506

Lomize, M. A., Pogozheva, I. D., Joo, H., Mosberg, H. I., Lomize, A. L., et al. (2012). OPM database and PPM web server: resources for positioning of proteins in membranes. *Nucleic Acids Res.* 40, D370-376. doi: 10.1093/nar/gkr703

Lu, M., Symersky, J., Radchenko, M., Koide, A., Guo, Y., Nie, R., et al. (2013). Structures of a Na+-coupled, substrate-bound MATE multidrug transporter. *Proc. Natl. Acad. Sci. U.S.A.* 110, 2099–2104. doi: 10.1073/pnas.1219901110

Lullien, V., Barker, D. G., de Lajudie, P., and Huguet, T. (1987). Plant gene expression in effective and ineffective root nodules of alfalfa (*Medicago sativa*). *Plant Mol. Biol.* 9, 469–478. doi: 10.1007/BF00015878

Marlow, V. L., Haag, A. F., Kobayashi, H., Fletcher, V., Scocchi, M., Walker, G. C., et al. (2009). Essential role for the BacA protein in the uptake of a truncated eukaryotic peptide in *Sinorhizobium meliloti*. *J. Bacteriol.* 191, 1519–1527. doi: 10.1128/JB.01661-08

Maróti, G., and Kondorosi, É. (2014). Nitrogen-fixing *Rhizobium*-legume symbiosis: are polyploidy and host peptide-governed symbiont differentiation general principles of endosymbiosis? *Front. Microbiol.* 5, 326. doi: 10.3389/fmicb.2014.00326

Miller, M. A., Pfeiffer, W., and Schwartz, T. (2010). *Creating the CIPRES Science Gateway for inference of large phylogenetic trees* (New Orleans, LA, USA: 2010 Gateway Computing Environments Workshop (GCE), 1–8.

Momonoi, K., Yoshida, K., Mano, S., Takahashi, H., Nakamori, C., Shoji, K., et al. (2009). A vacuolar iron transporter in tulip, TgVit1, is responsible for blue coloration in petal cells through iron accumulation. *Plant J.* 59, 437–447. doi: 10.1111/j.1365-313X.2009.03879.x

Narayanan, N., Beyene, G., Chauhan, R. D., Gaitán-Solís, E., Gehan, J., Butts, P., et al. (2019). Biofortification of field-grown cassava by engineering expression of an iron transporter and ferritin. *Nat. Biotechnol.* 37, 144–151. doi: 10.1038/s41587-018-0002-1

Narayanan, N., Beyene, G., Chauhan, R. D., Gaitán-Solis, E., Grusak, M. A., Taylor, N., et al. (2015). Overexpression of *Arabidopsis* VIT1 increases accumulation of iron in cassava roots and stems. *Plant Sci.* 240, 170–181. doi: 10.1016/j.plantsci.2015.09.007

Nguyen, L.-T., Schmidt, H. A., von Haeseler, A., and Minh, B. Q. (2015). IQ-TREE: A fast and effective stochastic algorithm for estimating maximum-likelihood phylogenies. *Mol. Biol. Evol.* 32, 268–274. doi: 10.1093/molbev/msu300

O'Brian, M. R. (2015). Perception and homeostatic control of iron in the rhizobia and related bacteria. *Annu. Rev. Microbiol.* 69, 229–245. doi: 10.1146/annurev-micro-091014-104432

O'Hara, G. W., Boonkerd, N., and Dilworth, M. J. (1988). Mineral constraints to nitrogen fixation. *Plant Soil* 108, 93–110. doi: 10.1007/BF02370104

Ofori, K. F., Antoniello, S., English, M. M., and Aryee, A. N. A. (2022). Improving nutrition through biofortification–A systematic review. *Front. Nutr.* 9, 1043655. doi: 10.3389/fnut.2022.1043655

Oldroyd, G. E. D. (2013). Speak, friend, and enter: signalling systems that promote beneficial symbiotic associations in plants. *Nat. Rev. Microbiol.* 11, 252–263. doi: 10.1038/nrmicro2990

Oldroyd, G. E. D., Murray, J. D., Poole, P. S., and Downie, J. A. (2011). The rules of engagement in the legume-rhizobial symbiosis. *Annu. Rev. Genet.* 45, 119–144. doi: 10.1146/annurev-genet-110410-132549

Ott, T., van Dongen, J. T., Gunther, C., Krusell, L., Desbrosses, G., Vigeolas, H., et al. (2005). Symbiotic leghemoglobins are crucial for nitrogen fixation in legume root nodules but not for general plant growth and development. *Curr. Biol.* 15, 531–535. doi: 10.1016/j.cub.2005.01.042

Pierre, O., Engler, G., Hopkins, J., Brau, F., Boncompagni, E., and Hérouart, D. (2013). Peribacteroid space acidification: a marker of mature bacteroid functioning in *Medicago truncatula* nodules. *Plant Cell Environ.* 36, 2059–2070. doi: 10.1111/pce.12116

Preisig, O., Zufferey, R., Thöny-Meyer, L., Appleby, C. A., and Hennecke, H. (1996). A high-affinity cbb3-type cytochrome oxidase terminates the symbiosis-specific respiratory chain of Bradyrhizobium japonicum. *J. Bacteriol.* 178, 1532–1538. doi: 10.1128/jb.178.6.1532-1538.1996

Rodríguez-Haas, B., Finney, L., Vogt, S., González-Melendi, P., Imperial, J., and González-Guerrero, M. (2013). Iron distribution through the developmental stages of *Medicago truncatula* nodules. *Metallomics* 5, 1247–1253. doi: 10.1039/c3mt00060e

Roux, B., Rodde, N., Jardinaud, M.-F., Timmers, T., Sauviac, L., Cottret, L., et al. (2014). An integrated analysis of plant and bacterial gene expression in symbiotic root nodules using laser-capture microdissection coupled to RNA sequencing. *Plant J.* 77, 817–837. doi: 10.1111/tpj.12442

Roy, S., Liu, W., Nandety, R. S., Crook, A., Mysore, K. S., Pislariu, C. I., et al. (2020). Celebrating 20 years of genetic discoveries in legume nodulation and symbiotic nitrogen fixation. *Plant Cell* 32, 15–41. doi: 10.1105/tpc.19.00279

Sankari, S., Babu, V. M. P., Bian, K., Alhhazmi, A., Andorfer, M. C., Avalos, D. M., et al. (2022). A haem-sequestering plant peptide promotes iron uptake in symbiotic bacteria. *Nat. Microbiol.* 7, 1453–1465. doi: 10.1038/s41564-022-01192-y

Schindelin, J., Arganda-Carreras, I., Frise, E., Kaynig, V., Longair, M., Pietzsch, T., et al. (2012). Fiji: an open-source platform for biological-image analysis. *Nat. Methods* 9, 676–682. doi: 10.1038/nmeth.2019

Schuldiner, S. (2014). Competition as a way of life for H(+)-coupled antiporters. *J. Mol. Biol.* 426, 2539–2546. doi: 10.1016/j.jmb.2014.05.020

Sharma, P., Tóth, V., Hyland, E. M., and Law, C. J. (2021). Characterization of the substrate binding site of an iron detoxifying membrane transporter from Plasmodium falciparum. *Malaria J.* 20, 295. doi: 10.1186/s12936-021-03827-7

Slavic, K., Krishna, S., Lahree, A., Bouyer, G., Hanson, K. K., Vera, I., et al. (2016). A vacuolar iron-transporter homologue acts as a detoxifier in *Plasmodium*. *Nat. Commun.* 7, 10403. doi: 10.1038/ncomms10403

Sorribes-Dauden, R., Peris, D., Martínez-Pastor, M. T., and Puig, S. (2020). Structure and function of the vacuolar Ccc1/VIT1 family of iron transporters and its regulation in fungi. *Comput. Struct. Biotechnol. J.* 18, 3712–3722. doi: 10.1016/j.csbj.2020.10.044

Suganuma, N., Nakamura, Y., Yamamoto, M., Ohta, T., Koiwa, H., Akao, S., et al. (2003). The *Lotus japonicus Sen1* gene controls rhizobial differentiation into nitrogen-fixing bacteroids in nodules. *Mol. Genet. Genomics* 269, 312–320. doi: 10.1007/s00438-003-0840-4

Tang, C., Robson, A. D., and Dilworth, M. J. (1992). The role of iron in the (brady) *Rhizobium* legume symbiosis. *J. Plant Nutr.* 15, 2235–2252. doi: 10.1080/01904169209364471

Tejada-Jiménez, M., Castro-Rodríguez, R., Kryvoruchko, I., Lucas, M. M., Udvardi, M., Imperial, J., et al. (2015). *Medicago truncatula* Natural Resistance-Associated Macrophage Protein1 is required for iron uptake by rhizobia-infected nodule cells. *Plant Physiol.* 168, 258–272. doi: 10.1104/pp.114.254672

Thomas, P. D., Ebert, D., Muruganujan, A., Mushayahama, T., Albou, L.-P., and Mi, H. (2022). PANTHER: Making genome-scale phylogenetics accessible to all. *Protein Sci.* 31, 8–22. doi: 10.1002/pro.4218

Udvardi, M. K., and Day, D. A. (1989). Electrogenic ATPase activity on the peribacteroid membrane of soybean (*Glycine max* L.) root nodules. *Plant Physiol.* 90, 982–987. doi: 10.1104/pp.90.3.982

Udvardi, M., and Poole, P. S. (2013). Transport and metabolism in legume-rhizobia symbioses. *Annu. Rev. Plant Biol.* 64, 781–805. doi: 10.1146/annurev-arplant-050312-120235

UniProt Consortium (2023). UniProt: the universal protein knowledgebase in 2023. *Nucleic Acids Res.* 51, D523–D531. doi: 10.1093/nar/gkac1052

Valimehr, S., Sanjarian, F., Sohi, H. H., Sharafi, A., and Sabouni, F. (2014). A reliable and efficient protocol for inducing genetically transformed roots in medicinal plant *Nepeta pogonosperma*. *Physiol. Mol. Biol. Plants* 20, 351–356. doi: 10.1007/s12298-014-0235-5

Varadi, M., Anyango, S., Deshpande, M., Nair, S., Natassia, C., Yordanova, G., et al. (2022). AlphaFold Protein Structure Database: massively expanding the structural coverage of protein-sequence space with high-accuracy models. *Nucleic Acids Res.* 50, D439–D444. doi: 10.1093/nar/gkab1061

Vasse, J., de Billy, F., Camut, S., and Truchet, G. (1990). Correlation between ultrastructural differentiation of bacteroids and nitrogen fixation in alfalfa nodules. *J. Bacteriol.* 172, 4295–4306. doi: 10.1128/jb.172.8.4295-4306.1990

Walton, J. H., Kontra-Kováts, G., Green, R. T., Domonkos, Á., Horváth, B., Brear, E. M., et al. (2020). The *Medicago truncatula* Vacuolar iron Transporter-Like proteins VTL4 and VTL8 deliver iron to symbiotic bacteria at different stages of the infection process. *New Phytol.* 228, 651–666. doi: 10.1111/nph.16735

Witty, J. F., Skøt, L., and Revsbech, N. P. (1987). Direct evidence for changes in the resistance of legume root nodules to O_2 diffusion. *J. Exp. Bot.* 38, 1129–1140. doi: 10.1093/jxb/38.7.1129

Yerushalmi, H., and Schuldiner, S. (2000). A common binding site for substrates and protons in EmrE, an ion-coupled multidrug transporter. *FEBS Lett.* 476, 1873–3468. doi: 10.1016/S0014-5793(00)01677-X

Yu, Y.-C., Dickstein, R., and Longo, A. (2021). Structural modeling and in *planta* complementation studies link mutated residues of the *Medicago truncatula* nitrate transporter NPF1.7 to functionality in root nodules. *Front. Plant Sci.* 12, 685334. doi: 10.3389/fpls.2021.685334

Zhang, Y., Xu, Y.-H., Yi, H.-Y., and Gong, J.-M. (2012). Vacuolar membrane transporters OsVIT1 and OsVIT2 modulate iron translocation between flag leaves and seeds in rice. *Plant J.* 72, 400–410. doi: 10.1111/j.1365-313X.2012.05088.x

frontiers | Frontiers in Plant Science

TYPE Original Research
PUBLISHED 05 January 2024
DOI 10.3389/fpls.2023.1326766

OPEN ACCESS

EDITED BY
Maria Jose Soto,
Spanish National Research Council (CSIC), Spain

REVIEWED BY
María Isabel Rubia,
Public University of Navarre, Spain
Ana Dominguez-Ferreras,
University of Warwick, United Kingdom
Marco Betti,
Sevilla University, Spain

*CORRESPONDENCE
Jesús Montiel
jmontiel@ccg.unam.mx
Jens Stougaard
stougaard@mbg.au.dk

RECEIVED 23 October 2023
ACCEPTED 12 December 2023
PUBLISHED 05 January 2024

CITATION
García-Soto I, Andersen SU, Monroy-Morales E, Robledo-Gamboa M, Guadarrama J, Aviles-Baltazar NY, Serrano M, Stougaard J and Montiel J (2024) A collection of novel *Lotus japonicus LORE1* mutants perturbed in the nodulation program induced by the *Agrobacterium pusense* strain IRBG74. *Front. Plant Sci.* 14:1326766. doi: 10.3389/fpls.2023.1326766

A collection of novel *Lotus japonicus LORE1* mutants perturbed in the nodulation program induced by the *Agrobacterium pusense* strain IRBG74

Ivette García-Soto[1], Stig U. Andersen[2], Elizabeth Monroy-Morales[1], Mariana Robledo-Gamboa[1], Jesús Guadarrama[1], Norma Yaniri Aviles-Baltazar[1], Mario Serrano[1], Jens Stougaard[2*] and Jesús Montiel[1*]

[1]Centro de Ciencias Genómicas, Universidad Nacional Autónoma de México (UNAM), Cuernavaca, Mexico, [2]Department of Molecular Biology and Genetics, Aarhus University, Aarhus, Denmark

The *Lotus japonicus* population carrying new *Lotus* retrotransposon 1 (*LORE1*) insertions represents a valuable biological resource for genetic research. New insertions were generated by activation of the endogenous retroelement *LORE1a* in the germline of the G329-3 plant line and arranged in a 2-D system for reverse genetics. *LORE1* mutants identified in this collection contributes substantially to characterize candidate genes involved in symbiotic association of *L. japonicus* with its cognate symbiont, the nitrogen-fixing bacteria *Mesorhizobium loti* that infects root nodules intracellularly. In this study we aimed to identify novel players in the poorly explored intercellular infection induced by *Agrobacterium pusense* IRBG74 sp. For this purpose, a forward screen of > 200,000 *LORE1* seedlings, obtained from bulk propagation of G329-3 plants, inoculated with IRBG74 was performed. Plants with perturbed nodulation were scored and the offspring were further tested on plates to confirm the symbiotic phenotype. A total of 110 *Lotus* mutants with impaired nodulation after inoculation with IRBG74 were obtained. A comparative analysis of nodulation kinetics in a subset of 20 mutants showed that most of the lines were predominantly affected in nodulation by IRBG74. Interestingly, additional defects in the main root growth were observed in some mutant lines. Sequencing of *LORE1* flanking regions in 47 mutants revealed that 92 *Lotus* genes were disrupted by novel *LORE1* insertions in these lines. In the IM-S34 mutant, one of the insertions was located in the 5´UTR of the LotjaGi5g1v0179800 gene, which encodes the AUTOPHAGY9 protein. Additional mutant alleles, named *atg9*-2 and *atg9*-3, were obtained in the reverse genetic collection. Nodule formation was significantly reduced in

these mutant alleles after *M. loti* and IRBG74 inoculation, confirming the effectiveness of the mutant screening. This study describes an effective forward genetic approach to obtain novel mutants in *Lotus* with a phenotype of interest and to identify the causative gene(s).

KEYWORDS

symbiosis, legume (nodules), mutant screening, autophagy, intercellular infection, *Lotus japonicus*

Introduction

Plant mutant collections have become a key resource to perform functional genomics and characterization of genes-of-interest in various biological processes. Mutagenized populations can be obtained with physical, chemical or biological mutagens (Chaudhary et al., 2019). The availability of mutant collections in the model legumes *Medicago truncatula* and *Lotus japonicus* (*Lotus*) have contributed importantly to understand the genetic networks that govern legume-rhizobia symbiosis (Roy et al., 2020). In the *M. truncatula* R108 line, a large mutant population was generated with the tobacco retrotransposon element Tnt1 (Tadege et al., 2008; Pislariu et al., 2012). In the *Lotus* accession Gifu, genotyping of plants regenerated from tissue culture (Madsen et al., 2005), identified new insertions of an endogenous *LORE1* retrotransposon and further investigation showed epigenetic activation of the *LORE1a* element in the germline (Fukai et al., 2008; Fukai et al., 2010). Subsequent studies exploited this discovery, generating a reverse genetic mutant collection of 134,682 individual plants from the G329-3 line carrying an active *LORE1a*. In this collection, information of the insertion sites was obtained by sequencing, facilitating identification and characterization of mutants disrupted in genes-of-interest (Fukai et al., 2012; Urbanski et al., 2012; Malolepszy et al., 2016).

Lotus establishes a mutualistic association with its cognate symbiont *Mesorhizobium loti*. The symbiotic association occurs in the rhizosphere, where both organisms exchange chemical signals for the specific recognition. This compatibility activates a symbiotic signaling pathway that allows intracellular rhizobial infection via root-hair infection threads (ITs) and initiation of the nodule organogenesis program. Bacteria migrate through the ITs towards the dividing cortical cells in the nodule primordia, that give rise to a nitrogen-fixing nodule. In the nodule cells, rhizobia are encapsuled into membranous structures called symbiosomes, where they convert atmospheric nitrogen into ammonia (Downie, 2014). *Lotus* is able to establish symbiotic associations with a broad spectrum of rhizobial species (Gossmann et al., 2012; Sandal et al., 2012; Zarrabian et al., 2022), and it was recently shown that is effectively nodulated by IRBG74, an *Agrobacterium pusense* strain isolated from *Sesbania cannabina* nodules (Cummings et al., 2009). IRBG74 induces massive root hair curling in *Lotus*, followed by intercellular infection of the epidermal cells (Montiel et al., 2021). Intercellular colonization is an entry mode observed in approximately 25% of the legume species investigated and although this group includes major legume crops, genetic control remains largely unexplored (Sprent, 2007). However, recent discoveries in intercellularly infected legumes such as *Arachys hypogaea*, *Aeschynomene evenia* and *Lotus*, have attracted attention to this entry mode and provided valuable information about the process (Chaintreuil et al., 2016; Peng et al., 2017; Bertioli et al., 2019; Chen et al., 2019; Karmakar et al., 2019; Montiel et al., 2021; Quilbe et al., 2021; Raul et al., 2022; Montiel et al., 2023). While intra- and intercellular rhizobial invasion share some genetic components and transcriptional responses, relevant differences were found among these processes (Quilbe et al., 2022).

Lotus is an optimal organism with abundant resources to analyze different plant-microbe interactions, such as germline activation of endogenous *LORE1*a retrotransposon, where new insertion sites can be tracked in the genome with a relatively simple and quick sequence-based method (Urbanski et al., 2012). Here we assess the potential use of a *LORE1a* activated population in a bulk forward screening. We present a collection of novel mutants impaired in intercellular symbiotic colonization by IRBG74 and compare the nodulation phenotype with that obtained by intracellular *M. loti* colonization. The genome mapping of the *LORE1* insertion sites allowed us to identify *ATG9* as a novel regulator in *Lotus*-rhizobia symbioses.

Materials and methods

Germination of *LORE1* seeds and mutant screening

Seeds from the line G329-3 were collected during several harvesting periods to obtain a mixed and balanced population. Batches with thousands of *LORE1* seeds were scarified with hydrochloric acid for 20 min, followed by several washes with distilled sterile water. The seeds were placed in square Petri dishes with moistened paper and two days later, transferred to autoclaved square boxes (40x40x40 cm) filled with Leca. The swollen seeds were inoculated with IRBG74 (O.D. 0.05) and the boxes were

maintained in a growth room with controlled temperature, photoperiod (21° C; 16:8 h), intensity light (100 µmol/m2/s). The plants were watered once per week with B & D solution (Broughton and Dilworth, 1971). This procedure was repeated for several months until approximately 200,000 plants were screened. We selected mutants with a visible nodulation phenotype such as: Nod-, hypernodulation or Fix-. This latter manifested by white nodules, reduced nodulation, short plant size and yellow leaves. The selected lines were kept at the greenhouse for seed production. Ten offspring plants from each mutant were subsequently tested by a nodulation assay in plate with IRBG74 (O. D. 0.05).

Identification of *LORE1* elements

To track the *LORE1* elements in the mutant collection, we followed the protocol previously described by Urbanski et al. (2012). First, total DNA was isolated from 3-5 plant of each mutant with hexadecyltrimethylammonium bromide (CTAB) (Rogers and Bendich, 1985). The DNA was quantified and shared with a Covaris S-series instrument to obtain 600-800 bp fragments. The DNA was blunted, end-repaired and adenylated with a T4 DNA polymerase, T4 DNA polynucleotide kinase and Taq polymerase, respectively, following the manufacturer´s instructions. A ligation was performed to incorporate a splinkerette intermediate adaptor (IA) to the DNA sequences (Mikkers et al., 2002), using a T4 DNA ligase. The flanking *LORE1* fragments were obtained by sequential PCR reactions. The first PCR products were amplified with the Splink1 and P2 oligonucleotides, obtaining amplicons of 500-600 bp, that were excised from the agarose gels and used as template for a nested PCR using the Splink2 and P3 primers (Supplementary Table S2). For each DNA sample, a unique P3 oligonucleotide harboring a molecular barcode was used. With this procedure, PCR products of 200-400 bp were amplified and pooled at equimolar concentrations for Illumina sequencing (Supplementary Table S2). The sequencing data was processed to detect the *LORE1*, adaptor and barcode sequences. These regions were trimmed and only the genomic region was mapped to the *L. japonicus* Gifu genome using bowtie2 with the following parameters: –end-to-end -X 500 -N 1 -L 28 -D 20 (Kamal et al., 2020). Only insertion with ≥ 4 reads were considered for the analysis.

Root growth and nodulation kinetics of *LORE1* mutants

The *L. japonicus* accession Gifu (Handberg and Stougaard, 1992) and *LORE1* lines were germinated as described above. For nodulation tests, seedlings of 3-5 days post-germination (dpg) were transferred to 12x12 cm square Petri dishes (10 seedlings per plate) containing 1.4% (w/v) agar slant with ¼ B & D medium (Broughton and Dilworth, 1971) and inoculated with 1 ml per plate of a bacterial suspension (*M. loti* R7A or IRBG74; OD600 = 0.05). The plants were kept in a growth room at 21° C with photoperiod (16/8 h). The nodule numbers were recorded weekly using a stereomicroscope. For the root growth dynamics, instead of B & D solution, the agar was supplemented with Gamborg's B-5 basal medium (Sigma-Aldrich, G5893) and the progression of the apical main root was monitored weekly.

Genotyping of *LORE1* lines

PCR reactions were performed to genotype the Nod- lines IM-A39, IM-N10 and IM-D22 using specific oligonucleotides for symbiotic genes (Supplementary Table S2), with the Phire Plant Direct PCR Mix (Thermofisher), following the manufacturer's instructions. Nested PCRs were done for *NFR5* in the IM-A39 mutant to flank the *LORE2* insertion and the PCR product was sequenced. The *LORE1* lines, 30164676 (*atg9*-2) and 30077209 (*atg9*-3), affected in the LotjaGi5g1v0179800 gene (*LjATG9*) were genotyped according to the *Lotus* base guidelines (Mun et al., 2016).

Results

Novel *LORE1* mutants affected in the *Lotus*-IRBG74 association

Progeny of the G329-3 line was successfully used to generate the *LORE1* reverse genetics mutant collection in *Lotus*, composed of 134,682 individual plants (Urbanski et al., 2012; Malolepszy et al., 2016). To explore the potential of *LORE1* for forward genetics, cuttings of the G329-3 line were cultivated and harvested in bulk. In this study, several batches of these seeds were used in a large-scale forward screen, searching for mutant plants perturbed in the symbiotic association with IRBG74, a *Rhizobium* sp. that induce nitrogen-fixing nodules in *Lotus* through intercellular infection (Montiel et al., 2021). More than 200,000 *LORE1* seedlings were inoculated in boxes with IRBG74 and plants with aberrant nodulation phenotypes at 6-8 weeks post-inoculation (wpi) were screened out. Focusing especially on Fix- mutants and delayed nodulation likely to carry mutations in genes required for intercellular infection, 1,200 putative mutants were selected and transferred to the greenhouse for seed production. Large-scale mutant screenings tend to have a variable proportion of false positive selection, therefore, to confirm the symbiotic phenotype of the selected lines, ten offspring plants from each mutant were inoculated with IRBG74 in plates (Figure 1). Since this is an ongoing project, the nodulation phenotype of the progeny of 629 mutants, selected in the first screening still needs to be validated. However, in the remaining 571 lines, the plate test confirmed the nodulation phenotype in 110 mutants (Figure 1, Supplementary Figure S1). In this mutant population, 105 lines showed a Fix- phenotype manifested in white nodule appearance, however, we also identified 4 Nod- mutants without visible nodules and 1 hypernodulating mutant (Supplementary Figure S1).

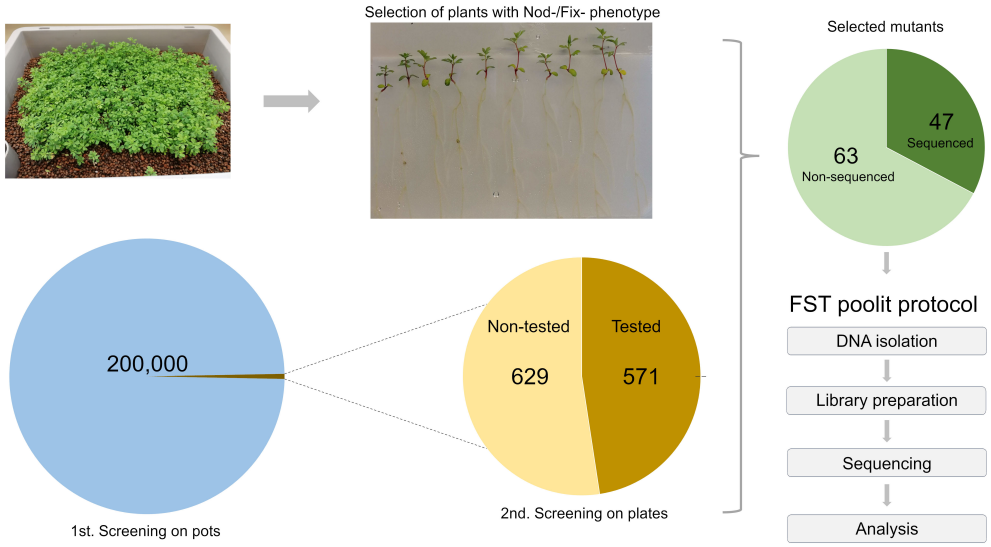

FIGURE 1
Scheme of the *LORE1* mutant screening to identify lines affected in the intercellular infection by IRBG74. Approximately 200,000 *LORE1* plants were inoculated with IRBG74, selecting 1,200 mutants with a Nod- or Fix- phenotype at 6-8 wpi. The offspring seeds of 571 selected lines were inoculated on plates (2nd screening), confirming the nodulation phenotype in 110 lines. For this study, we conducted the FST poolit method to identify the *LORE1* insertions sites in the genome of 47 selected mutants.

Differential symbiotic performance of *LORE1* mutants with *M. loti* and IRBG74

In this work, we identified 110 *LORE1* mutants affected in the nodulation performance with IRBG74. Since handling this number of mutant lines represents a technical challenge, we focused our attention on a subset of 20 randomly chosen mutants. First, we explored the specificity of the symbiotic phenotype, by analyzing the nodulation kinetics on plates at 2-6 weeks post-inoculation (wpi) with *M. loti* and IRBG74 (Supplementary Figures S2A-E), which colonize *Lotus* roots intra- and intercellularly, respectively (Montiel et al., 2021). In 12 lines, the number of pink nodules was significantly reduced at any timepoint with both rhizobial strains compared to Gifu (Figures 2A, B). However, nodule formation by *M. loti* was only affected in IM-53, IM-A19 and IM-D25 mutants. By contrast, the nodulation induced by IRBG74 was exclusively altered in IM-D08, IM-D11, IM-D26 and IM-N12 lines (Figures 2A, B, Supplementary Figures S2A-E). Since perturbances in the nodulation kinetics, nodule organogenesis and nitrogen fixation can negatively impact the plant growth, we measured the shoot length in the *LORE1* mutants at 6 wpi with both rhizobial strains. All the mutants tested showed a significantly shorter shoot length compared to Gifu at 6 wpi with IRBG74 (Figure 2A). On contrary, the aerial part was significantly affected in 11 lines inoculated with *M. loti* respect to Gifu (Figure 2A). These results suggest that all the mutants selected were affected in the *Lotus*-IRBG74, manifested by a delayed/reduced nodule formation or inefficient plant-growth promotion. Additionally, we observed significant differences in

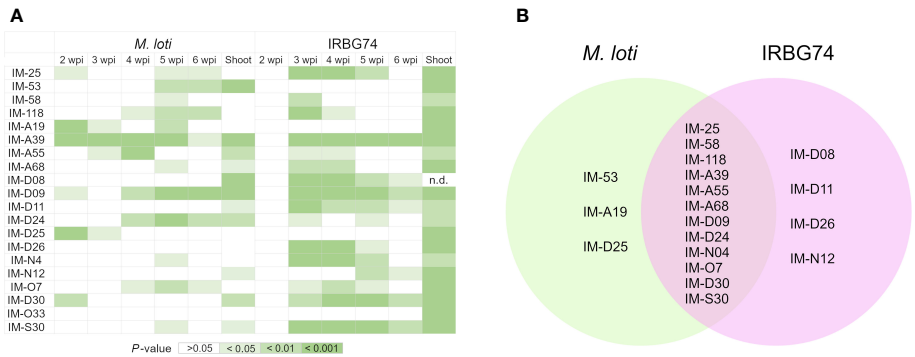

FIGURE 2
Significant reductions of nodule number and shoot length in *LORE1* mutants. **(A)** Graphical summary represented by shades of green of the significant differences observed by Mann–Whitney U-test for the parameters recorded in Supplementary Figures S2A-F. **(B)** Venn diagrams of the *LORE1* lines perturbed in the nodule formation induced by *M. loti* (green) and IRBG74 (pink).

the root growth of several mutants at 6 wpi with IRBG74. The length was reduced in 7 lines and increased in 5 mutants (Supplementary Figure S3).

LORE1 mutants with altered root and shoot growth

Our study revealed that most of the selected *LORE1* mutants were perturbed in the symbiotic program triggered by IRBG74 compared to *M. loti*. Nonetheless, during our analysis we noticed that certain mutants might be also affected in root development (Supplementary Figure S3). We explored whether any of these mutants have additional defects in their root growth under non-symbiotic conditions, by monitoring the main root length at 2-5 weeks post-germination (wpg) on plates supplemented with 12 mM KNO_3. In 14 lines, the root length was significantly shorter compared to Gifu plants of similar age at different timepoints. However, the length of the main root remained shorter throughout the analysis in the mutants IM-58, IM-D09, IM-N4, IM-O7, IM-O33 and IM-S30 (Figure 3). These results prompted us to measure the length of the aerial part in the plants grown in the above referred conditions. Although the shoot length was significantly different in 10 *LORE1* mutants compared to Gifu at 5 wpg, only in IM-58, IM-O33 and IM-S30 lines, the size was shorter (Supplementary Figure S4). Our data indicates that shoot and root growth is affected in several *LORE1* lines.

Genes disrupted by *LORE1* insertions

Mutants analyzed in this study, showed significant alterations in the root growth and plant-microbe associations. To get further insight into the genes associated to these phenotypes, the retrotransposon insertions were tracked in a subset of 20 mutants that were analyzed in more detail, along with 27 additional lines, randomly selected from the screening with IRBG74 (Figure 1, Supplementary Figure S1). For this purpose, we followed the FST poolit protocol that was previously developed to determine the insertion sites in the *LORE1* mutant collection (Urbanski et al., 2012; Malolepszy et al., 2016). The endogenous *LORE1* sequences and their respective position in the *Lotus* genome were successfully identified in all samples tested, confirming the effectiveness of the protocol (Supplementary Table S1). In 14 lines only the original *LORE1* elements were detected, however, in the remaining 33 mutants, 226 novel retrotransposon insertions were identified, 128 of them unique (Supplementary Table S1). These retrotransposons were distributed in introns, UTR, promoter and intergenic regions of the six chromosomes (Figures 4A, B). A total of 92 *Lotus* genes were disrupted in these 47 mutants and, each mutant line had in average 4.8 novel *LORE1* insertions (Figure 4C). Interestingly, an inspection of the expression profiles in the sequences disrupted by *LORE1* insertion in the *Lotus* database, revealed that certain genes were transcriptionally induced during symbiotic associations with rhizobia or pathogens. Therefore, these

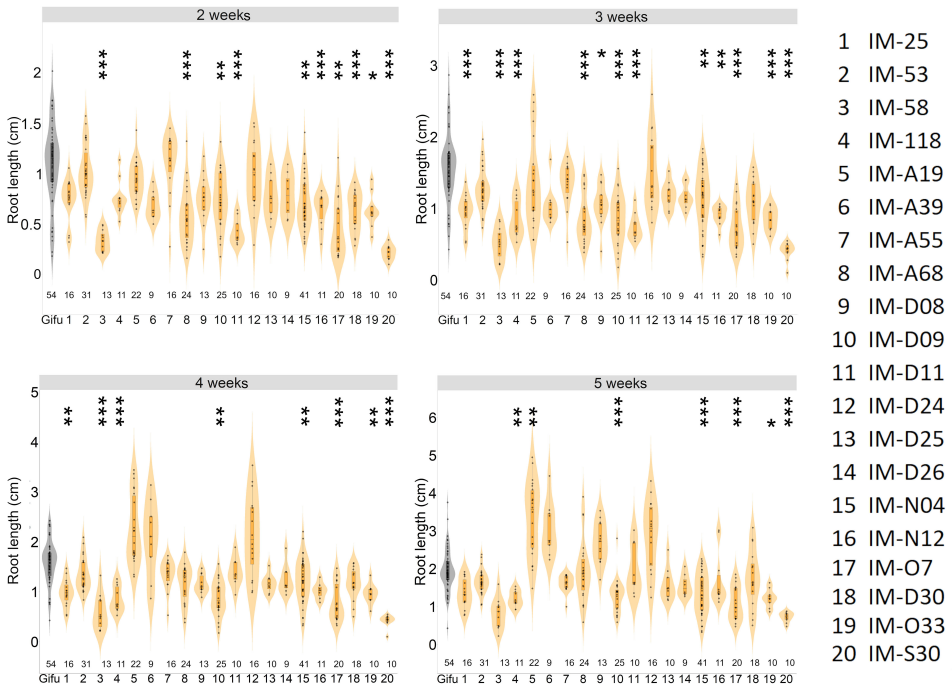

FIGURE 3
Differential root growth dynamics of *LORE1* mutants. The progression of main root growth on nitrogen-repleted medium was recorded in Gifu and *LORE1* lines at 2-5 weeks post-germination. In boxplots, the center line represents means values of 3 independent experiments; box limits, upper and lower quartiles; whiskers, 1.5× interquartile range; points represent individual data points. The number of plants tested is shown below the violin graphs. The asterisk indicates statistical significance between the *LORE1* mutants and Gifu according to Mann–Whitney U-test (*$P < 0.05$; **$P < 0.01$; ***$P < 0.001$).

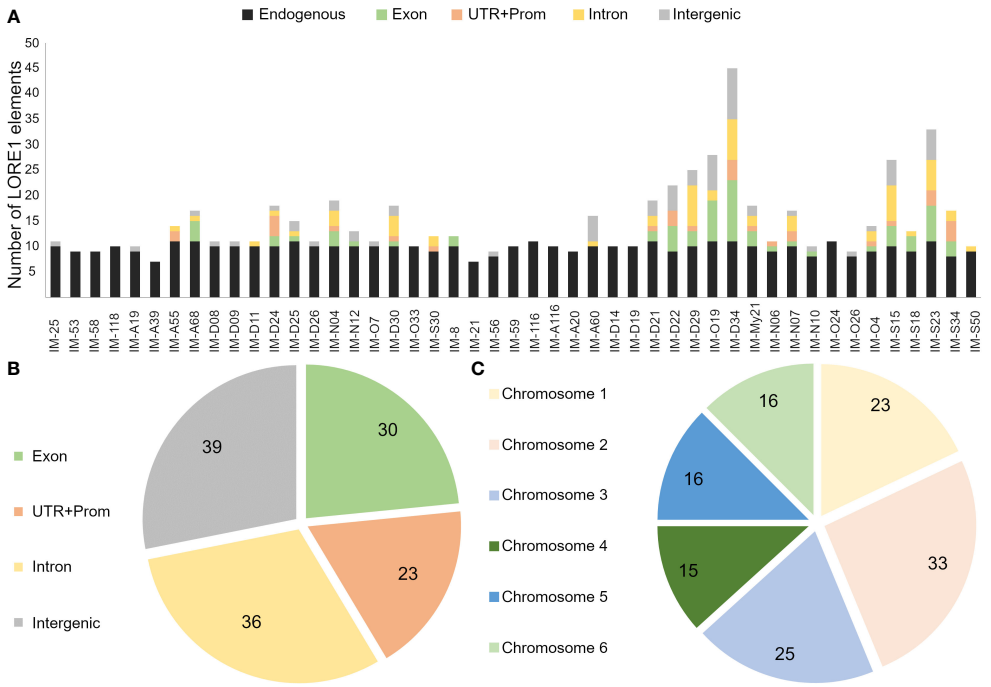

FIGURE 4
Distribution profile of retrotransposon elements in sequenced *LORE1* lines. **(A)** Number of different *LORE1* insertions detected in the genome of each mutant, including novel and endogenous elements. Venn diagrams with the number of unique *LORE1* elements found in exon, intron, UTR +Promoter, intergenic regions **(B)** and chromosomes **(C)**.

genes, interfered by *LORE1* elements, are potentially important for symbiosis (Supplementary Figure S5).

Additional mutations in *LORE1* lines

The nodulation kinetics showed that the IM-A39 mutant was unable to develop any nodules after *M. loti* and IRBG74 inoculation (Figure 2). Similarly, we noticed that IM-D22 and IM-N10 lines were Nod-. The *LORE1* mapping in these plants indicates that IM-D22 contained 13 novel *LORE1* insertions, one located in the first exon of *CYCLOPS*, a crucial transcription factor for the nodulation process (Yano et al., 2008). However, the IM-A39 mutant only had endogenous *LORE1* elements and the IM-N10 line contained one intergenic and one exonic insertion, that was not located in a known early symbiotic gene (Supplementary Table S1). These findings suggest that non-*LORE1*-mediated mutations occurred in IM-A39 and caused the Nod- phenotype. Nod- mutants have been previously documented by different research groups, and this condition is generally caused by the loss-of-function in the early symbiotic genes *NSP1, NSP2, NFR5, SYMRK, CCAMK, NIN* and *NFR1* (Schauser et al., 1999; Radutoiu et al., 2003; Kalo et al., 2005; Heckmann et al., 2006; Yano et al., 2008; Capoen et al., 2009; Singh et al., 2014). Specific primers were designed to amplify by PCR each gene from the start to the stop predicted codon, using as template genomic DNA. The expected amplicons were obtained for all the tested genes in the different genotypes, except for *NFR5* in IM-A39. In Gifu, IM-D22 and IM-N10 mutants, a PCR product of 1.7 Kb was amplified, while in IM-A39 the amplicon size was approximately 7 Kb (Figure 5). Sequencing of nested PCRs products for the *NFR5* gene in the IM-A39 line revealed a *LORE2* insertion within the gene. This finding indicates that additional genomic modifications occurred in some mutants.

Disruption of an *AUTOPHAGY9* gene affects the *Lotus*-rhizobia symbiosis

Identification of insertion sites in 47 selected *LORE1* mutants provided valuable information to discover genes associated with phenotype observed. This list was compared with a collection of homozygous mutants that we have developed in our group in recent years, by genotyping *LORE1* lines previously published (Malolepszy et al., 2016). We noticed that we had two additional mutant alleles for one of the insertions found in the IM-S34 line. This mutant contained a *LORE1* insertion in the 5´UTR of the predicted *AUTOPHAGY9* gene (*ATG9*), while the additional mutant alleles were affected by a retrotransposon element in the 5´UTR (*atg9*-2) and the second exon (*atg9*-3) (Figure 6A). This prompted us to evaluate if the symbiotic phenotype in the IM-S34 mutant (*atg9*-1) was caused by the disruption of *ATG9*. Importantly, the IM-S34 line had a low seed production and germination rate that impeded us in performing robust nodulation kinetics with *M. loti* and IRBG74. This phenotype was probably caused by additional *LORE1* elements detected in genes highly expressed in pod and seed (Supplementary Figure S6A). On contrary, *ATG9* was mainly expressed in nodules at

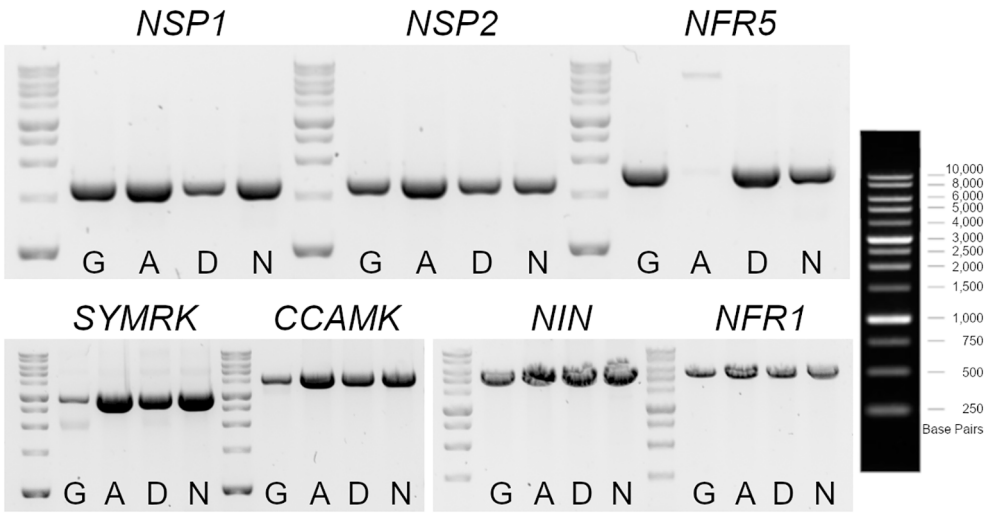

FIGURE 5
Genotyping of early symbiotic genes in *LORE1* mutants with a Nod- phenotype. Gel electrophoresis of PCR products amplified with specific oligonucleotides for *NSP1, NPS2, NFR5, SYMRK, CCAMK, NIN* and *NFR1*, using as template genomic DNA isolated from leaves of Gifu, IM-A39 (A), IM-D22 (D) and IM-N10 (N) plants. The amplicons encompass from the first to the last predicted codons for each gene. A larger fragment was obtained for the *NFR5* in the IM-A39 mutant, revealing a potential insertion within the gene.

21 dpi and induced in different root tissues at 10 dpi with *M. loti* (Supplementary Figure S6B; Frank et al., 2023).

The nodules numbers in the *atg9*-2 and *atg9*-3 mutants were recorded at 2-5 wpi with *M. loti* and IRBG74. In both mutants nodule development was delayed after IRBG74 inoculation, and the nodule numbers were significantly lower at 3-5 wpi with both rhizobial strains respect to Gifu (Figures 6B, C). Additionally, the nodules formed in these mutants were smaller and pale pink compared to Gifu (Figures 6D, E). The deficient nodulation in these mutants apparently had a negative impact on the growth of the plants harvested at 6 wpi with both inocula, since the shoot length was significantly shorter in *atg9*-2 and *atg9*-3 compared to Gifu (Figures 6F, H, I, K). Interestingly, the root length was affected in the mutants inoculated with IRBG74 but not with *M. loti* (Figures 6G, H, J, K). These results indicate that *LjATG9* directly or indirectly affects symbiotic program induced by *M. loti* and IRBG74.

Discussion

LORE1 lines: a valuable resource for mutant screening

The screening of legume mutants disturbed in the symbiotic association with rhizobia have provided relevant information on the complex genetic network required for rhizobial infection and nodule organogenesis in model legumes (Schauser et al., 1998; Catoira et al., 2001; Kawaguchi et al., 2002; Lombardo et al., 2006; Starker et al., 2006; Pislariu et al., 2012; Domonkos et al., 2013). In this study, we conducted a large forward mutant screen, with 200,000 *LORE1* lines, scoring plants affected in the nodulation program by IRBG74. A great advantage of this approach is the relatively simple and fast insertion site sequencing methodology for identification of causative *LORE1* insertions (Urbanski et al., 2012). Compared to map-based cloning, TILLING and whole genome resequencing (Hayashi et al., 2001; Sandal et al., 2002; Sandal et al., 2006; Uchida et al., 2011; Sandal et al., 2012), the FST poolit methods is cheap, robust and fast. Different reports indicate that *LORE1* elements have a significant higher preference for genic regions, representing 55-76% of the total novel insertions (Fukai et al., 2012; Urbanski et al., 2012; Malolepszy et al., 2016). Similarly, we observed in the 47 sequenced lines, that 71% of the novel *LORE1* copies were inserted in genic regions, distributed in the different chromosomes. We detected an average of 4.8 novel insertions per plant in our mutant collection, which is comparable to the 2.7-4.7 media described in previous studies (Fukai et al., 2012; Urbanski et al., 2012; Malolepszy et al., 2016). These results reflect the efficacy of the method employed and the persistence of the retrotransposon activity in the germline of the G329-3 line.

In our selected mutant collection, 92 *Lotus* genes with *LORE1* insertions were identified. The genes compromised belong to various molecular processes, where 63 of them showed the highest expression levels under symbiotic conditions. Interestingly, we detected in this gene list two members of the cellulose synthase family, LotjaGi6g1v0183200 and LotjaGi4g1v0062500. It was recently shown that mutants affected in a *CELLULOSE SYNTHASE-LIKE D1* (*CSLD1*) gene, develop abnormal root hairs and root nodule symbiosis (Karas et al., 2021). Among the genes affected by *LORE1* elements we also found LotjaGi3g1v0273500, which encodes a predicted RhoGEF protein that shares homology with LjSPK1. In Lotus, SPK1 interacts with ROP6 to coordinate the polarized growth of ITs (Liu et al., 2020). Additionally, we also identified known symbiotic players. The Nod- phenotype of the IM-D22 mutant, correlates with the *LORE1* element detected in the coding region of *CYCLOPS*, a key

10.3389/fpls.2023.1326766

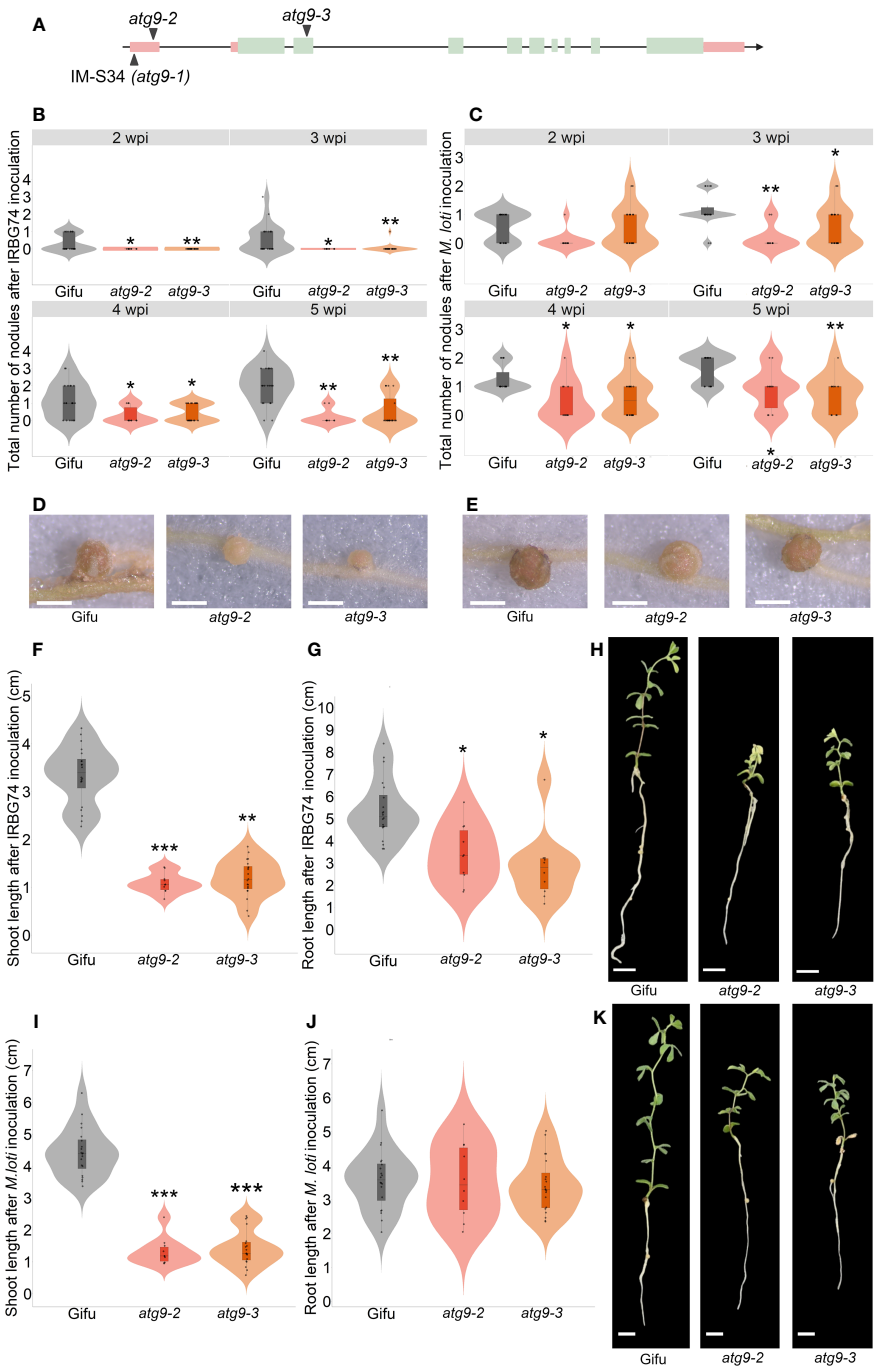

FIGURE 6
Nodulation, shoot and root phenotype of *atg9-2* and *atg9-3* mutants after inoculation with *M. loti* and IRBG74. **(A)** Scheme of the *LjATG9* gene structure. Pink rectangles, UTRs; Green rectangles, exons; Black lines, introns. Total number of nodules in Gifu (n=20), *atg9-2* (n=20) and *atg9-3* (n=10) at 2-6 wpi with IRBG74 **(B)** and *M. loti* **(C)**. Representative images of nodules formed in Gifu, *atg9-2* and *atg9-3* at 5 wpi with IRBG74 **(D)** and *M. loti* **(E)**. Scale, 1 mm. Root and shoot length measurements with representative images of Gifu, *atg9-2* and *atg9-3* at 6 wpi with IRBG74 **(F–H)** and *M. loti* **(I–K)**. Scale, 1 cm. In boxplots, the center line represents means values of 3 independent experiments; box limits, upper and lower quartiles; whiskers, 1.5× interquartile range; points represent individual data points. The asterisk indicates statistical significance between the *LORE1* mutants and Gifu according to Mann–Whitney U-test (*$P < 0.05$; **$P < 0.01$; ***$P < 0.001$).

transcription factor required for successful rhizobial infection and nodule organogenesis (Yano et al., 2008). However, we found that in 29% of the sequenced lines only the endogenous *LORE1* copies were detected and no additional *LORE1* insertions. This number is slightly higher to the 10-20% proportion observed in previous studies (Urbanski et al., 2012; Malolepszy et al., 2016). Therefore, the symbiotic phenotype in this set of mutants is likely mediated by non-*LORE1* mutations. This hypothesis is supported by the evidence obtained in the Nod- mutant IM-A39, where a *LORE2* element was detected in the coding region of *NFR5*, the NF receptor

(Radutoiu et al., 2003). This finding is not surprising since transposition of *LORE2* elements has been documented in regenerated Gifu plants (Fukai et al., 2008). In the Nod- mutant IM-N10, large insertions/deletions were not detected in the early symbiotic genes tested, however, we cannot exclude mutations in the flanking regions of the sequences or other mutations that might impact the ORF of the genes.

Novel LORE1 mutants interfered in the *Lotus*-IRBG74 symbiosis

In *Lotus*, the colonization by *M. loti* occurs via root-hair ITs, an intracellular infection process that has been extensively studied. However, a recent working model in *Lotus* was developed to study the intercellular infection in legumes, a largely unknown process that exists in approximately 25% of all the legume genera (Sprent, 2007). Although, the intra- and intercellular colonization in *Lotus* share some genetic components, remarkable differences have been observed among both processes (Quilbe et al., 2022). For instance, the *rinrk1* and *ern1* mutants show a more severe symbiotic phenotype with *M. loti* than with IRBG74 and by contrast, several cytoskeleton and cytokinin-related mutants are more affected in the intercellular infection (Copeland, 2021; Montiel et al., 2021). In this work, the large-scale mutant screening in boxes followed by a more stringent evaluation on plate led to the identification of 110 mutants potentially affected in the nodulation program induced by IRBG74, which colonizes *Lotus* intercellularly. A more detailed analysis in a subset of 20 mutants confirmed one of the selection criteria used in this study, since all the lines showed a significant shorter shoot length respect to Gifu after IRBG74 inoculation. Similarly, the nodule numbers were significantly reduced in 16 lines inoculated with IRBG74 in comparison to Gifu. Although the nodulation kinetics with IRBG74 was not affected in IM-53, IM-A19, IM-D25 and IM-O33 mutants, these lines showed symptoms of nitrogen starvation such as leaf chlorosis and shorter aerial part. Additionally, the nodule formation with *M. loti* was negatively impacted at different timepoints in IM-53, IM-A19 and IM-D25 lines. Only the nodulation performance of IM-O33 mutant was not affected with any rhizobial inoculum, and the compromised growth of the aerial part in this line is apparently not related to defects in mutualistic interactions with rhizobia, since the short size was also observed in nitrogen-replete conditions. The combined evidence indicates that our screening approaches showed a 95% success (19/20) to select novel mutants affected in the *Lotus*-rhizobia symbiosis, most of them perturbed in the symbiotic association of *Lotus* with IRBG74.

Role of *LjATG9* in nodulation

Autophagy is a complex coordinated process occurring in eukaryotic organisms, to degrade and recycle cytoplasmic material, which can be induced under adverse conditions, developmental processes, or pathogenic interactions (Wang et al., 2021). We found that in the IM-S34 mutant, a *LORE1* element was inserted in the 5´UTR of the *LjATG9* gene, a putative orthologue of *Arabidopsis thaliana ATG9*, which is a component of the autophagosome (Zhuang et al., 2017). The analysis performed in additional mutant alleles, *atg9*-2 and *atg9*-3, confirmed the relevance of *ATG9* in the symbiotic association of *Lotus* with *M. loti* and IRBG74. The role of autophagy has been marginally analyzed in the legume-rhizobia symbiosis, however, it was shown in *Phaseolus vulgaris* that silencing of the autophagy-related genes *PI3K* and *BECLIN1/ATG6*, results in aborted rhizobial infection in root hairs, and reduced nodule formation (Estrada-Navarrete et al., 2016). The recycling of cellular components during rhizobial infection and nodule organogenesis is likely to occur in this complex symbiotic process, however, further research is needed to unveil the precise mechanism of autophagy during legume-rhizobia symbiosis, including a deeper characterization of *LjATG9*.

Conclusion

L. japonicus is an excellent model legume with several characteristics that have facilitated the research of the legume-rhizobia symbiosis, including abundant expression data, genetic amenability and the Lotus Base, a portal that integrates transcriptomic and genomic data (Mun et al., 2016). These valuable features have been boosted with the generation of the *LORE1* mutant collection (Urbanski et al., 2012; Malolepszy et al., 2016). This resource has been widely employed by the scientific community to characterise genes-of-interest, since the retrotransposon elements can be tracked in the genome. In this study, we successfully exploited the germline activity of *LORE1a* and information in the *Lotus* base to identify novel mutants disturbed in the intercellular colonization of IRBG74 in *Lotus* roots. Importantly, the mapping of *LORE1* flanking sites revealed that uncharacterized genes transcriptionally upregulated during nodulation are likely associated to the phenotypes observed. These results reinforce the notion that certain molecular components are recruited by the plant host, depending on the infection mechanism, intracellular or intercellular. We also discovered that additional traits of interest can be tested with *LORE1* lines, such as plant development.

Data availability statement

The original contributions presented in the study are included in the article/Supplementary Material. Further inquiries can be directed to the corresponding authors.

Author contributions

IG-S: Conceptualization, Investigation, Methodology, Writing – original draft. SA: Conceptualization, Resources, Software, Supervision, Writing – review & editing. EM-M: Methodology, Writing – review & editing. MR-G: Methodology, Writing – review & editing. JG: Methodology, Writing – review & editing. NA-B:

Methodology, Writing – review & editing. MS: Funding acquisition, Resources, Writing – review & editing. JS: Conceptualization, Funding acquisition, Project administration, Resources, Supervision, Visualization, Writing – original draft, Writing – review & editing. JM: Conceptualization, Funding acquisition, Investigation, Methodology, Resources, Writing – original draft.

Funding

The author(s) declare financial support was received for the research, authorship, and/or publication of this article. This work was supported by the grant Engineering the Nitrogen Symbiosis for Africa made to the University of Cambridge by the Bill & Melinda Gates Foundation (ENSA; OPP11772165), the European Research Council (ERC) under the European Union's Horizon 2020 research and innovation programme (grant agreement no. 834221), the Dirección General de Asuntos del Personal Académico (DGAPA)-Universidad Nacional Autónoma de México (UNAM) – Programa de Apoyo a Proyectos de Investigación e Innovación Tecnológica (PAPIIT, grant IA200723). IG-S was granted with a PhD scholarship of CONACyT.

Acknowledgments

We thank Finn Pedersen and Nanna Walther with the assistance of *LORE1* mutant propagation at the greenhouse, and Noor de Jong, with the setup and screening of *LORE1* mutants.

Conflict of interest

The authors declare that the research was conducted in the absence of any commercial or financial relationships that could be construed as a potential conflict of interest.

The author(s) declared that they were an editorial board member of Frontiers, at the time of submission. This had no impact on the peer review process and the final decision.

Publisher's note

Supplementary material

The Supplementary Material for this article can be found online at: https://www.frontiersin.org/articles/10.3389/fpls.2023.1326766/full#supplementary-material

SUPPLEMENTARY TABLE 1
Mapping of *LORE1* elements in the mutant collection.

SUPPLEMENTARY TABLE 2
List of primers used for *LORE1* genome mapping and genotyping.

References

Bertioli, D. J., Jenkins, J., Clevenger, J., Dudchenko, O., Gao, D., Seijo, G., et al. (2019). The genome sequence of segmental allotetraploid peanut Arachis hypogaea. *Nat. Genet.* 51, 877–884. doi: 10.1038/s41588-019-0405-z

Broughton, W. J., and Dilworth, M. J. (1971). Control of leghemoglobin synthesis in snake beans. *Biochem. J.* 125, 1075–1080. doi: 10.1042/bj1251075

Capoen, W., Den Herder, J., Sun, J., Verplancke, C., De Keyser, A., De Rycke, R., et al. (2009). Calcium spiking patterns and the role of the calcium/calmodulin-dependent kinase CCaMK in lateral root base nodulation of Sesbania rostrata. *Plant Cell* 21, 1526–1540. doi: 10.1105/tpc.109.066233

Catoira, R., Timmers, A. C., Maillet, F., Galera, C., Penmetsa, R. V., Cook, D., et al. (2001). The HCL gene of Medicago truncatula controls Rhizobium-induced root hair curling. *Development* 128, 1507–1518. doi: 10.1242/dev.128.9.1507

Chaintreuil, C., Rivallan, R., Bertioli, D. J., Klopp, C., Gouzy, J., Courtois, B., et al. (2016). A gene-based map of the Nod factor-independent Aeschynomene evenia sheds new light on the evolution of nodulation and legume genomes. *DNA Res.* 23, 365–376. doi: 10.1093/dnares/dsw020

Chaudhary, J., Deshmukh, R., and Sonah, H. (2019). Mutagenesis approaches and their role in crop improvement. *Plants (Basel)* 8. doi: 10.3390/plants8110467

Chen, X., Lu, Q., Liu, H., Zhang, J., Hong, Y., Lan, H., et al. (2019). Sequencing of Cultivated Peanut, Arachis hypogaea, Yields Insights into Genome Evolution and Oil Improvement. *Mol. Plant* 12, 920–934. doi: 10.1016/j.molp.2019.03.005

Copeland, C. (2021). Same but different: examining the molecular mechanisms of intercellular rhizobial infection. *Plant Physiol.* 185, 754–756. doi: 10.1093/plphys/kiaa097

Cummings, S. P., Gyaneshwar, P., Vinuesa, P., Farruggia, F. T., Andrews, M., Humphry, D., et al. (2009). Nodulation of Sesbania species by Rhizobium (Agrobacterium) strain IRBG74 and other rhizobia. *Environ. Microbiol.* 11, 2510–2525. doi: 10.1111/j.1462-2920.2009.01975.x

Domonkos, A., Horvath, B., Marsh, J. F., Halasz, G., Ayaydin, F., Oldroyd, G. E., et al. (2013). The identification of novel loci required for appropriate nodule development in Medicago truncatula. *BMC Plant Biol.* 13, 157. doi: 10.1186/1471-2229-13-157

Downie, J. A. (2014). Legume nodulation. *Curr. Biol.* 24, R184–R190. doi: 10.1016/j.cub.2014.01.028

Estrada-Navarrete, G., Cruz-Mireles, N., Lascano, R., Alvarado-Affantranger, X., Hernandez-Barrera, A., Barraza, A., et al. (2016). An autophagy-related kinase is essential for the symbiotic relationship between phaseolus vulgaris and both rhizobia and arbuscular mycorrhizal fungi. *Plant Cell* 28, 2326–2341. doi: 10.1105/tpc.15.01012

Frank, M., Fechete, L. I., Tedeschi, F., Nadzieja, M., Norgaard, M. M. M., Montiel, J., et al. (2023). Single-cell analysis identifies genes facilitating rhizobium infection in Lotus japonicus. *Nat. Commun.* 14, 7171. doi: 10.1038/s41467-023-42911-1

Fukai, E., Dobrowolska, A. D., Madsen, L. H., Madsen, E. B., Umehara, Y., Kouchi, H., et al. (2008). Transposition of a 600 thousand-year-old LTR retrotransposon in the model legume Lotus japonicus. *Plant Mol. Biol.* 68, 653–663. doi: 10.1007/s11103-008-9397-2

Fukai, E., Soyano, T., Umehara, Y., Nakayama, S., Hirakawa, H., Tabata, S., et al. (2012). Establishment of a Lotus japonicus gene tagging population using the exon-targeting endogenous retrotransposon LORE1. *Plant J.* 69, 720–730. doi: 10.1111/j.1365-313X.2011.04826.x

Fukai, E., Umehara, Y., Sato, S., Endo, M., Kouchi, H., Hayashi, M., et al. (2010). Derepression of the plant Chromovirus LORE1 induces germline transposition in regenerated plants. *PloS Genet.* 6, e1000868. doi: 10.1371/journal.pgen.1000868

Gossmann, J. A., Markmann, K., Brachmann, A., Rose, L. E., and Parniske, M. (2012). Polymorphic infection and organogenesis patterns induced by a Rhizobium leguminosarum isolate from Lotus root nodules are determined by the host genotype. *New Phytol.* 196, 561–573. doi: 10.1111/j.1469-8137.2012.04281.x

Handberg, K., and Stougaard, J. (1992). Lotus japonicus, an autogamous, diploid legume species for classical and molecular genetics. *Plant J.* 2, 487–496. doi: 10.1111/j.1365-313X.1992.00487.x

Hayashi, M., Miyahara, A., Sato, S., Kato, T., Yoshikawa, M., Taketa, M., et al. (2001). Construction of a genetic linkage map of the model legume Lotus japonicus using an intraspecific F2 population. *DNA Res.* 8, 301–310. doi: 10.1093/dnares/8.6.301

Heckmann, A. B., Lombardo, F., Miwa, H., Perry, J. A., Bunnewell, S., Parniske, M., et al. (2006). Lotus japonicus nodulation requires two GRAS domain regulators, one of which is functionally conserved in a non-legume. *Plant Physiol.* 142, 1739–1750. doi: 10.1104/pp.106.089508

Kalo, P., Gleason, C., Edwards, A., Marsh, J., Mitra, R. M., Hirsch, S., et al. (2005). Nodulation signaling in legumes requires NSP2, a member of the GRAS family of transcriptional regulators. *Science* 308, 1786–1789. doi: 10.1126/science.1110951

Kamal, N., Mun, T., Reid, D., Lin, J. S., Akyol, T. Y., Sandal, N., et al. (2020). Insights into the evolution of symbiosis gene copy number and distribution from a chromosome-scale Lotus japonicus Gifu genome sequence. *DNA Res.* 27. doi: 10.1093/dnares/dsaa015

Karas, B. J., Ross, L., Novero, M., Amyot, L., Shrestha, A., Inada, S., et al. (2021). Intragenic complementation at the Lotus japonicus CELLULOSE SYNTHASE-LIKE D1 locus rescues root hair defects. *Plant Physiol.* 186, 2037–2050. doi: 10.1093/plphys/kiab204

Karmakar, K., Kundu, A., Rizvi, A. Z., Dubois, E., Severac, D., Czernic, P., et al. (2019). Transcriptomic analysis with the progress of symbiosis in 'Crack-entry' Legume arachis hypogaea highlights its contrast with 'Infection thread' Adapted legumes. *Mol. Plant Microbe Interact.* 32, 271–285. doi: 10.1094/MPMI-06-18-0174-R

Kawaguchi, M., Imaizumi-Anraku, H., Koiwa, H., Niwa, S., Ikuta, A., Syono, K., et al. (2002). Root, root hair, and symbiotic mutants of the model legume Lotus japonicus. *Mol. Plant Microbe Interact.* 15, 17–26. doi: 10.1094/MPMI.2002.15.1.17

Liu, J., Liu, M. X., Qiu, L. P., and Xie, F. (2020). SPIKE1 activates the GTPase ROP6 to guide the polarized growth of infection threads in lotus japonicus. *Plant Cell* 32, 3774–3791. doi: 10.1105/tpc.20.00109

Lombardo, F., Heckmann, A. B., Miwa, H., Perry, J. A., Yano, K., Hayashi, M., et al. (2006). Identification of symbiotically defective mutants of Lotus japonicus affected in infection thread growth. *Mol. Plant Microbe Interact.* 19, 1444–1450. doi: 10.1094/MPMI-19-1444

Madsen, L. H., Fukai, E., Radutoiu, S., Yost, C. K., Sandal, N., Schauser, L., et al. (2005). LORE1, an active low-copy-number TY3-gypsy retrotransposon family in the model legume Lotus japonicus. *Plant J.* 44, 372–381. doi: 10.1111/j.1365-313X.2005.02534.x

Malolepszy, A., Mun, T., Sandal, N., Gupta, V., Dubin, M., Urbanski, D., et al. (2016). The LORE1 insertion mutant resource. *Plant J.* 88, 306–317. doi: 10.1111/tpj.13243

Mikkers, H., Allen, J., Knipscheer, P., Romeijn, L., Hart, A., Vink, E., et al. (2002). High-throughput retroviral tagging to identify components of specific signaling pathways in cancer. *Nat. Genet.* 32, 153–159. doi: 10.1038/ng950

Montiel, J., Garcia-Soto, I., James, E. K., Reid, D., Cardenas, L., Napsucialy-Mendivil, S., et al. (2023). Aromatic amino acid biosynthesis impacts root hair development and symbiotic associations in Lotus japonicus. *Plant Physiol.* 193, 1508–1526. doi: 10.1093/plphys/kiad398

Montiel, J., Reid, D., Gronbaek, T. H., Benfeldt, C. M., James, E. K., Ott, T., et al. (2021). Distinct signaling routes mediate intercellular and intracellular rhizobial infection in Lotus japonicus. *Plant Physiol.* 185, 1131–1147. doi: 10.1093/plphys/kiaa049

Mun, T., Bachmann, A., Gupta, V., Stougaard, J., and Andersen, S. U. (2016). Lotus Base: An integrated information portal for the model legume Lotus japonicus. *Sci. Rep.* 6, 39447. doi: 10.1038/srep39447

Peng, Z., Liu, F., Wang, L., Zhou, H., Paudel, D., Tan, L., et al. (2017). Transcriptome profiles reveal gene regulation of peanut (Arachis hypogaea L.) nodulation. *Sci. Rep.* 7, 40066. doi: 10.1038/srep40066

Pislariu, C. I., Murray, J. D., Wen, J., Cosson, V., Muni, R. R., Wang, M., et al. (2012). A Medicago truncatula tobacco retrotransposon insertion mutant collection with defects in nodule development and symbiotic nitrogen fixation. *Plant Physiol.* 159, 1686–1699. doi: 10.1104/pp.112.197061

Quilbe, J., Lamy, L., Brottier, L., Leleux, P., Fardoux, J., Rivallan, R., et al. (2021). Genetics of nodulation in Aeschynomene evenia uncovers mechanisms of the rhizobium-legume symbiosis. *Nat. Commun.* 12, 829. doi: 10.1038/s41467-021-21094-7

Quilbe, J., Montiel, J., Arrighi, J. F., and Stougaard, J. (2022). Molecular mechanisms of intercellular rhizobial infection: novel findings of an ancient process. *Front. Plant Sci.* 13, 922982. doi: 10.3389/fpls.2022.922982

Radutoiu, S., Madsen, L. H., Madsen, E. B., Felle, H. H., Umehara, Y., Gronlund, M., et al. (2003). Plant recognition of symbiotic bacteria requires two LysM receptor-like kinases. *Nature* 425, 585–592. doi: 10.1038/nature02039

Raul, B., Bhattacharjee, O., Ghosh, A., Upadhyay, P., Tembhare, K., Singh, A., et al. (2022). Microscopic and transcriptomic analyses of dalbergoid legume peanut reveal a divergent evolution leading to nod-factor-dependent epidermal crack-entry and terminal bacteroid differentiation. *Mol. Plant Microbe Interact.* 35, 131–145. doi: 10.1094/MPMI-05-21-0122-R

Rogers, S. O., and Bendich, A. J. (1985). Extraction of DNA from milligram amounts of fresh, herbarium and mummified plant tissues. *Plant Mol. Biol.* 5, 69–76. doi: 10.1007/BF00020088

Roy, S., Liu, W., Nandety, R. S., Crook, A., Mysore, K. S., Pislariu, C. I., et al. (2020). Celebrating 20 years of genetic discoveries in legume nodulation and symbiotic nitrogen fixation. *Plant Cell* 32, 15–41. doi: 10.1105/tpc.19.00279

Sandal, N., Jin, H., Rodriguez-Navarro, D. N., Temprano, F., Cvitanich, C., Brachmann, A., et al. (2012). A set of Lotus japonicus Gifu x Lotus burttii recombinant inbred lines facilitates map-based cloning and QTL mapping. *DNA Res.* 19, 317–323. doi: 10.1093/dnares/dss014

Sandal, N., Krusell, L., Radutoiu, S., Olbryt, M., Pedrosa, A., Stracke, S., et al. (2002). A genetic linkage map of the model legume Lotus japonicus and strategies for fast mapping of new loci. *Genetics* 161, 1673–1683. doi: 10.1093/genetics/161.4.1673

Sandal, N., Petersen, T. R., Murray, J., Umehara, Y., Karas, B., Yano, K., et al. (2006). Genetics of symbiosis in Lotus japonicus: recombinant inbred lines, comparative genetic maps, and map position of 35 symbiotic loci. *Mol. Plant Microbe Interact.* 19, 80–91. doi: 10.1094/MPMI-19-0080

Schauser, L., Handberg, K., Sandal, N., Stiller, J., Thykjaer, T., Pajuelo, E., et al. (1998). Symbiotic mutants deficient in nodule establishment identified after T-DNA transformation of Lotus japonicus. *Mol. Gen. Genet.* 259, 414–423. doi: 10.1007/s004380050831

Schauser, L., Roussis, A., Stiller, J., and Stougaard, J. (1999). A plant regulator controlling development of symbiotic root nodules. *Nature* 402, 191–195. doi: 10.1038/46058

Singh, S., Katzer, K., Lambert, J., Cerri, M., and Parniske, M. (2014). CYCLOPS, a DNA-binding transcriptional activator, orchestrates symbiotic root nodule development. *Cell Host Microbe* 15, 139–152. doi: 10.1016/j.chom.2014.01.011

Sprent, J. I. (2007). Evolving ideas of legume evolution and diversity: a taxonomic perspective on the occurrence of nodulation. *New Phytol.* 174, 11–25. doi: 10.1111/j.1469-8137.2007.02015.x

Starker, C. G., Parra-Colmenares, A. L., Smith, L., Mitra, R. M., and Long, S. R. (2006). Nitrogen fixation mutants of Medicago truncatula fail to support plant and bacterial symbiotic gene expression. *Plant Physiol.* 140, 671–680. doi: 10.1104/pp.105.072132

Tadege, M., Wen, J., He, J., Tu, H., Kwak, Y., Eschstruth, A., et al. (2008). Large-scale insertional mutagenesis using the Tnt1 retrotransposon in the model legume Medicago truncatula. *Plant J.* 54, 335–347. doi: 10.1111/j.1365-313X.2008.03418.x

Uchida, N., Sakamoto, T., Kurata, T., and Tasaka, M. (2011). Identification of EMS-induced causal mutations in a non-reference Arabidopsis thaliana accession by whole genome sequencing. *Plant Cell Physiol.* 52, 716–722. doi: 10.1093/pcp/pcr029

Urbanski, D. F., Malolepszy, A., Stougaard, J., and Andersen, S. U. (2012). Genome-wide LORE1 retrotransposon mutagenesis and high-throughput insertion detection in Lotus japonicus. *Plant J.* 69, 731–741. doi: 10.1111/j.1365-313X.2011.04827.x

Wang, P., Wang, T., Han, J., Li, M., Zhao, Y., Su, T., et al. (2021). Plant autophagy: an intricate process controlled by various signaling pathways. *Front. Plant Sci.* 12, 754982. doi: 10.3389/fpls.2021.754982

Yano, K., Yoshida, S., Muller, J., Singh, S., Banba, M., Vickers, K., et al. (2008). CYCLOPS, a mediator of symbiotic intracellular accommodation. *Proc. Natl. Acad. Sci. U.S.A.* 105, 20540–20545. doi: 10.1073/pnas.0806858105

Zarrabian, M., Montiel, J., Sandal, N., Ferguson, S., Jin, H., Lin, Y. Y., et al. (2022). A promiscuity locus confers Lotus burttii nodulation with rhizobia from five different genera. *Mol. Plant Microbe Interact* 11, 1006–1017. doi: 10.1094/MPMI-06-22-0124-R

Zhuang, X., Chung, K. P., Cui, Y., Lin, W., Gao, C., Kang, B. H., et al. (2017). ATG9 regulates autophagosome progression from the endoplasmic reticulum in Arabidopsis. *Proc. Natl. Acad. Sci. U.S.A.* 114, E426–E435. doi: 10.1073/pnas.1616299114

frontiers | Frontiers in Plant Science

TYPE Original Research
PUBLISHED 11 January 2024
DOI 10.3389/fpls.2023.1334190

OPEN ACCESS

EDITED BY
Senjuti Sinharoy,
National Institute of Plant Genome Research (NIPGR), India

REVIEWED BY
Anindya Kundu,
National Institute of Agricultural Botany (NIAB), United Kingdom
Oswaldo Valdes-Lopez,
National Autonomous University of Mexico, Mexico

*CORRESPONDENCE
Julia Frugoli
jfrugol@clemson.edu

RECEIVED 06 November 2023
ACCEPTED 18 December 2023
PUBLISHED 11 January 2024

CITATION
Thomas J and Frugoli J (2024) Mutation of *BAM2* rescues the *sunn* hypernodulation phenotype in *Medicago truncatula*, suggesting that a signaling pathway like CLV1/BAM in *Arabidopsis* affects nodule number. *Front. Plant Sci.* 14:1334190. doi: 10.3389/fpls.2023.1334190

Mutation of *BAM2* rescues the *sunn* hypernodulation phenotype in *Medicago truncatula*, suggesting that a signaling pathway like CLV1/BAM in *Arabidopsis* affects nodule number

Jacklyn Thomas and Julia Frugoli*

Department of Genetics and Biochemistry, Clemson University, Clemson, SC, United States

The unique evolutionary adaptation of legumes for nitrogen-fixing symbiosis leading to nodulation is tightly regulated by the host plant. The autoregulation of nodulation (AON) pathway negatively regulates the number of nodules formed in response to the carbon/nitrogen metabolic status of the shoot and root by long-distance signaling to and from the shoot and root. Central to AON signaling in the shoots of *Medicago truncatula* is SUNN, a leucine-rich repeat receptor-like kinase with high sequence similarity with CLAVATA1 (CLV1), part of a class of receptors in *Arabidopsis* involved in regulating stem cell populations in the root and shoot. This class of receptors in *Arabidopsis* includes the BARELY ANY MERISTEM family, which, like CLV1, binds to CLE peptides and interacts with CLV1 to regulate meristem development. *M. truncatula* contains five members of the *BAM* family, but only *MtBAM1* and *MtBAM2* are highly expressed in the nodules 48 hours after inoculation. Plants carry mutations in individual *MtBAM*s, and several double *BAM* mutant combinations all displayed wild-type nodule number phenotypes. However, *Mtbam2* suppressed the *sunn-5* hypernodulation phenotype and partially rescued the short root length phenotype of *sunn*-5 when present in a *sunn-5* background. Grafting determined that *bam2* suppresses supernodulation from the roots, regardless of the *SUNN* status of the root. Overexpression of *MtBAM2* in wild-type plants increases nodule numbers, while overexpression of *MtBAM2* in some *sunn* mutants rescues the hypernodulation phenotype, but not the hypernodulation phenotypes of AON mutant *rdn1-2* or *crn*. Relative expression measurements of the nodule transcription factor MtWOX5 downstream of the putative *bam2 sunn-5* complex revealed disruption of meristem signaling; while both *bam2* and *bam2 sunn-5* influence *MtWOX5* expression, the expression changes are in different directions. We propose a genetic model wherein the specific root interactions of BAM2/SUNN are critical for signaling in nodule meristem cell homeostasis in *M. truncatula*.

KEYWORDS

nodulation, meristems, autoregulation of nodulation, *M. truncatula*, BAM, SUNN

1 Introduction

Legumes tightly control nitrogen-fixing symbioses leading to nodulation. The autoregulation of nodulation (AON) pathway negatively regulates the number of nodules formed in response to the metabolic status of the shoot (carbon) and root (nitrogen) (reviewed in Ferguson et al., 2019; Chaulagain & Frugoli, 2021). Genetic analysis has identified multiple genes that when mutated cause plants to hypernodulate, evidence of a network of regulation in AON from both the root and the shoot (reviewed in Roy et al., 2020).

In AON, very early after rhizobial infection, expression of a subset of genes encoding the CLAVATA3/Embryo Surrounding Region (CLE) peptides, *MtCLE12* and *MtCLE13* in *Medicago truncatula*, is induced (Mortier et al., 2010). In *Lotus japonicus*, a similar increase upon infection is observed in the LjCLE-root signaling (RS)1, LjCLE-RS2, and LjCLE-RS3 peptide-encoding genes (Okamoto et al., 2009; Nishida et al., 2016; Hastwell et al., 2017). These CLE peptides are 12–13 amino acids in length and are signaling peptides derived from the C-terminal region of pre-proproteins (Araya et al., 2016; Yamaguchi et al., 2016). In *Arabidopsis thaliana*, CLE function is associated with regulating cell proliferation and differentiation during development, especially in the shoot and root apical meristems. In *M. truncatula*, the MtCLE12 peptide has been shown genetically to be modified by an enzyme from the hydroxyproline *O*-arabinosyltransferase (HPAT) family encoded by the *M. truncatula ROOT DETERMINED NODULATION1* (*RDN1*) gene (Kassaw et al., 2017); the mutation of *RDN1* produces a supernodulation phenotype (Schnabel et al., 2011). After nodulation-suppressing CLE peptides are processed, they travel through the xylem to the shoot where they are perceived by a homo- or heterodimeric receptor complex, likely in the parenchyma cells of the vasculature (Kassaw et al., 2017).

Central to this receptor complex is a shoot-acting leucine-rich repeat (LRR) RLK, known as SUPER NUMERARY NODULES (SUNN) in M. truncatula, HYPERNODULATION ABBERANT ROOT FORMATION (HAR1) in L. japonicus, NODULE AUTOREGULATION RECEPTOR KINASE (NARK) in Glycine max, and SYMBIOSIS29 (SYM29) in Pisum sativum (Krusell et al., 2002; Searle et al., 2003; Schnabel et al., 2005). Mutations in the MtSUNN gene produce a hypernodulation phenotype and altered root development (Schnabel et al., 2005). A shoot-controlled increase in nodulation is also observed in the MtCORYNE Tnt1 insertion mutant (crn) of M. truncatula (Crook et al., 2016), as well as the klv mutant (Oka-Kira et al., 2005) and the clv2 mutant (Krusell et al., 2011) in L. japonicus. Bimolecular fluorescence analysis showed that SUNN forms heteromomers with homologous CLV1-interacting proteins CLAVATA2 (CLV2), CORYNE (CRN), and KLAVIER (KLV) (Oka-Kira et al., 2005; Miyazawa et al., 2010; Krusell et al., 2011; Crook et al., 2016). Genetic studies of a hypernodulating mutant in L. japonicus identified a root-responsive gene TOO MUCH LOVE (TML) that regulates nodule numbers in the root from shoot-derived signaling (Magori et al., 2009; Takahara et al., 2013). Knockdown of two TML genes, MtTML1 and MtTML2, showed increased nodule number, suggesting a role for these genes in AON (Gautrat et al., 2019).

Leucine-rich repeat receptor-like kinases (LRR-RLKs) are important in meristem development in most land plants. The similarity between symbiotic AON receptors and their *Arabidopsis* meristem regulating counterparts like RPK2 (Kinoshita et al., 2010) suggests that like the shoot apical meristem (SAM) and root apical meristem (RAM), LRR-RLK complexes are involved in AON signaling to nodule meristems (Krusell et al., 2002; Crook et al., 2016). Some (but not all) legume *CLV2* and *RPK2*-related mutants show defects in the SAM, but the *sunn Atclv1*-related mutants do not have SAM defects, indicating overlapping receptor complexes controlling SAM activity and nodule numbers in legumes (Krusell et al., 2002; Schnabel et al., 2005).

Since similar molecules regulate shoot, root, and nodule meristems, we wondered if BAMs, which have not yet been linked to AON in any legume, could be involved in the regulation of the nodule meristem. The *Arabidopsis* BAMs bind to a wider range of CLE peptides and show more diverse expression patterns compared to CLV1 (reviewed in Yamaguchi et al., 2016). We reasoned that studying *BAM* expression in *M. truncatula* could expand our understanding of plant receptor interacting partners' expression levels and location effects during signal transduction pathways. Since AtCLV1 forms a complex with AtBAMs, MtSUNN might form a complex with MtBAMs to control nodule numbers. Mutational and overexpression experiments of the *M. truncatula BAM* gene family reported below support a model in which the genetic interaction of BAM2 and SUNN provides a signal to limit nodulation.

2 Materials and methods

2.1 Phylogenetic analysis

The tree was constructed with MEGA X using the maximum likelihood method (Kumar et al., 2018) with bootstrap replicates n = 1,000. The analysis involved 21 amino acid sequences summarized in Supplementary Table 1 for a total of 1,107 positions in the final dataset, with AtCLV1 used to root the tree.

2.2 Mutant line screening

The *Tnt-1* mutant lines were isolated from populations of insertion lines obtained from the Nobel Foundation Medicago Mutant Database now located at https://medicagomutant.dasnr.okstate.edu/mutant/index.php described in Tadege et al. (2008). The following *Tnt-1* mutant pools were used in this study: *Mtbam1* (NF2153), *Mtbam2* (NF7126), *Mtbam3* (NF2071), *Mtbam4* (NF2835), *Mtbam5* (NF2488), and *sunn-5* (NF2262). Initial PCR screening from pools of *Tnt1* insertions in *M. truncatula BAMs* was carried out to identify plants carrying the insertion in a BAM gene using PCR from genomic DNA. Two primer sets for each gene were designed specifically for capturing

the wild-type allele and another specific to flanking regions of the *Tnt1* insert and *Tnt1* forward primer (see Supplementary Table 2). Plants identified as carrying an insertion were selfed, and the next generation was screened using PCR to obtain single homozygous mutants for all five *BAM*s from the *Tnt-1* pools. Each homozygous mutant was backcrossed to the parental R108 ecotype and reisolated, following the inheritance of the insertion via PCR.

2.3 PCR to identify single and double mutants and *sunn-5* structure

A leaf press was made by pressing a leaflet of each plant to a Plant Card (Whatman™, GE Healthcare UK Limited, Amersham, UK) according to the manufacturer's instructions for long-term storage. A 1.2-mm-diameter piece of Plant Card was excised and washed with Whatman™ FTA Purification Reagent (GE Healthcare UK Limited, UK) followed by TE-1 buffer according to the manufacturer's instructions and directly used in PCR. The 10-µL PCR used to identify single and double mutants contained 2 µL of gDNA (equivalent to 100 ng RNA), 1 mm each primer, 0.2 mm dNTPs, 1× colorless Go*Taq* buffer, and 1 U Go*Taq* (Promega, Madison, WI, USA) with cycling conditions of 95°C for 2 min followed by 40 cycles of 95°C for 5 sec, 55°C for 10 sec, and 72°C for 20 sec. Sequencing of *sunn-5* was performed using PCR products amplified from cDNA using pairs of gene-specific primers for sequences JF7092, JF7093, and JF7094 and a *Tnt-1* specific primer for JF7091 as referred to in Supplementary Figure 1. PCR conditions were 95°C for 2 min followed by 35 cycles of 95°C for 30 sec, 55°C for 30 sec, and 72°C for 4 min. Sequencing was performed by Arizona Life Sciences.

2.4 Plant crossing

Two pairs of fine-tip forceps (HL-14 #5, Buy in Coins Promotion) and straight-edge scalpels (scalpel blade handle 9303 #3 and scalpel blade 9311 #11, both from Microscopes America, Cumming, GA, USA) were used for keel petal incision and the removal of anthers from the unopened female flower bud and artificial cross-pollination (Veerappan et al., 2014). The mature pods from the successful cross-pollinations were wrapped using micro-perforated polythene sheets (MP1120160T, Prism Pak, Berwick PA, USA) to dry on the plant before harvesting at desiccation. The following crosses were successfully performed and the F2 was screened for double mutants: *bam2* × *bam3*, *bam2* × *bam4*, *bam5* × *bam4*, *bam2* × *sunn-5*, *bam3* × *sunn-5*, and *bam3* × *sunn-5*.

2.5 Plant growth conditions and materials

The identified homozygous *bam* mutants used for making genetic crosses were grown in a greenhouse, with supplemental lighting to create a 14:10 light:dark (L:D) cycle, a nightly minimum of 18°C, and a daily maximum between 21°C and 27°C. For nodulation screening, the following seeds were used: *M. truncatula* wild-type Jemalong A17; the AON-defective mutants *rdn1-2* (Schnabel et al., 2011), *sunn-1*, and *sunn-4* (Schnabel et al., 2005); and *M. truncatula* wild-type R108 and *Tnt1* mutants *bam1-5* (this work), *crn* (Crook et al., 2016), and *cra2* (Huault et al., 2014) in the R108 genetic background (Garmier et al., 2017). Seeds were removed from the pods and scarified in sulfuric acid for 8 min, rinsed five times in dH_2O, imbibed in dH_2O for 2–3 hours at room temperature, then placed at 4°C for 48–72 hours in the dark to synchronize germination, and allowed to germinate for 1 day at room temperature. This procedure as well as the growth in an aeroponic apparatus is described in Cai et al. (2023). Inoculation of all whole plants screened for nodulation phenotypes was carried out using *Sinorhizobium meliloti* RM41 (Luyten and Vanderleyden, 2000) for the R108 ecotype with 6 mL each of an OD_{600} = 0.2 culture, and data were collected 14 days post inoculation (dpi). The apparatus was subjected to 14:10 L:D conditions and maintained at room temperature. Nodule number comparisons of wild-type R108 plants and hypernodulating *sunn-5* plants to individual single *bams* plants, *bam* double-mutant plants, and *bam sunn-5* plants were carried out by visual count of individual plant roots using head-mounted magnification glasses.

Transgenic hairy root plants made with *Agrobacterium rhizogenes* containing the gene constructs described below or the empty vector were grown in TY (selection 25 µg/mL kanamycin) and used for hairy root transformation as described in Limpens et al. (2004). Inoculated seedlings were grown on plates containing modified HMF (Huo et al., 2006). The plates were incubated flat in the growth chamber at 20°C for 3 days to facilitate transformation and then moved to 25°C to facilitate root growth for 2–3 weeks. Transformed roots expressing the DsRED fluorescence marker were identified on the Olympus SZH-10 stereoscopic system (excitation 540 nm; emission detected at 570–625 nm), and untransformed roots were removed. The plants with transformed roots were then grown in perlite for 2 weeks before being used for the nodulation assay described in Kassaw et al. (2017) by inoculation using *Sinorhizobium medicae* strain ABS7 (Leong et al., 1985; Bekki et al., 1987) for A17 plants or *S. meliloti* RM41 as described in Kassaw and Frugoli (2012). Nodules were counted at 14 dpi.

Grafting was performed following the protocol of Kassaw and Frugoli (2012), and grafted plants were allowed to grow in the growth chamber at 20°C with a 16-hour photoperiod for 3 days to facilitate transformation and then moved to 25°C with a 16-hour photoperiod to facilitate root growth for 2–3 weeks. Plants were transferred to pots filled with washed, autoclaved perlite and maintained on a light bench with (14:10 L:D) cycle and temperatures between 21°C and 24°C. Plants were watered daily with a 100-fold dilution of water-soluble 20:10:20 (N:P: K) Peat-Lite Special fertilizer (Scotts Company, Marysville, OH, USA) for 5 days. After an additional 4 days of nutrient starvation induced by watering with water alone, the plants were used for inoculation experiments using *S. medicae Rm41*, and nodule number was assessed at 14 dpi. The survival rate for all grafted plants was approximately 40%–50% except for *sunn-5* shoot-to-*sunn-5*

root plants, which was approximately 10%–20%. The reduced survival of *sunn* self-grafts is common in both our laboratory and others due to disrupted auxin homeostasis in *sunn* mutants (van Noorden et al., 2006).

2.5.1 Creation of *BAM* overexpression constructs

The *MtBAM1*, *MtBAM2*, and *MtBAM3* sequences were amplified from *M. truncatula* R108 cDNA using overlap PCR with the primers listed in Supplementary Table 2. Using overlap extension PCR allowed for the cloning of large fragments by fusing two gene halves together to generate large transcripts for cloning (Simionatto et al., 2009). Each transcript was amplified using the following PCRs (10 µL) that contained 2 µL of cDNA (equivalent to 100 ng RNA), 1 mm of each primer, 0.2 mm dNTPs, 1× colorless Go*Taq* buffer, and 1 U Go*Taq* (Promega, Madison, WI, USA) with cycling conditions of 95°C for 2 min followed by 40 cycles of 95°C for 5 sec, 55°C for 10 sec, and 72°C for 20 sec. PCR products were gel extracted and purified using the Zymoclean gel DNA recovery kit (Zymo Research, Irvine, CA, USA). The PCR products were then digested with *Kpn*I and *Spe*I restriction enzymes and ligated into the *Kpn*I and *Spe*I sites of the pCDsRed/35S vector (Karimi et al., 2002) under the control of the 35S promoter using *Escherichia coli DH5α* cells. The construct was confirmed by sequencing and transferred to *A. rhizogenes* strain *ArQUA1* (Quandt and Hynes, 1993) by electroporation for use in hairy root transformation.

2.6 *A. rhizogenes*-mediated plant transformation

Seedlings were transformed as described by Limpens et al. (2004). The hypocotyls of 5-day-old seedlings were cut and transformed by lightly scraping on the surface of Luria–Bertani plates densely grown with *A. rhizogenes* strain *ArQUA1* (Quandt and Hynes, 1993) containing the appropriate binary vector and antibiotic selections at 30°C for 48 hours. After 5 days of cocultivation with the *A. rhizogenes* in the growth chamber at 23°C at 16:8 L:D, the seedlings were transferred to a nutrient-rich hairy root emergence medium (Limpens et al., 2004) containing 300 µg/mL cefotaxime (Phytotechnology Laboratories, St. Lenexa, KS, USA) sandwiched between two half-round Whatman filter papers grown under the same growth conditions. Five days later, the top filter papers were removed from the plates, and the seedlings were allowed to grow for an additional 5 days on the same emergence medium placed vertically in the same growth chamber. Transformed roots expressing the DsRED fluorescence marker were identified on Olympus SZH-10 stereoscopic system (excitation 540 nm; emission detected at 570–625 nm), untransformed roots were removed as described in Kassaw and Frugoli (2012), and plants were transferred to perlite. For acclimation to perlite, plants were watered for 5 days with a 100-fold dilution of water-soluble 20:10:20 Peat-Lite Special fertilizer (Scotts). Fertilization was then withdrawn, and the plants were hydrated with water alone for an additional 5 days to induce the nitrogen deficiency required for nodulation. Plants were then inoculated with *S. meliloti* RM41 or *S. medicae* ABS7 according to ecotype, with 6 mL each of an OD_{600} = 0.2 culture, and data were collected at 14 dpi.

2.7 Quantitative real-time PCR

For RNA extraction, the nodule-forming zone described in Schnabel et al. (2023a) was harvested from 10 plants for each genotype (*A17*, *sunn-1*, and *sunn-4*, *rdn2-1*, *cra2*, *R108*, *bam2*, *bam2 sunn-5*, and *sunn-5*) at multiple time points (0 hours, i.e., prior to inoculation, 12 hours post inoculation (hpi), and 48 hpi) and stored at −80°C. RNA was isolated from nodulating roots using the E.Z.N.A. Plant RNA Kit (Omega Bio-Tek, GA, USA) according to the manufacturer's instructions. Each RNA sample was digested with RNase-free DNase (Promega) treatment for 40 min to remove genomic DNA contamination. The iScript cDNA Synthesis Kit (Bio-Rad, Hercules, CA, USA) was used to synthesize cDNA from 1 µg of RNA in a 20-µL reaction. The cDNAs were then diluted to 40 µL. All experiments were performed using iTaq™ Universal SYBR® Green Supermix (Bio-Rad, CA, USA) and the Applied Biosystems QuantStudio 3 Real-Time PCR System. Each reaction was performed in triplicate, and results were averaged for a single biological replicate. The total reaction volume was 12.5 µL (5 µL of master mix including 0.5 µL of each primer [0.5 µM final concentration] and 2.0 µL of cDNA). Cycle threshold values were obtained using the QuantStudio 3 software, and expression was determined relative to the *internal reference PI4K* (see below). Intron spanning primers unique in the *M. truncatula* genome based on National Center for Biotechnology Information Primer-BLAST analysis were used (Supplementary Table 2). Relative expression levels of genes were assayed using the Pfaffl method (Pfaffl, 2001) relative to previously validated housekeeping reference gene phosphatidylinositol 3- and 4-kinase belonging to ubiquitin family (PI4K; Medtr3g091400 in MtV4.0) (Kakar et al., 2008). Data from the three biological replicates were used to estimate the mean and standard error.

2.8 Statistical analysis

Statistical difference analysis for pairwise mean comparison was calculated by the Tukey–Kramer honestly significant difference (HSD) using JMP Pro 13.1 (https://www.jmp.com/en_us/home.html). For qPCR, absolute quantification was used to compare the quantification cycle (Cq) values of test samples to those of standards (*PIK* internal reference) of known quantity plotted on a standard curve. The quantity was normalized to a unit amount of nucleic acid (i.e., concentrations). The statistical analysis tests for the probability that the relative expression RE ≠ 1 for data normalized to control.

3 Results

3.1 Phylogenetic and structural analysis of BAM proteins

A phylogenetic analysis by neighbor-joining was performed between the protein sequences of legume and *Arabidopsis* BAMs, with CLV1 and the related symbiotic kinases used to root the tree (Figure 1). There was not a one-to-one relationship between MtBAMs and AtBAMs; rather, they shared similarities with BAMs from other legume BAM-Like LRR kinases and *Arabidopsis*. For all the legumes, however, there were two BAM proteins with similarities to *At*BAM1 and *At*BAM2, including *Mt*BAM1 and *Mt*BAM2. The *Mt*BAM1 and *Mt*BAM2 proteins have 80% sequence similarity between them, while *Mt*BAM1 has 81% similarity to *At*BAM1, the highest shared similarity among all comparisons. *Mt*BAM3, *Mt*BAM4, and *Mt*BAM5 were closer phylogenetically to the *At*BAM3 protein with a 55%–56% similarity for each. The branching structure suggests that the five BAM genes in legumes arise from duplications of a BAM3 ortholog (Figure 1). To further pursue the idea that these duplicate genes might be specific for nodulation, the expression levels of each *MtBAM* in individual root tissues were examined during nodule development. Tissue level data from a Laser Capture Microdissection experiment (Schnabel et al., 2023b) and root segment transcriptome data from an unfixed roots experiment (Schnabel et al., 2023a) were examined, following nodule development at 0, 12, 24, 48, and 72 hpi (Figure 2). *MtBAM1* and *MtBAM2* were expressed in nodule meristems at 48 and 72 hpi at higher levels than the other *BAM* family members. *MtBAM1* and *MtBAM2* expression at 12 and 24 hpi was higher in the inner cortical cells at the xylem pole, the cells from which nodules arise (Libbenga and Harkes, 1973). In addition, *MtBAM1* and *MtBAM2* had higher expression in nodule meristems at 48 and 72 hpi compared to *MtBAM3*, *MtBAM4*, and *MtBAM5*. *MtBAM3*, *MtBAM4*, and *MtBAM5*; all displayed similarly low levels of expression throughout nodule formation, with no clear signature in an individual tissue in this experiment (Figure 2). The expression data suggest that *MtBAM1* and *MtBAM2* are most likely to be involved in early nodule formation.

3.2 Root length and nodule number phenotypes of *MtBAM* mutants are wild type

With the expression data in hand, we generated single homozygous mutants for the *BAM* genes in *M. truncatula* using PCR to follow the segregation of *Tnt1* insertions in lines isolated from pools of plants from the Nobel Foundation Medicago Mutant Database identified as containing an insertion in an *MtBAM* gene. The progeny of plants determined to be homozygous for a *Tnt-1* insertion in each *BAM* were tested for nodule number on an aeroponic chamber (see Materials and Methods). All the single *MtBAM* mutants had *Tnt1* insertions in approximately the same place in the LRR domains, and wild-type nodule numbers (Supplementary Figure 2A). Since other nodule regulatory mutants also have root length defects (Schnabel et al., 2005; Schnabel et al., 2010; Schnabel et al., 2011), single mutant plants were grown in the absence of rhizobia, and root length was measured at the equivalent development point to 14 dpi. None of the single *MtBAM* mutants displayed a root length phenotype different from the wild-type plants (Supplementary Figure 2B). Similar to the observation of no meristem defects in single *bam* mutants in

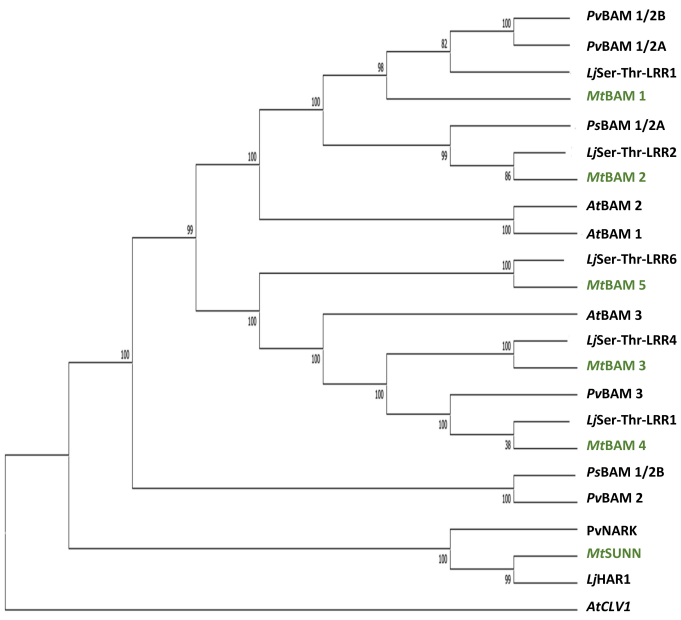

FIGURE 1
Relatedness of BAM receptor kinases between legumes and *Arabidopsis*. Phylogenetic tree created using the maximum likelihood method and rooted with *At*CLV1, with branches supported by at least 80% of the bootstrap replicates (n = 1,000). *Medicago truncatula* BAM proteins are highlighted in green. Accession numbers for genes in tree are in Supplementary Table 1.

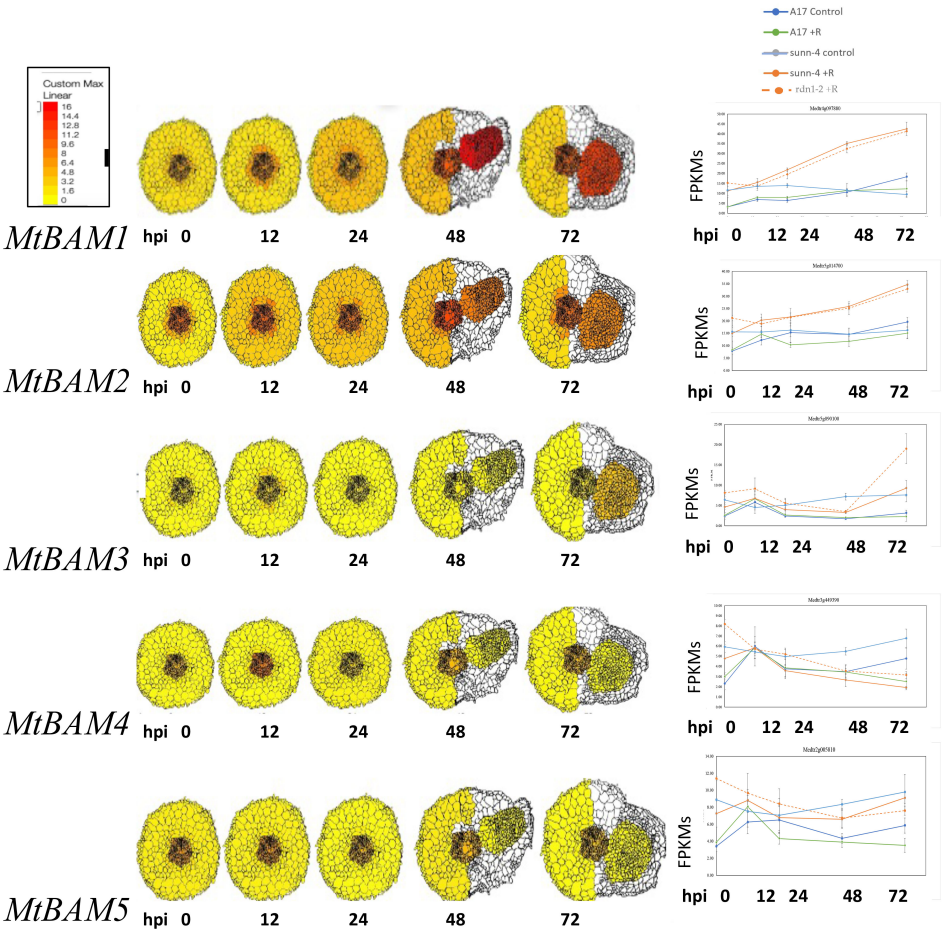

FIGURE 2
MtBAM expression in individual tissues and whole root segments during nodule formation. The tissue-specific expression patterns on the left for each *MtBAM* were created using ePlant and the data in Schnabel et al. (2023b) and a fixed maximum for comparison between genes across a time course at 0 to 72 hpi. The whole root expression traces for each *MtBAM* on the right are from the same time course and conditions, taken from the data in Schnabel et al. (2023a). Expression (FPKMs) of BAMs from 0 to 72 hpi are displayed as blue = A17 control, green = A17 + rhizobia, light blue = *sunn-4* control, orange = *sunn-4* + rhizobia, and orange dotted = *rdn1-2* + rhizobia.

Arabidopsis (DeYoung et al., 2006), no nodule number or root length phenotype was observed in the *M. truncatula* single *BAM* mutants. We also generated double mutants of *Mtbam2* with *Mtbam3* and *Mtbam4*, as well as an *Mtbam4;Mtbam5* double mutant, to determine if an effect is observable with the loss of more than one *BAM*, as is the situation with *Arabidopsis* mutants (DeYoung and Clark, 2008), but these also had no effect on nodule number or root length (Supplementary Figure 3). Interestingly, we were unable to obtain seeds from any cross of the *Mtbam1* mutant to any other *Mtbam* mutant, despite multiple attempts. Examining the ePlant database (Waese et al., 2017), transcriptomic data for *MtBAM1* show high levels of expression in tissues such as pods, flowers, stems, and developing seeds (Benedito et al., 2008). When attempting to make crosses with *bam1*, the stamen looked frail and opaque with few pollen granules visible (data not shown), and this may explain the lack of success generating *bam1 bamx* double mutants.

3.3 *Mtbam2* suppresses the *sunn-5* supernodulation phenotype in the double mutant

Since *Arabidopsis BAM*s were originally isolated by the effects observed in a *clv1* mutant background (DeYoung et al., 2006), we reasoned that mutations in *MtBAM* genes might only have noticeable effects on nodule number in a *sunn* mutant background. We created a set of *bam*/*sunn* double mutants by crossing and isolating F2 progeny using PCR confirmation of the phenotype: *bam2 sunn-5*, *bam3 sunn-5*, and *bam5 sunn-5*. We observed a suppressive effect on nodule number in the *bam2 sunn-5* double mutant (Figure 3A). We applied a slightly different observation to the root length phenotype; the *sunn-5* short root phenotype was partially rescued by *bam2* or *bam3*, but not *bam5* (Figure 3B). Because of the suppressive effect of *bam2* on both phenotypes of *sunn-5* plants, we investigated the mechanism further.

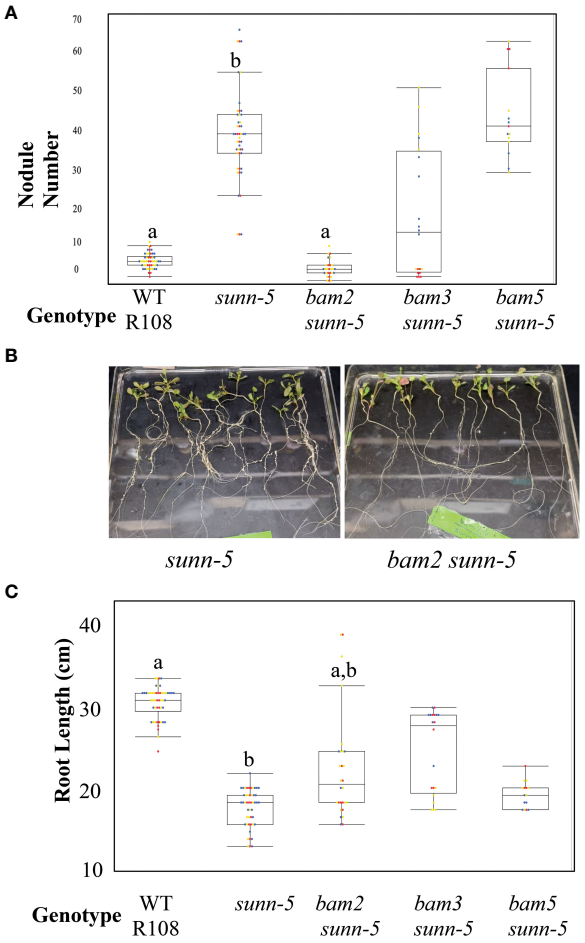

FIGURE 3
bam2 suppresses nodule number in *sunn-5* mutants, while *bam2* and *bam3* suppress root length defects. **(A)** Nodule number per plant at 14 dpi. Letters denote significance compared to wild-type **(B)** photos of *sunn-5* and *bam2 sunn-5* plants. **(C)** Root length in wild-type plants compared to *sunn-5* and *bam* double mutants at 14 days without rhizobia. Letters denote significance compared to wild type. Dots represent individual plants. Each dot color is associated with independent biological replicates: rep1 = red, rep2 = yellow, and rep3 = blue. Box plot mean is indicated with a line, while whiskers are ± standard error, pairwise comparison Tukey–Kramer honestly significant difference (HSD), p-value a:b > 0.001. p-value a: a,b > 0.001.

3.4 Grafting to determine localization (shoot or root) of *bam2* suppression of *sunn-5* phenotype

The *sunn* mutation has been shown to increase nodule number when a *sunn* mutant shoot is grafted onto wild-type shoots (Penmetsa et al., 2003). The same grafting experiment was employed to determine the location of the suppression observed in the *bam2 sunn5* double mutant. Since AON is a long-distance root to shoot to root regulatory pathway, a set of grafting experiments was designed to determine the location of the effect (Figure 4). Comparing the nodule number of plants created with a *bam2 sunn-5* shoot grafted onto a *sunn-5* root to that of a *sunn-5* shoot on a *bam2 sunn-5* root (Figure 4A), suppression of the *sunn-5* hypernodulation phenotype occurred when a *sunn-5* shoot genotype was grafted onto the *bam2 sunn-5* root genotype, indicating that the suppression is root derived (Figure 4A). Since the root is a double mutant, two possibilities arise—either *sunn-5* is required for the suppression, or *bam2* alone in the roots suppresses the nodule number phenotype of a *sunn-5* shoot. To resolve this, a second grafting experiment was designed (Figure 4B) in which the *sunn-5* shoot genotype was grafted onto a *bam2 sunn-5* root genotype and compared to a *sunn-5* shoot genotype grafted onto a *bam2* root genotype. Suppression of the *sunn-5* hypernodulation phenotype occurred in both graft combinations, suggesting that *bam2* can suppress nodule numbers from the roots, with or without *sunn-5* being present (Figure 4B).

3.5 Overexpression of *BAM2* increases nodulation in wild-type roots

In addition to phenotyping *bam* mutants, we observed nodule numbers in transgenic hairy roots overexpressing individual *MtBAM* genes driven by the CMV 35S promoter compared to control plants carrying empty vector constructs (Figure 5). Overexpression of *BAM1* and *BAM3* did not alter nodule numbers in wild-type plants of either ecotype, but overexpression of *BAM2* in wild-type transgenic hairy roots caused a significant increase in nodule number in both A17 (the ecotype used for genome sequencing) and R108 (an ecotype used for tissue culture-based transformation and the background of the *BAM* mutant lines). This confirms the specific involvement of *BAM2* in nodule number and that the effect is not ecotype specific.

3.6 The effect of overexpression of *BAM2* in a *sunn* mutant background is allele specific

Suppression of nodule number in *sunn-5* could arise from disruption of signaling downstream of SUNN, or it could arise from disruption of a signaling step at which BAM and SUNN interact (Meneely, 2020). We tested an allelic series of *sunn* mutants for indications of interaction between the proteins. The *sunn-5* mutant in the R108 background has been used in previous work (Crook et al., 2016; Nowak et al., 2019) and contains a *Tnt1* insertion (~2 kb in size) located 406 bp upstream of the ATG start codon in *SUNN* gene (El-Heba et al., 2015). Using PCR on cDNA (Supplementary Figure 1), we determined that this promoter insertion also removed 584 bases past the start site, resulting in a potential new start in the leucine-rich repeats, as well as a deletion of the end of the repeats, the transmembrane domain and into the kinase domain (Figure 6A); the ability to isolate RNA indicates that a truncated *SUNN* message is made. Additional *sunn* mutants exist in the A17 ecotype; the *sunn-1* allele in A17 produces a full transcript with only a change in an amino acid in the kinase

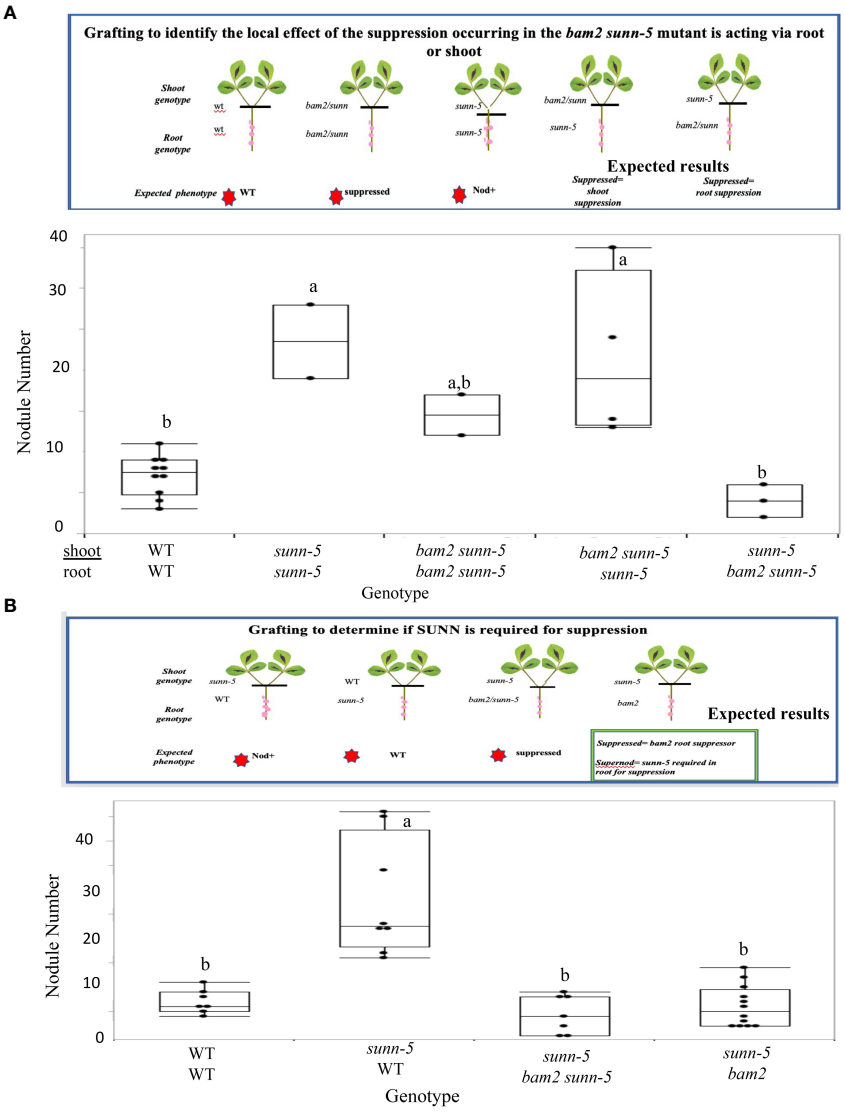

FIGURE 4
Suppression of the *sunn-5* phenotype by *bam2* is root derived and occurs regardless of *sunn-5* root genotype. **(A)** Nodule numbers formed on grafted plants to test root/shoot origin of suppression. Gene on top indicates shoot genotype; bottom indicates roots. Results are combined from two individual experiments. Box plot mean is indicated with a line (where more than three data points available), while whiskers are ± standard error, pairwise comparison Tukey–Kramer honestly significant difference (HSD). Letters indicate significance comparisons. p-value a:a,b > 0.01. p-value a:b > 0.001. **(B)** Nodule numbers formed on grafted plants to determine if SUNN is required. Experimental details are the same as in **(A)**.

domain, while the *sunn-4* allele contains a premature stop codon immediately after the signal sequence and is considered a null allele (Schnabel et al., 2005). The two alleles vary in nodule number; *sunn-1* plants have three to five times the nodules of wild-type plants, while *sunn-4* plants have a 10-fold increase in nodule number (Schnabel et al., 2010). A17 is difficult to cross with R108 due to multiple rounds of R108 selection for regeneration and differences in the genomes, which make genetic crosses problematic. Adding to the difficulties, the R108 ecotype nodulates best with a different strain of rhizobia (Hoffmann et al., 1997). Therefore, rather than making the mutants to test suppression, we chose to overexpress *BAM2* in the different alleles of *sunn* in their respective ecotypes, inoculated with the rhizobia best for each ecotype. In contrast to wild-type plants in which overexpression of *BAM2* increased nodule number, overexpression of *BAM2* in a *sunn-5* background suppressed nodule numbers to a wild-type level (Figure 6B). Overexpression of *BAM2* also suppresses the hypernodulation phenotype of a *sunn-1* mutant, which produces a full-length *sunn* message with a single amino acid change (Schnabel et al., 2005) but did not suppress hypernodulation in *sunn-4* null allele (Figure 6B). When *BAM1* and *BAM3* were overexpressed in the *sunn-4* and *sunn-5* mutants, no alteration to the hypernodulating *sunn* phenotype was observed for either mutant (Figure 6B), again confirming the effect is also specific to the *BAM2* gene. The *sunn-1* mutant appeared to increase nodule number in response to *BAM1* overexpression, but this was not statistically significant because of the distribution spread of nodule number in the empty vector control.

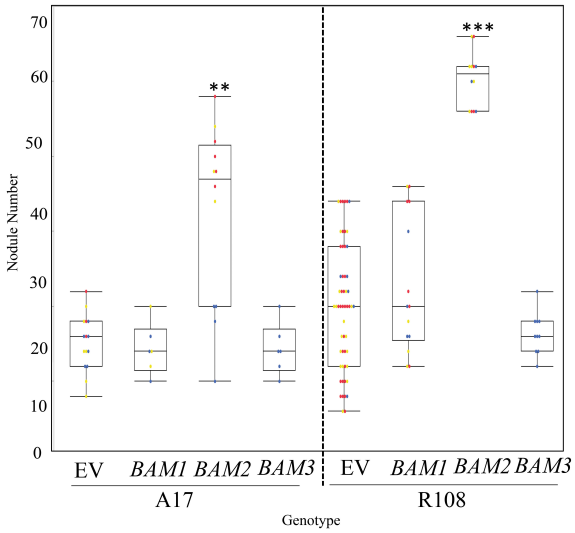

FIGURE 5
Overexpression of *MtBAM2* in wild-type A17 and R108 ecotypes increases nodule number. Nodule number in plants overexpressing *BAM1, BAM2,* or *BAM3* under the 35S promoter (see Materials and Methods) at 14 dpi. A17 ecotype plants are inoculated with *Sinorhizobium medicae* ABS7, and R108 ecotype plants with *Sinorhizobium meliloti* RM41. EV = empty vector control. Dots represent individual plants. Each dot color is associated with independent biological replicates: rep1 = red, rep2 = yellow, and rep3 = blue. Box plot mean is indicated with a line, while whiskers are ± standard error, pairwise comparison Tukey–Kramer honestly significant difference (HSD), p-value > 0.01. (**). p-value > 0.001. (***) denotes significance compared to EV control. Pictures of representative plants are in Supplementary Figure 4.

3.7 Overexpression of *BAM*s in other AON mutants

To determine if *BAM2* overexpression can suppress nodulation in other hypernodulators, we repeated the previous experiment with three mutants in different portions of the AON pathway. *RDN1* functions in the root early in the AON pathway upstream of *SUNN*, modifying the ligand for the SUNN receptor (Kassaw et al., 2017). The pseudokinase CRN displays an increase in nodule number when mutated and acts at the same point as SUNN in the AON pathway, forming heteromultimers with SUNN (Crook et al., 2016). In contrast, the CRA2 receptor kinase mutants signal in a different part of nodule number regulation, separate from SUNN, conveying information on nitrogen status to the AON pathway through signaling with CEP1 peptide (Laffont et al., 2019). The *cra2* mutant does not make nodules because the signal for nitrogen needs is not sent to the roots. None of the *BAM*s affected the hypernodulation phenotype of *rdn1-2* mutants when overexpressed; however, BAM2 overexpression suppressed the hypernodulation phenotype of *crn* mutants (Figure 7). Interestingly, overexpression of all *BAM*s tested resulted in the death of all *cra2* plants before nodulation could occur, while their empty vector controls remained alive (Figure 7), suggesting that there may be some effect unrelated to nodulation of excess *BAM2* in these plants.

3.8 Expression of genes downstream of *BAM/SUNN*

The *MtWOX5* transcription factor is downstream of *SUNN* signaling. Since *MtWOX5* has been implicated in nodule development in *M. truncatula* (Osipova et al., 2012), in this work, we examined expression levels in several mutant combinations. We examined the relative expression of *MtWOX5* during nodulation in both *bam2* and *bam2 sunn-5* plants by utilizing a time-course experiment using root segments to assess the relative expression of each marker gene at 0, 12, and 48 hpi. Previous work in our lab measured absolute expression for each gene in wild-type and *sunn-4* root segments, and we also used the ePlant resource to confirm the tissue-level expression of these genes. We examined the expression of *MtWOX5* at each time point in wild-type, *bam2*, and *bam2 sunn-5* plants using quantitative real-time PCR (Figure 8).

MtWOX5 expression is the strongest in developing nodules (Figure 8A) and may reflect the expression of the nodule meristem since the LCM resource colors the entire tissue. *MtWOX5* maintains a steady low-level expression throughout nodule development but is slightly higher in the inoculated roots compared to the non-inoculated controls (Figure 8B). In *sunn-4* roots, *MtWOX5* expression increases at 12 hpi and continues to increase to peak expression in this time course at 48 hpi (Figure 8B). In contrast, in a *bam2* background, *WOX5* expression as measured using real-time quantitative RT-PCR is greater at 0, 12, and 48 hpi compared to the wild-type control (Figure 8C). However, in the double-mutant *bam2 sunn-5* root segments, the highest level of relative expression of *MtWOX5* was observed at 0 hpi, with expression less than that of the wild-type control at 12 and 48 hpi in the double mutant (Figure 8D). Expression of the master regulator *MtWOX5* decreases after inoculation in the *bam2 sunn-5* mutant versus in the single *bam2* background in which *MtWOX5* increases and stays up after inoculation.

4 Discussion and conclusions

Phylogenetic analysis (Figure 1) suggests the expansion in the *BAM* gene family between *Arabidopsis* with three *BAM* genes, and *M. truncatula* with five suggests that if the expansion of the gene family resulted in new genes used for nodule meristems, *MtBAM4* and *MtBAM5* would be the best candidates based on their position with additional legume *BAM*s in a clade away from most of the rest of the *BAM*s. However, neither *BAM4* nor *BAM5* was expressed in nodules (Figure 2), while *MtBAM1–3* were expressed in nodules.

Since we did not identify nodule number or root length phenotype in any plants carrying a mutation in a single *bam* (Supplementary Figure 2) or any of the plants carrying two *bam* mutations (Supplementary Figure 3), mutation analysis of *BAM* genes alone did not identify a *BAM* specific to the regulation of nodule number. The lack of an observable effect from single *bam* mutants was not unexpected, as single *Atbams* showed no phenotype (DeYoung et al., 2006). While we did not investigate further, *MtBAM1* could be important to multiple developmental

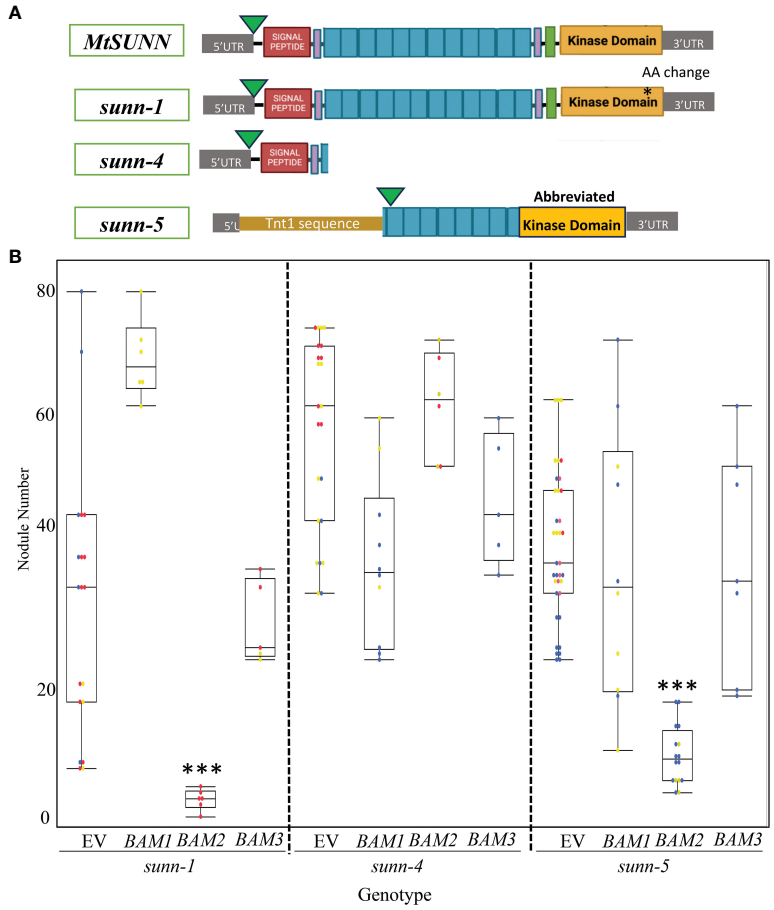

FIGURE 6
Results of overexpression of *MtBAM1*, *MtBAM2*, and *MtBAM3* in *sunn* mutants are allele specific. **(A)** Diagram of SUNN protein and effects of *sunn* alleles. Green arrow indicates Met used for start, purple boxes are paired Cys residues, turquoise boxes represent leucine-rich repeats (not to scale; there are 22), and green box is transmembrane domain. **(B)** Nodulation on plants overexpressing indicated *BAM* genes. EV = empty vector control. Dots represent individual plants. Each dot color is associated with independent biological replicates: rep1 = red, rep2 = yellow, and rep3 = blue. Box plot mean is indicated with a line, while whiskers are ± standard error, pairwise comparison Tukey–Kramer honestly significant difference (HSD). (***) denotes significance compared to EV, p-value > 0.001. Pictures of representative plants are in Supplementary Figure 4.

systems, as we were unable to generate any double mutants with this line. The discovery that adding a *bam2* mutation to a *sunn* mutation suppressed nodule number to wild-type levels (Figure 3) indicates *BAM2* is involved in nodule development, but visualization of this role is only possible when *SUNN* is disrupted. This effect is specific to *bam2* and not observed when *sunn-5* is combined with *bam3* or *bam5*. We were unable to test the mutations of *bam4* or *bam1*, as a double mutant with *sunn-5* could have a suppressive effect; however, *bam4* is not expressed in nodulating roots, making suppression unlikely. Since overexpression of *BAM2*, but not *BAM1* or *BAM3*, increases nodule number in wild-type plants (Figure 5), multiple lines of evidence support a specific role for *BAM2* in nodule number regulation.

The data support the action of BAM2 in nodulation as root specific rather than systemic. While SUNN signals from shoot to root to control nodule number (Penmetsa et al., 2003) and is central to AON (reviewed in Roy et al., 2020), *SUNN* is expressed throughout the plant in the vasculature (Schnabel et al., 2012), and the function of SUNN in the root has not yet been determined. The localization of the suppressor effect of *bam2* in the root (Figure 4A) is particularly interesting, as the SUNN protein is a systemic negative regulator of nodule number; *sunn-5* mutants hypernodulate because they cannot send a wild-type regulation signal to the roots to control nodule number. Nevertheless, the mutation in *bam2* in the roots of a *sunn-5* mutant allows the regulation to proceed, suggesting that the lack of *bam2* compensates for the lack of the SUNN signal from the shoots (Figure 4B). Further support of a local rather than systemic effect is the grafting experiment in which a *bam2* mutant in the shoot but not the root does not suppress the *sunn* hypernodulation phenotype (Figure 4A). All *sunn* mutants have normal nodulation if mutant roots are grafted to wild-type shoots (Penmetsa et al., 2003; Schnabel et al., 2010, Figure 4B), suggesting that whatever the function of SUNN in the root, a mutation of *sunn* in the root is not causal to hypernodulation. However, the addition of a *bam2* mutation in the root along with a *sunn* mutation changes the response to the shooting signal, supporting action locally in the root versus systemic action.

In *Arabidopsis*, the differentiation of stem cells in the root apical meristem and cell division in the root is controlled by CLE peptides

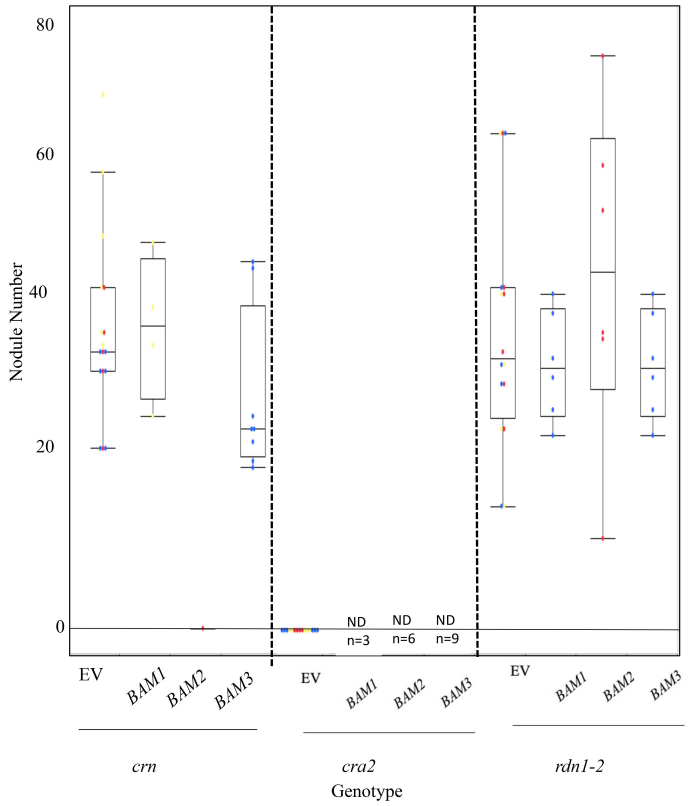

FIGURE 7
Results of overexpression of *MtBAM1*, *MtBAM2*, and *MtBAM3* in autoregulation of nodulation (AON) mutants *crn* and *rdn1-2* and *cra2* mutants. No significant nodule number phenotype was observed from the overexpression of *MtBAM1*, *MtBAM2*, or *MtBAM3* in any of the AON mutants. However, *MtBAM2* overexpression in *crn* resulted in almost all plants dying, with only one plant surviving the screening stage. No nodules formed on the sole surviving *crn*:p*MtBAM2* plant. All *cra2* plants overexpressing a *BAM* gene died before screening. EV = empty vector control. Dots represent individual plants. Each dot color is associated with independent biological replicates: rep1 = red, rep2 = yellow, and rep3 = blue. Box plot mean is indicated with a line, while whiskers are ± standard error.

(Willoughby and Nimchuk, 2021). Recent studies have shown that the SUNN ortholog CLV1 signals through a BAM protein complex to control CLE-mediated signaling of the root apical meristem (Wang et al., 2022) and root phloem development (Hu et al., 2022). Nodule primordia use many of the same regulatory genes, as lateral root primordia (Schiessl et al., 2019) contain a nodule meristem and develop vasculature at the time points used to measure gene expression in this work (48–72 hpi in our growth systems), making the involvement of a BAM quite likely.

In our system, both the *sunn-5* and *bam2* mutants make transcripts detectable by PCR of cDNA, but *sunn-5* is not likely to produce protein due to the lack of regulatory sequences around the possible alternate start in *sunn-5* (Figure 6), while the disruption of the coding sequence in all of the *bam Tnt1* insertion mutants occurs from insertion of the *Tnt-1* sequence in the middle of the LRR region, leading to a truncated protein (Supplementary Figure 1). In *Arabidopsis*, truncated BAM proteins lacking a kinase domain interfere with meristem homeostasis in a dominant negative manner because of the LRR repeats interacting with other proteins (Wang et al., 2018), but this is not observed in our system, suggesting that the insert in the LRR disrupts any dominant negative effect from the lack of a kinase domain.

The expression of *BAM2* in wild-type plant roots before nodulation (0 hpi in Figure 2, right panel) is approximately half the expression of *BAM2* in *sunn-4* mutant roots and *rdn1-2* hypernodulation mutant roots before nodulation begins. *BAM2* expression rises in roots of all inoculated plants over the 72-hpi time course, but the rise is larger in the hypernodulation mutants *sunn-4* and *rdn1-2*, and there is no reason not to expect the same pattern in *sunn-1* and *sunn-5* mutants given that the nodule number phenotypes of these mutants are similar to *rdn1-2*. If increased *BAM2* expression is observed in plant roots that hypernodulate, it is logical that overexpression of *BAM2* in wild-type roots increases nodule number. More interesting is the observation that adding more *BAM2* to *sunn* mutant roots already expressing higher levels of *BAM2* than wild-type decreases nodule number for *sunn-1* and *sunn-5* mutant roots but not *sunn-4* roots. The decrease in the *sunn-1* and *sunn-5* roots could be explained if the level of *BAM2* from the overexpression construct rises high enough to trigger RNA interference, acting like a *bam2* mutation, but the lack of suppression in *sunn-4* roots is perplexing. Because the expression of *BAM2* in these roots was not measured, it is not possible to rule out the explanation that the construct was not correctly expressed. However, the effect was seen in six plants tested in two independent

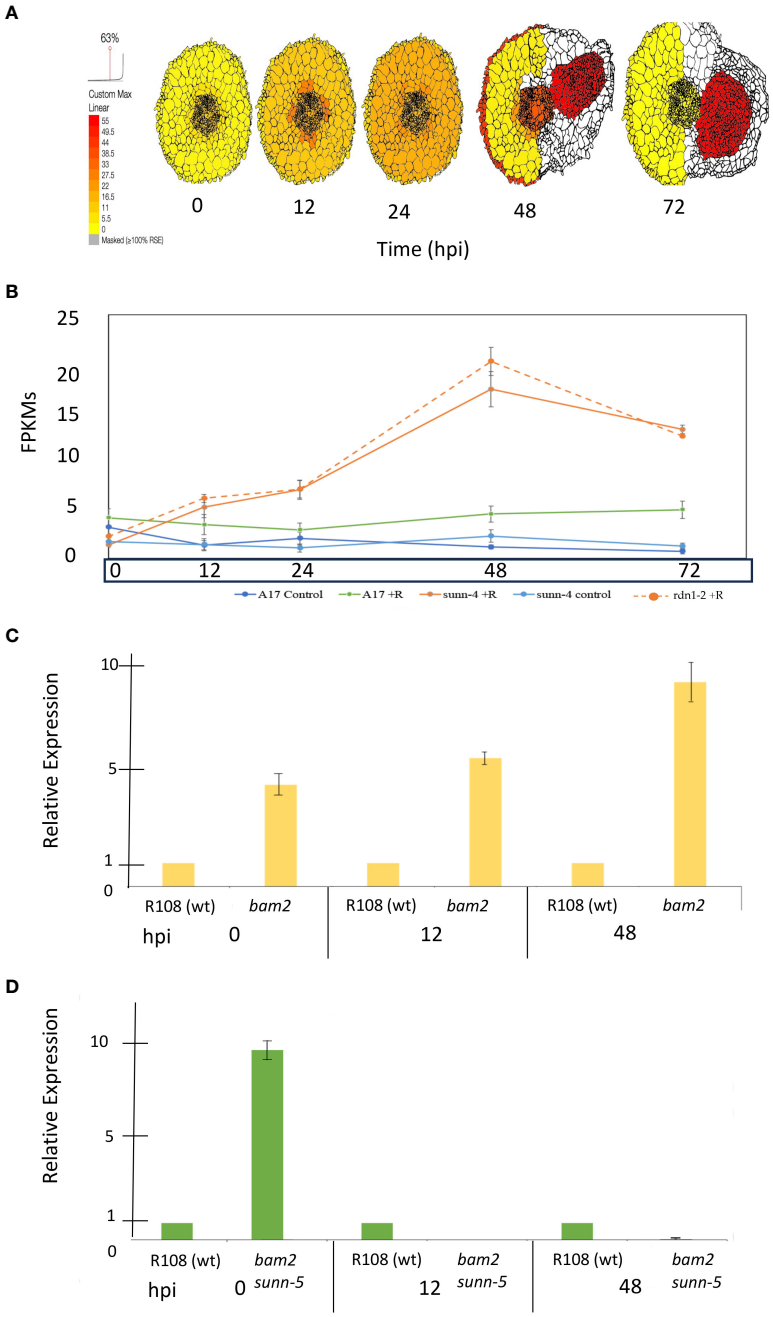

FIGURE 8
Expression of *MtWOX5* during nodule formation. **(A)** *MtWOX5* tissue-specific expression created using ePlant and the data in Schnabel et al. (2023b). **(B)** Whole root expression traces for *WOX5* from the same time course and conditions were taken from the data in Schnabel et al. (2023a). Expression (FPKMs) of *WOX5* from 0 to 72 hpi is displayed as blue = A17 control, green = A17 + rhizobia, light blue = *sunn-4* control, orange = *sunn-4* + rhizobia, and orange dotted = *rdn1-2* + rhizobia. **(C)** Expression of *MtWOX5* in *bam2* mutants and **(D)** *bam2 sunn-5* mutants. For each time point, relative expression was calculated by fold change compared to the wild-type control at that time point (see Materials and Methods). Data represent three biological and three technical replicates. Error bars represent ± standard error. Note that *WOX5* expression was undetectable in the *bam2 sunn-5* mutant at 12 hpi and barely detectable at 48 hpi.

experiments, giving confidence in the result. Since the transformations are performed in hairy roots in which auxin homeostasis is perturbed, it is possible that the extreme hypernodulation phenotype in the null allele is affected more by the hairy root environment than expression of *BAM* genes, given that the range of nodule numbers in Figure 6 is below the 125 average nodules per plant in *sunn-4* mutants on an aeroponic system in all conditions including the empty vector (Schnabel et al., 2010), adding difficulties to interpretation of the *sunn-4* results.

It is important to note that overexpression of wild-type *BAM2* did not suppress (or enhance) hypernodulation in the *crn* and *rdn1-2* AON mutant roots, even though the *rdn1-2* mutant has high *BAM2* expression compared to wild type, so the effect of the

mutation is not on the AON pathway itself: the suppression seems to be specific to plant roots carrying mutations in *SUNN*, with *sunn-4* as an exception. Relative expression measurements of *MtWOX5* add some insight into how the downstream nodulation signaling may be disrupted in *bam2* and *bam2 sunn-5* mutants. *MtWOX5* expression in the nodule apical meristem (NAM) (Osipova et al., 2011; Roux et al., 2014) provides molecular support for the derivation of nodule development programs from lateral root developmental programs (Hirsch and Larue, 1997; Mathesius et al., 2000; Bright et al., 2005; Desbrosses and Stougaard, 2011). *WOX5* gene is downstream from the CLE/CLV1/BAM signaling complex in *Arabidopsis* (Willoughby & Nimchuk, 2021), but other receptor kinases are involved in connecting CLE/CLV1/BAM signaling to WOX5 expression (Wang et al., 2022). The expression of *MtWOX5* is increased compared to the wild type at 0 hpi *bam2* mutants and *bam2 sunn-5* mutants but is the same as the wild type in *sunn-4* and *rdn1-2* hypernodulation mutants (Figure 8). In contrast to the steady higher expression observed in *sunn-4*, *rdn1-2*, and *bam2* mutants at 12 and 48 hpi, the *bam2 sunn5* mutant decreases *MtWOX5* expression below wild-type levels. Rather than eliminating nodule development, the lower expression is correlated with only a reduction of nodule number in *sunn-5* mutants. Likewise, even though *bam2* mutants have increased *MtWOX5* expression, the number of nodules is not affected, suggesting that other factors outside of *MtWOX5* are also involved in nodule number regulation.

In the event of genetic or environmental disruption, plants can initiate a genetic buffering mechanism called "active compensation" in which genes change their behavior to compensate for the disruption (Rodriguez-Leal et al., 2019). For example, in *Arabidopsis*, the weak *clv1* phenotype is genetically buffered by the paralogous BAM receptors through active compensation (Diss et al., 2014; Nimchuk et al., 2015). The loss of *CLV1* resulted in an increased expression of BAMs and a change in their expression domains, allowing for the compensation of *CLV1* loss (Nimchuk et al., 2015). In *Solanum lycopersicum*, the loss of *SlCLV3*, the tomato CLV3 ortholog, triggers an active compensation mechanism, by which the upregulation of *SlCLE9* buffers stem cell homeostasis in tomato (Rodriguez-Leal et al., 2019). Considering the related distance between *Arabidopsis* and tomato, genetic buffering of stem cells reflects a determining feature of indeterminate meristem development, including nodule meristems (Rodriguez-Leal et al., 2019). A similar effect may be happening with *BAM2* and *SUNN*.

We speculate that the loss of, or disruption to, the CLE/SUNN/BAM2 signaling in the roots alters signaling, affecting the nodule-specific transcription factor *MtWOX5*. We propose a genetic model, wherein the specific root interactions of BAM2/SUNN are critical for signaling in nodule meristem cell homeostasis in *M. truncatula*. Except for the perplexing *sunn-4* overexpression results, an anomaly to pursue in future studies, our data support the involvement of CLE/CLV1/BAM signaling influencing nodule number in *M. truncatula*.

Data availability statement

The original contributions presented in the study are included in the article/Supplementary Material. Further inquiries can be directed to the corresponding author.

Author contributions

JT: Data curation, Formal analysis, Investigation, Methodology, Writing – original draft, Writing – review & editing. JF: Conceptualization, Formal analysis, Funding acquisition, Methodology, Resources, Supervision, Visualization, Writing – review & editing.

Funding

The author(s) declare financial support was received for the research, authorship, and/or publication of this article. This work was supported by NSF 1733470 to JF.

Acknowledgments

We thank Elise Schnabel for the identification of the *BAM* mutant lines in the *Tnt1* pools and the Genetics and Biochemistry Teaching Lab for the use of their real-time PCR machine.

Conflict of interest

The authors declare that the research was conducted in the absence of any commercial or financial relationships that could be construed as a potential conflict of interest.

Publisher's note

Supplementary material

The Supplementary Material for this article can be found online at: https://www.frontiersin.org/articles/10.3389/fpls.2023.1334190/full#supplementary-material

References

Araya, T., von Wirén, N., and Takahashi, H. (2016). CLE peptide signaling and nitrogen interactions in plant root development. *Plant Mol. Biol.* 91 (6), 607–615. doi: 10.1007/s11103-016-0472-9

Bekki, A., Trinchant, J.-C., and Rigaud, J. (1987). Nitrogen fixation (C2H2 reduction) by Medicago nodules and bacteroids under sodium chloride stress. *Physiologia Plantarum* 71 (1), 61–67. doi: 10.1111/j.1399-3054.1987.tb04617.x

Benedito, V. A., Torres-Jerez, I., Murray, J. D., Andriankaja, A., Allen, S., Kakar, K., et al. (2008). A gene expression atlas of the model legume. *Medicago truncatula. Plant J.* 55 (3), 504–513. doi: 10.1111/j.1365-313X.2008.03519.x

Bright, L. J., Liang, Y., Mitchell, D. M., and Harris, J. M. (2005). The LATD gene of Medicago truncatula is required for both nodule and root development. *Mol. Plant-Microbe Interact.* 18 (6), 521–532. doi: 10.1094/MPMI-18-0521

Cai, J., Veerappan, V., Arildsen, K., Sullivan, C., Piechowicz, M., Frugoli, J., et al. (2023). A modified aeroponic system for growing small-seeded legumes and other plants to study root systems. *Plant Methods* 19 (1), 21. doi: 10.1186/s13007-023-01000-6

Chaulagain, D., and Frugoli, J. (2021). The regulation of nodule number in legumes is a balance of three signal transduction pathways. *Int. J. Mol. Sci.* 22 (3), 1117. doi: 10.3390/ijms22031117

Crook, A. D., Schnabel, E. L., and Frugoli, J. A. (2016). The systemic nodule number regulation kinase SUNN in *Medicago truncatula* interacts with MtCLV2 and MtCRN. *Plant J.* 88 (1), 108–119. doi: 10.1111/tpj.13234

Desbrosses, G. J., and Stougaard, J. (2011). Root nodulation: a paradigm for how plant-microbe symbiosis influences host developmental pathways. *Cell Host Microbe* 10 (4), 348–358. doi: 10.1016/j.chom.2011.09.005

DeYoung, B. J., Bickle, K. L., Schrage, K. J., Muskett, P., Patel, K., and Clark, S. E. (2006). The CLAVATA1-related BAM1, BAM2 and BAM3 receptor kinase-like proteins are required for meristem function in Arabidopsis. *Plant J.* 45 (1), 1–16. doi: 10.1111/j.1365-313X.2005.02592.x

DeYoung, B. J., and Clark, S. E. (2008). BAM receptors regulate stem cell specification and organ development through complex interactions with CLAVATA signaling. *Genetics* 180 (2), 895. doi: 10.1534/genetics.108.091108

Diss, G., Ascencio, D., DeLuna, A., and Landry, C. R. (2014). Molecular mechanisms of paralogous compensation and the robustness of cellular networks. *J. Exp. Zoology Part B: Mol. Dev. Evol.* 322 (7), 488–499. doi: 10.1002/jez.b.22555

El-Heba, G. A. A., Hafez, A., Elsahly, N., and Hussien, G. M. (2015). supn, a novel supernodulation mutant in *Medicago truncatula*. *Plant Gene* 4, 100–108. doi: 10.1016/j.plgene.2015.07.002

Ferguson, B. J., Mens, C., Hastwell, A. H., Zhang, M., Su, H., Jones, C. H., et al. (2019). Legume nodulation: The host controls the party. *Plant Cell Environ.* 42 (1), 41–51. doi: 10.1111/pce.13348

Garmier, M., Gentzbittel, L., Wen, J., Mysore, K. S., and Ratet, P. (2017). *Medicago truncatula:* genetic and genomic resources. *Curr. Protoc. Plant Biol.* 2 (4), 318–349. doi: 10.1002/cppb.20058

Gautrat, P., Mortier, V., Laffont, C., De Keyser, A., Fromentin, J., Frugier, F., et al. (2019). Unraveling new molecular players involved in the autoregulation of nodulation in *Medicago truncatula*. *J. Exp. Bot.* 70 (4), 1407–1417. doi: 10.1093/jxb/ery465

Hastwell, A. H., de Bang, T. C., Gresshoff, P. M., and Ferguson, B. J. (2017). CLE peptide-encoding gene families in *Medicago truncatula* and *Lotus japonicus*, compared with those of soybean, common bean and Arabidopsis. *Sci. Rep.* 7 (1), 1–13. doi: 10.1038/s41598-017-09296-w

Hirsch, A. M., and Larue, T. A. (1997). Is the Legume Nodule a Modified Root or Stem or an Organ sui generis? *Crit. Rev. Plant Sci.* 16 (4), 361–392. doi: 10.1080/07352689709701954

Hoffmann, B., Trinh, T. H., Leung, J., Kondorosi, A., and Kondorosi, E. (1997). A new Medicago truncatula line with superior in *vitro* regeneration, transformation, and symbiotic properties isolated through cell culture selection. *Mol. Plant-Microbe Interact.* 10 (3), 307–315. doi: 10.1094/MPMI.1997.10.3.307

Hu, C., Zhu, Y., Cui, Y., Zeng, L., Li, S., Meng, F., et al. (2022). A CLE–BAM–CIK signalling module controls root protophloem differentiation in Arabidopsis. *New Phytol.* 233 (1), 282–296. doi: 10.1111/nph.17791

Huault, E., Laffont, C., Wen, J., Mysore, K. S., Ratet, P., Duc, G., et al. (2014). Local and systemic regulation of plant root system architecture and symbiotic nodulation by a receptor-like kinase. *PloS Genet.* 10 (12), e1004891. doi: 10.1371/journal.pgen.1004891

Huo, X., Schnabel, E., Hughes, K., and Frugoli, J. (2006). RNAi phenotypes and the localization of a protein::GUS fusion imply a role for *Medicago truncatula PIN* genes in nodulation. *J. Plant Growth Regul.* 25 (2), 156–165. doi: 10.1007/s00344-005-0106-y

Kakar, K., Wandrey, M., Czechowski, T., Gaertner, T., Scheible, W.-R., Stitt, M., et al. (2008). A community resource for high-throughput quantitative RT-PCR analysis of transcription factor gene expression in. *Medicago truncatula. Plant Methods* 4 (1), 1–12. doi: 10.1186/1746-4811-4-18

Karimi, M., Inzé, D., and Depicker, A. (2002). GATEWAY vectors for Agrobacterium-mediated plant transformation. *Trends Plant Sci.* 7 (5), 193–195. doi: 10.1016/s1360-1385(02)02251-3

Kassaw, T. K., and Frugoli, J. A. (2012). Simple and efficient methods to generate split roots and grafted plants useful for long-distance signaling studies in *Medicago truncatula* and other small plants. *Plant Methods* 8 (1), 38. doi: 10.1186/1746-4811-8-38

Kassaw, T., Nowak, S., Schnabel, E., and Frugoli, J. (2017). *Root determined nodulation1* is required for *M. truncatula* CLE12, but not CLE13, peptide signaling through the SUNN receptor kinase. *Plant Physiol.* 174 (4), 2445–2456. doi: 10.1104/pp.17.00278

Kinoshita, A., Betsuyaku, S., Osakabe, Y., Mizuno, S., Nagawa, S., Stahl, Y., et al. (2010). RPK2 is an essential receptor-like kinase that transmits the CLV3 signal in Arabidopsis. *Development* 137 (22), 3911–3920. doi: 10.1242/dev.048199

Krusell, L., Madsen, L. H., Sato, S., Aubert, G., Genua, A., Szczyglowski, K., et al. (2002). Shoot control of root development and nodulation is mediated by a receptor-like kinase. *Nature* 420 (6914), 422–426. doi: 10.1038/nature01207

Krusell, L., Sato, N., Fukuhara, I., Koch, B. E. V., Grossmann, C., Okamoto, S., et al. (2011). The *Clavata2* genes of pea and *Lotus japonicus* affect autoregulation of nodulation. *Plant J.* 65 (6), 861–871. doi: 10.1111/j.1365-313X.2010.04474.x

Kumar, S., Stecher, G., Li, M., Knyaz, C., and Tamura, K. (2018). MEGA X: molecular evolutionary genetics analysis across computing platforms. *Mol. Biol. Evol.* 35 (6), 1547–1549. doi: 10.1093/molbev/msy096

Laffont, C., Huault, E., Gautrat, P., Endre, G., Kalo, P., Bourion, V., et al. (2019). Independent regulation of symbiotic nodulation by the SUNN negative and CRA2 positive systemic pathways. *Plant Physiol. 180(1) 559 LP –*, 570. doi: 10.1104/pp.18.01588

Leong, S. A., Williams, P. H., and Ditta, G. S. (1985). Analysis of the 5′ regulatory region of the gene for δ-aminolevulinic acid synthetase of. *Rhizobium meliloti. Nucleic Acids Res.* 13 (16), 5965–5976. doi: 10.1093/nar/13.16.5965

Libbenga, K. R., and Harkes, P. A. A. (1973). Initial proliferation of cortical cells in the formation of root nodules in P*isum sativum* L. *Planta* 114, 17–28. doi: 10.1007/BF00390281

Limpens, E., Ramos, J., Franken, C., Raz, V., Compaan, B., Franssen, H., et al. (2004). RNA interference in *Agrobacterium rhizogenes*-transformed roots of Arabidopsis and *Medicago truncatula*. *J. Exp. Bot.* 55 (399), 983–992. doi: 10.1093/jxb/erh122

Luyten, E., and Vanderleyden, J. (2000). Survey of genes identified in *Sinorhizobium meliloti* spp., necessary for the development of an efficient symbiosis. *Eur. J. Soil Biol.* 36 (1), 1–26. doi: 10.1016/S1164-5563(00)00134-5

Magori, S., Oka-Kira, E., Shibata, S., Umehara, Y., Kouchi, H., Hase, Y., et al. (2009). TOO MUCH LOVE, a root regulator associated with the long-distance control of nodulation in *Lotus japonicus*. *Mol. Plant-Microbe Interact.* 22 (3), 259–268. doi: 10.1094/MPMI-22-3-0259

Mathesius, U., Weinman, J. J., Rolfe, B. G., and Djordjevic, M. A. (2000). Rhizobia can induce nodules in white clover by "hijacking" mature cortical cells activated during lateral root development. *Mol. Plant-Microbe Interact.* 13 (2), 170–182. doi: 10.1094/MPMI.2000.13.2.170

Meneely, P. (2020). *Genetic analysis: genes, genomes, and networks in eukaryotes* (USA: Oxford University Press).

Miyazawa, H., Oka-Kira, E., Sato, N., Takahashi, H., Wu, G.-J., Sato, S., et al. (2010). The receptor-like kinase KLAVIER mediates systemic regulation of nodulation and non-symbiotic shoot development in *Lotus japonicus. Development* 137, 24, 4317 LP–4325. doi: 10.1242/dev.058891

Mortier, V., Den Herder, G., Whitford, R., Van de Velde, W., Rombauts, S., D'haeseleer, K., et al. (2010). CLE peptides control *Medicago truncatula* nodulation locally and systemically. *Plant Physiol.* 153 (1), 222 LP–237. doi: 10.1104/pp.110.153718

Nimchuk, Z. L., Zhou, Y., Tarr, P. T., Peterson, B. A., and Meyerowitz, E. M. (2015). Plant stem cell maintenance by transcriptional cross-regulation of related receptor kinases. *Development* 142 (6), 1043 LP–1049. doi: 10.1242/dev.119677

Nishida, H., Handa, Y., Tanaka, S., Suzaki, T., and Kawaguchi, M. (2016). Expression of the CLE-RS3 gene suppresses root nodulation in. *Lotus japonicus. J. Plant Res.* 129 (5), 909–919. doi: 10.1007/s10265-016-0842-z

Nowak, S., Schnabel, E., and Frugoli, J. (2019). The *Medicago truncatula* CLAVATA3-LIKE CLE12/13 signaling peptides regulate nodule number depending on the CORYNE but not the COMPACT ROOT ARCHITECTURE2 receptor. *Plant Signaling Behav.* 14 (6), 1598730. doi: 10.1080/15592324.2019.1598730

Oka-Kira, E., Tateno, K., Miura, K., Haga, T., Hayashi, M., Harada, K., et al. (2005). *klavier (klv)*, a novel hypernodulation mutant of *Lotus japonicus* affected in vascular tissue organization and floral induction. *Plant J.* 44 (3), 505–515. doi: 10.1111/j.1365-313X.2005.02543.x

Okamoto, S., Ohnishi, E., Sato, S., Takahashi, H., Nakazono, M., Tabata, S., et al. (2009). Nod factor/nitrate-induced CLE genes that drive HAR1-mediated systemic regulation of nodulation. *Plant Cell Physiol.* 50 (1), 67–77. doi: 10.1093/pcp/pcn194

Osipova, M. A., Dolgikh, E. A., and Lutova, L. A. (2011). Peculiarities of meristem-specific WOX5 gene expression during nodule organogenesis in legumes. *Russian J. Dev. Biol.* 42 (4), 226. doi: 10.1134/S1062360411010085

Osipova, M. A., Mortier, V., Demchenko, K. N., Tsyganov, V. E., Tikhonovich, I. A., Lutova, L. A., et al. (2012). WUSCHEL-RELATED HOMEOBOX5 gene expression and interaction of CLE peptides with components of the systemic control add two pieces to the puzzle of autoregulation of nodulation. *Plant Physiol.* 158 (3), 1329–1341. doi: 10.1104/pp.111.188078

Penmetsa, R. V., Frugoli, J. A., Smith, L. S., Long, S. R., and Cook, D. R. (2003). Dual genetic pathways controlling nodule number in *Medicago truncatula*. *Plant Physiol.* 131 (3), 998 LP–1008. doi: 10.1104/pp.015677

Pfaffl, M. W. (2001). A new mathematical model for relative quantification in real-time RT-PCR. *Nucleic Acids Res.* 29 (9), e45. doi: 10.1093/nar/29.9.e45

Quandt, J., and Hynes, M. F. (1993). Versatile suicide vectors which allow direct selection for gene replacement in gram-negative bacteria. *Gene* 127 (1), 15–21. doi: 10.1016/0378-1119(93)90611-6

Rodriguez-Leal, D., Xu, C., Kwon, C.-T., Soyars, C., Demesa-Arevalo, E., Man, J., et al. (2019). Evolution of buffering in a genetic circuit controlling plant stem cell proliferation. *Nat. Genet.* 51 (5), 786–792. doi: 10.1038/s41588-019-0389-8

Roux, B., Rodde, N., Jardinaud, M., Timmers, T., Sauviac, L., Cottret, L., et al. (2014). An integrated analysis of plant and bacterial gene expression in symbiotic root nodules using laser-capture microdissection coupled to RNA sequencing. *Plant J.* 77 (6), 817–837. doi: 10.1111/tpj.12442

Roy, S., Liu, W., Nandety, R. S., Crook, A., Mysore, K. S., Pislariu, C. I., et al. (2020). Celebrating 20 years of genetic discoveries in legume nodulation and symbiotic nitrogen fixation. *Plant Cell* 32 (1), 15 LP–15 41. doi: 10.1105/tpc.19.00279

Schiessl, K., Lilley, J. L., Lee, T., Tamvakis, I., Kohlen, W., Bailey, P. C., et al. (2019). NODULE INCEPTION recruits the lateral root developmental program for symbiotic nodule organogenesis in *Medicago truncatula*. *Curr. Biol.* 29 (21), 3657–3668. doi: 10.1016/j.cub.2019.09.005

Schnabel, E. L., Chavan, S. A., Gao, Y., Poehlman, W. L., Feltus, F. A., and Frugoli, J. A. (2023a). A *Medicago truncatula* autoregulation of nodulation mutant transcriptome analysis reveals disruption of the *SUNN* pathway causes constitutive expression changes in some genes, but overall response to Rhizobia resembles wild-type, including induction of *TML1* and *TML2*. *Curr. Issues Mol. Biol.* 45 (6), 4612–4631. doi: 10.3390/cimb45060293

Schnabel, E., Journet, E.-P., de Carvalho-Niebel, F., Duc, G., and Frugoli, J. (2005). The *Medicago truncatula SUNN* gene encodes a CLV1-like leucine-rich repeat receptor kinase that regulates nodule number and root length. *Plant Mol. Biol.* 58 (6), 809–822. doi: 10.1007/s11103-005-8102-y

Schnabel, E., Karve, A., Kassaw, T., Mukherjee, A., Zhou, X., Hall, T., et al. (2012). The *M. truncatula SUNN* gene is expressed in vascular tissue, similarly to *RDN1*, consistent with the role of these nodulation regulation genes in long distance signaling. *Plant Signaling Behav.* 7, 1–3. doi: 10.4161/psb.7.1.18491

Schnabel, E. L., Kassaw, T. K., Smith, L. S., Marsh, J. F., Oldroyd, G. E., Long, S. R., et al. (2011). The ROOT DETERMINED NODULATION gene regulates nodule number in roots of *Medicago truncatula* and defines a highly conserved, uncharacterized plant gene family. *Plant Physiol.* 157 (1), 328–340. doi: 10.1104/pp.111.178756

Schnabel, E., Mukherjee, A., Smith, L., Kassaw, T., Long, S., and Frugoli, J. (2010). The *lss* supernodulation mutant of *Medicago truncatula* reduces expression of the *SUNN* gene. *Plant Physiol.* 154 (3), 1390–1402. doi: 10.1104/pp.110.164889

Schnabel, E., Thomas, J., El-Hawaz, R., Gao, Y., Poehlman, W., Chavan, S., et al. (2023b). Laser capture microdissection transcriptome reveals spatiotemporal tissue gene expression patterns of *M. truncatula* roots responding to rhizobia. *Mol. Plant-Microbe Interact* 36 (12), 805–820. doi: 10.1094/MPMI-03-23-0029-R

Searle, I. R., Men, A. E., Laniya, T. S., Buzas, D. M., Iturbe-Ormaetxe, I., Carroll, B. J., et al. (2003). Long-distance signaling in nodulation directed by a CLAVATA1-like receptor kinase. *Science* 299 (5603), 109–112. doi: 10.1126/science.107793

Simionatto, S., Marchioro, S. B., Galli, V., Luerce, T. D., Hartwig, D. D., Moreira, Â.N., et al. (2009). Efficient site-directed mutagenesis using an overlap extension-PCR method for expressing *Mycoplasma hyopneumoniae* genes in *Escherichia coli*. *J. Microbiological Methods* 79 (1), 101–105. doi: 10.1016/j.mimet.2009.08.016

Tadege, M., Wen, J., He, J., Tu, H., Kwak, Y., Eschstruth, A., et al. (2008). Large-scale insertional mutagenesis using the *Tnt1* retrotransposon in the model legume *Medicago truncatula*. *Plant J.* 54 (2), 335–347. doi: 10.1111/j.1365-313X.2008.03418.x

Takahara, M., Magori, S., Soyano, T., Okamoto, S., Yoshida, C., Yano, K., et al. (2013). TOO MUCH LOVE, a novel kelch repeat-containing F-box protein, functions in the long-distance regulation of the legume–Rhizobium symbiosis. *Plant Cell Physiol.* 54 (4), 433–447. doi: 10.1093/pcp/pct022

van Noorden, G. E., Ross, J. J., Reid, J. B., Rolfe, B. G., and Mathesius, U. (2006). Defective long-distance auxin transport regulation in the *Medicago truncatula super numeric nodules* mutant. *Plant Physiol.* 140 (4), 1494–1506. doi: 10.1104/pp.105.075879

Veerappan, V., Kadel, K., Alexis, N., Scott, A., Kryvoruchko, I., Sinharoy, S., et al. (2014). Keel petal incision: a simple and efficient method for genetic crossing in *Medicago truncatula*. *Plant Methods* 10 (1), 11. doi: 10.1186/1746-4811-10-11

Waese, J., Fan, J., Pasha, A., Yu, H., Fucile, G., Shi, R., et al. (2017). ePlant: visualizing and exploring multiple levels of data for hypothesis generation in plant biology. *Plant Cell* 29 (8), 1806–1821. doi: 10.1105/tpc.17.00073

Wang, W., Hu, C., Li, X., Zhu, Y., Tao, L., Cui, Y., et al. (2022). Receptor-like cytoplasmic kinases PBL34/35/36 are required for CLE peptide-mediated signaling to maintain shoot apical meristem and root apical meristem homeostasis in Arabidopsis. *Plant Cell.* 34, 4, 1289–1307. doi: 10.1093/plcell/koab315

Wang, C., Yang, H., Chen, L., Yang, S., Hua, D., and Wang, J. (2018). Truncated BAM receptors interfere the apical meristematic activity in a dominant negative manner when ectopically expressed in Arabidopsis. *Plant Sci.* 269, 20–31. doi: 10.1016/j.plantsci.2018.01.003

Willoughby, A. C., and Nimchuk, Z. L. (2021). WOX going on: CLE peptides in plant development. *Curr. Opin. Plant Biol.* 163, 102056. doi: 10.1016/j.pbi.2021.102056

Yamaguchi, Y. L., Ishida, T., and Sawa, S. (2016). CLE peptides and their signaling pathways in plant development. *J. Exp. Bot.* 67 (16), 4813–4826. doi: 10.1093/jxb/erw208

frontiers | Frontiers in Plant Science

TYPE Mini Review
PUBLISHED 12 January 2024
DOI 10.3389/fpls.2023.1284720

OPEN ACCESS

EDITED BY
Chang Fu Tian,
China Agricultural University, China

REVIEWED BY
Dong Wang,
University of Massachusetts Amherst, United States
Senjuti Sinharoy,
National Institute of Plant Genome Research (NIPGR), India

*CORRESPONDENCE
Jian Feng
jfeng@genetics.ac.cn

RECEIVED 29 August 2023
ACCEPTED 27 December 2023
PUBLISHED 12 January 2024

CITATION
Shen L and Feng J (2024) NIN—at the heart of NItrogen-fixing Nodule symbiosis. *Front. Plant Sci.* 14:1284720. doi: 10.3389/fpls.2023.1284720

NIN—at the heart of NItrogen-fixing Nodule symbiosis

Lisha Shen[1] and Jian Feng[1,2,3]*

[1]Key Laboratory of Seed Innovation, Institute of Genetics and Developmental Biology, Chinese Academy of Sciences, Beijing, China, [2]College of Advanced Agricultural Sciences, University of Chinese Academy of Sciences, Beijing, China, [3]CAS–JIC Centre of Excellence for Plant and Microbial Science (CEPAMS), Institute of Genetics and Developmental Biology, Chinese Academy of Sciences, Beijing, China

Legumes and actinorhizal plants establish symbiotic relationships with nitrogen-fixing bacteria, resulting in the formation of nodules. Nodules create an ideal environment for nitrogenase to convert atmospheric nitrogen into biological available ammonia. NODULE INCEPTION (NIN) is an indispensable transcription factor for all aspects of nodule symbiosis. Moreover, NIN is consistently lost in non-nodulating species over evolutions. Here we focus on recent advances in the signaling mechanisms of NIN during nodulation and discuss the role of NIN in the evolution of nitrogen-fixing nodule symbiosis.

KEYWORDS

nitrogen-fixing symbiosis, *NODULE INCEPTION*, infection thread, nodule organogenesis, autoregulation of nodulation

Introduction

Nitrogen is an indispensable nutrient for plant growth. The earth's atmosphere contains approximately 78% nitrogen. However, atmospheric nitrogen (N_2) cannot be directly utilized by most plants. Only some plant species from Fabales, Fagales, Cucurbitales, and Rosales (FaFaCuRo) clades exhibit the ability to establish symbiotic interactions with soil nitrogen-fixing bacteria, which are referred to rhizobia or *Frankia* (Soltis et al., 1995; Kistner and Parniske, 2002). This mutualistic symbiosis occurs within specialized structures known as nodules. Rhizobia in nodules utilize the catalytic activity of nitrogenase to convert atmospheric dinitrogen into ammonium, which serves as a nitrogen source for the host plant. In return, the host plant reciprocates by providing rhizobia with carbon sources (Santi et al., 2013; Stambulska and Bayliak, 2019). The establishment of symbiotic interactions requires communications and signal processing between host plants and bacterial partners. These molecular dialogues have been extensively studied in legumes, with a particular focus on model plants such as *Medicago truncatula* and *Lotus japonicus* (Roy et al., 2020; Wang et al., 2022).

Initially, legumes produce and release flavonoid compounds into the rhizosphere in nitrogen-deficient soils, serving as a signal to attract and stimulate rhizobia to produce oligosaccharide, known as Nod factors, thereby initiating a dialogue with the host plant (Zipfel and Oldroyd, 2017). Subsequently, Nod factors are recognized by specific types of receptor kinases, including LjNFR1 (NOD FACTOR RECEPTOR)/MtLYK3 (LysM

RECEPTOR KINASE 3), LjNFR5/MtNFP (NOD FACTOR PERCEPTION), and LjSYMRK (SYMBIOTIC RECEPTOR LIKE KINASE)/MtDMI2 (DOSE NOT MAKE INFECTION), which form homomeric and heteromeric complexes on the plasma membrane of root hair cells, triggering the nitrogen-fixing symbiotic signaling pathway (Endre et al., 2002; Stracke et al., 2002; Limpens et al., 2003; Madsen et al., 2003; Radutoiu et al., 2003; Arrighi et al., 2006; Smit et al., 2007; Broghammer et al., 2012; Moling et al., 2014). The perception of Nod factors by receptor kinases located on the membrane transmits the signal to the cell interior, leading to periodic fluctuations in the calcium concentration, referred as calcium spiking, in the nuclei of epidermal root hair cells, which depends on the collaboration of nuclear membranes-localized calcium channel proteins LjPOLLUX/MtDMI1, LjCASTOR, MtCNGC15 (CYCLIC NUCLEOTIDE GATED CHANNEL) and MCA8 (*M. truncatula* calcium ATPase) (Ané et al., 2004; Imaizumi-Anraku et al., 2005; Charpentier et al., 2008; Capoen et al., 2011; Charpentier et al., 2016). The occurrence of nuclear calcium spiking serves as a hallmark event for the activation of the symbiotic signaling pathway (Oldroyd and Downie, 2004). Following that, a calcium and calmodulin-dependent serine/threonine protein kinase, LjCCaMK/MtDMI3, is activated upon to decode the calcium signals, resulting in the phosphorylation of transcription factor LjCYCLOPS/MtIPD3 (INTERACTING PROTEIN OF DMI3) (Lévy et al., 2004; Yano et al., 2008; Singh and Parniske, 2012; Miller et al., 2013; Yuan et al., 2022). Activated LjCYCLOPS/MtIPD3 forms a transcriptional complex with NSP1, NSP2 (NODULATION SIGNALING PATHWAY) and DELLA proteins. Then, this complex promotes the expression of key transcription factor *NIN*, thus initiating NIN-regulated transcriptional network (Singh et al., 2014; Jin et al., 2016). Notably, NIN is one of the earliest-activated transcription factors downstream of common symbiotic signaling pathway (Schiessl et al., 2019).

The transcription factor NIN belongs to a plant-specific RWP-RK protein family. NIN controls all aspects of symbiotic nodulation in legumes: rhizobial infection, nodule organogenesis, transition to nitrogen fixation, and regulation of nodule number in legumes and actinorhizal plants (Figure 1) (Schauser et al., 1999; Borisov et al., 2003; Marsh et al., 2007; Soyano et al., 2013; Soyano et al., 2014; Clavijo et al., 2015; Liu C.W. et al., 2019; Liu J. et al., 2019b; Bu et al., 2020; Feng et al., 2021). Moreover, *NIN* gene is consistently lost or unfunctional in some non-nodulating species of FaFaCuRo clades, suggesting that the nitrogen-fixing ability of plants may associate with functional NIN protein (Griesmann et al., 2018; van Velzen et al., 2018; Zhang et al., 2023). In this review, we focus on recent advances in understanding the regulatory mechanisms of NIN in nodule symbiosis and discuss the evolution of *NIN* function in nitrogen-fixing nodule (NFN) symbiosis.

The transcription factor NIN: structure and function

The transcription factor NIN was initially identified in *L. japonicus* by forward genetic screening (Schauser et al., 1999). *nin* mutations block the rhizobial entry at an early stage (Table 1) (Schauser et al., 1999; Borisov et al., 2003; Marsh et al., 2007; Feng et al., 2021). CYCLOPS activates *NIN* expression by binding to the CYCLOPS-responsive elements (CYC-RE or PACE) in the *NIN* promoter (Singh et al., 2014; Cathebras et al., 2022). The CYC-RE in *NIN* promoter is conserved in legumes (Liu C. W. et al., 2019). It was recently reported that a putative CYC-RE was also present in the promoter of one poplar *NIN* ortholog (Irving et al., 2022), suggesting that this element may be recruited before the origin of nodulation. Both CYC-RE and PACE are critical for *NIN* function during infection thread development (Figure 1B) (Liu J. et al., 2019; Akamatsu et al., 2022; Cathebras et al., 2022). Additionally, another cis-element CE (cytokinin response element-containing region) was reported to be essential for nodule organogenesis and *NIN* expression in the pericycle (Figure 1B) (Liu J. et al., 2019). The CE is not present outside nodulated legumes (Liu and Bisseling, 2020; Zhang et al., 2023), suggesting that original recruitment of *NIN* into nodulation may occur in CYC-RE, whereas CE-dependent induction of *NIN* in inner root cell layers may evolve later.

NIN protein is characterized by a conserved 60-amino acid-long sequence containing an RWPxRK motif, which exhibits conservation with the MID (minus dominance) protein, the first identified member possessing this motif (Ferris and Goodenough, 1997). The conserved RWPxRK motif was subsequently designated as the RWP-RK domain and categorized as a novel class of transcription factors (Schauser et al., 1999). Structure predictions and a series of protein-DNA binding assays demonstrate the DNA-binding capability of RWP-RK domain, allowing NIN to interact with specific DNA sequences located within the promoters of target genes. These NIN-regulated genes include early nodulation genes such as *NF-YA1* and *NF-YB1* (*NUCLEAR FACTOR-Y SUBUNIT A1*), *NPL* (*NODULATION PECTATE LYASE*), *CRE1* (*CYTOKININ RESPONSE 1*), *ASYMMETRIC LEAVES 2-LIKE 18*/*LATERAL ORGAN BOUNDARIES DOMAIN 16* (*ASL18*/*LBD16*), and late nodulation-associated genes such as leghemoglobins, thioredoxins, nodule-specific cysteine-rich (NCR) peptides and glycine-rich peptides (Figures 1C–F) (Xie et al., 2012; Soyano et al., 2013; Vernié et al., 2015; Soyano et al., 2019; Feng et al., 2021).

Another remarkable characteristic of NIN protein is the presence of PB1 (Phox and Bem1) domain at its C-terminal end, which mediates protein-protein interactions, allowing NIN to form dimers or oligomers (Figure 1B) (Sumimoto et al., 2007; Feng et al., 2021). NIN-like proteins (NLPs), named after its homology to NIN protein, share the RWP-RK and PB1 domains with NIN, but not its N-terminal nitrate binding domain (Liu et al., 2022). NLPs have been characterized as key regulators of nitrate signaling in land plants (Castaings et al., 2009; Konishi and Yanagisawa, 2013; Marchive et al., 2013; Chardin et al., 2014; Liu et al., 2017; Alvarez et al., 2020; Liu et al., 2022). Interestingly, *M. truncatula* NLP1 and *L. japonicus* NLP1/4 are required for the repression of nodulation by nitrate (Lin et al., 2018; Nishida et al., 2018; Nishida et al., 2021). MtNLP1 interacts with NIN through the PB1 domain, leading to suppression of NIN-activated *CRE1* expression (Lin et al., 2018). Adaptations in *NIN* promoter and functional changes to NIN protein enable its specific functions in NFN symbiosis.

NIN facilitates intracellular rhizobial infection

The infection thread is crucial for rhizobia invasion into host plant during nodulation. Upon recognition of Nod factors released by rhizobia, root hairs of host plant undergo curling, enclosing the rhizobia attached to the surface of root hairs (Esseling et al., 2003). Subsequently, cell wall surrounding the enclosed rhizobia is locally degraded, and the cytoskeleton in root hair undergoes rearrangement, resulting in the invagination of cell membrane and formation of a tubular structure known as infection thread. Rhizobia gain entry into plant cells through infection threads,

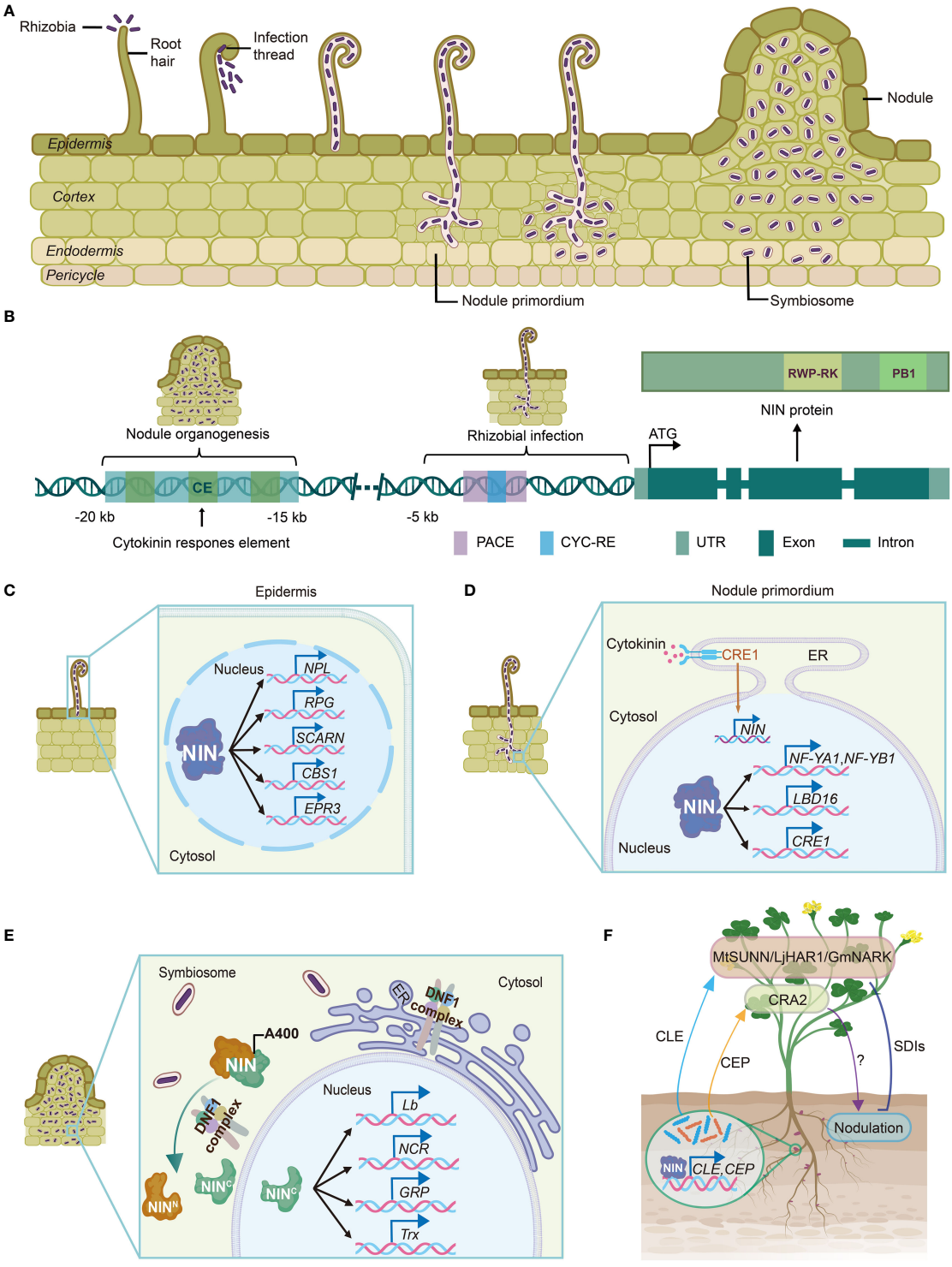

FIGURE 1 (Continued)

FIGURE 1 (Continued)
The transcription factor NIN plays essential roles in nitrogen-fixing nodulation. **(A)** Rhizobial infection and nodule organogenesis. Rhizobia enter the host plant through root hairs, which trap the bacteria inside. Afterwards, infection threads are formed and permit invasion of the rhizobia into inner root tissues. Nodule meristem initiates below the infection site in the cortex. The epidermal and cortical processes are coordinated to allow successful intracellular accommodation of rhizobia. Then infection threads then release membrane-bound rhizobia cells into nodule, where the bacteria differentiate and transit into nitrogen-fixing state. **(B)** *NIN* promoter harbors several cis-elements crucial for both rhizobial infection and nodule organogenesis. The CYC-RE and PACE elements in *LjNIN* promoter are required for infection thread development. The green boxes indicate three conserved regions identified in *MtNIN* promoter. The CE region in *MtNIN* promoter is essential for nodule organogenesis. **(C)** NIN facilitates rhizobial infection by regulating expression of infection-associated genes, such as *NPL*, *RPG*, *SCARN*, *CBS1* and *EPR3*. *NPL* encodes a pectate lyase enzyme involved in cell wall restructuring during rhizobia invasion. RPG is a critical determinant for the formation of infectosome, which is a protein complex essential for infection thread development. *SCARN* encodes a nodulation-specific component of the SCAR/WAVE complex. CBS1 contains a cystathionine-β-synthase (CBS) domain and a domain of unknown function. EPR3 is a LysM receptor that recognizes exopolysaccharides on the surface of rhizobia, promoting infection thread initiation. **(D)** NIN is essential for nodule organogenesis. NIN drives the expression of *NF-YA1* and *NF-YB1*, inducing cortical cell division and nodule primordium formation. NIN also controls the expression of *LBD16*, a key transcription factor involved in lateral root development, which has been hijacked to coordinate nodule development. Additionally, activated cytokinin receptor CRE1 promotes *NIN* expression in nodule primordium. Then, cortical NIN proteins activate *CRE1* expression, forming a positive feedback loop. **(E)** NIN determines the cellular state transition to nitrogen fixation. The DNF1-complex mediates the processing of NIN protein at A400, generating a C-terminal NIN fragment, which specifically activates a suit of genes involved in symbiosome development and nitrogen fixation, such as *Lb*, *NCR*, *GRP*, and *Trx*. **(F)** NIN controls AON signaling. NIN activates the expression of CLE and CEP peptides in root, which are subsequently transported to shoot. After perceived by MtSUNN/LjHAR1/GmNARK receptors, the CLE peptides activate the production of SDIs, which move back to root and suppress further nodulation. CEP peptides are recognized by shoot receptor CRA2, resulting in promotion of nodulation. Created with medpeer.cn. NIN, NODULE INCEPTION; CYC-RE, CYCLOPS-responsive element; PACE, Predisposition-Associated Cis-regulatory Element; CE, cytokinin response element-containing region; NPL, NODULATION PECTATE LYASE; RPG, RHIZOBIUM-DIRECTED POLAR GROWTH; EPR3, EXOPOLYSACCHARIDE RECEPTOR 3; ER, endoplasmic reticulum; NF-Y, NUCLEAR FACTOR-Y SUBUNIT; LBD16, LATERAL ORGAN BOUNDARIES DOMAIN 16; CRE1, CYTOKININ RESPONSE 1; DNF1, Defective in Nitrogen Fixation 1; Lb, leghemoglobin; NCR, nodule specific cysteine-rich; GRP, glycine-rich peptide; Trx, thioredoxin; AON, autoregulation of nodulation; CLE, CLAVATA3/EMBRYO SURROUNDING REGION; CEP, C-terminally

extending to the base of the root hair and subsequently penetrating the developing nodule primordia, which arise from differentiated cells composed of cortical cells, endodermis and pericycle (Figure 1A) (Oldroyd, 2013).

NIN is among the earliest-responding genes to rhizobia inoculation, suggesting its involvement in the initiation of bacterial infection, except rhizobial crack-entry infection in peanut (*Arachis hypogaea*) (Schiessl et al., 2019; Mergaert et al., 2020; Bhattacharjee et al., 2022). *NIN* loss of function leads to widespread defects in gene expression, highlighting its pivotal role in the gene regulatory network governing rhizobia infection (Liu C.W. et al., 2019). Notably, NIN controls many early genes associated with nodulation (Figure 1C). Among them, *NPL* encodes a pectate lyase enzyme involved in cell wall restructuring during rhizobia invasion (Xie et al., 2012). RPG (RHIZOBIUM-DIRECTED POLAR GROWTH) is a critical determinant for the formation of an exocyst complex (termed as infectosome) during bacterial infection (Arrighi et al., 2008; Lace et al., 2023). NIN directly binds to the *RPG* promoter and induce its expression (Li et al., 2023). *SCARN* (*SCAR-Nodulation*), a gene responsible for actin rearrangement during rhizobia infection, is induced by rhizobia in epidermal cells and directly regulated by NIN (Qiu et al., 2015). In addition, the absence of the membrane-localized protein CBS1 (cystathionine-β-synthase-like 1) results in the formation of an elevated number of microcolonies, whose expression is dependent on NIN (Sinharoy et al., 2016). NIN also promotes the expression of *EPR3* (*Exopolysaccharide Receptor 3*) in *L. japonicus*, a LysM receptor gene responsible for sensing rhizobia exopolysaccharides and facilitating the entry of rhizobia into host cells (Kawaharada et al., 2015; Kawaharada et al., 2017). These extensive regulations by NIN underscore its central role in orchestrating the early responses to rhizobia invasion in legumes.

NIN is essential for nodule organogenesis

As root hairs curl and entrap compatible rhizobia, cell divisions in the cortex, endodermis and pericycle are induced, triggering the formation of nodule primordia (Xiao et al., 2014). After successful invasion of legume plants by rhizobia, the initiation of root nodule organogenesis occurs in a coordinated manner to ensure accurate intrusion of infection thread into developing nodule primordium (Figure 1A) (Oldroyd and Downie, 2004). Mutants of *NF-YA1* and *NF-YB1*, members of nuclear factor-Y (NF-Y) transcription factor family, show abnormal infection thread development, delayed nodule formation, and smaller nodules, demonstrating their important roles in root nodule development (Laporte et al., 2013; Soyano et al., 2013). Further studies show that NIN directly binds to the promoter regions of *LjNF-YA1* and *LjNF-YB1* genes, promoting their expression (Figure 1D). Overexpression of *LjNIN* and *LjNF-YA1* genes induces cell division in the root cortex, resulting in the formation of nodule-like structures (Soyano et al., 2013). *ASL18/LBD16* is a key transcription factor that regulates lateral root development by activating expression of auxin synthesis-related genes, thus promoting auxin biosynthesis and influencing lateral root growth (Shahan and Benfey, 2020). Interestingly, the developmental program controlled by ASL18/LBD16 in lateral roots appears to be involved in root nodule organogenesis as well. NIN recruits the core developmental program of lateral roots to facilitate root nodule formation by promoting the expression of *ASL18/LBD16* (Figure 1D) (Schiessl et al., 2019; Soyano et al., 2019). These findings demonstrate that LBD16 and NF-Y transcription factors act downstream of NIN and work cooperatively to regulate root nodule development (Bishopp and Bennett, 2019).

TABLE 1 List of published *nin* alleles in nodulating plants.

Species	Allele	Mutant line	Background	Phenotypic defects			Mutagen	Genomic mutation	Effect of mutation	Reference
				Infection	Nodule organogenesis	Nitrogen fixation				
Lotus japonicus	*Ljnin-1*	96.1M2	Gifu	n/a	Nod-	n/a	*Ac* transposon insertion	Transposon insertion at C1459	*Ac* transposon insertion (unstable)	Schauser et al., 1999
	Ljnin-2	96.1M2 offspring 1	Gifu	n/a	Nod-	n/a	*Ac* transposon insertion	Transposon insertion at C1459	Frame shift	Schauser et al., 1999
	Ljnin-3	96.1M2 offspring 2	Gifu	n/a	Nod-	n/a	*Ac* transposon insertion	Transposon insertion at C1459	Frame shift	Schauser et al., 1999
	Ljnin-4	96.1M2 offspring 3	Gifu	n/a	Nod+	n/a	*Ac* transposon insertion	Transposon insertion at C1459	Amino acid insertion (V410-N411)	Schauser et al., 1999
	Ljnin-5	96.1M2 offspring 4	Gifu	n/a	Nod+	n/a	*Ac* transposon insertion	Transposon insertion at C1459	Amino acid insertion (N410)	Schauser et al., 1999
	Ljnin-6	KL773	Gifu	n/a	Nod+	n/a	*Ac* transposon insertion	Transposon insertion at C1459	Amino acid insertion (V410-N411)	Perry et al., 2009
	Ljnin-7	*sym47*	Gifu	Inf-	n/a	n/a	Lotus retrotransposon 1 insertion	Transposon insertion at G2599	n/a	Madsen et al., 2005
		KL577	n/a	n/a	Nod-	n/a	n/a	n/a	n/a	Sandal et al., 2006
	Ljnin-8	B21-1[a]; B47-B	Gifu	n/a	Inf-	n/a	EMS	C1785 to T	Q519 to stop condon	Murray et al., 2006; Perry et al., 2009
	Ljnin-9	SL5369[b]; SL5426[c]	Gifu	n/a	Nod+; Nod-	n/a	EMS	G1002 to A	V258 to M	Perry et al., 2009
		n/a	MG-20	n/a	Nod-	n/a	EMS	A nucleotide substitution from G2017 to A at splice donor site	n/a	Suzaki et al., 2012
	Ljnin-10	S46-1[d]	Gifu	n/a	Nod-	n/a	EMS	G1242 to A	A338 to T	Murray et al., 2006; Perry et al., 2009
	Ljnin-11	SL0605-2, 3[e]	Gifu	n/a	Nod-	n/a	EMS	G1848 to A	E540 to K	Perry et al., 2009

(Continued)

10.3389/fpls.2023.1284720

TABLE 1 Continued

Species	Allele	Mutant line	Background	Phenotypic defects			Mutagen	Genomic mutation	Effect of mutation	Reference
				Infection	Nodule organogenesis	Nitrogen fixation				
Lotus japonicus	*Ljnin-12*	SL1798-2, 4, 5	Gifu	n/a	Nod+	n/a	EMS	G1927 to A	R566 to K	Perry et al., 2009
	Ljnin-13	SL3012-1	Gifu	n/a	n/a	n/a	EMS	G2431 to A	G685 to R	Perry et al., 2009
	Ljnin-14	SL5800-3	Gifu	n/a	Nod-	n/a	EMS	G986 to A	E252 to E	Perry et al., 2009
	Ljnin-15	n/a	Gifu	Inf-	Nod+	n/a	Lotus retrotransposon 1 insertion	Transposon insertion at *NIN* promoter 143 bp of 3' PACE element	n/a	Cathebras et al., 2022
	daphne	n/a	MG-20	Inf+	Nod-	n/a	Carbon ion beam irradiation	A reciprocal chromosomal translocation at approximately 7 kb upstream of the start codon of *NIN*	Knock down	Yoro et al., 2014
Medicago truncatula	*Mtnin-1*	12S	A17	Inf-	Nod-	n/a	Fast neutron bombardment	An 11 bp deletion at 1850 bp	Frame shift leads to premature termination	Marsh et al., 2007
	Mtnin-2	Tnt148	R108	Inf-	Nod-	n/a	*Tnt1* transposon insertion	Transposon insertion at 20 bp upstream of the start codon of *NIN*	Knock down	Marsh et al., 2007
	Mtnin-3	Tnk148	R108	n/a	Nod-	n/a	*Tnt1* transposon insertion	Transposon insertion at 26 bp upstream of the start codon of *NIN*	n/a	Pislariu et al., 2012
	Mtnin-4	NF2728	R108	n/a	Nod-	n/a	*Tnt1* transposon insertion	Transposon insertion at 617 bp of *NIN*	n/a	Pislariu et al., 2012
	Mtnin-5	NF0532	R108	n/a	Nod-	n/a	*Tnt1* transposon insertion	Transposon insertion at 704 bp of *NIN*	n/a	Pislariu et al., 2012
	Mtnin-6	NF1317	R108	n/a	Nod-	n/a	*Tnt1* transposon insertion	Transposon insertion at 1196 bp of *NIN*	n/a	Pislariu et al., 2012
	Mtnin-7	NF1277	R108	n/a	Nod-	n/a	*Tnt1* transposon insertion	Transposon insertion at 1397 bp of *NIN*	n/a	Pislariu et al., 2012
	Mtnin-8	NF1263	R108	n/a	Nod-	n/a	*Tnt1* transposon insertion	Transposon insertion at 1664 bp of *NIN*	n/a	Pislariu et al., 2012

(Continued)

10.3389/fpls.2023.1284720

TABLE 1 Continued

Species	Allele	Mutant line	Background	Phenotypic defects			Mutagen	Genomic mutation	Effect of mutation	Reference
				Infection	Nodule organogenesis	Nitrogen fixation				
Medicago truncatula	*Mtnin-9*	NF3019	R108	n/a	Nod-	n/a	*Tnt1* transposon insertion	Transposon insertion at 1665 bp of *NIN*	n/a	Pislariu et al., 2012
	Mtnin-10	NF0117	R108	n/a	Nod-	n/a	*Tnt1* transposon insertion	Transposon insertion at 1977 bp of *NIN*	n/a	Pislariu et al., 2012
	Mtnin-11	NF3046	R108	n/a	Nod-	n/a	*Tnt1* transposon insertion	Transposon insertion at 2241 bp of *NIN*	n/a	Pislariu et al., 2012
	Mtnin-12	NF2640	R108	n/a	Nod-	n/a	*Tnt1* transposon insertion	Transposon insertion at 2628 bp of *NIN*	n/a	Pislariu et al., 2012
	Mtnin-13	NF0440	R108	n/a	Nod+	n/a	*Tnt1* transposon insertion	Transposon insertion at 2647 bp of *NIN*	Frame shift leads to PB1 deletion	Pislariu et al., 2012; Liu et al., 2021
	Mtnin-14	NF0825	R108	n/a	Nod-	n/a	*Tnt1* transposon insertion	Transposon insertion at 2819 bp of *NIN*	n/a	Pislariu et al., 2012
	Mtnin-15	NF2700	R108	n/a	Nod-	n/a	*Tnt1* transposon insertion	Transposon insertion at 2970 bp of *NIN*	n/a	Pislariu et al., 2012
	Mtnin-16	NF10547	R108	n/a	Nod+	n/a	*Tnt1* transposon insertion	Transposon insertion at 2669 bp of *NIN*	Frame shift leads to PB1 deletion	Veerappan et al., 2016; Liu et al., 2021
	daphne-like	FN8113	A17	Inf+	Nod-	n/a	Fast neutron bombardment	2.49 Mb chromosome 2 insertion at 4120 bp upstream of the start codon of *NIN*	n/a	Liu J. et al., 2019
Pisum sativum	*Psnin/ sym35*	SGENod$^-$1	SGE	Inf-	Nod-	n/a	EMS	C1657 to T	Q553 to stop condon	Tsyganov et al., 1999; Borisov et al., 2003
	Psnin/ sym35	SGENod$^-$3	SGE	Inf-	Nod-	n/a	EMS	C160 to T	Q54 to stop condon	Tsyganov et al., 1999; Borisov et al., 2003
		RisNod8	Finale	Inf-	Nod-	n/a	EMS	G1210 to A	E404 to K	Engvild, 1987; Borisov et al., 2003

(Continued)

10.3389/fpls.2023.1284720

TABLE 1 Continued

Species	Allele	Mutant line	Background	Phenotypic defects			Mutagen	Genomic mutation	Effect of mutation	Reference
				Infection	Nodule organogenesis	Nitrogen fixation				
Glycine max	*Gmnin1a*	n/a	Williams 82	n/a	Nod-	n/a	RNA interference	n/a	Knock down	Fu et al., 2021
	Gmnin1b	n/a	Williams 82	n/a	Nod+	n/a	RNA interference	n/a	Knock down	Fu et al., 2021
	Gmnin2a	n/a	Williams 82	n/a	Nod+	n/a	RNA interference	n/a	Knock down	Fu et al., 2021
	Gmnin2b	n/a	Williams 82	n/a	Nod+	n/a	RNA interference	n/a	Knock down	Fu et al., 2021
	Gmnin1b	n/a	Huachun 6	Inf+	Nod+	n/a	CRISPR-Cas9	C1774 deletion	Frame shift leads to premature termination	Bai et al., 2020; Fu et al., 2022
	Gmnin1a nin1b	n/a	Huachun 6	Inf+	Nod+	n/a	CRISPR-Cas9	1 bp insertion at G1773 of *NIN1a*	Frame shift leads to premature termination	Bai et al., 2020; Fu et al., 2022
								1 bp insertion at G1699 of *NIN1b*	Frame shift leads to premature termination	Bai et al., 2020; Fu et al., 2022
	Gmnin2a nin2b	n/a	Huachun 6	Inf+	Nod+	n/a	CRISPR-Cas9	83 bp insertion at G1564 of *NIN2a*	Frame shift leads to premature termination	Bai et al., 2020; Fu et al., 2022
								86 bp insertion at G1285 of *NIN2b*	Frame shift leads to premature termination	Bai et al., 2020; Fu et al., 2022
	Gmnin1a nin2a nin2b	n/a	Huachun 6	Inf-	Nod-	n/a	CRISPR-Cas9	14 bp deletion at G250 of *NIN1a*	Frame shift leads to premature termination	Bai et al., 2020; Fu et al., 2022
								Insertions at A1540 of *NIN2a*	Frame shift leads to premature termination	Bai et al., 2020; Fu et al., 2022
								G1264 and A1265 deletions and 86 bp insertion at G1285 of *NIN2b*	Frame shift leads to premature termination	Bai et al., 2020; Fu et al., 2022
	Gmnin1a nin1b nin2a nin2b	n/a	Huachun 6	Inf-	Nod-	n/a	CRISPR-Cas9	5 bp deletion at G255 of *NIN1a*	Frame shift leads to premature termination	Bai et al., 2020; Fu et al., 2022
								14 bp deletion at G256 of *NIN1b*	Frame shift leads to premature termination	Bai et al., 2020; Fu et al., 2022
								G1543 and A1544 deletions and 83 bp insertion at G1564 of *NIN2b*	Frame shift leads to premature termination	Bai et al., 2020; Fu et al., 2022
								Insertion at A1265 of *NIN2b*	Frame shift leads to premature termination	Bai et al., 2020; Fu et al., 2022

(Continued)

10.3389/fpls.2023.1284720

10.3389/fpls.2023.1284720

TABLE 1 Continued

Species	Allele	Mutant line	Background	Phenotypic defects			Mutagen	Genomic mutation	Effect of mutation	Reference
				Infection	Nodule organogenesis	Nitrogen fixation				
Cicer arietinum	*Carn4*	PM405	P502 (ICC 640)	n/a	Nod+	Fix-	γ-ray irradiation	A2189 deletion	Frame shift leads to PB1 deletion	Davis, 1986; Frailey et al., 2022
Parasponia andersonii	*Pannin*	B1	WU1.14	n/a	Nod-	n/a	CRISPR-Cas9	Deletions at T181 and A242 of *NIN*	Frame shift leads to stop condon at amino acid position 90	Bu et al., 2020
		B3	WU1.14	n/a	Nod-	n/a	CRISPR-Cas9	Deletion at T181 of *NIN*	Frame shift leads to stop condon at amino acid position 70	Bu et al., 2020

[a]Line contains in addition a *har1-1* mutation.
[b]Line SL5369 carries the mutant alleles *nin-9* and *nsp2-9*.
[c]Line SL5426 carries the mutant alleles *nfr1-6*, *nfr5-6* and *nin-9*.
[d]Line S46-1 carries the mutant alleles *castor-25*, *nin-10*, and *har1-1*.
[e]Lines SL0605-2,3 carry the mutant alleles *nin-11* and *symrk-9*.
n/a: not applicable.

Phytohormone cytokinin plays key roles in regulating various aspects of plant growth and development. Exogenous application of cytokinin has been shown to induce formation of nodule-like structures in leguminous plants (Gauthier-Coles et al., 2018). In *L. japonicus*, gain-of-function mutants *snf2* and *snf5* (*spontaneous nodule formation*) of the cytokinin receptor gene *LHK1* (*LOTUS HISTIDINE KINASE1*) exhibit a spontaneous nodule phenotype in the absence of rhizobia (Tirichine et al., 2007; Liu et al., 2018). Similarly, overexpression of gain-of-function *CRE1* mutant, a homolog of *LHK1* in *M. truncatula*, also induces rhizobia-free nodule formation (Jin et al., 2016). These results demonstrate the essential role of cytokinin signaling in nodule formation. Interestingly, the *NIN* gene is up-regulated by cytokinin treatment or *snf2* mutation. And spontaneous nodule formation in *snf2* mutants appears a NIN-dependent manner (Tirichine et al., 2007). Consistently, a distal element in *NIN* promoter, containing putative cytokinin B-type response regulator binding sites, is responsible for cytokinin-induced *NIN* expression, which is necessary for nodule organogenesis (Figure 1B) (Liu J. et al., 2019b). Furthermore, NIN protein is sufficient to activate the expression of *CRE1*, forming a positive feedback regulatory loop that promotes nodule development (Figure 1D) (Vernié et al., 2015). Alongside this, cytokinin and *NIN*-overexpression induced cortical cell divisions are dependent on the GRAS proteins MtSHR (SHORTROOT) and MtSCR (SCARECROW) (Dong et al., 2021). Together, these findings reveal the crucial role of NIN-dependent regulatory network governing root nodule formation in leguminous plants.

NIN determines the transition to nitrogen fixation

Symbiotic nitrogen fixation requires a low-oxygen environment for proper activity of nitrogenase (Kondorosi et al., 2013). However, the mechanism controlling the transition to nitrogen fixation remains elusive for years. While NIN has been extensively studied for its role in various aspects of nodule initiation and development, recent research reveals that NIN also regulates the transition of nodule cells into nitrogen-fixing state. Nodulation activated signal peptidase complex (SPC) mediates the processing of NIN protein, resulting in production of a C-terminal NIN fragment containing the DNA binding domain. The processed C-terminal product of NIN specifically activates a suite of genes associated with symbiosome development and nitrogen fixation [such as genes encoding leghemoglobins, nodule specific cysteine-rich (NCR) peptides and thioredoxins], thereby controlling the cell state transition (Figure 1E) (Feng et al., 2021). In addition, NIN and its close homolog NLP2 directly promote the expression of leghemoglobins, which buffer the oxygen concentration within nodules (Jiang et al., 2021). These findings demonstrate the important roles of NIN and NLP2 in creating suitable environment for nitrogen fixation.

NIN controls autoregulation of nodulation

Symbiotic nodulation is an energy-consuming process, and excessive nodule formation adversely affects regular development of host plant (Wang et al., 2021; Ke et al., 2022). To maintain energy balance between nitrogen fixation and other developmental processes, nodule number is tightly controlled by autoregulation of nodulation (AON) system. AON signaling pathway consists of root-derived signals, receptors in shoot and shoot-derived inhibitors (SDIs), which involve root-shoot-root communications determining optimal nodule numbers (Roy et al., 2020). Transcription factor NIN activates the expression of *CLE* (*CLAVATA3/EMBRYO SURROUNDING REGION*) peptides to initiate AON (Figure 1F) (Soyano et al., 2014; Laffont et al., 2020; Wang et al., 2020). The AON-related CLE peptides are widely present in legumes, including *M. truncatula* CLE12/13, *L. japonicus* CLE-RS1/2 (CLE-ROOT SIGNAL), as well as RIC1/2 (RHIZOBIUM INDUCED CLE) peptides in soybean (*Glycine max*) and common bean (*Phaseolus vulgaris*). As root-derived signals, these CLEs are transported through xylem to shoot (Okamoto et al., 2008; Mortier et al., 2010; Lim et al., 2011), where they are recognized by the leucine-rich-repeat receptor-like kinase (LRR-RLK), termed MtSUNN (SUPER NUMERIC NODULES) in *M. truncatula*, LjHAR1 (HYPER NODULATION ABERRANT ROOT FORMATION 1) in *L. japonicus*, and GmNARK (NODULE AUTOREGULATION RECEPTOR KINASE) in *G. max*. This perception triggers production of SDIs that move back to root suppressing further nodulation (Krusell et al., 2002; Nishimura et al., 2002; Searle et al., 2003; Schnabel et al., 2005; Tsikou et al., 2018). In contrast, *M. truncatula* CEP7 (C-terminally Encoded Peptide), which is induced by rhizobia and cytokinin, plays a crucial role in promoting rhizobia infections and nodule formation through the receptor MtCRA2 (COMPACT ROOT ARCHITECTURE 2) in shoots. Coordinated expression of *CLE* and *CEP* genes by NIN allows precise control of nodule number in plants (Figure 1F) (Laffont et al., 2020). In soybean, GmNINa activates the expression of *miR172c*, which relieves the transcriptional repression of *GmRIC1/2* by NNC1 (Nodule Number Control 1), thus activating AON pathway. Conversely, NNC1 represses *miR172c* expression, forming a negative feedback loop. NNC1 also interacts with GmNINa to antagonistically regulate the transcriptional activation of *GmRIC1/2*. Thus, the GmNINa-miR172c-NNC1 signaling axis systemically regulates nodulation and AON signaling (Wang et al., 2019).

Discussion

Symbiotic associations between plants and nitrogen-fixing microbes shape the global ecosystems during the evolution of life on earth. However, plants forming NFN symbiosis are restricted to the FaFaCuRo families (Griesmann et al., 2018; van Velzen et al., 2018; Zhang et al., 2023). Possibly because NFN symbiosis needs intensive energy to produce nodules and fuel nitrogen-fixing reactions. Alternatively, reduced immune responses allowing rhizobia invasion may make plants susceptible to disease (Mathesius, 2022). Recent phylogenomic studies propose a scenario of single gain of nodulation, followed by multiple losses (van Velzen et al., 2019). The emergence of master regulator NIN from a duplication event of NLP and subsequent evolutionary changes, such as the acquisition of specific promoter elements and/or amino acid substitutions, underscores its adaptive significance in driving the evolution of NFN symbiosis in legumes (Liu J. et al., 2019b; Cathebras et al., 2022; Zhang et al., 2023). More efforts are needed to decipher the molecular changes on NIN protein to enable occurrence of NFN symbiosis. We need to better understand the underlying mechanisms of NIN and NLP in regulating different biological processes that range from NFN symbiosis and nitrate signaling. Knowledge from analysis of fossil samples with root nodules and ancient DNA studies would also provide direct evidence for how the NFN symbiosis origins.

Since this initial discovery, *NIN* has been identified as essential for nodulation in nitrogen-fixing land plants. Besides legumes, NIN orthologs are also required for NFN symbiosis in actinorhizal plants *Parasponia andersonii* and *Casuarina glauca* (Clavijo et al., 2015; Bu et al., 2020). *P. andersonii* hosts rhizobia in thread-like structure, called fixation thread, which is equivalent to symbiosome in legumes that hosts its rhizobial partners. Both structures provide proper environments for nitrogen fixation (Behm et al., 2014). It would be interesting to explore whether the regulatory mechanisms on nodulation and nitrogen fixation mediated by NIN is conserved between legumes and actinorhizal plants. Furthermore, a novel NFN between seagrass *Posidonia oceanica* and N_2-fixing symbiont has been reported recently (Mohr et al., 2021). This finding makes it possible to test functional conservation of NIN in NFN symbiosis across land and aquatic plants. To obtain a complete picture of mechanisms that control the interactions between plants and nitrogen-fixing microorganisms, more plant-microbe systems are needed to be established. Future investigations of NFN symbiosis occurring across diverse plant species will expand our knowledge of molecular mechanisms for nitrogen-fixing signaling and will allow a strategic initiative towards the transfer of the nitrogen-fixing symbiosis to non-nodulating crops.

Author contributions

LS: Investigation, Validation, Writing – original draft, Writing – review & editing. JF: Conceptualization, Funding acquisition, Investigation, Project administration, Resources, Supervision, Validation, Visualization, Writing – review & editing.

Funding

The author(s) declare financial support was received for the research, authorship, and/or publication of this article. Research on this topic in Jian Feng's laboratory is supported by the National Key R&D Program of China (2022YFF1003201), the National Natural Science Foundation of China (32370261), and the Key Laboratory of Seed Innovation.

Acknowledgments

The authors thank members of Jian Feng's laboratory for continuous discussion. We apologize to our colleagues whose work could not be cited here owing to limited space.

Conflict of interest

The authors declare that the research was conducted in the absence of any commercial or financial relationships that could be construed as a potential conflict of interest.

Publisher's note

References

Akamatsu, A., Nagae, M., and Takeda, N. (2022). The *CYCLOPS response element* in the *NIN* promoter is important but not essential for infection thread formation during *Lotus japonicus*-rhizobia symbiosis. *Mol. Plant Microbe Interact.* 35 (8), 650–658. doi: 10.1094/MPMI-10-21-0252-R

Alvarez, J. M., Schinke, A. L., Brooks, M. D., Pasquino, A., Leonelli, L., Varala, K., et al. (2020). Transient genome-wide interactions of the master transcription factor NLP7 initiate a rapid nitrogen-response cascade. *Nat. Commun.* 11 (1), 1157. doi: 10.1038/s41467-020-14979-6

Ané, J. M., Kiss, G. B., Riely, B. K., Penmetsa, R. V., Oldroyd, G. E., Ayax, C., et al. (2004). *Medicago truncatula DMI1* required for bacterial and fungal symbioses in legumes. *Science* 303 (5662), 1364–1367. doi: 10.1126/science.1092986

Arrighi, J. F., Barre, A., Ben Amor, B., Bersoult, A., Soriano, L. C., Mirabella, R., et al. (2006). The *Medicago truncatula* lysine motif-receptor-like kinase gene family includes *NFP* and new nodule-expressed genes. *Plant Physiol.* 142 (1), 265–279. doi: 10.1104/pp.106.084657

Arrighi, J. F., Godfroy, O., de Billy, F., Saurat, O., Jauneau, A., and Gough, C. (2008). The *RPG* gene of *Medicago truncatula* controls *Rhizobium*-directed polar growth during infection. *Proc. Natl. Acad. Sci. U.S.A.* 105 (28), 9817–9822. doi: 10.1073/pnas.0710273105

Bai, M., Yuan, J., Kuang, H., Gong, P., Li, S., Zhang, Z., et al. (2020). Generation of a multiplex mutagenesis population *via* pooled CRISPR-Cas9 in soya bean. *Plant Biotechnol. J.* 18 (3), 721–731. doi: 10.1111/pbi.13239

Behm, J. E., Geurts, R., and Kiers, E. T. (2014). Parasponia: a novel system for studying mutualism stability. *Trends Plant Sci.* 19 (12), 757–763. doi: 10.1016/j.tplants.2014.08.007

Bhattacharjee, O., Raul, B., Ghosh, A., Bhardwaj, A., Bandyopadhyay, K., and Sinharoy, S. (2022). *Nodule INception*-independent epidermal events lead to bacterial entry during nodule development in peanut (*Arachis hypogaea*). *New Phytol.* 236 (6), 2265–2281. doi: 10.1111/nph.18483

Bishopp, A., and Bennett, M. J. (2019). Turning lateral roots into nodules. *Science* 366 (6468), 953–954. doi: 10.1126/science.aay8620

Borisov, A. Y., Madsen, L. H., Tsyganov, V. E., Umehara, Y., Voroshilova, V. A., Batagov, A. O., et al. (2003). The *Sym35* gene required for root nodule development in pea is an ortholog of *Nin* from *Lotus japonicus*. *Plant Physiol.* 131 (3), 1009–1017. doi: 10.1104/pp.102.016071

Broghammer, A., Krusell, L., Blaise, M., Sauer, J., Sullivan, J. T., Maolanon, N., et al. (2012). Legume receptors perceive the rhizobial lipochitin oligosaccharide signal molecules by direct binding. *Proc. Natl. Acad. Sci.* 109 (34), 13859–13864. doi: 10.1073/pnas.1205171109

Bu, F., Rutten, L., Roswanjaya, Y. P., Kulikova, O., Rodriguez-Franco, M., Ott, T., et al. (2020). Mutant analysis in the nonlegume *Parasponia andersonii* identifies NIN and NF-YA1 transcription factors as a core genetic network in nitrogen-fixing nodule symbioses. *New Phytol.* 226 (2), 541–554. doi: 10.1111/nph.16386

Capoen, W., Sun, J., Wysham, D., Otegui, M. S., Venkateshwaran, M., Hirsch, S., et al. (2011). Nuclear membranes control symbiotic calcium signaling of legumes. *Proc. Natl. Acad. Sci. U.S.A.* 108 (34), 14348–14353. doi: 10.1073/pnas.1107912108

Castaings, L., Camargo, A., Pocholle, D., Gaudon, V., Texier, Y., Boutet-Mercey, S., et al. (2009). The nodule inception-like protein 7 modulates nitrate sensing and metabolism in Arabidopsis. *Plant J.* 57 (3), 426–435. doi: 10.1111/j.1365-313X.2008.03695.x

Cathebras, C., Gong, X., Andrade, R. E., Vondenhoff, K., Keller, J., Delaux, P.-M., et al. (2022). A novel cis-element enabled bacterial uptake by plant cells. *BioRxiv* 28, 486070. doi: 10.1101/2022.03.28.486070

Chardin, C., Girin, T., Roudier, F., Meyer, C., and Krapp, A. (2014). The plant RWP-RK transcription factors: key regulators of nitrogen responses and of gametophyte development. *J. Exp. Bot.* 65 (19), 5577–5587. doi: 10.1093/jxb/eru261

Charpentier, M., Bredemeier, R., Wanner, G., Takeda, N., Schleiff, E., and Parniske, M. (2008). *Lotus japonicus* CASTOR and POLLUX are ion channels essential for perinuclear calcium spiking in legume root endosymbiosis. *Plant Cell* 20 (12), 3467–3479. doi: 10.1105/tpc.108.063255

Charpentier, M., Sun, J., Vaz Martins, T., Radhakrishnan, G. V., Findlay, K., Soumpourou, E., et al. (2016). Nuclear-localized cyclic nucleotide-gated channels mediate symbiotic calcium oscillations. *Science* 352 (6289), 1102–1105. doi: 10.1126/science.aae0109

Clavijo, F., Diedhiou, I., Vaissayre, V., Brottier, L., Acolatse, J., Moukouanga, D., et al. (2015). The *Casuarina NIN* gene is transcriptionally activated throughout *Frankia* root infection as well as in response to bacterial diffusible signals. *New Phytol.* 208 (3), 887–903. doi: 10.1111/nph.13506

Davis, T. M. (1988). Two genes that confer ineffective nodulation in chickpea (*Cicer arietinum* l.). *J. Hered.* 79 (6), 476–478. doi: 10.1093/oxfordjournals.jhered.a110555

Dong, W., Zhu, Y., Chang, H., Wang, C., Yang, J., Shi, J., et al. (2021). An SHR-SCR module specifies legume cortical cell fate to enable nodulation. *Nature* 589 (7843), 586–590. doi: 10.1038/s41586-020-3016-z

Endre, G., Kereszt, A., Kevei, Z., Mihacea, S., Kaló, P., and Kiss, G. B. (2002). A receptor kinase gene regulating symbiotic nodule development. *Nature* 417 (6892), 962–966. doi: 10.1038/nature00842

Engvild, K. C. (1987). Nodulation and nitrogen fixation mutants of pea, *Pisum sativum*. *Theor. Appl. Genet.* 74 (6), 711–713. doi: 10.1007/BF00247546

Esseling, J. J., Lhuissier, F. G., and Emons, A. M. (2003). Nod factor-induced root hair curling: continuous polar growth towards the point of nod factor application. *Plant Physiol.* 132 (4), 1982–1988. doi: 10.1104/pp.103.021634

Feng, J., Lee, T., Schiessl, K., and Oldroyd, G. E. D. (2021). Processing of NODULE INCEPTION controls the transition to nitrogen fixation in root nodules. *Science* 374 (6567), 629–632. doi: 10.1126/science.abg2804

Ferris, P. J., and Goodenough, U. W. (1997). Mating type in Chlamydomonas is specified by *mid*, the minus-dominance gene. *Genetics* 146 (3), 859–869. doi: 10.1093/genetics/146.3.859

Frailey, D. C., Zhang, Q., Wood, D. J., and Davis, T. M. (2022). Defining the mutation sites in chickpea nodulation mutants PM233 and PM405. *BMC Plant Biol.* 22 (1), 66. doi: 10.1186/s12870-022-03446-7

Fu, M., Sun, J., Li, X., Guan, Y., and Xie, F. (2022). Asymmetric redundancy of soybean nodule inception (NIN) genes in root nodule symbiosis. *Plant Physiol.* 188 (1), 477–489. doi: 10.1093/plphys/kiab473

Gauthier-Coles, C., White, R. G., and Mathesius, U. (2018). Nodulating legumes are distinguished by a sensitivity to cytokinin in the root cortex leading to pseudonodule development. *Front. Plant Sci.* 9. doi: 10.3389/fpls.2018.01901

Griesmann, M., Chang, Y., Liu, X., Song, Y., Haberer, G., Crook, M. B., et al. (2018). Phylogenomics reveals multiple losses of nitrogen-fixing root nodule symbiosis. *Science* 361 (6398), eaat1743. doi: 10.1126/science.aat1743

Imaizumi-Anraku, H., Takeda, N., Charpentier, M., Perry, J., Miwa, H., Umehara, Y., et al. (2005). Plastid proteins crucial for symbiotic fungal and bacterial entry into plant roots. *Nature* 433 (7025), 527–531. doi: 10.1038/nature03237

Irving, T. B., Chakraborty, S., Maia, L. G. S., Knaack, S., Conde, D., Schmidt, H. W., et al. (2022). An LCO-responsive homolog of *NODULE INCEPTION* positively regulates lateral root formation in Populus sp. *Plant Physiol.* 190 (3), 1699–1714. doi: 10.1093/plphys/kiac356

Jiang, S., Jardinaud, M. F., Gao, J., Pecrix, Y., Wen, J., Mysore, K., et al. (2021). NIN-like protein transcription factors regulate leghemoglobin genes in legume nodules. *Science* 374 (6567), 625–628. doi: 10.1126/science.abg5945

Jin, Y., Liu, H., Luo, D., Yu, N., Dong, W., Wang, C., et al. (2016). DELLA proteins are common components of symbiotic rhizobial and mycorrhizal signalling pathways. *Nat. Commun.* 7 (1), 12433. doi: 10.1038/ncomms12433

Kawaharada, Y., Kelly, S., Nielsen, M. W., Hjuler, C. T., Gysel, K., Muszyński, A., et al. (2015). Receptor-mediated exopolysaccharide perception controls bacterial infection. *Nature* 523 (7560), 308–312. doi: 10.1038/nature14611

Kawaharada, Y., Nielsen, M. W., Kelly, S., James, E. K., Andersen, K. R., Rasmussen, S. R., et al. (2017). Differential regulation of the *Epr3* receptor coordinates membrane-restricted rhizobial colonization of root nodule primordia. *Nat. Commun.* 8, 14534. doi: 10.1038/ncomms14534

Ke, X., Xiao, H., Peng, Y., Wang, J., Lv, Q., and Wang, X. (2022). Phosphoenolpyruvate reallocation links nitrogen fixation rates to root nodule energy state. *Science* 378 (6623), 971–977. doi: 10.1126/science.abq8591

Kistner, C., and Parniske, M. (2002). Evolution of signal transduction in intracellular symbiosis. *Trends Plant Sci.* 7 (11), 511–518. doi: 10.1016/s1360-1385(02)02356-7

Kondorosi, E., Mergaert, P., and Kereszt, A. (2013). A paradigm for endosymbiotic life: cell differentiation of *Rhizobium* bacteria provoked by host plant factors. *Annu. Rev. Microbiol.* 67, 611–628. doi: 10.1146/annurev-micro-092412-155630

Konishi, M., and Yanagisawa, S. (2013). Arabidopsis NIN-like transcription factors have a central role in nitrate signalling. *Nat. Commun.* 4, 1617. doi: 10.1038/ncomms2621

Krusell, L., Madsen, L. H., Sato, S., Aubert, G., Genua, A., Szczyglowski, K., et al. (2002). Shoot control of root development and nodulation is mediated by a receptor-like kinase. *Nature* 420 (6914), 422–426. doi: 10.1038/nature01207

Lace, B., Su, C., Invernot Perez, D., Rodriguez-Franco, M., Vernié, T., Batzenschlager, M., et al. (2023). RPG acts as a central determinant for infectosome formation and cellular polarization during intracellular rhizobial infections. *Elife* 12, e80741. doi: 10.7554/eLife.80741

Laffont, C., Ivanovici, A., Gautrat, P., Brault, M., Djordjevic, M. A., and Frugier, F. (2020). The NIN transcription factor coordinates CEP and CLE signaling peptides that regulate nodulation antagonistically. *Nat. Commun.* 11 (1), 3167. doi: 10.1038/s41467-020-16968-1

Laporte, P., Lepage, A., Fournier, J., Catrice, O., Moreau, S., Jardinaud, M.-F., et al. (2013). The CCAAT box-binding transcription factor NF-YA1 controls rhizobial infection. *J. Exp. Bot.* 65 (2), 481–494. doi: 10.1093/jxb/ert392

Lévy, J., Bres, C., Geurts, R., Chalhoub, B., Kulikova, O., Duc, G., et al. (2004). A putative Ca^{2+} and calmodulin-dependent protein kinase required for bacterial and fungal symbioses. *Science* 303 (5662), 1361–1364. doi: 10.1126/science.1093038

Li, X., Liu, M., Cai, M., Chiasson, D., Groth, M., Heckmann, A. B., et al. (2023). RPG interacts with E3-ligase CERBERUS to mediate rhizobial infection in *Lotus japonicus*. *PloS Genet.* 19 (2), e1010621. doi: 10.1371/journal.pgen.1010621

Lim, C. W., Lee, Y. W., and Hwang, C. H. (2011). Soybean nodule-enhanced CLE peptides in roots act as signals in GmNARK-mediated nodulation suppression. *Plant Cell Physiol.* 52 (9), 1613–1627. doi: 10.1093/pcp/pcr091

Limpens, E., Franken, C., Smit, P., Willemse, J., Bisseling, T., and Geurts, R. (2003). LysM domain receptor kinases regulating rhizobial Nod factor-induced infection. *Science* 302 (5645), 630–633. doi: 10.1126/science.1090074

Lin, J. S., Li, X., Luo, Z., Mysore, K. S., Wen, J., and Xie, F. (2018). NIN interacts with NLPs to mediate nitrate inhibition of nodulation in *Medicago truncatula*. *Nat. Plants* 4 (11), 942–952. doi: 10.1038/s41477-018-0261-3

Liu, J., and Bisseling, T. (2020). Evolution of NIN and NIN-like genes in relation to nodule symbiosis. *Genes (Basel)* 11 (7), 777. doi: 10.3390/genes11070777

Liu, C. W., Breakspear, A., Guan, D., Cerri, M. R., Jackson, K., Jiang, S., et al. (2019). NIN acts as a network hub controlling a growth module required for rhizobial infection. *Plant Physiol.* 179 (4), 1704–1722. doi: 10.1104/pp.18.01572

Liu, K. H., Liu, M., Lin, Z., Wang, Z. F., Chen, B., Liu, C., et al. (2022). NIN-like protein 7 transcription factor is a plant nitrate sensor. *Science* 377 (6613), 1419–1425. doi: 10.1126/science.add1104

Liu, K. H., Niu, Y., Konishi, M., Wu, Y., Du, H., Sun Chung, H., et al. (2017). Discovery of nitrate-CPK-NLP signalling in central nutrient-growth networks. *Nature* 545 (7654), 311–316. doi: 10.1038/nature22077

Liu, J., Rasing, M., Zeng, T., Klein, J., Kulikova, O., and Bisseling, T. (2021). NIN is essential for development of symbiosomes, suppression of defence and premature senescence in *Medicago truncatula* nodules. *New Phytol.* 230 (1), 290–303. doi: 10.1111/nph.17215

Liu, J., Rutten, L., Limpens, E., van der Molen, T., van Velzen, R., Chen, R., et al. (2019). A remote cis-regulatory region is required for *NIN* expression in the pericycle to initiate nodule primordium formation in *Medicago truncatula*. *Plant Cell* 31 (1), 68–83. doi: 10.1105/tpc.18.00478

Liu, H., Sandal, N., Andersen, K. R., James, E. K., Stougaard, J., Kelly, S., et al. (2018). A genetic screen for plant mutants with altered nodulation phenotypes in response to rhizobial glycan mutants. *New Phytol.* 220 (2), 526–538. doi: 10.1111/nph.15293

Madsen, E. B., Madsen, L. H., Radutoiu, S., Olbryt, M., Rakwalska, M., Szczyglowski, K., et al. (2003). A receptor kinase gene of the LysM type is involved in legumeperception of rhizobial signals. *Nature* 425 (6958), 637–640. doi: 10.1038/nature02045

Madsen, L. H., Fukai, E., Radutoiu, S., Yost, C. K., Sandal, N., Schauser, L., et al. (2005). LORE1, an active low-copy-number TY3-gypsy retrotransposon family in the model legume *Lotus japonicus*. *Plant J.* 44 (3), 372–381. doi: 10.1111/j.1365-313X.2005.02534.x

Marchive, C., Roudier, F., Castaings, L., Bréhaut, V., Blondet, E., Colot, V., et al. (2013). Nuclear retention of the transcription factor NLP7 orchestrates the early response to nitrate in plants. *Nat. Commun.* 4, 1713. doi: 10.1038/ncomms2650

Marsh, J. F., Rakocevic, A., Mitra, R. M., Brocard, L., Sun, J., Eschstruth, A., et al. (2007). *Medicago truncatula NIN* is essential for rhizobial-independent nodule organogenesis induced by autoactive calcium/calmodulin-dependent protein kinase. *Plant Physiol.* 144 (1), 324–335. doi: 10.1104/pp.106.093021

Mathesius, U. (2022). Are legumes different? Origins and consequences of evolving nitrogen fixing symbioses. *J. Plant Physiol.* 276, 153765. doi: 10.1016/j.jplph.2022.153765

Mergaert, P., Kereszt, A., and Kondorosi, E. (2020). Gene expression in nitrogen-fixing symbiotic nodule cells in *Medicago truncatula* and other nodulating plants. *Plant Cell* 32 (1), 42–68. doi: 10.1105/tpc.19.00494

Miller, J. B., Pratap, A., Miyahara, A., Zhou, L., Bornemann, S., Morris, R. J., et al. (2013). Calcium/calmodulin-dependent protein kinase is negatively and positively regulated by calcium, providing a mechanism for decoding calcium responses during symbiosis signaling. *Plant Cell* 25 (12), 5053–5066. doi: 10.1105/tpc.113.116921

Mohr, W., Lehnen, N., Ahmerkamp, S., Marchant, H. K., Graf, J. S., Tschitschko, B., et al. (2021). Terrestrial-type nitrogen-fixing symbiosis between seagrass and a marine bacterium. *Nature* 600 (7887), 105–109. doi: 10.1038/s41586-021-04063-4

Moling, S., Pietraszewska-Bogiel, A., Postma, M., Fedorova, E., Hink, M. A., Limpens, E., et al. (2014). Nod factor receptors form heteromeric complexes and are essential for intracellular infection in *Medicago* nodules. *Plant Cell* 26 (10), 4188–4199. doi: 10.1105/tpc.114.129502

Mortier, V., Den Herder, G., Whitford, R., Van de Velde, W., Rombauts, S., D'haeseleer, K., et al. (2010). CLE peptides control *Medicago truncatula* nodulation locally and systemically. *Plant Physiol.* 153 (1), 222–237. doi: 10.1104/pp.110.153718

Murray, J., Karas, B., Ross, L., Brachmann, A., Wagg, C., Geil, R., et al. (2006). Genetic suppressors of the *Lotus japonicus har1-1* hypernodulation phenotype. *Mol. Plant Microbe Interact.* 19 (10), 1082–1091. doi: 10.1094/MPMI-19-1082

Nishida, H., Nosaki, S., Suzuki, T., Ito, M., Miyakawa, T., Nomoto, M., et al. (2021). Different DNA-binding specificities of NLP and NIN transcription factors underlie nitrate-induced control of root nodulation. *Plant Cell* 33 (7), 2340–2359. doi: 10.1093/plcell/koab103

Nishida, H., Tanaka, S., Handa, Y., Ito, M., Sakamoto, Y., Matsunaga, S., et al. (2018). A NIN-LIKE PROTEIN mediates nitrate-induced control of root nodule symbiosis in *Lotus japonicus*. *Nat. Commun.* 9 (1), 499. doi: 10.1038/s41467-018-02831-x

Nishimura, R., Hayashi, M., Wu, G.-J., Kouchi, H., Imaizumi-Anraku, H., Murakami, Y., et al. (2002). HAR1 mediates systemic regulation of symbiotic organ development. *Nature* 420 (6914), 426–429. doi: 10.1038/nature01231

Okamoto, S., Ohnishi, E., Sato, S., Takahashi, H., Nakazono, M., Tabata, S., et al. (2008). Nod factor/nitrate-induced CLE genes that drive HAR1-mediated systemic regulation of nodulation. *Plant Cell Physiol.* 50 (1), 67–77. doi: 10.1093/pcp/pcn194

Oldroyd, G. E. (2013). Speak, friend, and enter: signalling systems that promote beneficial symbiotic associations in plants. *Nat. Rev. Microbiol.* 11 (4), 252–263. doi: 10.1038/nrmicro2990

Oldroyd, G. E., and Downie, J. A. (2004). Calcium, kinases and nodulation signalling in legumes. *Nat. Rev. Mol. Cell Biol.* 5 (7), 566–576. doi: 10.1038/nrm1424

Perry, J., Brachmann, A., Welham, T., Binder, A., Charpentier, M., Groth, M., et al. (2009). TILLING in *Lotus japonicus* identified large allelic series for symbiosis genes and revealed a bias in functionally defective ethyl methanesulfonate alleles toward glycine replacements. *Plant Physiol.* 151 (3), 1281–1291. doi: 10.1104/pp.109.142190

Pislariu, C. I., Murray, D., Wen, J., Cosson, V., Muni, R. R. D., Wang, M., et al. (2012). A *Medicago truncatula* tobacco retrotransposon insertion mutant collection with defects in nodule development and symbiotic nitrogen fixation. *Plant Physiol.* 159 (4), 1686–1699. doi: 10.1104/pp.112.197061

Qiu, L., Lin, J. S., Xu, J., Sato, S., Parniske, M., Wang, T. L., et al. (2015). SCARN a novel class of SCAR protein that is required for root-hair infection during legume nodulation. *PloS Genet.* 11 (10), e1005623. doi: 10.1371/journal.pgen.1005623

Radutoiu, S., Madsen, L. H., Madsen, E. B., Felle, H. H., Umehara, Y., Grønlund, M., et al. (2003). Plant recognition of symbiotic bacteria requires two LysM receptor-like kinases. *Nature* 425 (6958), 585–592. doi: 10.1038/nature02039

Roy, S., Liu, W., Nandety, R. S., Crook, A., Mysore, K. S., Pislariu, C. I., et al. (2020). Celebrating 20 years of genetic discoveries in legume nodulation and symbiotic nitrogen fixation. *Plant Cell* 32 (1), 15–41. doi: 10.1105/tpc.19.00279

Sandal, N., Petersen, T. R., Murray, J., Umehara, Y., Karas, B., Yano, K., et al. (2006). Genetics of symbiosis in *Lotus japonicus*: recombinant inbred lines, comparative genetic maps, and map position of 35 symbiotic loci. *Mol. Plant Microbe Interact.* 19 (1), 80–91. doi: 10.1094/ MPMI -19-0080

Santi, C., Bogusz, D., and Franche, C. (2013). Biological nitrogen fixation in non-legume plants. *Ann. Bot.* 111 (5), 743–767. doi: 10.1093/aob/mct048

Schauser, L., Roussis, A., Stiller, J., and Stougaard, J. (1999). A plant regulator controlling development of symbiotic root nodules. *Nature* 402 (6758), 191–195. doi: 10.1038/46058

Schiessl, K., Lilley, J. L. S., Lee, T., Tamvakis, I., Kohlen, W., Bailey, P. C., et al. (2019). *NODULE INCEPTION* recruits the lateral root developmental program for symbiotic nodule organogenesis in *Medicago truncatula*. *Curr. Biol.* 29 (21), 3657–3668.e3655. doi: 10.1016/j.cub.2019.09.005

Schnabel, E., Journet, E.-P., de Carvalho-Niebel, F., Duc, G., and Frugoli, J. (2005). The *Medicago truncatula SUNN* gene encodes a *CLV1*-like leucine-rich repeat receptor kinase that regulates nodule number and root length. *Plant Mol. Biol.* 58 (6), 809–822. doi: 10.1007/s11103-005-8102-y

Searle, I. R., Men, A. E., Laniya, T. S., Buzas, D. M., Iturbe-Ormaetxe, I., Carroll, B. J., et al. (2003). Long-distance signaling in nodulation directed by a CLAVATA1-like receptor kinase. *Science* 299 (5603), 109–112. doi: 10.1126/science.1077937

Shahan, R., and Benfey, P. N. (2020). A co-opted regulator of lateral root development controls nodule organogenesis in *Lotus*. *Dev. Cell* 52 (1), 6–7. doi: 10.1016/j.devcel.2019.12.009

Singh, S., Katzer, K., Lambert, J., Cerri, M., and Parniske, M. (2014). CYCLOPS, a DNA-binding transcriptional activator, orchestrates symbiotic root nodule development. *Cell Host Microbe* 15 (2), 139–152. doi: 10.1016/j.chom.2014.01.011

Singh, S., and Parniske, M. (2012). Activation of calcium- and calmodulin-dependent protein kinase (CCaMK), the central regulator of plant root endosymbiosis. *Curr. Opin. Plant Biol.* 15 (4), 444–453. doi: 10.1016/j.pbi.2012.04.002

Sinharoy, S., Liu, C., Breakspear, A., Guan, D., Shailes, S., Nakashima, J., et al. (2016). A *Medicago truncatula* cystathionine-b-synthase-like domain-containing protein is required for rhizobial infection and symbiotic nitrogen fixation. *Plant Physiol.* 170 (4), 2204–2217. doi: 10.1104/pp.15.01853

Smit, P., Limpens, E., Geurts, R., Fedorova, E., Dolgikh, E., Gough, C., et al. (2007). Medicago LYK3, an entry receptor in rhizobial nodulation factor signaling. *Plant Physiol.* 145 (1), 183–191. doi: 10.1104/pp.107.100495

Soltis, D. E., Soltis, P. S., Morgan, D. R., Swensen, S. M., Mullin, B. C., Dowd, J. M., et al. (1995). Chloroplast gene sequence data suggest a single origin of the predisposition for symbiotic nitrogen fixation in angiosperms. *Proc. Natl. Acad. Sci. U.S.A.* 92 (7), 2647–2651. doi: 10.1073/pnas.92.7.2647

Soyano, T., Hirakawa, H., Sato, S., Hayashi, M., and Kawaguchi, M. (2014). Nodule Inception creates a long-distance negative feedback loop involved in homeostatic regulation of nodule organ production. *Proc. Natl. Acad. Sci. U.S.A.* 111 (40), 14607–14612. doi: 10.1073/pnas.1412716111

Soyano, T., Kouchi, H., Hirota, A., and Hayashi, M. (2013). Nodule inception directly targets *NF-Y* subunit genes to regulate essential processes of root nodule development in *Lotus japonicus*. *PloS Genet.* 9 (3), e1003352. doi: 10.1371/journal.pgen.1003352

Soyano, T., Shimoda, Y., Kawaguchi, M., and Hayashi, M. (2019). A shared gene drives lateral root development and root nodule symbiosis pathways in *Lotus*. *Science* 366 (6468), 1021–1023. doi: 10.1126/science.aax2153

Stambulska, U. Y., and Bayliak, M. M. (2019). "Legume-rhizobium symbiosis: secondary metabolites, free radical processes, and effects of heavy metals," in *Co-Evolution of Secondary Metabolites*. Eds. J.-M. Merillon and K. G. Ramawat (Cham: Springer International Publishing), 1–32.

Stracke, S., Kistner, C., Yoshida, S., Mulder, L., Sato, S., Kaneko, T., et al. (2002). A plant receptor-like kinase required for both bacterial and fungal symbiosis. *Nature* 417 (6892), 959–962. doi: 10.1038/nature00841

Sumimoto, H., Kamakura, S., and Ito, T. (2007). Structure and function of the PB1 domain, a protein interaction module conserved in animals, fungi, amoebas, and plants. *Sci. STKE* 2007 (401), re6. doi: 10.1126/stke.4012007re6

Suzaki, T., Yano, K., Ito, M., Umehara, Y., Suganuma, N., and Kawaguchi, M. (2012). Positive and negative regulation of cortical cell division during root nodule development in *Lotus japonicus* is accompanied by auxin response. *Development* 139 (21), 3997–4006. doi: 10.1242/dev.084079

Tirichine, L., Sandal, N., Madsen, L. H., Radutoiu, S., Albrektsen, A. S., Sato, S., et al. (2007). A gain-of-function mutation in a cytokinin receptor triggers spontaneous root nodule organogenesis. *Science* 315 (5808), 104–107. doi: 10.1126/science.1132397

Tsikou, D., Yan, Z., Holt, D. B., Abel, N. B., Reid, D. E., Madsen, L. H., et al. (2018). Systemic control of legume susceptibility to rhizobial infection by a mobile microRNA. *Science* 362 (6411), 233–236. doi: 10.1126/science.aat6907

Tsyganov, V. E., Voroshilova, V. A., Kukalev, A. S., Jacobi, L. M., Azarova, T. S., Borisov, A. Y., et al. (1999). *Pisum sativum* L. genes *Sym14* and *Sym35* control infection thread growth initiation during the development of symbiotic nodules. *Russ. J. Genet.* 35 (3), 284–291.

van Velzen, R., Doyle, J. J., and Geurts, R. (2019). A resurrected scenario: single gain and massive loss of nitrogen-fixing nodulation. *Trends Plant Sci.* 24 (1), 49–57. doi: 10.1016/j.tplants.2018.10.005

van Velzen, R., Holmer, R., Bu, F., Rutten, L., van Zeijl, A., Liu, W., et al. (2018). Comparative genomics of the nonlegume *Parasponia* reveals insights into evolution of nitrogen-fixing rhizobium symbioses. *Proc. Natl. Acad. Sci.* 115 (20), E4700–E4709. doi: 10.1073/pnas.1721395115

Veerappan, V., Jani, M., Kadel, K., Troiani, T., Gale, R., Mayes, T., et al. (2016). Rapid identification of causative insertions underlying *Medicago truncatula Tnt1* mutants defective in symbiotic nitrogen fixation from a forward genetic screen by whole genome sequencing. *BMC Genomics* 17, 141. doi: 10.1186/s12864-016-2452-5

Vernié, T., Kim, J., Frances, L., Ding, Y., Sun, J., Guan, D., et al. (2015). The NIN transcription factor coordinates diverse nodulation programs in different tissues of the *Medicago truncatula* root. *Plant Cell* 27 (12), 3410–3424. doi: 10.1105/tpc.15.00461

Wang, D., Dong, W., Murray, J., and Wang, E. (2022). Innovation and appropriation in mycorrhizal and rhizobial symbioses. *Plant Cell* 34 (5), 1573–1599. doi: 10.1093/plcell/koac039

Wang, T., Guo, J., Peng, Y., Lyu, X., Liu, B., Sun, S., et al. (2021). Light-induced mobile factors from shoots regulate rhizobium-triggered soybean root nodulation. *Science* 374 (6563), 65–71. doi: 10.1126/science.abh2890

Wang, L., Sun, Z., Su, C., Wang, Y., Yan, Q., Chen, J., et al. (2019). A GmNINa-miR172c-NNC1 regulatory network coordinates the nodulation and autoregulation of nodulation pathways in soybean. *Mol. Plant* 12 (9), 1211–1226. doi: 10.1016/j.molp.2019.06.002

Wang, Z., Wang, L., Wang, Y., and Li, X. (2020). The NMN module conducts nodule number orchestra. *iScience* 23 (2), 100825. doi: 10.1016/j.isci.2020.100825

Xiao, T. T., Schilderink, S., Moling, S., Deinum, E. E., Kondorosi, E., Franssen, H., et al. (2014). Fate map of *Medicago truncatula* root nodules. *Development* 141 (18), 3517–3528. doi: 10.1242/dev.110775

Xie, F., Murray, J. D., Kim, J., Heckmann, A. B., Edwards, A., Oldroyd, G. E. D., et al. (2012). Legume pectate lyase required for root infection by rhizobia. *Proc. Natl. Acad. Sci.* 109 (2), 633–638. doi: 10.1073/pnas.1113992109

Yano, K., Yoshida, S., Muller, J., Singh, S., Banba, M., Vickers, K., et al. (2008). CYCLOPS, a mediator of symbiotic intracellular accommodation. *Proc. Natl. Acad. Sci. U.S.A.* 105 (51), 20540–20545. doi: 10.1073/pnas.0806858105

Yoro, E., Suzaki, T., Toyokura, K., Miyazawa, H., Fukaki, H., and Kawaguchi, M. (2014). A positive regulator of nodule organogenesis, NODULE INCEPTION, acts as a negative regulator of rhizobial infection in *Lotus japonicus*. *Plant Physiol.* 165 (2), 747–758. doi: 10.1104/pp.113.233379

Yuan, P., Luo, F., Gleason, C., and Poovaiah, B. W. (2022). Calcium/calmodulin-mediated microbial symbiotic interactions in plants. *Front. Plant Sci.* 13. doi: 10.3389/fpls.2022.984909

Zhang, Y., Fu, Y., Xian, W., Li, X., Feng, Y., Bu, F., et al. (2023). Comparative phylogenomics and phylotranscriptomics provide insights into the genetic complexity of nitrogen fixing root nodule symbiosis. *Plant Commun.* 100671. doi: 10.1016/j.xplc.2023.100671

Zipfel, C., and Oldroyd, G. E. (2017). Plant signalling in symbiosis and immunity. *Nature* 543 (7645), 328–336. doi: 10.1038/nature22009

Frontiers in
Plant Science

Cultivates the science of plant biology and its applications

The most cited plant science journal, which advances our understanding of plant biology for sustainable food security, functional ecosystems and human health.

Discover the latest Research Topics

See more →

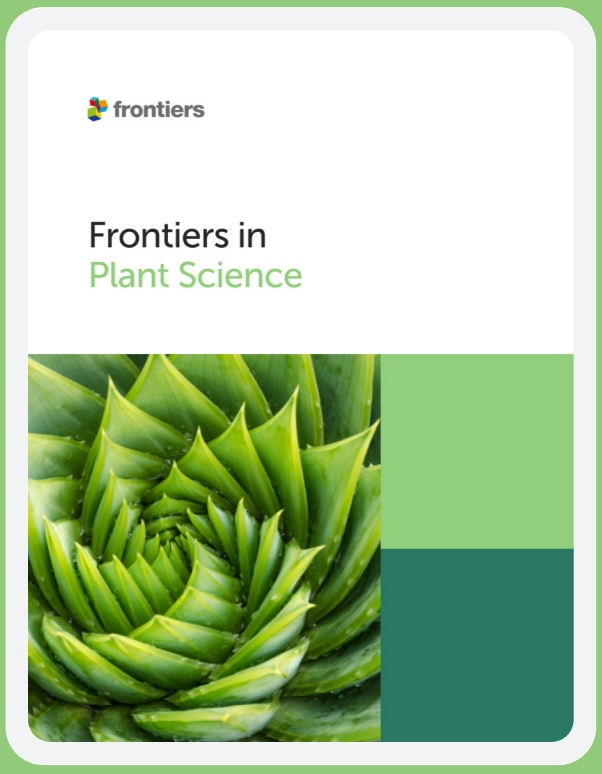

Frontiers

Avenue du Tribunal-Fédéral 34
1005 Lausanne, Switzerland
frontiersin.org

Contact us

+41 (0)21 510 17 00
frontiersin.org/about/contact